

REDUCTION OF NUCLEAR-SIZE RELATED UNCERTAINTIES IN
ATOMIC SPECTROSCOPY

**SIZE MATTERS: REDUCTION OF
NUCLEAR-SIZE RELATED UNCERTAINTIES IN
ATOMIC SPECTROSCOPY**

By LASZLO TIBOR ZALAVARI, B.Sc., M.Sc.

A Thesis Submitted to the School of Graduate Studies in Partial
Fulfilment of the Requirements for the Degree Doctor of Philosophy

McMaster University © Copyright by Laszlo Tibor Zalavari, April 2020

McMaster University DOCTOR OF PHILOSOPHY (2020) Hamilton,
Ontario (Physics and Astronomy)

TITLE: Size Matters: Reduction of Nuclear-Size Related Uncertainties in
Atomic Spectroscopy

AUTHOR: Laszlo Tibor Zalavari, B.Sc. (University of Sussex), M.Sc.
(Imperial College London)

SUPERVISOR: Dr Clifford Burgess

NUMBER OF PAGES: xxiii, 284

Public Abstract

The finite size of the nucleus shifts the bound-state energy of electrons (or muons) in atoms. Although these effects had been captured through a large number of nuclear-model independent “nuclear moments” closely related to the extent of the nucleus in the past, they introduce large uncertainties into theoretical predictions, which hinders testing fundamental subatomic processes in spectroscopic measurements. In this work it is shown that there is a more manageable number of parameters that control these effects because the above moments always appear in specific combinations. This allows for trading these combinations for differences between experimental values and their theoretically expected ones that assume the nucleus to have no size, which is the key in making predictions for atomic transitions that do not suffer from the large nuclear errors. A large set of such predictions are made for Hydrogen and the principles are applied to its muonic cousin as well.

Abstract

This work details how to use the Point-Particle Effective Field Theory (PPEFT) framework to make predictions for the nuclear-size contributions to spectroscopic transitions of atoms without the overbearing large uncertainties generally associated with such effects. After a lightning review of Quantum Field Theories, Effective Field Theories and their model-building algorithms, the backbones of the PPEFT formalism are laid down by considering the low-energy effective theories of lumps. Then, by drawing an analogy between a certain type of lumps and a freely propagating point-particle we build a PPEFT for nuclei, which we gradually couple to gauge and fermionic fields. We find that the consequences of having a nucleus in our theory are captured by a set of new near-nucleus boundary conditions its action implies for the surrounding fields, set up on a Gaussian spherical boundary with arbitrary radius, ϵ . Afterwards, we use this formalism to derive the effects of the finite size of the nucleus on bound-state energies in terms of Renormalization Group (RG)-invariant parameters that characterize the running of the PPEFT couplings in ϵ , implied by these new boundary conditions in order to keep physical quantities independent of this fictitious scale. Surprisingly, when comparing to formulae from the literature that express these same energy shifts in terms of nuclear moments there always appear to be fewer RG-invariants than moments. By fitting these handful of parameters using experimental data we then reduce the errors in nuclear-size effect predictions for other transitions by writing them in terms of differences between spectroscopic measurements and their corresponding energy differences predicted by those bound-state Quantum Electrodynamics calculations that assume nuclei to be point-like. Finally, we apply this algorithm to the systems: ${}^4_2\text{He}^+$, $\mu{}^4_2\text{He}^+$, H, and μH , where we make such predictions.

Acknowledgements

When I first received word of my offer from McMaster, I was ecstatic. It would be the first time that my wife, Juli and I would spend more than one year in the same place as we had moved around every year of our relationship one way or another. I had to share the news with her immediately, which was not too difficult, considering I was sitting in the cafe where she was working at the time. She took a break and we sat down to plan this next chapter of our lives in Canada. We started looking at places to stay, the university, I added Hamilton to my Weather app, *etc.* I also looked up Hamilton on Google Maps and saw that it had this big grid layout and with my naive European mind I thought: “This must mean it’s like Manhattan! It’s going to be a really beautiful, bustling, modern city”. That was the first lesson Hamilton had taught me, *always* check out a place before you move there!

Nevertheless, overall I had a good time at McMaster; I learned a lot, met a lot of wonderful people and made lots of friends and I even got married during my time here. It would not have been possible for me to finish this degree without the incredible amount of support I have received from family, friends and colleagues over the years. It is now time to thank all these people.

First, on the professional side, I would like to thank my supervisor, Dr Cliff Burgess for his patience with me during these four years. I know there had been some tough times and we had not always seen eye to eye, but I very much appreciate all that you have given me, starting with the opportunity to come to McMaster and Perimeter Institute. I have to extend this gratitude to Dr Sung-Sik Lee and Dr Duncan O’Dell who have also selflessly devoted their time to attend my committee meetings, comprehensive exam and my defense. I would also like to thank Dr Veronica Sanz and Dr Markus Rummel who believed in me and taught me that it is OK not to know everything.

Additionally, I would like to acknowledge and thank the hard work of the ladies in the Physics Office: Rose, Mara, Tina, Hope and Lyndsay, whose support in all matters has been an invaluable asset. Werner, thank you for the countless drives between McMaster and Perimeter and for always keeping us company.

Last but not least, I would like to thank my peers. Peter, you have certainly taught me a lot over the years and were always there to answer

my questions and explain things to me (sometimes many times over). I am eternally grateful for your help and patience, and I think you are a great researcher and person to work with, hope your dreams of becoming a professor come true, you deserve it. Markus, Greg, Josh, Dan, Sara, David and Mario thank you for coming to the group meetings and chiming in on my projects. Anton, James, Jon, Ryan, Wyatt, Yannick, Hank, Alex and Sriram thank you for teaching me lots of cool physics during the High-Energy Theory Journal Club sessions, I am team ETH 4 life! Ben, Carmen, James, Sarah and Connor, thank you guys for getting MAPSA off of the ground and thank you Jacqueline, Erica, Jon, Hamza, JC, Joey, Ashley for collectively representing all the grad students in trying to make our lives at the department better, don't forget to officially form the Water Fountain Committee in August, please! Sara, Matt, Lili and Ryan, it was a pleasure to organize the Physics Alumni Night with you guys, I could not have asked for a better team to do this. I am also indebted to Ryan Trepanier for his hard work in setting up the Graduate Student Ambassador program of which I was lucky enough to be a part of and hopefully have helped some students navigate their way into graduate studies at McMaster.

On the more personal side, I would like to start with thanking my wife. Juli, you are the most incredible person I have ever met and I am very lucky to be able to call you my partner as we wander through life together. Your humour always cheers me up, your adventurousness brings me out of my comfort zone to try new things and go to new places, your dedication and perseverance drives me to want to get better at everything I do and always improve myself, your love makes me feel happy, safe, warm and like I belong. I could not have done this program without your unwavering support, thank you for everything.

Next, none of what I have achieved would have been possible without my family. I would like to thank my mom and both dads for raising me to be who I am today. I can never repay you for all the love, hard work, and selflessness you have given me/ done for me but I will spend my life trying. Eszter, thank you for growing up to be an amazing sister, I will always be there for you for anything you need and hope that life will allow us to see each other more often in the future than it has in the past. Boti, take care of yourself, I hope you find your way through life. Petra, Kyra, you are great cousins, thank you for all the fun we had. Kriszti, Judit, thanks for being such great aunties. Nagymama, Nagypapa, Misi papa, Papus, Dede, Nagypapa (Imi bácsi) thank you for giving me such an awesome family and for being the best grandparents. My in-laws, thank you for always being so welcoming towards me and for all the help you have given us over the past few years, you make us feel home away from home.

Lastly, Bence, Flóri, Eszter, Gyuri, Marci, Ati, Dorca, Stefan and Tin thank you for being the living proofs of the sentiment that friendship knows no bounds and cares not about distance. I will always look forward to seeing you guys and trashing you all at table-tennis and losing to all of you at

Dixit. Jon, Alejandra, James, Greg, Peter, Wyatt, Josh, and Matt I am so happy that I have met you. Your friendship has been a pillar of support that I could always rely on and I will never forget all the fun times we had at the countless game nights and house parties.

Contents

1	Introduction	1
1.1	Objective and Outline of Thesis	1
1.2	Of QFTs and EFTs	3
1.2.1	The principle of decoupling	3
1.2.2	The QFT LEGO and Predictive Power	5
1.2.3	Wilsonian Actions and EFTs	9
1.2.4	Dimensional Analysis and the Robustness of EFTs	12
1.3	The PPEFT Framework	14
1.3.1	Lumps and Their Low-energy Degrees of Freedom	15
1.3.2	Implications of Lumps	19
1.4	PPEFT for Atoms	26
1.4.1	Relativistic, Free, Scalar Particle and Symmetries	27
1.4.2	Coupling to the photon	29
1.4.3	Coupling to the Electron	33
1.5	Nuclear-Size Effects in Atomic Bound-States	41
1.5.1	The success of QED	42
1.5.2	Moments...Moments Everywhere!	44
1.5.3	How PPEFT Can Help	48
2	Leading Finite-Size Effects of Scalar Nuclei on Bound Dirac Fermions	51
3	Subleading Finite-Size Effects of Scalar Nuclei	107
4	Leading Spin-Dependent Finite-Size Effects in Hydrogen	128
5	Summary, Conclusion and Outlook	274

List of Figures

Figure 1.1 Depiction of the three relevant scales in an effective theory of lumps	
Figure 2.1 Plot of the RG flow of $\hat{\lambda}_D^\pm := (Z\alpha)(\hat{c}_s \pm \hat{c}_v) \pm 1$ vs $\ln \epsilon/\epsilon_\star$ when $Z\alpha = 0$	51
Figure 2.2 Plot of the large- r normalizability condition defining combination, $\Gamma(1 + 2\zeta)\Gamma(-\zeta - Z\alpha\omega/\kappa)/(\Gamma(1 - 2\zeta)\Gamma(\zeta - Z\alpha\omega/\kappa))$ as a function of $Z\alpha/\omega$. The curves show the actual function and its single-pole and double-pole analytic approximations for the $n = 2, j = 1/2$ state	56
Figure 2.3 Plot of the relative error made as a function of mR when computing $\delta\omega/ \psi(0) ^2$ for a lepton orbiting a shell of positive charge, Ze and radius, R in the $n = 2, j = 1/2$ state, using the single-pole and double-pole approximations to the large- r normalizability condition, $C/A = \Gamma(1 + 2\zeta)\Gamma(-\zeta - Z\alpha\omega/\kappa)/(\Gamma(1 - 2\zeta)\Gamma(\zeta - Z\alpha\omega/\kappa))$	57
Figure 3.1 Plot of the RG flow of $B = (Z\alpha)^4(\hat{d}_s + \hat{d}_v)/4$ (solid blue) and $B = (Z\alpha)(\hat{c}'_s + \hat{c}'_{v\text{tot}})$ (dashed orange) vs $\ln \epsilon/\epsilon_\star$ with $\eta_+ = +1$	110
Figure 3.2 Plot of the RG flow of $B = (Z\alpha)^4(\hat{d}_s + \hat{d}_v)$ (solid blue) and $B = (Z\alpha)(\hat{c}'_s + \hat{c}'_{v\text{tot}})$ (dashed orange) vs $\ln \epsilon/\epsilon_\star$ with $\eta_+ = -1$	111
Figure 3.3 Plot of the RG flow of $B = (Z\alpha)^4(\hat{d}_s + \hat{d}_v)$ (solid blue) and $B = (Z\alpha)(\hat{c}'_s - \hat{c}'_{v\text{tot}})$ (dashed orange) vs $\ln \epsilon/\epsilon_\star^-$ with $\eta_- = -1$	111
Figure 3.4 Plot of the RG flow of $B = (Z\alpha)^4(\hat{d}_s + \hat{d}_v)$ (solid blue) and $B = (Z\alpha)(\hat{c}'_s - \hat{c}'_{v\text{tot}})$ (dashed orange) vs $\ln \epsilon/\epsilon_\star^-$ with $\eta_- = +1$	111
Figure 3.5 Example Feynman graphs of two Coulomb-photon (dashed vertical lines) exchange between an unexcited nucleus (single line on bottom) or an excited nucleus (bold line on bottom) and the orbiting lepton (top solid line)	118
Figure 4.1 Illustration of the two categories of RG flow described by $v(\epsilon)$ against the logarithmic variable $\ln(\epsilon/\epsilon_\star)$	160
Figure 4.2 A plot of how $\bar{\lambda}_+^{(1)}(\epsilon, \eta)$ runs as a function of ϵ with η fixed. The RG-invariant scale $\epsilon_{\star+}$ appearing here is the same one that also labels the running of the spin-independent interactions in $\bar{\lambda}_+^{(0)}$	180
Figure 4.3 The running of $\bar{\lambda}_-^{(1)}$ as a function of ϵ with η held fixed. The	

RG-invariant scale ϵ_{s-} is the same as the scale controlling the running of $\bar{\lambda}_-^{(0)}$ 181

List of Tables

Table 2.1	The first few harmonic numbers	63
Table 4.1	The order of magnitude of various nuclear contributions to atomic energy shifts in H and μH . This table highlights the contributions relevant to current experiments, and also how many RG-invariant parameters are relevant to a given experimental accuracy and what their leading contributions are to the energy shifts	144
Table 4.2	All about the fitting of the RG-invariants in atomic Hydrogen: reference transitions, point-like theoretical contributions, fitted values and errors	203
Table 4.3	Predictions of the finite-size energy contributions and their errors to the best measured (non-referenced) transitions in atomic Hydrogen	204
Table 4.4	The reference transitions, their point-like theoretical contributions and errors, and the fitted RG-invariant parameters and their uncertainties resulting from the fitting procedure	208
Table 4.5	Predictions of the finite-size effects and their errors in less accurately measured transitions of atomic Hydrogen	212
Table 4.6	Another set of predictions of the finite-size effects and their errors in less accurately measured transitions of atomic Hydrogen	213
Table 4.7	Predictions of finite-size contributions and their errors in measured linear combinations of atomic Hydrogen	214

List of Symbols

R	Radius of the region in which a lump solution concentrates its energy. For nuclei it is a scale of nuclear size, $R \sim 1$ fm
ϵ	Radius of the Gaussian pillbox where the alternative boundary conditions are set up
a_{exp}	The length scale of the macroscopic probe. In our applications to atomic bound-states it is the Bohr radius of the leptons orbiting the nucleus, $a_{\text{exp}} = a_B \sim (mZ\alpha)^{-1}$
Z	The atomic number
$\alpha := e^2/4\pi$	The fine-structure constant
e	Unit electric charge
m	Mass of the orbiting lepton
M	Mass of the nucleus
$y^\mu(s)$	Centre-of-mass coordinates of a lump
s	Arbitrary parameter along the nuclear world-line
$\Psi, \bar{\Psi}$	Field of a Dirac fermion and its conjugate
$A^\mu(x)$	Gauge field of a U(1) symmetry group
$\xi^\mu(s)$	Classically anticommuting Grassmann fields representing the nuclear spin degree of freedom
c	Speed of light
\hbar	Plancks constant

k_B	Boltzmann constant
$\eta_{\mu\nu}\eta^{\mu\nu}$	The Minkowski metric and its inverse
$\phi_a(x), \partial\phi_a(x), J_a(x)$	A generic field, its derivative and its source
$\mathcal{L}[\phi_a, \partial\phi_a]$	Lagrangian density functional
$S[\phi_a, \partial\phi_a]$	The action functional
C, P, T, \mathbb{Z}_n	Charge conjugation, parity, time reversal and n -rotation symmetries
$SU_C(3) \times SU_L(2) \times U_Y(1)$	Symmetry group of the Standard Model
$Z[J_a]$	Generating functional of a field theory
$\mathcal{D}\phi_a$	Functional measure of the path integral
$S_0[\phi_a, \partial\phi_a]$	The integrable part of the action, which usually only contains mass and kinetic terms
Δ	The operator sandwiched between two fields in the integrable part of the action
$S_{\text{int}}[\phi_a, \partial\phi_a]$	The non-integrable, interaction part of the action
$\phi(x)$	A real scalar field
m_ϕ	Mass of a real scalar field
λ	Dimensionless coupling of ϕ^4 theory
Λ	High-energy cut-off of a theory
E	Typical energy scale of an experiment and the energy of field excitations created by this experiment
ϕ_a^l, ϕ_a^h	The low-and high-energy parts of a field

S_0^l, S_{int}^l	Integrable and interacting parts of the action containing only low-energy field excitations
S_0^h, S_{int}^h	Integrable and interacting parts of the action containing only high-energy field excitations
S_{mix}	Part of the action resulting from the low-energy, high-energy split of the fields that contains both types of fields
$\langle e^{iS_{\text{int}}^h + iS_{\text{mix}}} \rangle_{\Omega}$	Expectation value of the operator in the angled brackets on the interacting vacuum state, $ \Omega\rangle$
$S_{\text{eff}}[\phi_a^l, \partial\phi_a^l, \partial\partial\phi_a^l, \dots]$	The low-energy effective action left behind after integrating out the high-energy degrees of freedom from the fields
\mathcal{L}_{eff}	The Lagrangian of the effective action, S_{eff}
\mathcal{L}_0	Part of the Lagrangian responsible for the integrable part of the generating functional
c_i	Effective coupling in the low-energy effective Lagrangian
\mathcal{O}_i	Placeholder for generic low-energy effective operator in the low-energy effective Lagrangian
$\not{A} = \gamma^\mu A_\mu$	The Dirac slash notation
g_i	Dimensionless coupling constant
$\bar{\phi}_a(x)$	The dimensionless version of a generic field
k^μ	Four-momentum of a wave-packet excitation of a field
$\bar{\mathcal{O}}_i[\bar{\phi}_a]$	Local dimensionless operator in the low-energy effective Lagrangian, \mathcal{L}_{eff}
$m_{\bar{\phi}_a}$	The mass of a generic field
S_a	Spin of a field, or the parameter on the world-line of a point-particle

\mathbb{N}^0	Set of positive integers including 0
H	Hamiltonian of a field theory with Lagrangian, \mathcal{L}
v	The vev of a given field that minimizes the Hamiltonian of the theory
$\varphi_a(x)$	Background configuration of the field, ϕ_a that asymptotically minimizes the Hamiltonian of the theory
\mathcal{B}_R	Ball of radius, R
$\hat{\phi}_a$	Fluctuations of the field ϕ_a around its background solution, φ_a
$\mathcal{O}[\varphi_a, \partial\varphi_a]$	The φ_a -dependent operator controlling the quantization of the fluctuations, $\hat{\phi}_a$ around this background configuration
$\hat{\phi}_{a,0}$	Fluctuations in the directions of the centre-of-mass coordinates, y^μ of the background solution, $\varphi_a(y - x)$ that turn out to be zero-modes of the operator, $\mathcal{O}[\varphi_a, \partial\varphi_a]$
\mathcal{P}	The world-line of a one-dimensional lump
\mathbb{M}^4	4-dimensional Minkowski spacetime
\mathbb{R}	The real line
$S_{p,0}, \mathcal{L}_{p,0}$	Action of a free blob and its corresponding Lagrangian, $\mathcal{L}_{p,0}$
y_{pt}	Generic low-energy degree of freedom of a lump background
$p^{(y_{\text{pt}})}$	Conjugate momenta to the generic low-energy degree of freedom of a blob, y_{pt}
S_B, \mathcal{L}_B	Bulk action and its corresponding Lagrangian
S_p, \mathcal{L}_p	The action and associated Lagrangian of a lump interacting with its surrounding fields

\mathcal{H}	Hamiltonian density to the Lagrangian density, \mathcal{L}_p
β, ω_β	Generic set of quantum numbers required to specify a state and the energy associated with that state
$\mathcal{Y}_L(\theta, \phi)$	Generic angular function arising in the the solutions to the bulk field equations of motion
L	Set of angular momentum quantum numbers
$\mathcal{C}_L, \mathcal{R}_{\mathcal{C},L}(r)$	The near-origin convergent radial function that solves the bulk field equations of motion, and its associated integration constant
$\mathcal{D}_L, \mathcal{R}_{\mathcal{D},L}(r)$	The near-origin divergent radial function that solves the bulk field equations of motion, and its associated integration constant
l, l_z	The orbital angular momentum quantum number and its projection that describe the various modes of scalar fields solving the Laplace equation in three spatial dimensions
j, j_z, ϖ	The total angular momentum quantum number, its projection, and the parity quantum number describing the various angular momentum modes of fermions in central potentials in three spatial dimensions
$\hat{\mathbf{n}}$	Unit normal to a three-dimensional Gaussian surface, which we always take to be a ball of radius ϵ , and so always set $\hat{\mathbf{n}} = \hat{\mathbf{r}}$
\mathcal{B}_ϵ	Ball of radius ϵ and boundary $\partial\mathcal{B}_\epsilon$
$S_{\partial\mathcal{B}_\epsilon}, \mathcal{L}_{\partial\mathcal{B}_\epsilon}$	Boundary action and the associated Lagrangian that contain parts of the boundary condition inferred from the presence of the lump
$\xi^\mu(s)$	Classically anticommuting field internal to the nucleus that represents its spin
$S_{p,0}, \mathcal{L}_{p,0}$	Action and Lagrangian of a relativistic free particle, and equivalently that of a free lump with only $y^\mu(s)$ as low-energy degrees of freedom

$SO^+(1,3), ISO^+(1,3)$	The proper orthochronous Lorentz- and Poincaré groups
$\Lambda^\mu{}_\nu$	Matrix in the fundamental representation of $SO^+(1,3)$
$f(s)$	An arbitrary well-behaved function
Q, \hat{Q}	Charge of the compact object under the U(1) symmetry and its boundary action equivalent
S_M	The Maxwell action
$A^\mu(x)$	The U(1) gauge field
$F_{\mu\nu}$	Field strength of $A^\mu(x)$
$h(x)$	The scalar function characterizing the U(1) gauge transformation
$S_{p,M}$	Action of a charged lump
P_A^μ	Conjugate momenta of the centre-of-mass coordinates incorporating the effect of the U(1) gauge field
τ	Proper time on the world-line of the compact object
b	PPEFT coupling that turns out to be the magnetic moment of a spinning nucleus
$S_{\partial\mathcal{B}_\epsilon, M}$	Boundary action of the charged lump
a_B	Bohr radius of a bound-state fermion
$S_{D, M}$	Action of a fermion minimally coupled to a U(1) gauge field
D_μ	Covariant derivative action on the fermion fields, $\Psi(x)$
S_{QED}	QED action

$\gamma^\mu, \gamma_5, \gamma^{\mu\nu}$	The 5 gamma matrices of the Dirac algebra and their Lorentz-algebra generators
$S_{p,QED}$	The action of a lump coupled to the full QED theory in the bulk
c_s, c_v	Effective couplings between the lump and the leptonic bulk field
$A_{\text{rad}}^\mu(x)$	Radiation component of the electromagnetic field
ω	Energy eigenvalue of the energy eigenstates of the bulk field equations of motion
$\psi_{njz\varpi}$	Fermionic energy eigenstates of central potentials
$\Omega_{jlz\varpi}(\theta, \phi)$	Spinor harmonics of fermions moving in a central potential
$\mathfrak{f}_{nj\varpi}, \mathfrak{g}_{nj\varpi}$	Solutions to the radial parts of the Dirac equation with a Coulomb potential
$\mathcal{M}_i, {}_1\mathcal{F}_1$	Confluent hypergeometric functions
ρ	Dimensionless variable of the radial Dirac equation
a, a', b, b', c	Various combinations of parameters in the radial Dirac equation
$\zeta, \mathfrak{K}, \kappa$	Parameters of the radial Dirac equation
n	The principal quantum number of leptonic bound-states
σ^i	The two-dimensional Pauli matrices
$\omega_{nj}^D, \kappa_{nj}^D, \mathcal{N}$	Dirac energy eigenvalues, their corresponding momenta and relativistic principal quantum number
B_ϵ	Matrix encoding the alternative near-nucleus boundary conditions imposed on the fermions by the nucleus

$S_{\partial\mathcal{B}_\epsilon, QED}$	Boundary action coupling the nucleus to the bulk theory of QED
\hat{c}_s, \hat{c}_v	Effective boundary action couplings between the nucleus and the leptonic bulk field
$S_{D,M}^{sym}$	The symmetric form of the minimally coupled Dirac action
nL_j	The spectroscopic notation of a state with principal quantum number n , orbital angular momentum quantum number, L and total angular momentum quantum number, j
$\rho_c(r), \rho_m(r)$	The charge- and magnetization distributions of the nucleus
μ_N	The magnetic moment of the nucleus
$\langle r^2 \rangle_e, \langle r^k \rangle_{e/m}$	The charge radius squared and the k^{th} electric (e) or magnetic (m) moment of the nucleus
$\langle r \rangle_{em}$	The integral over the weighted convolution of the magnetization- and charge distributions of the nucleus, known as the Zemach moment
$\delta E_{nS_{1/2}}^{\text{KKS}}$	The very first model-independent record of finite-size contributions to energy shifts
m_r	Reduced mass of the bound-state lepton
$\langle r^k \rangle_c, \langle r^k \rangle_m$	Model-independent nuclear moments of the charge- and magnetization distributions
$\delta E_{nS_{1/2}}^{\text{Zem}}$	The finite-size contribution to the hyperfine splitting of S -waves obtained by Zemach
g_p	Proton g -factor
$\langle r^k \rangle_{ij}$	The k^{th} convoluted moment of charge and magnetization distributions with $i, j = c, m$
$\delta E_{nS_{1/2}}^{\text{Fr}}$	The spin-independent finite-size contributions to $nS_{\frac{1}{2}}$ levels of low- Z atoms as obtained by Friar

$I_2^{\text{NR}}, I_3^{\text{NR}}, I_2^{\text{REL}}, I_3^{\text{REL}}$	Parametric integrals that lead to nuclear moments
H_{n-1}, γ	The harmonic numbers and the Euler-Mascheroni constant
$\delta E_{nP_{1/2}}^{\text{Fr}}$	Spin-independent energy shift to $nP_{\frac{1}{2}}$ states in low- Z atoms calculated by Friar
$\delta E_{nP_{3/2}}^{\text{Fr}}$	The spin-independent energy shift to $nP_{\frac{3}{2}}$ states in low- Z atoms calculated by Friar
$\delta E_{nS_{1/2}}^{\text{CPE}}$	The spin-independent nuclear-structure corrections to energy shifts calculated using Coulomb-exchange
$\langle r^3 \rangle_{cc}^{\text{eff}}, \langle r_{C1} \rangle, \langle r_{C2} \rangle$	Nuclear moments coming from the structure corrections in Coulomb-exchange calculations
$\delta E_{\text{spin}}^{\text{CPE}}$	The spin-dependent nuclear-structure correction to the hyperfine splitting of $nS_{\frac{1}{2}}$ states
$\langle r_{pp} \rangle$	Another nuclear moment coming from nuclear-structure calculations
$\delta\omega$	The energy shift perturbation around the Dirac-Coulomb energies associated with the finite size of the nucleus
\hat{g}_i, \hat{f}_i	Effective nuclear moments
ϵ_\star, y_\star	The RG-invariant parameters controlling the RG-flow of the spin-independent fermion-nucleus effective couplings
$\mathbf{A}(\mathbf{x}), \mathbf{A}_{\text{nuc}}(\mathbf{x})$	The electromagnetic vector-potential and the dipole-field
\mathcal{L}_{int}	Perturbation around the Dirac-Coulomb system
$\mathfrak{s} := em\mu_N/4\pi$	Small parameter controlling the perturbations caused by the magnetic-dipole field of the nucleus

- \mathbf{F}, \mathbf{F}_z Operators of the total atomic angular momentum and its projection with eigenvalues, F, F_z
- \mathbf{I}, \mathbf{J} The nuclear spin operator and the total leptonic angular momentum operator with eigenvalues I, j
- ϵ_F The RG-invariant scale controlling the spin-dependent finite-size effects

Declaration of Authorship

I have always admired science for its unique encouragement of the sharing and seeking of knowledge in a collaborative attempt to further our understanding of the world. As such, I believe it is most difficult to declare and claim in all honesty any one work to be the result of any one person's efforts. In light of this, I would like to point out the following contributions to the works contained in this thesis:

- PPEFT as a framework was conceived by Cliff Burgess and its application to Dirac fermions was concurrently developed mainly by him and Markus Rummel in the first paper presented. Peter Hayman and myself checked and confirmed all of the calculations in this paper, and vastly improved the accuracy of the conclusions by pointing out that the poles of the gamma functions in the large- r normalizability condition used to determine the energy due to finite size were very close to each other and so these functions both had to be expanded around these values in what we had dubbed the “double-pole approximation”. Peter Hayman and I have also developed the numerics to test these approximations, particularly on the examples provided in the appendices and compared them to what could be found in the literature. Additionally, a completely model-independent term in the mode-function ratios in the appendix of $-1/6n^2$ was found by me, which made these numerical tests possible.
- Although Cliff Burgess and Markus Rummel have provided many useful insights and guidance during its development, the second paper is almost entirely the work of Peter Hayman but its contents form an integral part of the third paper and so could not be dispensed. I have worked on this paper in its very early stages and helped derive the nuclear-size independent combinations of spectroscopic data and have checked some of the calculations.
- The last paper is a work of my own that has benefited from the scrutiny and physical insight of Cliff Burgess, Markus Rummel and Peter Hayman. Additionally, Peter Hayman has to be credited for relating the new RG-invariant parameter appearing in this work to the Zemach moment. Furthermore, it has to be noted that the dimensional regularization used for tracking the divergent integrals in matrix elements in Chapter 4 was a joint effort between Cliff Burgess

and I, and that it is thanks to Cliff Burgess that the final wording of this work delivers such a clear message.

Chapter 1

Introduction

1.1 Objective and Outline of Thesis

The main objectives of this thesis are to show that when applying the recently developed Point-Particle Effective Field Theory (PPEFT) framework [1]-[10] to atomic systems the effects of nuclear-size on the energy levels of the orbiting leptons are controlled by fewer parameters than naively expected from other calculations; and to leverage this fact in making predictions for such effects in spectroscopic measurements of the spinless Helium ion (${}^4_2\text{He}^+$), muonic spinless Helium ion ($\mu_2^4\text{He}^+$), Hydrogen (H) and muonic Hydrogen, μH .

To this end, three publications will be presented and the thesis will be organized as follows. Since PPEFT is an Effective Field Theory (EFT) we will begin by reviewing the bare minimum of concepts required to appreciate the differences between Quantum Field Theories (QFTs) and Effective Field Theories (EFTs), including their general model building procedure. Afterwards, we will develop an effective theory of lumps, which we will use to describe nuclei and build up an effective theory of atoms, commenting on the intricacies that arise, which will be addressed in detail in the main text. This will be followed by a brief introduction to the history and current status of finite-size effects in atomic energy levels. As such, the discussion presented in this chapter is aimed to introduce our formalism with enough technicality and clarity that the reader would feel comfortable in jumping right into reading the culminated works.

The second chapter presents the first paper, which details the construction of a PPEFT for atomic systems. In our formalism we model spinless nuclei as charged lumps of size $R \sim 1$ fm, mass, M and charge Ze with its only low-energy field being its centre-of-mass coordinates, $y^\mu(s)$ where s is an arbitrary parameter along the nuclear world-line. The orbiting leptons are taken to be Dirac fermions, $\Psi(x)$ of mass, m and charge $(-e)$ bound to the nucleus by an electromagnetic field, $A^\mu(x)$ at orbits of size of the leptonic Bohr radii, $a_B \sim (mZ\alpha)^{-1}$, where $\alpha := e^2/4\pi$ is the fine-structure constant. The effects of the nucleus on the surrounding fields are shown to be a set of alternative near-origin boundary conditions for the fields in

question and consistency of these new boundary conditions with the large- r normalizability condition of the leptonic bound-states are shown to lead to nuclear-size related energy shifts. This paper presents how the leading such effect – known as the proton charge radius term – can be captured through a single parameter in the PPEFT formalism. Additionally, the procedure necessary to obtain subleading size-related energy shifts using a set of parameters is outlined and these are explicitly matched to the leading and subleading nuclear-size predictions of some simpler nuclear models (*i.e.* UV completions in the field theory language).

In the third chapter, the second paper incorporates subleading interactions between the same nucleus and its surrounding fields to investigate in detail how the subleading nuclear-size effects can be captured in a PPEFT. This is achieved by taking into account higher-order operators in the nuclear action that arise suppressed by an additional power of $R/a_B \sim (mRZ\alpha)$ with respect to those responsible for the charge-radius term of the first paper. The importance of this paper cannot be overstated, as it reveals that despite the inclusion of these new interactions, *no* new effective parameters appear, rather the one responsible for the leading energy shift becomes more refined. We show in detail that comparing the size-related energy shifts written in terms of our effective parameter with that written as a function of the popular nuclear moments reveals that it is only ever certain linear combinations of these nuclear moments that enter energy shifts. Building on this finding, linear combinations of spectroscopic measurements of electronic and muonic atoms with spinless nuclei are devised in which to the accuracy of the first subleading finite-size effects these shifts either cancel, or can be written in terms of differences between experimental values of transitions and those theoretical contributions of their associated energy shifts that assume a point-like nucleus.

The fourth chapter constitutes the bulk of the thesis, presenting the paper that describes the algorithm used to extend the atomic PPEFT to include sources with arbitrary quantum-mechanical spin through the addition of a set of classically anti-commuting low-energy degrees of freedom, $\xi^\mu(s)$ to the nuclear action; thereby making it applicable to a much wider array of systems. To make the application of the PPEFT clear the rest of this paper focuses on the bound-states of atomic and muonic Hydrogen, and we find that to the precision of current experiments in these systems (1 kHz and 10^{-3} meV respectively) we only need to introduce a single new parameter in order to be able to account for spin-dependent finite-size effects. We then apply our previous techniques to fit the existing two parameters of the problem and find that in atomic Hydrogen it is possible to use these fitted values to compute the finite-size contributions to a number of previously measured transitions, which could potentially be improved in the future and act as a testing ground for fundamental theory. On the other hand, due to the extremely high precision of muonic hydrogen measurements and the large mass of the muon we see that in this system both further spin-independent and spin-dependent subleading finite-size effects

need to be captured in the PPEFT in order to be able to make predictions similar to those in atomic Hydrogen.

Finally, in the last chapter the main lessons from reading the atomic physics story through the PPEFT lens are summarized and a good number of possible directions for future research are discussed.

Note that throughout the entire thesis the spacetime metric is assumed to be flat with mostly positive entries $\eta_{\mu\nu} = \text{diag}(-, +, +, +)$ and the units are assumed to be natural, $c = \hbar = k_B = 1$, unless otherwise stated.

1.2 Of QFTs and EFTs

In this section we recap what we mean by an EFT, as it is vital to understand the emergence of this class of theories going forward.

First, the phenomena of decoupling is introduced through a few examples, followed by a hitch-hiker’s guide to the general model-building procedures of field theories. Second, the mathematical description of QFTs, path integrals are introduced and we combine this description with the essence of decoupling to show how EFTs emerge via Wilsonian renormalization. Lastly, the key differences between QFTs and EFTs in terms of their construction and predictive powers are summarized and are used as a segue into the effective theory of lumps.

1.2.1 The principle of decoupling

Let us begin by thinking about a multi-tiered cake with each layer boasting a different flavour. As we sample this cake tier by tier from the bottom up we notice that each level tastes different. Although we do not eat the whole of any one layer we can safely assume that the layers are homogeneous inasmuch that one flavour can only be found in a single level. Then, in order to appreciate any given one of the levels we do not need to know much if anything at all about other layers and flavours. As we munch on, there are various things we can notice: the texture of sponginess or creaminess; the overall taste such as sweet or savoury; the particular taste of chocolate or strawberry; and if we have a really fine palette probably most of the ingredients too. However, in order to appreciate any given layer of the cake we do not need to know anything about the others. We will now argue that this image of a cake is not so different from the world as we know it.

In this analogy, the various levels of the cake correspond to the different length-scales that can be physically probed one way or another, and the flavours represent the different physics needed to describe the given level. At the largest distances mankind can probe (say, the bottom layer of the cake) lies the observable universe, exhibiting some random structure. Zooming in on these structures corresponds to climbing up the cake’s layers, and as we do this we start to see emergence of smaller structures such as galaxy superclusters (the second tier). Zooming in on these we no-

tice galaxy clusters (third tier), then galaxies (fourth tier and so on), solar systems, stars, planets, continents and oceans, landscapes, cities, neighbourhoods, houses, people, dogs, insects, tissues, cells, atoms and finally quarks and other fundamental particles. Each of these structures tend to come with their own set of unique physical laws that help describe them and their interactions at the given length scale; this is what the flavours represent. At any given length scale, these physical laws can go from capturing very simple to very complex phenomena; this is the texture and flavour profile of the levels. What is surprising however is that just like appreciating the different levels of the cake in our example did not require prior knowledge of what all the other layers contain, we do not need to know what all these physical laws are and how they interplay with each other in order to make reliable predictions and describe the world at a given length scale. For example, in order to accurately describe projectile motion on Earth we do not need to know how our planet orbits the Sun nor that everything is made of atoms.

This ubiquitous phenomenon of Nature, whereby the sets of laws that provide precise descriptions of the world separate and become distinct depending on the length scales probed is known as *decoupling*. It is a uniquely interesting and useful feature of the universe as it allows for the construction of testable physical laws – *effective theories* – compartmentalized through the distance ranges over which they apply without prior knowledge of what is happening at all the other length scales.

As a more everyday example of decoupling, imagine driving in a very flat region (much like the Canadian Prairies) at night. At first, an extremely dim, tiny source of light somewhere very far away becomes observable. As time passes, the light seems to become brighter and its source bigger. Some time later the distance to the source becomes small enough that what was initially believed to be a single object splits into two distinct beams that approach at what seems to be the same speed. After some more time passes and once the light sources are very close it becomes clear that what was initially thought to be one single object – at first with one and later with two sources of light – had actually been two motorcycles travelling close together all along. The point is that at each step of separation from the motorbikes the effective description of the light source changes.

On a more physical note, two of the last century’s most cherished theories demonstrate decoupling in a beautiful way. On the one hand, General Relativity (GR) describes the physics of very massive and large-scale objects interacting under gravity; it conceives of the universe as an inherently 4-dimensional spacetime which curves under the influence of matter. GR is absolutely vital in describing how gravitation works in regions where the gravitational force is strong, such as at the orbital distance of Mercury from the Sun or near inspiralling binary systems that produce gravitational waves, yet in regions where gravity is much weaker such as on the surface of the Earth, the Newtonian description of gravity is perfectly sufficient to predict how apples fall from trees. Furthermore, GR is supposed to be

superseded by a quantum description of gravity in regions of ultra-strong gravitational forces such as inside black holes or ultra-short distances and even though a working theory of such a formalism does not yet exist, it is clear that it should match onto GR in some limit. In this sense, GR decouples from quantum gravity and in turn Newtonian gravity decouples from GR as the gravitational force becomes weaker and weaker.

On the other hand, QFT governs the interactions of subatomic, relativistic particles. At the time of writing, this formalism is believed to be the language in which the very short-distance laws of the world had been written and the foundation of this belief is the immense success of theories such as the Standard Model (SM) of particle physics and Quantum Electrodynamics (QED), extensively tested at colliders and in precision atomic spectroscopy experiments. However, even at distance scales probed today there is phenomenological evidence for Beyond the Standard Model (BSM) physics such as dark matter, neutrino masses, *etc.*, which indicate that the SM is not a complete story either, rather it is the theory obtained at some length scales as a decoupled effective description of the underlying theory of BSM. As an example of decoupling in the Standard Model consider the theory of weak interactions. The theory that describes weak decays at very short distances (equivalently, high-energies) is the full electroweak sector of SM with its symmetry breaking properties, in which these processes are mediated by the W and Z vector bosons. Nevertheless, on larger distance scales (*i.e.* at energies below the masses of these particles) weak phenomena had been very effectively described by 4-Fermi interactions, making powerful predictions for proton- and radioactive β -decay long before the Standard Model came to life. Decoupling in QED can be seen from the fact that in order to accurately predict the energy levels of the Hydrogen atom today one needs to use the full Dirac equation with its full QFT description, whereas in the early days it was sufficient to use the quantum mechanics of the non-relativistic (or large-distance) version of the Dirac description, the Schrödinger equation.

The general lesson to be learned here is that depending on the length scale a certain set of objects (be they fields, planets or others) are observed, or equivalently the energies at which their interactions are tested, the effective description of their interplay changes and becomes a theory unto itself. This is the phenomenon of decoupling.

1.2.2 The QFT LEGO and Predictive Power

Having described a few qualitative examples of theories decoupling from each other into effective descriptions at different scales, it is now time to elaborate on this process and make it more precise by studying its mathematical foundations. The first step towards this purpose is to discuss how theories are generated in the first place.

Based on empirical evidence, almost every QFT starts with a dimen-

sionless, Lorentz-invariant, local action,

$$S[\phi_a(x), \partial\phi_a(x)] = \int d^4x \mathcal{L}[\phi_a(x), \partial\phi_a(x)], \quad (1.1)$$

where \mathcal{L} is the Lagrangian (density) of the theory and $\phi_a(x)$ denotes a general set of fields. The action contains information about the dynamics and the interactions of the fields, which correspond to physical processes of the particles associated with these fields – such as propagation, scattering, *etc.* – calculable through Feynman diagrams once the fields have been quantized. These diagrams can be obtained from the generating functional of a QFT, which in very simple terms is merely the functional integral over the exponential of the action as we will define it below shortly. What is important for now is the observation that actions are the fundamental objects one needs to find in order to compute any observables and at a basic level there are three main ingredients that need to be combined in order to build them.

The first ingredient is known as the field content of the theory. It is the collection of the types of fields and corresponding particles such as scalars, fermions, vector bosons, *etc.* that the QFT should contain. In a very simple, yet abstract way these fields, $\phi_a(x)$ can be thought of as different types of LEGO bricks that are available to the model builder.

Second, the underlying symmetries of the theory (and their possible spontaneous- or explicit breaking), such as C, P, T, \mathbb{Z}_n , *etc.* invariance and gauge symmetries like $SU_C(3) \times SU_L(2) \times U_Y(1)$ need to be defined under whose transformations the theory will remain invariant. At the same time the representations such as fundamental, adjoint, conjugate, *etc.* of the fields under these symmetries, *i.e.* how they behave under the symmetry transformations need to be chosen. Along with locality and Lorentz-invariance, imposing the symmetries is extremely restrictive, as it confines the possible combinations of the fields to structures that remain invariant under all symmetry transformations. These structures can be divided into three groups: kinetic terms, recognized by single spacetime derivatives acting on the fields $\sim \partial\phi_a(x)$; mass terms, which are quadratic in a given field and contain no derivatives $\sim \phi_a(x)\phi_a(x)$; and interaction terms mixing more than two fields with or without derivatives $\sim \phi_a(x)\phi_b(x)\phi_c(x)$. Incidentally, the invariance of these objects under the symmetries means that the action built from them will transform in the trivial representation of all the symmetries and will have a vanishing variation under their transformations, $\delta S_{\text{sym.}} = 0$, leading to conserved currents. Following the analogy above, the set of symmetries under which the action needs to be invariant is like the set of instructions that come with the LEGO, outlining where each piece should go in order to be able to build something bigger.

Although establishing the field content, the symmetries and the representations is a restrictive process there are still infinitely many operators that can be formed that satisfy the above transformation criteria. As such, the last ingredient of building a QFT is cherry-picking those structures

that have desirable properties for a given theory. These qualities include particular interaction channels that feed certain types of processes, and renormalizability, which will be introduced momentarily. The final set of chosen interactions is entirely motivated by what combinations the model-builder thinks will accurately describe the physical system under study. Further tangling the LEGO analogy, although the pieces themselves and even their combinations are very versatile and can be combined in a huge number of ways, to build a QFT it is sufficient to chose only a handful of all the possibilities.

With the action in hand, the generating functional of a theory is defined as,

$$Z[J_a] := \int \mathcal{D}\phi_a e^{iS[\phi_a, \partial\phi_a] + \int d^4x J_a(x)\phi_a(x)}, \quad (1.2)$$

where $J_a(x)$ is known as a current term that sources a particle of type a at spacetime point x , and $\mathcal{D}\phi_a$ is known as the functional measure of the fields. Functional derivatives of this object can be related to physical observables such as correlation functions, decay rates, cross-sections and others and as such it is often referred to as the “Holy Grail” of a QFT, since once it is known in a closed form the observables fall right out.

Unfortunately, the generating functional only has a closed form for very few types of actions (we will call these parts of S “integrable” in the future), of which most notable are those of free theories where particles are only allowed to move around without affecting each other in any way, meaning that nothing interesting ever happens in these theories. The possibility of a closed expression for the generating functional of these theories lies in the fact that the only structures available to the model-builder from the previous paragraphs are the kinetic and mass terms, both of which are at most quadratic in the fields and as such lead to Gaussian integrals over the dummy integration variable, $\phi_a(x)$. In a little bit more detail what happens is that by integrating by parts we can bring the action into the form

$$iS_0[\phi_a, \partial\phi_a] = \int d^4x \phi_a(x)\Delta\phi_a(x), \quad (1.3)$$

where S_0 is the free-field action and Δ is an operator, and this schematically leads to a generating functional proportional to the root of the inverse of the determinant of the operator Δ ,

$$Z[J_a] = \int \mathcal{D}\phi_a e^{\int d^4x \{\phi_a\Delta\phi_a + J_a(x)\phi_a(x)\}} \propto \sqrt{\det(\Delta)^{-1}}. \quad (1.4)$$

We emphasize this because it will be an important point later when we look at the low-energy effective theory of lumps.

Of more phenomenological importance are interacting theories, where particles are allowed to talk to each other through the various channels encoded by the interaction terms of the action, although in most models these features spoil the integrability of the theory in the sense that the generating functional cannot be obtained in a closed form. However, not all is lost; if

the interactions between the particles can be assumed to be weak, it is possible to split the total action into two parts, $S = S_0[\phi_a, \partial\phi_a] + S_{\text{int}}[\phi_a, \partial\phi_a]$ and evolve the field operators in the interaction picture around the integrable part of the theory, $S_0[\phi_a, \partial\phi_a]$ and treat the non-integrable parts, $S_{\text{int}}[\phi_a, \partial\phi_a]$ as perturbations, allowing for the calculation of observables to arbitrarily high accuracy.

These calculations are carried out with the machinery of Feynman diagrams and they get increasingly more challenging as one includes higher and higher orders in the interactions of the perturbation. In addition to the computational obstacles posed by loops of virtual particles in these diagrams, they often also lead to infinities, which need to be regulated. Large-distance (a.k.a. low energy, a.k.a. infrared or IR) divergences can be often taken care of using infrared regulators such as the size of atomic spacing in a lattice or the low-energy sensitivity of detectors, while short-distance (a.k.a. high-energy, a.k.a. ultraviolet or UV) divergences are usually dealt with using renormalization techniques, whereby infinities are removed from physical observables, such as the masses of particles for example. Dealing with these pathologies through renormalization is closely related to the renormalizability of a theory.

In essence, renormalizability refers to how hard one has to work in order to make sense of all these infinities and it is determined by analyzing the superficial degree of divergence of a theory's Feynman diagrams to see how many of them fundamentally diverge. Under this umbrella, QFTs are divided into 3 categories: *super-renormalizable* theories, where interaction vertices reduce the divergence of diagrams; *renormalizable* theories, where vertices do not improve nor do they worsen the divergences of graphs and so only the types and number of external legs and the spacetime dimension of the theory matter for the divergence of any given diagram; and *non-renormalizable* theories, where interaction vertices increase the degree of divergence and so all amplitudes start to diverge if a sufficiently high number of the interaction terms are included. For super-renormalizable and renormalizable theories, one can measure a finite number of physical parameters through experiments and make predictions for observables to all orders in perturbation theory, provided that the loops do not pose a mathematical challenge. Although for non-renormalizable theories one formally needs to measure an infinite number of parameters to be able to make such predictions, to any given order in perturbation theory these theories still have predictive power, provided there is a sufficient number of measurements that the finite-number of parameters appearing to that order can be fixed. This is an important point, because all EFTs will technically be non-renormalizable as will be explained in the next section.

The general model-building algorithm for QFTs should now be clear. First the field content is established, then the theory's symmetries are laid down and representations are chosen. This is followed by picking desirable interactions between the fields that obey all the symmetries and to ensure

appropriate predictive power often only the renormalizable interactions are included in the model's action. As an example, imagine constructing ϕ^4 theory from scratch. The field content is a single, real scalar field, $\phi(x)$ of mass, m_ϕ , with only local interactions, and the symmetries comprise Lorentz-invariance and \mathbb{Z}_2 symmetry of the fields, *i.e.* the action should be invariant under $\phi \rightarrow -\phi$. After a little thought one realizes that the only possible, renormalizable theory that can be built with these criteria is given by,

$$S_{\phi^4} = - \int d^4x \frac{1}{2} (\partial_\mu \phi)(\partial^\mu \phi) + \frac{1}{2} m_\phi^2 \phi^2 + \frac{\lambda}{4!} \phi^4, \quad (1.5)$$

where λ is the dimensionless coupling constant of the interaction, assumed to be small for the purposes of perturbation theory.

1.2.3 Wilsonian Actions and EFTs

A common theme in the above examples of decoupling was the emergence of the effective theory as a large-distance limit of some other underlying theory – known as the UV completion – whose domain of validity encompasses shorter distance scales.

The QFTs built using the procedure outlined in the previous section are all UV complete in the sense that although they are not necessarily expected to be valid at arbitrarily short distances where new physics may come into play (known as the cut-off of the theory, Λ), they are assumed to be accurate and indisputably correct down to those scales. This is because by freely choosing the field content, the representations and the interactions, and turning a blind eye to everything else one explicitly excludes all other possible explanations of the system in a given distance regime. This is one of the crucial differences between EFTs and QFTs as will be explained shortly.

The emergence of an effective field theory can be understood through the renormalization group arguments developed by Wilson [11]. Starting on familiar ground, first let us build a QFT with high-energy cut-off, Λ and generating functional,

$$Z[J_a] = \int \mathcal{D}\phi_a e^{iS_0 + iS_{\text{int}} + i\int d^4x J_a(x)\phi_a(x)} \quad (1.6)$$

that is hypothesized to accurately describe the physics of a given system down to distance scales much shorter than what is accessible to the current generation of experiments running at energies, E . Notice that as prescribed above we have split the action into an integrable part, $S_0[\phi_a, \partial\phi_a]$ and an interaction part, $S_{\text{int}}[\phi_a, \partial\phi_a]$ that comprises of all the selected interaction terms.

To make contact with the experiments looking to find evidence that supports this particular model one needs to know what it looks like at the typical energy scales of said experiments, $E \ll \Lambda$ which can be worked out by coarse-graining the theory. This process starts with splitting the fields

into low-energy modes, $\phi_a^l(x)$ that are still accessible by the experiments and high-energy ones, $\phi_a^h(x)$ that are not, such that $\phi_a(x) = \phi_a^l(x) + \phi_a^h(x)$. Doing so divides the measure, $\mathcal{D}\phi_a \rightarrow \mathcal{D}\phi_a^l \mathcal{D}\phi_a^h$ and also complicates the originally simple-looking action as it gets cluttered with all sorts of high- and low-energy field interactions. In general, the action resulting from this mode-separation is of the form

$$S_0[\phi_a, \partial\phi_a] + S_{\text{int}}[\phi_a, \partial\phi_a] = \left\{ S_0^l[\phi_a^l, \partial\phi_a^l] + S_{\text{int}}^l[\phi_a^l, \partial\phi_a^l] \right\} + \left\{ S_0^h[\phi_a^h, \partial\phi_a^h] + S_{\text{int}}^h[\phi_a^h, \partial\phi_a^h] \right\} + S_{\text{mix}}[\phi_a^l, \phi_a^h, \partial\phi_a^l, \partial\phi_a^h], \quad (1.7)$$

where terms combine in such a way that the original form of the action (with integrable and interaction parts) appears for both the low- and high-energy modes separately (enclosed in braces) with additional interactions between these two types of modes, collected in S_{mix} . Although the functional measure now runs over the field configurations of both energy modes, the experiment is only able to excite the low-energy components of the fields, meaning that the current term for the high-energy modes can be turned off and set to zero. As a result of these artificial splittings, the generating functional morphs into

$$\begin{aligned} Z[J_a] &= \int \mathcal{D}\phi_a^l e^{iS_0^l + iS_{\text{int}}^l + i \int d^4x J_a(x) \phi_a^l(x)} \int \mathcal{D}\phi_a^h e^{iS_0^h + iS_{\text{int}}^h + iS_{\text{mix}}}, \\ &= \int \mathcal{D}\phi_a^l e^{iS_0^l + iS_{\text{int}}^l + i \int d^4x J_a(x) \phi_a^l(x)} \left[\int \mathcal{D}(\phi_a^h) e^{iS_0^h} \right] \frac{\int \mathcal{D}\phi_a^h e^{iS_0^h + iS_{\text{int}}^h + iS_{\text{mix}}}}{\int \mathcal{D}(\phi_a^h) e^{iS_0^h}}, \\ &= \int \tilde{\mathcal{D}}\phi_a^l e^{iS_0^l + iS_{\text{int}}^l + i \int d^4x J_a(x) \phi_a^l(x)} \left\{ \frac{\int \mathcal{D}\phi_a^h e^{iS_0^h + iS_{\text{int}}^h + iS_{\text{mix}}}}{\int \mathcal{D}\phi_a^h e^{iS_0^h}} \right\} \end{aligned} \quad (1.8)$$

where in the second line unity had been written in a funny way as the path integral over the integrable-theory action of the dummy variable, ϕ_a^h . The reason for doing so is that after a simple relabelling of the dummy high-energy modes in the denominator, the braces on the third line enclose the expectation value of the operator that is the exponential of $S_{\text{int}}^h + S_{\text{mix}}$ on the interacting vacuum state, $|\Omega\rangle$ such that

$$\left\{ \frac{\int \mathcal{D}\phi_a^h e^{iS_0^h} \times e^{iS_{\text{int}}^h + iS_{\text{mix}}}}{\int \mathcal{D}\phi_a^h e^{iS_0^h}} \right\} = \langle e^{iS_{\text{int}}^h + iS_{\text{mix}}} \rangle_{\Omega}, \quad (1.9)$$

which can be evaluated to arbitrary order in perturbation theory using Feynman diagrams. Simultaneously, the functional integral over the integrable-theory action in the numerator of unity (*i.e.* the square bracket on the second line) can be evaluated to a constant by the definition of integrability and in the above case this had been absorbed into the functional measure of the low-energy modes on the third line, $\mathcal{D}\phi_a^l \rightarrow \tilde{\mathcal{D}}\phi_a^l$.

Notice that it is only the high-energy modes that are integrated out in this way, while the low-energy modes are held fixed. What this means is

that the low-energy parts in the braces coming from S_{mix} factorize from the expectation value, while the high-energy modes are contracted, leading to calculable loops, whose results are finite. In this way, the operator $e^{iS_{\text{mix}}}$ containing the interactions between the low- and high-energy modes effectively introduces higher and higher powers of $\phi_a^1(x)$ and $\partial\phi_a^1(x)$ on the external legs of the calculated Feynman diagrams, generating all the possible interactions of these modes allowed by the initial symmetries imposed on the QFT. After the high-energy mode contributions are evaluated, these newly generated interactions gain non-zero coefficients and can be resummed into exponentials, leading to the generating functional of the effective low-energy theory,

$$Z[J_a] = \int \mathcal{D}\phi_a^1 e^{iS_{\text{eff}}[\phi_a^1, \partial\phi_a^1, \partial\partial\phi_a^1, \dots] + i \int d^4x J_a(x) \phi_a^1(x)}, \quad (1.10)$$

where $S_{\text{eff}}[\phi_a^1, \partial\phi_a^1, \partial\partial\phi_a^1, \dots]$ is the effective action that contains all possible interactions between the low-energy fields and their derivatives. There is more to the renormalization group story as detailed in [11] and many standard texts on QFT such as [12, 13, 14] but for the purposes of this discussion the above cartoon should suffice.

From a model-building perspective, constructing such a low-energy effective action is only marginally different from constructing a UV-complete QFT. The initial step is again to come up with a field content that is most likely to describe the physical system at the energy scales probed, followed by imposing symmetries and choosing representations. However, instead of cherry-picking any particularly appealing interactions like for a QFT, in an EFT all of the possible interactions between the fields and their derivatives are kept, making these theories necessarily non-renormalizable.

Of course, as to any good rule, there are exceptions to this one too [15]. First, total derivatives result in boundary terms that can be ignored given that the spacetime has no boundaries, and the fields remain finite near infinity and hide no topological surprises there and so writing these down is unnecessary. Second, we are only obliged to include at most $(N_{\text{IBP}} - 1)$ of N_{IBP} interactions related to each other through integrations by parts as these contribute to any processes in exactly the same way and including more of them than necessary only redefines the coefficients of the related terms. Lastly, we don't need to write down terms that are proportional to the field equations because these can be removed by field redefinitions.

In summary then, although EFTs naturally emerge as low-energy descriptions of given high-energy theories and these can be calculated in detail using the coarse-graining procedure outlined above, it is also possible to *build* EFTs provided the low-energy field content, representations and symmetries are known. This proceeds much the same way as the model-building algorithm for QFTs, however instead of a fixed set of interactions, all terms that are non-removable in the sense of the exceptions just listed must be included in the action. One then puts this polished low-energy action into a generating functional such that the theory is described in the

form (1.10). Note that the inclusion of all possible interactions forces EFTs to be non-renormalizable, however not all interactions in the effective theory are equally relevant for experiments, and in fact to a given precision only a certain number of them matter, as we will now argue.

1.2.4 Dimensional Analysis and the Robustness of EFTs

The easiest way to understand why not all EFT interactions are created equal is to carry out dimensional analysis on the Lagrangian of the effective model,

$$\mathcal{L}_{\text{eff}} = \mathcal{L}_0 + \sum_i c_i O_i[\phi_a, \partial\phi_a, \dots], \quad (1.11)$$

as opposed to working directly with its action, where \mathcal{L}_0 is the integrable part of the Lagrangian containing the canonically normalized single derivatives and the mass terms of the fields, c_i are coupling constants and O_i are local functional operators of the fields and their derivatives. When working in natural units, every quantity is assigned a mass (or equivalently energy) dimension: the mass dimension of a mass is of course, $[m] = 1$; distances have $[dx] = -1$; derivatives, $\partial_\mu \sim d/dx^\mu$ have $[\partial_\mu] = +1$ (this inverse relationship is why long distances can also be interpreted as small energies and vice versa); as previously mentioned, the action in these units needs to be dimensionless, *i.e.* $[S] = 0$; and last but not least, using the fact that the action is the integral of the Lagrangian density, $S = \int d^4x \mathcal{L}$ one finds that $[\mathcal{L}] = 4$. Then, using the canonically normalized kinetic terms it is also possible to determine the mass-dimensions of the fields, $\phi_a(x)$; for example the kinetic term for a real scalar field is $\frac{1}{2}\partial_\mu\phi\partial^\mu\phi$ which implies $[\phi(x)] = 1$, while that of a Dirac fermion is $\bar{\Psi}\not{\partial}\Psi$ leading to $[\Psi(x)] = 3/2$.

Having found the dimensions of all the fields in this way, it becomes possible to work out the dimensionality of the operators, O_i and through these also that of the coupling constants, $[c_i] = 4 - [O_i]$. For all of these c_i the natural mass scale is the UV cutoff, Λ , which can be explicitly factorized in order to trade them for dimensionless couplings, g_i ,

$$c_i := \Lambda^{4-[O_i]} g_i, \quad (1.12)$$

while for the fields the natural energy scale is that of the experiment, $E \ll \Lambda$ which excites them and produces their particles and so can be traded for dimensionless fields, $\bar{\phi}_a(x)$ as

$$\phi_a(x) := E^{[\phi_a]} \bar{\phi}_a(x). \quad (1.13)$$

Similarly, the derivatives acting on the fields in a given operator of \mathcal{L} produce factors of the experimental energy as well, because they tend to create plane-wave like configurations of the fields, $\phi_a(x) \sim e^{ik \cdot x}$ such that

$\partial\phi_a(x) \sim k\phi_a(x)$ where $|k| \sim E$. Finally, this allows for writing all the operators in \mathcal{L} in terms of dimensionless operators,

$$O_i[\phi_a, \partial\phi_a, \dots] := E^{[O_i]}\bar{O}_i[\bar{\phi}_a]. \quad (1.14)$$

Having traded all the couplings and fields for dimensionless ones and explicitly written the powers of the cut-off and the experimental energy scales in \mathcal{L} one can further trade the spacetime segment of the experiment for its Fourier space equivalent in terms of the experimental energy such that $\int d^4x \sim \frac{(2\pi)^4}{E^4}$, which grants writing the action schematically as,

$$S_{\text{eff}} = \int d^4x \mathcal{L}_{\text{eff}} \sim \bar{\phi}_a(x)\bar{\phi}_a(x) \left\{ 1 + \left(\frac{m_{\bar{\phi}_a}}{E}\right) \delta_{S_a, n/2} + \left(\frac{m_{\bar{\phi}_a}}{E}\right)^2 \delta_{S_a, n} \right\} + \sum_i \left(\frac{E}{\Lambda}\right)^{[O_i]-4} g_i \bar{O}_i[\bar{\phi}_a(x)]. \quad (1.15)$$

where S_a is the spin of the field, $\phi_a(x)$ and $n \in \mathbb{N}^0$ is an integer. The benefit of writing the action in this form is that it makes transparent that the effective interactions can be organized as a power series of the small, dimensionless quantity, $E/\Lambda \ll 1$ and as such is essentially a multipole expansion of operators where more complicated terms come suppressed by increasing powers of E/Λ .

Organizing S_{eff} this way divides the interactions into three categories depending on how they behave in the low-energy limit that is as $E \rightarrow 0$. Terms in effective actions accompanied by a negative power of E such as the mass terms and interactions with $[O_i] < 4$ become increasingly more important at lower energies and are called *relevant*; those interactions that appear independently from the E/Λ ratio and so have $[O_i] = 4$ are known as *marginal* and may or may not become important depending on their quantum corrections; and lastly there are the *irrelevant* terms in S_{eff} , which have $[O_i] > 4$ and are interactions that matter less and less as E is dialled down.

Thinking about these irrelevant operators naively we can realize that these are the interactions responsible for the non-renormalizability of EFTs because higher-order irrelevant operators contain increasingly more powers of the fields, which lead to increasingly more loops, always raising the superficial degree of divergence of any Feynman graphs they contribute to. However, this is no cause for alarm because thanks to the robustness of the effective action through the expansion in $E/\Lambda \ll 1$, to a given experimental accuracy with which observables of the theory can be probed it is only ever a finite number of effective interactions that contribute, and given enough measurements their couplings can be fit, retaining the predictive power of EFTs.

In this section we have applied dimensional analysis to establish that EFT actions are essentially multipole expansions of local functionals of field

operators, where higher-dimensional operators are suppressed by increasing powers of the small ratio, $E/\Lambda \ll 1$ between the large UV cut-off, Λ and the energy scale available to experiments, E . Furthermore, this analysis has helped us understand why the inclusion of all allowed interactions between the low-energy fields and their derivatives allowed by the symmetries makes EFTs non-renormalizable, but has also revealed that due to the robust expansion of S_{eff} in powers of $E/\Lambda \ll 1$, to a given accuracy of experimental probes it is sufficient to include the effects of only a finite number of effective operators. Then, by finding enough measurements to fit the couplings of these interactions with sufficient accuracy, EFTs can become efficient machines for grinding out predictions for a given energy regime of experiments.

This brings our short discussion of EFT methods to a close. We have found that in order to build an EFT one needs a high-energy scale, Λ and a low-energy scale, E with which the theory is probed in experiments and these scales need to be well separated such that $E \ll \Lambda$. Establishing a suitable low-energy field content, symmetries and representations then allows us to construct the most general, Lorentz-invariant effective local action by writing down all possible non-removable interactions between the fields and their derivatives that are allowed by the symmetries. Such an action comes in the form of a multipole expansion of the operators where terms of successive dimensions are suppressed by increasing powers of the ratio, $E/\Lambda \ll 1$, which makes the EFT robust in the sense that to any given experimental accuracy it is only a finite number of the effective interactions that play a role. In the next section we will use what we had learned here to find effective low-energy descriptions for compact objects.

1.3 The PPEFT Framework

Now you might say, “Wow! Good for us that we can build such effective theories thanks to decoupling and all, but what does this have to do with atoms and nuclear physics?”

The point is that to a large extent modern measurements of atomic spectra rely on a considerable amount of guesswork, because although the experiments are precise enough that nuclear effects need to be taken into account, there is no reliable UV theory for nuclei that predicts these effects. This necessitates modelling the nucleus in various ways, which introduces unwanted errors (we will say more about this in the coming sections).

Therefore, it would be really great if we could parameterize the effects of the nucleus without having to develop a working UV theory of nuclei and this is where EFTs can help, since they are specially designed to hide our ignorance of UV physics by using an appropriate low-energy description that systematically includes its effects to any desired experimental accuracy.

Atomic systems occupy a special place among EFTs in that there is an omnipresent, heavy, charged object of typical nuclear-scale size, $R \sim 1$ fm

in the theory that generates a background for the dynamics of all other particles, which is experimentally sampled at the much larger scale of the orbiting, bound fermion’s Bohr radius, $a_B \sim (mZ\alpha)^{-1} \gg R$, where m is the lepton mass, Z is the atomic number and α the fine-structure constant¹. The good thing about the EFT formalism is that we need not understand how this object got there, meaning that a full second-quantized treatment of the nucleus is overkill since we are not interested in its creation nor its possible destruction. It suffices to know what the low-energy degrees of freedom and the symmetries of the nucleus are to form a working EFT of atoms with an action organized into a multipole expansion of operators in powers of R/a_B .

In the proceeding sections then, we will briefly explore the effective theory of lumps following [15], because as we will see later they serve as the perfect candidates for what a nucleus is supposed to be, especially once they are coupled to the electromagnetic gauge field. We will begin by exploring what the low-energy degrees of freedom of such lumps can be and then look at what their presence implies for the other fields in the theory they are coupled to.

1.3.1 Lumps and Their Low-energy Degrees of Freedom

Background field configurations (a.k.a. “lumps” or “central objects”) naturally emerge in field theories as solutions to field equations that localize the energy density in some way, known as solitons. Usual examples of such solutions are one-dimensional kinks, domain walls and vortices. The wisdom of these examples is that the general picture we should have in mind is that a given field in the UV theory is subjected to interactions that alter the minimum-energy configurations for the field in some way.

To keep the discussion somewhat general, imagine building a renormalizable QFT as prescribed in the previous sections with Lagrangian $\mathcal{L}[\phi_a, \partial\phi_a]$ that has the corresponding Hamiltonian,

$$H = \int d^4x \dot{\phi}_a \left(\frac{\partial \mathcal{L}}{\partial (\partial_t \phi_a)} \right) - \mathcal{L}, \quad (1.16)$$

and varying the fields results in the field equations

$$\frac{\delta \mathcal{L}}{\delta \phi_a} = \partial_\nu \left(\frac{\partial \mathcal{L}}{\partial (\partial_\nu \phi_a)} \right) - \frac{\partial \mathcal{L}}{\partial \phi_a} = 0. \quad (1.17)$$

For later convenience let us also note the equation the derivative of the

¹In terms of the earlier discussion of EFTs, R corresponds to the high-energy cut-off where we no longer trust the description of the nucleus as a single charged particle, and a_B is related to the low energies at which the experiment runs.

fields obey by differentiating this equation,

$$\begin{aligned}
 \partial_\mu \frac{\delta \mathcal{L}}{\delta \phi_a} = 0 &= \partial_\mu \left[\partial_\nu \left(\frac{\partial \mathcal{L}}{\partial (\partial_\nu \phi_a)} \right) - \frac{\partial \mathcal{L}}{\partial \phi_a} \right], \\
 &= \left\{ \partial_\nu \left(\frac{\partial^2 \mathcal{L}}{\partial \phi_b \partial (\partial_\nu \phi_a)} \right) + \partial_\nu \left(\frac{\partial^2 \mathcal{L}}{\partial (\partial_\nu \phi_b) \partial (\partial_\rho \phi_a)} \right) \partial_\rho \right. \\
 &\quad \left. + \left(\frac{\partial^2 \mathcal{L}}{\partial (\partial_\nu \phi_b) \partial (\partial_\rho \phi_a)} \right) \partial_\nu \partial_\rho - \left(\frac{\partial^2 \mathcal{L}}{\partial \phi_b \partial \phi_a} \right) \right\} (\partial_\mu \phi_b), \quad (1.18)
 \end{aligned}$$

where we have first commuted the partial derivatives on the first term and then used the fact that \mathcal{L} only depends on the fields and their first derivatives when acting on it with ∂_μ and applying the chain rule. Lastly, let us note that the field theory we had written down was invariant under spacetime translations and so are the resulting equations of motion, which will become important momentarily.

Now, to minimize H we could proceed in one of two ways: we could try to find solutions to (1.17) that minimize the energy everywhere; or we could require them to minimize the energy on some boundary.

The first class of solutions corresponds to constant field configurations, $\phi_a(x) = v$ much like the vacuum expectation values of fields in scenarios containing spontaneous symmetry breaking, while the second one involves some non-trivial distribution of energy density in spacetime, $\phi_a(x) = \varphi_a(x)$. Pondering the implications of this second class a little more, we can realize that having a lump somewhere in the system is precisely such a solution with the two caveats: the surface we wish to minimize the energy on lies at infinity so that the lump exists somewhere in the bulk; and the energy is localized to a single region, say, a spatial ball \mathcal{B}_R of radius R .

The consequences of having translation-invariant equations of motion are that the solutions to these equations will depend on constants that describe where most of the energy is localized. Then, similarly to how rolling around the gutter of Mexican hat potentials does not change the vacuum expectation value of the fields, spacetime translations do not alter the profile of lump solutions but change these constants instead, which can therefore be thought of as the centre-of-mass coordinates, y^μ of the lumps, now written as $\varphi_a = \varphi_a(y - x)$.

Having found the solutions that minimize the energy of the system in this way we can now consider small fluctuations around it to develop the quantum theory and so we split the field into its classical background function plus small oscillations around it, $\phi_a(x) = \varphi_a(y - x) + \hat{\phi}_a(x)$, where $\hat{\phi}_a/\varphi_a \ll 1$. Taylor-expanding the Lagrangian in the small variable $\hat{\phi}_a(x)$

and its derivative then gives,

$$\begin{aligned}
 \mathcal{L} \left[\varphi_a + \hat{\phi}_a, \partial(\varphi_a + \hat{\phi}_a) \right] &= \mathcal{L}[\phi_a, \partial\phi_a]_{\varphi_a} + \hat{\phi}_a \left[\frac{\partial\mathcal{L}}{\partial\phi_a} \right]_{\varphi_a} + (\partial_\nu \hat{\phi}_a) \left[\frac{\partial\mathcal{L}}{\partial(\partial_\nu\phi_a)} \right]_{\varphi_a} \\
 &+ \frac{1}{2!} \left\{ \hat{\phi}_a^2 \left[\frac{\partial^2\mathcal{L}}{\partial\phi_a^2} \right]_{\varphi_a} + 2\hat{\phi}_a(\partial_\nu \hat{\phi}_a) \left[\frac{\partial\mathcal{L}}{(\partial\phi_a)\partial(\partial_\nu\phi_a)} \right]_{\varphi_a} \right. \\
 &\left. + (\partial_\rho \hat{\phi}_a)(\partial_\nu \hat{\phi}_a) \left[\frac{\partial^2\mathcal{L}}{\partial(\partial_\rho\phi_a)\partial(\partial_\nu\phi_a)} \right]_{\varphi_a} \right\} + \mathcal{O} \left[\hat{\phi}_a^3, \hat{\phi}_a^2(\partial\hat{\phi}_a), \hat{\phi}_a(\partial\hat{\phi}_a)^2, (\partial\hat{\phi}_a)^3 \right], \tag{1.19}
 \end{aligned}$$

where the φ_a subscript means that all quantities in the accompanying brackets are evaluated on the background solution, $\varphi_a(y-x)$. Integrating by parts on the third term ² reveals,

$$(\partial_\nu \hat{\phi}_a) \left[\frac{\partial\mathcal{L}}{\partial(\partial_\nu\phi_a)} \right]_{\varphi_a} + \hat{\phi}_a \left[\frac{\partial\mathcal{L}}{\partial\phi_a} \right]_{\varphi_a} = -\hat{\phi}_a \left[\partial_\nu \left(\frac{\partial\mathcal{L}}{\partial(\partial_\nu\phi_a)} \right) - \frac{\partial\mathcal{L}}{\partial\phi_a} \right]_{\varphi_a}, \tag{1.20}$$

that the linear terms of $\hat{\phi}_a$ and its derivative combine such that the coefficient of $\hat{\phi}_a$ becomes the equations of motion of $\varphi_a(y-x)$, *i.e.* (1.17) and so vanish in \mathcal{L} , pushing the appearance of the oscillations $\hat{\phi}_a$ to quadratic order in the action.

By rewriting the mixed $\hat{\phi}_a(\partial_\nu \hat{\phi}_a)$ term in (1.19) using

$$\begin{aligned}
 2\hat{\phi}_a(\partial_\nu \hat{\phi}_a) \left[\frac{\partial\mathcal{L}}{(\partial\phi_a)\partial(\partial_\nu\phi_a)} \right]_{\varphi_a} &= \partial_\nu \left\{ \hat{\phi}_a^2 \left[\frac{\partial\mathcal{L}}{(\partial\phi_a)\partial(\partial_\nu\phi_a)} \right]_{\varphi_a} \right\} \\
 &- \hat{\phi}_a^2 \partial_\nu \left[\frac{\partial\mathcal{L}}{(\partial\phi_a)\partial(\partial_\nu\phi_a)} \right]_{\varphi_a}, \tag{1.21}
 \end{aligned}$$

and dropping the total derivative, and integrating by parts on the two-derivative-term, $(\partial_\rho \hat{\phi}_a)(\partial_\nu \hat{\phi}_a)$ of the same expression, the quadratic piece in \mathcal{L} can be brought into the following symmetric form,

$$\begin{aligned}
 \hat{\phi}_a \mathcal{O}[\varphi_a, \partial\varphi_a] \hat{\phi}_a &:= \hat{\phi}_a \left\{ -\frac{1}{2} \left(\partial_\nu \left[\frac{\partial^2\mathcal{L}}{(\partial\phi_a)\partial(\partial_\nu\phi_a)} \right]_{\varphi_a} + \partial_\nu \left[\frac{\partial^2\mathcal{L}}{\partial(\partial_\nu\phi_a)\partial(\partial_\rho\phi_a)} \right]_{\varphi_a} \partial_\rho \right. \right. \\
 &\left. \left. + \left[\frac{\partial^2\mathcal{L}}{\partial(\partial_\nu\phi_a)\partial(\partial_\rho\phi_a)} \right]_{\varphi_a} \partial_\nu \partial_\rho - \left[\frac{\partial^2\mathcal{L}}{\partial\phi_a^2} \right]_{\varphi_a} \right) \right\} \hat{\phi}_a, \tag{1.22}
 \end{aligned}$$

where the equality defines the $\mathcal{O}[\varphi_a, \partial\varphi_a]$ operator that depends on the classical background configuration as the expression enclosed in braces on the right-hand side and this is used to quantize the fluctuations, $\hat{\phi}_a(x)$.

Now comes the important point: we can split the fluctuations into modes that oscillate in the directions of the centre-of-mass coordinates of

²We can do this with impunity because \mathcal{L} appears under a spacetime integral in the action, S and we assume boundary terms to vanish.

the lump, translating it in these directions such that $\hat{\phi}_{a,0} := y^\mu \partial_\mu \varphi_a$ and ones that are orthogonal to these directions. The utility of this decomposition lies in the fact that by virtue of (1.18) $\hat{\phi}_{a,0}$ are zero-modes of the operator $\mathcal{O}[\varphi_a, \partial\varphi_a]$ and as a result cannot be coarse-grained out of the theory when we test it at the low-energy regimes accessible to experiments that correspond to spatial scales, a_{exp} .

To see this, imagine that to leading order the $\hat{\phi}_a^3$ terms can be ignored in the action, which means that the path-integral can, in principle, be evaluated since it only involves Gaussian integrals in this case. However, as we had seen in (1.4) the result of these integrals involves the inverse of the determinant of the operator $\mathcal{O}[\varphi_a, \partial\varphi_a]$, which diverges if the zero modes are also included, and hence these modes cannot be integrated over and remain in the theory at lower energies as well.

Through these general considerations we see that effective theories involving lumps can be built by conceiving of the low-energy degrees of freedom of these background configurations such as the centre-of-mass coordinates, spin, *etc.* as fields in their own rights that interact with their surroundings. These surviving interactions come from couplings between the original fields in the high-energy theory, of which one has been assumed to be in its classical background configuration that asymptotically minimizes the system’s Hamiltonian, localizing the energy to a region, \mathcal{B}_R , and then integrating out all fluctuations around these solutions that are orthogonal to the low-energy degrees of freedom describing their energy-distribution. The physics of such backgrounds can then be probed at scales, $a_{\text{exp}} \gg R$, which warrants a multipole expansion of their effective action, where higher-order operators are systematically suppressed by increasing powers of R/a_{exp} once the symmetries of the low-energy theory have been established.

As the name “Point-Particle Effective Field Theory” suggests, we will be concentrating on the special class of such lumps that are one-dimensional in the low-energy theory and so behave as point-like objects³. These kinds of background solutions trace out a curve in spacetime, $\mathcal{P} : s \rightarrow y^\mu(s)$ – known as the world-line – that can be described by a single parameter, s mapping \mathbb{R} to the target space \mathbb{M}^4 through the centre-of-mass coordinates, $y^\mu(s)$.

In essence then, what we will mean by a PPEFT is this: there exists a localized (to a ball, \mathcal{B}_R of radius R) blob of energy somewhere in spacetime, whose interactions with its environment (at the experimental scale, $a_{\text{exp}} \gg R$) can be captured by assuming it to be a one-dimensional object with world-line, \mathcal{P} parameterized by a single variable s and a low-energy field content of centre-of-mass coordinates, $y^\mu(s)$ and other integral degrees of freedom such as spin, $\xi^\mu(s)$ coupling the bulk fields (*i.e.* the ones still in the path-integral) to its world-line through generic EFT interactions organized into a series of R/a_{exp} .

³As opposed to multi-dimensional ones such as strings, membranes, *etc.*

1.3.2 Implications of Lumps

Having found the low-energy degrees of freedom of a background solution, we are now ready to explore what the consequences of having such a solution are. For this discussion we will assume that the symmetries of the theory are known, which allows us to write the general low-energy effective action for a free blob as,

$$S_{p,0} = \int ds \mathcal{L}_{p,0}[y_{\text{pt}}(s), \dot{y}_{\text{pt}}(s), \dots], \quad (1.23)$$

where $y_{\text{pt}}(s)$ is a general set of low-energy fields that by the arguments of the previous section will always include the centre-of-mass coordinates, $y^\mu(s)$, the overdot represents differentiation with respect to the world-line parameter, s and the ellipses contain possible higher derivatives of these fields.

In cases where $\mathcal{L}_{p,0}$ is not too complicated it is now possible to figure out what physical parameters of the lump the lowest-order coefficients in $\mathcal{L}_{p,0}$ stand for by deriving the constraints on this theory. This proceeds [16, 17, 18] by finding the conjugate momenta for the internal degrees of freedom defined as,

$$p^{(y_{\text{pt}})} := \frac{\partial \mathcal{L}_{p,0}}{\partial \dot{y}_{\text{pt}}}, \quad (1.24)$$

and then attempting to rearrange the result to find the velocities, $\dot{y}_{\text{pt}}(s)$ as functions of these momenta. When this procedure fails, we obtain primary constraints that the theory has to obey, and it is in these primary constraints that one may easily relate the EFT couplings to physical parameters, such as mass for example. We will see this procedure more explicitly in the next section where we look at the physics of a free, scalar lump with no additional internal degrees of freedom apart from the centre-of-mass coordinates, $y^\mu(s)$.

A freely propagating blob is not too exciting on its own so to get some more interesting phenomena we introduce a general set of external fields, $\phi_a(x)$ into the bulk of the theory via the bulk action,

$$S_B = \int d^4x \mathcal{L}_B[\phi_a, \partial\phi_a, \dots]. \quad (1.25)$$

Here, if we want to consider a particular QFT, the bulk Lagrangian, \mathcal{L}_B can be a function of the fields and their first-derivatives only; but if we would rather have an EFT, S_B can be an effective action depending on the fields and all their derivatives. Now, to couple these new fields to the lump, we write down the most general PPEFT action consistent with the symmetries to a given order in the ratio R/a_{exp} by building interaction terms between the low-energy fields of the lump, the bulk fields, and all the possible derivatives of these. The lump action therefore modifies to an interacting one,

$$S_p = \int ds \mathcal{L}_p[y_{\text{pt}}, \dot{y}_{\text{pt}}, \phi_a, \partial\phi_a, \dots], \quad (1.26)$$

where the bulk fields, $\phi_a(x)$ and their derivatives are evaluated on the world-line of the blob. The physical significance of some of the effective couplings in this interacting lump action can also be revealed by finding its Hamiltonian,

$$\mathcal{H} := \dot{y}_{\text{pt}} \cdot p^{(y_{\text{pt}})} - \mathcal{L}_p, \quad (1.27)$$

for example the magnetic moment of an atom can be identified in this way, as will be shown in the appendices of Chapter 4.

Notice that S_B and S_p describe different sectors of the theory and so need to be combined to form the full theory with the complete action,

$$\begin{aligned} S &= S_p + S_B = \int d^4x \mathcal{L}_B[\phi_a, \partial\phi_a] + \int ds \mathcal{L}_p[y_{\text{pt}}, \dot{y}_{\text{pt}}, \phi_a, \partial\phi_a, \dots], \\ &= \int d^4x \left\{ \mathcal{L}_B[\phi_a, \partial\phi_a] + \int ds \delta^4(x - y) \mathcal{L}_p[y_{\text{pt}}, \dot{y}_{\text{pt}}, \phi_a, \partial\phi_a, \dots] \right\}, \end{aligned} \quad (1.28)$$

where in the second line we have introduced a 4-dimensional delta-function to place the two actions on the same footing; or said another way, to embed the lump world-line in the target-space of the bulk theory.

To see how the presence of the background solution affects the physics of the bulk fields in a simple setting, let us assume that \mathcal{L}_p only depends on the bulk fields but not their derivatives and require the total action to remain stationary under variations with respect to these fields, $\delta S/\delta\phi_a = 0$. This procedure leads to

$$\frac{\delta S}{\delta\phi_a} = \int d^4x \left\{ \frac{\partial\mathcal{L}_B}{\partial\phi_a} - \partial_\mu \left(\frac{\partial\mathcal{L}_B}{\partial(\partial_\mu\phi_a)} \right) + \int ds \delta^4(x - y) \frac{\partial\mathcal{L}_p}{\partial\phi_a} \right\} = 0, \quad (1.29)$$

and consequently gives rise to the equations of motion,

$$\partial_\mu \left(\frac{\partial\mathcal{L}_B}{\partial(\partial_\mu\phi_a)} \right) = \frac{\partial\mathcal{L}_B}{\partial\phi_a} + \int ds \delta^4(x - y) \frac{\partial\mathcal{L}_p}{\partial\phi_a}, \quad (1.30)$$

which contains our artificially introduced 4-dimensional delta-function. This can be further simplified by imposing a set of conditions on the centre-of-mass coordinates, namely by assuming the blob's world-line to be parameterized using proper time, τ we can set $-\dot{y}^2 = -\dot{y}_\mu\dot{y}^\mu = 1$, then we can boost to the rest-frame of the lump, which yields $\dot{y}^\mu = \delta_0^\mu$ with all higher derivatives vanishing and finally we can translate the background solution such that most of its energy is concentrated near the origin, which leads to $y^\mu = \tau\delta_0^\mu$. The idea behind these manipulations is that we can now get rid of the world-line integral in (1.30) and turn the interactions between the bulk fields and the centre-of-mass coordinates of the lump into specific components of the fields interacting at the origin,

$$\partial_\mu \left(\frac{\partial\mathcal{L}_B}{\partial(\partial_\mu\phi_a)} \right) = \frac{\partial\mathcal{L}_B}{\partial\phi_a} + \delta^3(\mathbf{x}) \frac{\partial\mathcal{L}_p}{\partial\phi_a} \Big|_{y^\mu = \tau\delta_0^\mu}. \quad (1.31)$$

Next, we turn to solving these equations to see what kind of fields can live outside the lump. When we exclude the origin from the problem, the field equations reduce to the usual equations of motion for the fields,

$$\partial_\mu \left(\frac{\partial \mathcal{L}_B}{\partial (\partial_\mu \phi_a)} \right) = \frac{\partial \mathcal{L}_B}{\partial \phi_a}, \quad (1.32)$$

which are usually some sort of first- or second-order differential equations that are generally solved by mode-expansions of the form,

$$\phi_a(t, r, \theta, \phi) = \sum_\beta e^{-i\omega_\beta t} \mathcal{Y}_L(\theta, \phi) \left\{ \mathcal{C}_L \mathcal{R}_{\mathcal{C},L}(r) + \mathcal{D}_L \mathcal{R}_{\mathcal{D},L}(r) \right\}, \quad (1.33)$$

where β is a set of quantum numbers that completely identify the state and its energy, ω_β , $\mathcal{Y}_L(\theta, \phi)$ is a set of angular functions appropriate for the field, L is a set of accompanying angular momentum labels⁴, and \mathcal{C}_L and \mathcal{D}_L are the integration constants multiplying the near-origin convergent radial solution, $\mathcal{R}_{\mathcal{C},L}(r)$ and the near-origin divergent radial solution, $\mathcal{R}_{\mathcal{D},L}(r)$ respectively.

Now, with our feet securely planted on the completely general solution to the equations of motion in the form (1.33), we can dive into finding the specific solutions that obey the full equation in (1.31), including the origin. This is achieved by imposing an adequate set of boundary conditions on the field that determine the integration constants \mathcal{C}_L and \mathcal{D}_L . We have previously required that fields fall-off sufficiently fast in the $r \rightarrow \infty$ limit that they remain finite and we can certainly stand by this requirement and impose it as a boundary condition at large- r . This will generally either kill the near-origin convergent solution by setting $\mathcal{C}_L = 0$ or turn into a constraint on the ratio of the integration constants, $\mathcal{D}_L/\mathcal{C}_L$. Another popular choice for boundary conditions, which is certainly familiar from lectures on quantum mechanics is boundedness at the origin, *i.e.* also requiring the solutions in (1.33) to be finite in the $r \rightarrow 0$ limit. We have shown in previous work [1, 2] that such a condition cannot be the correct one for non-relativistic Schrödinger fields moving in a $1/r^2$ potential or for charged, relativistic scalar fields moving in a Coulomb potential because both radial solutions can diverge in these scenarios. This suggests that we should also find an alternative for the general case now at hand.

So *what* condition should we impose and *where*? This is where the delta-function term derived from the lump action comes in, since one learns early on that to deal with such potentials one needs to integrate the equation they are involved in. Then, integrating (1.31) over a ball, \mathcal{B}_ϵ of vanishingly

⁴For example, in three spatial dimensions $\mathcal{Y}_L(\theta, \phi)$ are the scalar spherical harmonics for energy eigenstates of scalar fields obeying the Laplace equation, spinor spherical harmonics for fermions obeying the Dirac equation with a central field, *etc.* and the accompanying labels are: $\{l, l_z\}$ with orbital angular momentum quantum number l and projection l_z for the scalars; and $\{j, j_z, \varpi\}$ with total angular momentum (orbital plus spin) quantum number, j , its projection j_z and the state's parity, $\varpi = \pm$ for the spin-half fields.

small radius, ϵ (see Fig. 1.1 for an illustration) and so dropping all but the spatial-derivative and delta-function terms yields,

$$\begin{aligned} \int_{\mathcal{B}_\epsilon} d^3x \partial_i \left(\frac{\partial \mathcal{L}_B}{\partial (\partial_i \phi_a)} \right) &= \int_{\partial \mathcal{B}_\epsilon} d^2x \hat{\mathbf{n}}_i \left(\frac{\partial \mathcal{L}_B}{\partial (\partial_i \phi_a)} \right) \\ &= \int d^2\Omega_2 \epsilon^2 \left(\frac{\partial \mathcal{L}_B}{\partial (\partial_r \phi_a)} \right) \Big|_{r=\epsilon} = \frac{\partial \mathcal{L}_p}{\partial \phi_a} \Big|_{\substack{\dot{y}^\mu = \delta_0^\mu \\ \mathbf{x}=0}}, \\ \implies \int d^2\Omega_2 \epsilon^2 \left[\left(\frac{\partial \mathcal{L}_B}{\partial (\partial_r \phi_a)} \right) - \frac{1}{4\pi\epsilon^2} \left(\frac{\partial \mathcal{L}_p}{\partial \phi_a} \right) \right]_{\substack{\dot{y}^\mu = \delta_0^\mu \\ r=\epsilon}} &= 0, \quad (1.34) \end{aligned}$$

where in the first equality we have used Gauss' theorem to trade the volume integral over \mathcal{B}_ϵ to one on its surface, $\partial \mathcal{B}_\epsilon$ with unit normal vector, $\hat{\mathbf{n}}$ (taken to be $\hat{\mathbf{r}}$ in the second equality as is appropriate for a sphere), and on the third line we have assumed that the value of the field inside \mathcal{B}_ϵ is approximately equal to its value on the boundary such that $\phi_a(\epsilon) \approx \phi_a(0)$. Since the size of the Gaussian surface we have integrated over was arbitrary, we must have that

$$\left(\frac{\partial \mathcal{L}_B}{\partial (\partial_r \phi_a)} \right) \Big|_{r=\epsilon} = \frac{1}{4\pi\epsilon^2} \left(\frac{\partial \mathcal{L}_p}{\partial \phi_a} \right) \Big|_{\substack{\dot{y}^\mu = \delta_0^\mu \\ r=\epsilon}} \quad (1.35)$$

is the new near-source boundary condition we must impose on the fields. Notice that the left-hand side of (1.35) contains contributions from those terms in the bulk action S_B that required integrations by parts on the field when finding its equations of motion and the right-hand side only involves terms from the lump-action, S_p . As such, this condition relates the integration constants of (1.33) to the effective couplings appearing in S_p and its consistency with the large- r boundary conditions fully determines the solution to (1.31). Hence, it is only through these alternative near-source boundary conditions that the bulk fields learn about the presence of the lump in the theory and their knowledge of the background is reflected in the values of their integration constants.

All is not as well as it seems however, because there are two blatant problems with the above procedure, which we will address now.

Boundary Action

First, we had obtained from S_p a delta-function potential, which is not only ill-defined in three dimensions, it also forces us to evaluate the bulk fields at the origin; a region that exists inside the lump of size, R and so is a regime where we trust neither our effective description of this background solution nor the bulk field solutions valid external to R anymore. How then, can we make sense of the derivation of (1.35)?

A better argument has been developed in our earlier work [1] where we have first encountered this issue and we recount here the discoveries made there. Notice that the real implication of S_p is a condition on the

Gaussian surface, $\partial\mathcal{B}_\epsilon$ that relates the terms from the bulk action that contained spatial-derivatives of the fields to values of the fields themselves, both evaluated at $r = \epsilon$. This suggests that what we are really after is some data on this boundary that determines the fields and their derivatives on $\partial\mathcal{B}_\epsilon$ in a way that leads to the correct behaviour of the bulk fields outside of the source as inferred from S_p .

However, fixing the values of the fields and their derivatives on $\partial\mathcal{B}_\epsilon$ is risky business because these values need to be consistent with similar ones on other boundaries in the problem and they also depend on any possible sources outside of this surface not just the ones enclosed in it. This suggests that we should impose this data in a dynamical way that is allowed to change depending on the positions of all the sources and boundaries of the problem and this is precisely what can be achieved by an action principle. Motivated by this line of argument we introduce in place of S_p an effective boundary action, $S_{\partial\mathcal{B}_\epsilon}$ – with new, effective boundary couplings – whose sole purpose is to yield boundary conditions on $\partial\mathcal{B}_\epsilon$ that give rise to physics consistent with the presence of the lump under variation with respect to the fields. This boundary action can then be written as,

$$S_{\partial\mathcal{B}_\epsilon} := \int dt \int d^2\Omega_2 \epsilon^2 \mathcal{L}_{\partial\mathcal{B}_\epsilon} [y_{\text{pt}}, \dot{y}_{\text{pt}}, \phi_a(\epsilon), \dots] \quad (1.36)$$

where $\mathcal{L}_{\partial\mathcal{B}_\epsilon}$ is defined to have the same functional derivative under variations of ϕ_a as \mathcal{L}_p but with different effective couplings and all bulk fields evaluated at $r = \epsilon$, and the ellipses represent higher derivatives of the lump fields.

Then, the total action is again given by two parts, $S = S_B + S_{\partial\mathcal{B}_\epsilon}$ and as far as the region exterior to \mathcal{B}_ϵ is concerned there is a physical boundary at $\partial\mathcal{B}_\epsilon$. The fields that correctly take the effects of the lump into account can be found by requiring stationarity of the action S_B with respect to variations of the fields also satisfying the conditions obtained by requiring stationarity of the boundary action with respect to such variations. The variation of terms in S_B with respect to the fields that involve integrations by parts yield additional contributions to the boundary conditions not explicitly in $S_{\partial\mathcal{B}_\epsilon}$ through their boundary terms, which now don't all vanish thanks to the physical boundary, $\partial\mathcal{B}_\epsilon$, that is to say,

$$\begin{aligned} \delta S \supset \int d^4x \frac{\partial \mathcal{L}_B}{\partial(\partial_\mu \phi_a)} \partial_\mu (\delta \phi_a) &= - \int d^4x \partial_\mu \left(\frac{\partial \mathcal{L}_B}{\partial(\partial_\mu \phi_a)} \right) \delta \phi_a \\ &+ \int dt \int d^2\Omega_2 \epsilon^2 \delta \phi_a \frac{\partial \mathcal{L}_B}{\partial(\partial_r \phi_a)}. \end{aligned} \quad (1.37)$$

The term on the second line combines with $S_{\partial\mathcal{B}_\epsilon}$ under variation, yielding,

$$\begin{aligned} \delta S = \delta(S_B + S_{\partial\mathcal{B}_\epsilon}) &= - \int d^4x \delta \phi_a \left[\partial_\mu \left(\frac{\partial \mathcal{L}_B}{\partial(\partial_\mu \phi_a)} \right) - \frac{\partial \mathcal{L}_B}{\partial \phi_a} \right] \\ &+ \int dt d^2\Omega_2 \delta \phi_a \left[\frac{\partial \mathcal{L}_B}{\partial(\partial_r \phi_a)} + \frac{\partial \mathcal{L}_{\partial\mathcal{B}_\epsilon}}{\partial \phi_a} \right]_{r=\epsilon}, \end{aligned} \quad (1.38)$$

and requiring stationarity of the action under such variations, $\delta S/\delta\phi_a = 0$ forces the two terms on the right-hand side of the second equality to vanish separately, since they are on disjoint domains of the theory and so the fields must satisfy both

$$0 = \partial_\mu \left(\frac{\partial \mathcal{L}_B}{\partial(\partial_\mu \phi_a)} \right) - \frac{\partial \mathcal{L}_B}{\partial \phi_a}, \quad \text{and} \quad 0 = \left[\frac{\partial \mathcal{L}_B}{\partial(\partial_r \phi_a)} + \frac{\partial \mathcal{L}_{\partial \mathcal{B}_\epsilon}}{\partial \phi_a} \right]_{r=\epsilon}, \quad (1.39)$$

leading to the usual bulk field equations of motion and the boundary conditions on $\partial \mathcal{B}_\epsilon$ needed for them to correctly take into account the presence of the background solution.

This way of thinking about the problem has the added benefit that it avoids the evaluation of the fields inside the region where the microscopic details of the lump background solution become important, excluding in particular the origin, where parts of the bulk solutions (1.33) diverge. In this sense, S_p and its delta-function serve merely as a computational crutch that lets us identify the correct local interactions between the lump and the bulk fields that need to be translated into $S_{\partial \mathcal{B}_\epsilon}$ in order to capture the correct physics far away from the blob. Nevertheless, the couplings of the two actions, S_p and $S_{\partial \mathcal{B}_\epsilon}$ can be matched to one another⁵ by calculating the same physical observables at $a_{\text{exp}} \gg R$ from both, if this should be required.

This is a nicer story, but the question of *where* we should impose these conditions, *i.e.* what radius, ϵ we should choose for the surface on which we define $S_{\partial \mathcal{B}_\epsilon}$ still remains, since this was arbitrarily introduced into the theory. In order to escape sensitivity to boundary effects and have a well-controlled operator expansion in the usual sense of EFTs, we will choose $\epsilon \gg R$ as this will allow us to organize our lump-bulk interactions as a series in R/ϵ . To avoid similar issues with the observables calculated at a_{exp} we also choose $\epsilon \ll a_{\text{exp}}$.

Therefore, when we talk about PPEFT and its action what we really mean is that there exists a lump of size R probed at a scale a_{exp} surrounded by a spherical shell of size ϵ that obeys $R \ll \epsilon \ll a_{\text{exp}}$ on which we set up a boundary action whose variation combined with the boundary terms coming from the bulk action yield the boundary conditions required for the bulk fields to learn how they should behave around the given background solution; a condition inferred from the point-particle action, S_p .

Renormalization

The other issue that arises from (1.35) is that since both the fields and their derivatives are evaluated at the fictitious scale, ϵ , rearranging the equations to find the integration constants as functions of the PPEFT – or more precisely boundary action – couplings we find that these constants

⁵In the simple cases we will consider the point-particle couplings, c_i will be dimensional reductions of the boundary action couplings, \hat{c}_i such that the two are related by $\hat{c}_i := c_i/4\pi\epsilon^2$.

also explicitly depend on ϵ . This is a problem because physical quantities of interest often depend on the integration constants of the solutions in (1.33) and so by proxy appear to be functions of the unphysical parameter, ϵ . This would imply that observable quantities, such as the energies of atomic bound-states for example change, depending on what radius we choose for the imaginary boundary, $\partial\mathcal{B}_\epsilon$. Clearly this is completely absurd and unacceptable from a physical point of view and therefore it is imperative that we keep the integration constants independent of this artificial scale; the only question is how?

The way out is to realize that the ϵ -dependence of \mathcal{C}_L and \mathcal{D}_L is merely an illusion because any explicit terms of ϵ that may appear when we write them as functions of the PPEFT couplings using (1.35) get cancelled by implicit ϵ -dependences of these effective coupling constants. In this sense, the lump-bulk couplings exhibit a classical version of the renormalization group flow familiar from QFTs [12, 13, 14], in which the values of the coupling constants change depending on the size of $\partial\mathcal{B}_\epsilon$.

To find meaningful values of the integration constants then, we can analyze this RG-flow by rearranging the newly discovered near-source boundary conditions such as (1.35) or (1.39) for the coupling constants instead of the integration ones, and differentiating these with the operator $\epsilon \frac{d}{d\epsilon}$, while keeping \mathcal{C}_L and \mathcal{D}_L fixed in the sense that

$$\epsilon \frac{d}{d\epsilon} \mathcal{C}_L = \epsilon \frac{d}{d\epsilon} \mathcal{D}_L = 0. \quad (1.40)$$

Following this differentiation we integrate the result in order to tease out constants known as RG-invariants that pin-point which curve in the space of couplings our theory evolves on, but do not flow themselves. Comparing the result of the integration – written in terms of the RG-invariants – with the original ϵ -dependent function of the couplings we had started with (by rearranging conditions such as (1.35) and (1.39)) we find that the integration constants are actually only functions of the RG-invariant constants but not the fictitious scale, ϵ .

In this way, observables are saved from the threat of ever becoming functions of the unphysical quantity, ϵ and they turn out to be functions of the RG-invariant parameters themselves; a phenomenon known as dimensional transmutation. These constants are then possible to fit experimentally and using these fitted values it becomes possible to make predictions for other measurements, which we will heavily exploit when we look at atomic systems in Chapters 3 and 4.

To summarize, in this section we have discovered that the main implications of lump solutions lie in the boundary conditions they impose on the external fields on a Gaussian sphere of radius, $R \ll \epsilon \ll a_{\text{exp}}$ in the form of (1.35). Figure 1.1 illustrates these relevant scales in the problem and we should always have this image in the back of our mind going forward when we talk about EFTs of lumps. Strictly speaking these boundary conditions emerge in the form of (1.39) from an effective boundary ac-

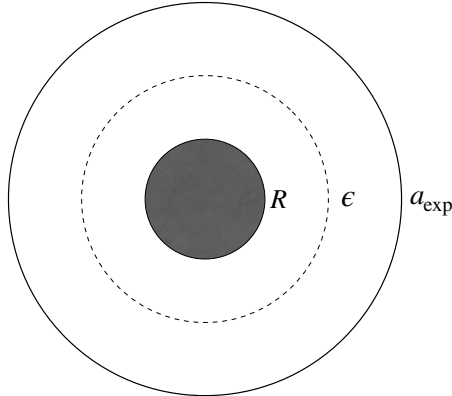


Figure 1.1: This picture shows the three relevant scales in an effective theory of lumps: R the size of the blob where its energy is concentrated; ϵ where the boundary conditions the lump implies for the bulk fields is set up; and a_{exp} the scale at which experiments probe the lump. These scales obey $R \ll \epsilon \ll a_{\text{exp}}$ and the fuzzy blob in the middle represents the lump that can be the result of very complicated physics.

tion $S_{\partial B_\epsilon}$ that allows these boundary conditions to change in a dynamical way in response to the presence of all sources pertaining to the fields, and whose construction relies on inferring the correct local interactions between the blob background and the bulk fields from the effective one-dimensional point-particle action, S_p , which is relatively easy to build. Furthermore, we have found that the coupling constants of these actions need to run in the renormalization group sense in order to keep observables that depend on the integration constants of (1.33) physical, and through dimensional transmutation these observables turn out to depend only on the RG-invariant parameters of this running. With these general ideas in mind we will now move onto finding the PPEFT of real atomic systems.

1.4 PPEFT for Atoms

So far we have seen that at low energies certain fields can develop background solutions that concentrate some energy to a centre-of-mass position, $y^\mu(s)$ in a ball of radius, R . We have christened these solutions “lumps/blobs” and found through general arguments that when they are probed at experimental scales of a_{exp} they interact with their surroundings through their low-energy degrees of freedom such as the coordinate fields, $y^\mu(s)$, their spin⁶, $\xi^\mu(s)$ and other internal degrees of freedom and these interactions can be conveniently captured by an effective action organized

⁶For simplicity of presentation we assume this nuclear spin, $\xi^\mu(s)$ to be zero for now. However, a major part of this thesis presented in Chapter 4 exhaustively discusses the inclusion of spinning nuclei in the PPEFT formalism and we comment on where this will be relevant at certain places in what follows.

into a multipole expansion of operators where higher-order interactions are suppressed by increasing powers of the ratio $R/a_{\text{exp}} \ll 1$. This action can then be used to construct a similar boundary action that dynamically imposes the necessary boundary conditions on the fields external to these backgrounds to allow them to adjust their behaviour to be consistent with the presence of such lumps.

In this section, we will explore the PPEFT for a simple class of blobs that have no low-energy degrees of freedom other than their centre-of-mass coordinates, $y^\mu(s)$ and will see that it is possible to conceive of such a theory as describing an atomic system with a spinless nucleus. We will proceed starting with the theory of a free lump (in what follows the names “lump/blob/nucleus/background solution” will be used interchangeably) and use it to infer the symmetries obeyed by such simple objects and then couple our blob to an electromagnetic field, which will allow us to demonstrate how the above formalism works in the familiar setting of electrostatics. In the last section we will further complement this system with fermionic bulk fields and see how these fields learn about the presence of the nucleus.

1.4.1 Relativistic, Free, Scalar Particle and Symmetries

Let us begin by studying a freely propagating, possibly relativistic spinless point-particle; a system well-studied in the gravitational literature [19, 20, 21]. The action for such a system is given by

$$S_{p,0} = \int ds \mathcal{L}_{p,0} = - \int ds \sqrt{-\dot{y}^2} M, \quad (1.41)$$

where $\dot{y}^2 = \eta_{\mu\nu} \dot{y}^\mu \dot{y}^\nu$ and as before, s is a parameter along the particle’s world-line, while $y^\mu(s)$ are the particle’s centre-of-mass coordinates, the overdot means differentiation with respect to the world-line parameter and M is a constant that will turn out to be the mass of the particle. This is a good starting point for us because a spinless nucleus has size, $R \sim 1$ fm and when viewed from afar, say from a scale $a_{\text{exp}} \gg R$ it appears to be exactly such a particle and so has a low-energy effective description akin to this system: its field-content consists of only the centre-of-mass coordinates, $y^\mu(s)$; and its only physically observable characteristic is its mass. Therefore, by studying the properties of this system we can learn surprisingly much about what the PPEFT corresponding to a nuclear lump should be like and can – in addition to the field content – also establish its symmetry properties.

The first symmetry that is readily apparent in this action is that of translation invariance. Moving the particle over by a constant, a^μ means translating its centre-of-mass coordinates such that $y'^\mu(s) = y^\mu(s) + a^\mu$ and this leaves the theory invariant thanks to the action only depending on the derivative $\dot{y}^\mu = \dot{y}'^\mu$. The emergence of this may seem surprising

but recall from our earlier discussion of lumps that we had started with a translation-invariant action before we integrated out the high-energy degrees of freedom. Once the blob had come to life, this symmetry was broken, because moving the lump around corresponded to physically distinct set-ups, leading to the translation-invariance of the high-energy theory becoming non-linearly realized as shifts in the coordinate fields, $y^\mu(s)$. To respect this symmetry, it then had to be true that the fields $y^\mu(s)$ only appear differentiated, *i.e.* through \dot{y}^μ in the effective actions for point-particles.

Another closely related and equally transparent symmetry of $S_{p,0}$ is Lorentz invariance, which can be seen by the contraction of all spacetime indices. This symmetry is inherited from the high-energy theory of the point-particle and is the unbroken subgroup of the full Poincaré group in the low-energy lump theory, $\text{SO}^+(1,3) \subset \text{ISO}^+(1,3)$. Again, a simple way to see that this symmetry survives the point-particle limit is that it is linearly realized on the low-energy degrees of freedom, since both the centre-of-mass coordinates, $y^\mu(s) \rightarrow \Lambda^\mu{}_\nu y^\nu(s)$ and spin, $\xi^\mu(s) \rightarrow \Lambda^\mu{}_\nu \xi^\nu(s)$ transform in the fundamental representation of the group, where $\Lambda^\mu{}_\nu$ is a proper, orthochronous Lorentz transformation.

The action of the other parts of the Lorentz group *i.e.* parity and time-reversal also leave this action invariant. This can be seen from the fact that the four-vectorial quantity \dot{y}^μ that changes under these transformations as

$$\text{P} : \begin{cases} \dot{y}^0 & \rightarrow & \dot{y}^0, \\ \dot{y}^i & \rightarrow & -\dot{y}^i, \end{cases} \quad \text{T} : \begin{cases} \dot{y}^0 & \rightarrow & -\dot{y}^0, \\ \dot{y}^i & \rightarrow & \dot{y}^i, \end{cases} \quad (1.42)$$

only appears contracted with another four-vectorial quantity – namely itself, \dot{y}^μ – that transforms the same way, leaving the resulting quantity invariant. Then, by the CPT-theorem the PPEFT action that is symmetric under P and T will also have to be symmetric under charge conjugation, C once the point-particle becomes charged under some gauge field.

A less obvious symmetry of the action of the free scalar particle is reparameterization invariance. This is the symmetry whereby choosing a different parameter to describe the trajectory of the particle the action is left unchanged and looks the same as in the old variable. This transformation is effected by taking $s \rightarrow f(s)$ for some arbitrary, well-behaved function, $f(s)$ and is most easily seen by explicitly writing out the transformation,

$$ds\sqrt{-\dot{y}^2} \rightarrow df \left(\frac{\partial f}{\partial s} \right) \left(\frac{\partial f}{\partial s} \right)^{-1} \sqrt{-\left(\frac{dy}{df} \right)^2} = df \sqrt{-\left(\frac{dy}{df} \right)^2}. \quad (1.43)$$

The last quality of the low-energy effective description of the nucleus we can extract from the action of the point-particle comes from the interpretation of the constant, M . To find what this parameter corresponds to we need to derive the constraints on the theory, and as we have advertised in the previous section this proceeds by way of finding the conjugate momenta to y^μ given by

$$p_\mu = \frac{\partial \mathcal{L}_{p,0}}{\partial \dot{y}^\mu} = M \frac{\dot{y}_\mu}{\sqrt{-\dot{y}^2}} \quad (1.44)$$

and then trying to rearrange this result to find the velocity, \dot{y}^μ as a function of p^μ . We run into an obstacle during this last manipulation due to the presence of the square-root, which necessitates calculating $p^2 = p_\mu p^\mu$ instead,

$$p^2 = -M^2 \tag{1.45}$$

from which \dot{y}^μ disappears, preventing us from writing it as function of p^μ . The result then is the constraint $p^2 + M^2 = 0$, which is no other than the correct dispersion relation for a relativistic particle, provided that the parameter M is associated with the mass of the particle. Since this last condition is a constraint, the free point-particle is forced to move on its mass-shell, as is worthy of a real particle. Furthermore, since M is a real quantity, we learn that the action has to be hermitian if it is to describe a unitary system⁷.

In summary, by studying the symmetry properties of the action of a relativistic scalar point-particle we have learned that the PPEFT action describing a nucleus has to be hermitian; translation and Lorentz-invariant; unaffected separately under P, T and consequently C transformations; and unchanged by reparameterizations of the world-line. Going forward, this will be a basic set of symmetries that we require from the low-energy actions of our one-dimensional lump.

1.4.2 Coupling to the photon

Next, we look at how a point-like-appearing object in our theory with the PPEFT properties just established couples to a U(1) gauge field. The reason for investigating this is twofold: it shows us how gauge symmetries can be incorporated into the PPEFT formalism, which is of practical importance to us since although atoms are neutral objects overall, nuclei are a collection of strongly bound neutrons and protons and therefore correspond to charged background solutions; and also reveals how the presence of a charged one-dimensional lump affects the surrounding electromagnetic gauge field through the near-nucleus boundary conditions it implies for this field.

Now then, let us imagine that there is a U(1) gauge field, $A^\mu(x)$ that lives in the bulk and that our point-particle is charged under this field with a total charge of Q . The dynamics of such a gauge field are described by the usual Maxwell action,

$$S_M = -\frac{1}{4} \int d^4x F_{\mu\nu} F^{\mu\nu}, \tag{1.46}$$

where $F_{\mu\nu} = \partial_\mu A_\nu - \partial_\nu A_\mu$ is the anti-symmetric field-strength tensor. As usual, this bulk action is invariant under gauge transformations of the form $A^\mu(x) \rightarrow A^\mu(x) + \partial^\mu h(x)$ for an arbitrary scalar function, $h(x)$ and this

⁷This condition can be relaxed depending on the physical situation, such as is the case when studying systems with sinks or sources of probability [8].

means that under such transformations the change in the Lagrangian can at most be a total derivative, since these leave the action and consequently the physics unchanged.

Recall, that for a PPEFT, S_M alone cannot be the whole story since it only describes the dynamics present in the bulk but says nothing about the existence of the lump and hence the total action of a charged lump with a U(1) gauge field will have to include an appropriate point-particle contribution as well in the form of the coupled nuclear action, $S_{p,M}$. If the point-particle was *uncharged* under the U(1) group, the total action would be $S = S_M + S_{p,0}$; an example of a boring free theory where nothing ever happens. The question to ask then is: what is $S_{p,M}$, the action for a one-dimensional lump *charged* under a U(1) group?

We can answer this using the model-building procedure developed in the earlier sections since we know that the low-energy field content is $\{y^\mu(s), A^\mu(x)\}$ and the symmetries are gauge invariance *and* the symmetries of a nuclear PPEFT we had inferred from $S_{p,0}$. Then, following our algorithm for building EFTs we find that the action for a charged spinless blob of size, R probed at a length scale, $a_{\text{exp}} \gg R$ is

$$S_{p,M} = - \int ds \left\{ \sqrt{-\dot{y}^2} M - Q \dot{y}^\mu A_\mu(y) + \dots \right\}, \quad (1.47)$$

where the bulk field, $A^\mu(x)$ is evaluated on the world-line, Q is a coupling constant that turns out to be the charge of the lump⁸ and the ellipses encode possible higher-dimensional operators suppressed by increasing powers of the ratio, R/a_{exp} that act as sources for the rest of the terms in a multipole expansion of the vector-potential⁹.

Note that $S_{p,M}$ is gauge-invariant, which can be easily established by looking at the last term under a gauge transformation with $\delta A^\mu(x) = \partial^\mu h(x)$, resulting in

$$\delta S = \delta \left(Q \int ds \dot{y}^\mu A_\mu(y) \right) = Q \int ds \dot{y}^\mu \partial_\mu h(x) \Big|_{x=y} = Q \int ds \frac{d}{ds} h(y), \quad (1.48)$$

which evaluates to a constant without physical significance.

The moral of this exercise then is that lumps can be charged under gauge fields by introducing gauge-invariant interactions between the low-energy degrees of freedom of the blob and the electromagnetic field, $A^\mu(x)$ and its various derivatives, evaluated on the world-line of the point-particle, just as we had claimed in the last section.

⁸One way to assert this is again by finding the constraints on the theory, which work out to be $P_A^2 + M^2 = 0$, where $P_A^\mu = p^\mu - QA^\mu$; the usual dispersion relation for a charged, relativistic scalar particle provided that M is interpreted as its mass and Q as its charge.

⁹For instance, as we will see later a lump with spin can interact with $A^\mu(x)$ through a term $S_p \supset i b \xi^\mu \xi^\nu F_{\mu\nu}$ that sources a magnetic-dipole field, where b is proportional to the blob's magnetic moment and as before, $\xi^\mu(s)$ is the spin of the lump.

Now that we know how to couple the gauge field to the point-particle, we can investigate how the charged lump affects the vector potential, *i.e.* what kind of potentials does the total action give rise to at the length scales of our experimental probes, a_{exp} that are much larger than the inherent size of the blob, R . In order to do this we need to work out the equations of motion for the gauge field as derived from $S = S_M + S_{p,M}$,

$$S = - \int d^4x \left\{ \frac{1}{4} F_{\mu\nu} F^{\mu\nu} + \int ds \left(\sqrt{-\dot{y}^2} M - Q \dot{y}^\mu A_\mu \right) \delta^4(x - y) \right\}, \quad (1.49)$$

where we have inserted a 4-dimensional delta-function to place S_M and $S_{p,M}$ under the same integral. Varying with respect to $A^\mu(x)$ leads to the field equation

$$\partial_\mu F^{\nu\mu} = \partial_\mu \partial^\nu A^\mu - \square A^\nu = Q \int ds \dot{y}^\nu \delta^4(x - y), \quad (1.50)$$

which can be simplified by exercising our freedom to choose Coulomb gauge *i.e.* to set $\partial_\mu A^\mu = 0$, assuming the solutions to be time-independent (and so $\partial^0 A^\mu = 0$ and $\partial^0 \partial^\mu h(x) = 0$) and utilizing the symmetries of the system to parameterize the nuclear world-line via its proper time, τ such that $\dot{y}^2 = -1$, then boost to the point-particle's rest frame (this sets $\dot{y}^\mu = \delta_0^\mu$) and finally translate the nucleus to the origin (which further picks out $y^\mu = \tau \delta_0^\mu$), which all come together to yield

$$\nabla^2 A^\nu = -Q \delta_0^\nu \delta^3(\mathbf{x}). \quad (1.51)$$

Following our procedure for finding the nuclear influence on the external fields we look for a solution to this differential equation away from the origin first, which turns out to be a sum over all angular momentum and radial modes allowed by the Laplace equation, $\nabla^2 A^0 = 0$ [22],

$$A^0(r, \theta, \phi) = \sum_{l=0}^{\infty} \sum_{l_z=-l}^l Y_l^{l_z}(\theta, \phi) \left\{ \mathcal{C}_{l,l_z} r^l + \mathcal{D}_{l,l_z} r^{-l-1} \right\} \quad (1.52)$$

where \mathcal{C}_{l,l_z} and \mathcal{D}_{l,l_z} are the integration constants of the near-origin convergent and divergent parts of the solution respectively, l is the angular momentum quantum number and l_z is its projection, while $Y_l^{l_z}(\theta, \phi)$ are the usual scalar spherical harmonics.

Although, this is the general form of the solution to (1.51), it is not *the* solution, since specifying the result completely requires fixing the integration constants and this is achieved by choosing boundary conditions on various surfaces. As we had discussed before we require there to be a boundary condition at $r \rightarrow \infty$ that asks the fields to remain finite in this limit, and imposing this large- r boundary condition on $A^0(r, \theta, \phi)$ sets $\mathcal{C}_{l,l_z} = 0$ for all of the angular momentum modes.

As we have learned from the last section the appropriate next step is integrating (1.51) over a ball, \mathcal{B}_ϵ of small radius, ϵ that obeys $R \ll \epsilon \ll a_{\text{exp}}$

which by using Gauss's theorem leads us to

$$\begin{aligned}
 \int_{\mathcal{B}_\epsilon} d^3x \nabla^2 A^0 &= \int_{\partial\mathcal{B}_\epsilon} d^2x \hat{\mathbf{n}} \cdot \nabla A^0 = \int d^2\Omega_2 \epsilon^2 \partial_r A^0 \Big|_{r=\epsilon} \\
 &= - \sum_{\ell, l_z} (\ell + 1) \mathcal{D}_{\ell, l_z} \epsilon^{-\ell} \int d^2\Omega_2 Y_\ell^{l_z} = -Q, \\
 \implies \mathcal{D}_{\ell, l_z} &= \frac{Q}{\sqrt{4\pi}} \delta_{\ell, 0} \delta_{l_z, 0},
 \end{aligned} \tag{1.53}$$

where $\hat{\mathbf{n}}$ is the unit normal vector of the surface $\partial\mathcal{B}_\epsilon$ that we have taken to be $\hat{\mathbf{r}}$ for the spherically symmetric Gaussian pillbox of our choosing. Hence, by integrating the delta-function piece in (1.51) to find an alternative near-origin boundary condition to boundedness we fix the second integration constant, which in turn yields the specific, spherically symmetric, time-independent solution to (1.51),

$$A^0(r) = \frac{Q}{4\pi r}, \tag{1.54}$$

which we recognize as the electromagnetic potential of a spherically symmetric charge-distribution with total associated charge, Q . For our PPEFT of a charged nucleus this is no other than the Coulomb-field of the nucleus with $Q = Ze$, where Z is the atomic number and e is the electric charge unit.

The same field can be derived by using the boundary action,

$$S_{\partial\mathcal{B}_\epsilon, M} = \int dt \int d^2\Omega_2 \hat{Q} A^0(\epsilon), \tag{1.55}$$

in place of $S_{p, M}$, where \hat{Q} is an effective coupling related to but not the same as Q . Varying the total action we find,

$$\begin{aligned}
 \delta S &= \delta(S_M + S_{\partial\mathcal{B}_\epsilon, M}) = -\frac{1}{2} \int d^4x F_{\mu\nu} \delta F^{\mu\nu} + \int dt \int d^2\Omega_2 \epsilon^2 \hat{Q} \delta A^0, \\
 &= - \int d^4x (\delta A^\mu) \partial^\nu F_{\mu\nu} + \int d^3x \hat{n}^\nu F_{\mu\nu} \delta A^\mu + \int dt \int d^2\Omega_2 \epsilon^2 \hat{Q} \delta A^0, \\
 &= - \int d^4x (\delta A^\mu) \partial^\nu F_{\mu\nu} + \int dt \int d^2\Omega_2 \epsilon^2 \left[F_{0r} + \hat{Q} \right]_{r=\epsilon} \delta A^0 \\
 &\quad + \int dt \int d^2\Omega_2 \epsilon^2 F_{jr} \Big|_{r=\epsilon} \delta A^j,
 \end{aligned} \tag{1.56}$$

from which we can read off the boundary condition for $A^0(\epsilon)$ to be ,

$$F_{0r} \Big|_{r=\epsilon} = \partial_0 A_r \Big|_{r=\epsilon} - \partial_r A_0 \Big|_{r=\epsilon} = \partial_r A^0 \Big|_{r=\epsilon} = -\hat{Q}. \tag{1.57}$$

Now using the bulk solution from (1.52) with $\mathcal{C}_{l, l_z} = 0$ we get,

$$\sum_{\ell, l_z} (\ell + 1) \mathcal{D}_{\ell, l_z} \epsilon^{-\ell-2} Y_\ell^{l_z}(\theta, \phi) = \hat{Q}, \tag{1.58}$$

from which we obtain,

$$\mathcal{D}_{l,l_z} = \delta_{l,0}\delta_{l_z,0}\sqrt{4\pi}\epsilon^2\hat{Q}, \quad (1.59)$$

by realizing that there is no angular-dependence on the right-hand side, and equating this to our earlier result from (1.53) also reveals,

$$\hat{Q} = \frac{Q}{4\pi\epsilon^2}, \quad (1.60)$$

and with this boundary coupling we recover the Coulomb field in (1.54).

The most important take-away from finding the solution to (1.51) is that the presence of the charged lump contributed to the gauge field equations of motion a delta-function potential, which eventually lead to a boundary condition on the Gaussian sphere of radius ϵ . This condition related the remaining integration constants $\mathcal{D}_{\ell,\ell_z}$ to the coupling constant, Q in $S_{p,M}$, and this is how the exact solution to (1.51) was found to be (1.54). We have also seen that we can avoid talking about what happens at the origin by introducing the boundary action, $S_{\partial B_{\epsilon,M}}$ with new effective couplings that upon variation lead to boundary conditions akin to those coming from integrating the equations of motion with the delta-function potential, and more importantly, when properly treated lead to the same specific external fields through a simple relation between the coupling of $S_{p,M}$ and $S_{\partial B_{\epsilon,M}}$.

In this section then, we have seen how to couple lump solutions to $U(1)$ gauge fields via introducing gauge-invariant interactions on the world-line of the lump between the low-energy degrees of freedom of the blob and the gauge field, $A^\mu(x)$ and its derivatives. We have also shown that the effect of the presence of the charged lump in the theory on $A^\mu(x)$ is to induce a boundary condition on a Gaussian sphere of radius $R \ll \epsilon \ll a_{\text{exp}}$ near the origin that helps determine the specific solution to its field equations. It is only through this boundary condition that the bulk field learned about the existence of the lump and as argued before this turns out to be true for other types of external fields as we will now show for fermions.

1.4.3 Coupling to the Electron

Now that we can create charged lumps we are in a good position to start studying atoms, because we can now create electromagnetically bound-states between the blob and other oppositely charged fields. Of particular interest to us is when these orbiting particles are Dirac fermions, $\Psi(x)$ of mass m and charge $(-e)$ such as electrons and muons that interact with the nucleus at the scales of their Bohr radii, $a_{\text{exp}} := a_B \sim (mZ\alpha)^{-1}$, where $\alpha := e^2/4\pi$ is the fine-structure constant and $a_B \gg R$.

Chalking up everything we have learned in the previous sections we see that atoms can be described in our newly developed formalism by a PPEFT with field content $\{A^\mu(x), \Psi(x), y^\mu(s), \xi^\mu(s), \dots\}$, where the ellipses represent other possible internal nuclear degrees of freedom. Furthermore,

the symmetries of such a bound system comprise of Poincaré-, gauge- and reparameterization-invariance, C, P and T conservation and hermiticity; and the effective action of the nucleus can be systematically organized into a multipole expansion of operators between the low-energy fields allowed by these symmetries with higher-order terms suppressed by increasing powers of the ratio, $R/a_B \sim (mRZ\alpha)$ and resolving increasingly finer nuclear details. In fact, the utility of the PPEFT formalism lies precisely in this statement, because it shows that the nuclear-size-related effects can be efficiently tracked by a robust low-energy effective action whose implications are simple (relative to the increasingly difficult QED calculations, which we will discuss in the later sections) boundary conditions that can be imposed in a first-quantized language on the fermion fields, instead of having to rely on complicated processes involving their second-quantized versions.

In the last section we have worked out how the presence of the nucleus affects the gauge field and found that $A^\mu(x)$ learns about its presence through a near-nucleus boundary condition that helps determine what kind of electromagnetic potential arises around such a background. In detail, this condition related the PPEFT couplings to the integration constants that arose in the solutions to the Maxwell equations; specifying them to yield the correct $A^\mu(x)$ around the charged blob. The final piece of the puzzle in describing atoms as a PPEFT is throwing the fermion field at this system and finding their bound-state solutions along with their new near-nucleus boundary conditions.

First, let us introduce the charged fermions to the bulk of the theory via the action,

$$S_{D,M} = - \int d^4x \bar{\Psi} [\not{D} + m] \Psi, \quad (1.61)$$

where the slash denotes contraction with the Dirac gamma matrices $\not{\partial} = \gamma^\mu \partial_\mu$ with $D_\mu \Psi(x) = [\partial_\mu + ieA_\mu(x)]\Psi(x)$ the covariant derivative for a field of charge $(-e)$ that minimally couples the electron to the photon, and where $\bar{\Psi} = \Psi^\dagger(i\gamma^0)$ is the Dirac conjugate to the field, $\Psi(x)$. The combination of the free dynamics of the Maxwell field described by S_M and this minimally coupled Dirac action form the renormalizable bulk theory of Quantum Electrodynamics (QED),

$$S_B = S_{D,M} + S_M = S_{QED} = - \int d^4x \left\{ \frac{1}{4} F_{\mu\nu} F^{\mu\nu} + \bar{\Psi} [\not{D} + m] \Psi \right\}, \quad (1.62)$$

central to the modern theory of atoms.

So much for the bulk, but what about the nucleus? As before, to include the presence of the nuclear background configuration we need to couple its low-energy degrees of freedom to the bulk fields in a way that preserves all the symmetries we have mentioned above and form the low-energy effective action, $S_{P,QED}$. The most general Poincaré-, gauge- and reparameterization-invariant, hermitian, C, P, T conserving action we can write down for the theory of a charged spinless nucleus with field content $\{y^\mu(s), A^\mu(x), \Psi(x)\}$

is then

$$S_{p,QED} = - \int ds \left\{ M\sqrt{-\dot{y}^2} - (Ze)\dot{y}^\mu A_\mu + \bar{\Psi} \left[c_s\sqrt{-\dot{y}^2} + ic_v\dot{y}^\mu\gamma_\mu \right] \Psi + \dots \right\}, \quad (1.63)$$

where c_s and c_v are effective couplings of dimension, $(length)^2$ and the ellipses denote interactions with higher-dimensional couplings that – thanks to the robustness of EFTs – are suppressed by more powers of R/a_B than those written. The total action of this system is then given by the sum of S_{QED} and $S_{p,QED}$,

$$S = S_{QED} + S_{p,QED} = - \int d^4x \left\{ \frac{1}{4}F_{\mu\nu}F^{\mu\nu} + \bar{\Psi} [\not{D} + m] \Psi + \int ds \delta^4(x - y) \left(M\sqrt{-\dot{y}^2} - (Ze)\dot{y}^\mu A_\mu + \bar{\Psi} \left[c_s\sqrt{-\dot{y}^2} + ic_v\dot{y}^\mu\gamma_\mu \right] \Psi + \dots \right) \right\}, \quad (1.64)$$

where we have again introduced a 4-dimensional delta-function to place all contributions on the same footing.

Again, to see what new near-nucleus boundary conditions the charged central object imposes on the bulk fields thereby asserting its presence, we need to find their equations of motion and we start with that of the gauge-field,

$$\partial_\mu F^{\nu\mu} = (Ze) \int ds \delta^4(x - y) \dot{y}^\nu - ie\bar{\Psi}\gamma^\nu\Psi. \quad (1.65)$$

The second term here, $ie\bar{\Psi}\gamma^\nu\Psi$ comes from the interaction between the fermionic and the gauge fields and so should be accounted for in a perturbative second-quantized treatment of the fields with the use of Feynman graphs. Put another way, we wish to include the first term coming from the nucleus in the interaction-picture evolution of the gauge-field, *i.e.* use it to determine the classical solution around which $A^\mu(x)$ is quantized, while we retain its coupling to the electron field as a dynamic interaction that allows for processes that change particle number, which gives rise to radiation-field components, $A_{\text{rad}}^\mu(x)$ in the solutions (*c.f.* the discussion below (1.4)). The position-space solution to (1.65) in the nuclear rest-frame placed at the origin at zeroth-order in the radiation field is then given by the Coulomb-field familiar from (1.54)

$$A^0(r) = \frac{Ze}{4\pi r}, \quad (1.66)$$

and so not much changes due to the inclusion of the electrons as far as this field is concerned.

On the other hand, varying the total action with respect to $\bar{\Psi}$ to find the equations of motion for Ψ yields,

$$[\not{D} + m] \Psi + \int ds \delta^4(x - y) \left[c_s\sqrt{-\dot{y}^2} + ic_v\dot{y}^\mu\gamma_\mu \right] \Psi = 0, \quad (1.67)$$

which can be simplified to

$$[\not{D} + m] \Psi + \delta^3(\mathbf{x}) [c_s - ic_v \gamma^0] \Psi = 0, \quad (1.68)$$

by parameterizing the lump's world-line with proper-time, boosting to the nuclear rest-frame and translating it to the origin, as is our go-to procedure by now.

For atomic applications we are interested in bound-state solutions to these equations, which are energy eigenstates with the standard unitary time-evolution factor, $\Psi(t, \mathbf{x}) = e^{-i\omega t} \psi(\mathbf{x})$, where ω is the energy of the state and for these solutions the equations of motion become,

$$\begin{aligned} [-i\gamma^0 (\omega - eA_0) + \gamma^i \partial_i + ie\gamma^i A_i + m] \psi(\mathbf{x}) \\ + \delta^3(\mathbf{x}) [c_s - ic_v \gamma^0] \psi(\mathbf{x}) = 0. \end{aligned} \quad (1.69)$$

Away from the effects of the nucleus (1.69) reduces to

$$[-i\gamma^0 (\omega - eA_0) + \gamma^i \partial_i + ie\gamma^i A_i + m] \psi(\mathbf{x}) = 0, \quad (1.70)$$

which for central potentials such as the one in (1.66) is solved by the ansatz [23],

$$\psi_{njz\varpi}(r, \theta, \phi) := \begin{pmatrix} \Omega_{jlz\varpi}(\theta, \phi) \mathfrak{f}_{nj\varpi}(r) \\ i\Omega_{jl'j_z-\varpi}(\theta, \phi) \mathfrak{g}_{nj\varpi}(r) \end{pmatrix}, \quad (1.71)$$

where $n = 1, 2, \dots$ is the principal quantum number, $j = 1/2, 3/2, \dots$ is the total angular momentum quantum number with projection $j_z = -j, -j+1, \dots, j-1, j$, $l = j - \varpi/2$ and $l' = j + \varpi/2$ are the orbital angular momentum quantum numbers, while $\varpi = \pm$ is the state's parity quantum number. The spinor harmonics, $\Omega_{jlz\varpi}$ are defined in terms of the scalar spherical harmonics as,

$$\Omega_{jlz\varpi} := \begin{pmatrix} \varpi \sqrt{\frac{l+\varpi j_z + \frac{1}{2}}{2l+1}} Y_{l, j_z - \frac{1}{2}}(\theta, \phi) \\ \sqrt{\frac{l-\varpi j_z + \frac{1}{2}}{2l+1}} Y_{l, j_z + \frac{1}{2}}(\theta, \phi) \end{pmatrix}, \quad (1.72)$$

while the radial solutions specific to the Coulomb potential sourced by the spinless nucleus in (1.66) work out to be,

$$\begin{aligned} \mathfrak{f}_{nj\varpi}(r) &= \sqrt{m + \omega} e^{-\rho/2} \left\{ \mathcal{C}_{j,\varpi} \rho^{\zeta-1} \left[\mathcal{M}_1 - \left(\frac{a}{c}\right) \mathcal{M}_2 \right] \right. \\ &\quad \left. + \mathcal{D}_{j,\varpi} \rho^{-\zeta-1} \left[\mathcal{M}_3 - \left(\frac{a'}{c}\right) \mathcal{M}_4 \right] \right\}, \\ \mathfrak{g}_{nj\varpi}(r) &= -\sqrt{m - \omega} e^{-\rho/2} \left\{ \mathcal{C}_{j,\varpi} \rho^{\zeta-1} \left[\mathcal{M}_1 + \left(\frac{a}{c}\right) \mathcal{M}_2 \right] \right. \\ &\quad \left. + \mathcal{D}_{j,\varpi} \rho^{-\zeta-1} \left[\mathcal{M}_3 + \left(\frac{a'}{c}\right) \mathcal{M}_4 \right] \right\}, \end{aligned} \quad (1.73)$$

where $\mathcal{C}_{j,\varpi}$ and $\mathcal{D}_{j,\varpi}$ are integration constants and the functions \mathcal{M}_i are given in terms of confluent hypergeometric functions¹⁰ $\mathcal{M}(\beta, \gamma; z) := {}_1\mathcal{F}_1[\beta; \gamma; z]$ with different arguments:

$$\begin{aligned}\mathcal{M}_1 &:= \mathcal{M}(a, b; \rho), & \mathcal{M}_2 &:= \mathcal{M}(a+1, b; \rho), \\ \mathcal{M}_3 &:= \mathcal{M}(a', b'; \rho), & \mathcal{M}_4 &:= \mathcal{M}(a'+1, b'; \rho).\end{aligned}\quad (1.74)$$

The various parameters appearing in (1.73) and (1.74) are defined by

$$\begin{aligned}a &:= \zeta - \frac{Z\alpha\omega}{\kappa}, & a' &:= -\left(\zeta + \frac{Z\alpha\omega}{\kappa}\right), & b &:= 1 + 2\zeta, & b' &:= 1 - 2\zeta, \\ c &:= \mathfrak{K} - \frac{Z\alpha m}{\kappa}, & \rho &:= 2\kappa r, & \kappa &:= \sqrt{m^2 - \omega^2}, & \zeta &:= \sqrt{\mathfrak{K}^2 - (Z\alpha)^2},\end{aligned}\quad (1.75)$$

where \mathfrak{K} is the Dirac quantum number, defined by

$$\mathfrak{K} := \mp \left(j + \frac{1}{2}\right) \quad \text{for parity } \pm \text{ states.} \quad (1.76)$$

The completely general solution to (1.68) with potential (1.66) away from the origin is then,

$$\Psi(x) = \sum_{n=1}^{\infty} \sum_{j=\frac{1}{2}}^{n-\frac{1}{2}} \sum_{j_z=-j}^j \sum_{\varpi=\pm} e^{-i\omega_{njj_z\varpi} t} \psi_{njj_z\varpi}(r, \theta, \phi), \quad (1.77)$$

where we have now also affixed the quantum numbers to the mode-energy, $\omega_{njj_z\varpi}$.

Note that this form of the solution assumes the standard representation of the Dirac gamma matrices [23, 24],

$$\gamma^0 = -i \begin{pmatrix} \mathbb{1} & 0 \\ 0 & -\mathbb{1} \end{pmatrix}, \quad \gamma^i = -i \begin{pmatrix} 0 & \sigma^i \\ -\sigma^i & 0 \end{pmatrix}, \quad (1.78)$$

with the fifth gamma matrix defined as $\gamma_5 := -i\gamma^0\gamma^1\gamma^2\gamma^3 = -\begin{pmatrix} 0 & \mathbb{1} \\ \mathbb{1} & 0 \end{pmatrix}$ and its related matrices given by

$$\gamma_5\gamma^0 = -i \begin{pmatrix} 0 & \mathbb{1} \\ -\mathbb{1} & 0 \end{pmatrix}, \quad \gamma_5\gamma^i = -i \begin{pmatrix} \sigma^i & 0 \\ 0 & -\sigma^i \end{pmatrix}, \quad (1.79)$$

while the Lorentz-algebra generators are defined as $\gamma^{\mu\nu} := -\frac{i}{4}[\gamma^\mu, \gamma^\nu]$, explicitly written as,

$$\gamma^{0i} = \frac{i}{2} \begin{pmatrix} 0 & \sigma^i \\ \sigma^i & 0 \end{pmatrix}, \quad \gamma^{ij} = \frac{1}{2}\epsilon^{ijk} \begin{pmatrix} \sigma^k & 0 \\ 0 & \sigma^k \end{pmatrix}, \quad (1.80)$$

¹⁰These are discussed in more detail and generality in the appendices of Chapter 4, and are defined as the series ${}_1\mathcal{F}_1[\beta; \gamma; z] := \sum_{i=0}^{\infty} \frac{(\beta)_i}{i!(\gamma)_i} z^i$, where $(a)_i = a(a+1)\cdots(a+i-1)$ with $(a)_0 := 1$ are the Pochhammer symbols.

where $\mathbb{1}$ is the 2×2 identity matrix and the σ^i are the usual Pauli matrices,

$$\sigma^x = \begin{pmatrix} 0 & 1 \\ 1 & 0 \end{pmatrix}, \quad \sigma^y = \begin{pmatrix} 0 & -i \\ i & 0 \end{pmatrix}, \quad \sigma^z = \begin{pmatrix} 1 & 0 \\ 0 & -1 \end{pmatrix}. \quad (1.81)$$

All of the mode-functions in (1.77) obey the equation (1.68) independently and since they all couple to the nucleus differently through their angular momenta they must also individually satisfy their own set of large- r and near-nucleus boundary conditions. In the $r \rightarrow \infty$ limit any bound-state mode with fixed quantum numbers $\{n, j, j_z, \varpi\}$ must be normalizable, which translates to the following constraint on their integration constant ratios,

$$-\left(\frac{\mathcal{D}_{j,\varpi}}{\mathcal{C}_{j,\varpi}}\right) = \frac{\Gamma[1 + 2\zeta] \Gamma[-\zeta - (Z\alpha\omega/\kappa)]}{\Gamma[1 - 2\zeta] \Gamma[\zeta - (Z\alpha\omega/\kappa)]}, \quad (1.82)$$

arising purely from the need for the combination of radial functions in (1.73) to be well-behaved in this limit.

For later use we note that the standard near-nucleus condition that is normally imposed – appropriate only for truly point-like nuclei – is finiteness at the origin, which demands the near-nucleus divergent solutions in (1.73) to be killed by setting $\mathcal{D}_{j,\varpi} = 0$. Consistency of this condition with (1.82) leads to the Dirac-Coulomb energy levels,

$$\omega_{nj}^D = m \sqrt{1 - \left(\frac{\kappa_{nj}^D}{m}\right)^2} \quad (1.83)$$

with

$$\kappa_{nj}^D = \frac{mZ\alpha}{\mathcal{N}} \quad \text{and} \quad \mathcal{N} = n \sqrt{1 - \frac{2(n - |\mathfrak{K}|)(Z\alpha)^2}{n^2(\zeta + |\mathfrak{K}|)}}, \quad (1.84)$$

found as the locations of the poles of the mode-energy dependent Gamma function in the denominator of (1.82), which show that the point-like energies of the Dirac-Coulomb modes are actually degenerate in their parity and j_z quantum numbers. This is important because as we will see in the coming chapters these are the values we will perturb around by assuming the nucleus to have a finite size, and these perturbations break the degeneracy in ϖ .

Proceeding with our program, we next have to find the alternative boundary conditions for the modes $\psi_{nj j_z \varpi}(\mathbf{x})$ near the nucleus by integrating (1.69) over a ball, \mathcal{B}_ϵ of radius, ϵ satisfying $R \ll \epsilon \ll a_B$. By ignoring all but the derivative and delta-function terms this calculation gives

$$\begin{aligned} \int d^3x \{ \boldsymbol{\gamma} \cdot \nabla \psi \} &= \int_{\partial\mathcal{B}_\epsilon} d^2x \hat{\mathbf{n}} \cdot \boldsymbol{\gamma} \psi = \int d^2\Omega_2 \epsilon^2 \gamma^r \psi(\epsilon) = -[c_s - i\gamma^0 c_v] \psi(0), \\ \implies \int d^2\Omega_2 \epsilon^2 \left[\gamma^r + \frac{c_s}{4\pi\epsilon^2} - i\gamma^0 \frac{c_v}{4\pi\epsilon^2} \right] \psi(\epsilon) &= \int d^2\Omega_2 \epsilon^2 \mathcal{B}_\epsilon \psi(\epsilon) = 0, \end{aligned} \quad (1.85)$$

where on the second line we have assumed that inside \mathcal{B}_ϵ the value of the field is approximately equal to its value on the boundary such that $\psi(\epsilon) \approx \psi(0)$. Since our choice of a Gaussian surface was completely arbitrary we have also defined the matrix operator $B_\epsilon := [\gamma^r + c_s/4\pi\epsilon^2 - i\gamma^0 c_v/4\pi\epsilon^2]$ that encodes the near-source boundary conditions on the Gaussian pillbox, $\partial\mathcal{B}_\epsilon$ in a compact way

$$B_\epsilon \psi_{njz\varpi}(\epsilon) = \begin{pmatrix} \frac{c_s}{4\pi\epsilon^2} - \frac{c_v}{4\pi\epsilon^2} & -i\sigma^r \\ i\sigma^r & \frac{c_s}{4\pi\epsilon^2} + \frac{c_s}{4\pi\epsilon^2} \end{pmatrix} \begin{pmatrix} \Omega_{jlz\varpi}(\theta, \phi) \mathfrak{f}_{nj\varpi}(r) \\ i\Omega_{jlz-\varpi}(\theta, \phi) \mathfrak{g}_{nj\varpi}(r) \end{pmatrix} = 0, \quad (1.86)$$

where in the first equality we have made use of the explicit representation in eqs. (1.78) through (1.80) and used (1.71) for the form of the mode-functions.

Since we would like to avoid evaluating $\Psi(x)$ at the origin, where its solutions external to the boundary $\partial\mathcal{B}_\epsilon$ are no longer valid and we do not trust our low-energy effective description of the nucleus, we can arrive at the same boundary condition for this mode and others by defining the boundary action,

$$S_{\partial\mathcal{B}_\epsilon, QED} := \int dt \int d^2\Omega_2 \epsilon^2 \bar{\Psi}(\epsilon) \left[\frac{\hat{c}_s}{2} - i\gamma^0 \frac{\hat{c}_v}{2} \right] \Psi(\epsilon), \quad (1.87)$$

where \hat{c}_s and \hat{c}_v are new effective couplings. Notice that this definition does not contain the γ^r term and to obtain that piece we need to realize that for $\bar{\Psi}$ to really be the conjugate field to Ψ we need the bulk derivative term in $S_{B, QED}$ to have a symmetric form which we obtain by the replacement

$$S_{D, M} \rightarrow S_{D, M}^{sym} = - \int d^4x \bar{\Psi} \left[\frac{\overrightarrow{D}}{2} - \frac{\overleftarrow{D}}{2} + m \right] \Psi, \quad (1.88)$$

where the arrows indicate the direction of differentiation, because upon variation with respect to $\bar{\Psi}$ the derivative acting on this field will yield

$$\begin{aligned} \delta S_{D, M}^{sym} &\supset \delta \left\{ \int d^4x \bar{\Psi} \frac{\overleftarrow{D}}{2} \Psi \right\} = \int d^4x \frac{\partial_\mu}{2} (\gamma^\mu (\delta\bar{\Psi}) \Psi) - \int d^4x (\delta\bar{\Psi}) \frac{\not{\partial}}{2} \Psi, \\ &= \int d^3x (\delta\bar{\Psi}) \frac{\hat{n}_\mu}{2} \gamma^\mu \Psi - \int d^4x (\delta\bar{\Psi}) \frac{\not{\partial}}{2} \Psi, \\ &= \int dt \int d^2\Omega_2 \epsilon^2 (\delta\bar{\Psi}) \frac{1}{2} \gamma^r \Psi - \int d^4x (\delta\bar{\Psi}) \frac{\not{\partial}}{2} \Psi, \end{aligned} \quad (1.89)$$

where \hat{n}^μ is the unit normal vector to the spherical Gaussian surface, $\partial\mathcal{B}_\epsilon$ of our choosing; containing the γ^r term we are after. With this new symmetric set-up the total PPEFT action becomes $S = S_M + S_{D, M, sym} + S_{\partial\mathcal{B}_\epsilon, QED}$ and takes the form

$$\begin{aligned} S = - \int d^4x &\left\{ \frac{1}{4} F_{\mu\nu} F^{\mu\nu} + \bar{\Psi} \left[\frac{\overrightarrow{D}}{2} - \frac{\overleftarrow{D}}{2} + m \right] \Psi \right\} \\ &+ \int dt \int d^2\Omega_2 \epsilon^2 \bar{\Psi} \left[\frac{\hat{c}_s}{2} - i\frac{\hat{c}_v}{2} \gamma^0 \right] \Psi, \end{aligned} \quad (1.90)$$

and varying it with respect to $\bar{\Psi}$ leads to

$$\begin{aligned} \delta S_{\bar{\Psi}} = & - \int d^4x (\delta\bar{\Psi}) [\not{D} + m] \Psi \\ & + \frac{1}{2} \int dt \int d^2\Omega_2 \epsilon^2 (\delta\bar{\Psi}) [\gamma^r + \hat{c}_s - i\hat{c}_v\gamma^0] \Psi. \end{aligned} \quad (1.91)$$

Requiring the action to be stationary under such variations forces the two terms on the right-hand side to vanish separately since they live on different domains of the theory, giving us the far-field (that is excluding the origin) equations of motion familiar from (1.68)

$$[\not{D} + m] \Psi(x) = 0, \quad (1.92)$$

and the boundary condition,

$$B_\epsilon \Psi(x) = \begin{pmatrix} \hat{c}_s - \hat{c}_v & -i\sigma^r \\ i\sigma^r & \hat{c}_s + \hat{c}_v \end{pmatrix} \Psi(x) = 0, \quad (1.93)$$

which both individually vanish for the different Dirac-Coulomb modes. Lastly, notice that the forms of the two boundary conditions in (1.86) and (1.93) are so similar that calculating the same physical quantities from both will result in the identification $\hat{c}_s = c_s/4\pi\epsilon^2$, $\hat{c}_v = c_v/4\pi\epsilon^2$.

The alternative near-nucleus boundary condition in (1.93) written using the explicit representation of the Dirac matrices suggests that for every bound-state mode we could obtain two conditions relating the integration constant ratio $\mathcal{D}_{j\varpi}/\mathcal{C}_{j\varpi}$ present in the radial solutions of (1.73); one for the top and one for the bottom component of (1.93). However, notice that if the matrix encoding these boundary conditions, B_ϵ is invertible it is possible to multiply (1.93) by this inverse and this would enforce the radial solutions to be trivial. Then, to avoid such solutions B_ϵ must be non-invertible, *i.e.* it has to have a vanishing determinant, which in the standard gamma matrix representation can be read off from (1.93) to be,

$$\det(B_\epsilon) = (\hat{c}_s - \hat{c}_v)(\hat{c}_s + \hat{c}_v) - 1 = 0. \quad (1.94)$$

This relationship between the coupling constants informs us that the two conditions obtained from the top and bottom components of (1.93) are in fact not independent and so it is enough to take into account either one of them.

Now, we could use (1.93) to find $\mathcal{D}_{j\varpi}/\mathcal{C}_{j\varpi}$ in terms of the coupling constants \hat{c}_s , \hat{c}_v , and the fictitious scale, ϵ . We would then need to find how the coupling constants run in this parameter in order to keep the integration constant ratio physical, depending on at most the RG-invariant parameters of this coupling flow. Then, we would perturb (1.82) around the Dirac-Coulomb energies of (1.83) to find the energy shift associated with the new value of $\mathcal{D}_{j\varpi}/\mathcal{C}_{j\varpi}$ acquired through the new near-nucleus boundary condition in (1.93), and would be able to write this energy shift

also as a function of the RG-invariant parameters, which we could in turn fit using experimental data to make predictions for the same energy shift in other levels. This is precisely the topic of the papers presented in the rest of the thesis and so we will not prod this problem any further at present.

In this section, we have seen that lumps of size R that have no other internal degrees of freedom than their centre-of-mass coordinates, $y^\mu(s)$ can be effectively described as point-particles at the large experimental scales, $a_{\text{exp}} \gg R$. Capitalizing on this analogy we have explored the symmetry properties of such blobs by looking at the well-studied action of the relativistic free particle and found that the PPEFT action of such simple blobs must be Poincaré- and reparameterization-invariant, separately C, P and T conserving and hermitian. We then charged these blobs under a U(1) gauge field by appending the PPEFT action with gauge-invariant interactions between the low-energy degrees of freedom of the lump and the gauge field, $A^\mu(x)$ that preserve all the other symmetries of the theory and found the alternative near-source boundary conditions for the field implied by the presence of the lump. This condition picked out the specific allowed solution around the lump by relating the integration constants appearing in the solutions to the field equations of $A^\mu(x)$ to the PPEFT couplings of the lump action. Lastly, we have introduced fermions into the theory and found the near-nucleus boundary conditions the charged blob implied for them and outlined what we intend to do with these conditions in the presented work to turn them into physical predictions for energy shifts of leptonic bound-states related to the finite size of the nucleus.

1.5 Nuclear-Size Effects in Atomic Bound-States

In the previous section we have seen that atoms can be described as theories that involve a charged lump (namely, the nucleus) of size $R \sim 1$ fm giving rise to a Coulomb potential with which it binds oppositely charged fermions to itself at scales of the Bohr radii of these fermions, $a_B \sim (mZ\alpha)^{-1}$. The influence of this background solution on the fermions in addition to the Coulomb potential it sources for them can be captured through a boundary action that is a result of a multipole expansion in powers of $R/a_B \sim (mRZ\alpha)$ of the ever-more intricate interactions between the low-energy degrees of freedom of the nucleus and the surrounding bulk fields. Varying the total action with respect to the fermion fields reveals that the presence of the nucleus asserts a new set of near-source boundary conditions on these fields that relates the integration constants in the solutions to their equations of motion to the couplings of the boundary action and thereby takes into account the finite size of the nucleus. This is apparent in two ways: the couplings of the effective action come with increasing powers of $(mRZ\alpha)$ and so trading them for the integration constants introduces

terms in the physical observables that are also expanded in powers of this combination; and the standard boundary condition that the new one replaces assumes a point-like nucleus and so deviating from such a condition takes into account that the nucleus had a finite size. It is worth emphasizing this point again: *PPEFT provides a low-energy effective description of nuclei that systematically computes the finite-size effects of these objects on physical observables in a first-quantized language.*

So far so good, but before we dive into exploring how this works in detail it is worthwhile to recount how such effects have been calculated in the past and explain why our way of computing them is useful. In order to do this we will take a short detour to marvel at the beauty and success of QED and by extension the Standard Model and then study the history of finite-size effects on atomic spectroscopy.

1.5.1 The success of QED

Quantum Electrodynamics is the renormalizable QFT of an electromagnetically interacting fermion field, $\Psi(x)$ with action presented in the previous section in (1.62), repeated here for convenience,

$$S_{QED} = - \int d^4x \left\{ \frac{1}{4} F_{\mu\nu} F^{\mu\nu} + \bar{\Psi} [\not{D} + m] \Psi \right\}, \quad (1.95)$$

with $F_{\mu\nu}$ the field strength of the electromagnetic gauge field, $A^\mu(x)$. It is one of the most successful theories of modern physics and one of the roots of its success lies in its renormalizability, since it means that there is a finite number of Feynman diagrams that lead to infinities, which can therefore all be absorbed into the physical mass, m of the fermion and the photon-fermion coupling, $(-e)$, a.k.a. the charge of the fermion. The facts that it has such few parameters and that we are well-suited to construct experiments that can probe its predictions are added bonuses that also contributed to the hype around this theory. By measuring these quantities in the laboratory one can make – in principle arbitrarily – accurate predictions for the consequences of all sorts of matter-light interactions, such as the cross-sections for scattering processes, the anomalous magnetic moments of leptons, atomic bound-state energies and many more, and these calculations can be found in most standard textbooks on the subject of QFT [12, 13, 14, 23, 24].

One could argue that the study of QED began with the birth of Quantum Mechanics (QM), because at low-energies where the excitations of the fermion fields are non-relativistic particles QM emerges as an effective theory of QED through an expansion of the Dirac fields in $v/c \ll 1$, where v is the velocity of the fermion and c the speed of light [23]. This effective theory of QED has taught us many surprising features of Nature, starting with an accurate model of the quantization of atomic bound-states and explaining the spectrum of the Hydrogen atom using the Bohr model. Since that early golden era the theory of bound-states as described by QM had

been overtaken by the more superior theory of QED, which was able to explain the famous Lamb shift of the $2P_{\frac{1}{2}}$ and $2S_{\frac{1}{2}}$ states due to vacuum polarization using the QFT framework. After the QFT revolution both the experimental and theoretical fields of bound-states had undergone an impressive evolution as a result of which people today can predict and measure energy levels with such unprecedented precision that their calculations need to rely on the full theory of the Standard Model¹¹. For a review of the modern treatment of atomic bound-states see [25] as an example.

However, with high precision comes big responsibility; at the high-energy frontier, due to this unparalleled accuracy of modern laser spectroscopy techniques atomic bound-states have become the testing ground for fundamental theories. The exciting aspect of these experiments is that as technology progresses and physical quantities are measured to ever-increasing precision, any deviations from QED and the Standard Model would signal that our understanding of Nature is somehow incomplete, opening the door to the wildest dreams of model-builders. However, so far any inconsistencies between bound-state QED and experiments have been resolved either by invoking the full machinery of the Standard Model and/or by finding more accurate values for the natural constants, such as the fine-structure constant, α or the Rydberg constant, Ry . In this sense, QED and the Standard Model have withstood the tests of time and live on to make valuable predictions that can either be proven wrong by experiments, which would no doubt please many Beyond the Standard Model theorists; or proven right, bringing everyone who has ever understood QED the joy of knowing that we can accurately describe some aspect of Nature to a new decimal place.

This gleeful outlook is overshadowed by the fact that our understanding of the strong interactions that make up nuclei is – ironically – rather weak. There are no *ab initio* calculations that people can perform that would accurately describe nuclei and yield testable predictions for the structure of such objects. This is a major roadblock in using atomic spectroscopy as a test of fundamental physics because at the experimental level of precision attainable today the effects of nuclear forces and substructures are measurable and important. Without such predictions people are forced to model nuclei in various ways, introducing parameters that in turn need to be fit using experimental data. In and of itself this would not be a problem, however as we will show in the next section there is a large amount of these parameters and there are far fewer measurements that can be used to fit them to the accuracy required to test the predictions of fundamental theory. This mismatch between parameters and accurate measurements leads to large uncertainties associated with these nuclear structure contributions to the extent that their uncertainties cloud the effects we would like to

¹¹As far as “low” energies are concerned QED is a great theory, however we know that it is the full theory of the Standard Model that rules particle physics and as experimentalists become able to probe energy levels to higher-and-higher accuracies the full machinery of this UV completion to QED becomes necessary to take into account.

measure. Let us now look at just how dire this situation is.

1.5.2 Moments...Moments Everywhere!

For the longest time, only numerical studies possessed the computational power necessary to incorporate nuclear-substructure effects – such as those related to the finite sizes of nuclei – into atomic energy shift calculations, because closed forms for such phenomena exist only in a few cases. This was problematic because the calculation of such effects rested in the hands of a few select groups of physicists, who themselves always had to commit to specific nuclear models (not necessarily the same one between the various teams) and their calculations involved the nuclear structure to all orders in small quantities such as α , making it impossible to discern at what orders in these quantities the effects of finite size played a role. The nuclear models devised and used consisted of specific charge- and magnetization-distributions $\rho_c(\mathbf{x})$ and $\rho_m(\mathbf{x})$ that in our conventions we normalize as

$$Ze = \int d^3\mathbf{x}' \rho_c(\mathbf{x}'), \quad \mu_N = \int d^3\mathbf{x}' \rho_m(\mathbf{x}'), \quad (1.96)$$

where the integrals run over the expanse of these distributions and μ_N is the size of the nuclear magnetic moment with the nuclear g -factor included (and so is *not* simply the nuclear magneton for Hydrogen for example).

Naturally, this was quite upsetting and people were hard at work to find some way to characterize these nuclear-structure contributions without relying on any given model. The first such model-independent parameterization of a finite-size effect was written down by Karplus, Klein and Schwinger for Hydrogen in [26], where the energy shift of the $nS_{\frac{1}{2}}$ state due to the finite size of the nucleus was written as,

$$\delta E_{nS_{1/2}}^{\text{KKS}} \approx \frac{2}{3n^3} (Z\alpha)^4 m_r^3 \langle r^2 \rangle_c, \quad (1.97)$$

where $m_r = mM/(m + M)$ is the reduced mass with m the leptonic and M the nuclear masses respectively and $\langle r^2 \rangle_c$ is what is known as a nuclear charge moment that in today's folklore is referred to as the charge-radius squared. The importance of this result was to show that nuclear-size effects can be captured in terms of such nuclear moments as $\langle r^2 \rangle_c$, which are defined to be weighted integrals over $\rho_c(\mathbf{x})$ and $\rho_m(\mathbf{x})$ and in our conventions are given by

$$\langle r^k \rangle_c = \frac{1}{Ze} \int d^3\mathbf{x}' r^k \rho_c(\mathbf{x}'), \quad \langle r^k \rangle_m = \frac{1}{\mu_N} \int d^3\mathbf{x}' r^k \rho_m(\mathbf{x}'), \quad (1.98)$$

where $\langle r^k \rangle_m$ is the k^{th} magnetic moment of the nucleus.

Followed by the calculation in [26] another exception to the model-specific computations was produced by Zemach in [27], where he had writ-

ten¹² the nuclear-size correction to the hyperfine splitting of $nS_{\frac{1}{2}}$ levels of Hydrogen as,

$$\delta E_{nS_{1/2}}^{Zem} \approx \left[\left(\frac{8}{3n^3} \right) \frac{g_p m^2 (Z\alpha)^4}{2M} \left(\frac{m_r}{m} \right)^3 \right] (-2)m_r (Z\alpha) \langle r \rangle_{cm}, \quad (1.99)$$

including a weighted integral over the convolution of the charge and magnetization distributions known today as the first Zemach moment. These Zemach-type convoluted integrals are given in terms of the charge and magnetization distributions by

$$\langle r^k \rangle_{cm} = \frac{1}{\mu_N (Ze)} \int d^3 \mathbf{x}' \int d^3 \mathbf{y}' |\mathbf{x}' - \mathbf{y}'|^k \rho_c(\mathbf{x}') \rho_m(\mathbf{y}'), \quad (1.100)$$

and can be generalized to include any pair of distributions with appropriate changes to the denominator.

Finally, inspired by these calculations some 20 years later Friar systematically categorized spin-independent finite-size effects in [28], through an impressive calculation of third-order perturbation theory for low- Z atoms, controlled by the small parameter $(Z\alpha) \ll 1$ as a function of such model-independent nuclear moments and showed that to accurately capture finite-size related energy shifts to a given order in this parameter it is sufficient to include only a certain number (rapidly increasing with factors of $Z\alpha$) of these nuclear moments. In our conventions his result out to and including terms proportional to $(Z\alpha)^6$ (but ignoring higher-order contributions) for the positive-parity $nS_{\frac{1}{2}}$ states reads,

$$\begin{aligned} \delta E_{nS_{1/2}}^{Fr} \approx & \frac{2}{3} (Z\alpha)^4 \frac{m_r^3}{n^3} \left\{ \langle r^2 \rangle_c - \frac{1}{2} m_r (Z\alpha) \langle r^3 \rangle_{cc} - (Z\alpha)^2 \left[\frac{\langle r^3 \rangle_c \langle r^{-1} \rangle_c}{3} - I_2^{\text{REL}} \right. \right. \\ & \left. \left. - I_3^{\text{REL}} + \langle r^2 \rangle_c \left(H_{n-1} + \gamma - \frac{13n^2 + 4n - 9}{4n^2} + \left\langle \ln \left[\frac{2m_r (Z\alpha)r}{n} \right] \right\rangle_c \right) \right] \right. \\ & \left. + m_r^2 (Z\alpha)^2 \left[I_2^{\text{NR}} + I_3^{\text{NR}} + \langle r^5 \rangle_c \langle r^{-1} \rangle_c + \langle r^3 \rangle_c \langle r \rangle_c + \frac{\langle r^4 \rangle_c}{10n^2} \right. \right. \\ & \left. \left. + \frac{2}{3} \langle r^2 \rangle_c \left(\left\langle r^2 \ln \left[\frac{2m_r (Z\alpha)r}{n} \right] \right\rangle_c + \langle r^2 \rangle_c \left\{ H_{n-1} + \gamma - \frac{4n+3}{3n} \right\} \right) \right] \right\}, \quad (1.101) \end{aligned}$$

for the negative parity $nP_{\frac{1}{2}}$ states reads,

$$\delta E_{nP_{1/2}}^{Fr} \approx \frac{n^2 - 1}{3n^5} (Z\alpha)^4 m_r^3 \left\{ \frac{1}{2} (Z\alpha)^2 \langle r^2 \rangle_c + \frac{1}{15} (Z\alpha)^2 m_r^2 \langle r^4 \rangle_c \right\}, \quad (1.102)$$

¹²Zemach's original paper presented this effect for the ground-state of Hydrogen and without any reduced mass factors. Here we are paraphrasing his result based on [25] to include such reduced mass factors and generalize it to arbitrary $nS_{\frac{1}{2}}$ states of Hydrogen.

and for the $nP_{\frac{3}{2}}$ state is given by,

$$\delta E_{nP_{3/2}}^{\text{Fr}} \approx \left(\frac{n^2 - 1}{45n^5} \right) (Z\alpha)^6 m_r^5 \langle r^4 \rangle_c. \quad (1.103)$$

Here, H_n are the harmonic numbers defined as $H_n := \sum_{k=1}^n 1/k$, γ is Euler's constant, and $I_2^{\text{NR}}, I_3^{\text{NR}}, I_2^{\text{REL}}, I_3^{\text{REL}}$ are parametric integrals that contain further moments. Although the particular forms of these integrals can be found in [28], their only contribution to our current discussion is that they yield previously unwritten moments and so we do not repeat them here but rather make the conservative assumption that they each contribute only a single insofar unmentioned moment to the energy shift, $\delta E_{nS_{1/2}}^{\text{Fr}}$.

Note that these results are purely quantum mechanical and as such do not yet take into account nuclear polarizabilities, non-trivial nuclear recoil¹³ and effects of second-quantization such as vacuum polarization and self-energy corrections. For a long time these effects were included in bound-state QED calculations as perturbations around these above results that appeared suppressed by extra powers of α (without Z) due to loop processes [25, 29, 30], and as such did not result in any new nuclear moments. Then, because for our discussion only the astounding number of these moments matters, we do not discuss these contributions here in detail, but will do so in Chapters 3 and 4 when we compare our RG-invariants to these moments. This old-fashioned approach then predicts there to be upward of a total of 14 nuclear moments that need to be experimentally determined in order to accurately predict finite-size energy shifts at order $(Z\alpha)^6$.

In more modern approaches that dominate the recent literature [31, 32, 33, 34] nuclear-structure effects are calculated in one fell-swoop using all the bells and whistles of bound-state QED. This momentum-space approach uses diagrammatic techniques to compute Feynman diagrams that exchange two or more Coulomb photons (these are particular types of graphs whose all-order sum results in the dominant Coulomb interaction of the atomic system) between the nucleus and the orbiting lepton and then artificially splits the resulting integrals into elastic and inelastic parts. The elastic contributions assume the nucleus to remain unexcited during the Coulomb exchange and constitute the parts of the nuclear-structure shifts that are traditionally referred to as finite-size effects such as those of (1.97) and (1.99), and eqs. (1.101) through (1.103); certain recoil corrections; and mixtures of the two. On the other hand, the inelastic parts of the structure effects take into account nuclear polarizability by summing over the excited nuclear states. The reason this splitting between the two types of corrections is arbitrary is that as can be seen from the discussion of these effects for deuterium in [35, 34] some inelastic contributions are also related to cer-

¹³By “non-trivial nuclear recoil” we mean contributions other than those that arise as a result of the replacement of the lepton mass, m by its reduced mass, m_r . It should be noted though that [28] does include a contribution for the leading such non-trivial effect.

tain weighted integrals of charge distributions and as such should always be considered together.

Then, in our work here we will adopt the results of this more modern approach and following [34, 36, 25] we write the spin-independent energy shifts that take into account finite-size effects along with their recoil- and polarizability corrections for $nS_{\frac{1}{2}}$ states out to and including terms of order $(Z\alpha)^6$ as,

$$\begin{aligned} \delta E_{nS_{1/2}}^{\text{CPE}} \approx & \frac{2}{3}(Z\alpha)^4 \frac{m_r^3}{n^3} \left\{ \langle r^2 \rangle_c - \frac{1}{2} m_r (Z\alpha) \langle r^3 \rangle_{cc}^{\text{eff}} - (Z\alpha)^2 \langle r^2 \rangle_c \left[H_{n-1} + \gamma - \frac{1}{n} \right. \right. \\ & + \frac{9}{4n^2} - 3 + \ln \left[\frac{2m_r(Z\alpha)}{n} \right] + \ln[\langle r_{c2} \rangle] \left. \right] + m_r^2 (Z\alpha)^2 \left[\frac{\langle r^4 \rangle_c}{15n^5} \right. \\ & \left. \left. + \frac{2}{3} \langle r^2 \rangle_c \langle r^2 \rangle_c \left(H_{n-1} + \gamma - \frac{1}{n} + 2 + \ln \left[\frac{2m_r(Z\alpha)}{n} \right] + \ln[\langle r_{c1} \rangle] \right) \right] \right\}, \end{aligned} \quad (1.104)$$

where $\langle r^3 \rangle_{cc}^{\text{eff}}$ is an effective radius that takes into account the inelastic contributions of the two-photon Coulomb exchange¹⁴, and $\langle r_{c2} \rangle, \langle r_{c1} \rangle$ are again other nuclear moments, whose definitions from [34] we do not repeat here as they do not qualitatively contribute to our discussion.

It is important to note that [34] primarily focuses on deuterium but makes several useful comments for other nuclei such as atomic- and muonic-Hydrogen. It turns out that these latter systems are special in that the α^6 polarizability corrections to their finite-size effects vanish, which is not true for other nuclei such as deuterium, and the form of these corrections can be found in [34]. We do not write these here for two reasons: the systems we will be interested in in this thesis are ${}^4_2\text{He}^+, \mu_2^4\text{He}^+, \text{H}$ and μH and as we have just mentioned for the latter two these corrections vanish, while for the former two they turn out to be too small to contribute to current experiments; and these effects turn out to depend on the principal quantum number the same way as do the other finite-size effects, which means that we could group them together into effective moments the same way we had done so for $\langle r^3 \rangle_{cc}^{\text{eff}}$. At the same time, the polarizability contributions to $nP_{\frac{1}{2}}$ and $nP_{\frac{3}{2}}$ states in the systems of interest to us are also too small and as such the finite-size effects in these states preserve their form from (1.102) and (1.103).

Similarly, the spin-dependent finite-size effects have also been calculated for Hydrogen using this more modern approach and they have been written in terms of momentum-space integrals over the proton form-factors in [37],

¹⁴There is a cancellation between the original $\langle r^3 \rangle_{cc}$ term in (1.101) (known as the Friar moment) and a certain part of the polarizability [35] but since the inelastic contributions at this order depend on the lepton quantum numbers the same way as the elastic contributions they can be combined to define the effective nuclear moment, $\langle r^3 \rangle_{cc}^{\text{eff}}$.

and a position-space equivalent has been recently presented in [38] to be

$$\begin{aligned} \delta E_{\text{spin}}^{\text{CPE}} = & \left(\frac{8}{3n^3} \right) \frac{g_p m^2 (Z\alpha)^4}{2M} \left(\frac{m_r}{m} \right)^3 \left\{ (-2)m_r (Z\alpha) \langle r \rangle_{cm} + \frac{4}{3} (Z\alpha)^2 m^2 \langle r^2 \rangle_c \right. \\ & \times \left[-\frac{1}{n} + \gamma + H_{n-1} + \ln \left[\frac{2(Z\alpha)m \langle r_{pp} \rangle}{n} \right] + \frac{\langle r^2 \rangle_m}{4 \langle r^2 \rangle_c n^2} \right] \left. \right\} + \dots, \end{aligned} \quad (1.105)$$

with the ellipses standing for terms of $(Z\alpha)^7$ or higher and where $\langle r_{pp} \rangle$ is again some moment from [38] whose definition does not add to our discussion and so we do not repeat it here.

As we can see, although these more compact photon-exchange calculations depend on fewer model-independent nuclear parameters, they still require upward of 8 nuclear moments to be fitted experimentally in order to be able to predict finite-size effects at order $(Z\alpha)^6$. The issue with this is that accurate enough measurements for fitting these parameters accurately enough not to introduce large uncertainties in the predictions are few and far between with only 3 available in H [25, 39, 40] and only 2 in μH [41] for example. What makes matters worse is that fitting the $\langle r^2 \rangle_c$ term of (1.104) using the more precise measurements of muonic atoms of the past decade [42] has initially lead to a different value than the one suggested by CODATA derived from experiments using electrons [43]. This became known as the proton charge radius puzzle – for some recent reviews see for example [44, 45, 46] – and has ignited a lively reevaluation of all the effects of bound-state QED as well as the proposition of many Beyond the Standard Model Physics models. However, it must be noted that as new electronic experiments seemed to start yielding results conforming to the muonic measurements, the CODATA group recently has adjusted their recommended value for the proton charge radius [47].

1.5.3 How PPEFT Can Help

All in all, we see that while using nuclear moments is certainly a viable way for characterizing finite-size effects, the large number of these moments that need to be inferred experimentally due to a lack of first-principles calculations makes using them somewhat unreliable when it comes to nuclear errors. It would be great then, if we could reduce the number of these parameters, preferably to such an extent that the few accurate measurements we have would be enough to fit them in such a way that their implied predictions would be unclouded by the large uncertainties of nuclear structure.

This is where EFT methods, and in particular the above developed PPEFT formalism can help. As we had seen, we can describe atoms as a system of a lump of size, $R \sim 1$ fm, mass, M and charge Ze binding fermions, $\Psi(x)$ of mass, m and charge $(-e)$ to itself through electromagnetic interactions mediated by a U(1) gauge field, $A^\mu(x)$ at orbits of size, $a_B \sim (mZ\alpha)^{-1}$. This theory contains as a bulk action, the dynamics of

QED and a one-dimensional effective action that contains all possible interactions between the low-energy degrees of freedom of the nucleus and the bulk fields that are hermitian and symmetric under Poincaré-, gauge-, reparameterization-, C-, P- and T-transformations. Through the magic of EFTs such an effective action comes organized into a multipole expansion of operators where higher-order operators are suppressed by increasing powers of the small ratio, $R/a_B \sim (mRZ\alpha)$; and through it the nucleus affects the surrounding bulk fields only through a set of new near-nucleus boundary conditions that tie its effective couplings to the integration constants of the solutions to the bulk field equations of motion. Since the effective nuclear action appears as an expansion in powers of $(mRZ\alpha)$ it is clear that the effective couplings of this action are related to the finite size of the nucleus, and by writing physical observables in terms of the integration constants and using the implied near-source boundary conditions to trade these constants for the effective couplings, we can capture the effects of finite nuclear-size on the observables of interest.

Of particular importance for bound-states are the energies of the orbiting leptons. Writing shifts of these levels in terms of the integration constants of the bulk fields and then trading these constants for the couplings as outlined in the previous sections will introduce a dependence of this observable not just on the PPEFT couplings but also the fictitious scale, ϵ where the new boundary conditions are set up. Then, to ensure that the bound-state energies remain physical the effective couplings will rush to the rescue and assume an implicit dependence on ϵ that is exactly right to cancel these apparent dependences. The running of the couplings will then turn out to be characterized by a handful of RG-invariant parameters, which will therefore enter physical observables through dimensional transmutation. By inspection we will then be able to relate these RG-invariant scales to the nuclear moments of the previous section and see that it is only ever certain combinations of the many moments shown that enter into energy shifts and so they depend on fewer parameters than when written in terms of nuclear moments.

Since the nuclear-size dependent energy shifts turn out to depend on only a few parameters it will be possible to devise linear combinations of spectroscopic measurements from which the finite-size effects cancel to the accuracy we will work. Alternatively, it becomes possible to fit these handful of parameters and use them to make predictions for the finite-size energy shifts of other transitions, which therefore only depend on the precision of the experimental data we had used for the fitting and the accuracy of the theoretical contributions to these measurements that assume a point-like nucleus. As such, by designing more accurate experiments and calculating point-like bound-state QED effects to higher precision will only improve our predictions over time, diminishing the large nuclear-structure uncertainties of the past.

In summary, PPEFT reveals that nuclear-size contributions to energy

shifts are governed by fewer parameters than naively believed, which plays to the benefit of reducing the large uncertainties associated with these effects that have been stumping the progress of tests of fundamental theory in ultra-precise spectroscopic measurements. On this note, let us now dive in and see how all of this works out in detail.

Chapter 2

Leading Finite-Size Effects of Scalar Nuclei on Bound Dirac Fermions

Paper presented

C. P. Burgess, Peter Hayman, Markus Rummel and László Zalavári

“Point-particle effective field theory III: relativistic fermions and the Dirac equation”

J. High Energ. Phys. **2017**, 7 (2017).

doi:10.1007/JHEP09(2017)007

Summary

In this paper we continue the initiated efforts in [1, 2] to apply the PPEFT framework to various systems. While the motivation for studying the Schrödinger equation with a $1/r^2$ potential in [1] and the equations of motion of a charged relativistic scalar field in a Coulomb potential in [2] were purely technical, in this paper we apply PPEFT to our first physically well-motivated system: atoms. This is made possible by the fact that nuclei are charged, heavy, compact objects of size $R \sim 1$ fm that lend themselves well to a PPEFT treatment since from the scales of atomic orbits, $a_B \sim (mZ\alpha)^{-1}$ they appear to be point-like objects and can therefore be described through the effective theory of one-dimensional lumps we have developed above in Section 1.4. On the other hand, the bulk of the theory contains (for the first time for us) a fermionic field, $\Psi(x)$ with mass, m and charge, $(-e)$ bound to this nucleus through the effects of a U(1) gauge field, $A^\mu(x)$, whose dynamics are assumed to be described by the QED action of (1.62), as is appropriate in modern treatments of atomic bound-states.

In such an EFT, general nuclei correspond to background solutions with mass, M , charge, Ze , magnetic dipole moment, μ_N and higher-order elec-

tromagnetic moments, interacting with their surroundings only through their centre-of-mass coordinates, $y^\mu(s)$, their spin, $\xi^\mu(s)$, and other internal degrees of freedom. Their trajectory in spacetime is given by a one-dimensional path that maps \mathbb{R} to \mathbb{M}^4 , $\mathcal{P} : s \rightarrow y^\mu(s)$, where s is an arbitrary parameter along the nuclear world-line. The effective low-energy action, S_p of such a nucleus contains the most general interactions between its low-energy degrees of freedom and the surrounding bulk fields that are hermitian and allowed by Poincaré-, gauge-, reparameterization-, C-, P- and T-transformations, and comes organized into a multipole expansion of operators with higher-order terms suppressed by increasing powers of the small ratio, $R/a_B \sim (mRZ\alpha)$ and resolving ever-finer nuclear-size related details.

Since in [1, 2] we had already observed that the presence of the nucleus induces alternative near-source boundary conditions for the bulk fields and have already treated the electromagnetic field under the assumptions that the source only has charge but no other multipole moments, our current purpose is to understand how the presence of a nucleus with similar restrictions affects the fermion field and what new fermionic boundary conditions its existence leads to. Therefore, in this paper we take the nucleus to have zero spin, $\xi^\mu(s) = 0$ and no other electromagnetic properties other than its charge, which restricts our attention to systems such as ${}^4_2\text{He}^+$ and other Hydrogen-like systems with doubly magic nuclei.

To a large extent we have already summarized the set-up of this paper in our discussion of coupling a scalar nucleus to fermions in Section 1.4.3. The electromagnetic field sourced by the nucleus is found to be the Coulomb field in (1.66), while the solution to the Dirac-equation with this potential is given by (1.71) with the radial functions written in (1.73). The large- r boundary condition on these modes turns out to be (1.82) by normalizability, while the traditional near-nucleus boundary condition of boundedness at the origin forces $\mathcal{D}_{j\varpi} = 0$, yielding the Dirac-Coulomb energies, ω_D of (1.83). The alternative boundary conditions that emerge due to the presence of the nucleus are given in (1.86) and these introduce a perturbation around ω_D related to finite-nuclear size that can be calculated from (1.82) by taking $\omega = \omega_D + \delta\omega$, while keeping $\mathcal{D}_{j\varpi}/\mathcal{C}_{j\varpi} \neq 0$. We concentrate on such energy shifts of the $j = 1/2$ states as these are located closest to the nucleus and feel the effects of its finite size the most.

We use the boundary conditions in (1.86) to find this ratio of integration constants as a function of the effective fermion-nucleus couplings. This inadvertently introduces a dependence on the fictitious parameter, ϵ – the radius of the boundary on which the alternative boundary conditions have been set up – of the energy shift. Then to keep this energy perturbation physical we analyze (1.86) as if it was a running equation that told us how the PPEFT couplings have to depend on ϵ in order to achieve this.

In this paper, instead of using the RG-invariant parameters to characterize the running and then trading the apparent ϵ -dependence of $\mathcal{D}_{j\varpi}/\mathcal{C}_{j\varpi}$ for a dependence on these parameters, we write it as a function of “effective

moments”, \hat{g}_i, \hat{f}_i in a double series expansion of $\epsilon/a_B \approx m\epsilon Z\alpha$ and $(Z\alpha)^2$, using $\mathfrak{g}_{n\frac{1}{2}+}/\mathfrak{f}_{n\frac{1}{2}+} \approx (Z\alpha) [\hat{g}_1 + \hat{g}_2(m\epsilon Z\alpha) + \hat{g}_3(Z\alpha)^2 + \dots]$ and a similar expression for the negative-parity modes in the boundary condition.

Lastly, we compare our leading energy shift result written as a function of these effective moments to that written in terms of nuclear moments, namely the shift in (1.101) and find that $(1 + 2\hat{g}_1)\epsilon^2 = \langle r^2 \rangle_c/3$ and also compare our predictions for subleading effects in terms of \hat{g}_i, \hat{f}_i to those made by specific nuclear models.



Point-particle effective field theory III: relativistic fermions and the Dirac equation

C.P. Burgess, Peter Hayman, Markus Rummel and László Zalavári

*Department of Physics & Astronomy, McMaster University,
1280 Main Street West, Hamilton Ontario L8S 4M1, Canada*

*Perimeter Institute for Theoretical Physics,
31 Caroline Street North, Waterloo Ontario N2L 2Y5, Canada*

*E-mail: cburgess@perimeterinstitute.ca, haymanpf@mcmaster.ca,
rummelm@mcmaster.ca, zalavar1@mcmaster.ca*

ABSTRACT: We formulate point-particle effective field theory (PPEFT) for relativistic spin-half fermions interacting with a massive, charged finite-sized source using a first-quantized effective field theory for the heavy compact object and a second-quantized language for the lighter fermion with which it interacts. This description shows how to determine the near-source boundary condition for the Dirac field in terms of the relevant physical properties of the source, and reduces to the standard choices in the limit of a point source. Using a first-quantized effective description is appropriate when the compact object is sufficiently heavy, and is simpler than (though equivalent to) the effective theory that treats the compact source in a second-quantized way. As an application we use the PPEFT to parameterize the leading energy shift for the bound energy levels due to finite-sized source effects in a model-independent way, allowing these effects to be fit in precision measurements. Besides capturing finite-source-size effects, the PPEFT treatment also efficiently captures how other short-distance source interactions can shift bound-state energy levels, such as due to vacuum polarization (through the Uehling potential) or strong interactions for Coulomb bound states of hadrons, or any hypothetical new short-range forces sourced by nuclei.

KEYWORDS: Effective Field Theories, Nonperturbative Effects, Renormalization Group

ARXIV EPRINT: [1706.01063](https://arxiv.org/abs/1706.01063)

Contents

1	Introduction	2
2	Action and field equations	4
2.1	Action and field equations	4
2.2	Bulk solutions	5
3	Fermionic boundary conditions and the point-particle action	7
3.1	Source-bulk matching	7
3.2	RG evolution	9
3.2.1	Non-relativistic limit	10
3.2.2	Relativistic running when $Z\alpha = 0$	10
3.2.3	Relativistic running when $Z\alpha \neq 0$	13
3.3	Higher-order interactions	15
4	Bound-state energy shifts	16
4.1	Energy-shift calculations	16
4.2	Leading and first-subleading energy shifts	20
4.3	Subleading $(Z\alpha)^2$ energy shifts	23
5	Examples	25
5.1	Explicit charge distributions	25
5.1.1	Relations to moments	25
5.1.2	Specific charge distributions	27
5.2	Other applications	29
6	Summary	30
A	Gamma-matrix conventions	32
A.1	Polar coordinates	33
A.2	Spinor harmonics	35
B	Dirac solutions	37
B.1	Exterior (Coulomb) solutions	37
B.2	Interior solutions for given charge distributions	40
B.2.1	Charged-shell model	40
B.2.2	General charge distribution	42
B.2.3	Uniform charge distribution	47

1 Introduction

Nature is full of examples where small but massive compact objects (of linear size R) interact with and control the motions of lighter neighbours within a much larger surrounding domain (of size $a \gg R$). Examples include nuclei and atoms, stars and solar systems as well as legions of others. For such systems familiar arguments (such as the multipole expansion) show that only a few features of the compact object are often relevant to understanding motions in their larger environment. This simplicity usually emerges once observables are expanded in powers of small ratios like R/a .

Effective field theories [1–4] are the natural language for exploiting this kind of simplicity, though these are usually only formulated in a second-quantized language with all species of particles represented by their respective quantum field. For instance two-body contact interactions between two species of particles in a fully second-quantized framework would be represented in terms of their respective fields by terms like $g(\psi^*\psi)(\chi^*\chi)$ in an effective Lagrangian.

Our companion papers [5, 6] explore how to formulate such effective theories using instead a first-quantized language for the heavy compact object, reserving the second-quantized language for the lighter particles with which it interacts.¹ In this mixed first-quantized/second-quantized (one-two) language, if the heavy (χ) particle is in a position eigenstate situated at $\mathbf{x} = 0$ then the two-body contact interaction mentioned above instead has the form $g(\psi^*\psi) \delta^3(x)$. This kind of formulation would be appropriate when the mass of the compact object is sufficiently large. In such situations all information about the source enters observables through the boundary conditions that are implied for the light fields at the position of the heavy compact object; boundary conditions that are completely determined by the source’s first-quantized effective action.

This type of one-two formulation can have several advantages. One of these is the more direct connection it provides to the study of particle motion within a central (e.g. Coulomb or gravitational) potential, for which many useful tools are known (particularly for bound states). In this they are complementary to a fully second-quantized (two-two) formulation, such as for NRQED or NRQCD [13–19], in which induced quantities — like the nuclear Coulomb potential or solar gravitational field — arise as a resummation of a particular class of interactions that dominate in some limits. By contrast, in the mixed one-two framework such classical fields are included into the zeroth order description about which one perturbs.

Furthermore, relating the near-source boundary conditions to the source action takes the guesswork out of small- r boundary conditions, and shows in particular why linear ‘Robin’ boundary conditions are so generic at low energies (see also [20, 21]). More generally, they show how to handle singular potentials (like $V(r) \propto r^p$ with $p \leq -2$) unambiguously, despite the generic absence in these cases (for a clear introduction to the ambiguities

¹Similar methods have been developed to handle compact gravitating systems, such as for gravitational-wave emission by inspiralling compact objects [7] and gravitational back-reaction in extra-dimensional models to [8–12].

otherwise hit for the inverse-square potential, see for example, [22]) of smooth solutions at the origin.

The study in [5, 6] considered both nonrelativistic and spinless relativistic particles orbiting the massive compact object, focussing in particular on unusual effects that arise if the compact source size, R , is small enough that relativistic kinematics is relevant for the matching problem to the interior physics of the source *even for bound states whose total energy, ω , is nonrelativistic: $m - \omega \ll m$* . This mixed relativistic/nonrelativistic regime occurs when $mR \ll v \ll 1$, where $v \sim Z\alpha$ is the speed of the orbiting particle (whose mass is m). (Here we take the source charge to be Ze and $\alpha = e^2/4\pi$ is the usual fine-structure constant.)

In particular, for relativistic spinless particles an interesting regime was identified for which energy shifts of S -wave states due to the source's finite size scale as

$$\delta\omega_{\text{KG}} \sim \frac{(Z\alpha)^2 R}{m} \left(\frac{mZ\alpha}{n} \right)^3 \propto (Z\alpha)^5 m^2 R, \quad (1.1)$$

where the last factor is the S -wave Schrödinger-Coulomb wave-function at the origin $|\psi(0)|^2 \propto (mZ\alpha/n)^3$. Effects like this, scaling linearly with R , are unusual and so lead to the question of whether similar shifts occur for the spin-half electrons and muons that arise in conventional and muonic atoms.

We here address this question by extending the discussion of [5, 6] to spin-half systems, finding that although many of the features of the Klein-Gordon problem of [6] also carry over to the Dirac field studied here the scaling of (1.1) does not: the corresponding leading Dirac expression instead gives the standard result:

$$\delta\omega_D \sim Z\alpha R^2 \left(\frac{mZ\alpha}{n} \right)^3 \propto (Z\alpha)^4 m^3 R^2. \quad (1.2)$$

At first sight this difference in scaling may seem surprising, since spin-dependent effects in orbital energies might be expected to be suppressed by $v \sim Z\alpha$ leading one to expect Dirac and Klein-Gordon predictions to agree at leading order in $Z\alpha$. Although this expectation is true for most observables, it proves not to be true when tracking finite-size effects because relativistic effects are not small at radii $r \sim R$ once $R \lesssim Z\alpha/m \sim (Z\alpha)^2 a_B$ (where a_B is the Bohr radius). Indeed the ratio of $\delta\omega_{\text{KG}}$ and $\delta\omega_D$ given above is of order $Z\alpha/mR$, which is order unity for electrons (for which $mR \sim Z\alpha$ even though both are separately small).

Along the way we show how to formulate the near-source boundary condition for fermions, and why these differ from those that arise for bosons. We identify how the couplings for two-body contact interactions run, even at the classical level, and how this running goes over to the running found in [5, 6] in the non-relativistic limit. This running properly captures how effective theories can sometimes generate scattering lengths that are much larger than the size R of the underlying object, and corresponds to the first-quantized version of a similar discussion found in [15–19].

Another result from [5, 6] carries over to fermions: the fixed point of the running is *not* at $c_s = c_v = 0$ for charged sources (for which $Z\alpha \neq 0$). It turns out this nontrivial

fixed point is precisely what is required in order for the fixed point to reproduce standard results for the Dirac equation in the presence of specific nuclear charge distributions. That is, when we compare the PPEFT approach to explicit solutions to the Dirac equation in the presence of a finite-size charge distribution, we find that matching produces contact interactions for the PPEFT that sit precisely at the infrared fixed point of the RG flow. This shows why energy-level shifts take on a particular model-independent form (proportional to the charge-radius $r_p^2 = \langle r^2 \rangle$ and higher moments [23, 24] — see also [25]) in the special case where the nucleus is modelled as a specific charge distribution.

In what follows we specialize for simplicity to parity-preserving interactions and spinless compact central objects, and so strictly speaking the interactions we find suffice in themselves to describe finite-size effects in the He^+ ion or muonic states in even-even nuclei [24, 26–45]. The effects we find also apply to nuclei with spin (such as hydrogen) once the effective theory of the first-quantized source is supplemented by the extra interactions that a nuclear spin allows. (We intend to return to discuss spinning sources more fully in a later paper.)

In section 2 we set the stage by introducing the point-particle effective action in the context of Dirac fermions. In section 3 we derive the boundary condition and the induced renormalization group running in the presence and absence of a Coulomb potential. This leads to the discussion of bound state energy shifts implied by the boundary condition in section 4. We discuss applications of PPEFT for fermions in section 5 and conclude in section 6. We discuss various technicalities in the appendix.

2 Action and field equations

To make things concrete we focus on describing a relativistic spin-half charged particle interacting with a small charged source. The system of interest consists of a 3+1 dimensional ‘bulk’ action coupled to a 0+1 dimensional ‘point-particle’ action representing the small source (e.g. the nucleus of an atom),

$$S_{\text{tot}} = \int d^4x \mathcal{L}_B + \int_{\mathcal{W}} d\tau L_p = \int d^4x \left[\mathcal{L}_B + \int_{\mathcal{W}} d\tau \delta^4(x - y(\tau)) L_p \right], \quad (2.1)$$

where \mathcal{W} indicates the integration is over the world-line, $y^\mu(\tau)$, of the source. In the final equality \mathcal{L}_B and L_p are both regarded as being functions of the bulk fields evaluated at an arbitrary spacetime point, x^μ . L_p is also a function of the ‘brane-localized’ position field, $y^\mu(\tau)$.

2.1 Action and field equations

Taking the bulk dynamics to be QED with a fermion of charge $-e$, the bulk action becomes

$$S_B = - \int d^4x \left[\frac{1}{4} F_{\mu\nu} F^{\mu\nu} + \bar{\psi} (\not{D} + m) \psi \right], \quad (2.2)$$

with $D_\mu \psi = (\partial_\mu + ieA_\mu) \psi$. This should be considered in the spirit of a Wilson action, and so in principle also includes an infinite series of subdominant local terms involving more powers of the fields and their derivatives (whose effects are not important in what follows).

The point-particle action is similarly given by an expansion in these fields, for which (for a spinless, parity-preserving source) the leading parity-even terms are²

$$S_p = - \int_{\mathcal{W}} d\tau \left[M - Q A_\mu \dot{y}^\mu + c_s \bar{\psi} \psi + i c_v \bar{\psi} \gamma_\mu \psi \dot{y}^\mu - \tilde{h} \nabla \cdot \mathbf{E} + \dots \right], \quad (2.3)$$

where the over-dot denotes differentiation with respect to proper time, the coefficients c_s , c_v and \tilde{h} all have dimension length-squared and the ellipses indicate terms suppressed by more than two powers of length. Notice that terms involving more than two powers of ψ first arise suppressed by a coupling with dimension (length)⁵, and so are nominally subdominant to several terms involving only two powers of ψ but more derivatives than those written above.

Specializing to the rest frame for a motionless source, $\dot{y}^\mu(\tau) = \delta_0^\mu$, with charge $Q = Ze$ the bulk field equations become

$$(\mathcal{D} + m)\psi + \mathcal{J} = 0 \quad \text{and} \quad \partial_\mu F^{\mu\nu} - ie \bar{\psi} \gamma^\nu \psi + j^\nu = 0, \quad (2.4)$$

where

$$\mathcal{J} := - \frac{\partial L_p}{\partial \bar{\psi}} = \left(c_s + i c_v \gamma^0 \right) \psi \delta^3(x) + \dots, \quad (2.5)$$

and

$$j^\nu := \frac{\partial L_p}{\partial A_\nu} = Ze \left(1 + \frac{r_p^2}{6} \nabla^2 \right) \delta^3(x) \delta_0^\nu. \quad (2.6)$$

This last equality trades the parameter \tilde{h} for the mean-square charge radius: $r_p^2 = \langle r^2 \rangle$ of the source charge distribution using $\tilde{h} = \frac{1}{6} Ze r_p^2$.

2.2 Bulk solutions

We seek solutions to the bulk equations with a motionless point charge situated at the origin. The Maxwell equation is straightforwardly solved for the given source by choosing $\mathbf{A} = 0$ and electrostatic potential

$$A^0 = Ze \left[\frac{1}{4\pi r} - \frac{r_p^2}{6} \delta^3(x) \right]. \quad (2.7)$$

Here the first term is the usual homogeneous solution to the Poisson equation, normalized using the boundary condition at small radial distance, $r = \epsilon$, corresponding to nonzero electric flux

$$\oint_{r=\epsilon} d^2\Omega \mathbf{n} \cdot \mathbf{E} = Ze. \quad (2.8)$$

This boundary condition can be obtained by integrating the Maxwell equation over a small Gaussian pillbox of vanishingly small radius $r = \epsilon$. By contrast, the second term in (2.7) is the particular integral arising when solving $\nabla \cdot \mathbf{E} = -\nabla^2 A^0 = \frac{1}{6} Ze r_p^2 \nabla^2 \delta^3(x)$.

²Our metric is mostly plus and our Dirac conventions in rectangular and polar coordinates are given in appendix A.

We wish to repeat the above arguments for the Dirac field, whose field equation is

$$\begin{aligned} 0 &= (\not{D} + m)\psi + (c_s + ic_v\gamma^0)\psi\delta^3(x) \\ &= \left[-i\gamma^0\left(\omega + \frac{Z\alpha}{r}\right) + \vec{\gamma}\cdot\nabla + m\right]\psi + (c_s + ic_{v\text{tot}}\gamma^0)\psi\delta^3(x), \end{aligned} \quad (2.9)$$

where the second line specializes to energy eigenstates,³ $\psi(t) = \psi e^{-i\omega t}$, and to gauge potentials of the form (2.7). The parameter $c_{v\text{tot}}$ denotes the total localized combination

$$c_{v\text{tot}} := c_v + \frac{Ze^2}{6}r_p^2 = c_v + \frac{2\pi}{3}Z\alpha r_p^2. \quad (2.10)$$

This implies ψ_L and ψ_R are related by

$$\begin{aligned} &\left[-\left(\omega + \frac{Z\alpha}{r}\right) - i\sigma_k\partial_k\right]\psi_R + m\psi_L + (c_s\psi_L + ic_{v\text{tot}}\gamma^0\psi_R)\delta^3(x) = 0 \\ \text{and } &\left[-\left(\omega + \frac{Z\alpha}{r}\right) + i\sigma_k\partial_k\right]\psi_L + m\psi_R + (c_s\psi_R + ic_{v\text{tot}}\gamma^0\psi_L)\delta^3(x) = 0. \end{aligned} \quad (2.11)$$

Outside the source these equations become $(\not{D} + m)\psi = 0$ which (see appendix B for a summary in the present conventions) for rotationally and parity invariant situations have solutions of the parity-even form

$$\Psi^+ = \begin{pmatrix} \psi_L^+ \\ \psi_R^+ \end{pmatrix} = \begin{pmatrix} f_+(r)U^+(\theta, \phi) + ig_+(r)U^-(\theta, \phi) \\ f_+(r)U^+(\theta, \phi) - ig_+(r)U^-(\theta, \phi) \end{pmatrix}, \quad (2.12)$$

and parity-odd form

$$\Psi^- = \begin{pmatrix} \psi_L^- \\ \psi_R^- \end{pmatrix} = \begin{pmatrix} f_-(r)U^-(\theta, \phi) + ig_-(r)U^+(\theta, \phi) \\ f_-(r)U^-(\theta, \phi) - ig_-(r)U^+(\theta, \phi) \end{pmatrix}. \quad (2.13)$$

Here U^\pm are the spinor harmonics that combine the particle's spin-half with orbital angular momenta $\ell = j \mp \frac{1}{2}$ to give total angular momentum $j = \frac{1}{2}, \frac{3}{2}, \dots$.

The functions $f_\pm(r)$ and $g_\pm(r)$ are found by explicitly solving the radial part of the Dirac equation in the presence of a potential $A_0(r)$. For a Coulomb potential with source charge Ze these radial equations are (see appendix B for details)

$$f'_+ = \left(m + \omega + \frac{Z\alpha}{r}\right)g_+ \quad \text{and} \quad g'_+ + \frac{2g_+}{r} = \left(m - \omega - \frac{Z\alpha}{r}\right)f_+, \quad (2.14)$$

together with

$$g'_- = \left(m - \omega - \frac{Z\alpha}{r}\right)f_- \quad \text{and} \quad f'_- + \frac{2f_-}{r} = \left(m + \omega + \frac{Z\alpha}{r}\right)g_-. \quad (2.15)$$

³Speaking of 'energy eigenstates' for a relativistic field is shorthand for evaluating matrix elements of the form $\langle 0|\psi(x)|n\rangle$, between the vacuum and an energy eigenstate. The energy ω is the energy of $|n\rangle$ (relative to the vacuum) and can be found in the usual way from the poles in the correlation functions like $\langle \bar{\psi}(x)\psi(y)\rangle$.

These have as their general solutions

$$\begin{aligned}
 f_{\pm} &= \sqrt{m + \omega} e^{-\rho/2} \rho^{\zeta-1} \\
 &\times \left\{ A_{\pm} \mathcal{M} \left[\zeta - \frac{Z\alpha\omega}{\kappa}, 2\zeta + 1; \rho \right] + C_{\pm} \rho^{-2\zeta} \mathcal{M} \left[-\zeta - \frac{Z\alpha\omega}{\kappa}, -2\zeta + 1; \rho \right] \right. \\
 &\quad - A_{\pm} \left(\frac{\zeta - Z\alpha\omega/\kappa}{K - Z\alpha m/\kappa} \right) \mathcal{M} \left[\zeta - \frac{Z\alpha\omega}{\kappa} + 1, 2\zeta + 1; \rho \right] \\
 &\quad \left. + C_{\pm} \left(\frac{\zeta + Z\alpha\omega/\kappa}{K - Z\alpha m/\kappa} \right) \rho^{-2\zeta} \mathcal{M} \left[-\zeta - \frac{Z\alpha\omega}{\kappa} + 1, -2\zeta + 1; \rho \right] \right\}, \tag{2.16}
 \end{aligned}$$

and

$$\begin{aligned}
 g_{\pm} &= -\sqrt{m - \omega} e^{-\rho/2} \rho^{\zeta-1} \\
 &\times \left\{ A_{\pm} \mathcal{M} \left[\zeta - \frac{Z\alpha\omega}{\kappa}, 2\zeta + 1; \rho \right] + C_{\pm} \rho^{-2\zeta} \mathcal{M} \left[-\zeta - \frac{Z\alpha\omega}{\kappa}, -2\zeta + 1; \rho \right] \right. \\
 &\quad + A_{\pm} \left(\frac{\zeta - Z\alpha\omega/\kappa}{K - Z\alpha m/\kappa} \right) \mathcal{M} \left[\zeta - \frac{Z\alpha\omega}{\kappa} + 1, 2\zeta + 1; \rho \right] \\
 &\quad \left. - C_{\pm} \left(\frac{\zeta + Z\alpha\omega/\kappa}{K - Z\alpha m/\kappa} \right) \rho^{-2\zeta} \mathcal{M} \left[-\zeta - \frac{Z\alpha\omega}{\kappa} + 1, -2\zeta + 1; \rho \right] \right\}. \tag{2.17}
 \end{aligned}$$

Here A_{\pm} and C_{\pm} are integration constants, $\mathcal{M}[a, b; z] = 1 + (a/b)z + \dots$ are the standard confluent hypergeometric functions, ω is the mode energy and κ and ζ are defined by

$$\kappa = \sqrt{(m - \omega)(m + \omega)} \quad \text{and} \quad \zeta = \sqrt{\left(j + \frac{1}{2}\right)^2 - (Z\alpha)^2}, \tag{2.18}$$

with κ real because of our focus on bound states: $m > \omega$. The parity of the solution enters the above formulae only through the parameter $K = \mp(j + \frac{1}{2})$ where (perversely) standard conventions match negative (positive) K to parity-even (parity-odd) states.

3 Fermionic boundary conditions and the point-particle action

The next step is to formalize the boundary conditions at the surface of a spherical Gaussian pillbox of radius $r = \epsilon$, along the lines of what is done in (2.8) for the Maxwell field. We now show how these relate the constants c_s and c_v of the source action to the ratios g_+/f_+ and f_-/g_- at $r = \epsilon$. These boundary conditions are again obtained from the source action by integrating the equations of motion over the interior of the pillbox using the delta-function.

3.1 Source-bulk matching

That is, given the action

$$S = - \int_P d^4x \left[\sqrt{-g} \bar{\psi} (\not{D} + m) \psi + \sqrt{-\hat{g}} \bar{\psi} N \psi \delta^3(x) \right], \tag{3.1}$$

where $\hat{g}_{ab} = g_{\mu\nu} \partial_a x^\mu \partial_b x^\nu$ is the induced metric on the world-volume of the source and $N = c_s + i c_v \text{tot} \gamma^0$ is the Dirac matrix specified by the source action S_p , the equation of motion satisfied by ψ is

$$\sqrt{-g} (\not{D} + m) \psi + \sqrt{-\hat{g}} N \psi \delta^3(x) = 0, \tag{3.2}$$

so integrating over the small Gaussian pillbox, P , of radius ϵ centred on the source then gives (in the limit $\epsilon \rightarrow 0$ of vanishingly small pillbox)

$$\lim_{\epsilon \rightarrow 0} \int_{\partial P} d^2x \sqrt{-g} n_\mu \gamma^\mu \psi = \lim_{\epsilon \rightarrow 0} \int d\theta d\phi \epsilon^2 \sin \theta \gamma^r \psi = -\sqrt{-\hat{g}} N \psi(0). \quad (3.3)$$

Here n_μ is an outward-pointing unit normal to the pillbox so $n_\mu dx^\mu = dr$, and the integral of the $m\psi$ term vanishes as $\epsilon \rightarrow 0$. Our conventions on gamma-matrices in polar coordinates are given in appendix A.

For spherically symmetric configurations (in the limit where ϵ is much smaller than all other scales of interest) this implies the boundary condition

$$\int_{r=\epsilon} d^2\Omega \left[\epsilon^2 \gamma^r + \frac{1}{4\pi} (c_s + i c_{v \text{ tot}} \gamma^0) \right] \psi = 0. \quad (3.4)$$

Notice this boundary condition is trivially satisfied pretty much anywhere in the absence of a source, for a small enough pillbox. This is because no source means $c_s = c_v = r_p = 0$ and ψ varies slowly enough to be approximately constant across the pillbox. In this case the integral over all directions for γ^r on the surface of the pillbox gives zero trivially.

The boundary condition on the Gaussian pillbox can be written as $\int d^2\Omega B_\epsilon \psi(\epsilon) = 0$ where

$$B_\epsilon := \gamma^r + \hat{c}_s + i \hat{c}_v \gamma^0 = \begin{pmatrix} \hat{c}_s & \hat{c}_v - i\sigma^r \\ \hat{c}_v + i\sigma^r & \hat{c}_s \end{pmatrix}. \quad (3.5)$$

The dimensionless coefficients $\hat{c}_s = c_s/(4\pi\epsilon^2)$ and $\hat{c}_v = c_{v \text{ tot}}/(4\pi\epsilon^2)$ can be interpreted as the coefficients of a term in a ‘boundary action’ defined on the codimension-one surface of the Gaussian pillbox,

$$S_{\text{bound}} = - \int_{\partial P} d^3x \bar{\psi} \left(\hat{c}_s + i \hat{c}_v \gamma^0 + \dots \right) \psi. \quad (3.6)$$

The subscript ϵ on B_ϵ is meant to emphasize that the constants \hat{c}_a (and in general also the original couplings c_i themselves) also must carry an implicit ϵ -dependence if physical quantities are to remain unchanged as ϵ is varied (more about which below).

To see what these boundary conditions mean we write them out separately for ψ_L and ψ_R , leading to

$$-\hat{c}_s \int_\epsilon d^2\Omega \psi_L^\pm = \int_\epsilon d^2\Omega (\hat{c}_v - i\sigma^r) \psi_R^\pm \quad \text{and} \quad - \int_\epsilon d^2\Omega (\hat{c}_v + i\sigma^r) \psi_L^\pm = \hat{c}_s \int_\epsilon d^2\Omega \psi_R^\pm. \quad (3.7)$$

Notice that these can be found from one another by making the replacements $\psi_L \leftrightarrow \psi_R$ together with $(\hat{c}_v, \hat{c}_s) \leftrightarrow (-\hat{c}_v, -\hat{c}_s)$. Acting on bulk solutions (2.12) and (2.13) and evaluating the angular integrations, these give

$$\hat{c}_s + \hat{c}_v = \frac{c_s + c_{v \text{ tot}}}{4\pi\epsilon^2} = \left(\frac{g_+}{f_+} \right)_{r=\epsilon} \quad \text{and} \quad \hat{c}_s - \hat{c}_v = \frac{c_s - c_{v \text{ tot}}}{4\pi\epsilon^2} = \left(\frac{f_-}{g_-} \right)_{r=\epsilon}. \quad (3.8)$$

In what follows we determine $c_s(R)$ and $c_v(R)$ from several hypothetical UV completions for the structure of the source of size R , and then regard (3.8) as a boundary condition that selects the exterior solution appropriate for the source of interest. This emphasizes that it is only through boundary conditions like (3.8) that the physics of a specific source can influence the exterior solution, and so enter into physical observables.

3.2 RG evolution

The radius of the Gaussian pillbox, $r = \epsilon$, is not a physical scale and so must drop out of predictions for observables (unlike the physical size, R , of the underlying source, say). In detail, this happens because any explicit ϵ -dependence arising in a calculation of an observable cancels an implicit ϵ -dependence buried within the ‘bare’ quantities c_s and c_v . Following the procedure of [5, 6] (which in turn builds on [46–50]), we next determine what the ϵ -independence of observables implies for the ϵ -dependence of c_s and c_v .

First we establish what is needed to ensure physical quantities remain independent of ϵ . Boundary conditions like (3.8) affect observables by determining the ratio of the integration constants that arise when integrating the bulk field equations. For instance, writing the general solutions, (2.16) and (2.17), to the radial part of the Dirac field equation in the form

$$f_{\pm}(r) = A_{\pm}f_{1\pm}(r) + C_{\pm}f_{2\pm}(r) \quad \text{and} \quad g_{\pm}(r) = A_{\pm}g_{1\pm}(r) + C_{\pm}g_{2\pm}(r), \quad (3.9)$$

it is the two ratios C_+/A_+ and C_-/A_- that are determined by a boundary condition like the specification of $(g_{\pm}/f_{\pm})_{r=\epsilon}$. Energy levels for states of either parity are determined by demanding the resulting value for the appropriate C/A be consistent with what is required for C/A by normalizability of the modes at infinity. Scattering amplitudes are similarly determined by C/A . It follows that physical predictions are ϵ -independent if $c_s(\epsilon)$ and $c_v(\epsilon)$ are chosen to ensure C/A is ϵ -independent for both parity choices.

At some level (3.8) says it all. Rather than reading (3.8) as fixing f_{\pm}/g_{\pm} at a specific radius given known values of c_s and c_v we can instead read the equations

$$c_s(\epsilon) = \left[\frac{g_+(\epsilon)}{f_+(\epsilon)} + \frac{f_-(\epsilon)}{g_-(\epsilon)} \right] 2\pi\epsilon^2 \quad \text{and} \quad c_{v \text{ tot}}(\epsilon) = \left[\frac{g_+(\epsilon)}{f_+(\epsilon)} - \frac{f_-(\epsilon)}{g_-(\epsilon)} \right] 2\pi\epsilon^2, \quad (3.10)$$

as giving $c_s(\epsilon)$ and $c_{v \text{ tot}}(\epsilon)$ for known functions $f_{\pm}(r)$ and $g_{\pm}(r)$. This means that the ϵ -dependence of the right-hand-side of (3.10) is simply given by the r -dependence of $f_{\pm}(r)$ and $g_{\pm}(r)$ using (3.9), with $r = \epsilon$. Because C_{\pm} and A_{\pm} are r -independent the above conditions tell us what c_s and $c_{v \text{ tot}}$ must do to keep them also ϵ -independent.

Our greatest interest is when ϵ is much smaller than the typical scale a of the external problem (such as the Bohr radius, for applications to atoms), and in this limit it suffices to use the leading small- r form of the solutions f_{\pm} and g_{\pm} when computing the ϵ -dependence of c_s and $c_{v \text{ tot}}$. In this regime solutions are usually well described by power laws, with (3.9) reducing to

$$f_{\pm}(r) = A_{\pm} \left(\frac{r}{a} \right)^{\zeta-1} + C_{\pm} \left(\frac{r}{a} \right)^{-\zeta-1} \quad \text{and} \quad g_{\pm}(r) = A_{\pm} \left(\frac{r}{a} \right)^{\zeta-1} + C_{\pm} \left(\frac{r}{a} \right)^{-\zeta-1}. \quad (3.11)$$

For such solutions the choice of C_{\pm}/A_{\pm} controls the precise radius at which one of these solutions dominates the other one, and as a result the RG evolution of the couplings implied by (3.10) in this regime describes the cross-over between these two types of evolution.

3.2.1 Non-relativistic limit

We start by examining this running for parity-even states in the nonrelativistic limit, which corresponds to the evolution found in [5, 6] using the Schrödinger equation.

The radial equations for parity-even states are given by (2.14) which imply in the nonrelativistic limit (for which the energy and mass are approximately equal, $\omega \simeq m$, and much larger than all other scales) that $g_+ \simeq f'_+/(2m) \ll f_+$. Using this in the second of eqs. (2.14) and dropping subdominant terms gives the Schrödinger equation (in the presence of a Coulomb potential), with Schrödinger field $\varphi(r) = f_+(r)$.

In this limit the Dirac spinor is approximately given by

$$\psi \simeq \frac{1}{\sqrt{2}} \begin{pmatrix} \varphi \\ \varphi \end{pmatrix}, \quad (3.12)$$

so in the nonrelativistic limit the combination appearing in the source action is

$$c_v \bar{\psi} \psi + i c_v \bar{\psi} \gamma^0 \psi \simeq (c_s + c_v) \varphi^* \varphi =: h \varphi^* \varphi, \quad (3.13)$$

where $h = c_s + c_v$ is the coupling for the analogous effective Schrödinger contact interaction.

Defining the quantity $\lambda := 2m h_{\text{tot}} = 2m (h + \frac{2\pi}{3} Z\alpha r_p^2)$, the nonrelativistic limit of the boundary condition (3.8) therefore is

$$\lambda = 2m h_{\text{tot}} = 2m(c_s + c_{v \text{ tot}}) = 8\pi m \epsilon^2 \left(\frac{g_+}{f_+} \right)_{r=\epsilon} \simeq 4\pi \epsilon^2 \left(\frac{\varphi'}{\varphi} \right)_{r=\epsilon}, \quad (3.14)$$

in agreement with the boundary condition found for a Schrödinger field coupled to a source with Lagrangian density $\mathcal{L}_p = -h \varphi^* \varphi \delta^3(x)$ [5, 6]. These references also show that restricting to s -wave ($\ell = 0$) configurations and using the small- r asymptotic form $\varphi_1(r) \propto r^\ell$ and $\varphi_2(r) \propto r^{-\ell-1}$ implies that for small ϵ the evolution of h given in (3.14) satisfies the differential RG equation

$$\epsilon \frac{d\hat{\lambda}}{d\epsilon} = \frac{1}{2} (1 - \hat{\lambda}^2) \quad \text{where} \quad \hat{\lambda} := \frac{\lambda}{2\pi\epsilon} + 1 = \frac{mh}{\pi\epsilon} + 1, \quad (3.15)$$

in which the last equalities define $\hat{\lambda}$.

The evolution of $\hat{\lambda}$ evidently has two fixed points, at $\hat{\lambda}_* = \pm 1$, and these respectively correspond to $\lambda_* = 0$ and $\lambda_* = -4\pi\epsilon$. Comparing with (3.14) shows these forms for λ_* are equivalent to having $\varphi(r) \propto r^0$ and $\varphi(r) \propto r^{-1}$ (i.e. r^ℓ and $r^{-\ell-1}$ for $\ell = 0$), showing the crossover described below (3.11).

3.2.2 Relativistic running when $Z\alpha = 0$

A similar story relates the solutions f and g to solutions of the Klein-Gordon equation in the relativistic case, as is most easily seen in the absence of the Coulomb interaction ($Z\alpha = 0$), as we now show.

Parity-even case. When $Z\alpha = 0$ the first of eqs. (2.14) again gives g_+ as the derivative of f_+ :

$$g_+ = \frac{f'_+}{m + \omega}, \quad (3.16)$$

for a mode of energy ω . Using this in the second equation then shows f_+ satisfies the Klein-Gordon equation. This shows that the r -dependence of the ratio g_+/f_+ is proportional to the ratio χ'/χ for a Klein-Gordon field:

$$\left(\frac{g_+}{f_+}\right)_{r=\epsilon} = \frac{1}{m + \omega} \left(\frac{\chi'}{\chi}\right)_{r=\epsilon}. \quad (3.17)$$

But refs. [5, 6] show (even for $Z\alpha \neq 0$) that if we define the quantity

$$\lambda = 4\pi\epsilon^2 \left(\frac{\chi'}{\chi}\right)_{r=\epsilon}, \quad (3.18)$$

for χ a general $\ell = 0$ solution to the Klein-Gordon equation, then $\hat{\lambda} := (\lambda/2\pi\epsilon) + 1$ satisfies the RG equation

$$\epsilon \frac{d}{d\epsilon} \left(\frac{\hat{\lambda}}{\zeta_s}\right) = \frac{\zeta_s}{2} \left[1 - \left(\frac{\hat{\lambda}}{\zeta_s}\right)^2\right] \quad (3.19)$$

for ϵ small enough to use the small- r asymptotic solution for $\chi(r)$. Here $\zeta_s := \sqrt{1 - 4(Z\alpha)^2}$. As $Z\alpha \rightarrow 0$ it follows λ as defined in (3.18) again satisfies the RG equation (3.15).

These considerations show that when $Z\alpha$ vanishes, if we define the quantity

$$\lambda_D^+ := (m + \omega)(c_s + c_v) = (m + \omega)4\pi\epsilon^2 \left(\frac{g_+}{f_+}\right) = 4\pi\epsilon^2 \left(\frac{\chi'}{\chi}\right), \quad (3.20)$$

for parity-even $j = \frac{1}{2}$ states, then $\hat{\lambda}_D^+ := (\lambda_D^+/2\pi\epsilon) + 1$ satisfies the same RG equation, eq. (3.15), as does $\hat{\lambda}$ in the Klein-Gordon case. Notice that in the nonrelativistic limit we have $\lambda_D^+ \rightarrow 2m(c_s + c_v)$ in agreement with the $Z\alpha \rightarrow 0$ limit of (3.14).

Parity-odd case. A similar argument goes through for the parity-odd $j = \frac{1}{2}$ states. Parity-odd states satisfy the radial equations (2.15) and so when $Z\alpha = 0$ we have

$$f_- = \frac{g'_-}{m - \omega}. \quad (3.21)$$

Repeating the arguments of the parity-odd case then shows that $g_- = \chi$ satisfies the Klein-Gordon equation and so implies that $\hat{\lambda}_D^- = (\lambda_D^-/2\pi\epsilon) + 1$ satisfies (for small ϵ) the same RG equation, (3.15) as do the parity-even and Klein-Gordon cases, provided we define

$$\lambda_D^- := (m - \omega)(c_s - c_v) = (m - \omega)4\pi\epsilon^2 \left(\frac{f_-}{g_-}\right) = 4\pi\epsilon^2 \left(\frac{\chi'}{\chi}\right). \quad (3.22)$$

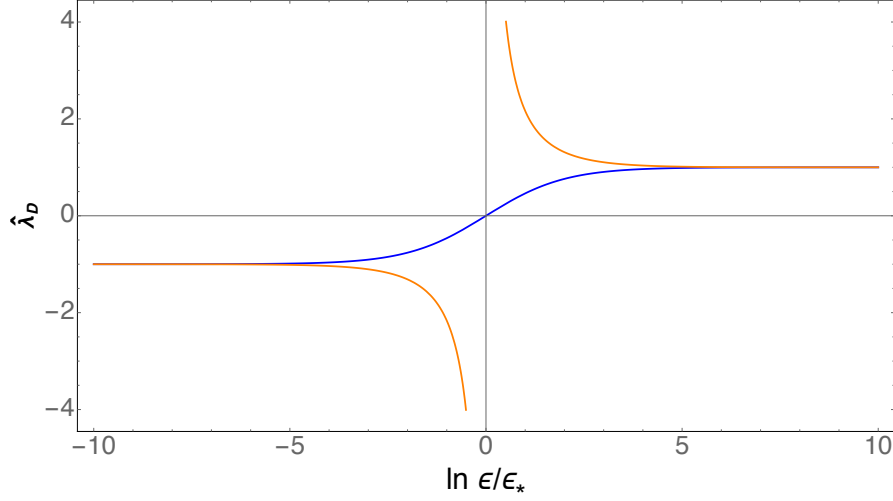


Figure 1. Plot of the RG flow of $\hat{\lambda}_D^\pm$ (as defined in the main text) vs $\ln \epsilon/\epsilon_*$ when $Z\alpha = 0$. A representative of each of the two RG-invariant classes of flows is shown, and ϵ_* is chosen as the place where $\hat{\lambda} = 0$ or $\hat{\lambda} \rightarrow \infty$, depending on which class of flows is of interest.

Flow patterns. The flow obtained by integrating (3.15) is given (for ϵ small enough that f and g are dominated by their near-source asymptotic forms) by

$$\hat{\lambda}_D^\pm(\epsilon) = \frac{\hat{\lambda}_0^\pm(\epsilon + \epsilon_{0\pm}) + (\epsilon - \epsilon_{0\pm})}{(\epsilon + \epsilon_{0\pm}) + \hat{\lambda}_0^\pm(\epsilon - \epsilon_{0\pm})} = \left(\frac{\epsilon + \epsilon_{*\pm}}{\epsilon - \epsilon_{*\pm}} \right)^{\eta_\pm}, \quad (3.23)$$

a flow that is shown in figure 1. In the first equality the integration constant is chosen using the initial condition $\lambda_D^\pm(\epsilon_{0\pm}) = \lambda_0^\pm$, while in the second equality $\eta_\pm = \text{sign}(|\hat{\lambda}_D^\pm| - 1)$ and the RG-invariant quantities $\epsilon_{*\pm}$ are defined as the scales where the $\hat{\lambda}_D^\pm$ approach zero (or diverge). Which of these one uses depends on whether the RG trajectory of interest has $|\hat{\lambda}_D^\pm|$ greater than or smaller than 1. In either case $\epsilon_{*\pm}$ is given explicitly by inverting the first equality of (3.23):

$$\frac{\epsilon_{*\pm}}{\epsilon_{0\pm}} = \lim_{\lambda_D^\pm \rightarrow 0} \frac{\hat{\lambda}_D^\pm \hat{\lambda}_0^\pm - 1 - (\hat{\lambda}_D^\pm - \hat{\lambda}_0^\pm)}{\hat{\lambda}_D^\pm \hat{\lambda}_0^\pm - 1 + (\hat{\lambda}_D^\pm - \hat{\lambda}_0^\pm)} = \eta_\pm \left(\frac{\hat{\lambda}_0^\pm - 1}{\hat{\lambda}_0^\pm + 1} \right). \quad (3.24)$$

As shown in detail in [5, 6], the ϵ -independence of physical quantities implies they depend only on $\lambda_D^\pm(\epsilon)$ and ϵ through RG-invariant quantities like $\epsilon_{*\pm}$.

For $\epsilon \gg \epsilon_{*\pm}$ (though ϵ not so large as to invalidate the small- r expansion of the mode functions at $r = \epsilon$) the flow approaches the fixed point at $\hat{\lambda}_D^\pm = +1$, with $\hat{\lambda}_D^\pm - 1 \propto \epsilon_{*\pm}/\epsilon$. Because $\hat{\lambda}_D^\pm - 1 \propto (c_s \pm c_v)/\epsilon$ this implies c_s and c_v simply become independent of ϵ in this limit.

For small ϵ the flow emerges from the repulsive fixed point at $\hat{\lambda}_D^\pm = -1$ with $\hat{\lambda}_D^\pm + 1 \simeq -2\eta_\pm(\epsilon/\epsilon_{*\pm})$ with (as before) $\eta_\pm = \text{sign}(|\hat{\lambda}_D^\pm| - 1)$. Consequently for small ϵ the couplings c_s and c_v evolve *linearly* with ϵ (as opposed to the naive quadratic behaviour expected on

dimensional grounds):

$$\begin{aligned} c_s(\epsilon) &= \frac{1}{2} \left(\frac{\lambda_D^+}{m+\omega} + \frac{\lambda_D^-}{m-\omega} \right) = -\frac{4\pi m\epsilon}{m^2 - \omega^2} + \mathcal{O}(\epsilon^2) \\ \text{and } c_v(\epsilon) &= \frac{1}{2} \left(\frac{\lambda_D^+}{m+\omega} - \frac{\lambda_D^-}{m-\omega} \right) = \frac{4\pi\omega\epsilon}{m^2 - \omega^2} + \mathcal{O}(\epsilon^2). \end{aligned} \quad (3.25)$$

The flow describes the transition between these two asymptotic states, and clearly no source coupling ($c_s = c_v = 0$) is an RG-invariant fixed point, and it is also RG-invariant to have $c_v = 0$ while c_s runs (corresponding to $\epsilon_{\star+} = \epsilon_{\star-}$).

As a concrete example, suppose matching to a UV completion were to give the predictions

$$c_v = g_v R^2 \quad \text{and} \quad c_s = g_s R^2 \quad \text{at } \epsilon = R, \quad (3.26)$$

for a microscopic scale $1/R \gg \omega \geq m$ and dimensionless constants $|g_v|, |g_s| \lesssim \mathcal{O}(1)$. Then $\lambda_D^\pm(R) = (m \pm \omega)(g_s \pm g_v)R^2$ while the signs $\eta_\pm = \text{sign}(\hat{\lambda}_D^\pm - 1)$ are $\eta_+ = \text{sign}(g_s + g_v)$ and $\eta_- = \text{sign}(g_v - g_s)$. Then the RG-invariant scales are $\epsilon_{\star\pm}/R = \eta_\pm(\hat{\lambda}_D^\pm - 1)/(\hat{\lambda}_D^\pm + 1)$ and so

$$\frac{\epsilon_{\star\pm}}{R} = \eta_\pm \left[\frac{(m \pm \omega)(g_s \pm g_v)R/4\pi}{1 + (m \pm \omega)(g_s \pm g_v)R/4\pi} \right], \quad (3.27)$$

hence $\epsilon_{\star\pm} \gg R$ requires $(g_s \pm g_v)R \simeq -4\pi/(m \pm \omega)$. Unlike for the nonrelativistic case there is always an ω for which this can be satisfied, but because $\omega R \ll 1$ this is only possible in the effective theory if $g_s \pm g_v$ is sufficiently large and has the right sign.

For general ϵ the running couplings are

$$\hat{\lambda}_D^\pm(\epsilon) = \left(\frac{\epsilon + \epsilon_{\star\pm}}{\epsilon - \epsilon_{\star\pm}} \right)^{\eta_\pm} = \frac{\epsilon + (\epsilon + R)(m \pm \omega)(g_s \pm g_v)R/4\pi}{\epsilon + (\epsilon - R)(m \pm \omega)(g_s \pm g_v)R/4\pi}, \quad (3.28)$$

which has the right limits for both large and small ϵ . Consequently

$$c_s(\epsilon) \pm c_v(\epsilon) = \frac{2\pi\epsilon}{m \pm \omega} \left(\hat{\lambda}_D^\pm - 1 \right) = \frac{(g_s \pm g_v)R^2}{1 + (1 - R/\epsilon)(m \pm \omega)(g_s \pm g_v)R/4\pi}, \quad (3.29)$$

which shows how the flow for $\epsilon \gg \epsilon_{\star\pm}$ is towards constant c_s and c_v , asymptoting to limits renormalized relative to their values at $\epsilon = R$.

3.2.3 Relativistic running when $Z\alpha \neq 0$

We repeat the analysis of section 3.2.2 this time for the case $Z\alpha \neq 0$ as is relevant to the Coulomb problem.

Parity even. The running in the parity even case is determined by equation (3.8). The small radius expansion of the mode functions f (2.16) and g (2.17) yields to leading order

$$\begin{aligned} \hat{c}_s + \hat{c}_v &= \left(\frac{g_+}{f_+} \right)_{r=\epsilon} \\ &\simeq -\sqrt{\frac{m-\omega}{m+\omega}} \frac{[(1-\zeta)\kappa + (m+\omega)Z\alpha] (2\kappa\epsilon)^{2\zeta} + [(1+\zeta)\kappa + (m+\omega)Z\alpha] \frac{C_+}{A_+}}{[(1+\zeta)\kappa + (m-\omega)Z\alpha] (2\kappa\epsilon)^{2\zeta} + [(1-\zeta)\kappa + (m-\omega)Z\alpha] \frac{C_+}{A_+}}. \end{aligned} \quad (3.30)$$

The RG running can be found by calculating the derivative $d(\hat{c}_s + \hat{c}_v)/d\epsilon$ and after inverting (3.30) inserting $\epsilon^{2\zeta}$ as a function of $\hat{c}_s + \hat{c}_v$:

$$\epsilon \frac{d(\hat{c}_s + \hat{c}_v)}{d\epsilon} = -Z\alpha \left[\left(\hat{c}_s + \hat{c}_v + \frac{1}{Z\alpha} \right)^2 - \left(\frac{\zeta}{Z\alpha} \right)^2 \right]. \quad (3.31)$$

Defining the quantity

$$\hat{\lambda}_D^+ := Z\alpha(\hat{c}_s + \hat{c}_v) + 1, \quad (3.32)$$

the RG equation (3.31) takes the form

$$\epsilon \frac{d}{d\epsilon} \left(\frac{\hat{\lambda}_D^+}{\zeta} \right) = \zeta \left[1 - \left(\frac{\hat{\lambda}_D^+}{\zeta} \right)^2 \right], \quad (3.33)$$

which has the solution

$$\frac{\hat{\lambda}_D^+}{\zeta} = \frac{\hat{\lambda}_{D0}^+/\zeta + \tanh[\zeta \ln(\epsilon/\epsilon_0)]}{1 + (\hat{\lambda}_{D0}^+/\zeta) \tanh[\zeta \ln(\epsilon/\epsilon_0)]} = \frac{(\lambda_{D0}^+ + \zeta)(\epsilon/\epsilon_0)^{2\zeta} + (\lambda_{D0}^+ - \zeta)}{(\lambda_{D0}^+ + \zeta)(\epsilon/\epsilon_0)^{2\zeta} - (\lambda_{D0}^+ - \zeta)}. \quad (3.34)$$

Parity odd. Similarly to the parity even case we can write (3.8) as

$$\begin{aligned} \hat{c}_s - \hat{c}_v &= \left(\frac{f_-}{g_-} \right)_{r=\epsilon} \quad (3.35) \\ &\simeq -\sqrt{\frac{m+\omega}{m-\omega}} \frac{[(1-\zeta)\kappa - (m-\omega)Z\alpha](2\kappa\epsilon)^{2\zeta} + [(1+\zeta)\kappa - (m-\omega)Z\alpha] \frac{C_-}{A_-}}{[(1+\zeta)\kappa - (m+\omega)Z\alpha](2\kappa\epsilon)^{2\zeta} + [(1-\zeta)\kappa - (m+\omega)Z\alpha] \frac{C_-}{A_-}}. \end{aligned}$$

Repeating the procedure of the previous subsection we then find the running to be

$$\epsilon \frac{d(\hat{c}_s - \hat{c}_v)}{d\epsilon} = Z\alpha \left[\left(\hat{c}_s - \hat{c}_v - \frac{1}{Z\alpha} \right)^2 - \left(\frac{\zeta}{Z\alpha} \right)^2 \right]. \quad (3.36)$$

Again, one can define the quantity

$$\hat{\lambda}_D^- := Z\alpha(\hat{c}_s - \hat{c}_v) - 1, \quad (3.37)$$

in terms of which the RG equation (3.36) takes the form

$$\epsilon \frac{d}{d\epsilon} \left(\frac{\hat{\lambda}_D^-}{\zeta} \right) = -\zeta \left[1 - \left(\frac{\hat{\lambda}_D^-}{\zeta} \right)^2 \right], \quad (3.38)$$

which has the solution

$$\frac{\hat{\lambda}_D^-}{\zeta} = \frac{\hat{\lambda}_{D0}^-/\zeta - \tanh(\zeta \ln(\epsilon/\epsilon_0))}{1 - (\hat{\lambda}_{D0}^-/\zeta) \tanh(\zeta \ln(\epsilon/\epsilon_0))} = \frac{(\lambda_{D0}^- + \zeta) + (\lambda_{D0}^- - \zeta)(\epsilon/\epsilon_0)^{2\zeta}}{(\lambda_{D0}^- + \zeta) - (\lambda_{D0}^- - \zeta)(\epsilon/\epsilon_0)^{2\zeta}}. \quad (3.39)$$

Fixed points. From the running equations (3.33) and (3.38), it is clear that there are fixed points when $\hat{\lambda}_D^+ = \pm\zeta$, and when $\hat{\lambda}_D^- = \pm\zeta$. However, from the solutions (3.34) and (3.39), we see that the fixed points of λ_D^\pm are coupled. The fixed point obtained in the limit $\epsilon \rightarrow \infty$ (which we call the IR fixed point) corresponds to $\lambda_D^+ = +\zeta$ and $\lambda_D^- = -\zeta$, so that

$$\hat{c}_s = 0 \quad \text{and} \quad \hat{c}_v = \frac{\zeta - 1}{Z\alpha} \quad (\text{IR}). \quad (3.40)$$

The UV fixed point is similarly defined as the limit $\epsilon \rightarrow 0$ and is given by $\lambda_D^+ = -\zeta$ and $\lambda_D^- = +\zeta$, so that

$$\hat{c}_s = 0 \quad \text{and} \quad \hat{c}_v = -\left(\frac{\zeta + 1}{Z\alpha}\right) \quad (\text{UV}). \quad (3.41)$$

For later purposes (when comparing to results for specific nuclear charge distributions) we remark that the IR fixed point implies the following linear combination of the couplings c_s and c_v evaluates at $\epsilon = R$ to

$$(c_s + c_v)_{IR} \simeq -2\pi Z\alpha R^2, \quad (3.42)$$

which uses $\zeta \simeq 1 - \frac{1}{2}(Z\alpha)^2$.

The attentive reader may also be puzzled as to why the running for $Z\alpha \rightarrow 0$ does not coincide with the $Z\alpha = 0$ running found earlier. The reason for this is the observation that the limits $\epsilon \rightarrow 0$ and $Z\alpha \rightarrow 0$ do not commute, due to the appearance of factors of $1/(1 - \zeta) \simeq 1/(Z\alpha)^2$ within the hypergeometric functions that furnish the Dirac-Coulomb solutions. (Related to this, mode functions can asymptote to r^p at small r where $p \propto (Z\alpha)^2$, again displaying non-commuting small- r and $Z\alpha \rightarrow 0$ limits.) As discussed in later sections, this makes the evaluation of energy shifts for bound states for specific values for $Z\alpha$ and nuclear size R somewhat subtle, since care must be taken to work to a consistent order in small quantities.

3.3 Higher-order interactions

For some applications it is insufficient to work only to lowest order in the nuclear size, and so we pause here to classify some of the next-to-leading interactions according to their dimension:

$$S_p = \int d^4x \left[\mathcal{L}_0 + \mathcal{L}_1 + \mathcal{L}_3 + \mathcal{L}_4 + \mathcal{L}_5 + \dots \right], \quad (3.43)$$

where the operators appearing in \mathcal{L}_n have engineering dimension (mass) ^{n} . In this notation $\mathcal{L}_0 + \mathcal{L}_1 + \mathcal{L}_3$ represent the terms already written in (2.3), so we now enumerate the dimension-4 interactions. At this order the operators consistent with invariance under rotations, gauge transformations and C, P and T are \mathbf{E}^2 , \mathbf{B}^2 and ${}^4\bar{\psi}\gamma^0 D_0\psi$. We therefore take

$$\mathcal{L}_4 = -\left[\frac{1}{2}(\tilde{h}_E \mathbf{E}^2 + \tilde{h}_B \mathbf{B}^2) + c_h \bar{\psi} D_0 \psi + i c_t \bar{\psi} \gamma^0 D_0 \psi \right] \delta^3(x), \quad (3.44)$$

⁴A spatial derivative, $\bar{\psi} \vec{\gamma} \cdot \nabla \psi$, need not be included separately since it is redundant — i.e. it can be recast in terms of one of those already written by a field redefinition and/or an integration by parts.

where c_t , c_h and the ‘polarizabilities’ \tilde{h}_E and \tilde{h}_B are new effective couplings having dimension (length)³. For instance the time derivative appearing in the last of these terms contains contributions to the Dirac equation that resemble a correction to c_v by an amount $\delta c_v \propto c_t \omega$. For nonrelativistic bound states and for $c_v \propto R^2$ and $c_t \propto R^3$ such corrections look like $mR^3 |\phi(0)|^2$ contributions to the energy shift, and so contribute to some of the subleading corrections discussed below.

One can continue in this way to as high a dimension as one wishes. Notice that the first interaction to involve more than two Dirac fields — such as ‘three-body’ interactions, like $c_{3b} (\bar{\psi} \psi) (\bar{\psi} \psi) \delta^3(x)$ — arises once we consider effective couplings with dimension (length)⁵.

Effectively, we can parametrize the boundary condition as

$$\left(\frac{g_+}{f_+} \right)_{r=R} = \xi_g Z\alpha \quad \text{with} \quad \xi_g = \hat{g}_1 + \hat{g}_2(mRZ\alpha) + \hat{g}_3(Z\alpha)^2 + \dots \quad (3.45)$$

Any microscopic source physics can only influence parity-even physical observables through their contributions to the constants \hat{g}_i , only a few of which are relevant to any given order in the small expansion parameters. This makes these parameters useful proxies for specific models of source physics, and their values are computed in appendix B for several simple examples. Although quantities like \hat{g}_2 can be traded for parameters like c_t and/or h_E we do not pursue this connection explicitly here.

4 Bound-state energy shifts

With a view to computing nuclear-size effects on atomic energy levels we next turn to the implications source contact interactions have for the energy of states bound to the source. Our assumptions of rotation invariance in S_p restricts us for simplicity to atoms with spherically symmetric nuclei. What we find also applies to nuclei with spin but must be supplemented by spin-dependent nuclear-size effects (such as nuclear-size effects for hyperfine splitting [23]).

4.1 Energy-shift calculations

Bound-state energies are computed by reconciling the implications for the integration constants, C_{\pm}/A_{\pm} , appearing in (3.9) (or in more detail (2.16) and (2.17)) as imposed by the small- r and large- r boundary conditions. At small r the relevant boundary conditions are (3.8), which we repeat here for convenience

$$\hat{c}_s + \hat{c}_v = \frac{c_s + c_{v \text{ tot}}}{4\pi\epsilon^2} = \left(\frac{g_+}{f_+} \right)_{r=\epsilon} \quad \text{and} \quad \hat{c}_s - \hat{c}_v = \frac{c_s - c_{v \text{ tot}}}{4\pi\epsilon^2} = \left(\frac{f_-}{g_-} \right)_{r=\epsilon}, \quad (4.1)$$

and the implications of these for C_{\pm}/A_{\pm} — as found using (2.16) and (2.17) — must be consistent with normalizability at large r , which implies

$$- \frac{C_{\pm}}{A_{\pm}} = \frac{\Gamma(1 + 2\zeta)}{\Gamma(1 - 2\zeta)} \frac{\Gamma(-\zeta - Z\alpha\omega/\kappa)}{\Gamma(\zeta - Z\alpha\omega/\kappa)}. \quad (4.2)$$

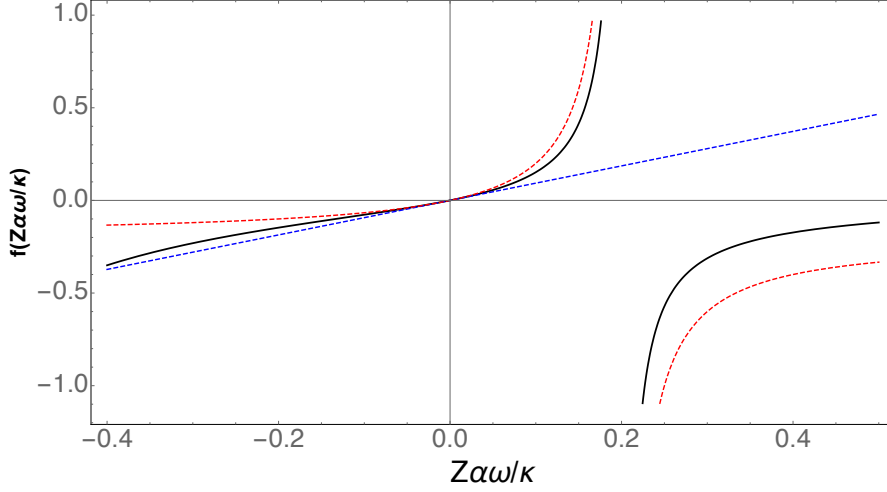


Figure 2. The black curve plots the right-hand side of eq. (4.2) $f(Z\alpha\omega/\kappa) = \Gamma(1 + 2\zeta)\Gamma(-\zeta - Z\alpha\omega/\kappa)/(\Gamma(1 - 2\zeta)\Gamma(\zeta - Z\alpha\omega/\kappa))$ vs $Z\alpha\omega/\kappa$, with the zero of energy chosen to be the eigenvalue of the $n = 2$ and $j = \frac{1}{2}$ states. Standard Dirac energy levels correspond to places where the plotted quantity vanishes, while finite-size effects of the source correspond to those energies for which (4.2) instead equals a specified nonzero (positive) value. The dashed curves show two approximations to (4.2) that provide useful analytic expressions for energy shifts. The blue (red) curve shows the single-pole (double-pole) approximation to (4.2), described in the main text. In order to better display the shape of these curves, for plotting purposes we use $\zeta = 0.9$ (and so $Z\alpha \sim 0.45$) and for concreteness expand about the pole at $n = 2$.

In the absence of a source the Dirac energy eigenvalues are given by solutions to $C_{\pm}/A_{\pm} = 0$, which (4.2) shows is satisfied when $\zeta - Z\alpha\omega/\kappa = -N$ with $N = 0, 1, 2, \dots$. This returns the standard Dirac energy eigenvalues

$$\begin{aligned} \omega_N &= m \left[1 + \frac{(Z\alpha)^2}{(n + \zeta - j - \frac{1}{2})^2} \right]^{-1/2} \\ &\simeq m \left[1 - \frac{(Z\alpha)^2}{2n^2} - \frac{[4n - 3(j + 1/2)]}{8n^4(j + 1/2)} (Z\alpha)^4 + \mathcal{O}[(Z\alpha)^6] \right], \end{aligned} \quad (4.3)$$

where $n = N + (j + \frac{1}{2}) = 1, 2, 3, \dots$ is the usual principal quantum number.

In the presence of a finite-sized source we instead solve for ω by equating the right-hand side of (4.2) to the nonzero value of C/A obtained by fixing f/g using the boundary condition (3.8) at nonzero $r = \epsilon$. In practice this is done in two steps: (i) computing the value of C/A implied from the microscopic physics of the source (as parametrized by S_p , say); and (ii) solving (4.2) for ω as a function of nonzero C/A , given a known form for C/A . We next consider each of these steps in turn.

Solving for $\delta\omega$. Solving for $\delta\omega = \omega - \omega_N$ with given C/A requires no knowledge of source structure since the right-hand side of (4.2) is dictated purely by the known solutions to the Coulomb-Dirac equation. Although this is easily done numerically, there are also accurate analytic approximations that are very useful (particularly when tracking the dependence of the result on external parameters), which are summarized briefly here.

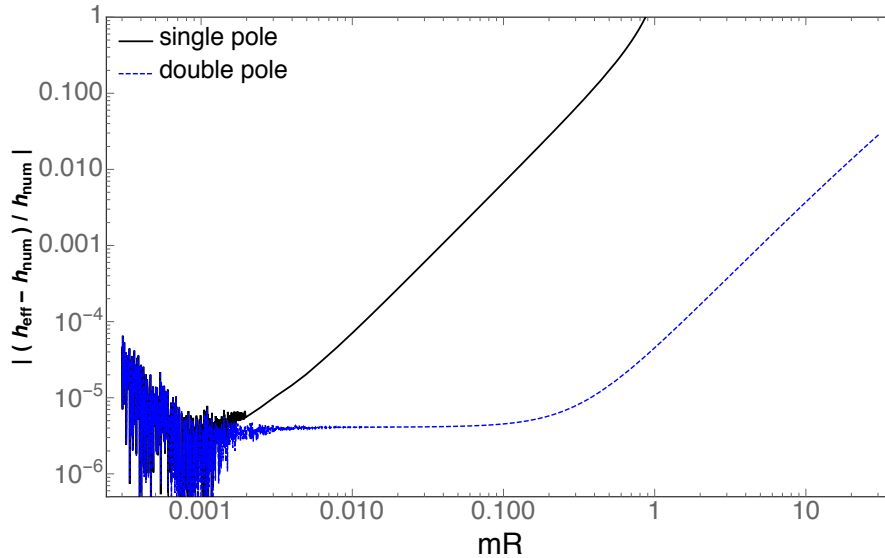


Figure 3. A plot of the relative error made when computing $\delta\omega/|\psi(0)|^2$ for nonzero C/A using two analytic approximations single pole (black solid) and double-pole (blue dashed) to the right-hand side of eq. (4.2) as described in the main text. The plot’s horizontal axis is mR , where m is the mass of the orbiting fermion and R is the size of the source. For plotting purposes we use $Z\alpha = 1/137$ and compute the shifts to the parity-even $j = \frac{1}{2}$ state with $n = 2$ assuming the source to be a shell of positive charge with radius R .

Figure 2 plots the right-hand side of (4.2) against energy with the zero of energy chosen to be the Dirac energy eigenvalue for a point-like source corresponding to a particular whole number N . Also plotted are two approximate forms, corresponding to approximating $\Gamma(-N + \delta z) \simeq (-)^N/[N! \delta z]$ in just the denominator (*single-pole approximation*) or in both the denominator and numerator (*double-pole approximation*). As the figure shows, because of the presence of a nearby pole in the numerator the first of these approximations turns out only to have a radius of convergence of order $(1 - \zeta) \sim (Z\alpha)^2$ and so is only of use for extremely small δz .

The double-pole approximation turns out to be much better than the single-pole one (particularly given that the left-hand side, $\mathcal{Q} := -(C/A)$, of (4.2) turns out to be positive for small δz), and suffices for identifying the leading energy shift and its first subleading correction. This can be seen in figure 3, which compares the solution obtained for $\delta\omega$ using these approximate formulae to numerical results. For the purposes of these comparisons the source is assumed to be a fixed charged shell of radius R , whose energy eigenvalues can be computed exactly, and the state whose energy is perturbed is taken to be a parity-even S state (similar results obtain for parity-odd states). The plots show that the error obtained when using the double-pole approximation is order $(Z\alpha)^2$ out to $mR \lesssim \mathcal{O}(1)$, for reasons identified below when we seek to compute $\mathcal{O}(Z\alpha)^2$ terms.

Concretely, the double-pole approximates the right-hand side of (4.2) using the leading Laurent expansion near the poles of the Gamma functions,

$$G(x_N + \delta x) := \frac{\Gamma(1 + 2\zeta)}{\Gamma(1 - 2\zeta)} \frac{\Gamma[y(x) - 2\zeta]}{\Gamma[y(x)]} \simeq \frac{4(1 - \zeta) \delta x}{(N + 2)(N + 1)(2 - 2\zeta - \delta x)}, \quad (4.4)$$

which uses $y(x) = \zeta - x$ and $x = Z\alpha\omega/\kappa$ and so $y(x_N + \delta x) = -N + \delta y = -N - \delta x$ where $x_N = N + \zeta$ corresponds to the Dirac-Coulomb energy eigenvalue (4.3) for a point source. To proceed we regard $\mathcal{Q} := -(C/A)$ as a function of $f(\epsilon)/g(\epsilon)$ and ω and evaluate it at $\omega = \omega_N$, equating the result to (4.4). This allows δx (and hence also $\delta\omega$) to be solved for explicitly as

$$\delta x = \frac{Z\alpha m^2 \delta\omega}{(m^2 - \omega_N^2)^{3/2}} \simeq \frac{n(n+1)\mathcal{Q}/2}{1 + n(n+1)\mathcal{Q}/[2(Z\alpha)^2]}, \quad (4.5)$$

where (because our later focus is on $j = \frac{1}{2}$) we trade N for the principal quantum number, $n = N + 1$, and write $1 - \zeta \simeq \frac{1}{2}(Z\alpha)^2$. (The single-pole approximation differs from the above by taking the denominator to be unity, and only gives the leading contribution reliably in the limit $mR \ll 1$, if R is the typical size of the source.)

It is useful to extract the naive Coulomb wave-function at the origin from $\delta\omega$ by writing

$$\delta\omega = \frac{h_{\text{eff}}}{\pi} \left(\frac{mZ\alpha}{n} \right)^3, \quad (4.6)$$

where tracking through the definitions gives

$$h_{\text{eff}} = \frac{\pi c_n^{3/2} \delta x}{Z\alpha m^2} \simeq \frac{\pi c_n^{3/2}}{Z\alpha m^2} \left[\frac{\frac{1}{2} n(n+1)\mathcal{Q}}{1 + \frac{1}{2} n(n+1)\mathcal{Q}/(Z\alpha)^2} \right], \quad (4.7)$$

where we write $m^2 - \omega_N^2 = c_n(Z\alpha m/n)^2$ and so

$$c_n^{3/2} = 1 + \frac{3(n-1)(Z\alpha)^2}{2n^2} + \mathcal{O}(Z\alpha)^4, \quad (4.8)$$

which can be taken as unity for the leading and $\mathcal{O}(Z\alpha)$ correction but not once order $(Z\alpha)^2$ contributions are required. As we shall see, for $\mathcal{O}(Z\alpha)^2$ corrections (4.4) must also be revisited to include also subleading terms in δx .

Determining $\mathcal{Q} = -C/A$. To use the above formulae in practice we require an expression for how $\mathcal{Q} = -C/A$ depends on the properties of the source. If the UV completion were a specific classical distribution, $\rho(r)$, of radius R then C/A would be fixed by demanding continuity of f/g between the exterior and interior solutions at $r = R$ (examples of this are discussed in more detail below). In general, knowledge of C/A is equivalent to knowledge of f/g at some radius, since this is ultimately the only way the physics of the source influences exterior phenomena.

What is required then is an explicit expression for C_{\pm}/A_{\pm} as a function of $f_{\pm}(\epsilon)/g_{\pm}(\epsilon)$. In principle this is obtained by taking the ratio of expression (2.16) and (2.17) for the exterior solution (for each parity) and solving the resulting equations for C_+/A_+ and C_-/A_- . This is efficient and easy to implement numerically and once this is done f_{\pm}/g_{\pm} at $r = \epsilon$ can be traded for constants in the source action through boundary conditions like (3.8).

Analytic expressions⁵ for the required relation for C_{\pm}/A_{\pm} can also be found when ϵ is small enough to justify keeping only the leading small- r asymptotic form for the confluent

⁵Such analytic expressions are useful (even when numerical results are easy) for tracking the leading parametric dependence of energy shifts on external variables.

hypergeometric functions in (2.16) and (2.17). Specializing to states with $j = \frac{1}{2}$ — i.e. parity-even (S) states f_+ and g_+ and parity-odd (P) states f_- and g_- — since these are the states most sensitive to finite-size effects of the source, we find the leading small- ϵ form

$$\frac{C_{\pm}}{A_{\pm}} = \frac{[\zeta \pm 1 + Z\alpha X] - [(\zeta \mp 1)X - Z\alpha](f_{\pm}/g_{\pm})}{[\zeta \mp 1 - Z\alpha X] - [(\zeta \pm 1)X + Z\alpha](f_{\pm}/g_{\pm})} (2\kappa\epsilon)^{2\zeta}, \quad (4.9)$$

where f_{\pm}/g_{\pm} is evaluated at $r = \epsilon$ and X is defined by $X := \sqrt{(m - \omega)/(m + \omega)}$. As we shall see, it is the factor of 2 in the exponent of $(2\kappa\epsilon)^{2\zeta}$ that is responsible for the main differences between the Dirac case and the Klein-Gordon problem studied in [6] (for which instead $(2\kappa\epsilon)^{\zeta_s}$ appeared). This factor has its origins in the spin-orbit coupling that mixes two different orbital angular momenta into each state having fixed j .

4.2 Leading and first-subleading energy shifts

For detailed studies of the influence of nuclei on atomic energy levels one expands all contributions to bound state energies as a dual series in the small parameters $(Z\alpha)^2$ and $m\epsilon Z\alpha \sim \epsilon/a_B$, where $a_B = 1/(mZ\alpha)$ is the Bohr radius and $\epsilon \simeq R$ where $R \simeq 1$ fm is a typical nuclear size. In practice, comparison with experiments on atomic energy levels requires both the leading contribution and its subleading $\mathcal{O}(mRZ\alpha)$ correction, and for electronic atoms $(Z\alpha)^2$ corrections are also required since for R of order a Fermi these are comparable in size to $(mRZ\alpha)$ corrections. Our purpose in this section is to identify as generally as possible how these terms depend parametrically on the properties of the source.

Although (4.9) is sufficient for some applications, a more accurate approximation turns out to be required in order to track the leading subdominant coefficients in this kind of expansion. Increased accuracy is required for bound-state calculations because nominally independent variables like κ and X become specific powers of $Z\alpha$ once evaluated at the lowest-order bound-state energies $\omega = \omega_N$. For instance, using (4.3) in the definitions implies

$$\rho_{nj} = 2\kappa_N\epsilon = \frac{2m\epsilon Z\alpha}{n} \left[1 + \mathcal{O}(Z\alpha)^2\right] \quad \text{and} \quad X_{nj} = \frac{Z\alpha}{2n} \left[1 + \mathcal{O}(Z\alpha)^2\right], \quad (4.10)$$

and so higher powers of these compete with powers of $Z\alpha$ arising elsewhere (such as from the expansion of ζ). Extracting a particular order in $Z\alpha$ is further complicated by the appearance of factors of $(1 - \zeta)^{-1} \propto (Z\alpha)^{-2}$ in the expansion of the confluent hypergeometric functions $\mathcal{M}[a, 1 - 2\zeta; \rho]$, due to the singularity of $\mathcal{M}[a, b; z]$ as b approaches a nonpositive integer.

We next identify the leading and subleading $\mathcal{O}(mRZ\alpha)$ and $\mathcal{O}(Z\alpha)^2$ contributions to the energy shift. To do so we use the exact expressions, (2.16) and (2.17), for the general Dirac-Coulomb solution and solve for the integration constants $\mathcal{Q} = -(C/A)$ in terms of f/g evaluated at $r = \epsilon = R$, finding

$$\mathcal{Q} = -\frac{C}{A} = \left\{ \left[\frac{(Q_{20} + Q_{10})g + X(-Q_{20} + Q_{10})f}{(Q_{21} + Q_{11})g + X(-Q_{21} + Q_{11})f} \right] \rho^{2\zeta} \right\}_{r=R} \quad (4.11)$$

where (as before) $X := \sqrt{(m - \omega)/(m + \omega)}$ and

$$\begin{aligned} Q_{10} &:= \mathcal{M}(\zeta - x, 1 + 2\zeta; \rho), & Q_{11} &:= \mathcal{M}(-\zeta - x, 1 - 2\zeta; \rho), \\ Q_{20} &:= -\left(\frac{\zeta - x}{K - \hat{x}}\right) \mathcal{M}(\zeta - x + 1, 1 + 2\zeta; \rho) \\ \text{and } Q_{21} &:= \left(\frac{\zeta + x}{K - \hat{x}}\right) \mathcal{M}(-\zeta - x + 1, 1 - 2\zeta; \rho), \end{aligned} \quad (4.12)$$

with $x = Z\alpha\omega/\kappa$ while $\hat{x} = Z\alpha m/\kappa$. These are to be evaluated at the lowest-order solution, $x = x_N = N + \zeta$, where $N = n - 1$ and $\zeta \simeq 1 + \frac{1}{2}(Z\alpha)^2$ for $j = \frac{1}{2}$ states, and we work only to subdominant order in $mRZ\alpha$ and $(Z\alpha)^2$. Eq. (4.11) agrees with (4.9) at lowest order in ρ , for which $\mathcal{M}[a, b; \rho] = 1$.

Since $\rho = 2\kappa_N R \propto mRZ\alpha$ working to fixed order in $Z\alpha$ allows us to expand \mathcal{M} in powers of ρ , but when doing so must be careful about factors of $1/(1 - \zeta) \propto (Z\alpha)^{-2}$ appearing in the coefficients of the hypergeometric series. Such terms only arise when b of $\mathcal{M}[a, b; \rho]$ is a negative integer and so only are a factor in Q_{11} and Q_{21} . Since all powers of ρ involve the factor mR our guiding principle when expanding in ρ is to keep terms involving only a single subdominant power of $Z\alpha$. This also allows us to neglect all subdominant powers of $1 - \zeta \propto (Z\alpha)^2$ in any ρ -dependent terms. Using $\zeta \simeq 1 - \frac{1}{2}(Z\alpha)^2$ and $x \simeq x_N = N + \zeta \simeq N + 1$ one finds

$$Q_{10} := \mathcal{M}(\zeta - x, 1 + 2\zeta; \rho) \simeq 1 - \left(\frac{N}{3}\right) \rho + \frac{N(N-1)}{24} \rho^2 + \dots, \quad (4.13)$$

and

$$\begin{aligned} Q_{20} &:= -\left(\frac{\zeta - x}{K - x}\right) \mathcal{M}(\zeta - x + 1, 1 + 2\zeta; \rho) \\ &\simeq -\left(\frac{N}{N+1-K}\right) \left[1 - \left(\frac{N-1}{3}\right) \rho + \frac{(N-1)(N-2)}{24} \rho^2 + \dots\right], \end{aligned} \quad (4.14)$$

while

$$\begin{aligned} Q_{11} &:= \mathcal{M}(-\zeta - x, 1 - 2\zeta; \rho) \\ &\simeq 1 + (N+2) \rho - \left[\frac{(N+2)(N+1)}{2(1-\zeta)}\right] \frac{\rho^2}{2} + \left[\frac{N(N+2)(N+1)}{2(1-\zeta)}\right] \frac{\rho^3}{3!} + \dots, \end{aligned} \quad (4.15)$$

and

$$\begin{aligned} Q_{21} &:= \left(\frac{\zeta + x}{K - x}\right) \mathcal{M}(-\zeta - x + 1, 1 - 2\zeta; \rho) \\ &\simeq -\left(\frac{N+2}{N+1-K}\right) \left\{1 + (N+1) \rho - \left[\frac{(N+1)N}{2(1-\zeta)}\right] \frac{\rho^2}{2} \left[\frac{N(N+1)(N-1)}{2(1-\zeta)}\right] \frac{\rho^3}{3!} + \dots\right\}. \end{aligned} \quad (4.16)$$

Parity-even leading energy shifts. Collecting results and specializing to the parity-even $j = \frac{1}{2}$ S states (i.e. those with $K = -1$) gives the leading contribution (unsuppressed by any additional powers of $Z\alpha$)

$$\frac{1}{2} n(n+1) \mathcal{Q}_+ \simeq \left[\frac{2(1+2\xi_g)}{1-2(1+2\xi_g)(mR)^2}\right] (mRZ\alpha)^2 \quad (\text{leading order}) \quad (4.17)$$

where ξ_g contains the entire contribution of the physics of the source, through (3.45).

Using (4.17) in the double-pole approximation (4.7) then gives

$$\begin{aligned} h_{\text{eff}}^+ &\simeq \frac{\pi}{Z\alpha m^2} \left[\frac{\frac{1}{2}n(n+1)\mathcal{Q}_+}{1 + \frac{1}{2}n(n+1)\mathcal{Q}_+/(Z\alpha)^2} \right] \\ &= 2\pi Z\alpha R^2(1 + 2\hat{g}_1) \quad (\text{leading order}), \end{aligned} \quad (4.18)$$

where we use $\xi_g \simeq \hat{g}_1$ because at leading order consistency requires also dropping subleading terms in ξ_g . Notice the cancellation here of the spurious $(mR)^2$ terms in the denominator of (4.17); a cancellation that is missed if only the single-pole approximation is used (thereby showing that physical energy shifts lie beyond its domain of validity).

Parity-even subleading $\mathcal{O}(mRZ\alpha)$ energy shifts. Including also subdominant terms linear in $Z\alpha$ requires keeping corrections coming from the expansion of the higher orders in ρ , leading to

$$\frac{1}{2}n(n+1)\mathcal{Q}_+ \simeq \left[\frac{1 + 2\xi_g - \Delta_1^+}{1 - 2(1 + 2\xi_g - \Delta_1^+)(mR)^2 + \Delta_2^+} \right] 2(mRZ\alpha)^2 \quad (\text{subleading order}) \quad (4.19)$$

where we use $\xi_g = \hat{g}_1 + \hat{g}_2(mRZ\alpha)$ in the explicitly written terms, but it suffices to use only $\xi_g = \hat{g}_1$ in the quantities

$$\begin{aligned} \Delta_1^+ &:= 2(n-1) \left(\hat{g}_1 + \frac{2n-1}{6n} \right) \frac{mRZ\alpha}{n} \\ \text{and } \Delta_2^+ &:= \left[1 + 2n(1 + \hat{g}_1) \right] \frac{mRZ\alpha}{n}. \end{aligned} \quad (4.20)$$

Consequently the double-pole approximation gives

$$\begin{aligned} h_{\text{eff}}^+ &\simeq \frac{\pi}{Z\alpha m^2} \left[\frac{\frac{1}{2}n(n+1)\mathcal{Q}_+}{1 + \frac{1}{2}n(n+1)\mathcal{Q}_+/(Z\alpha)^2} \right] \\ &\simeq 2\pi Z\alpha R^2 \left[(1 + 2\hat{g}_1)(1 - \Delta_2^+) + 2\hat{g}_2(mRZ\alpha) - \Delta_1^+ \right] \\ &= 2\pi Z\alpha R^2 \left\{ 1 + 2\hat{g}_1 + 2\hat{g}_2(mRZ\alpha) - \left[1 + 8n^2 \left(1 + \frac{3}{2}\hat{g}_1(\hat{g}_1 + 2) \right) \right] \frac{mRZ\alpha}{3n^2} \right\}, \end{aligned} \quad (4.21)$$

which includes all corrections that are down only by a single power of $Z\alpha$ (but drops $(Z\alpha)^2$ everywhere). Later sections verify that this expression captures specific special cases in the literature.

Parity-odd leading energy shift. We next turn to parity-odd $j = \frac{1}{2}P$ states (for which $K = +1$). In this case following the same steps reveals the leading contribution to be

$$\mathcal{Q}_- \simeq - \left(\frac{n-1}{2n} \right) \left[\xi_f - \frac{2}{3}(mRZ\alpha) \right] \left(\frac{2mRZ\alpha}{n} \right)^2 \quad (\text{leading order}) \quad (4.22)$$

where the entire contribution of source physics is through

$$X \left(\frac{f_-}{g_-} \right)_{r=R} = \frac{\xi_f}{2n} \quad \text{with} \quad \xi_f = \hat{f}_1(mRZ\alpha) + \hat{f}_2(mRZ\alpha)^2 + \hat{f}_3(Z\alpha)^2 + \dots \quad (4.23)$$

with (as before) $X = \sqrt{(m-\omega)/(m+\omega)}$.

Dropping all subdominant powers of $Z\alpha$ (and for consistency restricting the source contribution to $\xi_f \simeq \hat{f}_1(mRZ\alpha)$) gives the leading parity-odd energy shift

$$h_{\text{eff}}^- \simeq -\frac{\pi(n^2-1)}{n^2} \left(\hat{f}_1 - \frac{2}{3} \right) (Z\alpha)^2 mR^3 \quad (\text{leading order}). \quad (4.24)$$

As usual, this is smaller than the parity-even result because it is suppressed by the spin-orbit coupling required to link the P states to $\ell = 0$ orbital angular momentum.

Parity-odd subleading $\mathcal{O}(mRZ\alpha)$ energy shift. Even though small, for some special cases (such as the charged shell described below) it happens that $\hat{f}_1 = \frac{2}{3}$ and so the leading contribution to parity-odd states vanishes. Such cases are dominated by the subleading contribution, for which

$$\frac{1}{2} n(n+1) \mathcal{Q}_- \simeq -\frac{n^2-1}{n^2} \left[\frac{\xi_f - \frac{2}{3}(mRZ\alpha) + \Delta_1^-}{1 + (n^2-1)(mR/n)^2[\xi_f - \frac{2}{3}(mRZ\alpha)] - \Delta_2^-} \right] (mRZ\alpha)^2 \quad (4.25)$$

where we can use $\xi_f = \hat{f}_1(mRZ\alpha) + \hat{f}_2(mRZ\alpha)^2$ in the explicitly written factors, but stop at $\xi_f \simeq \hat{f}_1(mRZ\alpha)$ in

$$\begin{aligned} \Delta_1^- &\simeq \left[(n-2) - (2n-3)\hat{f}_1 \right] \frac{(mRZ\alpha)^2}{3n} \\ \text{and} \quad \Delta_2^- &= \frac{1}{2} \left[\hat{f}_1 - \frac{2(n+1)}{n} \right] (mRZ\alpha), \end{aligned} \quad (4.26)$$

leading to

$$\begin{aligned} h_{\text{eff}}^- &\simeq \frac{\pi}{Z\alpha m^2} \left[\frac{\frac{1}{2}n(n+1)\mathcal{Q}_-}{1 + \frac{1}{2}n(n+1)\mathcal{Q}_-/(Z\alpha)^2} \right] \\ &\simeq -\frac{\pi(n^2-1)}{n^2} Z\alpha R^2 \left[\frac{\xi_f - \frac{2}{3}(mRZ\alpha) + \Delta_1^-}{1 - \Delta_2^-} \right] \quad (\text{subleading order}) \quad (4.27) \\ &\simeq -\frac{\pi(n^2-1)}{n^2} (Z\alpha)^2 mR^3 \left\{ \left(\hat{f}_1 - \frac{2}{3} \right) \left[1 + \left(\frac{\hat{f}_1}{2} - \frac{5}{3} \right) (mRZ\alpha) \right] \right. \\ &\quad \left. + \left(\hat{f}_2 - \frac{1}{9} \right) (mRZ\alpha) \right\}. \end{aligned}$$

4.3 Subleading $(Z\alpha)^2$ energy shifts

This section computes the subdominant $\mathcal{O}(Z\alpha)^2$ energy shifts for parity even and parity odd cases. Because factors of mR do not accompany the subleading powers of $Z\alpha$ it suffices to drop all nontrivial powers of ρ from the get-go and instead focus on the subdominant powers of $(Z\alpha)^2$. Because of this we can evaluate \mathcal{Q} directly using (4.9), which is repeated here for convenience

$$\mathcal{Q} \simeq \frac{[K - \zeta - Z\alpha X]g + [(K + \zeta)X - Z\alpha]f}{[K + \zeta - Z\alpha X]g + [(K - \zeta)X - Z\alpha]f} (2\kappa R)^{2\zeta}. \quad (4.28)$$

N	0	1	2	3	4	5	6	7	8
H_N	0	1	3/2	11/6	25/12	137/60	49/20	363/140	761/280

Table 1. First few harmonic numbers.

This is to be expanded to order $(Z\alpha)^2$, using $\zeta \simeq 1 - \frac{1}{2}(Z\alpha)^2$ and

$$\begin{aligned} \omega \rightarrow \omega_N &= m \left[1 + \frac{(Z\alpha)^2}{(N + \zeta)^2} \right]^{-1/2} \\ &\simeq m \left[1 - \frac{(Z\alpha)^2}{2n^2} - \frac{(4n-3)(Z\alpha)^4}{8n^4} + \mathcal{O}[(Z\alpha)^6] \right], \end{aligned} \quad (4.29)$$

and

$$\kappa \rightarrow \kappa_N = \sqrt{(m - \omega_N)(m + \omega_N)} \simeq m \left[\frac{Z\alpha}{n} + \frac{(n-1)(Z\alpha)^3}{2n^3} + \mathcal{O}[(Z\alpha)^5] \right], \quad (4.30)$$

so in particular

$$(2\kappa_N R)^2 \simeq \left[1 + \frac{(n-1)(Z\alpha)^2}{n^2} + \mathcal{O}[(Z\alpha)^4] \right] \left(\frac{2mRZ\alpha}{n} \right)^2. \quad (4.31)$$

Similarly

$$X \rightarrow X_N = \sqrt{\frac{m - \omega_N}{m + \omega_N}} \simeq \frac{Z\alpha}{2n} + \frac{(2n-1)(Z\alpha)^3}{8n^3} + \mathcal{O}[(Z\alpha)^5]. \quad (4.32)$$

Using the corresponding terms in the source expansion $\xi_g \simeq \hat{g}_1 + \hat{g}_3(Z\alpha)^2$ then gives \mathcal{Q}_+ for parity-even ($K = -1$) states as

$$\begin{aligned} \frac{n(n+1)\mathcal{Q}_+}{2} &\simeq (mRZ\alpha)^2 \left\{ 2(1 + 2\hat{g}_1) \left[1 - (Z\alpha)^2 \ln \left(\frac{2mRZ\alpha}{n} \right) \right] \right. \\ &\quad + \left[\frac{(6n^2 - n - 3) - (2n^3 - 4n^2 + n + 3)2\hat{g}_1 - 4n^2(n+1)\hat{g}_1^2}{2n^2(n+1)} \right] (Z\alpha)^2 \\ &\quad \left. + 4\hat{g}_3(Z\alpha)^2 + \mathcal{O}[(Z\alpha)^4] \right\}. \end{aligned} \quad (4.33)$$

To work systematically to relative order $(Z\alpha)^2$ we must keep track of the factor of c_N in h_{eff}

$$h_{\text{eff}} \simeq \frac{\pi c_N^{3/2} \delta x}{Z\alpha m^2} \simeq \frac{\pi \delta x}{Z\alpha m^2} \left[1 + \frac{3(n-1)(Z\alpha)^2}{2n^2} \right], \quad (4.34)$$

and it is also necessary to refine the double-pole approximation, by keeping subdominant terms in the Gamma-function expansion:

$$\Gamma(y) = \Gamma(\delta y - N) \simeq \frac{(-)^N}{N!} \left[\frac{1}{\delta y} + H_N - \gamma + \mathcal{O}(\delta y) \right], \quad (4.35)$$

where the harmonic numbers (see also table 1) are defined by

$$H_N = \sum_{k=1}^N \frac{1}{k} = \int_0^1 dx \frac{1-x^N}{1-x}, \quad (4.36)$$

and the integral representation shows in particular that $H_0 = 0$. γ is the Euler-Mascheroni constant

$$\gamma = \lim_{N \rightarrow \infty} [H_N - \ln N] = 0.57721\ 56649\ 01532\ 86060\ 65120\ \dots$$

Tracking only the m -independent $(Z\alpha)^2$ terms the leading contributions then are

$$h_{\text{eff}}^+ \simeq \pi Z\alpha R^2 \left\{ 2(1 + 2\hat{g}_1) \left[1 - (Z\alpha)^2 \left[\ln \left(\frac{2mRZ\alpha}{n} \right) + H_{n+1} + \gamma \right] \right] \right. \\ \left. + \left[4\hat{g}_3 + 5 + 8\hat{g}_1 - 2\hat{g}_1^2 + (1 + 2\hat{g}_1) \frac{12n^2 - n - 9}{2n^2(n+1)} \right] (Z\alpha)^2 + \mathcal{O}[(Z\alpha)^4] \right\}. \quad (4.37)$$

The first term agrees with the leading result found earlier, and to these can be added the subleading ($mRZ\alpha$) corrections found in eq. (4.21) above.

Some implications of these formulae are explored in the next sections.

5 Examples

As ever, the power in using an effective action to describe the short-distance properties of the source lies in its generality. That is, coefficients like c_s , r_p and c_v can be used to describe the leading contributions due to *any* localized source physics, provided only that this physics arises over small enough scales, R , to make an expansion in powers of R/a useful (where a is a typical macroscopic scale — such as the Bohr radius of an exterior orbit). This ensures the model-independence of parametrizing physical quantities like energy shifts in terms of these parameters.

This section emphasizes this point by indicating how several kinds of microscopic source physics contribute to effective couplings in the source action, S_p , and how the above expressions reproduce familiar results in specific instances.

5.1 Explicit charge distributions

Perhaps the simplest example of microscopic source physics that can be parametrized by S_p is the situation where the source is an explicit static charge distribution, $\rho(x)$, rather than a point charge. Examples of this form are studied in the literature, with sensitivity to source structure often estimated by tracking how energy shifts alter as $\rho(x)$ is varied through a plausible range of configurations [24, 26–37, 51, 52].

5.1.1 Relations to moments

The leading terms in the source-dependent energy shift in this case have been calculated by perturbing the interior solution around the Coulomb problem and are known⁶ to be given by [24]

$$h_{\text{eff}} = \frac{2\pi}{3} Z\alpha \left[r_p^2 - \frac{Z\alpha\mu}{2} \langle r^3 \rangle_{(2)} + (Z\alpha\mu)^2 F_{NR} + (Z\alpha)^2 F_{REL} \right], \quad (5.1)$$

⁶See also [25] for a discussion of the limits of this expansion.

where μ is the reduced mass (so $\mu \rightarrow m$ in the infinite-source-mass limit used here) and

$$\langle r^3 \rangle_{(2)} = \int d^3x d^3y |\mathbf{x}|^3 \rho(\mathbf{y} - \mathbf{x}) \rho(\mathbf{y}), \quad (5.2)$$

while F_{NR} and F_{REL} are given in terms of various charge moments in [24].

This result is model-independent inasmuch as the expressions for the coefficients of the series are universal functions of these moments, with the energy shift due to various charge distributions just differing in the values these distributions predict for the moments themselves. This is a more limited sense of ‘model-independence’ than we use here, since the model-independence of the predictions of the effective action apply not just to static charge distributions, but essentially to *any* kind of source physics that is sufficiently localized. (This model-independence of EFT methods for atomic measurements is emphasized within the 2nd-quantized framework in [41–45, 53].)

We verify in appendix B that for a general static charge distribution, $\rho(x)$, the quantity \hat{g}_1 that dominates how source physics appears in g_+/f_+ is related to the rms charge density, $r_p^2 = \langle r^2 \rangle$, by

$$(1 + 2\hat{g}_1)R^2 = \frac{r_p^2}{3}, \quad (5.3)$$

which implies that the leading energy shift given by (4.18) becomes

$$h_{\text{eff}}^+ \simeq \frac{2\pi}{3} Z\alpha r_p^2, \quad (5.4)$$

as required for consistency with (5.1). On the other hand, the boundary condition (3.8) shows how the parameter \hat{g}_1 is also interchangeable with one combination of c_s and $c_{v \text{ tot}}$ through

$$\left(c_s + c_{v \text{ tot}} \right)_{\epsilon=R} = c_s + c_v + \frac{2\pi}{3} Z\alpha r_p^2 = 4\pi R^2 \left(\frac{g_+}{f_+} \right)_{r=R} = 4\pi \hat{g}_1 Z\alpha R^2. \quad (5.5)$$

This implies

$$c_s + c_v = -2\pi Z\alpha R^2, \quad (5.6)$$

i.e. the infrared fixed point found in (3.42). Note the difference from the Schrödinger running where we found that $h = 0$ is a fixed point that parametrizes a trivial boundary condition.

The subdominant ($mRZ\alpha$) contribution also provides a relation between \hat{g}_2 and the higher moment $\langle r^3 \rangle_{(2)}$. Comparing (4.21) with (5.1) and using (5.3) shows

$$\langle r^3 \rangle_{(2)} \simeq -6R^3 \left\{ 2\hat{g}_2 - \left[1 + 8n^2 \left(1 + \frac{3}{2} \hat{g}_1 (\hat{g}_1 + 2) \right) \right] \frac{1}{3n^2} \right\}. \quad (5.7)$$

Although we do not have a general proof of this result, we can verify it for specific charge distributions. These higher terms can be related to higher-dimension interactions — such as those of (3.44) — in S_p , using matching conditions similar to (5.5), although we do not pursue this here.

5.1.2 Specific charge distributions

The detailed calculations done for specific charge distributions [24, 51, 52] provide useful checks on the higher-order terms, since these must agree on the series coefficients for the specific charge distributions studied. To provide this check we compute the couplings \hat{g}_i and \hat{f}_i for various charge distributions in appendix B, and we here use these in the above expressions for h_{eff} to verify agreement where overlap is possible.

Spherical charged shell. The simplest such example is that of a charged shell, for which

$$\rho = \sigma \delta(r - R) = \frac{Ze}{4\pi R^2} \delta(r - R) \quad (5.8)$$

which is convenient since the interior solution can be solved exactly in closed form. (We have checked that our numerical results for this case agree with those of [52].) For this distribution the rms charge radius is $r_p^2 = R^2$ and $\langle r^3 \rangle_{(2)} = 16R^3/5$.

For the parity-even state the boundary parameters appearing in $g_+(R)/f_+(R)$ work out to be

$$\hat{g}_1 = -\frac{1}{3}, \quad \hat{g}_2 = -\frac{2}{45} + \frac{1}{6n^2} \quad \text{and} \quad \hat{g}_3 = -\frac{1}{45}, \quad (5.9)$$

while for the parity-odd state the analogous parameters are

$$\hat{f}_1 = +\frac{2}{3}, \quad \hat{f}_2 = +\frac{2}{45} \quad \text{and} \quad \hat{f}_3 = +\frac{1}{3}. \quad (5.10)$$

Using these values to compute the leading and subleading $(mRZ\alpha)$ and $(Z\alpha)^2$ energy shifts then gives

$$\begin{aligned} h_{\text{eff}}^+ &\simeq \pi Z\alpha R^2 \left\{ 2(1 + 2\hat{g}_1) \left[1 - (Z\alpha)^2 \left[\ln \left(\frac{2mRZ\alpha}{n} \right) + H_{n+1} + \gamma \right] \right] \right. \\ &\quad + 4\hat{g}_2(mRZ\alpha) - \left[1 + 8n^2 \left(1 + \frac{3}{2}\hat{g}_1(\hat{g}_1 + 2) \right) \right] \frac{2mRZ\alpha}{3n^2} \\ &\quad + \left[4\hat{g}_3 + 5 + 8\hat{g}_1 - 2\hat{g}_1^2 + (1 + 2\hat{g}_1) \frac{12n^2 - n - 9}{2n^2(n+1)} \right] (Z\alpha)^2 \\ &\quad \left. + \mathcal{O}[(mRZ\alpha)^2, mR(Z\alpha)^2, (Z\alpha)^4] \right\} \\ &\rightarrow \frac{2\pi Z\alpha R^2}{3} \left\{ 1 - \frac{8}{5}(mRZ\alpha) - \left[\ln \left(\frac{2mRZ\alpha}{n} \right) \right. \right. \\ &\quad \left. \left. + H_{n+1} + \gamma - \frac{91}{30} - \frac{12n^2 - n - 9}{4n^2(n+1)} \right] (Z\alpha)^2 + \dots \right\} \\ &\quad (\text{charged shell}), \end{aligned} \quad (5.11)$$

for parity-even states. Notice the correct result for r_p^2 and the cancellation of the n -dependence (and agreement with) the second moment $\langle r^3 \rangle_{(2)}$ for this distribution. This expression also agrees well with numerical evaluation (as illustrated in figure 3).

In this case, because $\hat{f}_1 = \frac{2}{3}$, the leading parity-odd energy shift vanishes, leaving a result that is smaller than would naively be expected. The energy shifts predicted by the

parameters \hat{f}_i in this case are

$$\begin{aligned}
 h_{\text{eff}}^- &\simeq -\frac{\pi(n^2-1)}{n^2}(Z\alpha)^2 mR^3 \left\{ \left(\hat{f}_1 - \frac{2}{3} \right) \left[1 + \left(\frac{\hat{f}_1}{2} - \frac{5}{3} \right) (mRZ\alpha) \right] \right. \\
 &\qquad \qquad \qquad \left. + \left(\hat{f}_2 - \frac{1}{9} \right) (mRZ\alpha) \right\} \\
 &\rightarrow +\frac{\pi(n^2-1)}{45n^2}(Z\alpha)^3 m^2 R^4 \quad (\text{charged shell}). \tag{5.12}
 \end{aligned}$$

Both of these results also depend on n in the way indicated by numerical evaluation.

Uniform spherical distribution. A second go-to example is the case of a uniform charge distribution, although in this case the interior solution cannot be computed in closed form. We have verified that our solutions agree in this case with the numerical results given in [52]. Analytic expressions for the series expansion of the energy shifts are also given in [51], and we have verified that our results agree with these (and with [24]) in this case.

Evaluating the boundary condition $g_+(R)/f_+(R)$ using the interior solutions returns the following values

$$\hat{g}_1 = -\frac{2}{5}, \quad \hat{g}_2 = -\frac{116}{1575} + \frac{1}{6n^2} \quad \text{and} \quad \hat{g}_3 = -\frac{736}{17325}, \tag{5.13}$$

while the same calculation for the parity-odd states gives

$$\hat{f}_1 = \frac{2}{3}, \quad \hat{f}_2 = +\frac{32}{315} \quad \text{and} \quad \hat{f}_3 = +\frac{2}{5}. \tag{5.14}$$

Used in the parity-even energy shift, these values return the leading and sub-leading results

$$\begin{aligned}
 h_{\text{eff}}^+ &\simeq \pi Z\alpha R^2 \left\{ 2(1+2\hat{g}_1) \left[1 - (Z\alpha)^2 \left[\ln \left(\frac{2mRZ\alpha}{n} \right) + H_{n+1} + \gamma \right] \right] \right. \\
 &\quad + 4\hat{g}_2(mRZ\alpha) - \left[1 + 8n^2 \left(1 + \frac{3}{2}\hat{g}_1(\hat{g}_1+2) \right) \right] \frac{2mRZ\alpha}{3n^2} \\
 &\quad + \left[4\hat{g}_3 + 5 + 8\hat{g}_1 - 2\hat{g}_1^2 + (1+2\hat{g}_1) \frac{12n^2-n-9}{2n^2(n+1)} \right] (Z\alpha)^2 \\
 &\quad \left. + \mathcal{O}[(mRZ\alpha)^2, mR(Z\alpha)^2, (Z\alpha)^4] \right\} \\
 &\rightarrow \frac{2\pi Z\alpha R^2}{5} \left\{ 1 - \frac{80}{63}(mRZ\alpha) - \left[\ln \left(\frac{2mRZ\alpha}{n} \right) \right. \right. \\
 &\quad \left. \left. + H_{n+1} + \gamma - \frac{22697}{6930} - \frac{12n^2-n-9}{4n^2(n+1)} \right] (Z\alpha)^2 + \dots \right\} \\
 &\quad (\text{uniform sphere}). \tag{5.15}
 \end{aligned}$$

These agree with the coefficients given explicitly in [51]. The first two terms also agree with [24] since the rms radius is $r_p^2 = \frac{3}{5}R^2$ for this distribution, while the second moment is $\langle r^3 \rangle_{(2)} = \frac{32}{21}R^3$ and so

$$\frac{Z\alpha m \langle r^3 \rangle_{(2)}}{2r_p^2} = \frac{1}{2} \frac{32}{21} \frac{5}{3} (mRZ\alpha) = \frac{80}{63} (mRZ\alpha). \tag{5.16}$$

5.2 Other applications

A point-particle effective action like S_p can be used to parametrize *any* short-range source physics and so need not be limited to describing the effects of finite nuclear size. This section summarizes a few such examples.

Vacuum polarization. A standard contribution to atomic energy levels that also can be captured using S_p is the contribution (or parts of the contribution) due to vacuum polarization. It is well-known that the effects of vacuum polarization on the field of a point charge, Ze , can be described by the Uehling potential [54–57], of the form

$$U(r) = \frac{2\alpha Ze}{3\pi r} \int_1^\infty \frac{du}{u^2} \sqrt{u^2 - 1} \left(1 + \frac{1}{2u^2}\right) e^{-2ur/\alpha}, \quad (5.17)$$

in which m is the mass of the particle circulating within the loop. Since the range of this interaction is of order $R \sim m^{-1}$ the electron and muon vacuum polarizations fall into the category of physical effects acting over much smaller distances than typical sizes of orbits in ordinary atoms. The same is true for the influence of the muonic vacuum polarization within muonic atoms (but because $m_e \sim \alpha m_\mu$ it is not true for the shifts on muonic atom energies due to electron vacuum polarization).

Such a potential shifts the energy of atomic states with low angular momentum that sample the potential near the nucleus, by an amount that is proportional (in the Schrödinger limit) to the wave-function at the origin: $|\varphi(0)|^2$. Using the notation of earlier sections, the resulting energy shift has size

$$h_{\text{eff}} = -\frac{4Z\alpha^2}{15m^2}, \quad (5.18)$$

where m is the mass of the particle in the loop. Since the photon line of the vacuum polarization does not flip helicity, the arguments of earlier sections imply that this leading energy shift is correctly captured (at order $(Z\alpha)^2/m^2$) in all low-energy observables through a contribution to the effective couplings in (2.3) of size

$$c_s = 0 \quad \text{and} \quad c_{v \text{ tot}} = -\frac{4Z\alpha^2}{15m^2}. \quad (5.19)$$

Strong interactions and anti-protonic atoms. When the particle orbiting a nucleus is affected by the strong interaction (such as for a π^- , K^- or \bar{p}) then it experiences a short-range ($R \sim m_\pi^{-1}$) strong interaction with the nucleus in addition to the usual Coulomb potential. These are often described in the literature in terms of explicit nuclear potentials, which though concrete introduce an element of model-dependence into the treatment.

For such situations a more model-independent approach is to use the contact interactions appearing in (2.3) to capture the effects of these strong interactions on energy shifts and nuclear scattering amplitudes. This has the advantage of using only the short range of the force to organize the calculation, and so allows the disentangling of effects that rely only on this from those that instead depend on the detailed form assumed for any hypothetical nuclear potential.

Ref. [6] shows how parametrizing these strong interactions in terms of the lowest-dimension contact interaction allows the derivation of a relation between the strong-interaction induced shifts in atomic energy levels and the scattering length for collisions with the nucleus, that reproduce the standard Deser formula [58] (derived using nuclear potentials in the 1950s).

The leading effects of the nuclear force on antiprotons in protonium [59, 60] can similarly be captured through the contact interactions of (2.3), though for protonium the existence of a relatively quick annihilation channel reduces the practical utility of using measurements of the energy shifts to learn about the nuclear interaction. But because this annihilation can also be described in the effective point-source action through the addition of imaginary parts to the effective couplings c_s and c_v one use for S_p in this case is to compute the dependence of the annihilation rate on the principal quantum number n for S and P states. Thinking of the annihilation rate as the imaginary part of the energy eigenvalue shows that this n -dependence should be the same as for the energy shifts found in earlier sections, and this indeed reproduces what is found when modelling annihilation using nuclear potentials [61].

The virtue of rederiving this result using S_p is that the effective field theory shows why the result is robust, and not an artefact of model-dependent details.

Exotic interactions. A fairly obvious use for contact interactions in the point-particle action is to parametrize the effects of any hypothetical new forces acting between nuclei and electrons or muons, and in particular forces that differ in strength between these two (since these can be captured through species-dependent values for c_s and c_v , unlike for r_p). Indeed the observation that the existence of such short-range interactions could, in principle, explain the proton radius puzzle [38–40] has led to efforts to better understand their size [53] and to the proposal of exotic interactions of this type [62–65].

6 Summary

In this paper, we introduce the PPEFT of Dirac fermions using a first-quantized language for the heavy compact object and a second-quantized language for the lighter fermion with which it interacts. This formalism can be advantageous to the fully second-quantized framework in the limit of the compact object being much heavier than the light interacting particle, i.e. the heavy compact object can be regarded as being in a position eigenstate to first approximation.

This formalism was previously introduced for bosons [5, 6] where it was found that energy shifts due to the finite size R of the source scale linearly in R which is unusual. This does not carry over to fermions, i.e. energy shifts scale as R^2 . The absence of such unusual energy shifts means that there is no additional term that could account for the proton-radius-puzzle.

Our PPEFT allows one to parametrize the currently measurable energy shifts and their leading corrections due to the finite size of the nucleus for nuclei with zero nuclear spin. Other applications include parametrizing strong interactions between the orbiting particle and the nucleus and anti-protonic atoms as well as hypothetical new forces acting between nuclei and electrons or muons.

In general, energy shifts are found by comparing the ratio of integration constants, C/A , appearing in the mode expansions (2.16) and (2.17) for the radial solutions to the Dirac equation found in two ways. On one hand normalizability at large r implies C/A is given by (4.2), while on the other hand it is fixed by the boundary condition for the ratio of radial functions, f/g , evaluated at a small radius $r = \epsilon$ near where the small source intervenes. The expression for C/A given $f/g|_{r=\epsilon}$ can be found either by working numerically with the exact mode functions, or analytically using (4.9) if ϵ is small enough that the mode functions are well-approximated by their small- r asymptotic forms.

The main contribution of the PPEFT construction given here is to express f/g at $r = \epsilon$ in terms of general effective couplings, such as c_s and c_v using the conditions given in eqs. (3.8). This leads to a low-energy expansion applicable to *generic* source physics provided only that the size of the source is sufficiently small. In the explicit calculations presented here ‘generic’ is in practice restricted for simplicity to parity conserving and rotationally invariant sources, rather than considering different source models one at a time. Results for specific models of the source can then be found by evaluating c_s and c_v explicitly using the model, such as along the lines as was done in the text for specific charge distributions.

What sets the size of ϵ ? The above procedure works for boundary conditions at *any* small radius $r = \epsilon$, provided that ϵ is much smaller than the applications of interest (such as the Bohr radius, for atomic examples) while also being larger than the actual size R of the source. The effective couplings — e.g. c_s and c_v — themselves also depend on ϵ in precisely the way required to ensure that physical quantities do not; an evolution computed for c_s and c_v explicitly in section 3.2. Once c_s and c_v are specified by matching to a specific model at $r = R$, their size at larger $r = \epsilon$ is dictated by this evolution.

Finally, we give explicit formulae for energy shifts in the Dirac-Coulomb case as a double series in powers of $mRZ\alpha$ and $(Z\alpha)^2$, given a similar expansion for the boundary conditions f/g of the form

$$\frac{1}{Z\alpha} \left(\frac{g_+}{f_+} \right)_{r=R} = \hat{g}_1 + \hat{g}_2(mRZ\alpha) + \hat{g}_3(Z\alpha)^2 + \dots, \quad (6.1)$$

and

$$2n\sqrt{\frac{m-\omega}{m+\omega}} \left(\frac{f_-}{g_-} \right)_{r=R} = \hat{f}_1(mRZ\alpha) + \hat{f}_2(mRZ\alpha)^2 + \hat{f}_3(Z\alpha)^2 + \dots, \quad (6.2)$$

with ‘plus’ and ‘minus’ referring to positive and negative parity eigenstates. The parameters \hat{f}_i and \hat{g}_i can be determined directly from a particular model of the underlying source and can be traded for parameters in the effective Lagrangian (like c_s and c_v , with higher orders also depending on their higher-dimensional counterparts).

Given such a boundary condition we write the energy shift to electrostatic bound states in terms of an effective δ -function potential:

$$\delta\omega^\pm = \frac{h_{\text{eff}}^\pm}{\pi} \left(\frac{mZ\alpha}{n} \right)^3, \quad (6.3)$$

where the effective coupling h_{eff}^{\pm} is given order by order in $(Z\alpha)^2$ and $(mRZ\alpha)$ by:

$$\begin{aligned}
 h_{\text{eff}}^+ \simeq & \pi Z\alpha R^2 \left\{ 2(1 + 2\hat{g}_1) \left[1 - (Z\alpha)^2 \left[\ln \left(\frac{2mRZ\alpha}{n} \right) + H_{n+1} + \gamma \right] \right] \right. \\
 & + \left[4\hat{g}_3 + 5 + 8\hat{g}_1 - 2\hat{g}_1^2 + (1 + 2\hat{g}_1) \frac{12n^2 - n - 9}{2n^2(n+1)} \right] (Z\alpha)^2 \\
 & \left. + \left[2\hat{g}_2 - \frac{1}{3n^2} \left[1 + 8n^2 \left(1 + \frac{3}{2} \hat{g}_1(\hat{g}_1 + 2) \right) \right] \right] (mRZ\alpha) + \dots \right\}, \quad (6.4)
 \end{aligned}$$

and

$$\begin{aligned}
 h_{\text{eff}}^- \simeq & -\frac{\pi(n^2 - 1)}{n^2} (Z\alpha)^2 mR^3 \left\{ \left(\hat{f}_1 - \frac{2}{3} \right) \left[1 + \left(\frac{\hat{f}_1}{2} - \frac{5}{3} \right) (mRZ\alpha) \right] \right. \\
 & \left. + \left(\hat{f}_2 - \frac{1}{9} \right) (mRZ\alpha) + \dots \right\}. \quad (6.5)
 \end{aligned}$$

These expressions apply for general \hat{f}_i and \hat{g}_i out to subdominant order $mRZ\alpha$ and $(Z\alpha)^2$, and so suffice for modern comparisons with precision measurements. As such they provide a model-independent description of source effects, allowing them to be efficiently parameterized when comparing modern measurements (for an example of the precision now possible, see [66]) with other precision corrections, such as those of QED.

Finally, we have verified explicitly that these expressions reproduce those in the literature when specialized to the case where the source is modelled as an explicit charge distribution, and for comparison purposes give expressions for the leading values of \hat{f}_i and \hat{g}_i for several simple models considered elsewhere.

Acknowledgments

We thank Paddy Fox, Richard Hill, Bob Holdom, Marko Horbatsch, Friederike Metz, Bernie Nickel, Sasha Penin, Ryan Plestid, Maxim Pospelov, Ira Rothstein, Andrew Tolley and Michael Trott for helpful discussions and Ross Diener, Leo van Nierop, Claudia de Rham and Matt Williams for their help in understanding singular fields and classical renormalization. This research was supported in part by funds from the Natural Sciences and Engineering Research Council (NSERC) of Canada and by a postdoctoral fellowship from the National Science Foundation of Belgium (FWO). Research at the Perimeter Institute is supported in part by the Government of Canada through Industry Canada, and by the Province of Ontario through the Ministry of Research and Information (MRI).

A Gamma-matrix conventions

When necessary we use the following representation for the tangent-frame gamma matrices:

$$\gamma^0 = -i\beta = -i \begin{pmatrix} 0 & I \\ I & 0 \end{pmatrix}, \quad \gamma_k = -i \begin{pmatrix} 0 & \sigma_k \\ -\sigma_k & 0 \end{pmatrix}, \quad (A.1)$$

where σ_k are the Pauli matrices,

$$\sigma_1 = \begin{pmatrix} 0 & 1 \\ 1 & 0 \end{pmatrix}, \quad \sigma_2 = \begin{pmatrix} 0 & -i \\ i & 0 \end{pmatrix} \quad \text{and} \quad \sigma_3 = \begin{pmatrix} 1 & 0 \\ 0 & -1 \end{pmatrix}, \quad (\text{A.2})$$

and I is the 2-by-2 unit matrix. The gamma matrices are defined to satisfy the Dirac algebra $\{\gamma^\mu, \gamma^\nu\} = 2\eta^{\mu\nu}$ where $\eta^{\mu\nu}$ is the inverse Minkowski metric, given (in rectangular coordinates) by $\text{diag}(-+++)$.

Similarly

$$\gamma_5 = -i\gamma^0\gamma^1\gamma^2\gamma^3 = \begin{pmatrix} I & 0 \\ 0 & -I \end{pmatrix}, \quad (\text{A.3})$$

and $\bar{\psi} := \psi^\dagger\beta = i\psi^\dagger\gamma^0$. The chirality projection matrices are

$$\gamma_L = \frac{1}{2}(1 + \gamma_5) \quad \text{and} \quad \gamma_R = \frac{1}{2}(1 - \gamma_5) \quad \text{so} \quad \psi = \begin{pmatrix} \psi_L \\ \psi_R \end{pmatrix}. \quad (\text{A.4})$$

As usual, the Pauli matrices satisfy

$$\{\sigma_i, \sigma_j\} = 2\delta_{ij} \quad \text{and} \quad [\sigma_i, \sigma_j] = 2i\epsilon_{ijk}\sigma_k, \quad (\text{A.5})$$

and so defining $\gamma^{\mu\nu} := \frac{1}{2}[\gamma^\mu, \gamma^\nu]$ we have

$$\gamma_{0k} = \frac{1}{2}[\gamma_0, \gamma_k] = \frac{1}{2} \begin{pmatrix} -2\sigma_k & 0 \\ 0 & 2\sigma_k \end{pmatrix} = \begin{pmatrix} -\sigma_k & 0 \\ 0 & \sigma_k \end{pmatrix}, \quad (\text{A.6})$$

while

$$\gamma_{jk} = \frac{1}{2}[\gamma_j, \gamma_k] = \frac{1}{2} \begin{pmatrix} [\sigma_j, \sigma_k] & 0 \\ 0 & [\sigma_j, \sigma_k] \end{pmatrix} = i\epsilon_{jkl} \begin{pmatrix} \sigma_l & 0 \\ 0 & \sigma_l \end{pmatrix}. \quad (\text{A.7})$$

Consequently the spin parts of the boost and rotation generators are block-diagonal in this basis, since

$$B_j := -\frac{i}{2}\gamma_{0j} = \frac{i}{2} \begin{pmatrix} \sigma_j & 0 \\ 0 & -\sigma_j \end{pmatrix} \quad \text{and} \quad \Sigma_j := -\frac{i}{4}\epsilon_{jkl}\gamma^{kl} = \frac{1}{2} \begin{pmatrix} \sigma_j & 0 \\ 0 & \sigma_j \end{pmatrix}. \quad (\text{A.8})$$

A.1 Polar coordinates

Our conventions for spherical polar coordinates $\{r, \theta, \phi\}$ are standard, with (as usual)

$$x = r \sin \theta \cos \phi, \quad y = r \sin \theta \sin \phi \quad \text{and} \quad z = r \cos \theta. \quad (\text{A.9})$$

The differentials therefore satisfy

$$\begin{pmatrix} dx \\ dy \\ dz \end{pmatrix} = \begin{pmatrix} \sin \theta \cos \phi & \cos \theta \cos \phi & -\sin \phi \\ \sin \theta \sin \phi & \cos \theta \sin \phi & \cos \phi \\ \cos \theta & -\sin \theta & 0 \end{pmatrix} \begin{pmatrix} dr \\ r d\theta \\ r \sin \theta d\phi \end{pmatrix} \quad (\text{A.10})$$

in terms of which the flat 3D metric is

$$g_{ij} dx^i dx^j = dx^2 + dy^2 + dz^2 = dr^2 + r^2(d\theta^2 + \sin^2 \theta d\phi^2) =: (\mathbf{e}^r)^2 + (\mathbf{e}^\theta)^2 + (\mathbf{e}^\phi)^2. \quad (\text{A.11})$$

This last equality defines the normalized frame of basis 1-forms, \mathbf{e}_r , \mathbf{e}_θ and \mathbf{e}_ϕ , so that an orthonormal frame is given by

$$\mathbf{e}^r = dr, \quad \mathbf{e}^\theta = r d\theta \quad \text{and} \quad \mathbf{e}^\phi = r \sin \theta d\phi. \quad (\text{A.12})$$

We implicitly work in a gauge with $\partial_\mu A^\mu = 0$. For later use notice the inverse of (A.10) is

$$\begin{pmatrix} dr \\ r d\theta \\ r \sin \theta d\phi \end{pmatrix} = \begin{pmatrix} \sin \theta \cos \phi & \sin \theta \sin \phi & \cos \theta \\ \cos \theta \cos \phi & \cos \theta \sin \phi & -\sin \theta \\ -\sin \phi & \cos \phi & 0 \end{pmatrix} \begin{pmatrix} dx \\ dy \\ dz \end{pmatrix}. \quad (\text{A.13})$$

The radial gamma matrices are then defined by

$$\begin{aligned} \gamma^\theta &= \gamma^1 e_x^\theta + \gamma^2 e_y^\theta + \gamma^3 e_z^\theta \\ &= \frac{1}{r} [(\gamma^1 \cos \phi + \gamma^2 \sin \phi) \cos \theta - \gamma^3 \sin \theta] \\ &= -\frac{i}{r} \begin{pmatrix} 0 & \sigma^\theta \\ -\sigma^\theta & 0 \end{pmatrix}, \end{aligned} \quad (\text{A.14})$$

with

$$\sigma^\theta := (\sigma_x \cos \phi + \sigma_y \sin \phi) \cos \theta - \sigma_z \sin \theta = \begin{pmatrix} -\sin \theta & e^{-i\phi} \cos \theta \\ e^{i\phi} \cos \theta & \sin \theta \end{pmatrix}. \quad (\text{A.15})$$

Similarly

$$\begin{aligned} \gamma^\phi &= \gamma^1 e_x^\phi + \gamma^2 e_y^\phi + \gamma^3 e_z^\phi \\ &= \frac{1}{r \sin \theta} [-\gamma^1 \sin \phi + \gamma^2 \cos \phi] \\ &= -\frac{i}{r \sin \theta} \begin{pmatrix} 0 & \sigma^\phi \\ -\sigma^\phi & 0 \end{pmatrix}, \end{aligned}$$

with

$$\sigma^\phi := -\sigma_x \sin \phi + \sigma_y \cos \phi = \begin{pmatrix} 0 & -ie^{-i\phi} \\ ie^{i\phi} & 0 \end{pmatrix}, \quad (\text{A.16})$$

and (for completeness)

$$\begin{aligned} \gamma^r &= \gamma^1 e_x^r + \gamma^2 e_y^r + \gamma^3 e_z^r \\ &= (\gamma^1 \cos \phi + \gamma^2 \sin \phi) \sin \theta + \gamma^3 \cos \theta \\ &= -i \begin{pmatrix} 0 & \sigma^r \\ -\sigma^r & 0 \end{pmatrix}, \end{aligned} \quad (\text{A.17})$$

with

$$\begin{aligned} \sigma^r &:= (\sigma_x \cos \phi + \sigma_y \sin \phi) \sin \theta + \sigma_z \cos \theta = \begin{pmatrix} \cos \theta & e^{-i\phi} \sin \theta \\ e^{i\phi} \sin \theta & -\cos \theta \end{pmatrix} \\ &= \frac{1}{r} \begin{pmatrix} z & x - iy \\ x + iy & -z \end{pmatrix} = \frac{\mathbf{r}}{r} \cdot \vec{\sigma}. \end{aligned} \quad (\text{A.18})$$

Finally

$$\sigma^\theta \sigma^\phi = -\sigma^\phi \sigma^\theta = i \begin{pmatrix} \cos \theta & e^{-i\phi} \sin \theta \\ e^{i\phi} \sin \theta & -\cos \theta \end{pmatrix} = i\sigma^r, \quad (\text{A.19})$$

and so

$$\gamma^{\theta\phi} = \gamma^\theta \gamma^\phi = -\gamma^\phi \gamma^\theta = \frac{1}{r^2 \sin \theta} \begin{pmatrix} \sigma^\theta \sigma^\phi & 0 \\ 0 & \sigma^\theta \sigma^\phi \end{pmatrix} = \frac{i}{r^2 \sin \theta} \begin{pmatrix} \sigma^r & 0 \\ 0 & \sigma^r \end{pmatrix}, \quad (\text{A.20})$$

which also implies

$$\gamma_{\theta\phi} = g_{\theta\theta} g_{\phi\phi} \gamma^\theta \gamma^\phi = ir^2 \sin \theta \begin{pmatrix} \sigma^r & 0 \\ 0 & \sigma^r \end{pmatrix}. \quad (\text{A.21})$$

For future reference notice also that with the convention $\epsilon^{0r\theta\phi} = +\det e_a^\mu = +1/(r^2 \sin \theta)$ the above imply

$$\gamma^{0r} = -\gamma^{r0} = \gamma^0 \gamma^r = \begin{pmatrix} \sigma^r & 0 \\ 0 & -\sigma^r \end{pmatrix} \quad \text{and} \quad \gamma_{\theta\phi} \gamma_5 = ir^2 \sin \theta \begin{pmatrix} \sigma^r & 0 \\ 0 & -\sigma^r \end{pmatrix}, \quad (\text{A.22})$$

and so

$$\gamma^{\mu\nu} = -\frac{i}{2} \epsilon^{\mu\nu\lambda\rho} \gamma_{\lambda\rho} \gamma_5. \quad (\text{A.23})$$

Solutions to the Dirac equation, $(\mathcal{D} + m)\psi = 0$ also solve

$$0 = (\mathcal{D} - m)(\mathcal{D} + m)\psi = (\mathcal{D}^2 - m^2)\psi = \left[D_\mu D^\mu - m^2 + \frac{ie}{2} \gamma^{\mu\nu} F_{\mu\nu} \right] \psi, \quad (\text{A.24})$$

which is the Klein-Gordon equation supplemented by a spin term, whose explicit form is

$$+ \frac{ie}{2} \gamma^{\mu\nu} F_{\mu\nu} = +ie \gamma^{r0} F_{r0} = -\frac{iZ\alpha}{r^2} \begin{pmatrix} \sigma^r & 0 \\ 0 & -\sigma^r \end{pmatrix}, \quad (\text{A.25})$$

and we use the definition of the fine-structure constant: $\alpha := e^2/(4\pi)$. Once a solution, χ , to (A.24) is found, then the corresponding electron-type solution to the Dirac equation $(\mathcal{D} + m)\psi = 0$ is $\psi = (\mathcal{D} - m)\chi$ [and similarly the corresponding positron-type solution to $(\mathcal{D} - m)\psi = 0$ would be $\psi = (\mathcal{D} + m)\chi$].

A.2 Spinor harmonics

When solving the Dirac equation we define quantities having definite quantum numbers (j and j_z) for \mathbf{J} and J_z , leading to the following 2-component spinors

$$U_{jj_z}^+(\theta, \phi) := \begin{bmatrix} \sqrt{(j+j_z)/(2j)} Y_{j-\frac{1}{2}j_z-\frac{1}{2}}(\theta, \phi) \\ \sqrt{(j-j_z)/(2j)} Y_{j-\frac{1}{2}j_z+\frac{1}{2}}(\theta, \phi) \end{bmatrix}$$

and

$$U_{jj_z}^-(\theta, \phi) := \begin{bmatrix} \sqrt{(j+1-j_z)/[2(j+1)]} Y_{j+\frac{1}{2}j_z-\frac{1}{2}}(\theta, \phi) \\ -\sqrt{(j+1+j_z)/[2(j+1)]} Y_{j+\frac{1}{2}j_z+\frac{1}{2}}(\theta, \phi) \end{bmatrix}. \quad (\text{A.26})$$

Notice that the property $Y_{\ell\ell_z}(\pi - \theta, \phi + \pi) = (-)^\ell Y_{\ell\ell_z}(\theta, \phi)$ implies parity acts on these combinations oppositely: $\hat{\Pi} U_{jj_z}^\pm = (-)^{j\mp\frac{1}{2}} U_{jj_z}^\pm$. Furthermore, notice also that $\sigma^r U_{jj_z}^\pm =$

U_{jjz}^\mp . Indeed the result $\sigma^r U_{jjz}^\pm = \eta U_{jjz}^\mp$ with $\eta^2 = 1$ is a consequence of the properties (i) $\sigma^r = \hat{\mathbf{r}} \cdot \boldsymbol{\sigma}$ is parity odd; (ii) $(\sigma^r)^2 = 1$; and (iii) $[\mathbf{J}, \sigma^r] = 0$, so only a direct calculation determines $\eta = 1$ rather than $\eta = -1$.

We directly evaluate for the case of most interest: $j = \frac{1}{2}$. For this purpose we use the explicit forms

$$\begin{aligned} Y_{00} &= \frac{1}{\sqrt{4\pi}}, & Y_{10} &= \sqrt{\frac{3}{4\pi}} \cos \theta = \sqrt{\frac{3}{4\pi}} \frac{z}{r} \\ Y_{1\pm 1} &= \mp \sqrt{\frac{3}{8\pi}} e^{\pm i\phi} \sin \theta = \mp \sqrt{\frac{3}{8\pi}} \frac{x \pm iy}{r}, \end{aligned} \quad (\text{A.27})$$

in the definitions of the $U_{\frac{1}{2}jz}^\pm$ to find

$$\begin{aligned} U_{\frac{1}{2}\frac{1}{2}}^+(\theta, \phi) &:= \begin{bmatrix} Y_{00}(\theta, \phi) \\ 0 \end{bmatrix} = \frac{1}{\sqrt{4\pi}} \begin{bmatrix} 1 \\ 0 \end{bmatrix} \\ U_{\frac{1}{2}-\frac{1}{2}}^+(\theta, \phi) &:= \begin{bmatrix} 0 \\ Y_{00}(\theta, \phi) \end{bmatrix} = \frac{1}{\sqrt{4\pi}} \begin{bmatrix} 0 \\ 1 \end{bmatrix}, \end{aligned} \quad (\text{A.28})$$

and

$$\begin{aligned} U_{\frac{1}{2}\frac{1}{2}}^-(\theta, \phi) &:= \frac{1}{\sqrt{3}} \begin{bmatrix} Y_{10}(\theta, \phi) \\ -\sqrt{2} Y_{11}(\theta, \phi) \end{bmatrix} = \frac{1}{\sqrt{4\pi} r} \begin{bmatrix} z \\ x + iy \end{bmatrix} = \frac{1}{\sqrt{4\pi}} \begin{bmatrix} \cos \theta \\ e^{i\phi} \sin \theta \end{bmatrix} \\ U_{\frac{1}{2}-\frac{1}{2}}^-(\theta, \phi) &:= \frac{1}{\sqrt{3}} \begin{bmatrix} \sqrt{2} Y_{1-1}(\theta, \phi) \\ -Y_{10}(\theta, \phi) \end{bmatrix} = \frac{1}{\sqrt{4\pi} r} \begin{bmatrix} x - iy \\ -z \end{bmatrix} = \frac{1}{\sqrt{4\pi}} \begin{bmatrix} e^{-i\phi} \sin \theta \\ -\cos \theta \end{bmatrix}, \end{aligned} \quad (\text{A.29})$$

which are also what is found explicitly by acting on $U_{\frac{1}{2}jz}^+$ with the explicit matrix

$$\sigma^r = \frac{\mathbf{r}}{r} \cdot \vec{\sigma} = \frac{1}{r} \begin{pmatrix} z & x - iy \\ x + iy & -z \end{pmatrix}. \quad (\text{A.30})$$

Similarly, acting with σ^r on $U_{\frac{1}{2}jz}^-$ gives

$$\begin{aligned} \sigma^r U_{\frac{1}{2}\frac{1}{2}}^-(\theta, \phi) &:= \frac{1}{\sqrt{4\pi} r^2} \begin{pmatrix} z & x - iy \\ x + iy & -z \end{pmatrix} \begin{bmatrix} z \\ x + iy \end{bmatrix} = \frac{1}{\sqrt{4\pi}} \begin{bmatrix} 1 \\ 0 \end{bmatrix} = U_{\frac{1}{2}\frac{1}{2}}^+ \\ \sigma^r U_{\frac{1}{2}-\frac{1}{2}}^-(\theta, \phi) &:= \frac{1}{\sqrt{4\pi} r^2} \begin{pmatrix} z & x - iy \\ x + iy & -z \end{pmatrix} \begin{bmatrix} x - iy \\ -z \end{bmatrix} = \frac{1}{\sqrt{4\pi}} \begin{bmatrix} 0 \\ 1 \end{bmatrix} = U_{\frac{1}{2}-\frac{1}{2}}^+. \end{aligned} \quad (\text{A.31})$$

For later purposes we also evaluate the spatial derivatives explicitly using $\vec{\sigma} \cdot \nabla = \sigma_k \partial_k = \sigma_x \partial_x + \sigma_y \partial_y + \sigma_z \partial_z$ as well as $\vec{\sigma} \cdot \nabla f(r) = f'(r) \vec{\sigma} \cdot \nabla r = f'(r) \vec{\sigma} \cdot \mathbf{r}/r = f'(r) \sigma^r$. This trivially gives

$$\sigma_k \partial_k U_{\frac{1}{2}jz}^+ = 0, \quad (\text{A.32})$$

while

$$\sigma_k \partial_k U_{\frac{1}{2}\frac{1}{2}}^- = \frac{2}{r} U_{\frac{1}{2}\frac{1}{2}}^+ \quad \text{and} \quad \sigma_k \partial_k U_{\frac{1}{2}-\frac{1}{2}}^- = \frac{2}{r} U_{\frac{1}{2}-\frac{1}{2}}^+, \quad (\text{A.33})$$

in agreement with an algebraic evaluation.

B Dirac solutions

This appendix collects several exact and approximate solutions to the Dirac equation that are used in the main text.

B.1 Exterior (Coulomb) solutions

Bound states for the Dirac equation are found as usual by demanding that the boundary condition (normalizability) at infinity be compatible with the boundary condition at the origin.

Energy eigenvalues. If the boundary condition at the origin is the usual one (for which we discard the singular solution to the radial equation — see below) the energy eigenvalues are

$$\begin{aligned}\omega_N &= m \left[1 + \frac{(Z\alpha)^2}{(N + \zeta)^2} \right]^{-1/2} = m \left[1 + \frac{(Z\alpha)^2}{\left[N + \sqrt{\left(j + \frac{1}{2}\right)^2 - (Z\alpha)^2} \right]^2} \right]^{-1/2} \\ &= m \left[1 + \frac{(Z\alpha)^2}{\left(n + \zeta - j - \frac{1}{2}\right)^2} \right]^{-1/2},\end{aligned}\tag{B.1}$$

where $j = \frac{1}{2}, \frac{3}{2}, \dots$ and the principal quantum number is defined by $n = N + \left(j + \frac{1}{2}\right) = 1, 2, 3, \dots$. We define $\zeta = \frac{1}{2}\sqrt{1 + 4j(j+1) - 4(Z\alpha)^2}$ or

$$\zeta := \sqrt{\left(j + \frac{1}{2}\right)^2 - (Z\alpha)^2},\tag{B.2}$$

so $\zeta \rightarrow 1$ as $Z\alpha \rightarrow 0$ when $j = \frac{1}{2}$. This implies

$$\left(j + \frac{1}{2} + \zeta\right) \left(j + \frac{1}{2} - \zeta\right) = \left(j + \frac{1}{2}\right)^2 - \zeta^2 = (Z\alpha)^2.\tag{B.3}$$

The standard derivation shows that for $N \neq 0$ (that is, except for $n = j + \frac{1}{2}$) each state with fixed n and j comes with two-fold degeneracy corresponding to parity $s = \pm$. The most famous example is $N = 1$ and $j = \frac{1}{2}$, which corresponds to $n = 2$ and $j = \frac{1}{2}$ in which case the degeneracy is between the $2S_{1/2}$ and $2P_{1/2}$ states that get split by the Lamb shift. This two-fold degeneracy does *not* occur for $N = 0$, corresponding to the $n = j + \frac{1}{2}$ states like $1S_{1/2}$ (the ground state), $2P_{3/2}$, $3D_{5/2}$ and so on. (Notice that here S , P and D do not strictly correspond to specifying ℓ but instead give the parity value s for the corresponding state.)

Parity eigenstates. Normally, atomic states are given as parity eigenstates, which involves combining ψ_L and ψ_R since the action of parity is

$$\mathcal{P} \begin{bmatrix} \psi_L(\theta, \phi) \\ \psi_R(\theta, \phi) \end{bmatrix} \mathcal{P}^{-1} = \begin{pmatrix} 0 & i \\ i & 0 \end{pmatrix} \begin{bmatrix} \psi_L(\pi - \theta, \phi + \pi) \\ \psi_R(\pi - \theta, \phi + \pi) \end{bmatrix}.\tag{B.4}$$

We expect a unique solution for each choice of parity, j and j_z quantum numbers, while the above just relates the radial functions for left- and right-handed fields to one another. The Dirac equation reads

$$-i(D_0 + \sigma_k D_k)\psi_R + m\psi_L = 0 \quad \text{and} \quad -i(D_0 - \sigma_k D_k)\psi_L + m\psi_R = 0, \quad (\text{B.5})$$

and so

$$i\sigma_k \nabla_k \psi_L = \left(\omega + \frac{Z\alpha}{r}\right)\psi_L - m\psi_R \quad \text{and} \quad i\sigma_k \nabla_k \psi_R = -\left(\omega + \frac{Z\alpha}{r}\right)\psi_R + m\psi_L. \quad (\text{B.6})$$

To identify the parity eigenstates we expand in terms of the spinor harmonics U^+ and U^- of appendix A and define the radial functions $f(r)$ and $g(r)$ using the following ansätze:

$$\begin{aligned} \psi_L^+ &= f_+(r) U_{j j_z}^+(\theta, \phi) + i g_+(r) U_{j j_z}^-(\theta, \phi) \\ \text{and } \psi_R^+ &= f_+(r) U_{j j_z}^+(\theta, \phi) - i g_+(r) U_{j j_z}^-(\theta, \phi) \\ \psi_L^- &= f_-(r) U_{j j_z}^-(\theta, \phi) + i g_-(r) U_{j j_z}^+(\theta, \phi) \\ \text{and } \psi_R^- &= f_-(r) U_{j j_z}^-(\theta, \phi) - i g_-(r) U_{j j_z}^+(\theta, \phi), \end{aligned} \quad (\text{B.7})$$

where the superscript on ψ and subscripts on f and g are the parity eigenlabel $p = \pm$. Using this in either of (B.6) gives the same conditions relating g and f . For the parity even states the relations are

$$f'_+ = \left(m + \omega + \frac{Z\alpha}{r}\right) g_+ \quad \text{and} \quad g'_+ + \frac{2g_+}{r} = \left(m - \omega - \frac{Z\alpha}{r}\right) f_+, \quad (\text{B.8})$$

while for parity odd states these relations instead become

$$g'_- = \left(m - \omega - \frac{Z\alpha}{r}\right) f_- \quad \text{and} \quad f'_- + \frac{2f_-}{r} = \left(m + \omega + \frac{Z\alpha}{r}\right) g_-, \quad (\text{B.9})$$

as used in the main text.

Coulomb-Dirac solutions. To solve the radial Dirac equations, (B.8) and (B.9), for general radius we introduce the two functions

$$\begin{aligned} Q_1 &= \frac{1}{2} e^{\rho/2} \rho^{1-\zeta} \left(\frac{f}{\sqrt{m+\omega}} - \frac{g}{\sqrt{m-\omega}} \right) \\ Q_2 &= \frac{1}{2} e^{\rho/2} \rho^{1-\zeta} \left(\frac{f}{\sqrt{m+\omega}} + \frac{g}{\sqrt{m-\omega}} \right) \end{aligned} \quad (\text{B.10})$$

where $\rho = 2\kappa r$ and $\kappa = \sqrt{m^2 - \omega^2}$. Some manipulation shows that these satisfy the following second-order linear ODEs

$$\begin{aligned} \rho Q_1'' + (2\zeta + 1 - \rho) Q_1' - \left(\zeta - \frac{Z\alpha\omega}{\kappa} \right) Q_1 &= 0 \\ \rho Q_2'' + (2\zeta + 1 - \rho) Q_2' - \left(\zeta + 1 - \frac{Z\alpha\omega}{\kappa} \right) Q_2 &= 0, \end{aligned} \quad (\text{B.11})$$

which hold for *either* sign of the parity quantum number. The parameter ζ is as defined in (B.2). The most general solutions to these equations are given as linear combinations of confluent hypergeometric functions $\mathcal{M}(a, b; \rho) = 1 + (a/b)\rho + \dots$, thereby introducing a total of four integration constants.

The Dirac equation imposes two relations between the four constants. Hence, we can express the solutions Q_1 and Q_2 as

$$Q_1 = A \mathcal{M} \left[\zeta - \frac{Z\alpha\omega}{\kappa}, 2\zeta + 1; \rho \right] + C \rho^{-2\zeta} \mathcal{M} \left[-\zeta - \frac{Z\alpha\omega}{\kappa}, -2\zeta + 1; \rho \right] \quad (\text{B.12})$$

$$Q_2 = -A \left(\frac{\zeta - Z\alpha\omega/\kappa}{K - Z\alpha m/\kappa} \right) \mathcal{M} \left[\zeta - \frac{Z\alpha\omega}{\kappa} + 1, 2\zeta + 1; \rho \right] \\ + C \left(\frac{\zeta + Z\alpha\omega/\kappa}{K - Z\alpha m/\kappa} \right) \rho^{-2\zeta} \mathcal{M} \left[-\zeta - \frac{Z\alpha\omega}{\kappa} + 1, -2\zeta + 1; \rho \right], \quad (\text{B.13})$$

where $K = \mp(j + \frac{1}{2})$ for states with parity ± 1 . A and C are the two remaining integration constants, and are chosen so that the function multiplying A is bounded as $\rho \rightarrow 0$ while the function multiplying C diverges there.

The corresponding expressions for f and g are then given by

$$f = \sqrt{m + \omega} e^{-\rho/2} \rho^{\zeta-1} \left\{ A \mathcal{M} \left[\zeta - \frac{Z\alpha\omega}{\kappa}, 2\zeta + 1; \rho \right] + C \rho^{-2\zeta} \mathcal{M} \left[-\zeta - \frac{Z\alpha\omega}{\kappa}, -2\zeta + 1; \rho \right] \right. \\ \left. - A \left(\frac{\zeta - Z\alpha\omega/\kappa}{K - Z\alpha m/\kappa} \right) \mathcal{M} \left[\zeta - \frac{Z\alpha\omega}{\kappa} + 1, 2\zeta + 1; \rho \right] \right. \\ \left. + C \left(\frac{\zeta + Z\alpha\omega/\kappa}{K - Z\alpha m/\kappa} \right) \rho^{-2\zeta} \mathcal{M} \left[-\zeta - \frac{Z\alpha\omega}{\kappa} + 1, -2\zeta + 1; \rho \right] \right\}, \quad (\text{B.14})$$

and

$$g = -\sqrt{m - \omega} e^{-\rho/2} \rho^{\zeta-1} \left\{ A \mathcal{M} \left[\zeta - \frac{Z\alpha\omega}{\kappa}, 2\zeta + 1; \rho \right] + C \rho^{-2\zeta} \mathcal{M} \left[-\zeta - \frac{Z\alpha\omega}{\kappa}, -2\zeta + 1; \rho \right] \right. \\ \left. + A \left(\frac{\zeta - Z\alpha\omega/\kappa}{K - Z\alpha m/\kappa} \right) \mathcal{M} \left[\zeta - \frac{Z\alpha\omega}{\kappa} + 1, 2\zeta + 1; \rho \right] \right. \\ \left. - C \left(\frac{\zeta + Z\alpha\omega/\kappa}{K - Z\alpha m/\kappa} \right) \rho^{-2\zeta} \mathcal{M} \left[-\zeta - \frac{Z\alpha\omega}{\kappa} + 1, -2\zeta + 1; \rho \right] \right\}. \quad (\text{B.15})$$

Normalisation of the state for $\rho \rightarrow \infty$ demands A and C must be related by

$$\frac{A}{C} = - \frac{\Gamma(1 - 2\zeta)}{\Gamma(1 + 2\zeta)} \frac{\Gamma(\zeta - Z\alpha\omega/\kappa)}{\Gamma(-\zeta - Z\alpha\omega/\kappa)} \quad (\text{B.16})$$

which follows from the large- ρ form of the confluent hypergeometric functions \mathcal{M} . When $C = 0$ this condition reproduces the energy eigenvalue given in (B.1). Alternative boundary conditions at $r \rightarrow 0$ change the bound state energy levels (and any other physical implications) entirely by changing what they imply for A/C .

As the above formulae attest, such alternative boundary conditions governing A/C can be imposed by demanding that the ratio f/g take a specific value at a particular radius $r = \epsilon$. (For instance, for particles orbiting a known charge distribution that extends out

to radius $r = R$, it is continuity of the internal with the external solution at $r = R$ that imposes the required condition:

$$\frac{g_{\text{out}}(R, K)}{f_{\text{out}}(R, K)} = \frac{g_{\text{in}}(R, K)}{f_{\text{in}}(R, K)} \quad (\text{B.17})$$

where f_{out} and g_{out} are the Coulomb solutions described above, valid for $r > R$, and f_{in} and g_{in} are given by the solution to the Dirac equation for the charge distribution for $r \leq R$. The next sections provide several representative solutions for simple charge distributions.

B.2 Interior solutions for given charge distributions

This section collects several simple solutions appropriate to the interior for several kinds of charge distributions, and gives the approximate series solutions in the general case.

B.2.1 Charged-shell model

In this case consider an exactly solvable model of a charge distribution against which later results can be compared. The model assumes a charge distribution that makes up a spherical shell, with surface density σ . That is,

$$\rho = \sigma \delta(r - R) = \frac{Ze}{4\pi R^2} \delta(r - R) \quad (\text{B.18})$$

where R is the radius of the shell, and the second equality assumes the total charge is Ze . The corresponding electromagnetic potential found by integrating Maxwell's equations then is

$$A^0 = \frac{Ze}{4\pi r} \quad \text{if } r > R \quad \text{and} \quad A^0 = \frac{Ze}{4\pi R} \quad \text{if } r < R. \quad (\text{B.19})$$

The Dirac equation outside the shell therefore sees only the Coulomb potential and so is the one whose solutions are given above. The solution inside the shell is essentially the free Dirac equation, though in the presence of a nonzero constant A^0 . That is, it is equivalent to (A.24), which now reads

$$0 = (\not{D} - m)(\not{D} + m)\psi = \left[D_\mu D^\mu - m^2 + \frac{ie}{2} \gamma^{\mu\nu} F_{\mu\nu} \right] \psi = [D_\mu D^\mu - m^2] \psi, \quad (\text{B.20})$$

where the spatial derivatives are $D_i = \partial_i$ while the time derivative (acting on an energy eigenstate) is

$$D_0 = \partial_t + ieA_0 = -i \left(\omega + \frac{Z\alpha}{4\pi R} \right). \quad (\text{B.21})$$

This has as solutions the usual spherical Bessel functions

$$A j_\ell(kr) + B y_\ell(kr), \quad (\text{B.22})$$

and $B = 0$ if we demand ψ be bounded at $r = 0$. Specializing to $j = \frac{1}{2}$ the appropriate solutions are $f_+ = A_+ j_0(kr)$, $f_- = B_- j_1(kr)$, $g_+ = B_+ j_1(kr)$ and $g_- = A_- j_0(kr)$. Since f'_+ and g'_- vanish at the origin it follows that g_+ and f_- must vanish there and this is automatic because these only involve $\ell = 1$. When evaluated at $r = R$ then

$$\frac{g_+(R)}{f_+(R)} = \left(\frac{B_+}{A_+} \right) \frac{j_1(kR)}{j_0(kR)}, \quad (\text{B.23})$$

and

$$\frac{f_-(R)}{g_-(R)} = \left(\frac{B_-}{A_-} \right) \frac{j_1(kR)}{j_0(kR)}. \quad (\text{B.24})$$

Finally, the Dirac equation says $f'_+ = (m + W)g_+$ and $g'_- = (m - W)f_-$ where $W = \omega + Z\alpha/R$. Using

$$j_0(x) = \frac{\sin x}{x} \simeq 1 + \mathcal{O}(x^2) \quad \text{and} \quad j_1(x) = \frac{\sin x}{x^2} - \frac{\cos x}{x} \simeq \frac{x}{3} + \mathcal{O}(x^3), \quad (\text{B.25})$$

so $j'_0(x) = -j_1(x)$ we find $f'_+ = (m + W)g_+$ implies $-kA_+ = (m + W)B_+$ and $g'_- = (m - W)f_-$ implies $-kA_- = (m - W)B_-$. This allows the boundary condition to be written

$$\begin{aligned} \frac{g_+(R)}{f_+(R)} &= - \left(\frac{k}{m + W} \right) \frac{j_1(kR)}{j_0(kR)} = - \sqrt{\frac{W - m}{W + m}} \left[\frac{\sin(kR) - kR \cos(kR)}{kR \sin(kR)} \right] \\ &= - \frac{1}{3} (W - m)R \left[1 + \frac{(kR)^2}{15} + \frac{2(kR)^4}{315} + \dots \right], \end{aligned} \quad (\text{B.26})$$

where we use $(\sin x - x \cos x)/(x \sin x) = \frac{1}{3}x + \frac{1}{45}x^3 + \frac{2}{945}x^5 + \dots$.

To make contact with the series in powers of $(Z\alpha)^2$ and $mRZ\alpha$ we evaluate at a bound-state energy and use

$$\begin{aligned} (kR)^2 &= [(\omega + m)R + Z\alpha][(\omega - m)R + Z\alpha] \\ &\simeq (2mR + Z\alpha)Z\alpha + \mathcal{O}[(mRZ\alpha)^2 \text{ or } (Z\alpha)^3 mR], \end{aligned}$$

and

$$\begin{aligned} (W - m)R &= (\omega - m)R + Z\alpha \\ &\simeq -\frac{1}{2n^2}(Z\alpha)^2 mR + Z\alpha = Z\alpha \left[1 - \frac{mRZ\alpha}{2n^2} + \mathcal{O}[(Z\alpha)^3 mR] \right], \end{aligned} \quad (\text{B.27})$$

so that

$$\frac{g_+(R)}{f_+(R)} \simeq -\frac{Z\alpha}{3} \left[1 + \left(\frac{2}{15} - \frac{1}{2n^2} \right) (mRZ\alpha) + \frac{(Z\alpha)^2}{15} + \dots \right], \quad (\text{B.28})$$

which drops terms in the brackets that are of order $mR(Z\alpha)^3$, $(mRZ\alpha)^2$ and $(Z\alpha)^4$.

Similarly, for the parity-odd case

$$\begin{aligned} \frac{f_-(R)}{g_-(R)} &= - \left(\frac{k}{m - W} \right) \frac{j_1(kR)}{j_0(kR)} = + \sqrt{\frac{W + m}{W - m}} \left[\frac{\sin(kR) - kR \cos(kR)}{kR \sin(kR)} \right] \\ &= \frac{(W + m)R}{3} \left[1 + \frac{(kR)^2}{15} + \frac{2(kR)^4}{315} + \dots \right], \end{aligned} \quad (\text{B.29})$$

and so again using the bound-state energy and the above approximate expressions we have

$$\begin{aligned} \sqrt{\frac{m - \omega}{m + \omega}} \left[\frac{f_-(R)}{g_-(R)} \right] &\simeq \left(\frac{Z\alpha}{2n} \right) \frac{1}{3} (2mR + Z\alpha) \left[1 + \frac{Z\alpha}{15} (2mR + Z\alpha) + \dots \right] \\ &\simeq \frac{1}{3n} (mRZ\alpha) + \frac{2}{45} (mRZ\alpha)^2 + \frac{(Z\alpha)^2}{6n} + \mathcal{O}[mR(Z\alpha)^3; (Z\alpha)^4]. \end{aligned} \quad (\text{B.30})$$

These imply $g_+/f_+ \simeq -\frac{1}{3}(W - m)R \simeq -\frac{1}{3}(Z\alpha)$ in the parity-even case for both the nonrelativistic and relativistic limits, while $f_-/g_- \simeq \frac{2}{3}mR$ in the nonrelativistic limit ($mR \gg Z\alpha$) while in the relativistic limit (for which $Z\alpha/R \gg \omega \simeq m$) we instead find $f_-/g_- \simeq \frac{1}{3}Z\alpha$.

Expansion coefficients. For comparison with the results for other charge distributions used in the main text it is useful to quote the above results in terms of parameters \hat{g}_i and \hat{f}_i appearing in the expansion

$$\left(\frac{g_+}{f_+}\right)_{r=R} = Z\alpha \left[\hat{g}_1 + \hat{g}_2(mRZ\alpha) + \hat{g}_3(Z\alpha)^2 + \dots \right], \quad (\text{B.31})$$

and

$$\sqrt{\frac{m-\omega}{m+\omega}} \left(\frac{f_-}{g_-}\right)_{r=R} = \frac{1}{2n} \left[\hat{f}_1(mRZ\alpha) + \hat{f}_2(mRZ\alpha)^2 + \hat{f}_3(Z\alpha)^2 + \dots \right]. \quad (\text{B.32})$$

With these definitions the above calculation shows that the charged shell predicts for the parity-even state we have

$$\hat{g}_1 = -\frac{1}{3}, \quad \hat{g}_2 = -\frac{2}{45} + \frac{1}{6n^2} \quad \text{and} \quad \hat{g}_3 = -\frac{1}{45}, \quad (\text{B.33})$$

while for the parity-odd state the parameters are

$$\hat{f}_1 = +\frac{2}{3}, \quad \hat{f}_2 = +\frac{2}{45} \quad \text{and} \quad \hat{f}_3 = +\frac{1}{3}. \quad (\text{B.34})$$

B.2.2 General charge distribution

Next, we evaluate the interior solution for a general distribution $\rho(r)$ for $r \leq R$ by evaluating as a series in kR . This is generally sufficient since $kR \simeq mRZ\alpha$ or $Z\alpha$ in the cases $mR \gg Z\alpha$ and $mR \ll Z\alpha$. The goal will be to determine f/g at $r = R$ as a function of the first few derivatives of ρ at $r = 0$.

To this end assume a charge distribution of the form

$$\rho = \rho(r) \quad \text{with} \quad \rho(R) = 0 \quad \text{for} \quad r \geq R, \quad (\text{B.35})$$

where R is the radius of the distribution and

$$4\pi \int_0^\infty dr r^2 \rho(r) = Ze. \quad (\text{B.36})$$

The corresponding electromagnetic potential satisfies $\mathbf{E} = -\nabla A^0$ and so $\nabla \cdot \mathbf{E} = -\nabla^2 A^0 = \rho$ and so

$$\nabla^2 A_0 = \frac{1}{r^2} \partial_r \left(r^2 \partial_r A_0 \right) = \rho \quad (\text{B.37})$$

and so

$$A^0 = \frac{Ze}{4\pi r} \quad \text{if} \quad r > R. \quad (\text{B.38})$$

For $r < R$ we use dimensionless variable $u = r/R$ so $A_0(u)$ satisfies

$$\frac{1}{u^2} \left(u^2 A_0' \right)' = R^2 \rho, \quad (\text{B.39})$$

and if we demand that ρ and A_0 must be analytic at $u = 0$ we may impose $\rho(-u) = \rho(u)$ (and similarly for $A_0(u)$) and so write (with a small abuse of notation)

$$\begin{aligned}\rho(u) &= \frac{3Ze}{4\pi R^3} \left[\rho_0 + \rho_2 u^2 + \rho_4 u^4 + \dots \right] \\ A_0(u) &= A_0(0) + A_2 u^2 + A_4 u^4 + \dots .\end{aligned}\tag{B.40}$$

Note that the coefficients ρ_{2k} are not completely independent of each other, since the charge density must satisfy $Ze = \int d^3x \rho(r)$, and so we must have

$$\frac{1}{3} = \sum_{k=0}^{\infty} \frac{\rho_{2k}}{2k+3}.\tag{B.41}$$

Inserting (B.40) into the Maxwell equation leads to

$$6A_2 + 20A_4 u^2 + \dots + k(k+1)A_k u^{k-2} + \dots = \frac{3Ze}{4\pi R} \left[\rho_0 + \rho_2 u^2 + \dots + \rho_k u^k + \dots \right],\tag{B.42}$$

and so

$$A_2 = \frac{Ze\rho_0}{8\pi R}, \quad A_4 = \frac{3Ze\rho_2}{80\pi R} \quad \text{and} \quad A_k = \frac{3Ze\rho_{k-2}}{4\pi k(k+1)R},\tag{B.43}$$

while continuity at $r = R$ demands

$$A_0(0) + A_2 + A_4 + \dots = -\frac{Ze}{4\pi R},\tag{B.44}$$

and so

$$\begin{aligned}eA_0(r) &= eA_0(0) + \frac{Z\alpha}{R} \left[\frac{\rho_0}{2} u^2 + \frac{3\rho_2}{20} u^4 + \dots + \frac{3\rho_{k-2}}{k(k+1)} u^k + \dots \right] \\ &= \frac{Z\alpha}{R} \left[-1 + \frac{\rho_0}{2} (u^2 - 1) + \frac{3\rho_2}{20} (u^4 - 1) + \dots + \frac{3\rho_{k-2}}{k(k+1)} (u^k - 1) + \dots \right],\end{aligned}\tag{B.45}$$

where $u = r/R$. These identify the parameters — i.e. $A_0(0)$, ρ_0 , ρ_2 and so on — that govern the leading form of the interior solutions to the Dirac equation.

We now solve the Dirac equation explicitly. The solution outside the shell sees only the Coulomb potential and so is the one given in earlier appendices. The solution inside the shell we solve in the presence of the above nonzero potential $A_0(u)$, perturbatively in u .

Parity-even states. For parity-even states the functions f_+ and g_+ satisfy (B.8), which reads

$$\partial_r f_+ = \left[m + \omega - eA_0(r) \right] g_+ \quad \text{and} \quad \partial_r g_+ + \frac{2g_+}{r} = \left[m - \omega + eA_0(r) \right] f_+,\tag{B.46}$$

so in terms of $u = r/R$ we find

$$\begin{aligned}f'_+ &= R \left[m + \omega - eA_0(u) \right] g_+ \\ &= \left\{ (m + \omega)R - eA_0(0)R - Z\alpha \left[\left(\frac{\rho_0}{2} \right) u^2 + \left(\frac{3\rho_2}{20} \right) u^4 + \dots \right] \right\} g_+,\end{aligned}\tag{B.47}$$

and

$$\begin{aligned} \left(g'_+ + \frac{2g_+}{u}\right) &= R[m - \omega + eA_0(u)]f_+ \\ &= \left\{ (m - \omega)R + eA_0(0)R + Z\alpha \left[\left(\frac{\rho_0}{2}\right)u^2 + \left(\frac{3\rho_2}{20}\right)u^4 + \dots \right] \right\} f_+. \end{aligned} \quad (\text{B.48})$$

Writing

$$\begin{aligned} f_+ &= f_0^+ + \frac{1}{2}f_2^+u^2 + \frac{1}{4}f_4^+u^4 + \dots \\ g_+ &= \mathfrak{g}_1^+u + \frac{1}{3}\mathfrak{g}_3^+u^3 + \frac{1}{5}\mathfrak{g}_5^+u^5 + \dots, \end{aligned} \quad (\text{B.49})$$

then (B.47) implies

$$\begin{aligned} f_2^+u + f_4^+u^3 + \dots &= \left\{ (m + \omega)R - eA_0(0)R - Z\alpha \left[\left(\frac{\rho_0}{2}\right)u^2 + \left(\frac{3\rho_2}{20}\right)u^4 + \dots \right] \right\} \\ &\quad \times \left[\mathfrak{g}_1^+u + \frac{1}{3}\mathfrak{g}_3^+u^3 + \dots \right], \end{aligned} \quad (\text{B.50})$$

and so

$$\begin{aligned} f_2^+ &= [(m + \omega)R - eA_0(0)R]\mathfrak{g}_1^+ = M_+\mathfrak{g}_1^+ \\ f_4^+ &= [(m + \omega)R - eA_0(0)R]\frac{\mathfrak{g}_3^+}{3} - \left(\frac{Z\alpha\rho_0}{2}\right)\mathfrak{g}_1^+ = \left(\frac{M_+}{3}\right)\mathfrak{g}_3^+ - \left(\frac{Z\alpha\rho_0}{2}\right)\mathfrak{g}_1^+ \\ f_6^+ &= [(m + \omega)R - eA_0(0)R]\frac{\mathfrak{g}_5^+}{5} - \frac{Z\alpha}{2}\left(\frac{\rho_0\mathfrak{g}_3^+}{3} + \frac{3\rho_2\mathfrak{g}_1^+}{10}\right), \end{aligned} \quad (\text{B.51})$$

and so on, where we define

$$M_{\pm} := [m \pm (\omega - eA_0(0))]R. \quad (\text{B.52})$$

Similarly (B.48) implies

$$\begin{aligned} 3\mathfrak{g}_1^+ + \frac{5}{3}\mathfrak{g}_3^+u^2 + \frac{7}{5}\mathfrak{g}_5^+u^4 + \dots &= \left\{ M_- + Z\alpha \left[\left(\frac{\rho_0}{2}\right)u^2 + \left(\frac{3\rho_2}{20}\right)u^4 + \dots \right] \right\} \\ &\quad \times \left[f_0^+ + \frac{1}{2}f_2^+u^2 + \dots \right] \end{aligned} \quad (\text{B.53})$$

and so

$$\begin{aligned} \mathfrak{g}_1^+ &= \left(\frac{M_-}{3}\right)f_0^+ \\ \mathfrak{g}_3^+ &= \frac{3}{10}(M_-f_2^+ + Z\alpha\rho_0f_0^+) \\ \mathfrak{g}_5^+ &= \frac{5}{7}\left[\left(\frac{M_-}{4}\right)f_4^+ + \left(\frac{Z\alpha\rho_0}{4}\right)f_2^+ + \left(\frac{3Z\alpha\rho_2}{20}\right)f_0^+\right], \end{aligned} \quad (\text{B.54})$$

and so on.

These equations fix all coefficients in terms of the unknown normalization f_0^+ as well as $A_0(0)$ and the ρ_i which are assumed to be known. The series for the solution at $r = R$ then takes the form

$$f_+(R) = f_0^+ \left[1 + \frac{f_2^+}{2f_0^+} + \frac{f_4^+}{4f_0^+} + \dots \right] \quad \text{and} \quad g_+(R) = f_0^+ \left[\frac{g_1^+}{f_0^+} + \frac{g_3^+}{3f_0^+} + \frac{g_5^+}{5f_0^+} + \dots \right], \quad (\text{B.55})$$

where

$$\begin{aligned} \frac{g_1^+}{f_0^+} &= \frac{M_-}{3} \\ \frac{f_2^+}{2f_0^+} &= M_+ \left(\frac{g_1^+}{2f_0^+} \right) = \frac{M_+ M_-}{6} = -\frac{1}{6} (k_0 R)^2 \\ \frac{g_3^+}{3f_0^+} &= \left(\frac{M_-}{5} \right) \frac{f_2^+}{2f_0^+} + \frac{Z\alpha \rho_0}{10} = \frac{Z\alpha \rho_0}{10} + \frac{M_+ M_-^2}{30} = \frac{Z\alpha \rho_0}{10} - \frac{M_-}{30} (k_0 R)^2 \\ \frac{f_4^+}{4f_0^+} &= \left(\frac{M_+}{12} \right) \frac{g_3^+}{f_0^+} - \left(\frac{Z\alpha \rho_0}{8} \right) \frac{g_1^+}{f_0^+} = \frac{Z\alpha \rho_0}{8} \left(\frac{M_+}{5} - \frac{M_-}{3} \right) + \frac{(k_0 R)^4}{120} \\ \frac{g_5^+}{5f_0^+} &= \left(\frac{M_-}{7} \right) \frac{f_4^+}{4f_0^+} + \left(\frac{Z\alpha \rho_0}{14} \right) \frac{f_2^+}{2f_0^+} + \frac{3Z\alpha \rho_2}{140} \\ &= -\frac{Z\alpha \rho_0 M_-^2}{168} + \frac{M_-}{840} (k_0 R)^4 - \frac{13Z\alpha \rho_0}{840} (k_0 R)^2 + \frac{3Z\alpha \rho_2}{140} \\ \frac{f_6^+}{6f_0^+} &= \left(\frac{M_+}{6} \right) \frac{g_5^+}{5f_0^+} - \left(\frac{Z\alpha \rho_0}{12} \right) \frac{g_3^+}{3f_0^+} + \left(\frac{Z\alpha \rho_2}{40} \right) \frac{g_1^+}{f_0^+} \\ &= \frac{Z\alpha \rho_2}{40} \left(\frac{M_+}{7} + \frac{M_-}{3} \right) - \frac{(Z\alpha \rho_0)^2}{120} + \frac{Z\alpha \rho_0}{5040} (k_0 R)^2 (19M_- - 13M_+) - \frac{(k_0 R)^6}{5040} \end{aligned} \quad (\text{B.56})$$

and so on. These last equalities define

$$k_0^2 := \left[\omega - eA_0(0) \right]^2 - m^2 \quad \text{so that} \quad (k_0 R)^2 = -M_+ M_-, \quad (\text{B.57})$$

and because $M_- \sim \mathcal{O}(Z\alpha)$ and $M_+ \sim \mathcal{O}[mR + Z\alpha]$ we see that the expansion is controlled by powers of $mRZ\alpha$ and $(Z\alpha)^2$.

The boundary condition of interest in this case is $g_+(R)/f_+(R)$ which is given by

$$\begin{aligned} \left(\frac{g_+}{f_+} \right)_{r=R} &= \frac{g_1^+ + \frac{1}{3}g_3^+ + \frac{1}{5}g_5^+ + \dots}{f_0^+ + \frac{1}{2}f_2^+ + \frac{1}{4}f_4^+ + \dots} \\ &\simeq \left[\frac{g_1^+}{f_0^+} + \frac{g_3^+}{3f_0^+} + \frac{g_5^+}{5f_0^+} + \dots \right] \left[1 - \left(\frac{f_2^+}{2f_0^+} + \frac{f_4^+}{4f_0^+} + \frac{f_6^+}{6f_0^+} + \dots \right) + \dots \right]. \end{aligned} \quad (\text{B.58})$$

Consequently

$$\begin{aligned} \left(\frac{g_+}{f_+} \right)_{r=R} &= \left\{ \frac{M_-}{3} \left[1 - \frac{(k_0 R)^2}{10} \right] + \frac{Z\alpha \rho_0}{10} \left[1 - \frac{5M_-^2}{84} - \frac{13(k_0 R)^2}{84} \right] \right. \\ &\quad \left. + \frac{3Z\alpha \rho_2}{140} [1 + \dots] + \dots \right\} \end{aligned}$$

$$\begin{aligned}
 & \times \left\{ 1 + \frac{1}{6}(k_0 R)^2 + \frac{Z\alpha \rho_0}{8} \left(\frac{M_-}{3} - \frac{M_+}{5} \right) - \frac{Z\alpha \rho_2}{40} \left(\frac{M_+}{7} + \frac{M_-}{3} \right) \right. \\
 & \quad \left. + \frac{(Z\alpha \rho_0)^2}{120} + \dots \right\} \\
 & = \frac{M_-}{3} \left[1 + \frac{(k_0 R)^2}{15} \right] + \frac{Z\alpha \rho_0}{10} \left[1 + \frac{5M_-^2}{63} + \frac{2(k_0 R)^2}{21} \right] + \frac{(Z\alpha \rho_0)^2}{8} \left(\frac{M_-}{18} - \frac{M_+}{50} \right) \\
 & \quad + Z\alpha \rho_2 \left[1 + \dots \right] + \dots . \tag{B.59}
 \end{aligned}$$

where $(k_0 R)^2 = -M_+ M_-$ with $M_- \sim \mathcal{O}(Z\alpha)$ and $M_+ \sim \mathcal{O}[mR + Z\alpha]$ and drop any terms that are suppressed by more than just $mRZ\alpha$ or $(Z\alpha)^2$ relative to the leading term.

Notice in particular that higher coefficients ρ_i enter suppressed only by $Z\alpha$. We now show that these terms of order $Z\alpha$ sum to give the result required to have the energy shift be controlled by the mean-square charge distribution

$$r_p^2 := \frac{1}{Ze} \int d^3x r^2 \rho(x) = 3R^2 \sum_{k=0}^{\infty} \frac{\rho_{2k}}{2k+5}. \tag{B.60}$$

To see if this is so we track these terms explicitly using

$$\frac{\mathbf{g}_k^+}{k\mathbf{f}_0^+} = \frac{3Z\alpha \rho_{k-3}}{k(k-1)(k+2)} + (\text{other terms}) \quad \text{for } k = 3, 5, 7, \dots \tag{B.61}$$

The leading contribution to g_+/f_+ then is

$$\begin{aligned}
 \frac{g_+}{f_+} & = \frac{M_-}{3} + Z\alpha \sum_{k=0}^{\infty} \frac{3\rho_{2k}}{(2k+2)(2k+3)(2k+5)} + \dots \\
 & = \frac{eA_0(0)R}{3} + Z\alpha \sum_{k=0}^{\infty} \frac{3\rho_{2k}}{(2k+2)(2k+3)(2k+5)} + \dots \tag{B.62}
 \end{aligned}$$

so using

$$eA_0(0)R = -Z\alpha \left[1 + \sum_{k=0}^{\infty} \frac{3\rho_{2k}}{(2k+2)(2k+3)} \right], \tag{B.63}$$

we have

$$\begin{aligned}
 \frac{g_+}{f_+} & = Z\alpha \left[-\frac{1}{3} + \sum_{k=0}^{\infty} \left(\frac{3\rho_{2k}}{(2k+2)(2k+3)(2k+5)} - \frac{\rho_{2k}}{(2k+2)(2k+3)} \right) \right] + \dots \\
 & = Z\alpha \left[-\frac{1}{3} - \sum_{k=0}^{\infty} \frac{\rho_{2k}}{(2k+3)(2k+5)} \right] + \dots \tag{B.64}
 \end{aligned}$$

This contributes to the effective coupling h_{eff}^+ the amount

$$\begin{aligned}
 h_{\text{eff}}^+ & \approx 2\pi Z\alpha R^2 \left\{ 1 + \frac{2}{Z\alpha} \left(\frac{g_+}{f_+} \right) \right\} = 2\pi Z\alpha R^2 \left\{ \frac{1}{3} - 2 \sum_{k=0}^{\infty} \frac{\rho_{2k}}{(2k+3)(2k+5)} \right\} \\
 & = 2\pi Z\alpha R^2 \sum_{k=0}^{\infty} \frac{\rho_{2k}}{2k+3} \left\{ 1 - \frac{2}{2k+5} \right\} = 2\pi Z\alpha R^2 \sum_{k=0}^{\infty} \frac{\rho_{2k}}{2k+5} \tag{B.65} \\
 & = \frac{2\pi}{3} Z\alpha r_p^2.
 \end{aligned}$$

Parity-odd states. For parity-odd states the functions f_- and g_- satisfy (B.9), which reads

$$\partial_r g_- = \left[m - \omega + eA_0(r) \right] f_- \quad \text{and} \quad \partial_r f_- + \frac{2f_-}{r} = \left[m + \omega - eA_0(r) \right] g_-, \quad (\text{B.66})$$

which has the same form as did the parity-even case if we make the replacements $f_+ \leftrightarrow g_-$, $f_- \leftrightarrow g_+$ and $\omega - eA_0 \leftrightarrow -(\omega - eA_0)$. This implies the solutions have the same form with $\mathfrak{g}_i^\pm \leftrightarrow \mathfrak{f}_i^\mp$ as well as $M_+ \leftrightarrow M_-$ and $\rho_i \leftrightarrow -\rho_i$.

Consequently for parity-odd states we have

$$\begin{aligned} \left(\frac{f_-}{g_-} \right)_{r=R} &= \frac{\mathfrak{f}_1^- + \frac{1}{3}\mathfrak{f}_3^- + \frac{1}{5}\mathfrak{f}_5^- + \dots}{\mathfrak{g}_0^- + \frac{1}{2}\mathfrak{g}_2^- + \frac{1}{4}\mathfrak{g}_4^- + \dots} \\ &\simeq \left[\frac{\mathfrak{f}_1^-}{\mathfrak{g}_0^-} + \frac{\mathfrak{f}_3^-}{3\mathfrak{g}_0^-} + \frac{\mathfrak{f}_5^-}{5\mathfrak{g}_0^-} + \dots \right] \left[1 - \left(\frac{\mathfrak{g}_2^-}{2\mathfrak{g}_0^-} + \frac{\mathfrak{g}_4^-}{4\mathfrak{g}_0^-} + \dots \right) + \dots \right] \\ &= \frac{M_+}{3} \left[1 + \frac{(k_0 R)^2}{15} \right] - \frac{Z\alpha \rho_0}{10} \left[1 + \frac{5M_+^2}{63} + \frac{2(k_0 R)^2}{21} \right] + \frac{(Z\alpha \rho_0)^2}{8} \left(\frac{M_+}{18} - \frac{M_-}{50} \right) \\ &\quad - Z\alpha \rho_2 \left[1 + \dots \right] + \dots \end{aligned} \quad (\text{B.67})$$

B.2.3 Uniform charge distribution

A special case of the previous section is the case of a constant charge distribution

$$\rho = \frac{3Ze}{4\pi R^3} \quad \text{for } r \leq R, \quad (\text{B.68})$$

and so represents the special case $\rho_0 = 1$ and $\rho_k = 0$ for all $k \neq 0$. For this distribution the rms radius and the moment $\langle r^3 \rangle_{(2)}$ are given explicitly by

$$r_p^2 = \frac{1}{Ze} \int d^3x r^2 \rho(x) = \frac{3}{R^3} \int_0^R dr r^4 = \frac{3R^2}{5}, \quad (\text{B.69})$$

and

$$\begin{aligned} \langle r^3 \rangle_{(2)} &= \frac{1}{(Ze)^2} \int d^3x d^3y |\mathbf{x}|^3 \rho(\mathbf{y} - \mathbf{x}) \rho(\mathbf{y}) = \frac{1}{(Ze)^2} \int d^3z d^3y |\mathbf{z} + \mathbf{y}|^3 \rho(\mathbf{z}) \rho(\mathbf{y}) \\ &= \frac{1}{2} \left(\frac{3}{R^3} \right)^2 \int_0^R dz \int_0^R dy \int_{-1}^1 d \cos \theta y^2 z^2 (y^2 + z^2 + 2yz \cos \theta)^{3/2} \\ &= \frac{1}{10} \left(\frac{3}{r^3} \right)^2 \int_0^R dz \int_0^R dy yz (|y+z|^5 - |y-z|^5) \\ &= \frac{1}{5} \left(\frac{3}{r^3} \right)^2 \int_0^R dz z \left\{ \int_0^z dy [5y^2 z^4 + 10y^4 z^2 + y^6] + \int_z^R dy [5y^5 z + 10y^3 z^3 + yz^5] \right\} \\ &= \frac{1}{5} \left(\frac{3}{r^3} \right)^2 \int_0^R dz z \left[-\frac{1}{42} z^8 + \frac{1}{2} R^2 z^6 + \frac{5}{2} R^4 z^4 + \frac{5}{6} R^6 z^2 \right] = \frac{32}{21} R^3. \end{aligned} \quad (\text{B.70})$$

The electrostatic potential coefficients for this charge distribution are

$$A_2 = \frac{Ze}{8\pi R} \quad \text{and} \quad A_k = 0 \quad \text{for } k > 2, \quad (\text{B.71})$$

and so in the continuity condition this gives

$$A_0(0) + A_2 = -\frac{Ze}{4\pi R} \quad \text{and so} \quad eA_0(0) = -\frac{3Z\alpha}{2R}. \quad (\text{B.72})$$

The complete electrostatic potential therefore is

$$eA_0(r) = \frac{Z\alpha}{R} \left[-1 + \frac{1}{2}(u^2 - 1) \right], \quad (\text{B.73})$$

where $u = r/R$. Consequently

$$M_{\pm} = mR \pm \left(\omega R + \frac{3Z\alpha}{2} \right) = (m \pm W)R \pm \frac{Z\alpha}{2}, \quad (\text{B.74})$$

and so

$$(k_0R)^2 = -M_+M_- = \left(WR + \frac{Z\alpha}{2} \right)^2 - (mR)^2. \quad (\text{B.75})$$

Finally, evaluating at bound-state energies $\omega \simeq m \left[1 - \frac{1}{2}(Z\alpha/n)^2 + \dots \right]$, we have $M_- \simeq -\frac{3}{2}Z\alpha + \frac{1}{2}mR(Z\alpha/n)^2 + \mathcal{O}[mR(Z\alpha)^4]$ and $M_+ \simeq \frac{3}{2}Z\alpha + 2mR \left[1 - (Z\alpha/2n)^2 + \mathcal{O}[(Z\alpha)^4] \right]$ so their product is $(k_0R)^2 = -M_+M_- \simeq \frac{9}{4}(Z\alpha)^2 + 3mRZ\alpha \left[1 + \mathcal{O}[(Z\alpha)^2] \right]$. The boundary condition therefore becomes

$$\begin{aligned} \left(\frac{g_+}{f_+} \right)_{r=R} &= \frac{M_-}{3} \left[1 + \frac{(k_0R)^2}{15} \right] + \frac{Z\alpha}{10} \left[1 + \frac{5M_-^2}{63} + \frac{2(k_0R)^2}{21} \right] + \frac{(Z\alpha)^2}{8} \left(\frac{M_-}{18} - \frac{M_+}{50} \right) \dots \\ &= -Z\alpha \left[\frac{2}{5} + \left(\frac{116}{1575} - \frac{1}{6n^2} \right) mRZ\alpha + \frac{736}{17325}(Z\alpha)^2 + \dots \right]. \end{aligned} \quad (\text{B.76})$$

Similarly, the parity-odd expression is

$$\begin{aligned} \left(\frac{f_-}{g_-} \right)_{r=R} &= \frac{M_+}{3} \left[1 + \frac{(k_0R)^2}{15} \right] - \frac{Z\alpha \rho_0}{10} \left[1 + \frac{5M_+^2}{63} + \frac{2(k_0R)^2}{21} \right] \\ &\quad + \frac{(Z\alpha \rho_0)^2}{8} \left(\frac{M_+}{18} - \frac{M_-}{50} \right) + \dots \\ &= \frac{2mR}{3} + \frac{2Z\alpha}{5} + \dots \end{aligned} \quad (\text{B.77})$$

Expansion coefficients. For comparison, in terms of the parameters \hat{g}_i and \hat{f}_i found in

$$\left(\frac{g_+}{f_+} \right)_{r=R} = Z\alpha \left[\hat{g}_1 + \hat{g}_2(mRZ\alpha) + \hat{g}_3(Z\alpha)^2 + \dots \right], \quad (\text{B.78})$$

and

$$\sqrt{\frac{m-\omega}{m+\omega}} \left(\frac{f_-}{g_-} \right)_{r=R} = \frac{1}{2n} \left[\hat{f}_1(mRZ\alpha) + \hat{f}_2(mRZ\alpha)^2 + \hat{f}_3(Z\alpha)^2 + \dots \right], \quad (\text{B.79})$$

we have

$$\hat{g}_1 = -\frac{2}{5}, \quad \hat{g}_2 = -\frac{116}{1575} + \frac{1}{6n^2} \quad \text{and} \quad \hat{g}_3 = -\frac{736}{17325}, \quad (\text{B.80})$$

while for the parity-odd state the parameters are

$$\hat{f}_1 = \frac{2}{3}, \quad \hat{f}_2 = +\frac{32}{315} \quad \text{and} \quad \hat{f}_3 = +\frac{2}{5}. \quad (\text{B.81})$$

Open Access. This article is distributed under the terms of the Creative Commons Attribution License ([CC-BY 4.0](https://creativecommons.org/licenses/by/4.0/)), which permits any use, distribution and reproduction in any medium, provided the original author(s) and source are credited.

References

- [1] S. Weinberg, *Phenomenological lagrangians*, *Physica A* **96** (1979) 327 [[INSPIRE](#)].
- [2] H. Georgi, *Effective field theory*, *Ann. Rev. Nucl. Part. Sci.* **43** (1993) 209 [[INSPIRE](#)].
- [3] C.P. Burgess, *Introduction to effective field theory*, *Ann. Rev. Nucl. Part. Sci.* **57** (2007) 329 [[hep-th/0701053](#)] [[INSPIRE](#)].
- [4] C.P. Burgess, *Quantum gravity in everyday life: general relativity as an effective field theory*, *Living Rev. Rel.* **7** (2004) 5 [[gr-qc/0311082](#)] [[INSPIRE](#)].
- [5] C.P. Burgess, P. Hayman, M. Williams and L. Zalavari, *Point-particle effective field theory I: classical renormalization and the inverse-square potential*, *JHEP* **04** (2017) 106 [[arXiv:1612.07313](#)] [[INSPIRE](#)].
- [6] C.P. Burgess, P. Hayman, M. Rummel, M. Williams and L. Zalavari, *Point-particle effective field theory II: relativistic effects and Coulomb/inverse-square competition*, *JHEP* **07** (2017) 072 [[arXiv:1612.07334](#)] [[INSPIRE](#)].
- [7] W.D. Goldberger and I.Z. Rothstein, *An effective field theory of gravity for extended objects*, *Phys. Rev. D* **73** (2006) 104029 [[hep-th/0409156](#)] [[INSPIRE](#)].
- [8] C.P. Burgess, D. Hoover, C. de Rham and G. Tasinato, *Effective field theories and matching for codimension-2 branes*, *JHEP* **03** (2009) 124 [[arXiv:0812.3820](#)] [[INSPIRE](#)].
- [9] A. Bayntun, C.P. Burgess and L. van Nierop, *Codimension-2 brane-bulk matching: examples from six and ten dimensions*, *New J. Phys.* **12** (2010) 075015 [[arXiv:0912.3039](#)] [[INSPIRE](#)].
- [10] F. Niedermann and R. Schneider, *Fine-tuning with brane-localized flux in 6D supergravity*, *JHEP* **02** (2016) 025 [[arXiv:1508.01124](#)] [[INSPIRE](#)].
- [11] C.P. Burgess, R. Diener and M. Williams, *EFT for vortices with dilaton-dependent localized flux*, *JHEP* **11** (2015) 054 [[arXiv:1508.00856](#)] [[INSPIRE](#)].
- [12] C.P. Burgess, R. Diener and M. Williams, *The gravity of dark vortices: effective field theory for branes and strings carrying localized flux*, *JHEP* **11** (2015) 049 [[arXiv:1506.08095](#)] [[INSPIRE](#)].
- [13] W.E. Caswell and G.P. Lepage, *Effective lagrangians for bound state problems in QED, QCD, and other field theories*, *Phys. Lett. B* **167** (1986) 437.
- [14] G.T. Bodwin, E. Braaten and G.P. Lepage, *Rigorous QCD analysis of inclusive annihilation and production of heavy quarkonium*, *Phys. Rev. D* **51** (1995) 1125 [*Erratum ibid.* **D 55** (1997) 5853] [[hep-ph/9407339](#)] [[INSPIRE](#)].
- [15] S. Weinberg, *Nuclear forces from chiral Lagrangians*, *Phys. Lett. B* **251** (1990) 288 [[INSPIRE](#)].
- [16] D.B. Kaplan, M.J. Savage and M.B. Wise, *Nucleon-nucleon scattering from effective field theory*, *Nucl. Phys. B* **478** (1996) 629 [[nucl-th/9605002](#)] [[INSPIRE](#)].
- [17] T. Mehen and I.W. Stewart, *A momentum subtraction scheme for two nucleon effective field theory*, *Phys. Lett. B* **445** (1999) 378 [[nucl-th/9809071](#)] [[INSPIRE](#)].

- [18] A.V. Manohar and I.W. Stewart, *Renormalization group analysis of the QCD quark potential to order v^2* , *Phys. Rev. D* **62** (2000) 014033 [[hep-ph/9912226](#)] [[INSPIRE](#)].
- [19] E. Braaten and H.W. Hammer, *Universality in few-body systems with large scattering length*, *Phys. Rept.* **428** (2006) 259 [[cond-mat/0410417](#)] [[INSPIRE](#)].
- [20] D.M. Jacobs, *An artificial boundary approach for short-ranged interactions*, *J. Phys. A* **49** (2016) 295203 [[arXiv:1511.03954](#)] [[INSPIRE](#)].
- [21] G. Allwright and D.M. Jacobs, *Robin boundary conditions are generic in quantum mechanics*, [arXiv:1610.09581](#).
- [22] A.M. Essin and D.J. Griffiths, , *Am. J. Phys.* **74** (2006) 109.
- [23] A.C. Zemach, *Proton structure and the hyperfine shift in hydrogen*, *Phys. Rev.* **104** (1956) 1771 [[INSPIRE](#)].
- [24] J.L. Friar, *Nuclear finite size effects in light muonic atoms*, *Annals Phys.* **122** (1979) 151 [[INSPIRE](#)].
- [25] F. Hagelstein and V. Pascalutsa, *Breakdown of the expansion of finite-size corrections to the hydrogen Lamb shift in moments of charge distribution*, *Phys. Rev. A* **91** (2015) 040502.
- [26] J.L. Friar and J.W. Negele, *Theoretical and experimental determination of nuclear charge distributions*, *Adv. Nucl Phys.* **8** (1975) 219.
- [27] E. Borie and G.A. Rinker, *The energy levels of muonic atoms*, *Rev. Mod. Phys.* **54** (1982) 67.
- [28] K. Pachucki, *Theory of the Lamb shift in muonic hydrogen*, *Phys. Rev. A* **53** (1996) 4.
- [29] K. Pachucki, *Proton structure effects in muonic hydrogen*, *Phys. Rev. A* **60** (1999) 3593.
- [30] D. Andrae, *Finite nuclear charge distributions in electronic structure calculations for atoms and molecules*, *Phys. Rept.* **336** (2000) 413.
- [31] E. Borie, *Lamb shift in muonic hydrogen*, *Phys. Rev. A* **71** (2005) 032508 [[physics/0410051](#)] [[INSPIRE](#)].
- [32] M.O. Distler, J.C. Bernauer and T. Walcher, *The RMS charge radius of the proton and Zemach moments*, *Phys. Lett. B* **969** (2011) 343.
- [33] C.E. Carlson and M. Vanderhaeghen, *Higher-order proton structure corrections to the Lamb shift in muonic hydrogen*, *Phys. Rev. A* **84** (2011) 020102.
- [34] A. Antognini et al., *Theory of the 2S-2P Lamb shift and 2S hyperfine splitting in muonic hydrogen*, *Ann. Phys.* **331** (2013) 127.
- [35] U.D. Jentschura, *Lamb shift in muonic hydrogen. I. Verification and update of theoretical predictions*, *Ann. Phys.* **326** (2011) 500.
- [36] T.P. Gorringe and D.W. Hertzog, *Precision muon physics*, *Prog. Part. Nucl. Phys.* **84** (2015) 73 [[arXiv:1506.01465](#)] [[INSPIRE](#)].
- [37] M.I. Eides, H. Grotch and V.A. Shelyuto, *Theory of light hydrogen-like atoms*, *Phys. Rept.* **342** (2001) 63 [[hep-ph/0002158](#)] [[INSPIRE](#)].
- [38] R. Pohl, R. Gilman, G.A. Miller and K. Pachucki, *Muonic hydrogen and the proton radius puzzle*, *Ann. Rev. Nucl. Part. Sci.* **63** (2013) 175 [[arXiv:1301.0905](#)] [[INSPIRE](#)].
- [39] C.E. Carlson, *The proton radius puzzle*, *Prog. Part. Nucl. Phys.* **82** (2015) 59 [[arXiv:1502.05314](#)] [[INSPIRE](#)].

- [40] R. Pohl et al., *The size of the proton*, *Nature* **466** (2010) 213 [INSPIRE].
- [41] A. Pineda, *The chiral structure of the Lamb shift and the definition of the proton radius*, *Phys. Rev. C* **71** (2005) 065205 [hep-ph/0412142] [INSPIRE].
- [42] R.J. Hill and G. Paz, *Model independent analysis of proton structure for hydrogenic bound states*, *Phys. Rev. Lett.* **107** (2011) 160402.
- [43] C. Peset and A. Pineda, *Model-independent determination of the Lamb shift in muonic hydrogen and the proton radius*, *Eur. Phys. J. A* **51** (2015) 32 [arXiv:1403.3408] [INSPIRE].
- [44] C. Peset and A. Pineda, *The Lamb shift in muonic hydrogen and the proton radius from effective field theories*, *Eur. Phys. J. A* **51** (2015) 156 [arXiv:1508.01948] [INSPIRE].
- [45] T. Liu, A.A. Penin and A. Rayyan, *Coulomb artifacts and bottomonium hyperfine splitting in lattice NRQCD*, *JHEP* **02** (2017) 084 [arXiv:1609.07151] [INSPIRE].
- [46] W.D. Goldberger and M.B. Wise, *Renormalization group flows for brane couplings*, *Phys. Rev. D* **65** (2002) 025011 [hep-th/0104170] [INSPIRE].
- [47] C. de Rham, *Classical renormalization of codimension-two brane couplings*, *AIP Conf. Proc.* **957** (2007) 309 [arXiv:0710.4598] [INSPIRE].
- [48] E. Dudas, C. Papineau and V.A. Rubakov, *Flowing to four dimensions*, *JHEP* **03** (2006) 085 [hep-th/0512276] [INSPIRE].
- [49] C.P. Burgess, C. de Rham and L. van Nierop, *The hierarchy problem and the self-localized Higgs*, *JHEP* **08** (2008) 061 [arXiv:0802.4221] [INSPIRE].
- [50] R. Diener and C.P. Burgess, *Bulk stabilization, the extra-dimensional Higgs portal and missing energy in Higgs events*, *JHEP* **05** (2013) 078 [arXiv:1302.6486] [INSPIRE].
- [51] B. Nickel, *Nuclear size effects on hydrogenic atom energies: a semi-analytic formulation*, *J. Phys. B* **46** (2013) 015001.
- [52] R.T. Deck, J.G. Amar and G. Fralick, *Nuclear size corrections to the energy levels of single-electron and -muon atoms*, *J. Phys. B* **38** (2005) 2173.
- [53] R.J. Hill and G. Paz, *Model independent extraction of the proton charge radius from electron scattering*, *Phys. Rev. D* **82** (2010) 113005 [arXiv:1008.4619] [INSPIRE].
- [54] E.A. Uehling, *Polarization effects in the positron theory*, *Phys. Rev.* **48** (1935) 55 [INSPIRE].
- [55] W. Pauli and M.E. Rose, *Remarks on the polarization effects in the positron theory*, *Phys. Rev.* **49** (1936) 462 [INSPIRE].
- [56] E.H. Wichmann and N.M. Kroll, *Vacuum polarization in a strong Coulomb field*, *Phys. Rev.* **101** (1956) 843 [INSPIRE].
- [57] A.M. Frolov, *On the interaction between two point electric charges*, arXiv:1111.2303 [INSPIRE].
- [58] S. Deser, M.L. Goldberger, K. Baumann and W.E. Thirring, *Energy level displacements in π mesonic atoms*, *Phys. Rev.* **96** (1954) 774 [INSPIRE].
- [59] E. Klempt, F. Bradamante, A. Martin and J.M. Richard, *Antinucleon nucleon interaction at low energy: scattering and protonium*, *Phys. Rept.* **368** (2002) 119 [INSPIRE].
- [60] ATHENA collaboration, N. Zurlo et al., *Evidence for the production of slow antiprotonic hydrogen in vacuum*, *Phys. Rev. Lett.* **97** (2006) 153401 [arXiv:0708.3717] [INSPIRE].

- [61] C.J. Batty, *Antiprotonic-hydrogen atoms*, *Rep. Prog. Phys.* **52** (1989) 1165.
- [62] D. Tucker-Smith and I. Yavin, *Muonic hydrogen and MeV forces*, *Phys. Rev. D* **83** (2011) 101702 [[arXiv:1011.4922](#)] [[INSPIRE](#)].
- [63] V. Barger, C.-W. Chiang, W.-Y. Keung and D. Marfatia, *Proton size anomaly*, *Phys. Rev. Lett.* **106** (2011) 153001 [[arXiv:1011.3519](#)] [[INSPIRE](#)].
- [64] B. Batell, D. McKeen and M. Pospelov, *New parity-violating muonic forces and the proton charge radius*, *Phys. Rev. Lett.* **107** (2011) 011803 [[arXiv:1103.0721](#)] [[INSPIRE](#)].
- [65] J.D. Carroll, A.W. Thomas, J. Rafelski and G.A. Miller, *Non-perturbative relativistic calculation of the muonic hydrogen spectrum*, *Phys. Rev. A* **84** (2011) 012506 [[arXiv:1104.2971](#)] [[INSPIRE](#)].
- [66] C.G. Parthey et al., *Improved measurement of the Hydrogen 1S-2S transition frequency*, *Phys. Rev. Lett.* **107** (2011) 203001 [[arXiv:1107.3101](#)] [[INSPIRE](#)].

Chapter 3

Subleading Finite-Size Effects of Scalar Nuclei

Paper presented

C. P. Burgess, P. Hayman, Markus Rummel, and László Zalavári

“Reduced theoretical error in ^4He spectroscopy”

Phys. Rev. A **98**, 052510 (2018).

doi: 10.1103/PhysRevA.98.052510

Copyright 2018 by the American Physical Society

Summary

This paper builds on the PPEFT of atoms with scalar nuclei developed in Section 1.4 and used to capture the leading finite-size effects of the nucleus on leptonic bound-states in the paper presented in Chapter 2. It expands the PPEFT action to one higher order in the small ratio, $R/a_B \sim (mRZ\alpha)$, thereby capturing all interactions between the centre-of-mass coordinates of the nucleus and the bulk fields that obey the atomic symmetries and come with effective couplings of dimension, $(length)^3$.

This inclusion allows us to investigate the finite-size effects of the nucleus on the fermionic bound-states to relative order $(mRZ\alpha)$ and $(Z\alpha)^2$ with respect to that of the leading term explored in the previous chapter. In terms of the nuclear structure corrections of the literature presented in (1.104) and (1.102) this corresponds to being able to capture the Friar-moment, nuclear polarizability and relativistic corrections to the charge-radius term. The phenomenological importance of this expansion is that it enables us to take into account all nuclear-size related energy shifts necessary to match the current experimental precision in both electronic and muonic $^4\text{He}^+$.

The new terms in the action involve derivatives of the lepton fields and

in order to get a sensible low-energy limit we extract the rapidly oscillating mass term from the energy eigenstates, which allows us to write down a controlled low-energy PPEFT action. Following this, we examine the alternative near-source boundary conditions of fermions implied by this updated nuclear action and analyze the running of the effective couplings in the small parameter, ϵ – the radius of the Gaussian sphere on which the new boundary conditions had been set up – required to keep observables such as the energy shift independent of this fictitious parameter. We find that the RG-flow of the higher-order couplings is controlled by the same RG-invariant parameters, $\{\epsilon_\star, y_\star\}$ as that of the leading-order ones, where ϵ_\star is a length-scale where the appropriate combinations of PPEFT couplings either blows up or vanishes, depending on the value of $y_\star = \pm$. In this way, y_\star distinguishes between two types of flows, while ϵ_\star picks out a specific curve among those that share the same value of y_\star . Now, since there is no new RG-invariant parameter in the running of the new couplings, these equations simply help us determine the existing ones to a higher accuracy.

Committing to writing all energy shift formulae in terms of RG-invariant parameters, we use the running equations to determine the ratio of integration constants, $\mathcal{D}_{j\varpi}/\mathcal{C}_{j\varpi}$ in terms of these quantities. During this analysis, we make contact with the effective moments \hat{g}_i, \hat{f}_i that we have used as proxies for capturing the subleading nuclear-size effects in the previous paper, and write them as ϵ -dependent functions of the RG-invariants. Substituting these functions into the energy shift formulae of Chapter 2 that captured subleading effects we find that the energy shift to this improved accuracy depends purely on ϵ_\star and y_\star .

Comparing energy shift formulae as written in terms of our RG-invariants with those written in terms of nuclear moments from the literature reveals that in order for ϵ_\star to be interpreted as a length-scale we must have $y_\star = +1$ and it also allows us to infer what combination of nuclear moments ϵ_\star corresponds to at the given accuracy.


Finally, using our RG-invariant-dependent energy shift expressions we devise linear combinations of spectroscopic measurements in atomic and muonic Hydrogen-like atoms with scalar nuclei from which the finite-size effects cancel to the accuracy we work. Additionally, we also detail the procedure for fitting ϵ_\star as a function of the difference between an experimentally measured transition and its corresponding energy shift associated with theoretical bound-state QED contributions that assume a point-like nucleus. We then describe how this value can be used to make predictions for the nuclear-size effects of other spectroscopic transitions.

Through the PPEFT formalism then, we can see that finite-size effects in leptonic bound-state energies to subleading $(mRZ\alpha)$ and $(Z\alpha)^2$ orders relative to the charge-radius squared term are captured by a single parameter instead of the numerous nuclear moments used in the literature. This allows us to make predictions for energy shifts in which the uncertainty associated with nuclear-size effects are minimized because they are controlled only by the smallest experimental and point-nucleus theoretical

errors, which will certainly improve with time.

Reduced theoretical error for ${}^4\text{He}^+$ spectroscopy

C. P. Burgess,^{*} P. Hayman,[†] Markus Rummel,[‡] and László Zalavári[§]
Physics & Astronomy, McMaster University, Hamilton, Ontario, Canada L8S 4M1
and Perimeter Institute for Theoretical Physics, Waterloo, Ontario, Canada N2L 2Y5

 (Received 19 September 2017; revised manuscript received 17 September 2018; published 19 November 2018)

We apply point-particle effective field theory to electronic and muonic ${}^4\text{He}^+$ ions, and use it to identify linear combinations of spectroscopic measurements for which the theoretical uncertainties are much smaller than for any particular energy levels. The error is reduced because these combinations are independent of all short-range physics effects up to a given order in the expansion in the small parameters R/a_B and $Z\alpha$ (where R and a_B are the ion's nuclear and Bohr radii). In particular, the theory error is not limited by the precision with which nuclear matrix elements can be computed, or compromised, by the existence of any novel short-range interactions, should these exist. These combinations of ${}^4\text{He}$ measurements therefore provide particularly precise tests of quantum electrodynamics. The restriction to ${}^4\text{He}$ arises because our analysis assumes a spherically symmetric nucleus, but the argument used is more general and extendable to both nuclei with spin, and to higher orders in R/a_B and $Z\alpha$.

DOI: [10.1103/PhysRevA.98.052510](https://doi.org/10.1103/PhysRevA.98.052510)

I. INTRODUCTION

Atomic systems have historically been an important testing ground for quantum electrodynamics (QED), even providing one of the very first observations of a relativistic quantum effect with the Lamb shift [1]. Muonic atoms have further proved an excellent means of honing our understanding of QED by contrasting with electronic measurements. For muonic atoms, the leading QED radiative correction is due to electron-loop vacuum polarization [2] in contrast to the electron's leading self-energy correction, and finite-size effects are enhanced by a factor $(m_\mu/m_e)^3 \sim 8 \times 10^6$. Indeed, experiments in the 1970's found a discrepancy between theoretical and measured values for certain transitions in heavy muonic atoms [3,4]. This motivated much research, and after a few years improvements in the theory [5–8] and in experiments [9,10] resolved the discrepancy and improved our understanding of QED [11]. Today, a very similar situation can be found in the “proton-radius” problem [12], wherein the root-mean-squared charge radius inferred from the leading nuclear contributions to atomic energy shifts in hydrogen and muonic hydrogen appears to depend on the flavor of the orbiting lepton.

Recent laser spectroscopy of muonic atoms [13] has opened the door to new high-precision tests of QED, constituting tests of the theory at the two- and three-loop levels [14]. However, the small size of these higher-order QED corrections to atomic levels makes them compete with more mundane energy shifts, such as those due to the finite size of

the nucleus. Consequently, uncertainties in computing nuclear contributions to atomic energy shifts are important components of the theoretical error budget when comparing with experiments. These theoretical uncertainties are made even worse if there should also be new short-range interactions between the nucleus and muon, such as have been motivated [15] by the proton-radius problem. Until it is understood whether this problem is solved by a better understanding of the experimental errors or through the existence of new physics, this discrepancy must be treated as an unknown unknown when assessing the theory error.

A better understanding of the nature of short-distance nucleus-lepton interactions is therefore an important prerequisite for exploiting the precision of spectroscopic measurements, both for the extraction of the best value of the Rydberg and to test QED. This is where effective field theory (EFT) in general [16,17], and the point-particle effective field theory (PPEFT) framework in particular, can help [18–20]. EFTs allow one to write a small set of effective interactions that capture the effects of *all* short-distance contributions to atomic energy levels (including both nuclear-scale physics and any hypothetical new short-range forces), order by order in powers of the relevant small size R of the physics in question. For nuclear physics R would be of order the nuclear radius, while for a new short-range force it would instead be the force's range. The existence of these effective interactions allows a robust parametrization of the contributions of short-distance physics to atomic energy levels, without having to understand the details of its microscopic origin.

Of course, knowing the underlying microscopic physics in question (such as the structure of the relevant nucleus), it becomes possible to compute the size of these effective interactions from first principles. In this language, the uncertainties in nuclear-structure calculations enter into predictions through any inaccuracy in the values so inferred for the effective interactions. One of the points of this paper is to show how

^{*}cburgess@perimeterinstitute.ca

[†]haymanpf@mcmaster.ca

[‡]rummelm@mcmaster.ca

[§]zalavarl@mcmaster.ca

to relate such calculations to the effective couplings of the PPEFT framework in particular.

We also take an entirely different tack. Instead of trying to reduce the inaccuracy of these effective couplings through more precise nuclear calculations, in this paper we also use the generality of the EFT parametrization to identify combinations of spectroscopic measurements from which all of the relevant short-distance effective couplings drop out to a fixed order in the expansion in $R/a_b = m\epsilon Z\alpha$ and $Z\alpha$ (where m is the mass of the orbiting particle, Z is the nuclear charge, α is the fine-structure constant, and a_b is the relevant Bohr radius). These combinations are particularly interesting because the absence of short-distance contributions to them means that the theoretical error for these observables is controlled by powers of R/a_b or $Z\alpha$ rather than by the larger uncertainties arising from (say) nuclear physics. A similar approach has been used to cancel dependence on nuclear effects for the hyperfine splitting in hydrogen [21] (as well as to highlight nuclear isotope dependence, among other reasons [13,22]), however our approach has the advantage of being systematic, and can be applied in principle to any spinning or spinless nucleus. We can also extend our results to higher orders, as we illustrate by identifying nuclear-free combinations to higher order in $Z\alpha$ than has been done previously.

The key observation of this work is that the short-distance PPEFT couplings only enter into spectroscopic measurements through a single (mass-dependent) length scale $\epsilon_{\star,e,\mu}$ (where the e and μ are used to distinguish between the scale that applies to electrons versus muons). As a result, a single spectroscopic measurement for each fermion-type suffices to predict the finite-size contribution to all other energy shifts. Working to order $m^4 R^3 (Z\alpha)^5 \approx 10^{-2}$ eV $\approx 10^3$ GHz for muonic atoms (as is relevant for the newest generation of muonic helium experiments [12]), we use this approach to predict

$$\widehat{\Delta E}_{nS_{1/2-n}P_{1/2}} = \frac{8[2 + \alpha(\eta_{n0}^{(\mu)} - \eta_{n1}^{(\mu)})]}{n^3[2 + \alpha(\eta_{20}^{(\mu)} - \eta_{21}^{(\mu)})]} \widehat{\Delta E}_{2S_{1/2-2}P_{1/2}} \quad (1)$$

and

$$\begin{aligned} \widehat{\Delta E}_{n_1S_{1/2-n_2}S_{1/2}} \\ = 2\widehat{\Delta E}_{2S_{1/2-2}P_{1/2}} \left(\frac{2 + \alpha\eta_{n_10}^{(\mu)}}{n_1^2} - \frac{2 + \alpha\eta_{n_20}^{(\mu)}}{n_2^2} \right), \end{aligned} \quad (2)$$

where

$$\widehat{\Delta E}_{1\rightarrow 2} := \Delta E_{1\rightarrow 2} - \Delta E_{1\rightarrow 2}^{\text{EM}} = \Delta E_{1\rightarrow 2}^{\text{PP}} + \Delta E_{1\rightarrow 2}^{\text{PPQED}} \quad (3)$$

is the difference between the total $n_1X_{j_1-n_2}Y_{j_2}$ transition ($\Delta E_{1\rightarrow 2}$) and the purely pointlike contributions to the same difference ($\Delta E_{1\rightarrow 2}^{\text{EM}}$). [Equivalently, this is the difference between the finite-size correction to the $n_1X_{j_1}$ and $n_2Y_{j_2}$ states ($\Delta E_{1\rightarrow 2}^{\text{PP}}$), plus the difference between the combined finite-size-QED corrections to the same states ($\Delta E_{1\rightarrow 2}^{\text{PPQED}}$)]. Here, $\eta_{n\ell}$ are computable n - and ℓ -dependent coefficients associated with the combined finite-size-QED contributions given explicitly for electrons in (64) below.

For electrons, we also work to order $m^4 R^3 (Z\alpha)^5$, but now this is closer to 10^{-12} eV $\approx 10^0$ kHz, and so we must also include terms of order $m^3 R^2 (Z\alpha)^6 \approx 10^{-11}$ eV ≈ 10 kHz since

the smaller electron mass makes those scales comparable. In this case, we predict for the same transitions

$$\begin{aligned} \widehat{\Delta E}_{nS_{1/2-n}P_{1/2}} \\ = \frac{8}{n^3} \widehat{\Delta E}_{2S_{1/2-2}P_{1/2}} \left\{ 1 + (Z\alpha)^2 \left[N(n) - \frac{n^2 - 1}{4n^2} \right] \right\} \end{aligned} \quad (4)$$

and

$$\begin{aligned} \widehat{\Delta E}_{n_1S-n_2S} \\ = \widehat{\Delta E}_{2S_{1/2-2}P_{1/2}} \left\{ \frac{1}{n_1^3} - \frac{1}{n_2^3} + (Z\alpha)^2 \left[\frac{N(n_1)}{n_1^3} - \frac{N(n_2)}{n_2^3} \right] \right\}, \end{aligned} \quad (5)$$

in which we define

$$\begin{aligned} N(n) := \frac{12n^2 - n - 9}{4n^2(n+1)} - H_{n+1} + \frac{5}{4} + \frac{\eta_{n0}^{(e)}}{2Z} \\ - \frac{\eta_{20}^{(e)}}{2Z} - \ln\left(\frac{2}{n}\right). \end{aligned} \quad (6)$$

Moreover, even without solving for ϵ_{\star} explicitly, our knowledge of how this one parameter enters into energy shifts allows us to write linear combinations of measurements from which it cancels altogether, thus defining relations between energy shifts that are entirely free of nuclear physics. For muons, we identify

$$\begin{aligned} \frac{n_1^2}{2 + \alpha(\eta_{n_10}^{(\mu)} - \eta_{n_21}^{(\mu)})} \widehat{\Delta E}_{n_1S_{1/2-n_1}P_{3/2}} \\ = \frac{n_2^2}{2 + \alpha(\eta_{n_20}^{(\mu)} - \eta_{n_21}^{(\mu)})} \widehat{\Delta E}_{n_2S_{1/2-n_2}P_{3/2}}, \end{aligned} \quad (7)$$

while for electrons,

$$\begin{aligned} \frac{24n_1^5}{n_1^2 - 1} \Delta E_{n_1P_{1/2-n_1}P_{3/2}} \\ = \frac{1}{F[n_1] - F[n_2]} (n_1^3 \Delta E_{n_1S_{1/2-n_1}P_{1/2}} - n_2^3 \Delta E_{n_2S_{1/2-n_2}P_{1/2}}), \end{aligned} \quad (8)$$

where

$$F[n] := \frac{12n^2 - n - 9}{2n^2(n+1)} - \frac{n^2 - 1}{24n^2} + 2 \ln n - 2H_{n+1} + \frac{\eta_{n0}^{(e)}}{Z}. \quad (9)$$

We organize our presentation as follows. Section II sets up the PPEFT framework required to draw the above conclusions, starting with a summary of the relevant near-nucleon boundary conditions and how these are related to the PPEFT effective description of the nucleus. This section also deals with various conceptual issues, such as deriving the appropriate renormalization-group- (RG-) invariant nuclear length scale ϵ_{\star} . Next, Sec. III computes how this RG-invariant parameter captures various microscopic models for nuclei, including the moments of fixed charge distributions and nuclear polarizabilities. Once it is established how these contribute to atomic energy levels only through the one RG-invariant combination ϵ_{\star} , we identify combinations of atomic transition

frequencies from which this one nucleus-sensitive parameter cancels out. There are a great many such combinations, and each represents a quantity for which nuclear uncertainties are negligible at the level of present-day experimental measurements. Section IV applies the formulas of the previous sections to the helium ion using the only available experimental data, the $2S_{1/2}-2P_{1/2}$ transition. The result is a prediction for the $1S-2S$ transition of $\nu_{1S-2S} = 9.868\,561\,009(1) \times 10^9$ MHz, which is roughly four times less precise than predictions in the literature [23]. Our precision is, however, entirely dominated by the experimental error, and so can only improve with future experiments, while never relying on the inherently uncertain choice of a particular model of the nucleus. Finally, some conclusions are briefly summarized in Sec. V.

II. PPEFT FOR SPINLESS NUCLEI

We present in this section a brief summary of EFT methods, as needed to discuss nuclear effects on the energy levels of electrons and muons orbiting spinless nuclei, such as ${}^4\text{He}$. EFTs are designed to exploit any hierarchies of scales in a problem to most efficiently compute a system's properties. As applied to atoms, EFTs such as nonrelativistic QED (NRQED) [16] are usually used to exploit the hierarchy between the electron-muon mass and the much smaller size of typical bound-state energies. For PPEFT the hierarchy exploited is the large ratio between the small size R of the nucleus and the much larger size a_b of the atomic Bohr radius. The expansion of observables in powers of R/a_b reveals them not to depend on most of the nuclear details, but only on a set of “generalized multipole moments,” similar to the way that ordinary multipole moments control the expansion of the electrostatic field of a compact charge distribution.

A. PPEFT including subleading order

This section reviews how to set up and solve for atomic energies within the PPEFT framework.

1. Bulk system

Before describing the nuclear degrees of freedom, we start by defining the long-distance, “bulk,” fields whose properties the nucleus perturbs. We take the bulk system to be defined by QED, describing the renormalizable coupling of charge $-e$ fermions to photons,¹

$$S_B = - \int d^4x \left[\bar{\Psi} (\not{D} + m) \Psi + \frac{1}{4} F_{\mu\nu} F^{\mu\nu} \right], \quad (10)$$

where $\not{D} = \gamma^\mu D_\mu$ with γ^μ denoting the usual Dirac gamma matrices and $D_\mu \Psi = (\partial_\mu + ieA_\mu)\Psi$, as appropriate for fermions of charge $-e$, while $F_{\mu\nu} = \partial_\mu A_\nu - \partial_\nu A_\mu$. It is often useful to zoom in on the nonrelativistic limit of this bulk physics by taking m to be much larger than the energies of interest, and NRQED is the natural field-theoretic language for doing so. For later purposes it suffices to notice that this

¹Our metric has $(-+++)$ signature, so γ^0 is anti-Hermitian while the spatial γ^i are Hermitian.

limit can be formally derived by performing a field redefinition that simplifies the large- m limit. This is done for electrons and muons by redefining $\Psi \rightarrow \exp[mt\gamma^0]\Xi$, and assuming Ξ to vary appreciably only over distances and times much larger than $1/m$. The point of this redefinition is to ensure S_B has a well-defined large- m limit since the term $m\bar{\Psi}\Psi = m\bar{\Xi}\Xi$ then precisely cancels the rest-mass part of the time derivative $\bar{\Psi}\gamma^0\partial_t\Psi = -m\bar{\Xi}\Xi + \dots$, leaving interactions that can be expanded in powers of derivatives divided by m .

2. Nuclear properties

If proceeding in the spirit of NRQED, nuclear properties could be included into the theory by adding its field Φ , preferably already within a nonrelativistic framework that exploits expansions in inverse powers of the nuclear mass M .

Within PPEFT, however, nuclear properties are instead identified by writing the *first-quantized* action for the nucleus that includes all possible local interactions between its center-of-mass coordinate $y^\mu(\tau)$ and the “bulk” fields $A_\mu(x)$ and $\Psi(x)$, respectively describing the electromagnetic potential and the Dirac field of the orbiting particle. This first-quantized framework is completely equivalent to the second-quantized one restricted to single-particle states and is more convenient when working purely within the single-nucleus sector, such as when describing an atom, for which most of the bells and whistles of quantum field theory for the nucleus are overkill.

For a spherically symmetric nucleus such as helium (or other doubly magic nuclei) restricted to parity-preserving interactions, this leads to [20]

$$\begin{aligned} S_p = - \int_{\mathcal{W}} d\tau & \left[M - Ze A_\mu \dot{y}^\mu + c_s \bar{\Psi} \Psi + i c_v \bar{\Psi} \gamma_\mu \Psi \dot{y}^\mu \right. \\ & + \tilde{h} \dot{y}^\mu \partial^\nu F_{\mu\nu} + i d_s \dot{y}^\mu \bar{\Psi} D_\mu \Psi + d_v \dot{y}^\mu \dot{y}^\nu \bar{\Psi} \gamma_\mu D_\nu \Psi \\ & \left. + \frac{1}{2} (d_E + d_B) \dot{y}^\mu \dot{y}^\nu F_{\mu\lambda} F_\nu^\lambda + \frac{1}{4} d_B F_{\mu\nu} F^{\mu\nu} + \dots \right]. \end{aligned} \quad (11)$$

Here, \mathcal{W} denotes the world line $y^\mu(\tau)$ of the nuclear center of mass, along which τ is its proper time with derivative $\dot{y}^\mu := dy^\mu/d\tau$, at which all bulk fields are evaluated; as above, $D_\mu \Psi = (\partial_\mu + ieA_\mu)\Psi$.

The first line describes the physics of a point source with mass M and charge Ze . The couplings c_s , c_v , and \tilde{h} in the second line have dimensions of $[\text{length}]^2$, and so are expected to be order R^2 in size, up to dimensionless $O(1)$ coefficients. Similarly the couplings d_s , d_v , d_E , and d_B have dimension $[\text{length}]^3$ and should be order R^3 and so on, with the ellipses containing all terms suppressed by more than three powers of R .

Since our focus is on energy shifts due to finite nuclear size, for simplicity of presentation we neglect kinematic nuclear recoil effects since the suppression of these corrections by powers of m/M make their contributions to nuclear size effects smaller than the order to which we work. This amounts to assuming the nucleus to be at rest within the atomic rest frame: $\dot{y}^\mu = \delta_0^\mu$. Recoil corrections are, however, easily included within this framework by instead using (and quantizing) the full nuclear 4-velocity $\dot{y}^\mu = \gamma\{1, \mathbf{v}\}$, where $\gamma = (1 - \mathbf{v}^2)^{-1/2}$.

With a static nucleus the above action becomes

$$S_p = - \int_{\mathcal{W}} dt \left[M - Ze A_0 + c_s \bar{\Psi} \Psi + i c_v \bar{\Psi} \gamma_0 \Psi - \tilde{h} \nabla \cdot \mathbf{E} + i d_s \bar{\Psi} D_0 \Psi + d_v \bar{\Psi} \gamma_0 D_0 \Psi + \frac{1}{2} d_e \mathbf{E}^2 + \frac{1}{2} d_b \mathbf{B}^2 + \dots \right]. \quad (12)$$

In the absence of any Ψ terms, the four pure electromagnetic interactions would establish the particle to have electric charge Ze , charge radius r_p with $\tilde{h} = \frac{1}{6} Ze r_p^2$, and so on. The complete response of the atom to the nucleus, including nuclear polarizabilities [24], also requires direct couplings to Ψ , however, we see below how to relate these couplings to other nuclear properties, such as the polarizabilities and order- R^3 Friar moment contributions to the nuclear electrostatic form factor [25].

Because our interest is in largely nonrelativistic applications for which kinematic effects arise as powers of $1/m$, just as for the bulk it can be convenient to rescale $\Psi = \exp[m t \gamma^0] \Xi$, to remove the rapidly oscillating phase associated with the rest mass. Having a reasonable large- m limit after doing so requires the coefficients c_s and c_v to contain contributions proportional to m that cancel those terms in S_p involving time derivatives $\partial_t \Psi = m \gamma^0 \Psi + \dots$, leading to

$$c_s \bar{\Psi} \Psi + i c_v \bar{\Psi} \gamma_0 \Psi + i d_s \bar{\Psi} D_0 \Psi + d_v \bar{\Psi} \gamma_0 D_0 \Psi = (c_s - d_v m) \bar{\Xi} \Xi + i (c_v + d_s m) \bar{\Xi} \gamma_0 \Xi + \dots, \quad (13)$$

and so suggesting writing $c_s = d_v m + \tilde{c}_s$ and $c_v = -d_s m + \tilde{c}_v$, and so on. In what follows, we make these replacements but drop the “tilde” on c_s and c_v to avoid notational clutter. Once this is done, all time derivatives acting on Ψ in S_p can be treated as giving $\partial_t \Psi \rightarrow -i(\omega - m)\Psi$.

3. Electromagnetic response

The purely electromagnetic terms in (12) influence atomic energy levels through the change they introduce in the electromagnetic field sourced by the atomic nucleus. The naive way to compute the modified electric field represents the action (12) as a delta function, leading to the formal perturbative modification

$$\mathbf{E} \simeq \mathbf{E}_c + \tilde{h} \nabla \delta^3(\mathbf{r}) + d_e \mathbf{E}_c \delta^3(\mathbf{r}), \quad (14)$$

in which $\mathbf{E}_c = (Ze/4\pi r^2)\hat{\mathbf{r}}$ denotes the lowest-order (Coulomb) field, with $\hat{\mathbf{r}} = \mathbf{r}/r$ being the radial unit vector.

What makes the above expression naive is the divergence of \mathbf{E}_c at the support of the delta function. A more precise way to formulate this (for which the PPEFT formalism is designed [18–20]) is to recast the influence of S_p on A_μ in terms of a boundary condition at a regularization surface at small but nonzero radius $r = \epsilon$. The couplings \tilde{h} and d_e are regarded as depending implicitly on ϵ in such a way as to ensure that physical quantities do not depend on the precise value chosen for ϵ .

What counts for energy shifts is the scalar potential implied by (14). Keeping the regularization in mind, the

result is

$$A_0(r) = -\frac{Ze}{4\pi r} + \tilde{h} \delta^{(3)}(\mathbf{r}) + \frac{d_e Ze}{(4\pi)^2 \epsilon^2} f_\epsilon(r), \quad (15)$$

where the function $f_\epsilon(r)$ is any regularization consistent with $\nabla f_\epsilon = 4\pi \hat{\mathbf{r}} \delta^3(\mathbf{r})$ in the small- ϵ limit [such as $f_\epsilon(r) = -\Theta(\epsilon - r)/\epsilon^2$ where $\Theta(x)$ is the Heaviside step function].

A similar story goes through for the magnetic field, for which the Maxwell equation gets modified by S_p to become

$$\nabla \times \mathbf{B} = d_b \nabla \times [\mathbf{B} \delta^{(3)}(x)]. \quad (16)$$

Because of the absence of nuclear spin (and so also magnetic moment) dictated by our spherical-symmetry assumption, nontrivial solutions to this arise only suppressed by powers of $v/c \sim Z\alpha$ and so are negligible to the order we work. This allows the neglect of the vector potential \mathbf{A} in the calculations described below, in particular ensuring the magnetic polarizability d_b contributes negligibly to atomic energies at the order we work.

To these must be added the corrections to the Dirac field due to the boundary-condition change it also experiences.

4. Fermion response

To study atomic helium in this framework, we examine QED involving the Dirac and electromagnetic quantum fields, subject to the boundary conditions implied [18–20] by the presence of S_p . In this language, it is only through these boundary conditions, and the modification (15), that the nucleus affects atomic energy levels. More and more detailed nuclear contributions correspond to adding more and more complicated interactions to S_p , in what amounts to a “generalized multipole expansion” of the nucleus.

In this framework, QED interactions are included perturbatively as usual, with bound-state energies obtained from the positions of poles of the two-point function $\langle 0 | T \Psi(x) \bar{\Psi}(x') | 0 \rangle$. These are determined in part by computing the modes $\psi_n(x) = \langle 0 | \Psi(x) | n \rangle$ everywhere away from the nucleus. Perturbation theory is set up as usual, with the unperturbed system neglecting QED and nuclear corrections to A_0 , i.e., using for ψ_n solutions to the Dirac equation with a Coulomb potential:

$$(\not{D} + m)\psi = \left[-\gamma^0 \left(\omega + \frac{Z\alpha}{r} \right) + \vec{\gamma} \cdot \vec{\nabla} + m \right] \psi = 0, \quad (17)$$

for energy eigenstates $\psi \propto e^{-i\omega t}$.

This has well-known solutions of definite parity and total angular momentum given by

$$\psi^\pm = \begin{pmatrix} f_\pm(r) U_{jj_z}^\pm(\theta, \phi) + i g_\pm(r) U_{jj_z}^\mp(\theta, \phi) \\ f_\pm(r) U_{jj_z}^\pm(\theta, \phi) - i g_\pm(r) U_{jj_z}^\mp(\theta, \phi) \end{pmatrix}, \quad (18)$$

where ψ^+ and ψ^- denote parity eigenstates, $U_{jj_z}^\pm$ are the Dirac spinor harmonics with definite total angular momentum $j = \ell \pm \frac{1}{2}$, and the parity eigenvalue is $\hat{\Pi} U_{jj_z}^\pm = (-)^{j \mp \frac{1}{2}} U_{jj_z}^\pm$.

To lowest order the functions $f_{\pm}(r)$ and $g_{\pm}(r)$ solve the radial part of the Dirac-Coulomb equation, and for a source with charge Ze have the form

$$f_{\pm} = \sqrt{m+\omega} e^{-\rho/2} \rho^{\zeta-1} \left\{ A_{\pm} \mathcal{M}\left[\zeta - \frac{Z\alpha\omega}{\kappa}, 2\zeta + 1; \rho\right] + C_{\pm} \rho^{-2\zeta} \mathcal{M}\left[-\zeta - \frac{Z\alpha\omega}{\kappa}, -2\zeta + 1; \rho\right] \right. \\ \left. - A_{\pm} \left(\frac{\zeta - Z\alpha\omega/\kappa}{K - Z\alpha m/\kappa}\right) \mathcal{M}\left[\zeta - \frac{Z\alpha\omega}{\kappa} + 1, 2\zeta + 1; \rho\right] + C_{\pm} \left(\frac{\zeta + Z\alpha\omega/\kappa}{K - Z\alpha m/\kappa}\right) \rho^{-2\zeta} \mathcal{M}\left[-\zeta - \frac{Z\alpha\omega}{\kappa} + 1, -2\zeta + 1; \rho\right] \right\} \quad (19)$$

and

$$g_{\pm} = -\sqrt{m-\omega} e^{-\rho/2} \rho^{\zeta-1} \left\{ A_{\pm} \mathcal{M}\left[\zeta - \frac{Z\alpha\omega}{\kappa}, 2\zeta + 1; \rho\right] + C_{\pm} \rho^{-2\zeta} \mathcal{M}\left[-\zeta - \frac{Z\alpha\omega}{\kappa}, -2\zeta + 1; \rho\right] \right. \\ \left. + A_{\pm} \left(\frac{\zeta - Z\alpha\omega/\kappa}{K - Z\alpha m/\kappa}\right) \mathcal{M}\left[\zeta - \frac{Z\alpha\omega}{\kappa} + 1, 2\zeta + 1; \rho\right] - C_{\pm} \left(\frac{\zeta + Z\alpha\omega/\kappa}{K - Z\alpha m/\kappa}\right) \rho^{-2\zeta} \mathcal{M}\left[-\zeta - \frac{Z\alpha\omega}{\kappa} + 1, -2\zeta + 1; \rho\right] \right\}, \quad (20)$$

where A_{\pm} and C_{\pm} are integration constants, $\mathcal{M}[a, b; z] = 1 + (a/b)z + \dots$ are the standard confluent hypergeometric functions, ω is the mode energy, while $\rho = 2\kappa r$ where κ and ζ are defined by

$$\kappa = \sqrt{(m-\omega)(m+\omega)} \quad \text{and} \\ \zeta = \sqrt{\left(j + \frac{1}{2}\right)^2 - (Z\alpha)^2}. \quad (21)$$

In what follows, κ is real because we study atomic bound states which satisfy $m > \omega$. The parity of the state often enters through the parameter $K = \mp(j + \frac{1}{2})$ where the upper (lower) sign in K corresponds to state ψ^+ (or ψ^-).

In this language, the entire influence of nuclear-scale physics on the orbiting fermion arises through the boundary condition implied by the point-particle action (12) for the bulk fields Ψ and A_{μ} near the origin [18–20]. Nuclear contributions to QED corrections similarly enter through the boundary conditions satisfied by the propagators built from these modes in the relevant graphs.

5. Near-nucleus boundary conditions

The main result (explained in some detail for the Dirac equation in [20]) governing how nuclear properties perturb atomic levels relates the parameters of S_p to the near-nucleus value of the ratios $(g_+/f_+)_{r=\epsilon}$ and $(f_-/g_-)_{r=\epsilon}$ of the radial modes evaluated at a small (but arbitrary) distance $r = \epsilon$ outside the nucleus: $R \leq \epsilon \ll a_b$ (with R the smallest radius where an external extrapolation is valid and a_b denoting the relevant atomic Bohr radius). The ratios g_+/f_+ and f_-/g_- at $r = \epsilon$ determine the physical integration constant that arises in the general solution to the radial equation, which in turn controls the dependence of atomic observables.²

²Notice that specifying f_{\pm}/g_{\pm} at $r = \epsilon$ generically implies the radial functions need not remain bounded at the origin, which is the traditional choice for boundary conditions there. But, this is not a fundamental worry because the growth of the radial solution eventually gets cut off once the interior of the nucleus is reached and the asymptotic solution of the Coulomb-Dirac equation no longer approximates the real physics.

It is convenient when stating the boundary conditions to write the ratios $(g_{\pm}/f_{\pm})_{r=\epsilon}$ in a way that makes manifest the small parameters in the problem: the two small quantities $\epsilon/a_b = m\epsilon Z\alpha$ and $(Z\alpha)^2$. This is most conveniently done by writing

$$\left(\frac{g_+}{f_+}\right)_{r=\epsilon} = \xi_g Z\alpha \quad \text{and} \quad X\left(\frac{f_-}{g_-}\right)_{r=\epsilon} = \frac{\xi_f}{2n}, \quad (22)$$

where $X := \sqrt{(m-\omega)/(m+\omega)}$ is included for later notational simplicity, while n is the state's principal quantum number and/or atomic energy levels $\omega = m - (Z\alpha)^2 m/(2n^2) + \dots$. The quantities ξ_f and ξ_g then have the expansions

$$\xi_g := \hat{g}_1(\epsilon) + (m\epsilon Z\alpha)\hat{g}_2(\epsilon) + (Z\alpha)^2\hat{g}_3(\epsilon) + \dots, \\ \xi_f := (m\epsilon Z\alpha)\hat{f}_1(\epsilon) + (m\epsilon Z\alpha)^2\hat{f}_2(\epsilon) + (Z\alpha)^2\hat{f}_3(\epsilon) + \dots, \quad (23)$$

where the ellipses involve terms involving more powers of $(m\epsilon Z\alpha)$ and/or $(Z\alpha)^2$ than those written, and the dependence on n follows directly from the ω dependence of the radial Dirac equation. The dimensionless coefficients $\hat{g}_i(\epsilon)$ and $\hat{f}_i(\epsilon)$ are normalized in (22) so as to ensure that \hat{g}_1 are order unity in applications to atomic energy levels.

6. Energy shifts

Before determining how \hat{f}_i and \hat{g}_i depend on nuclear parameters, we briefly summarize how these quantities are related to shifts in atomic energy levels. As shown in detail in [20], the ratio of integration constants A_{\pm}/C_{\pm} appearing in the solutions (19) and (20) can be determined if f_{\pm}/g_{\pm} is regarded as being specified at $r = \epsilon$. For bound states, imposing normalizability at infinity overdetermines the eigenvalue problem in the usual way, leading to standard predictions for the bound-state energy levels. Writing the shift in these energies relative to the standard Dirac energies (obtained when $C_{\pm} = 0$) due to the deviations in \hat{f}_i and \hat{g}_i [20] as δE

gives the nucleus-dependent shift to the $j = \frac{1}{2}$ positive- and negative-parity energy levels as

$$\begin{aligned} \delta E_{1/2}^+ \simeq & \frac{m^3 \epsilon^2 (Z\alpha)^4}{n^3} \left\{ 2(1 + 2\hat{g}_1) + \left[2\hat{g}_2 - \frac{8}{3} - 4\hat{g}_1(\hat{g}_1 + 2) \right] (m\epsilon Z\alpha) + \left[4\hat{g}_3 + 5 + 8\hat{g}_1 - 2\hat{g}_1^2 \right. \right. \\ & \left. \left. + (1 + 2\hat{g}_1) \left\{ \frac{12n^2 - n - 9}{2n^2(n+1)} - 2 \ln \left(\frac{2m\epsilon Z\alpha}{n} \right) - 2H_{n+1} - 2\gamma \right\} \right] (Z\alpha)^2 + \dots \right\} \end{aligned} \quad (24)$$

for parity-even states and

$$\begin{aligned} \delta E_{1/2}^- \simeq & -\frac{(n^2 - 1)}{n^5} m^4 \epsilon^3 (Z\alpha)^5 \left(\hat{f}_1 - \frac{2}{3} \right) \\ & + \frac{n^2 - 1}{2n^5} m^3 \epsilon^2 (Z\alpha)^6 (1 - 2\hat{f}_3) + \dots \end{aligned} \quad (25)$$

for parity-odd states. In these expressions, the ellipses contain terms suppressed by higher powers of $(m\epsilon Z\alpha)$ and $(Z\alpha)^2$. Here, γ is the Euler-Mascheroni constant and H_n are the harmonic numbers $H_m = 1 + \frac{1}{2} + \frac{1}{3} + \dots + \frac{1}{m}$, and so $H_1 = 1$, $H_2 = \frac{3}{2}$, $H_3 = \frac{11}{6}$, and so on.

We include in the above all contributions relevant to the current generation of experiments involving electrons and muons orbiting a ${}^4\text{He}$ nucleus. Recall that for muons, $(m\epsilon Z\alpha) \gg (Z\alpha)^2$ when ϵ is a typical nuclear size, but for electrons $(m\epsilon Z\alpha) \simeq (Z\alpha)^2$. Consequently, for muonic atoms it suffices to keep terms of order $m^4 \epsilon^3 (Z\alpha)^5$ while dropping terms of size $m^3 \epsilon^2 (Z\alpha)^6$, but for electrons these terms must both be kept. This means the coefficients \hat{g}_1 , \hat{g}_2 , and \hat{f}_1 are in principle of interest for muonic He, while all of \hat{g}_1 , \hat{g}_2 , \hat{g}_3 , \hat{f}_1 , and \hat{f}_3 are relevant for electrons. It is for this reason that the contribution to δE^- from \hat{f}_2 is not written in (25). Similarly, the leading contributions for $j = \frac{3}{2}$ are the same size as terms neglected above, and so can be dropped in what follows.

Later sections evaluate these formulas using \hat{f}_i and \hat{g}_i as computed with several simple specific models of nuclei, and in this way we verify that they include the results of standard calculations in the literature. In particular, they contain the various moments encountered when doing so with the nucleus modeled as a static charge distribution, reducing to well-known formulas for finite-size corrections to the Dirac-Coulomb energies [2,20,25–29]. However, as we see below, the real power of the above expressions (24) and (25) is in their generality since once computed in terms of the parameters in S_p they capture the effects of arbitrary short-distance physics localized at the nucleus.³

B. Matching and RG invariance

The influence of the nucleus on atomic levels (or on low-energy lepton scattering) is completely determined by the near-nucleus boundary condition for the modes ψ at $r = \epsilon$, and so is ultimately parametrized by the dependence of the coefficients $\hat{g}_i(\epsilon)$ and $\hat{f}_i(\epsilon)$ on nuclear parameters. The mapping of nuclear physics to atomic physics is completely captured

³The interactions of S_p specialize to rotational and parity invariance, but nothing in principle forbids extending these interactions to include nuclear spin and parity-violating interactions.

by describing this dependence, and the point of the PPEFT formalism is to parametrize this dependence efficiently so as to exploit the hierarchy of scales $R \lesssim \epsilon \ll a_B$.

1. Connecting boundary conditions to S_p

The main consequence of S_p for atomic levels comes from the boundary condition it implies at $r = \epsilon$ for the radial functions $f_{\pm}(r)$ and $g_{\pm}(r)$. These are worked out at leading nontrivial order in [20], and the result is extended to include the subdominant interactions of (12) in [30]. The boundary conditions that follow from these references are

$$\begin{aligned} \hat{c}'_s + \hat{c}'_{v \text{ tot}} - \frac{(Z\alpha)}{2n^2} (\hat{d}_s + \hat{d}_v) (m\epsilon Z\alpha) \\ = \left(\frac{g_+}{f_+} \right)_{r=\epsilon} \\ = Z\alpha [\hat{g}_1(\epsilon) + (m\epsilon Z\alpha) \hat{g}_2(\epsilon) + (Z\alpha)^2 \hat{g}_3(\epsilon) + \dots] \end{aligned} \quad (26)$$

for the parity-even states and

$$\begin{aligned} \hat{c}'_s - \hat{c}'_{v \text{ tot}} - \frac{(Z\alpha)}{2n^2} (\hat{d}_s - \hat{d}_v) (m\epsilon Z\alpha) \\ = \left(\frac{f_-}{g_-} \right)_{r=\epsilon} \\ = \frac{1}{2nX} [(m\epsilon Z\alpha) \hat{f}_1(\epsilon) + (m\epsilon Z\alpha)^2 \hat{f}_2(\epsilon) \\ + (Z\alpha)^2 \hat{f}_3(\epsilon) + \dots] \end{aligned} \quad (27)$$

for the parity-odd states. Here, the hatted quantities are $\hat{c}'_{s,v \text{ tot}} := c'_{s,v \text{ tot}} / 4\pi \epsilon^2$ while $\hat{d}_{s,v} := d_{s,v} / 4\pi \epsilon^3$, and so are dimensionless. Primes denote the combinations

$$c'_{s,v} := c_{s,v} - \frac{(Z\alpha) d_{s,v}}{\epsilon}. \quad (28)$$

Finally, the subscript “tot” represents the combination

$$c_{v \text{ tot}} := c_v - e\tilde{h} - \frac{d_e Z\alpha}{3\epsilon}. \quad (29)$$

The parameters c_v and $e\tilde{h}$ naturally combine in this way since both of these effective interactions introduce a delta-function potential in the nonrelativistic Schrödinger limit [18,20].

The final step is to solve the above boundary condition to relate the quantities \hat{f}_i and \hat{g}_i to the parameters c_s , c_v , d_s , d_v , \tilde{h} , and d_e . This allows a determination of which nuclear parameters govern which atomic energy shifts. Before doing so, we first show how to deal with the apparent arbitrariness associated with the ubiquitous ϵ dependence of the boundary conditions. Doing so allows an efficient identification of the physical quantities, and in particular allows a clean counting of the number of nuclear parameters that enter into energy shifts at any given order.

2. Renormalization-group running

Recall that the position $r = \epsilon$, where the boundary conditions (26) and (27) are imposed, is basically arbitrary, so long as it lies outside the nucleus and is much smaller than the atomic Bohr radius. This makes it odd that expressions like (24) and (25) for physical energy shifts appear to make them depend on ϵ . The purpose of this section is to show why this dependence is really an illusion because it is canceled by an ϵ dependence that is implicit in the effective couplings c_s , c_v , and so on. This section develops renormalization-group (RG) tools for determining this dependence explicitly, thereby allowing a determination of the physical RG-invariant content of the effective couplings.

To this end, it is important to realize that equations like (26) and (27) can be read in two ways. First, they can be read as giving the ϵ dependence required of the effective couplings in order to ensure that physical quantities remain ϵ independent. This is done by equating it to the ϵ dependence that is explicit on the right-hand side (through the evaluation of the bulk solution for f_{\pm}/g_{\pm}). The condition that physical quantities be independent of ϵ in this language corresponds to demanding that the ratio of integration constants A_{\pm}/C_{\pm} be ϵ independent (and so RG invariant as ϵ is varied).

Once this is done, the ϵ dependence on both sides of Eqs. (26) and (27) becomes identical, and then the second way to read these equations is to equate the RG-invariant

coefficients on both sides. This then gives the ratio of integration constants A_{\pm}/C_{\pm} in terms of RG-invariant parameters. But, because energy shifts can be computed from A_{\pm}/C_{\pm} , this also gives predictions for the energy shifts in terms of the RG-invariant characterizations of the coupling flow.

To start this off, we take the small- r asymptotic form of the solutions given in (19) and (20) and use these to evaluate g_+/f_+ and f_-/g_- on the right-hand sides of Eqs. (26) and (27). This leads to the following expressions:

$$\begin{aligned} \hat{c}'_s + \hat{c}'_{v, \text{tot}} - \frac{(Z\alpha)}{2n^2}(\hat{d}_s + \hat{d}_v)(m\epsilon Z\alpha) \\ = -X \frac{\{(g_{02}^+ + g_{03}^+\rho) + (g_{12}^+ + g_{13}^+\rho)\frac{C_{\pm}}{A_{\pm}}\rho^{-2\zeta}\}}{\{(f_{02}^+ + f_{03}^+\rho) + (f_{12}^+ + f_{13}^+\rho)\frac{C_{\pm}}{A_{\pm}}\rho^{-2\zeta}\}} \end{aligned} \quad (30)$$

and

$$\begin{aligned} \hat{c}'_s - \hat{c}'_{v, \text{tot}} - \frac{(Z\alpha)}{2n^2}(\hat{d}_s + \hat{d}_v)(m\epsilon Z\alpha) \\ = -\frac{1}{X} \frac{\{(f_{02}^- + f_{03}^-\rho) + (f_{12}^- + f_{13}^-\rho)\frac{C_{\pm}}{A_{\pm}}\rho^{-2\zeta}\}}{\{(g_{02}^- + g_{03}^-\rho) + (g_{12}^- + g_{13}^-\rho)\frac{C_{\pm}}{A_{\pm}}\rho^{-2\zeta}\}}, \end{aligned} \quad (31)$$

where (as before) $X := \sqrt{(m-\omega)/(m+\omega)}$ while $\rho = 2\kappa\epsilon = 2m\epsilon\sqrt{1-\omega^2/m^2} \simeq 2m\epsilon Z\alpha/n$. Finally, the coefficients are given by

$$\begin{aligned} g_{02}^+ &:= -\left(j + \frac{1}{2}\right) + \zeta - \frac{Z\alpha}{X}, & g_{12}^+ &:= -\left(j + \frac{1}{2}\right) - \zeta - \frac{Z\alpha}{X}, \\ f_{02}^+ &:= -\left(j + \frac{1}{2}\right) - \zeta - Z\alpha X, & f_{12}^+ &:= -\left(j + \frac{1}{2}\right) + \zeta - Z\alpha X, \end{aligned} \quad (32)$$

and

$$\begin{aligned} f_{02}^- &:= \left(j + \frac{1}{2}\right) - \zeta - Z\alpha X, & f_{12}^- &:= \left(j + \frac{1}{2}\right) + \zeta - Z\alpha X, \\ g_{02}^- &:= \left(j + \frac{1}{2}\right) + \zeta - \frac{Z\alpha}{X}, & g_{12}^- &:= \left(j + \frac{1}{2}\right) - \zeta - \frac{Z\alpha}{X}, \end{aligned} \quad (33)$$

and

$$\begin{aligned} g_{03}^+ &:= \frac{(\zeta - Z\alpha\omega/\kappa)(\zeta - Z\alpha/X)}{2\zeta + 1}, & g_{13}^+ &:= \frac{(\zeta + Z\alpha\omega/\kappa)(\zeta + Z\alpha/X)}{-2\zeta + 1}, \\ f_{03}^+ &:= \frac{(\zeta - Z\alpha\omega/\kappa)(-\zeta - Z\alpha X - 2)}{2\zeta + 1}, & f_{13}^+ &:= \frac{(\zeta + Z\alpha\omega/\kappa)(-\zeta + Z\alpha X + 2)}{-2\zeta + 1}, \\ f_{03}^- &:= \frac{(\zeta - Z\alpha\omega/\kappa)(-\zeta - Z\alpha X)}{2\zeta + 1}, & f_{13}^- &:= \frac{(\zeta + Z\alpha\omega/\kappa)(-\zeta + Z\alpha X)}{-2\zeta + 1}, \\ g_{03}^- &:= \frac{(\zeta - Z\alpha\omega/\kappa)(2 + \zeta - Z\alpha/X)}{2\zeta + 1}, & g_{13}^- &:= \frac{(\zeta + Z\alpha\omega/\kappa)(-2 + \zeta + Z\alpha/X)}{-2\zeta + 1}. \end{aligned} \quad (34)$$

These equations show that it is the series in integer powers of ρ on the right-hand side that corresponds to the expansion in powers of $m\epsilon Z\alpha$ on the left-hand side. Temporarily working to lowest order in this expansion leads to the expression found in [20] for the running of the couplings \hat{c}_s and $\hat{c}_{v, \text{tot}}$:

$$\hat{c}_s + \hat{c}_{v, \text{tot}} = -X \left(\frac{g_{02}^+ + g_{12}^+ \frac{C_{\pm}}{A_{\pm}} \rho^{-2\zeta}}{f_{02}^+ + f_{12}^+ \frac{C_{\pm}}{A_{\pm}} \rho^{-2\zeta}} \right), \quad (35)$$

with coefficients given in (32). Similarly,

$$\hat{c}_s - \hat{c}_{v, \text{tot}} = -\frac{1}{X} \left(\frac{f_{02}^- + f_{12}^- \frac{C_-}{A_-} \rho^{-2\zeta}}{g_{02}^- + g_{12}^- \frac{C_-}{A_-} \rho^{-2\zeta}} \right), \quad (36)$$

with coefficients given in (33).

These expressions give the RG evolution of $\hat{c}'_s \pm \hat{c}'_{v, \text{tot}}$ as functions of ϵ . It is convenient to rewrite the result as

$$\hat{c}'_s \pm \hat{c}'_{v, \text{tot}} = \bar{\lambda}_\pm, \quad (37)$$

where the $\bar{\lambda}^\pm$ are given by

$$\bar{\lambda}_\pm := \frac{1}{Z\alpha} \left[\pm \zeta \frac{(\epsilon/\epsilon_\star^\pm)^{2\zeta} + \eta_\pm}{(\epsilon/\epsilon_\star^\pm)^{2\zeta} - \eta_\pm} + K \right], \quad (38)$$

where $K := \mp(j + \frac{1}{2})$, with upper (lower) sign corresponding to parity even (odd). Equation (38) defines two types of RG evolution, distinguished by the parameter $\eta_\pm := \text{sgn}[(Z\alpha)\bar{\lambda}_\pm - K] - 1$. $\eta_\pm = 1$ corresponds to a class of evolution for which $\bar{\lambda}_\pm$ never passes through $-K/Z\alpha$ and is unbounded (diverging at $\epsilon = \epsilon_\star^\pm$). $\eta_\pm = -1$ represents a class of evolution for which $\bar{\lambda}_\pm$ is bounded and passes through $-K/Z\alpha$ once (at $\epsilon = \epsilon_\star^\pm$).

This evolution can also be recast in differential form by differentiating while requiring C_\pm/A_\pm to be ϵ independent, and reexpressing the result in terms of $\bar{\lambda}_\pm$. Equation (38) trades the constants C_\pm/A_\pm for convenient RG-invariant integration constants ϵ_\star^\pm , obtained by integrating the differential evolution.

How is this picture changed once we include the $m\epsilon Z\alpha$ corrections? It turns out that the functions $\bar{\lambda}_\pm(\epsilon)$ are very useful in this case too because the functional form (38) appears in the coefficients of each power of ρ in (30) and (31). In particular, the generalization of (35) and (36) to next order in $m\epsilon Z\alpha$ has the form

$$\begin{aligned} \hat{c}'_s \pm \hat{c}'_{v, \text{tot}} - \frac{(Z\alpha)}{2n^2} (\hat{d}_s \pm \hat{d}_v) (m\epsilon Z\alpha) \\ = \bar{\lambda}_\pm + \frac{1}{n} [C_0^\pm + C_1^\pm \bar{\lambda}_\pm + C_2^\pm \bar{\lambda}_\pm^2] (2m\epsilon Z\alpha), \end{aligned} \quad (39)$$

where, evaluating X and κ using the lowest-order Coulomb energy, $\omega/m \approx 1 - \frac{1}{2}(Z\alpha/n)^2$,

$$\begin{aligned} C_0^+ &:= \frac{X(g_{02}^+ g_{13}^+ - g_{03}^+ g_{12}^+)}{f_{02}^+ g_{12}^+ - f_{12}^+ g_{02}^+} \approx \frac{8n^2 + 1}{12n} (Z\alpha) + \dots, \\ C_1^+ &:= \frac{f_{02}^+ g_{13}^+ - f_{03}^+ g_{12}^+ - f_{12}^+ g_{03}^+ + f_{13}^+ g_{02}^+}{f_{02}^+ g_{12}^+ - f_{12}^+ g_{02}^+} \approx 2n + \dots, \\ C_2^+ &:= \frac{f_{02}^+ f_{13}^+ - f_{03}^+ f_{12}^+}{X(f_{02}^+ g_{12}^+ - f_{12}^+ g_{02}^+)} \\ &\approx \frac{n}{Z\alpha} + \frac{8n^2 - 2n + 1}{4n} (Z\alpha) + \dots, \end{aligned} \quad (40)$$

and

$$\begin{aligned} C_0^- &:= \frac{f_{02}^- f_{13}^- - f_{03}^- f_{12}^-}{X(g_{02}^- f_{12}^- - g_{12}^- f_{02}^-)} \approx \frac{n}{3(Z\alpha)} + \dots, \\ C_1^- &:= \frac{g_{02}^- f_{13}^- - g_{03}^- f_{12}^- - g_{12}^- f_{03}^- + g_{13}^- f_{02}^-}{g_{02}^- f_{12}^- - g_{12}^- f_{02}^-} \approx \frac{2n}{3} + \dots, \end{aligned}$$

$$C_2^- := \frac{X(g_{02}^- g_{13}^- - g_{03}^- g_{12}^-)}{g_{02}^- f_{12}^- - g_{12}^- f_{02}^-} \approx -\frac{8n^2 - 3}{12n} (Z\alpha) + \dots \quad (41)$$

Here, ellipses indicate higher powers of $Z\alpha$.

Equating the coefficients of each power of $m\epsilon Z\alpha$ in (39) dictates separately the running of \hat{c}'_s , $\hat{c}'_{v, \text{tot}}$ [given by (37)], and \hat{d}_s and \hat{d}_v . The running of \hat{d}_s and \hat{d}_v is given by

$$\begin{aligned} Z\alpha(\hat{d}_s + \hat{d}_v) = & -\frac{8n^2 + 1}{3} (Z\alpha) - 8n^2 \bar{\lambda}_+ \\ & - \left(\frac{4n^2}{Z\alpha} + (8n^2 - 2n + 1)(Z\alpha) \right) \bar{\lambda}_+^2 \end{aligned} \quad (42)$$

and

$$Z\alpha(\hat{d}_s - \hat{d}_v) = -\frac{4n^2}{3(Z\alpha)} - \frac{8n^2}{3} \bar{\lambda}_- + \frac{8n^2 - 3}{3} (Z\alpha) \bar{\lambda}_-^2. \quad (43)$$

Interestingly, the running of all of the effective couplings are controlled by the two functions $\bar{\lambda}_\pm(\epsilon)$. As a result, the flow of all couplings is described in principle by the same two RG-invariant constants ϵ_\star^\pm . These two parameters encode the information contained in C_\pm/A_\pm in the solutions f_\pm and g_\pm . As we see below, only one of these two quantities is independent for a parity-preserving nucleus since $\epsilon_\star^+ = \epsilon_\star^- =: \epsilon_\star$.

These functions are plotted in Figs. 1 and 2 (for parity even) and in Figs. 3 and 4 (for parity odd). In each case, the two classes of flows identified by $\eta_\pm := \text{sgn}[(Z\alpha)\bar{\lambda}_\pm - K] - 1$. These figures show that the RG-invariant quantities ϵ_\star^\pm give the value of ϵ for which $(Z\alpha)\bar{\lambda}_\pm \mp K$ approaches infinity (when $\eta_\pm = +1$) or 0 (when $\eta_\pm = -1$).

III. NUCLEAR UNCERTAINTIES

Having established in the previous section why the precise value of ϵ carries no physical information, we turn in this section to connecting the RG-invariant parameters ϵ_\star^\pm to explicit nuclear properties. This is done in the first subsection

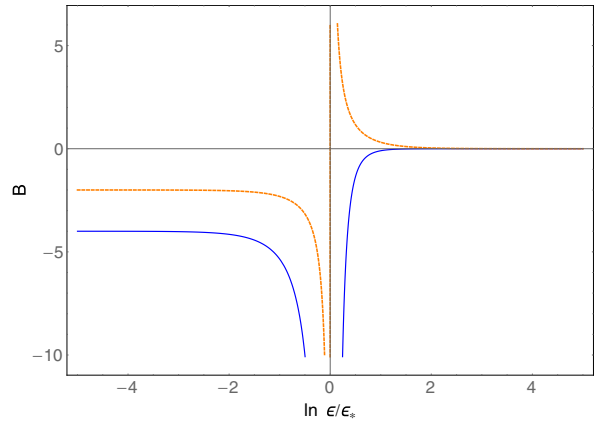


FIG. 1. Plot of the RG flow of $B = (Z\alpha)^4(\hat{d}_s + \hat{d}_v)/4$ (solid blue) and $B = (Z\alpha)(\hat{c}'_s + \hat{c}'_{v, \text{tot}})$ (dashed orange) vs $\ln \epsilon/\epsilon_\star$, with $\eta_+ = +1$.

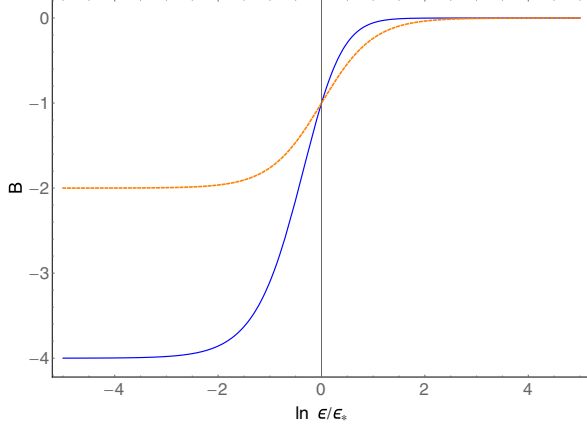


FIG. 2. Plot of the RG flow of $B = (Z\alpha)^4(\hat{d}_s + \hat{d}_v)$ (solid blue) and $B = (Z\alpha)(\hat{c}'_s + \hat{c}'_{v,\text{tot}})$ (dashed orange) vs $\ln \epsilon/\epsilon_*$, with $\eta_+ = -1$.

by computing the energy shift as a function of ϵ_*^\pm , and then comparing this result to the results of explicit simple models of the nucleus. The upshot of this section is the observation that a single parameter ϵ_* := $\epsilon_*^+ = \epsilon_*^-$ accounts for the energy shifts found using explicit calculations with these models, with $\eta_+ = \eta_- = +1$.

Furthermore, the parameter ϵ_* required to obtain this agreement does not depend on the quantum numbers $\{n, l, m\}$ of the state whose energy is being computed, as is intuitively plausible given that ϵ_* captures the properties of the nucleus and these should not depend on which particular electron (or muon) state that is used to probe them.

Finally, the above statements are equally true at lowest order and when higher-order contributions are included in powers of $Z\alpha$ and/or $mRZ\alpha$. Working to subdominant order does not introduce new parameters beyond ϵ_* into the result, it just determines the value of ϵ_* with more precision than at lower order.

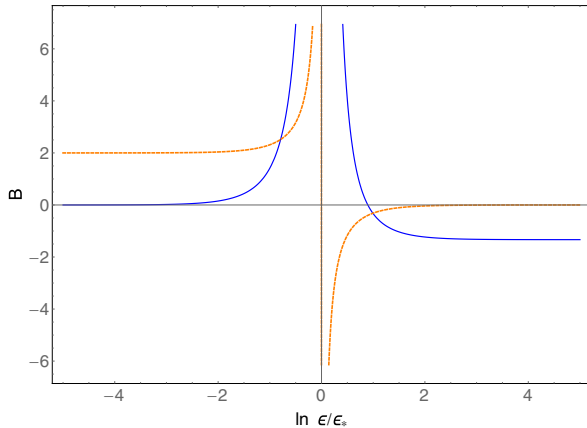


FIG. 3. Plot of the RG flow of $B = (Z\alpha)^4(\hat{d}_s - \hat{d}_v)$ (solid blue) and $B = (Z\alpha)(\hat{c}'_s - \hat{c}'_{v,\text{tot}})$ (dashed orange) vs $\ln \epsilon/\epsilon_*$, with $\eta_- = +1$.

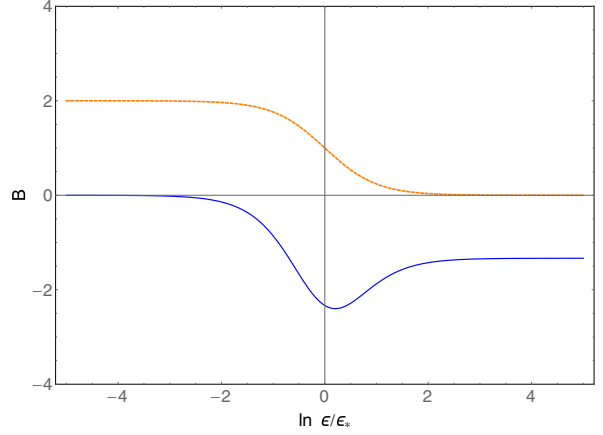


FIG. 4. Plot of the RG flow of $B = (Z\alpha)^4(\hat{d}_s - \hat{d}_v)/4$ (solid blue) and $B = (Z\alpha)(\hat{c}'_s - \hat{c}'_{v,\text{tot}})$ (dashed orange) vs $\ln \epsilon/\epsilon_*$, with $\eta_- = -1$.

The upshot to the order we work is that all calculations are captured by an RG-invariant scale ϵ_* of the following form:

$$\epsilon_*^2 = (Z\alpha)^2 [R_0^2 + R_1^2(Z\alpha) + R_2^2(Z\alpha)^2 + \dots]. \quad (44)$$

The length scales R_i are generalized nuclear moments whose values can weakly depend on m (e.g., logarithmically), and are computed below for several models of interest. Notice in particular that the overall factor $(Z\alpha)^2$ ensures ϵ_* is much smaller than the R_i , which turn out to be typical nuclear scales.

Finally, the second subsection in this part of the paper asks for observable combinations of energy levels from which ϵ_* drops out. Such combinations must always exist when there are more observables than there are nuclear parameters. What is crucial is that the numbers R_0 , R_1 , and R_2 above are *not* independent parameters in this sense since they enter into all observables, for *both* electronic and muonic atoms, purely through the single combination ϵ_* . Because of the explicit appearance of m , and the implicit dependence of the R_i on lepton mass, ϵ_* will be numerically different between electronic and muonic atoms.

A. Moments and polarizabilities

We start by making contact with nuclear models, computing the value of ϵ_*^\pm required to reproduce energy-shift calculations in the literature [and justifying Eq. (44)].

1. RG-invariant energy shifts

Consider first the energy shifts for atomic energy levels as a function of the RG-invariant parameters ϵ_*^\pm and η^\pm . The calculation is greatly simplified given the knowledge that ϵ_*^\pm proves to be much smaller than typical nuclear sizes [in retrospect due to the explicit factor $\epsilon_* \propto Z\alpha$ implied by (44)].

Expanding Eqs. (37), (38), (42), and (43) in the limit of small ϵ_*/ϵ , and specializing to $j = \frac{1}{2}$, we have

$$\begin{aligned}\hat{g}_1 &= -\frac{1}{2} + \frac{2\eta_+}{(Z\alpha)^2} \left(\frac{\epsilon_*^+}{\epsilon}\right)^2, \\ \hat{g}_2 &= -\frac{n^2-1}{6n^2} + \frac{4\eta_+}{(Z\alpha)^2} \left(\frac{\epsilon_*^+}{\epsilon}\right)^2 + \frac{8}{(Z\alpha)^4} \left(\frac{\epsilon_*^+}{\epsilon}\right)^4, \\ \hat{g}_3 &= -\frac{1}{8} - \frac{\eta_+}{(Z\alpha)^2} \left(\frac{\epsilon_*^+}{\epsilon}\right)^2 [1 + 2\ln(\epsilon_*^+/\epsilon)] \\ &\quad + \frac{2}{(Z\alpha)^4} \left(\frac{\epsilon_*^+}{\epsilon}\right)^4,\end{aligned}\quad (45)$$

while

$$\begin{aligned}\hat{f}_1 &= \frac{2}{3}, \\ \hat{f}_3 &= \frac{1}{2} - \frac{2\eta_-}{(Z\alpha)^2} \left(\frac{\epsilon_*^-}{\epsilon}\right)^2.\end{aligned}\quad (46)$$

Using these in the energy shifts, Eqs. (24) and (25), then gives the parity-even $j = \frac{1}{2}$ shift

$$\begin{aligned}\delta E_{nS_{1/2}} &\simeq \frac{4m^3(Z\alpha)^2}{n^3} \eta_+ (\epsilon_*^+)^2 \left\{ 2 + \left[\frac{12n^2 - n - 9}{2n^2(n+1)} \right. \right. \\ &\quad \left. \left. - 2\ln\left(\frac{2m\epsilon_*^+ Z\alpha}{n}\right) - 2H_{n+1} - 2\gamma + 4 \right] \right. \\ &\quad \left. \times (Z\alpha)^2 + \dots \right\},\end{aligned}\quad (47)$$

while the parity-odd $j = \frac{1}{2}$ state shifts by

$$\delta E_{nP_{1/2}} \simeq 2 \frac{n^2-1}{n^5} m^3 (Z\alpha)^4 \eta_- (\epsilon_*^-)^2 (1 + \dots).\quad (48)$$

As mentioned earlier, the nuclear shifts to $j = \frac{3}{2}$ states and higher are smaller than the order to which we work.

2. Fixed charge distributions

The simplest nuclear model treats it as a simple static charge distribution $\rho(\mathbf{r})$ and energy shifts for Dirac fermions orbiting such distributions have been computed in the limit where the radius R of the distribution is much smaller than atomic size a_b [2,20,25–29].

For such models in the limit $R \ll a_b$, the finite-size energy shift to leading and subleading order in R/a_b is parametrized by just three moments of the charge distribution. Expressions for this shift (as found by Refs. [2,20,25–29]) agree with (47) and (48) when $\eta := \eta_+ = \eta_- = +1$ and the RG-invariant parameter $\epsilon_*^+ = \epsilon_*^- =: \epsilon_*$ is given by

$$\epsilon_*^2 = \frac{(Z\alpha)^2}{12} \left(r_p^2 + \frac{1}{2} r_f^3 m Z\alpha + a_{\text{rel}}^2 (Z\alpha)^2 \right),\quad (49)$$

which corresponds to the generalized moments

$$R_0^2 = \frac{r_p^2}{12}, \quad R_1^2 = m \frac{r_f^3}{24}, \quad \text{and} \quad R_2^2 = \frac{a_{\text{rel}}^2}{12}.\quad (50)$$

The nuclear moments r_p^2 , r_f^3 , and a_{rel}^2 above are defined as follows.

At order $m^3 R^2 (Z\alpha)^4$, the only moment that appears is the charge radius

$$r_p^2 := \frac{1}{Ze} \int d^3\mathbf{r} r^2 \rho.\quad (51)$$

At order $m^4 R^3 (Z\alpha)^5$ only the Friar (or third Zemach) moment appears

$$r_f^3 := \frac{1}{(Ze)^2} \int d^3\mathbf{r} d^3\mathbf{r}' \rho(\mathbf{r}) \rho(\mathbf{r}') |\mathbf{r} - \mathbf{r}'|^3.\quad (52)$$

Finally, at order $m^3 R^2 (Z\alpha)^6$, there is one more moment that arises which we call a_{rel} . This moment has a more complicated structure, for which several authors have presented different but equivalent formulations [25,28,31]. Following [31], we write

$$a_{\text{rel}}^2 = r_p^2 \left[1 + \frac{1}{2} \ln(12) - \ln(Z\alpha) + \ln\left(\frac{r_{c1}}{r_p}\right) \right],\quad (53)$$

with the parameter r_{c1} [cf. Eq. (66) in [31]] given by

$$\begin{aligned}\ln \frac{r_{c1}}{r_p} - 1 &= \frac{6}{r_p^2} \int_0^\infty dr \ln(r/r_p) \frac{d}{dr} r^3 \\ &\quad \times \left\{ 2\pi\rho(r)[V^{(2)}(r)]^2 - [V(r)]^2 V^{(2)}(r) \right. \\ &\quad \left. - \frac{1}{r^2} \left[\frac{r}{2} + \frac{r_p^2}{6r} \right] \right\},\end{aligned}\quad (54)$$

where $V(r) \approx 1/r$, $V^{(2)}(r) \approx -r/2 - r_p^2/6r$, and $\rho(r)$ is the nuclear charge distribution.

This example illustrates several things. First, it shows that agreement with calculated energy shifts requires the parity-even and parity-odd RG invariants to be the same. This seems a reasonable consequence of the assumed parity invariance of the nuclear couplings: odd- and even-parity electrons (or muons) see the same nucleus. Furthermore, this example shows how moving past leading order does not introduce new independent RG-invariant parameters into the energy shifts. Instead, it provides a more accurate determination of the value of the single RG invariant ϵ_* . Finally, ϵ_* is independent of the lepton-state quantum numbers $jj_z\Pi$.

3. Nuclear polarizability

In general, nuclear contributions to atomic energy shifts arise that cannot be simply parametrized in terms of a static nuclear charge distribution, such as those due to “inelastic” Coulomb exchanges. These typically involve sums over intermediate nuclear states and so sample nuclear degrees of freedom outside of their ground state, and contain the effects of nuclear polarizability. A representative example of how such a calculation proceeds is sketched in Appendix A.

The upshot of these calculations is that they contribute (to within the accuracy we work here) to atomic energy shifts in a way that depends on the quantum numbers of the atomic state in the same way as does the charge-radius contribution. As a result, these contributions can also be captured by a shift in the value of the RG-invariant scale ϵ_* with $\eta = +1$.

In terms of the parametrization of Eq. (44) the calculations of Refs. [24,31–34] give contributions that first arise at order

$m^3 R^2 (Z\alpha)^5$ for muonic atoms, and $m^4 R^3 (Z\alpha)^5$ for electronic atoms. For muons, the inelastic two-photon exchange introduces a new contribution $R_1^2 \supset -\tilde{\alpha}'_{\text{pol}}/6$, where $\tilde{\alpha}'_{\text{pol}}$ is a generalized (mass-dependent) nuclear polarizability given by [35,36]

$$\tilde{\alpha}'_{\text{pol}} := \int_{E_T} dE \sqrt{\frac{m}{2E}} |\langle \phi_N | \vec{d} | E \rangle|^2, \quad (55)$$

where $|\phi_N\rangle$ is the nuclear ground state, $|E\rangle$ is the nuclear excited state with energy $E - M$, \vec{d} is the nuclear dipole operator (divided by the elementary charge), and E_T is the nuclear threshold excitation energy (which for helium [37] is ~ 20 MeV). Furthermore, at order $m^4 R^3 (Z\alpha)^5$, the nuclear polarizability also adjusts the value of R_1^2 , so that $R_1^2 \supset m\tilde{r}_F^3/24$, where now \tilde{r}_F^3 is a generalized Friar moment. For muonic atoms [24],

$$\tilde{r}_{F,\mu}^3 = -\frac{1}{(Ze)^2} \int d^3r \int d^3r' |r - r'|^3 \langle \phi_N | \hat{\rho}^\dagger(r) \hat{\rho}(r') | \phi_N \rangle, \quad (56)$$

where $\hat{\rho}(r)$ is the (un-normalized) nuclear charge density operator, and $|\phi_N\rangle$ is again the nuclear ground state [note that the matrix element $\langle \phi_N | \hat{\rho}^\dagger(r) \hat{\rho}(r') | \phi_N \rangle$ is distinct from $\rho(r)\rho(r') = \langle \phi_N | \hat{\rho}^\dagger(r) | \phi_N \rangle \langle \phi_N | \hat{\rho}(r') | \phi_N \rangle$, which appears in (52)]. For electronic atoms, the static dipole polarizability also arises at this order, and so [36]

$$\tilde{r}_{F,e}^3 = -\frac{\tilde{\alpha}_{\text{pol}}}{6} - \frac{1}{(Ze)^2} \int d^3r \times \int d^3r' |r - r'|^3 \langle \phi_N | \hat{\rho}^\dagger(r) \hat{\rho}(r') | \phi_N \rangle, \quad (57)$$

where

$$\tilde{\alpha}_{\text{pol}} = \frac{2}{3} \int dE \left\{ \frac{19}{6} |\langle \phi_N | \vec{d} | E \rangle|^2 + 5 |\langle \phi_N | \vec{d} \ln(2E/m) | E \rangle|^2 \right\} \quad (\text{muons}) \quad (58)$$

is the weighted static electric nuclear polarizability. Finally, R_2^2 is also altered, although in this case the exact form of the inelastic exchange is not known for helium [31]. However, for both electrons and muons it is expected to be well described by a local interaction due to the high excitation energy of the ${}^4\text{He}$ nucleus relative to atomic scales, and so should appear as some generalized a_{rel} which we denote \tilde{a}_{rel} , in analogy with the generalized Friar moment. Altogether, inclusion of nuclear polarizability effects can be encoded simply by the contributions

$$R_0^2 = \frac{r_F^2}{12}, \quad R_1^2 = -\frac{\tilde{\alpha}'_{\text{pol}}}{6} + m \frac{\tilde{r}_F^3}{24}, \quad \text{and} \quad R_2^2 = \frac{\tilde{a}_{\text{rel}}}{12}, \quad (59)$$

where $\tilde{\alpha}'_{\text{pol}}$ is defined in (58) for muons, and is 0 for electrons.

The bottom line is again that these contributions represent particular kinds of contributions to ϵ_* , and are not contributing to atomic energy shifts as independent parameters. Consequently, assessments of nuclear errors involved in each of these kinds of processes can be interpreted as contributions to the total theoretical uncertainty in microscopic predictions for ϵ_* .

However, the real power of the above expressions in terms of ϵ_* is in their very broad generality. Although specific kinds of nuclear physics contribute to the value of ϵ_* , the same would also be true for *arbitrary* short-distance physics, regardless of whether this has nuclear origins or not. Because the PPEFT framework parametrizes all possible interactions localized at the nucleus consistent with symmetries, the contribution to atomic energies of these couplings (through their RG-invariant parametrizations ϵ_* and η) are guaranteed to capture any short-distance physics that shares these symmetries to the given order in R/a_B , regardless of the details of how that physics might be modeled.

B. Nucleus-independent combinations

Exploitation of more precise measurements of atomic level spacings is currently hampered by theoretical uncertainties associated with predicting the energy shifts due to nuclear physics. Ongoing efforts are underway to improve the theoretical prediction for these nuclear shifts, and in the language of PPEFT these can be regarded as improving the theoretical prediction for the RG-invariant parameter ϵ_* . In this view, the various individual contributions to nuclear level shifts, e.g., charge radius, Friar moment, polarizability, and so on, all enter together only through this single parameter.⁴

The fact that the nucleus can only influence atomic levels through ϵ_* suggests another approach towards reducing theoretical error for precision atomic measurements. Rather than trying to reduce the theoretical error by computing this parameter more accurately, why not instead identify combinations of observables from which the parameter ϵ_* cancels out? Any such combination is a quantity for which the theoretical error is much smaller since it does not depend at all on any nuclear uncertainties.

To formalize this, we write the energy levels of hydrogenic atoms as

$$E_{nj\pm} = E_{nj}^{\text{Dirac}} + \delta E_{nj\pm}^{\text{QED}} + \delta E_{nj\pm}^{\text{PP}} + \delta E_{nj\pm}^{\text{PPQED}}, \quad (60)$$

where quantum numbers n , j and parity \pm are used as labels. Here, E^{Dirac} is the energy eigenvalue predicted by the Dirac-Coulomb solution, and δE^{QED} contains all QED radiative corrections in the limit of a point nucleus. δE^{PP} is the nucleus-dependent contribution given above, and δE^{PPQED} contains the influence of nonzero nuclear size on all QED radiative corrections.

When comparing to the literature, such as the three-photon contributions evaluated in Ref. [31], it is the ‘‘high-energy’’ parts of graphs whose effects can be captured by a shift in the parameters of the effective theory, which in the present instance means shifting the value of ϵ_*^2 in $\delta E_{nj\pm}^{\text{PP}}$. The same cannot be done for the ‘‘low-energy’’ parts that correspond to graphs evaluated within the effective theory using nucleus-modified propagators and so these contributions

⁴Since ϵ_* depends explicitly on the lepton mass [cf. the R_2^3 term in (44)], strictly speaking there is a single parameter controlling electron-type atoms and another one for muonic atoms, and any evidence for a difference in these parameters for electrons and muons is evidence for the presence of a nonzero size for the parameter R_2^3 .

are either already included in the perturbative expansion of the energy shifts [Eqs. (24) and (25)], or else grouped into $\delta E_{nj\pm}^{\text{PPQED}}$.

Both of δE^{PP} and δE^{PPQED} suffer from systematic uncertainties arising from nuclear physics (and the proton radius problem, should this prove not to be due to experimental error). But, because δE^{PPQED} starts out with higher powers of α it only depends on the lowest-order R_0^2 contributions⁵ to ϵ_* , unlike δE^{PP} which in principle depends on all of the parameters R_0^2 through to R_2^2 of Eq. (44).

However, it is differences $\Delta E_{1\rightarrow 2} := E_{n_1, j_1, \pm_1} - E_{n_2, j_2, \pm_2}$ between energy levels that are measured spectroscopically. For these quantities we therefore write

$$\Delta E_{1\rightarrow 2} = \Delta E_{1\rightarrow 2}^{\text{EM}} + \Delta E_{1\rightarrow 2}^{\text{PP}} + \Delta E_{1\rightarrow 2}^{\text{PPQED}}, \quad (61)$$

in which the Dirac-Coulomb and point-source QED effects are grouped together into the term labeled “EM.” Because $\Delta E_{1\rightarrow 2}^{\text{EM}}$ is calculable with negligible error, we focus below on the nucleus-dependent combination

$$\widehat{\Delta E}_{1\rightarrow 2} := \Delta E_{1\rightarrow 2} - \Delta E_{1\rightarrow 2}^{\text{EM}} = \Delta E_{1\rightarrow 2}^{\text{PP}} + \Delta E_{1\rightarrow 2}^{\text{PPQED}}. \quad (62)$$

Our goal is to identify linear combinations of these observables from which the parameter ϵ_* cancels. With upcoming experiments in mind we do so explicitly here for muonic atoms up to the accuracy of $m^4 R^3 (Z\alpha)^5$ required to see the Friar moment. For electrons we go to the same accuracy, which is slightly more involved due to the necessity of keeping terms at both order $m^4 R^3 (Z\alpha)^5$ and $m^3 R^2 (Z\alpha)^6$ since these are similar in size (due to the numerical coincidence $m_e R \sim Z\alpha$).

1. Predicted energy differences

In order to pursue this program, we need complete expressions for the ϵ_* dependence of all relevant levels, including both the δE^{PP} and δE^{PPQED} contributions. Since to the desired accuracy ϵ_* does not appear at all within δE^{PP} for the energies of $j > \frac{1}{2}$ states, we focus on itemizing all relevant contributions for $j = \frac{1}{2}$.

The mixed nuclear-QED contribution has been evaluated at the order required, and we simply quote the result here. For both electrons and muons the leading result is given by [38,39]

$$\begin{aligned} \delta E^{\text{PPQED}} &= \frac{4\eta_{nl}^{(e)}}{n^3} m_\mu^3 \alpha (Z\alpha)^2 \epsilon_{*\mu}^2 \quad (\text{muons}) \\ &= \frac{4\eta_{nl}^{(\mu)}}{n^3} m_e^3 \alpha (Z\alpha)^3 \epsilon_{*e}^2 \quad (\text{electrons}), \end{aligned} \quad (63)$$

with the dimensionless coefficients $\eta_{nl}^{(a)}$ depending on the quantum numbers of the lepton state. In these expressions, the subscripts “ $a = \mu, e$ ” on ϵ_{*a} is meant to underline that it is evaluated using the muon mass in its $R_2^3 m Z\alpha$ contribution.

⁵Apart from logarithms (see, e.g., [31]) inasmuch as other nuclear scales aside from R_0 can appear logarithmically in low-energy contributions. When this occurs, we write a contribution of the form $\ln(mR_x)$ as $\ln(mR_0) + \ln(R_x/R_0)$ and absorb the m -independent factor $\ln(R_x/R_0)$ into the R_2^2 term of (44).

We identify the ϵ_* dependence by trading the dependence on r_p^2 given in the literature for ϵ_* using only the leading R_0^2 contribution from Eq. (49): $\epsilon_*^2 = \frac{1}{12} (Z\alpha)^2 r_p^2$.

For electronic atoms η_{nl} is given by [38]

$$\eta_{nl}^{(e)} := (8 \ln 2 - 10) \delta_{l0} \quad (\text{electron}), \quad (64)$$

which vanishes for $l \neq 0$ since the wave function must have support at the position of the nucleus because the Bohr radius for the orbit $a_b \sim (Z\alpha m_e)^{-1}$ is much larger than the Compton wavelength $\lambda_c \sim m_e^{-1}$ of the virtual electrons in the QED loop. The same is not true for muons since αm_μ is comparable to m_e , and so for muonic atoms $\eta_{nl}^{(\mu)}$ need not vanish for $l \neq 0$. The precise value of $\eta_{nl}^{(\mu)}$, given in [39], is not required in what follows.

Collecting results we have the following:

Muons. Here, we have the nonzero nuclear-dependent energy shifts to the desired order⁶

$$\delta E_{nS_{1/2}}^{\text{PP}} + \delta E_{nS_{1/2}}^{\text{PPQED}} = \frac{4m_\mu^3 (Z\alpha)^2}{n^3} (2 + \eta_{n0}^{(\mu)} \alpha) \epsilon_{*\mu}^2 \quad (65)$$

while

$$\delta E_{nP_{1/2}}^{\text{PP}} + \delta E_{nP_{1/2}}^{\text{PPQED}} = m_\mu^3 (Z\alpha)^2 \eta_{n1}^{(\mu)} \alpha \epsilon_{*\mu}^2 \quad (66)$$

and

$$\delta E_{nP_{3/2}}^{\text{PP}} + \delta E_{nP_{3/2}}^{\text{PPQED}} = m_\mu^3 (Z\alpha)^2 \eta_{n1}^{(\mu)} \alpha \epsilon_{*\mu}^2. \quad (67)$$

Combining these expressions provides the following expressions for the measurable energy differences for the lowest angular momentum states:

$$\widehat{\Delta E}_{nS_{1/2}-nP_{1/2}} = \frac{4m_\mu^3 (Z\alpha)^2}{n^3} [2 + (\eta_{n0}^{(\mu)} - \eta_{n1}^{(\mu)}) \alpha] \epsilon_{*\mu}^2, \quad (68)$$

$$\widehat{\Delta E}_{nS_{1/2}-nP_{3/2}} = \frac{4m_\mu^3 (Z\alpha)^2}{n^3} [2 + (\eta_{n0}^{(\mu)} - \eta_{n1}^{(\mu)}) \alpha] \epsilon_{*\mu}^2, \quad (69)$$

while

$$\widehat{\Delta E}_{nP_{1/2}-nP_{3/2}} = 0. \quad (70)$$

Electrons. The corresponding formulas for electrons are

$$\begin{aligned} \delta E_{nS_{1/2}}^{\text{PP}} + \delta E_{nS_{1/2}}^{\text{PPQED}} &= \frac{4m_e^3 (Z\alpha)^2}{n^3} \epsilon_{*e}^2 \left\{ 2 + \left[\frac{12n^2 - n - 9}{2n^2(n+1)} - 2 \ln \left(\frac{2m_e \epsilon_{*e} Z\alpha}{n} \right) \right. \right. \\ &\quad \left. \left. - 2H_{n+1} - 2\gamma + 4 + \frac{\eta_{n0}^{(e)}}{Z} \right] (Z\alpha)^2 \right\}, \end{aligned} \quad (71)$$

as well as

$$\delta E_{nP_{1/2}}^{\text{PP}} + \delta E_{nP_{1/2}}^{\text{PPQED}} = 2 \left(\frac{n^2 - 1}{n^5} \right) m_e^3 (Z\alpha)^4 \epsilon_{*e}^2, \quad (72)$$

but now $\delta E_{nP_{3/2}}^{\text{PP}} = \delta E_{nP_{3/2}}^{\text{PPQED}} = 0$ to the order of interest.

⁶We switch to spectroscopic notation where states are labeled by j and parity, so the labels S, P, D, F, \dots are proxies for parity. Thus, S (or P) are parity-even (-odd) states with spin $j = \frac{1}{2}$, while D (or F) are parity-even (-odd) with spin $j = \frac{3}{2}$ and so on.

The corresponding energy differences for electrons are therefore

$$\widehat{\Delta E}_{nS_{1/2}-nP_{3/2}} = \frac{4m_e^3(Z\alpha)^2}{n^3} \epsilon_{*e}^2 \left\{ 2 + \left[\frac{12n^2 - n - 9}{2n^2(n+1)} - 2 \ln \left(\frac{2m_e \epsilon_{*e} Z\alpha}{n} \right) - 2H_{n+1} - 2\gamma + 4 + \frac{\eta_{n0}^{(e)}}{Z} \right] (Z\alpha)^2 \right\}, \quad (73)$$

as well as

$$\widehat{\Delta E}_{nS_{1/2}-nP_{1/2}} = \frac{4m_e^3(Z\alpha)^2}{n^3} \epsilon_{*e}^2 \left\{ 2 + \left[\frac{12n^2 - n - 9}{2n^2(n+1)} - 2 \ln \left(\frac{2m_e \epsilon_{*e} Z\alpha}{n} \right) - 2H_{n+1} - 2\gamma + 4 + \frac{\eta_{n0}^{(e)}}{Z} - \frac{n^2 - 1}{2n^2} \right] (Z\alpha)^2 \right\} \quad (74)$$

and

$$\widehat{\Delta E}_{nP_{1/2}-nP_{3/2}} = 2 \left(\frac{n^2 - 1}{n^5} \right) m_e^3 (Z\alpha)^4 \epsilon_{*e}^2. \quad (75)$$

In essence, these expressions imply that the nuclear-size contributions to a great many energy electronic and muonic levels can be parametrized in terms of just two parameters, ϵ_{*e} and $\epsilon_{*\mu}$. By eliminating these parameters, we can derive relations that directly connect measurable quantities. The relations derived in this way are therefore known with smaller theoretical errors since they are entirely independent of nuclear uncertainties.

2. Levels with $n = 2$

We start by concentrating on the energy levels that have already been measured, and so restrict our attention to the special case $n = 2$.

Focusing first on muonic atoms, the nuclear contribution to the differences between the three levels $2S_{1/2}$, $2P_{1/2}$, and $2P_{3/2}$ is controlled by the single parameter $\epsilon_{*\mu}$. This means there must be a nucleus-independent combination relating the two independent energy differences. This can be taken to be (70): $\widehat{\Delta E}_{nP_{1/2}-nP_{3/2}} = 0$ is a statement unclouded by nuclear uncertainties, in particular for $n = 2$.

Alternatively, (68) provides an accurate experimental determination of ϵ_* for muonic helium:

$$\epsilon_{*\mu}^2 = \frac{\widehat{\Delta E}_{2S_{1/2}-2P_{1/2}}}{m_\mu^3 (Z\alpha)^2 \left[1 + \frac{1}{2} (\eta_{20}^{(\mu)} - \eta_{21}^{(\mu)}) \alpha \right]} + O[(Z\alpha)^4]. \quad (76)$$

Turning now to the ${}^4\text{He}^+$ ion, the nuclear contribution to the two independent differences between the $2S_{1/2}$, $2P_{1/2}$, and $2P_{3/2}$ levels is controlled by the single parameter ϵ_{*e} , again suggesting there is a nucleus-independent combination.

This can be found by using (74) to eliminate ϵ_{*e} and using the result in (75) to predict the $2P_{1/2}-2P_{3/2}$ transition in terms of the $2S_{1/2}-2P_{1/2}$ transition:

$$\widehat{\Delta E}_{2P_{1/2}-2P_{3/2}} = \frac{3}{16} (Z\alpha)^2 \widehat{\Delta E}_{2S_{1/2}-2P_{1/2}} + O[(Z\alpha)^7]. \quad (77)$$

We write the error in this expression as $(Z\alpha)^7$ rather than $(Z\alpha)^8$ because the corrections to (75) arise at relative order $(mRZ\alpha)$, though for electrons this is numerically closer to order $(Z\alpha)^8$. Alternatively, using the $2S_{1/2}-2P_{1/2}$ to predict the $2S_{1/2}-2P_{3/2}$ difference leads to the equivalent prediction

$$\widehat{\Delta E}_{2S_{1/2}-2P_{3/2}} = \widehat{\Delta E}_{2S_{1/2}-2P_{1/2}} \left[1 + \frac{3}{16} (Z\alpha)^2 + O[(Z\alpha)^4] \right]. \quad (78)$$

While naively ϵ_{*e} might be obtained from (75), leading to

$$\epsilon_{*e}^2 = \frac{16}{3m_e^3 (Z\alpha)^4} \widehat{\Delta E}_{2P_{1/2}-2P_{3/2}} + O[(Z\alpha)^4], \quad (79)$$

this determines it with larger relative error than it would have been by solving for ϵ_{*e} from one of the other two energy differences. Taking this latter approach instead leads (see Appendix B, including the result for general n) to

$$\begin{aligned} m_e^2 \epsilon_{*e}^2 &\simeq \frac{1}{m_e (Z\alpha)^2} \widehat{\Delta E}_{2S_{1/2}-2P_{1/2}} \\ &\times \left\{ 1 + \frac{(Z\alpha)^2}{2} \left[\ln \left(\frac{\widehat{\Delta E}_{2S_{1/2}-2P_{1/2}}}{m_e} \right) - \frac{3}{2} + 2\gamma - \frac{\eta_{20}}{Z} \right] \right\} \\ &+ O \left((Z\alpha)^2 \frac{\widehat{\Delta E}_{2S_{1/2}-2P_{1/2}}}{m_e} \right), \end{aligned} \quad (80)$$

and the correction is now down by $(Z\alpha)^4$ relative to the leading term.

3. More general n

The relations found above for the special case $n = 2$ might not be all that surprising. However, should experiments access transitions with higher n , the fact that all nuclear contributions are controlled by the single parameter ϵ_* becomes ever more predictive. This section makes a start at some of the nuclear-free relations that can be derived in this way for general n .

Muons. We start with muons, which are simpler. A start is the prediction for the general $nS_{1/2}-nP_{1/2}$ shift for any n given measurements of this shift for $n = 2$. For $n = 2$, we use (69) to infer the value of $\epsilon_{*\mu}$, which when substituted into (68) for general n , gives

$$\widehat{\Delta E}_{nS_{1/2}-nP_{1/2}} = \frac{8 \left[2 + \alpha (\eta_{n0}^{(\mu)} - \eta_{n1}^{(\mu)}) \right]}{n^3 \left[2 + \alpha (\eta_{20}^{(\mu)} - \eta_{21}^{(\mu)}) \right]} \widehat{\Delta E}_{2S_{1/2}-2P_{1/2}}. \quad (81)$$

Similarly, generic muonic S-S transitions become

$$\widehat{\Delta E}_{n_1S_{1/2}-n_2S_{1/2}} = 2 \left(\frac{2 + \alpha \eta_{n_1 0}^{(\mu)}}{n_1^2} - \frac{2 + \alpha \eta_{n_2 0}^{(\mu)}}{n_2^2} \right) \widehat{\Delta E}_{2S_{1/2}-2P_{1/2}}. \quad (82)$$

A similar argument relates the $S_{1/2}-P_{3/2}$ transitions for general n :

$$\begin{aligned} &\frac{n_1^2}{2 + \alpha (\eta_{n_1 0}^{(\mu)} - \eta_{n_2 1}^{(\mu)})} \widehat{\Delta E}_{n_1S_{1/2}-n_1P_{3/2}} \\ &= \frac{n_2^2}{2 + \alpha (\eta_{n_2 0}^{(\mu)} - \eta_{n_2 1}^{(\mu)})} \widehat{\Delta E}_{n_2S_{1/2}-n_2P_{3/2}}. \end{aligned} \quad (83)$$

Electrons. Similar expressions hold for electronic atoms. The prediction for the $nS_{1/2}-nP_{1/2}$ shift for any n in terms of this shift for $n = 2$ obtained by using (80) to infer the value of ϵ_{*e} used in (74) gives

$$\widehat{\Delta E}_{nS_{1/2}-nP_{1/2}} = \frac{8}{n^3} \widehat{\Delta E}_{2S_{1/2}-2P_{1/2}} \times \left\{ 1 + (Z\alpha)^2 \left[N(n) - \frac{n^2 - 1}{4n^2} \right] \right\}, \quad (84)$$

in which we define

$$N(n) := \frac{12n^2 - n - 9}{4n^2(n+1)} - H_{n+1} + \frac{5}{4} + \frac{\eta_{n0}^{(e)}}{2Z} - \frac{\eta_{20}^{(e)}}{2Z} - \ln\left(\frac{2}{n}\right). \quad (85)$$

The predictions for electronic S - S transitions is similarly

$$\widehat{\Delta E}_{n_1S-n_2S} = \widehat{\Delta E}_{2S_{1/2}-2P_{1/2}} \left\{ \frac{1}{n_1^3} - \frac{1}{n_2^3} + (Z\alpha)^2 \left[\frac{N(n_1)}{n_1^3} - \frac{N(n_2)}{n_2^3} \right] \right\}. \quad (86)$$

The nucleus-free prediction for the difference between the P states for electronic atoms becomes

$$\frac{n_1^5}{n_1^2 - 1} \widehat{\Delta E}_{n_1P_{1/2}-n_1P_{3/2}} = \frac{n_2^5}{n_2^2 - 1} \widehat{\Delta E}_{n_2P_{1/2}-n_2P_{3/2}}. \quad (87)$$

This situation is somewhat more complicated for electronic S -wave states, but using

$$n_1^3 \widehat{\Delta E}_{n_1S_{1/2}-n_1P_{1/2}} - n_2^3 \widehat{\Delta E}_{n_2S_{1/2}-n_2P_{1/2}} = 4m_e^3 (Z\alpha)^4 \epsilon_{*e}^2 (F[n_1] - F[n_2]), \quad (88)$$

where

$$F[n] := \frac{12n^2 - n - 9}{2n^2(n+1)} - \frac{n^2 - 1}{24n^2} + 2 \ln n - 2H_{n+1} + \frac{\eta_{n0}^{(e)}}{Z}, \quad (89)$$

the difference becomes

$$\frac{1}{F[n_1] - F[n_2]} (n_1^3 \widehat{\Delta E}_{n_1S_{1/2}-n_1P_{1/2}} - n_2^3 \widehat{\Delta E}_{n_2S_{1/2}-n_2P_{1/2}}) - \frac{24n_1^5}{n_1^2 - 1} \widehat{\Delta E}_{n_1P_{1/2}-n_1P_{3/2}} = 0, \quad (90)$$

which is again free of nuclear uncertainties. It is clear that a great many such relations can be derived in the same way.

IV. NUMERICAL EXAMPLE

At the moment, data [40] are only available for the $2P_{1/2}-2S_{1/2}$ transition in ${}^4\text{He}^+$. With this transition, we can use (86) to predict the $1S-2S$ transition in hydrogenic helium, which is relevant for upcoming experiments [41]. Subtracting the pointlike physics listed in [23], we compute

$$\widehat{\Delta E}_{2S_{1/2}-2P_{1/2}}^{(\text{exp})} = -2.58(5) \times 10^{-9} \text{ Ry}, \quad (91)$$

in units of the Rydberg energy. Here, the number in parentheses is the error on the last digit. The predicted $1S-2S$ transition

is then

$$\Delta E_{2S-1S} = 2.999\,706\,711\,8(4) \text{ Ry} \\ = 9.868\,561\,009(1) \times 10^9 \text{ MHz}, \quad (92)$$

where in the last line, we used $\text{Ry} = 3.289\,841\,960\,355 \times 10^{15} \text{ Hz}$ from the 2014 CODATA review [13]. Our prediction agrees with [41] and [23], however, the error we report is nominally a few times larger than they report (three times [41] and four times [23]). What is important in our case is that the error is completely independent of nuclear uncertainties, and is dominated by the experimental error. Our result will therefore only improve as future experiments improve their precision, and will never be hindered by a particular choice of nuclear model.

V. CONCLUSION

We here apply the PPEFT framework to muonic and electronic atoms with spinless nuclei, which produce systematic parametrizations of the energy level shifts due to *all* short-range physics, including (but not limited to) uncertainties in evaluating nuclear contributions. Our parametrization cleanly identifies a single mass-dependent length scale ϵ_* that encodes the effect of all nuclear physics on atomic energy levels.

That is, in discussions of finite-size contributions to atomic energy shifts, one often writes (see, e.g., [24])

$$\Delta E = \delta_{\text{QED}} + \delta_{\text{FS},r^2}(r_p^2) + \delta_{\text{FS,Other}}, \quad (93)$$

where δ_{QED} is all of the non-finite-size-dependent contributions, $\delta_{\text{FS},r^2}(r_p^2)$ is all the finite-size terms that are proportional to the squared charge radius, and $\delta_{\text{FS,Other}}$ is all the other finite-size contributions. Our observation is that at the level of atomic energy shifts, this division is artificial. The real division is

$$\Delta E = \delta_{\text{QED}} + \delta_{\epsilon_*}, \quad (94)$$

where δ_{QED} is all point-nucleus contributions (as above), and δ_{ϵ_*} is all finite-size contributions, which is a known function of the one length scale ϵ_* . The separation of ϵ_* into different sources (such as moments of the nuclear charge distribution, and nuclear polarizability) is a theoretical exercise (although certainly a worthy one) that always needs supplementary information, such as input from theoretical models and scattering data. However, ϵ_* is just one number, so once it is determined from a single measurement, it can be used to predict the finite-size contribution of all other measurements.

As a practical application of this observation, we use two different strategies to make predictions about spectroscopic transition for electronic and muonic atoms that are free of ϵ_* . For these observables our formulas reduce the theoretical error in tests of QED by eliminating any uncertainties arising from explicit models of the nucleus. The same predictions are also independent of any potential short-range new physics (should this prove to be responsible for the proton-radius problem) allowing tests of QED using only muonic ${}^4\text{He}$ whose validity is undiminished by the existence of such forces.

Our first strategy is using a single measurement to solve for ϵ_* , and then use that to predict all other measurements. Doing so, we find explicitly predictions for the following transitions:

For muonic atoms, we find

$$\widehat{\Delta E}_{nS_{1/2}-nP_{1/2}} = \frac{8[2 + \alpha(\eta_{n0}^{(\mu)} - \eta_{n1}^{(\mu)})]}{n^3[2 + \alpha(\eta_{20}^{(\mu)} - \eta_{21}^{(\mu)})]} \widehat{\Delta E}_{2S_{1/2}-2P_{1/2}} \quad (95)$$

and

$$\widehat{\Delta E}_{n_1S_{1/2}-n_2S_{1/2}} = 2\left(\frac{2 + \alpha\eta_{n_10}^{(\mu)}}{n_1^2} - \frac{2 + \alpha\eta_{n_20}^{(\mu)}}{n_2^2}\right) \widehat{\Delta E}_{2S_{1/2}-2P_{1/2}}, \quad (96)$$

while electronic atoms produce

$$\begin{aligned} \widehat{\Delta E}_{nS_{1/2}-nP_{1/2}} &= \frac{8}{n^3} \widehat{\Delta E}_{2S_{1/2}-2P_{1/2}} \left\{ 1 + (Z\alpha)^2 \right. \\ &\quad \left. \times \left[N(n) - \frac{n^2 - 1}{4n^2} \right] \right\} \end{aligned} \quad (97)$$

and

$$\begin{aligned} \widehat{\Delta E}_{n_1S-n_2S} &= \widehat{\Delta E}_{2S_{1/2}-2P_{1/2}} \left\{ \frac{1}{n_1^3} - \frac{1}{n_2^3} + (Z\alpha)^2 \right. \\ &\quad \left. \times \left[\frac{N(n_1)}{n_1^3} - \frac{N(n_2)}{n_2^3} \right] \right\}, \end{aligned} \quad (98)$$

with $N(n)$ defined in (85).

Our second approach is to avoid solving for ϵ_* altogether, and instead find general linear combinations of measurements for which it falls out. In this way, we predict the following: For muonic systems,

$$\begin{aligned} &\frac{n_1^2}{2 + \alpha(\eta_{n_10}^{(\mu)} - \eta_{n_21}^{(\mu)})} \widehat{\Delta E}_{n_1S_{1/2}-n_1P_{3/2}} \\ &= \frac{n_2^2}{2 + \alpha(\eta_{n_20}^{(\mu)} - \eta_{n_21}^{(\mu)})} \widehat{\Delta E}_{n_2S_{1/2}-n_2P_{3/2}}, \end{aligned} \quad (99)$$

while for electronic systems,

$$\begin{aligned} &\frac{1}{F[n_1] - F[n_2]} (n_1^3 \Delta E_{n_1S_{1/2}-n_1P_{1/2}} - n_2^3 \Delta E_{n_2S_{1/2}-n_2P_{1/2}}) \\ &- \frac{24n_1^5}{n_1^2 - 1} \Delta E_{n_1P_{1/2}-n_1P_{3/2}} = 0, \end{aligned} \quad (100)$$

where $F[n]$ is defined in (89).

Using the only available data for the helium ion (the $2S-2P$ Lamb shift in ordinary ${}^4\text{He}^+$), we use (86) to predict a $1S-2S$ transition $\nu_{1S-2S} = 9.868\,561\,009(1) \times 10^9$ MHz. While our uncertainty in this prediction is roughly four times the uncertainty in the literature, our error is dominated by the experimental precision of the $2S-2P$ measurement. Consequently, our predictions will become more and more precise as experiments improve, and remain unencumbered by the inherent uncertainty in choice of nuclear model.

Although we here address only spinless nuclei, it is certainly possible to include nuclei with spin in the PPEFT framework, and work is ongoing to do so. Although nuclear spin changes the counting of parameters in the energy shift formulas above, the principle remains exactly the same and we expect in this case also to be able to build observables from which short-range contributions completely drop out.

ACKNOWLEDGMENTS

We thank R. Hill, B. Holdom, M. Horbatsch, T. Jacobson, R. Koniuk, B. Nickel, S. Penin, M. Pospelov, I. Rothstein, K. Zuber, and K. Pachucki for discussions and A. Antognini, F. Kottman, and R. Pohl for very helpful correspondence. We thank the organizers of the workshop ‘Precision Measurements and Fundamental Physics: the Proton Radius and Beyond’ held at the Mainz Institute for Theoretical Physics (MITP), for providing such stimulating environs where part of this work was completed. This research was supported in part by funds from the Natural Sciences and Engineering Research Council (NSERC) of Canada. Research at the Perimeter Institute is supported in part by the Government of Canada through Industry Canada, and by the Province of Ontario through the Ministry of Research and Information (MRI).

APPENDIX A: POLARIZABILITY IN A NUCLEAR MODEL

To illustrate how nuclear polarizabilities enter into the PPEFT framework, this appendix considers a relatively simple nuclear model, following Refs. [24,34]. The model works with nucleons and leptons with states $|NJJ_z; njj_z\rangle$ representing the nuclear (upper case) quantum numbers and lepton (lower case) quantum numbers. The Hamiltonian of the system is

$$H = H_N + H_f + \Delta H, \quad (A1)$$

where H_N is the Hamiltonian of the nucleus (whose details never need be explicitly written, with the basis of nuclear states $|NJJ_z\rangle$ assumed known), H_f is the Schrödinger or Dirac-Coulomb Hamiltonian for the lepton interacting with a point-source Coulomb potential, and ΔH is given by

$$\Delta H = \frac{Z\alpha}{r} - Z\alpha \int d^3r' \frac{\hat{q}(\mathbf{r}')}{|\mathbf{r} - \mathbf{r}'|}, \quad (A2)$$

where \hat{q} is the electric charge operator written in terms of the quantum nuclear degrees of freedom (such as the nucleon positions and charges). The perturbation subtracts out the point-source Coulomb interaction appearing in H_f and replaces it with the more realistic nuclear electromagnetic source distribution.

Working perturbatively in ΔH leads to a graphical expansion that includes those of Fig. 5. Of these, the leftmost graph is linear in the nonpointlike Coulomb-nuclear coupling ΔH , and involves one factor of the nuclear charge-density operator \hat{q} evaluated within the nuclear ground state $\langle 0|\Delta H|0\rangle$. It is this type of graph that gives the contributions that look like the charge radius r_p^2 of the nuclear charge distribution $\rho(\mathbf{r}) = \langle 0|\hat{q}(\mathbf{r})|0\rangle$.

Terms quadratic in this same nuclear charge distribution, such as the Friar moment r_F^3 of (52), arise from the second graph in Fig. 5 that are quadratic in ΔH but also only involve the nucleus in its ground state. The first two types of graphs therefore have counterparts for leptons interacting with a specified charge distribution and so can be expected to contribute to energy shifts in the same way, leading to contributions to ϵ_* of the form given in (49).

It is the final graph of Fig. 5 (and its crossed counterpart) that contains the nuclear polarizability and so is not simply captured by static moments of a given nuclear distribution

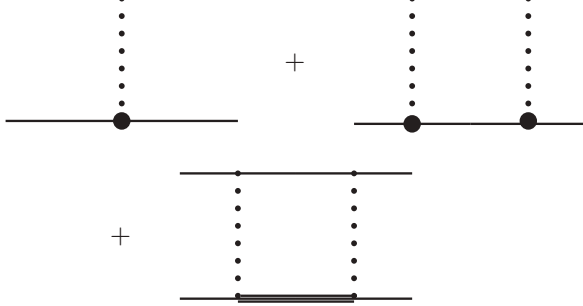


FIG. 5. Graphs arising from the perturbative expansion of nuclear electromagnetic interactions. The upper solid line represents the atomic lepton, dotted lines represent the Coulomb part of the electromagnetic field, and the lower solid line represents the nucleus in its ground state. The fat dot vertex includes a nonpointlike momentum-dependent correction to the Coulomb vertex, while the fat solid line represents the propagation of an excited nuclear state. Crossed graphs are also present even though they are not drawn.

$\rho(\mathbf{r}) = \langle 0 | \hat{\rho}(\mathbf{r}) | 0 \rangle$. For the nuclear sector, this graph contributes a contribution involving a sum over nuclear states involving the off-diagonal matrix elements $|\langle N | \hat{\rho}(\mathbf{r}) | 0 \rangle|^2$.

Explicitly, in [34] Friar gives the following expression for the atomic energy shift due to such a polarizability:

$$\delta E_{\text{pol}} = -\frac{4\pi}{3}(Z\alpha)^2 |\phi_n(0)|^2 \sum_{N \neq 0} \left[\sqrt{\frac{2m}{\omega_N}} |\langle N | \mathbf{D} | 0 \rangle|^2 + \frac{m}{4} \int d^3x \int d^3y \langle 0 | \rho(\mathbf{y}) | N \rangle \langle N | \rho(\mathbf{x}) | 0 \rangle |\mathbf{x} - \mathbf{y}|^3 \right], \quad (\text{A3})$$

where \mathbf{D} is the nucleon electric dipole operator $\mathbf{D} = \int d^3x \mathbf{x} \rho(\mathbf{x})$, and ω_N is the excitation energy of the intermediate nuclear state while $\phi_n(0)$ is the lepton's wave function at the origin.

For the main text what is important about this calculation is that it depends on the lepton quantum numbers in precisely the same way as does the charge radius r_p^2 , and so can be interpreted as a shift in the value of ϵ_* . The leading (dipole) polarizability term goes as $(Z\alpha)^2 |\phi_n(0)|^2 R^2$ and so is a contribution to the R_1^2 contribution of ϵ_* in the parametrization of (44).

By comparison, the second term (and Friar moment correction) can be seen to go as relative order $(mRZ\alpha)$ and so are also contributions to R_1^2 in (44). Contributions to R_2^2 in (44) also arise in explicit calculations, typically as relativistic kinematic corrections to lower-order terms.

APPENDIX B: SOLVING FOR ϵ_*

This Appendix fills in the details that give the expression for ϵ_* in situations where the energy shifts also depend logarithmically on ϵ_* . This arises in the main text when writing an expression for ϵ_* in terms of the $2S_{1/2}-2P_{1/2}$ level shift, for example. We do so in this appendix for general n .

We start by writing the $nS_{1/2}-nP_{1/2}$ shift as

$$\widehat{\Delta E}_{nS_{1/2}-nP_{1/2}} = \frac{4m_e^3 (Z\alpha)^4}{n^3} \epsilon_*^2 \{ \chi_n - \ln[(m_e \epsilon_* e)^2] \}, \quad (\text{B1})$$

where

$$\chi_n := \frac{2}{(Z\alpha)^2} - 2 \ln \left(\frac{2Z\alpha}{n} \right) + \frac{12n^2 - n - 9}{2n^2(n+1)} - 2H_{n+1} - 2\gamma + 4 + \frac{\eta_{n0}^{(e)}}{Z} - \frac{2(n^2-1)}{n^2}, \quad (\text{B2})$$

and rearrange to obtain

$$\frac{n^3}{4m_e (Z\alpha)^4} \widehat{\Delta E}_{2S_{1/2}-2P_{1/2}} = m_e^2 \epsilon_*^2 \{ \chi_n - \ln[(m_e \epsilon_* e)^2] \}. \quad (\text{B3})$$

We wish to solve this equation for ϵ_* , but it has no closed-form solution. However, the solution does have a name: it is called the Lambert W function. In terms of this we have

$$m_e^2 \epsilon_*^2 = \exp \left[W \left(-\frac{n^3}{4m_e (Z\alpha)^4} \widehat{\Delta E}_{2S_{1/2}-2P_{1/2}} e^{-\chi_n} \right) + \chi_n \right]. \quad (\text{B4})$$

To turn this into something useful, we use some approximate forms for W in various limits. The first observation is that the argument of the W function is order $e^{-1/(Z\alpha)^2}$ (coming from the χ_n) and so is very small. Also, the energy shift in question is positive, so this argument is negative. In this limit, $W[z]$ is double valued, and the branch of interest is the one satisfying $W[z] < -1$, denoted by $W_m[z]$. In the limit of small negative argument,

$$W_m[z] \simeq -\ln \left(-\frac{1}{z} \right) - \ln \left[\ln \left(-\frac{1}{z} \right) \right] - \frac{\ln[\ln(-1/z)]}{\ln(-1/z)} \dots, \quad (\text{B5})$$

so that

$$\begin{aligned} & W \left(-\frac{n^3}{4m_e (Z\alpha)^4} \widehat{\Delta E}_{nS_{1/2}-nP_{1/2}} e^{-\chi_n} \right) + \chi_n \\ & \simeq \ln \left(\frac{n^3}{4m_e (Z\alpha)^4} \widehat{\Delta E}_{nS_{1/2}-nP_{1/2}} \right) \\ & - \ln \left[\chi_n - \ln \left(\frac{n^3}{4m_e (Z\alpha)^4} \widehat{\Delta E}_{nS_{1/2}-nP_{1/2}} \right) \right] \\ & - \frac{(Z\alpha)^2}{2} \ln \left(\frac{2}{(Z\alpha)^2} \right) + \dots, \end{aligned} \quad (\text{B6})$$

where the dots contain terms suppressed by order $(Z\alpha)^4$ and higher. Consequently,

$$\begin{aligned} m_e^2 \epsilon_*^2 & \simeq \frac{n^3}{8m_e (Z\alpha)^2} \widehat{\Delta E}_{nS_{1/2}-nP_{1/2}} \\ & \times \left\{ 1 + (Z\alpha)^2 \left[\hat{\chi}_n + \frac{1}{2} \ln \left(\frac{n^3}{4m_e (Z\alpha)^4} \widehat{\Delta E}_{nS_{1/2}-nP_{1/2}} \right) \right] \right\} \\ & + O \left((Z\alpha)^2 \frac{n^3 \widehat{\Delta E}_{nS_{1/2}-nP_{1/2}}}{4m_e} \right), \end{aligned} \quad (\text{B7})$$

where

$$\hat{\chi}_n := \frac{1}{2} \ln[2(Z\alpha)^4/n^2] - \frac{12n^2 - n - 9}{4n^2(n+1)} + H_{n+1} + \gamma - 2 - \frac{\eta_{n0}}{2Z} + \frac{n^2 - 1}{4n^2} \quad (\text{B8})$$

(defined by $\chi_n = [2/(Z\alpha)^2](1 - \hat{\chi}_n)$), and the correction is down by $(Z\alpha)^4$ relative to the leading term.

Finally, plugging this into (73) for the $nS_{1/2-n}P_{3/2}$ shift, we predict

$$\begin{aligned} \widehat{\Delta E}_{nS_{1/2-n}P_{3/2}} &\approx \widehat{\Delta E}_{nS_{1/2-n}P_{1/2}} \left\{ 1 + (Z\alpha)^2 \left[\hat{\chi}_n + \frac{1}{2} \ln \left(\frac{n^3}{4m_e(Z\alpha)^4} \widehat{\Delta E}_{nS_{1/2-n}P_{1/2}} \right) \right] \right\} \\ &\times \left\{ 1 + (Z\alpha)^2 \left[\frac{12n^2 - n - 9}{4n^2(n+1)} - \frac{1}{2} \ln \left(\frac{n \widehat{\Delta E}_{nS_{1/2-n}P_{1/2}}}{2m_e} \right) - H_{n+1} - \gamma + 2 + \frac{\eta_{n0}}{2Z} \right] \right\} \\ &= \widehat{\Delta E}_{nS_{1/2-n}P_{1/2}} \left\{ 1 + (Z\alpha)^2 \left[\frac{n^2 - 1}{4n^2} \right] + O((Z\alpha)^4) \right\}, \end{aligned} \quad (\text{B9})$$

which is exactly the result (77) used in the main text.

-
- [1] W. E. Lamb and R. C. Retherford, Fine structure of the hydrogen atom by a microwave method, *Phys. Rev.* **72**, 241 (1947).
- [2] J. L. Friar and J. W. Negele, Theoretical and experimental determination of nuclear charge distributions, *Adv. Nucl. Phys.* **8**, 219 (1975); E. Borie and G. A. Rinker, The energy levels of muonic atoms, *Rev. Mod. Phys.* **54**, 67 (1982); K. Pachucki, Theory of the Lamb shift in muonic hydrogen, *Phys. Rev. A* **53**, 2092 (1996); Proton structure effects in muonic hydrogen, *60*, 3593 (1999); D. Andrae, Finite nuclear charge distributions in electronic structure calculations for atoms and molecules, *Phys. Rep.* **336**, 413 (2000); E. Borie, Lamb shift in muonic hydrogen, *Phys. Rev. A* **71**, 032508 (2005); M. O. Distler, J. C. Bernauer, and T. Walcher, The RMS charge radius of the proton and Zemach moments, *Phys. Lett. B* **696**, 343 (2011); C. E. Carlson and M. Vanderhaeghen, Higher-order proton structure corrections to the Lamb shift in muonic hydrogen, *Phys. Rev. A* **84**, 020102(R) (2011); U. D. Jentschura, Lamb shift in muonic hydrogen. I. verification and update of theoretical predictions, *Ann. Phys. (NY)* **326**, 500 (2011); A. Antognini, F. Kottmann, F. Biraben, P. Indelicato, F. Nez and R. Pohl, Theory of the $2S$ - $2P$ Lamb shift and $2S$ hyperfine splitting in muonic hydrogen, *ibid.* **331**, 127 (2013); T. P. Gorringe and D. W. Hertzog, Precision muon physics, *Prog. Part. Nucl. Phys.* **84**, 73 (2015); arXiv:1506.01465; S. G. Karshenboim, V. G. Ivanov, and E. Y. Korzinin, Relativistic recoil corrections to the electron-vacuum-polarization contribution in light muonic atoms, *Phys. Rev. A* **85**, 032509 (2012).
- [3] H. K. Walter *et al.*, Test of quantum-electrodynamical corrections in muonic atoms, *Phys. Lett. B* **40**, 197 (1972).
- [4] M. S. Dixit, H. L. Anderson, C. K. Hargrove, R. J. Mckee, D. Kessler, H. Mes, and Albert C. Thompson, Experimental Test of the Theory of Muonic Atoms, *Phys. Rev. Lett.* **27**, 878 (1971).
- [5] M. K. Sundaresan and P. J. S. Watson, Higher-Order Vacuum Polarization Corrections in Muonic Atoms, *Phys. Rev. Lett.* **29**, 15 (1972).
- [6] J. Blomqvist, Vacuum polarization in exotic atoms, *Nucl. Phys. B* **48**, 95 (1972).
- [7] L. Wilets and G. A. Rinker, Jr., Estimate of the $(Z\alpha)^2\alpha^2$ Vacuum Polarization Term in Muonic Pb, *Phys. Rev. Lett.* **34**, 339 (1975).
- [8] G. A. Rinker and L. Wilets, Vacuum Polarization in High-Z, Finite-Size Nuclei, *Phys. Rev. Lett.* **31**, 1559 (1973).
- [9] M. S. Dixit, A. L. Carter, E. P. Hincks, D. Kessler, J. S. Wadden, C. K. Hargrove, R. J. McKee, H. Mes, and H. L. Anderson, New Muonic-Atom Test of Vacuum Polarization, *Phys. Rev. Lett.* **35**, 1633 (1975).
- [10] T. Dubler, K. Kaeser, B. Robert-Tissot, L. A. Schaller, L. Schellenberg, and H. Schneuwly, Precision test of vacuum polarization in heavy muonic atoms, *Nucl. Phys. A* **294**, 397 (1978).
- [11] J. L. Vuilleumier, W. Dey, R. Engfer, H. Schneuwly, H. K. Walter and A. Zehnder, Test of electron screening and vacuum polarization in heavy muonic atoms, *Z. Phys. A* **278**, 109 (1976).
- [12] K. A. Woodle, A. Badertscher, V. W. Hughes, D. C. Lu, M. W. Ritter, M. Gladisch, H. Orth, G. zu Putlitz, M. Eckhause, J. Kane, and F. G. Mariani, Measurement of the Lamb shift in the $N = 2$ state of muonium, *Phys. Rev. A* **41**, 93 (1990); R. Pohl *et al.*, The size of the proton, *Nature (London)* **466**, 213 (2010); R. Pohl, R. Gilman, G. A. Miller, and K. Pachucki, Muonic hydrogen and the proton radius puzzle, *Annu. Rev. Nucl. Part. Sci.* **63**, 175 (2013); A. Antognini *et al.*, Proton structure from the measurement of $2s$ - $2p$ transition frequencies of muonic hydrogen, *Science* **339**, 417 (2013); C. E. Carlson, The proton radius puzzle, *Prog. Part. Nucl. Phys.* **82**, 59 (2015); R. Pohl, Laser spectroscopy of muonic hydrogen and the puzzling proton, *J. Phys. Soc. Jpn.* **85**, 091003(E) (2016); J. Downie, The proton radius puzzle, *EPJ Web Conf.* **113**, 05021 (2016); J. J. Krauth *et al.*, The proton radius puzzle, arXiv:1706.00696v2.
- [13] A. Antognini *et al.*, Illuminating the proton radius conundrum: the μHe^+ Lamb shift, *Can. J. Phys.* **89**, 47 (2011); C. G. Parthey, A. Matveev, J. Alnis, B. Bernhardt, A. Beyer, R. Holzwarth, A. Maistrou, R. Pohl, K. Predehl, T. Udem, T. Wilken, N. Kolachevsky, M. Abgrall, D. Rovera, C. Salomon, P. Laurent, and T. W. Hänsch, Improved Measurement of the Hydrogen $1S - 2S$ Transition Frequency, *Phys. Rev. Lett.* **107**, 203001 (2011); N. T. Amaro and F. D. Antognini, The Lamb-shift experiment in muonic helium, *Hyperfine Interact.* **212**, 195 (2012); A. Antognini *et al.*, Experiments towards resolving the proton charge radius puzzle, *EPJ Web Conf.* **113**, 01006 (2016); R. Pohl *et al.*, Laser spectroscopy of muonic atoms and ions, *JPS Conf. Proc.* **18**, 011021 (2017).

- [14] See, e.g., P. J. Mohr, D. B. Newell, and B. N. Taylor, CODATA recommended values of the fundamental physical constants: 2014, *Rev. Mod. Phys.* **88**, 035009 (2016).
- [15] V. Barger, C. W. Chiang, W. Y. Keung, and D. Marfatia, Proton Size Anomaly, *Phys. Rev. Lett.* **106**, 153001 (2011); D. Tucker-Smith and I. Yavin, Muonic hydrogen and MeV forces, *Phys. Rev. D* **83**, 101702 (2011); B. Batell, D. McKeen, and M. Pospelov, New Parity-Violating Muonic Forces and the Proton Charge Radius, *Phys. Rev. Lett.* **107**, 011803 (2011); A. De Rújula, QED confronts the radius of the proton, *Phys. Lett. B* **697**, 26 (2011); C. E. Carlson and B. C. Rislow, New physics and the proton radius problem, *Phys. Rev. D* **86**, 035013 (2012); R. Onofrio, Proton radius puzzle and quantum gravity at the Fermi scale, *Europhys. Lett.* **104**, 20002 (2013); L.-B. Wang and W.-T. Ni, Proton radius puzzle and large extra dimensions, *Mod. Phys. Lett. A* **28**, 1350094 (2013); S. G. Karshenboim, D. McKeen, and M. Pospelov, Constraints on muon-specific dark forces, *Phys. Rev. D* **90**, 073004 (2014); Constraints on muon-specific dark forces, **90**, 079905(E) (2014); D. Robson, Solution to the proton radius puzzle, *Int. J. Mod. Phys. E* **23**, 1450090 (2015); P. Brax and C. Burrage, Explaining the proton radius puzzle with disformal scalars, *Phys. Rev. D* **91**, 043515 (2015).
- [16] W. E. Caswell and G. P. Lepage, Effective lagrangians for bound state problems in QED, QCD, and other field theories, *Phys. Lett. B* **167**, 437 (1986); C. Peset and A. Pineda, The Lamb shift in muonic hydrogen and the proton radius from effective field theories, *Eur. Phys. J. A* **51**, 156 (2015); A. A. Krutov *et al.*, *J. Exp. Theor. Phys.* **120**, 73 (2015).
- [17] A. Pineda, Chiral structure of the Lamb shift and the definition of the proton radius, *Phys. Rev. C* **71**, 065205 (2005); R. J. Hill and G. Paz, Model independent extraction of the proton charge radius from electron scattering, *Phys. Rev. D* **82**, 113005 (2010); C. Peset and A. Pineda, Model-independent determination of the Lamb shift in muonic hydrogen and the proton radius, *Eur. Phys. J. A* **51**, 32 (2015); M. Horbatsch and E. A. Hessels, Evaluation of the strength of electron-proton scattering data for determining the proton charge radius, *Phys. Rev. C* **93**, 015204 (2016); G. Lee, J. R. Arrington, and R. J. Hill, Extraction of the proton radius from electron-proton scattering data, *Phys. Rev. D* **92**, 013013 (2015).
- [18] C. P. Burgess, P. Hayman, M. Williams, and L. Zalavari, Point-particle effective field theory I: Classical renormalization and the inverse-square potential, *J. High Energy Phys.* **04** (2017) 106.
- [19] C. P. Burgess, P. Hayman, M. Rummel, M. Williams, and L. Zalavari, Point-particle effective field theory II: Relativistic effects and coulomb/inverse-square competition, *J. High Energy Phys.* **07** (2017) 072.
- [20] C. P. Burgess, P. Hayman, M. Rummel, and L. Zalavari, Point-particle effective field theory III: Relativistic fermions and the dirac equation, *J. High Energy Phys.* **09** (2017) 007.
- [21] S. G. Karshenboim and V. G. Ivanov, Hyperfine structure of the ground and first excited states in light hydrogen-like atoms and high-precision tests of QED, *Eur. Phys. J. D* **19**, 13 (2002).
- [22] See, e.g., M. Weitz, A. Huber, F. Schmidt-Kaler, D. Leibfried, W. Vassen, C. Zimmermann, K. Pachucki, T. W. Hänsch, L. Julien, and F. Biraben, Precision measurement of the $1S$ ground-state Lamb shift in atomic hydrogen and deuterium by frequency comparison, *Phys. Rev. A* **52**, 2664 (1995); S. G. Karshenboim, Precision physics of simple atoms: QED tests, nuclear structure and fundamental constants, *Phys. Rep.* **422**, 1 (2005).
- [23] V. A. Yerokhin and V. M. Shabaev, Lamb shift of $n = 1$ and $n = 2$ states of hydrogen-like atoms, $1 \leq Z \leq 110$, *J. Phys. Chem. Ref. Data* **44**, 033103 (2015).
- [24] C. Ji, N. Nevo Dinur, S. Bacca, and N. Barnea, Nuclear Polarization Corrections to the $\mu^4\text{He}^+$ Lamb Shift, *Phys. Rev. Lett.* **111**, 143402 (2013).
- [25] J. L. Friar, Nuclear finite size effects in light muonic atoms, *Ann. Phys. (NY)* **122**, 151 (1979).
- [26] M. I. Eides, H. Grotch, and V. A. Shelyuto, Theory of light hydrogenlike atoms, *Phys. Rep.* **342**, 63 (2001).
- [27] A. C. Zemach, Proton structure and the hyperfine shift in hydrogen, *Phys. Rev.* **104**, 1771 (1956).
- [28] B. Nickel, Nuclear size effects on hydrogenic atom energies: a semi-analytic formulation, *J. Phys. B: At. Mol. Opt. Phys.* **46**, 015001 (2013).
- [29] R. T. Deck, J. G. Amar, and G. Fralick, Nuclear size corrections to the energy levels of single-electron and -muon atoms, *J. Phys. B: At. Mol. Opt. Phys.* **38**, 2173 (2005).
- [30] C. P. Burgess, P. Hayman, and M. Rummel, Point-Particle Effective Field Theory and Subleading Finite-Size Effects in Nuclear Spin-0 Atoms (unpublished).
- [31] K. Pachucki, V. Patkóš, and V. A. Yerokhin, Three-photon exchange nuclear structure correction in hydrogenic systems, *Phys. Rev. A* **97**, 062511 (2018).
- [32] M. I. Eides, H. Grotch, and V. A. Shelyuto, Lamb shift in light muonic atoms, in *Theory of Light Hydrogenic Bound States*, Springer Tracts in Modern Physics (Springer, Berlin, 2007), Vol. 222.
- [33] M. I. Eides, H. Grotch, and V. A. Shelyuto, Nuclear size and structure corrections, in *Theory of Light Hydrogenic Bound States*, Springer Tracts in Modern Physics (Springer, Berlin, 2007), Vol. 222.
- [34] J. L. Friar, Nuclear polarization corrections to μ - d atoms in zero-range approximation, *Phys. Rev. C* **88**, 034003 (2013).
- [35] C. Ji, S. Bacca, N. Barnea, O. J. Hernandez, and N. Nevo-Dinur, Ab initio calculation of nuclear structure corrections in muonic atoms, *J. Phys. G: Nucl. Part. Phys.* **45**, 9 (2018).
- [36] K. Pachucki and A. M. Moro, Nuclear polarizability of helium isotopes in atomic transitions, *Phys. Rev. A* **75**, 032521 (2007).
- [37] G. Audi, F. G. Kondev, M. Wang, W. J. Huang, and S. Naimi, The NUBASE2016 evaluation of nuclear properties, *Chin. Phys. C* **41**, 030001 (2017).
- [38] M. I. Eides, H. Grotch, and V. A. Shelyuto, in *Nuclear Size and Structure Corrections* (Springer, Berlin, 2007), pp. 109–130.
- [39] M. I. Eides, H. Grotch, and V. A. Shelyuto, in *Lamb Shift in Light Muonic Atoms* (Springer, Berlin, 2007), pp. 131–159; See also Ref. [2c].
- [40] A. van Wijngaarden, F. Holuj, and G. F. W. Drake, Lamb shift in He^+ : Resolution of a discrepancy between theory and experiment, *Phys. Rev. A* **63**, 012505 (2000).
- [41] M. Herrmann, M. Haas, U. D. Jentschura, F. Kottmann, D. Leibfried, G. Saathoff, C. Gohle, A. Ozawa, V. Batteiger, S. Knünz, N. Kolachevsky, H. A. Schüssler, T. W. Hänsch, and T. Udem, Feasibility of coherent xuv spectroscopy on the $1S$ - $2S$ transition in singly ionized helium, *Phys. Rev. A* **79**, 052505 (2009).

Chapter 4

Leading Spin-Dependent Finite-Size Effects in Hydrogen

Paper presented

L. Zalavari, C. P. Burgess, P. Hayman and M. Rummel

“*Precision Nuclear-Spin Effects in Atoms: EFT Method for Reducing Theory Errors*”,

Submitted to *Physical Review A* for publication,

arXiv:2008.09718 [hep-ph].

Summary

In this latest instalment of the atomic PPEFT odyssey we address one of the major missing components of the formalism developed so far; the extension to nuclei with spin. A slightly more involved summary of the results of the paper we are about to present can be found in [9].

Inspired by supersymmetric treatments of spinning point-particles, as done for instance in [48], we capture the effects of nuclear spin by appending the field content of the nucleus by a set of classically anti-commuting Grassmann fields, $\xi^\mu(s)$ that satisfy $\{\xi^\mu, \xi^\nu\} = 0$. Classically, the inclusion of these internal low-energy degrees of freedom leads to new primary constraints on the theory and once the point-particle degrees of freedom are quantized the quantum operators associated with these Grassmann fields, $\hat{\xi}^\mu$ satisfy anticommutation relations of the form $\{\hat{\xi}^\mu, \hat{\xi}^\nu\} \propto \eta^{\mu\nu}$ and turn out to span a multi-dimensional Hilbert space, whose dimension is chosen when particular representations of their anticommutation algebra are assumed. Then, in order to capture fermionic nuclei we choose a representation of this algebra in terms of Dirac matrices and later project out the anti-particle sector of the Hilbert-space.

Next, in order to capture the leading spin-dependent finite-size corrections to leptonic bound-states we append the PPEFT action derived in

Chapter 3 with all Grassmann-even interactions between the new fields and the already existing fields of the problem, $\{y^\mu(s), A^\mu(x), \Psi(x)\}$ that obey atomic symmetries and have coupling dimension up to and including $(length)^2$. We find only a single new interaction between $\xi^\mu(s)$ and $A^\mu(x)$ with coupling dimension $(length)$, and four others at $(length)^2$ including couplings to the leptons.

The rest of the paper works out various consequences of the nuclear spin, assuming a nucleus at rest, which automatically projects out the anti-nucleus solutions and effectively halves the dimensionality of the nuclear Hilbert-space. In this frame, there are only two new interactions relative to the ones included in Chapter 4: the operator with dimension $(length)$ between the spin and gauge fields; and one $(length)^2$ term contracting the nuclear spin with that of the fermion's.

The new interaction between spin and $A^\mu(x)$ sets up new near-nucleus boundary conditions for $\mathbf{A}(\mathbf{x})$ that result in a magnetic dipole field, $\mathbf{A}_{\text{nuc}}(\mathbf{x})$, whose effects we treat perturbatively around the Dirac-Coulomb problem with perturbation $\mathcal{L}_{\text{int}} = -e\gamma^0\boldsymbol{\gamma} \cdot \mathbf{A}_{\text{nuc}}$, expanding our calculations to linear order in the small quantity, $\mathfrak{s} := me\mu_N/4\pi \ll 1$. In order to do this efficiently, we couple the spin of the nucleus, \mathbf{I} to the total angular momentum of the lepton, \mathbf{J} to form the total atomic angular momentum $\mathbf{F} = \mathbf{I} + \mathbf{J}$, whose eigenfunctions diagonalize the fixed- j subspaces of the Dirac-Coulomb modes degenerate under the perturbation. We then create the coupled nuclear-Dirac-Coulomb modes that have the same form of radial functions as in (1.73) (though their energies and integration constants can now depend on the F quantum number of the \mathbf{F}^2 operator) but instead of the previously obtained spherical spinor harmonics in (1.71) their angular dependence is instead given by eigenfunctions of the operators, \mathbf{F}^2 and \mathbf{F}_z .

It turns out that spin-dependent finite-size effects arise in two places: coming from matrix elements of \mathcal{L}_{int} between the coupled nuclear-Dirac-Coulomb modes; but also coming from expanding the physical integration constant ratio, $\mathcal{D}_{Fj\varpi}/\mathcal{C}_{Fj\varpi}$ in powers of \mathfrak{s} in the energy shift formulae derived from (1.82) in the previous papers. The first of these results in divergent integrals, whose behaviour we track through dimensional regularization, while the second allows these divergences to be absorbed into the new fermionic PPEFT coupling constant using the boundary conditions, and also gives rise to a new RG-invariant parameter, ϵ_F that turns out to account for the leading spin-dependent finite-size energy shifts.

The expansion of the ratio of integration constants in powers of \mathfrak{s} also allows for the near-source boundary conditions implied by the presence of the nucleus on the nuclear-Dirac-Coulomb modes set up on the usual Gaussian surface at fictitious radial scale, ϵ to be expanded in this parameter. The $\mathcal{O}(\mathfrak{s})$ boundary condition relates the first correction of the integration constant ratio to the new spin-dependent fermion-nucleus coupling. As such, the new coupling is not only burdened by having to absorb the infinities coming from matrix elements but also by an ϵ -dependence necessary to

keep the energy shifts at leading order in \mathfrak{s} independent of this unphysical scale. The RG-flow of this parameter turns out to depend on the old (spin-independent) RG-invariant parameters as well and is further complicated by the first-order state-corrections to the nuclear-Dirac-Coulomb modes.

Having dealt with all of the issues regarding infinities and unphysical parameter dependences we use the new RG-invariant scale to compute how the leading spin-dependent finite-size energy shift depends on ϵ_F , which we then also compare to expressions that use nuclear moments to capture these effects and find that ϵ_F is related to the first Zemach-moment, $\langle r \rangle_{cm}$ of (1.99). Combining this result with that of Chapter 3 we now see that in cases of nuclei with spin, it is sufficient to use two RG-invariant parameters to capture all finite-size related energy shifts to relative subleading spin-independent contributions of $(mRZ\alpha)$ and $(Z\alpha)^2$ to the charge-radius term and leading order in the spin-dependent ones.

This number is still significantly lower than that of nuclear moments and hence allows us to use the handful of extremely precise measurements available in any given system to fit the “true” nuclear parameters with the same methods as outlined in the previous chapter, and the errors of these parameters will be controlled by the uncertainties of the most precise experimental values and the theoretical contributions to the measured transitions that assume a point-like nucleus.

Carrying out this fitting for atomic Hydrogen we make a large number of predictions for existing measurements, whose uncertainty is dominated by the uncomputed terms of point-like bound-state QED effects and in this way we push past the error floor presented by nuclear-size effects, making these transitions good targets for tests of fundamental theory once more. We do a similar fitting for muonic Hydrogen, although due to the large mass of the muon further subleading nuclear-size effects need to be calculated than has been done here and therefore show that our predictions are only competitive with current ones using nuclear moments but are not necessarily superior, except in that our formalism makes it easier to improve on these results.

PREPARED FOR SUBMISSION TO JHEP

Precision Nuclear-Spin Effects in Atoms: EFT Methods for Reducing Theory Errors

L. Zalavari, C.P. Burgess, P. Hayman and M. Rummel

^a*Department of Physics & Astronomy, McMaster University, Hamilton, Ontario, L8S 4M1, Canada*

^b*Perimeter Institute for Theoretical Physics, Waterloo, Ontario, N2L 2Y5, Canada*

E-mail: zalavar1@mcmaster.ca, cburgess@perimeterinstitute.ca,
haymanpf@mcmaster.ca, rummelm@mcmaster.ca

ABSTRACT: We use effective field theory to compute the influence of nuclear structure on precision calculations of atomic energy levels. As usual, the EFT’s effective couplings correspond to the various nuclear properties (such as the charge radius, nuclear polarizabilities, Friar and Zemach moments *etc.*) that dominate its low-energy electromagnetic influence on its surroundings. By extending to spinning nuclei the arguments developed for spinless ones in [arXiv:1708.09768](https://arxiv.org/abs/1708.09768), we use the EFT to show – to any fixed order in $Z\alpha$ (where Z is the atomic number and α the fine-structure constant) and the ratio of nuclear to atomic size – that nuclear properties actually contribute to electronic energies through fewer parameters than the number of these effective nuclear couplings naively suggests. Our result is derived using a position-space method for matching effective parameters to nuclear properties in the EFT, that more efficiently exploits the simplicity of the small-nucleus limit in atomic systems. By showing that precision calculations of atomic spectra depend on fewer nuclear uncertainties than naively expected, this observation allows the construction of many nucleus-independent combinations of atomic energy differences whose measurement can be used to test fundamental physics (such as the predictions of QED) because their theoretical uncertainties are not limited by the accuracy of nuclear calculations. We provide several simple examples of such nucleus-free predictions for Hydrogen-like atoms.

Contents

1	Introduction	2
1.1	The EFT framework	3
1.2	Parameter counting for atomic energy shifts	8
2	PPEFT for sources with spin	14
2.1	Spin on a world-line	15
2.2	Implications for the electromagnetic field	17
2.3	Lepton mode functions	18
2.4	Near-nucleus fermion boundary conditions	30
3	Renormalization	35
3.1	Cancellation of ϵ -dependence	35
3.2	Cancellation of η -dependence	43
3.3	Matching to nuclear moments	46
4	Predictions for energy shifts	52
4.1	Isolating finite-nucleus effects	52
4.2	Atomic Hydrogen	59
4.3	Muonic Hydrogen	65
5	Summary and Outlook	69
A	Spin formalism	74
B	Fermionic boundary conditions	79
C	Finite-size energy shift	84
D	Perturbing in the magnetic dipole	86
E	Evaluation of matrix elements	90
F	RG evolution	110
G	List of symbols	120

1 Introduction

Modern experimental techniques allow exquisitely accurate measurements of atomic transition frequencies. For simple atoms it is hoped that these measurements can be turned into a test of fundamental theory by comparing with equally precise predictions; modern alternatives to the classic comparisons between theory and experiment for the Lamb shift in Hydrogen [1] – [26].

The sad fact that atomic nuclei are not point charges is a major obstruction to this program, because atomic energy shifts due to nuclear structure can be larger than the fundamental corrections to be measured. Furthermore, the intricacies of the strong interactions make *ab initio* predictions of nuclear properties necessarily inaccurate, often making nuclear uncertainties the dominant theoretical error when predicting atomic energy levels [27] – [62].

In this paper we provide the details for (and provide broader applications of the results of) [63], which aims to push past this floor in theoretical error by systematically identifying combinations of energy differences from which all of the effects of nuclear physics cancel. Because the accuracy with which such observables can be predicted is not limited by nuclear uncertainties (by construction), their measurement can provide a potentially telling test of fundamental theory. Given N_{exp} well-measured transitions involving a specific type of atom and N_{nuc} parameters governing nuclear contributions to atomic energies, there are $N_{\text{exp}} - N_{\text{nuc}}$ independent observables for which a nucleus-free prediction can be made.

While this counting is not so remarkable an observation in itself, what is perhaps more surprising is how small N_{nuc} turns out to be. In the applications made here, for instance, precisely two nuclear parameters suffice even though our predictions are accurate enough to include the effects of the nuclear charge radius, nuclear Friar and Zemach moments, nuclear polarizabilities, effects of multiple photon exchange, and so on. Only two parameters turn out to capture all of these different nuclear effects in our examples because atomic energy shifts only sample nuclear physics at extremely low energies relative to typical nuclear scales.

The precise value for N_{nuc} depends on the accuracy that is required. This accuracy is most precisely specified when atomic energy levels are expressed as a perturbative expansion about the leading Bohr formula (for the binding energy of a nonrelativistic

point-like lepton¹ to a static, charge Ze point nucleus),

$$\varepsilon_n = -\frac{(Z\alpha)^2 m_r}{2n^2}, \quad (1.1)$$

where $m_r = mM/(m + M) = m + \mathcal{O}(m^2/M)$ is the reduced mass, with M the nuclear mass and m the relevant lepton mass, while $n = 1, 2, \dots$ is the usual principal quantum number. This expansion comes in powers of four small quantities: the lepton speed $v_e \sim Z\alpha$; the fine-structure constant² $\alpha = e^2/4\pi$ (which enters without Z in QED radiative corrections, for instance); the ratio of lepton to nuclear mass, m/M ; and the ratio $R/a_B \sim mRZ\alpha$ of nuclear and atomic length scales, where $R \sim 1$ fm is a measure of nuclear radius (more about which below) and $a_B \sim (Z\alpha m)^{-1}$ is the Bohr radius.

In terms of this expansion Ref. [64] found when working out to order $m^3 R^2 (Z\alpha)^6$ and $m^4 R^3 (Z\alpha)^5$ that only $N_{\text{nuc}} = 1$ parameter was required (for each type of nucleus) to capture *all* dependence of leptonic energy levels on nuclear substructure, at least for spinless nuclei.³ In this paper we extend this analysis to include nuclear-spin effects to the same order, and find all effects of nuclear substructure require only a single new parameter (so $N_{\text{nuc}} = 2$). Furthermore, since this accuracy provides a precision of about 0.01 kHz it is sufficient (with two exceptions) for current measurement precision with elemental Hydrogen. The corresponding precision for muonic Hydrogen is about 10^{-3} meV, and so is close to (but, as discussed at length in §4.3, not quite) accurate enough for these measurements as well. A summary of this parameter counting as a function of expansion order can be found in Table 1.

Our construction of nucleus-free combinations relies on identifying combinations of observables for which the R/a_B corrections cancel order-by-order in α and $Z\alpha$, and our tool for finding these exploits the fact that the expansion in R/a_B is most efficiently captured using an appropriate effective field theory (EFT), described in detail below.

1.1 The EFT framework

It has long been known that these expansions are efficiently organized using EFT methods, since both the expansion in powers of v_e and R/a_B arise as low-energy approximations. In quantum field theory the expansion in powers of $v_e \sim Z\alpha$ can be systematized

¹For simplicity of language we speak in the main text about ordinary atoms – *i.e.* electrons orbiting nuclei – but our analysis applies equally well to muonic atoms. At various points in the text we point out how the larger muon mass changes the relative size of different contributions.

²Unless otherwise stated we use fundamental units, for which $\hbar = c = k_B = 1$.

³More precisely, although one parameter captures all nuclear effects for either an electron or a muon orbiting a spinless nucleus, the parameter differs for the two so measurements of electrons cannot be used to infer nuclear contributions to muonic atoms without additional information from nuclear models.

Abs. order	Rel. order	$j = 1/2$	$j = 3/2$	H (kHz)	muonic H (meV)
$m^3 R^2 (Z\alpha)^4$	chg. rad.	✓	✗	1.7×10^3	6.1×10^1
$m^4 R^3 (Z\alpha)^5$	$(mRZ\alpha)$	✓	✗	2.6×10^{-2}	2.0×10^{-1}
$m^5 R^4 (Z\alpha)^6$	$(mRZ\alpha)^2$	✓	✓	4.2×10^{-7}	6.6×10^{-4}
$m^3 R^2 (Z\alpha)^6$	$(Z\alpha)^2$	✓	✗	8.9×10^{-2}	3.2×10^{-3}
$m^4 R^3 (Z\alpha)^7$	$(mRZ\alpha)(Z\alpha)^2$	✓	✗	1.4×10^{-6}	1.1×10^{-5}
$m^3 R^2 (Z\alpha)^8$	$(Z\alpha)^4$	✓	✗	4.7×10^{-6}	1.7×10^{-7}
$m\mathfrak{s}(Z\alpha)^3$	hfs	✓	✓	5.3×10^5	9.4×10^1
$m^2 R\mathfrak{s}(Z\alpha)^4$	LO	✓	✗	1.1×10^1	4.0×10^{-1}
$m^3 R^2 \mathfrak{s}(Z\alpha)^5$	$(mRZ\alpha)$	✓	✗	2.2×10^{-4}	1.7×10^{-3}
$m^4 R^3 \mathfrak{s}(Z\alpha)^6$	$(mRZ\alpha)^2$	✓	✓	4.6×10^{-9}	7.1×10^{-6}
$m^2 R\mathfrak{s}(Z\alpha)^6$	$(Z\alpha)^2$	✓	✗	5.8×10^{-4}	2.1×10^{-5}
$m^3 R^2 \mathfrak{s}(Z\alpha)^7$	$(mRZ\alpha)(Z\alpha)^2$	✓	✗	1.2×10^{-8}	9.0×10^{-8}
$m^2 R\mathfrak{s}(Z\alpha)^8$	$(Z\alpha)^4$	✓	✗	3.1×10^{-8}	1.1×10^{-9}
$m\mathfrak{s}^2(Z\alpha)^4$	hfs ²	✓	✓	4.3×10^{-2}	1.6×10^{-3}
$m^2 R\mathfrak{s}^2(Z\alpha)^5$	LO	✓	✗	8.8×10^{-7}	6.7×10^{-6}
$m^3 R^2 \mathfrak{s}^2(Z\alpha)^6$	$(mRZ\alpha)$	✓	✗	1.8×10^{-11}	2.8×10^{-8}
$m^4 R^3 \mathfrak{s}^2(Z\alpha)^7$	$(mRZ\alpha)^2$	✓	✓	3.7×10^{-16}	1.2×10^{-10}
$m^2 R\mathfrak{s}^2(Z\alpha)^7$	$(Z\alpha)^2$	✓	✗	4.7×10^{-11}	3.6×10^{-10}
$m^3 R^2 \mathfrak{s}^2(Z\alpha)^8$	$(mRZ\alpha)(Z\alpha)^2$	✓	✗	9.6×10^{-16}	1.5×10^{-12}
$m^2 R\mathfrak{s}^2(Z\alpha)^9$	$(Z\alpha)^4$	✓	✗	2.5×10^{-15}	1.9×10^{-14}

Table 1: The order of magnitude of various nuclear contributions to atomic energy shifts. Double lines separate blocks involving different powers of nuclear moments, μ_N , where $\mathfrak{s} \sim \mathcal{O}(me\mu_N/4\pi) \sim \mathcal{O}(mRZ\alpha)$ – with m the lepton mass, R a measure of nuclear size and α the fine-structure constant – is more precisely defined in eq. (2.35). The checks and crosses indicate if a term of the given order actually arises (excluding recoil effects and QED radiative corrections, which do not introduce new parameters) for lepton states with $j = \frac{1}{2}$ and $j = \frac{3}{2}$. New parameters enter when integration constants for new modes are required, and cyan shading indicates the order where this first arises, for different choices for j and powers of \mathfrak{s} . The final two columns evaluate the numerical size implied by the powers of \mathfrak{s} , $Z\alpha$ and $mRZ\alpha$, for ordinary Hydrogen (electrons) and for muonic Hydrogen, using assumptions spelled out in the text below. Green boxes flag terms required to achieve an accuracy of order 0.001 kHz for Hydrogen (or 10^{-3} meV for muonic Hydrogen). The yellow square flags a term not computed here, which is likely to be relevant to muonic Hydrogen experiments.

using non-relativistic quantum electrodynamics (NRQED) [65], and efficiently allows the inclusion of second-quantized radiative corrections with the standard Schrödinger treatment of Coulomb bound states. One way to think about our formalism is as a version of NRQED where the projection onto the single-nucleus sector is achieved using first-quantized methods. This allows the matching of the nuclear-size effective couplings to be performed very efficiently, using a near-nucleus boundary condition.

We do *not* explicitly start from NRQED here (though our formalism is also easily adapted to the non-relativistic fields of NRQED), since it is equally easy to treat the light lepton relativistically. So we instead choose to perturb around the relativistic Dirac-Coulomb system, rather than the nonrelativistic Schrödinger-Coulomb system. We do so because our main EFT focus is on those interactions that capture the R/a_B expansion.

If the nucleus⁴ were a point particle its leading relativistic electromagnetic interactions with leptons and photons would be described by the renormalizable QED lagrangian

$$S_{\Phi_{QED}} = - \int d^4x \left\{ \frac{1}{4} F_{\mu\nu} F^{\mu\nu} + \bar{\Psi} [\not{D} + m] \Psi + \bar{\Phi} [\not{D} + M] \Phi \right\}, \quad (1.2)$$

for electromagnetic field strength $F_{\mu\nu} = \partial_\mu A_\nu - \partial_\nu A_\mu$, Dirac lepton field Ψ and spin-half nucleus field Φ (with $D_\mu \Psi = \partial_\mu \Psi + ieA_\mu \Psi$ and $D_\mu \Phi = \partial_\mu \Phi - iZeA_\mu \Phi$). Here $M \gg m$ is the mass of the nucleus where (as above) m is the lepton mass. In reality (1.2) gets supplemented by additional renormalizable terms involving other light fields (such as any other light leptons), as well as by nonrenormalizable terms describing shorter-wavelength physics that is already integrated out (such as those describing the weak interactions and so on).

From an EFT perspective the R/a_B expansion is captured by a subset of the higher-dimensional terms not listed explicitly in (1.2). The ones that are relevant are those — see *e.g.* [66–69] — consistent with the symmetries of the strong interactions (like electromagnetic gauge invariance, parity, and so on), that couple Φ to Ψ and A_μ non-minimally, such as

$$S_{\text{nuc}} = - \int d^4x \left\{ \frac{\tilde{c}_d}{2} (\bar{\Phi} \gamma^{\mu\nu} \Phi) F_{\mu\nu} + \tilde{c}_s (\bar{\Psi} \Psi) (\bar{\Phi} \Phi) + \tilde{c}_v (\bar{\Psi} \gamma^\mu \Psi) (\bar{\Phi} \gamma_\mu \Phi) + \dots \right\}. \quad (1.3)$$

Here $\gamma^{\mu\nu} := -\frac{i}{4} [\gamma^\mu, \gamma^\nu]$ and effective couplings like \tilde{c}_d and \tilde{c}_v have dimensions $(\text{length})^p$ for positive p . EFT methods exploit the fact that such interactions capture the low-energy effects obtained by integrating out *any* kinds of nuclear degrees of freedom besides the nucleus' overall spin and position.

⁴For concreteness this discussion proceeds assuming a spin-half nucleus but our effective theory works for arbitrary nuclear spin.

The effective couplings obtained in this way dominate the low-energy interactions of finite-sized nuclei at wavelengths much longer than nuclear size. Of the couplings given above $\tilde{c}_d \propto R$ captures the anomalous nuclear magnetic moment, $\tilde{c}_v \propto R^2$ is related to its electromagnetic charge radius and so on. The precise interpretation of parameters like \tilde{c}_d , \tilde{c}_s and \tilde{c}_v is found using matching calculations that compare the predictions of $S_{\Phi QED} + S_{\text{nuc}}$ for lepton-nucleus and photon-nucleus scattering, either with measurements or (in principle) with *ab initio* predictions of the Standard Model (in practice this is where calculations using nuclear models come in).

The arguments of this paper are easiest to make using a variant of the above EFT that is better adapted to atomic calculations. Rather than treating the nucleus using the second-quantized field Φ the variant we prefer instead uses a first-quantized description (described in more detail in refs. [70–72]). A first-quantized EFT description of the nucleus is more efficient because an atom includes only a single nucleus, making the rest of the multi-particle Fock space accessed by Φ unnecessary. In principle one integrates out all multi-particle degrees of freedom to arrive at an EFT that contains only nuclear collective coordinates: its centre-of-mass position and nuclear spin, interacting with the second-quantized fields Ψ and A_μ .

The resulting EFT is worked out for spinless nuclei in refs. [64, 72], where the only relevant nuclear degree of freedom is the position operator that describes the nucleus' world-line, \mathcal{P} : $x^\mu = y^\mu(s)$. In this effective theory the remaining second-quantized degrees of freedom are described by

$$S_{QED} = - \int d^4x \left\{ \frac{1}{4} F_{\mu\nu} F^{\mu\nu} + \bar{\Psi} [\not{D} + m] \Psi \right\}, \quad (1.4)$$

to which one adds the action describing couplings to the nuclear degrees of freedom:

$$\begin{aligned} S_p &= - \int_{\mathcal{P}} ds \left\{ \sqrt{-\dot{y}^2} M - Ze \dot{y}^\mu A_\mu + c_s \sqrt{-\dot{y}^2} (\bar{\Psi}\Psi) + ic_v \dot{y}^\mu (\bar{\Psi}\gamma_\mu\Psi) + \dots \right\} \\ &= - \int d^4x \int_{\mathcal{P}} ds \left\{ \sqrt{-\dot{y}^2} M - Ze \dot{y}^\mu A_\mu + c_s \sqrt{-\dot{y}^2} (\bar{\Psi}\Psi) \right. \\ &\quad \left. + ic_v \dot{y}^\mu (\bar{\Psi}\gamma_\mu\Psi) + \dots \right\} \delta^4[x - y(s)], \end{aligned} \quad (1.5)$$

where the second line emphasizes that in the first line the ‘bulk’ fields $\Psi(x)$ and $A_\mu(x)$ are evaluated along the nuclear world-line $x^\mu = y^\mu(s)$. \dot{y}^μ here represents dy^μ/ds where s is an arbitrary parameter along the world-line. Quantization proceeds by evaluating the functional integral of $\exp[i(S_{QED} + S_p)]$ with respect to $y^\mu(s)$ (which in particular captures the response of nuclear recoil – more about which below) as well as $\Psi(x)$ and $A_\mu(x)$.

In this language the Φ -dependent part of eqs. (1.2) and (1.3) are replaced by S_p , and the spin-independent part of effective couplings — *e.g.* \tilde{c}_s, \tilde{c}_v of (1.3) — are captured by the effective couplings — *e.g.* c_s, c_v of (1.5) — within S_p . For this to be possible S_p is again required to be the most general local action consistent with the field content and symmetries, which in this case now also include arbitrary reparametrizations of the world-line parameter s . On dimensional grounds the effective couplings c_s and c_v are of order R^2 , and the ellipses in (1.5) contain interactions with couplings having dimension (length) ^{p} for $p > 2$, with those — like the ones describing nuclear polarizability — arising at order R^3 (but not involving nuclear spin) considered in detail in [64].

Physical interpretation is simpler if the world-line parameter s is chosen to be proper time, τ (in which case $\dot{y}^2 = \eta_{\mu\nu} \dot{y}^\mu \dot{y}^\nu = -1$). With this choice then $\dot{y}^\mu = \gamma(1, \mathbf{v})$ with $\gamma := dt/d\tau = (1 - \mathbf{v}^2)^{-1/2}$ and $\mathbf{v} := d\mathbf{y}/dt$, so once evaluated in the atomic center-of-mass frame (1.5) becomes

$$\begin{aligned}
 S_p &= - \int_{\mathcal{P}} d\tau \left\{ M - Ze\gamma(A_0 + \mathbf{v} \cdot \mathbf{A}) + c_s (\bar{\Psi}\Psi) \right. \\
 &\quad \left. + ic_v \gamma \left[(\bar{\Psi}\gamma_0\Psi) + \mathbf{v} \cdot (\bar{\Psi}\boldsymbol{\gamma}\Psi) \right] + \dots \right\} \\
 &= - \int d^4x \left\{ \sqrt{1 - \mathbf{v}^2} \left[M + c_s (\bar{\Psi}\Psi) \right] - Ze(A_0 + \mathbf{v} \cdot \mathbf{A}) \right. \\
 &\quad \left. + ic_v \left[(\bar{\Psi}\gamma_0\Psi) + \mathbf{v} \cdot (\bar{\Psi}\boldsymbol{\gamma}\Psi) \right] + \dots \right\} \delta^3[\mathbf{x} - \mathbf{y}(\tau)].
 \end{aligned} \tag{1.6}$$

The terms of (1.5) and (1.6) involving M and Ze are recognizable as describing the rest mass and Coulomb coupling of a point nucleus, while the subsequent terms carry the leading information about nuclear substructure.

The \mathbf{v} -dependent terms of (1.6) contain the nuclear recoil effects, with $M\sqrt{1 - \mathbf{v}^2}$ capturing the usual relativistic kinematics $E = \sqrt{\mathbf{p}^2 + M^2}$. \mathbf{v} -dependent terms that also involve c_s or c_v contain mixed nuclear-size/recoil contributions. Their size can be estimated given that, in atoms, the nuclear momenta are of order $|\mathbf{p}| \sim Z\alpha m$, and so $|\mathbf{v}| \sim Z\alpha m/M$. Similarly the leptonic matrix element $\langle \bar{\Psi}\boldsymbol{\gamma}\Psi \rangle \sim |\psi(0)|^2 \mathbf{v}_e$ is of order $(Z\alpha m)^3 (Z\alpha)$ and so $c_v \mathbf{v} \cdot \bar{\Psi}\boldsymbol{\gamma}\Psi$ contributes to energies a shift of order $c_v (Z\alpha)^5 m^4/M$. Given that the non-recoil term implies $c_v \sim Z\alpha R^2$ is a measure of the nuclear charge radius, the energy shift is $m^4 R^2 (Z\alpha)^6/M$. Since we work here to an accuracy of order $m^4 R^3 (Z\alpha)^5$ and $m^3 R^2 (Z\alpha)^6$, we must keep the leading mixed recoil/nuclear-size effects in what follows.⁵ Because recoil effects do not change the parameter counting given below, we put them aside temporarily and return to them in §4.

⁵Recoil effects for point nuclei must of course also be included, as we do in what follows.

Dropping recoil effects, in the nuclear rest frame (with the nucleus situated at the origin) one finds

$$S_p = - \int d^4x \left\{ M - Ze A_0 + c_s (\bar{\Psi}\Psi) + ic_v (\bar{\Psi}\gamma_0\Psi) + \dots \right\} \delta^3(\mathbf{x}). \quad (1.7)$$

This first-quantized, point-particle EFT (or PPEFT) treatment of the central object has been tested in a variety of other systems with compact central sources [64, 73–75], and found to reproduce in a simpler way many standard results. In particular, ref. [64] shows that its application to spinless nuclei – including some of the order- R^3 terms shown as ellipses in (1.5) and (1.7) – correctly captures the nuclear charge radius, Friar moment, polarizability *etc.* that provide the leading contributions to shifts in atomic energy levels.

A major purpose of the present paper is to extend the action (1.6) to include nuclear spin — leading *e.g.* to eq. (2.5) — and to explore the consequences of new terms for atomic energies.

1.2 Parameter counting for atomic energy shifts

In principle, the above discussion allows existing calculations of atomic energy shifts due to nuclear size to be described in two steps. First use an explicit nuclear model to compute effective couplings like c_s or c_v (which can be mapped to the various nuclear moments encountered in the literature). Second, compute the dependence of atomic energies on these effective couplings. Ref. [64] elaborates on this process in the special case of spinless nuclei.

A virtue of proceeding in this way is its economy of effort: for a specific nuclear model the first step need be taken only once, with the results usable in the second step for any number of different type of observables (provided these are at low enough energies to allow the assumed expansion in powers of R). Alternatively the second step can be done once to obtain how a specific observable depends on the effective couplings, with only the first step needing to be repeated to calculate these couplings using a variety of different nuclear models.

For the present purposes, however, we focus specifically on step two (which we generalize to include nuclei with spin). We do so because the PPEFT formulation of the nucleus provides insight into the number of independent ways that nuclear structure (or, equivalently, the effective couplings, c_s , c_v and so on) can contribute to atomic energy shifts. In particular it provides a systematic way to identify observables that do not depend at all on the nuclear effective couplings.

Tracing how effective couplings appear in low-energy atomic observables is particularly transparent in the first-quantized language. This is because in this formalism

observables like energy shifts turn out to acquire their dependence on nuclear properties purely through the near-nucleus boundary conditions satisfied by the external fields Ψ and A_μ , which in turn depends on the effective couplings like c_s, c_v . This boundary condition is found by integrating the equations of motion for these fields over a small ball centred at the nuclear position (possibly weighted by spherical harmonics). It is *only* because these boundary conditions depend on couplings like c_s and c_v that observables like atomic energy levels are sensitive to nuclear structure.

For a familiar example of this general argument, consider the field equations for A_0 obtained from the action $S_{QED} + S_p$ as given in (1.4) and (1.7). The field A_0 satisfies (in Coulomb gauge: $\nabla \cdot \mathbf{A} = 0$)

$$\nabla^2 A_0 - ie \bar{\Psi} \gamma_0 \Psi = Ze \delta^3(\mathbf{x}). \quad (1.8)$$

Treating the $A_\mu \bar{\Psi} \gamma^\mu \Psi$ term of S_{QED} — as well as all but the first two terms on the right-hand side of (1.7) — as perturbations then allows (to leading order) the dropping of the $\bar{\Psi} \gamma_0 \Psi$ term in (1.8). Integrating what's left over a small Gaussian pillbox centred at the origin gives the standard Gaussian boundary condition⁶

$$\int d^2\Omega \left(\mathbf{e}_r \cdot \nabla A_0 \right) \Big|_{r=0^+} = 4\pi \lim_{r \rightarrow 0^+} r^2 \partial_r A_0 = Ze, \quad (1.9)$$

where \mathbf{e}_r denotes the outward-pointing radial unit normal. This boundary condition fixes an integration constant of the Coulomb solution in the usual way to ensure $A^0 = Ze/(4\pi r)$. (Higher electromagnetic multipole moments are similarly found from higher-derivative terms in S_p that are linear in A_μ [76].)

Now comes the main point. The argument just given applies equally well for the field Ψ , and also once interactions are included in the equations of motion.⁷ By changing the boundary conditions at the origin the presence of the interactions in S_p necessarily alters the mode functions and energy eigenvalues of the fields Ψ and A_μ , and this is how effective couplings like c_s or c_v end up affecting electronic properties. This observation is useful because it means that many effective couplings can only appear in observables in a limited way, as is now argued.

To see why parameters like c_s or c_v (and by extension the various nuclear moments) only appear in specific combinations in observables, imagine finding the mode functions for Ψ by separating variables in its field equation in spherical coordinates. One then seeks a basis of solutions of the form $u_L(t, r, \theta, \varphi) = \mathcal{R}_L(\kappa r) Y_L(\theta, \varphi) e^{-i\omega t}$, where κ is

⁶In our metric conventions the usual electrostatic potential is $A^0 = -A_0$.

⁷As explored in more detail in [70–72, 76], once S_p is not linear in the bulk fields this procedure necessarily involves regularizing coincident divergences at the source position, and renormalizing effective couplings in S_p . (See also [77–82] for similar discussions in another context.)

a function of the mode’s energy, ω , while $Y_L(\theta, \varphi)$ represent appropriate spherical harmonics for which L denotes the collection of angular-momentum labels relevant to the problem (*e.g.* for spinless fields $L = \{l, l_z\}$ is a pair of integers in three spatial dimensions). The radial mode then satisfies an ordinary second-order differential equation, whose general solution has the form

$$\mathcal{R}_L(\kappa r) = \mathcal{C}_L \mathcal{R}_L^{\mathcal{C}}(\kappa r) + \mathcal{D}_L \mathcal{R}_L^{\mathcal{D}}(\kappa r), \quad (1.10)$$

with two integration constants, \mathcal{C}_L and \mathcal{D}_L , corresponding to the two basis solutions, $\mathcal{R}_L^{\mathcal{C}}(\kappa r)$ and $\mathcal{R}_L^{\mathcal{D}}(\kappa r)$, for each value of κ and each choice of angular-momentum quantum numbers L . The boundary condition at the origin fixes the value of $\mathcal{D}_L/\mathcal{C}_L$ and once the interactions in (1.7) are included in the action this value also depends on effective couplings like c_s and c_v . This is in practice how effective interactions localized at the nucleus ultimately modify physics far from the nucleus, and in particular influence the shapes and energies of the electronic energy eigenmodes. Furthermore, it is *only* through such boundary conditions that these eigenmodes ‘learn’ about non-pointlike nuclear-physics effects.

The above discussion is important because it shows that effective couplings typically only enter into electronic energy shifts through the values they imply for the ratio $\mathcal{D}_L/\mathcal{C}_L$ for each choice for L . Furthermore, at low orders in the R/a_B expansion only a few angular momenta contribute at all, because of the suppression near the nucleus of higher- L wave-functions. This leads to one of our main points:

If there are more effective couplings in S_p than there are relevant integration constants $\mathcal{C}_L, \mathcal{D}_L$, then the effective couplings cannot all appear independently in observables: all that matters for experiments are the values of $\mathcal{D}_L/\mathcal{C}_L$.

For spinless nuclei ref. [64] shows that out to orders $m^4 R^3 (Z\alpha)^5$ and $m^3 R^2 (Z\alpha)^6$ (but not including order $m^5 R^4 (Z\alpha)^6$) all nuclear-size contributions — *i.e.* the charge radius, the Friar moment [29], the electromagnetic nuclear polarizabilities, leading recoil corrections and a few others — contribute to atomic energy shifts only through their contributions to one parameter: the value of $\mathcal{D}_L/\mathcal{C}_L$ for S -wave modes. This is only one parameter because this ratio has a predictable dependence on κ (and so also on the principal quantum number $n = 1, 2, \dots$). Because the couplings c_i capture *all* possible nuclear-size effects, it follows that (to this order in $Z\alpha$ and $R/a_B = mRZ\alpha$) *all* nuclear finite-size effects can enter into atomic energy levels only through a single independent parameter: the S -wave value of $\mathcal{D}_L/\mathcal{C}_L$ (for details see [64]).

A similar statement applies at higher orders. Starting at order $m^5 R^4 (Z\alpha)^6$ the ratio $\mathcal{D}_L/\mathcal{C}_L$ for the P -wave modes is also required when computing atomic energies, so to

this order (for spinless nuclei) all nuclear effects only enter atomic energies through *two* independent parameters. One can continue on in this way to any order and identify the number of independent nuclear contributions that can robustly arise. In all cases there are fewer contributions than would be naively expected by counting nuclear effective couplings (like c_s , c_v , *etc*) allowed at this order in R (or by counting nuclear ‘moments’ within specific nuclear models, as is the usual calculational practice).

This paper

With the above logic in mind, we now can state what the present paper achieves. We first extend the analysis of [64] to include nonzero nuclear spin. This allows us to broaden the applicability of these conclusions to general single-lepton atoms and ions, and in particular to those of most practical interest: Hydrogen (and muonic Hydrogen). We find that the inclusion of spin introduces additional constants, but to any fixed order it remains true that nuclear-size effects enter into atomic energies through fewer parameters than might be expected based on nuclear modelling. Our more detailed conclusions regarding the number of relevant parameters at any given order are summarized in Table 1, which contains a list of contributions to atomic energy shifts due to nuclear finite-size effects. The Table is organized into three blocks, each containing terms that involve specific powers of the nuclear magnetic moment, μ_N (which enters through the small dimensionless parameter $\mathfrak{s} \propto m_e \mu_N$). Successive rows in each block list higher-order terms additionally suppressed by powers of $Z\alpha$ or $R/a_B = mRZ\alpha$. (The first block – independent of magnetic moments – reproduces in particular the results of [64] for spinless nuclei.)

The Table’s 2nd column gives the suppression of each term relative to the leading-order contribution that shares the same power of \mathfrak{s} . The leading contribution independent of \mathfrak{s} is the usual charge-radius term. For terms involving at least one power of \mathfrak{s} the entry marked ‘LO’ contains the leading dependence on finite nuclear size R at this order in \mathfrak{s} . (The term before this one depends on nuclear size only through μ_N , which need not vanish even for a point nucleon).

The third and fourth columns of Table 1 indicate with a check or a cross whether or not this size a contribution actually arises when computed using Dirac-Coulomb wavefunctions (and neglecting QED radiative corrections⁸ that are suppressed by additional powers of α). These two columns differ in the value they assume for the lepton’s total angular momentum quantum number, j , with column 3 giving the dominant result for

⁸These radiative corrections are included within our formalism, as are recoil corrections, because all of Ψ , A_μ and y^μ are fully dynamic quantum operators. We discuss radiative and recoil corrections in more detail in §4, but what is important is this: they do not introduce any new parameters (though they do of course depend on the bulk-field mode functions, and so on the existing parameters, $\mathcal{D}_L/\mathcal{C}_L$).

$j = \frac{1}{2}$ and column 4 giving the same for $j = \frac{3}{2}$. Comparing these columns shows the angular-momentum suppression expected for nuclear effects due to the suppression of the wave-function outside the nucleus near the origin. For instance $j = \frac{3}{2}$ states are irrelevant for contributions lower-order than $m^5 R^4 (Z\alpha)^6$, but once this order is reached a new constant enters because the value of $\mathcal{D}_L/\mathcal{C}_L$ for $j = \frac{3}{2}$ contributes observably.

The final two columns give an indication of the numerical size of each term, with column 5 providing the numbers for ordinary (electronic) Hydrogen while column 6 does so for muonic Hydrogen. Electronic and muonic Hydrogen differ only in the value of the lepton mass that is used in the corresponding estimate, which implies that the combination mR is not particularly small for muonic Hydrogen (and so $R/a_B \sim Z\alpha$, rather than being much smaller). For illustration purposes squares are shaded green if the resulting estimate is of order 0.001 kHz or larger (for Hydrogen) or of order 10^{-3} meV or more for muonic Hydrogen. The given numerical values evaluate R using the charge radius, $R = r_p = 0.84087$ fm, for \mathfrak{s} -independent contributions, but use the Zemach radius, $R = r_z = 1.082$ fm for \mathfrak{s} -dependent contributions [13]. The yellow square flags a term not computed here that might also contribute observably for muonic Hydrogen.

Only terms on rows shaded green are required if one works only to this accuracy, and Table 1 shows that in this case nuclear finite-size effects enter through just two independent constants. One controls the contributions independent of nuclear spin (and contains in particular the contributions of the charge radius, Friar moment, nuclear polarizabilities, leading recoil corrections and more [64]) and the second, spin-dependent, parameter captures the nuclear Zemach moment. The nuclear magnetic moment also enters into atomic energies at this order, though we do not count this as an unknown nuclear parameter because its value is accurately determined by other means.

We see from the Table that the conclusions of [64] also apply for spinning nuclei, though with one additional constant required at the accuracy discussed above. This is so despite there being many more parameters apparently relevant in the first-quantized action, S_p , and in explicit calculations using nuclear models [29]. Of course, this does not mean that the parameters of nuclear models are not intrinsically independent; what it says is that only a small number of combinations of them ever appear in observables *at the extremely low energies relevant to atomic energy levels*. As discussed below, the two constants through which they appear to this order for spin-half nuclei can be captured by $\mathcal{D}_L/\mathcal{C}_L$ for S -wave modes for the two different values of total atomic angular momentum quantum number: F (where $\mathbf{F} = \mathbf{I} + \mathbf{J}$ as usual combines nuclear spin and electronic total angular momentum).

Why care that the many moments of nuclear models (or parameters in the action S_p) can only enter atomic energies through their contributions to the (comparatively

fewer) mode constants $\mathcal{D}_L/\mathcal{C}_L$? This observation is useful because theoretical calculations of nuclear moments are notoriously difficult and in some cases introduce the dominant theoretical uncertainties in calculations of atomic energy levels. These uncertainties can be larger than the size of other small effects whose measurement might ultimately provide new tests of fundamental physics. Robustly knowing that these uncertainties only enter atomic levels in a small number of independent ways opens up ways to remove nuclear uncertainties from some precision atomic measurements. This can be done in several ways: simply use experiments to determine the relevant nuclear parameters (which, as argued above, are fewer than the naive number of nuclear moments); or combine observables in such a way that nuclear contributions completely cancel, whose results are not subject at all to uncertainties associated with nuclear (or other short-distance) physics.

We illustrate how this can be done in practice by identifying the values of the two independent nuclear parameters using two particularly well-measured atomic energy-level differences, with results for these parameters summarized in Table 2 for atomic Hydrogen and Table 4 for muonic Hydrogen. These values are then used to predict the nuclear component of other transition frequencies working at the order indicated by green entries in Table 1. These predictions are presented for the best-measured transitions of atomic Hydrogen in Table 3, while results for the much broader list of transitions compiled in [6] are given in Tables 5 through 7. Each of these tables gives the finite-nuclear-size contribution as computed for these transitions, together with an estimate of the errors involved, at the orders listed in green in Table 1, as summarized in §4.

As these tables show, at present the largest uncertainty comes from the error in the theoretical prediction for the two reference transitions as computed using a point-like nucleus (or the ‘point-like’ theory, for short). What is important is that the size of all of these errors can improve in a way that does not depend on nuclear physics. Although the required calculations are challenging in practice, improved computations for a point-like nucleus are in principle straightforward to perform. The same is true for the ‘truncation’ error given in Column 5 of the Tables, and of course experimental errors do not require improvements in nuclear-physics calculations. As these errors improve, so do the overall theoretical errors in the predictions like those in Column 2 of the Tables. Errors in nuclear calculations play no role in our predictions because all relevant nuclear parameters are taken directly from atomic observations.

We find in this way a broad and robust class of predictions whose intrinsic error is not set by our ability to compute with nuclear models. In the language of earlier paragraphs, given precise measurements for N_{exp} leptonic energy differences (for a specific nucleus), we make $N_{\text{exp}} - 2$ model-independent predictions for how nuclei shift atomic

energies, essentially by eliminating the two independent nuclear parameters. What is important is that the error in these predictions is controlled only by the accuracy of the experiments used to determine the two parameters, plus the error implied by working only to a fixed order in the small quantities $Z\alpha$ and $\mathfrak{s} \sim R/a_B = mRZ\alpha$ in both the ‘point-like’ theory contributions and the effective couplings.

The rest of this paper is organized as follows. §2 derives the point-particle effective action for central sources with spin, keeping effective interactions with couplings out to dimension (length)². To the order we work the main difference relative to [64] is the presence of the dipole nuclear magnetic field, and we use standard perturbation theory to establish its consequences for atomic energy levels.

In particular, §2.4 then explores the near-nucleus boundary conditions implied for the electron field by the relevant contact interactions at the nucleus, §3 gives a discussion of the associated divergences in these calculations in the near-nucleus limit, and derives the renormalization-group (RG) evolution of the new effective couplings. These contact interactions also shift electronic energy levels in a way that competes with the effects of the nuclear magnetic dipole field. These sections show in detail why (for each nuclear isotope) only two parameters (plus the nuclear magnetic moment) are required to describe all nucleus-dependent shifts to the order we work.

Next, §4 collects expressions for nucleus-dependent atomic energy shifts. §4.2 uses the existing experimental data for Hydrogen to fit the two relevant nuclear parameters, and applies these to make predictions for nuclear-size effects for other transitions, with prediction errors that are independent of the limitations of nuclear models. §4.3 briefly discusses the same steps for muonic Hydrogen. Finally, §5 summarizes our conclusions and comments on possible future directions. Several appendices outline useful calculational details, and in particular Appendix G provides a list of notation used.

2 PPEFT for sources with spin

To set up the position-space point-particle effective theory (PPEFT) for spinning nuclei we couple second-quantized electron and photon fields to the first-quantized nuclear centre-of-mass and spin degrees of freedom. The resulting action is the sum of a ‘bulk’ part and a ‘point-particle’ part, $S = S_B + S_p$, where the bulk part consists of standard quantum electrodynamics (QED), as in (1.4) (repeated here, for convenience),

$$S_B = - \int d^4x \left\{ \frac{1}{4} F_{\mu\nu} F^{\mu\nu} + \bar{\Psi} (\not{D} + m) \Psi \right\}. \quad (2.1)$$

As before, $F_{\mu\nu}$ is the field strength for the electromagnetic gauge potential $A_\mu(x)$, and $\Psi(x)$ is the spin-half Dirac field of the orbiting lepton with mass m and charge $q = -e$

(with covariant derivative $D_\mu = \partial_\mu + ieA_\mu$).

Our main focus here is in the formulation of S_p for the first-quantized nucleus, with the new feature relative to refs. [64, 70–72] being the inclusion of the nuclear spin degrees of freedom in the first-quantized nuclear action, S_p .

2.1 Spin on a world-line

The classical and quantum dynamics of first-quantized spinless relativistic particles propagating in spacetime is discussed in many textbooks [83–85]. The extension to first-quantized spinning particles started in the early days of supersymmetry where it was found that first-quantized supersymmetric systems built using Grassmann (classically anti-commuting) fields described spinning particles [86–91].

Classical Grassman variables naturally arise when describing spin because on quantization they furnish finite-dimensional representations of rotations in the quantum Hilbert space (as is seen explicitly below). The particle’s total spin quantum number, s , is then fixed in terms of the dimension, $2s + 1$, of this representation. We here follow this lead and use such a Grassmann field to describe nuclear spin, introducing a 4-vector of new Grassmann fields, $\xi^\mu(s)$, on the nuclear world-line, which at the classical level satisfies $\{\xi^\mu, \xi^\nu\} = 0$.

Kinematics

Supplementing the unperturbed action for the centre-of-mass motion of the nucleus with the free action for ξ^μ gives

$$S_{p0} = - \int ds \left\{ \sqrt{-\dot{y}^2} M + i\xi^\mu \dot{\xi}_\mu - (Ze)\dot{y}^\mu A_\mu \right\}, \quad (2.2)$$

where s is an arbitrary world-line parameter.

Once quantized, the classical anticommutation relation becomes modified⁹ to become [89]:

$$\left\{ \hat{\xi}^\mu, \hat{\xi}^\nu \right\} = -\frac{1}{2} \eta^{\mu\nu}. \quad (2.3)$$

A technical complication arises when quantizing because this is a constrained classical system, whose canonical positions and momenta are not all independent of one another. Quantization requires the toolkit put together by Dirac in [92] and others [84, 93–95] for constrained systems, combined with standard techniques for anti-commuting objects summarised (for instance) in [96, 97].

The system’s Hilbert space (as usual) furnishes a representation of this algebra, and we choose the spin of the nucleus when we choose the dimension of the representation

⁹See Appendix A for more details and for our Dirac matrix conventions.

that is of interest. For spin- $\frac{1}{2}$ fermions, we use a 4-dimensional¹⁰ representation in terms of Dirac matrices,

$$\hat{\xi}^\mu = \frac{i}{2} \Gamma^\mu, \quad (2.4)$$

since the Clifford algebra identity $\{\Gamma^\mu, \Gamma^\nu\} = 2\eta^{\mu\nu}$ then ensures (2.3) is satisfied. We use the notation Γ^μ (rather than γ^μ) here to emphasize that these matrices act in the spin-space of the nucleus and reserve γ^μ for the matrices that act on the bulk electron field Ψ .

Interactions

The EFT program for a first-quantized and spinning nucleus then asks for all possible local interactions on the world-line that can be written using the fields $y^\mu(s)$, $\xi^\mu(s)$ as well as the ‘bulk’ fields $A_\mu(x = y(s))$ and $\Psi(x = y(s))$. One must write down all allowed operators to a given order to capture all spin-dependent effects consistent with the assumed symmetries (which for the applications below we take, as before, to be the symmetries of the strong and electromagnetic interactions).

We require the point-particle localized interactions to be hermitian (this is not always required for localized sources, see *e.g.* [73], but is appropriate for the present application); to be Grassmann-even; to be invariant under Poincare transformations; to be electromagnetic gauge-invariant; to preserve separately C, P and T transformations; and arbitrary reparameterizations of the nuclear world-line: $s \rightarrow s' = f(s)$. Then, keeping only interactions out to order $(\text{length})^2$, the most general interactions work out to be

$$\begin{aligned} S_p = S_{p0} + \int ds \left\{ i\mu_N \sqrt{-\dot{y}^2} \xi^\mu \xi^\nu F_{\mu\nu} + ic_{\text{em}} \dot{y}^\mu \xi^\rho \xi^\sigma \partial_\mu F_{\rho\sigma} \right. \\ \left. - \bar{\Psi} \left[\sqrt{-\dot{y}^2} (c_s + ic_2 \epsilon_{\alpha\beta\gamma\delta} \xi^\alpha \xi^\beta \xi^\gamma \xi^\delta \gamma_5 + ic_F \xi^\mu \xi^\nu \gamma_{\mu\nu}) \right. \right. \\ \left. \left. + i\dot{y}^\mu (c_v \gamma_\mu + c_3 \epsilon_{\alpha\beta\gamma\delta} \xi^\alpha \xi^\beta \xi^\gamma \xi^\delta \gamma_5 \gamma_\mu) \right] \Psi + \dots \right\}, \end{aligned} \quad (2.5)$$

where S_{p0} is as given in (2.2) and (as above) $y^\mu(s)$ is the bosonic centre-of-mass position of the source, $\xi^\mu(s)$ is the Grassmann coordinate representing nuclear spin, while overdots denote derivatives with respect to the world-line parameter. The quantities μ_N , c_{em} , c_s , c_2 , c_v , c_F , c_3 and so on are the effective couplings that arise to this order, where μ_N has dimension (length) and the rest have dimension $(\text{length})^2$.

We next turn to the boundary conditions for A_μ and Ψ that are implied by this action, starting first with the electromagnetic field. We specialize when doing so to spin-half nuclei (both for concreteness’s sake and with a view to applications to Hydrogen).

¹⁰This becomes two-dimensional once antiparticle states are projected out.

2.2 Implications for the electromagnetic field

Varying A_μ in the action $S_B + S_p$ yields the field equation

$$\begin{aligned}
 \partial_\nu F^{\mu\nu} &= -ie\bar{\Psi}\gamma^\mu\Psi + Ze \int ds \dot{y}^\mu \delta^4[x - y(s)] + i\mu_N \partial_\nu \int ds \sqrt{-\dot{y}^2} \left[\hat{\xi}^\mu, \hat{\xi}^\nu \right] \delta^4[x - y(s)] \\
 &\quad - ic_{\text{em}} \partial_\sigma \partial_\nu \int ds \left[\hat{\xi}^\mu, \hat{\xi}^\nu \right] \dot{y}^\sigma \delta^4[x - y(s)] \\
 &= -ie\bar{\Psi}\gamma^\mu\Psi + Ze \delta_0^\mu \delta^3(\mathbf{x}) + \mu_N \Gamma^{\mu\nu} \partial_\nu \delta^3(\mathbf{x}) - c_{\text{em}} \Gamma^{\mu\nu} \partial_0 \partial_\nu \delta^3(\mathbf{x}),
 \end{aligned} \tag{2.6}$$

where the second line uses the spin-half version of (2.4) as well as the definition $\Gamma^{\mu\nu} := -\frac{i}{4} [\Gamma^\mu, \Gamma^\nu]$; we specialize to the nuclear rest-frame with nucleus situated at the origin – *i.e.* $\dot{\mathbf{y}}(s) = \mathbf{y}(s) = 0$ – and we parameterize the world-line using proper time (*i.e.* $s = \tau$, with $-\dot{y}^2 = 1$ and $\dot{y}^\mu = \delta_0^\mu$). Specialization to the rest frame simplifies the discussion by excluding nuclear recoil effects that are suppressed by inverse powers of the nuclear mass, since these are not required for the applications we have in mind. But there is no reason why such effects cannot also be included as corrections to the second equality of (2.6), which would instead be obtained by evaluating the first equation in the atomic centre-of-mass frame.

Neglect of inverse powers of nuclear mass also simplifies the above by allowing the removal of its antiparticle states, leaving the two spin states of the non-relativistic nucleus at the origin, familiar from atomic physics. This is achieved by projecting out the anti-particle solutions from the nuclear states (as described in Appendix A). Together with dropping nuclear recoil this also means the only matrices to survive unsuppressed by nuclear velocity are

$$\Gamma^0 \rightarrow -i \mathbf{1} \quad \text{and} \quad \Gamma_5 \Gamma_k \rightarrow -i \tau_k \quad \text{and} \quad \Gamma^{ij} \rightarrow \frac{1}{2} \epsilon^{ijk} \tau_k, \tag{2.7}$$

which are 2×2 matrices acting in nuclear spin-space, for which our conventions use τ_k to denote the Pauli matrices (with the same matrices acting in electron-spin space being denoted σ_k).

With these choices the electromagnetic field equations (2.6) become

$$\begin{aligned}
 \nabla \cdot \mathbf{E} &= \partial_\nu F^{0\nu} = -ie\bar{\Psi}\gamma^0\Psi + Ze \delta^3(\mathbf{x}), \\
 (-\partial_t \mathbf{E} + \nabla \times \mathbf{B})^i &= \partial_\nu F^{i\nu} = -ie\bar{\Psi}\gamma^i\Psi + \mu_N \epsilon^{ilk} I_k \partial_l \delta^3(\mathbf{x}),
 \end{aligned} \tag{2.8}$$

where $\mathbf{I} := \frac{1}{2} \boldsymbol{\tau}$ denotes the nuclear spin vector, which is an operator in the space of nuclear spins. These show that the nuclear part of the electromagnetic current 4-vector is:

$$j^0 = Ze \delta^3(\mathbf{x}), \quad j^i = \mu_N \epsilon^{ilk} I_k \partial_l \delta^3(\mathbf{x}). \tag{2.9}$$

Following standard practice, we work perturbatively in quantum-field interactions like $eA_\mu \bar{\Psi} \gamma^\mu \Psi$, whose contributions can be tracked by evaluating the appropriate Feynman graphs for QED. In principle we would like also *not* to perturb in the nucleus-generated electromagnetic fields, and so include these in the evolution of interaction-picture fields. The boundary conditions for the interaction-picture fields therefore are derived by following the arguments leading to (1.9), but using the contributions of both the currents j^0 and j^i of (2.9) on the right-hand side of eqs. (2.8).

In interaction picture (and in Coulomb gauge) the solution to the Maxwell equations that satisfy the nucleus-dependent boundary conditions generated by the right-hand side of (2.8) gives (1.9) as before (for the electrostatic potential), while use of the j^i boundary condition¹¹ generates the standard magnetic dipole field [98, 99],

$$A^0 = A_{\text{nuc}}^0 = \frac{Ze}{4\pi r}, \quad \mathbf{A} = \mathbf{A}_{\text{nuc}} + \mathbf{A}_{\text{rad}} = \frac{\boldsymbol{\mu} \times \mathbf{r}}{4\pi r^3} + \mathbf{A}_{\text{rad}}, \quad (2.10)$$

where¹² $\boldsymbol{\mu} := \mu_N \mathbf{I}$ is the nuclear magnetic moment¹³ and $\mathbf{A}_{\text{rad}}(\mathbf{r}, t)$ denotes the operator-valued radiation component of the interaction-picture electromagnetic field (whose boundary conditions are the standard, nucleus-independent, ones).

2.3 Lepton mode functions

The previous sections show that the A_μ -dependent terms in the action (2.5) alter the interaction-picture electromagnetic field only by capturing the nuclear magnetic moment (and by doing so give a physical interpretation for the effective coupling μ_N). Repeating the above exercise for the electron field reveals more information, however, leading to the field equation:

$$0 = (\not{D} + m) \Psi + \int ds \delta^4[x - y(s)] \left\{ \sqrt{-\dot{y}^2} \left(c_s + ic_2 \epsilon_{\mu\nu\rho\sigma} \hat{\xi}^\mu \hat{\xi}^\nu \hat{\xi}^\rho \hat{\xi}^\sigma \gamma_5 + ic_F \hat{\xi}^\mu \hat{\xi}^\nu \gamma_{\mu\nu} \right) + i\dot{y}^\mu \left(c_v \gamma_\mu + c_3 \epsilon_{\mu\nu\rho\sigma} \hat{\xi}^\mu \hat{\xi}^\nu \hat{\xi}^\rho \hat{\xi}^\sigma \gamma_5 \gamma_\mu \right) \right\} \Psi, \quad (2.11)$$

where, as before, the lepton covariant derivative is $D_\mu \Psi = (\partial_\mu + ieA_\mu) \Psi$. Using again the representation (2.4) and specializing to the nuclear rest frame (and parameterizing

¹¹In detail, the A_0 boundary condition is obtained as before by straight-up integration of the field equation over a small spherical Gaussian pillbox of radius ϵ , while the boundary condition for \mathbf{A} comes from a similar integration, but weighted by an $l = 1$ spherical harmonic [76].

¹²Notice μ_N here denotes the nuclear magnetic moment (*not* the nuclear magneton) including the nuclear g -factor.

¹³That is, (2.10) is the classical solution obtained using the boundary condition that formally follows from (2.8) with \mathbf{I} regarded as a specified function. For first-quantized nuclei we may treat \mathbf{I} as an operator in the knowledge that \mathbf{A}_{nuc} ultimately appears within an expectation value between two nuclear spins (as we see explicitly below).

using proper time) then gives

$$0 = [\gamma^0 (\partial_0 + ieA_0) + \gamma^i (\partial_i + ieA_i) + m] \Psi + \delta^3(\mathbf{x}) \left[c_s - ic_v \gamma^0 + \frac{c_F}{2} \epsilon^{ijk} I_k \gamma_{ij} \right] \Psi, \quad (2.12)$$

where the terms involving c_2 and c_3 are proportional to $\Gamma_5 := -i\Gamma^0\Gamma^1\Gamma^2\Gamma^3$ and so vanish in the nuclear rest frame – *c.f.* eqs. (2.7) – and (as above) $\mathbf{I} := \frac{1}{2} \boldsymbol{\tau}$ is the nuclear spin (acting in nuclear-spin space).

As above, our perturbative treatment of quantum-field interactions allows the term $\mathbf{A}_{\text{rad}} \cdot \bar{\Psi} \boldsymbol{\gamma} \Psi$ to be dropped in the interaction-picture evolution of the fields, though the nucleus-generated Coulomb and magnetic-dipole fields do appear in the interaction-picture evolution of the field operator Ψ . Away from the nuclear position eq. (2.12) then boils down to the Dirac equation in the presence of a Coulomb potential and a dipole magnetic field:

$$0 = [-i\gamma^0 (\omega - eA_0^{\text{nuc}}) + \boldsymbol{\gamma} \cdot \nabla + m] \psi + ie\boldsymbol{\gamma} \cdot \mathbf{A}_{\text{nuc}} \psi, \quad (2.13)$$

where A_0^{nuc} and \mathbf{A}_{nuc} are the Coulomb and magnetic-dipole contributions given in (2.10).

The delta-function terms in (2.12) contribute once the equation is integrated over a small sphere of radius ϵ that includes the nucleus (possibly weighted by spherical harmonics¹⁴). For example (as described in more detail in Appendix B), for S -wave modes integrating over a small sphere (of radius ϵ) about the position of the delta function implies a boundary condition

$$0 = \int d^2\Omega_2 \epsilon^2 [\gamma^r + \hat{c}_s - i\gamma^0 \hat{c}_v + \hat{c}_F \mathbf{I} \cdot \boldsymbol{\Sigma}] \psi(\epsilon), \quad (2.14)$$

for fields at $r = \epsilon$, where the couplings \hat{c}_i are related to the couplings appearing in S_p by $\hat{c}_i = c_i/(4\pi\epsilon^2)$ and Σ_k is defined by $\gamma^{ij} = \epsilon^{ijk} \Sigma_k$, where $\gamma^{\mu\nu} := -\frac{i}{4}[\gamma^\mu, \gamma^\nu]$. This near-nucleus boundary condition fixes some of the integration constants that arise when integrating (2.13), and thereby allows them to depend on c_s , c_v and c_F . It is through this dependence that nuclear properties alter atomic energy levels.

Two new steps are required in order to compute the effects of the nucleus on electronic levels. First the Dirac equation (2.13) must be solved away from the nucleus in the presence of the dipole magnetic field, which is done in this section by perturbing in the magnetic moment μ_N . The second step (performed in §2.4 below) takes these solutions and imposes the near-nucleus boundary conditions implied by (2.14) to determine some of the integration constants found when solving (2.13). In particular these

¹⁴For the S -wave modes of later interest no weighting by spherical harmonics is necessary.

solutions are *not* assumed to be bounded at the origin, and indeed the boundary conditions following from (2.14) are only consistent with boundedness when the effective couplings c_s , c_v , *etc.* all vanish. The full effect of spin-dependent finite-size nuclei on atomic energy levels receives contributions from both of these two steps, as we now see.

2.3.1 Dirac-Coulomb modes

We start by reviewing the properties of modes, $u(\mathbf{x}, t)$, of the Dirac equation in the presence of a Coulomb potential but without a dipole magnetic field. Denoting mode energy by ω one seeks solutions of the form $u(\mathbf{x}, t) = e^{-i\omega t}\psi(\mathbf{x})$. Away from the origin the function ψ satisfies:

$$0 = \left[-i\gamma^0 (\omega - eA_0^{\text{nuc}}) + \boldsymbol{\gamma} \cdot \nabla + m \right] \psi. \quad (2.15)$$

where (as above) A_0^{nuc} is the Coulomb potential of eq. (2.10).

The standard Dirac-Coulomb Hamiltonian mode functions separate in polar coordinates, and are labelled by the quantum numbers $|njz\varpi\rangle$ where n is the principal quantum number, $j = \frac{1}{2}, \frac{3}{2}, \dots$ and $j_z = -j, -j+1, \dots, j-1, j$, stand for total electronic angular momentum, and $\varpi = \pm$ is the parity quantum number.¹⁵ Working in a basis for which γ^0 is diagonal, the corresponding mode functions are Dirac spinors [72, 100]:

$$\psi = \begin{pmatrix} \Omega_{jlj_z\varpi}(\theta, \phi) \mathbf{f}_{nj}(r) \\ i\Omega_{j'l'j_z\varpi}(\theta, \phi) \mathbf{g}_{nj}(r) \end{pmatrix}, \quad (2.16)$$

where $\Omega_{jlj_z\varpi}$ denotes a 2-component spinor spherical harmonic,

$$\Omega_{jlj_z\varpi} := \begin{pmatrix} \varpi \sqrt{\frac{l+\varpi j_z + \frac{1}{2}}{2l+1}} Y_{l, j_z - \frac{1}{2}}(\theta, \phi) \\ \sqrt{\frac{l-\varpi j_z + \frac{1}{2}}{2l+1}} Y_{l, j_z + \frac{1}{2}}(\theta, \phi) \end{pmatrix}, \quad (2.17)$$

with total, orbital and projected total angular momentum quantum numbers (j, l, j_z) . Here the orbital quantum numbers l and l' are related to j and parity by $l = j - \frac{1}{2}\varpi$ and $l' = j + \frac{1}{2}\varpi$. $Y_{l_z}(\theta, \phi)$ are the usual scalar spherical harmonics.

The functions $\mathbf{f}_{nj}(r)$ and $\mathbf{g}_{nj}(r)$ are the solutions to the radial part of the Dirac equation (more about which below). Skipping details – see [64] for an enumeration of more steps using much the same formalism, but for spinless nuclei – the radial functions

¹⁵Strictly speaking the parity of a state is $(-)^l$ where $l := j - \frac{1}{2}\varpi$, so ϖ *determines* the parity, but need not be equal to it for all j . This distinction does not matter in practice for the states of most interest, for which $j = \frac{1}{2}$.

are given by

$$\begin{aligned} \mathfrak{f}_{nj}(r) &= \sqrt{m+\omega} e^{-\rho/2} \left\{ \mathcal{C} \rho^{\zeta-1} \left[\mathcal{M}_1 - \left(\frac{a}{c}\right) \mathcal{M}_2 \right] + \mathcal{D} \rho^{-\zeta-1} \left[\mathcal{M}_3 - \left(\frac{a'}{c}\right) \mathcal{M}_4 \right] \right\}, \\ \mathfrak{g}_{nj}(r) &= -\sqrt{m-\omega} e^{-\rho/2} \left\{ \mathcal{C} \rho^{\zeta-1} \left[\mathcal{M}_1 + \left(\frac{a}{c}\right) \mathcal{M}_2 \right] + \mathcal{D} \rho^{-\zeta-1} \left[\mathcal{M}_3 + \left(\frac{a'}{c}\right) \mathcal{M}_4 \right] \right\}, \end{aligned} \quad (2.18)$$

where \mathcal{C} and \mathcal{D} are integration constants and the functions \mathcal{M}_i are given in terms of confluent hypergeometric functions – defined in (E.16) – $\mathcal{M}(\beta, \gamma; z) := {}_1\mathcal{F}_1[\beta; \gamma; z]$ with different arguments:

$$\begin{aligned} \mathcal{M}_1 &:= \mathcal{M}(a, b; \rho), \quad \mathcal{M}_2 := \mathcal{M}(a+1, b; \rho), \\ \mathcal{M}_3 &:= \mathcal{M}(a', b'; \rho), \quad \mathcal{M}_4 := \mathcal{M}(a'+1, b'; \rho). \end{aligned} \quad (2.19)$$

The various parameters appearing in (2.18) and (2.19) are defined by

$$\begin{aligned} a &:= \zeta - \frac{Z\alpha\omega}{\kappa}, \quad a' := -\left(\zeta + \frac{Z\alpha\omega}{\kappa}\right), \quad b := 1 + 2\zeta, \quad b' := 1 - 2\zeta, \\ c &:= \mathfrak{K} - \frac{Z\alpha m}{\kappa}, \quad \rho := 2\kappa r, \quad \kappa := \sqrt{m^2 - \omega^2}, \quad \zeta := \sqrt{\mathfrak{K}^2 - (Z\alpha)^2}, \end{aligned} \quad (2.20)$$

where \mathfrak{K} is the Dirac quantum number, defined by

$$\mathfrak{K} := -\varpi \left(j + \frac{1}{2}\right) = \mp \left(j + \frac{1}{2}\right) \quad \text{for parity } \pm \text{ states.} \quad (2.21)$$

For later purposes we note that only \mathcal{M}_1 and \mathcal{M}_2 are bounded at the origin, and so the radial functions are bounded at the origin only when $\mathcal{D} = 0$, as is usually chosen when working with a point-like spinless nucleus.

Bound states have $\omega < m$ and for these normalizability at large r requires the integration constants to be related by

$$-\left(\frac{\mathcal{D}}{\mathcal{C}}\right) = \frac{\Gamma[1+2\zeta] \Gamma[-\zeta - (Z\alpha\omega/\kappa)]}{\Gamma[1-2\zeta] \Gamma[\zeta - (Z\alpha\omega/\kappa)]}. \quad (2.22)$$

The Dirac-Coulomb bound-state energies are then determined by choosing ω to ensure that (2.22) is consistent with the condition on \mathcal{D}/\mathcal{C} that comes from the near-nucleus boundary condition (described in more detail in §2.4).

As mentioned earlier, for a point-like spinless nucleus – *i.e.* in the absence of the nucleus-dependent $\delta^3(\mathbf{x})$ terms in (2.12) – these boundary conditions simply state that

the solution is bounded at the origin, which implies $\mathcal{D} = 0$. Using $\mathcal{D} = 0$ in (2.22) then implies the standard point-nucleus Dirac-Coulomb energy spectrum $\omega = \omega_{nj}^D$, where

$$\omega_{nj}^D = m\sqrt{1 - \left(\frac{\kappa_{nj}^D}{m}\right)^2} \quad (2.23)$$

with

$$\kappa_{nj}^D = \frac{mZ\alpha}{\mathcal{N}} \quad \text{and} \quad \mathcal{N} = n\sqrt{1 - \frac{2(n - |\mathfrak{K}|)(Z\alpha)^2}{n^2(\zeta + |\mathfrak{K}|)}}. \quad (2.24)$$

Here $n = 1, 2, \dots$ is the usual principal quantum number.

More generally, when \mathcal{D}/\mathcal{C} is nonzero but small the solution obtained by solving (2.22) for ω becomes¹⁶ $\omega_{nFj\varpi} = \omega_{nj}^D + \delta\omega_{nFj\varpi}$ with $\delta\omega_{nFj\varpi}$ given [64] by eq. (C.10) of Appendix C.

In what follows it is important to keep in mind that the mode energy, ω , is *not* the same as the physical single-particle energy measured in atomic systems. The entire energy relevant to experiments includes many corrections, and (to the order required here) takes the form

$$\omega_{nFj\varpi} = \omega_{nj}^D + \delta\omega_{nFj\varpi} + \varepsilon_{nFj\varpi}^{\text{mag}} + \varepsilon_{nFj\varpi}^{\text{QED}} + \varepsilon_{nFj\varpi}^{\text{rec}}. \quad (2.25)$$

The first of these is the single-particle Dirac-Coulomb spectrum of (2.23), while $\delta\omega_{nFj\varpi}$ denotes the shift in the mode spectrum coming from having $\mathcal{D}/\mathcal{C} \neq 0$ when solving eq. (2.22). As we see explicitly below, nonzero values for \mathcal{D}/\mathcal{C} arise when nuclei are not point-like, and so provide part of the influence of nuclear structure on atomic spectra.

The contribution $\varepsilon_{nFj\varpi}^{\text{mag}} = \varepsilon_{nFj\varpi}^{(1)} + \varepsilon_{nFj\varpi}^{(ho)}$ contains the influence of the nuclear magnetic field, \mathbf{A}_{nuc} , which to the accuracy desired here can be computed perturbatively. The first-order effects we denote by $\varepsilon_{nFj\varpi}^{(1)}$, whose calculation is described at length below. This term contains both spin-dependent point-nucleus contributions (such as the hyperfine splitting) and spin-dependent finite-size nuclear effects. Higher-order contributions, denoted $\varepsilon_{nFj\varpi}^{(ho)}$, are also relevant [116], though for current precision their form for point nuclei is sufficient.

The next contribution arises when perturbing in the radiation component of the electromagnetic field, $\varepsilon_{nFj\varpi}^{\text{QED}} = \varepsilon_{nFj\varpi}^{\text{pt-QED}} + \varepsilon_{nFj\varpi}^{N\text{-QED}}$, with $\varepsilon_{nFj\varpi}^{\text{pt-QED}}$ describing standard QED corrections (such as the Lamb shift) as computed for point nuclei, and $\varepsilon_{nFj\varpi}^{N\text{-QED}}$ describing nuclear-size effects in these QED corrections.

¹⁶The subscript F anticipates that $\delta\omega$ depends on the total atomic angular momentum quantum number, F , through its dependence on the quantity \mathcal{D}/\mathcal{C} .

The final contribution in (2.25) contains recoil corrections (those terms suppressed by powers of m/M that are not simply the result of using the reduced mass in the non-relativistic problem). As described above – *c.f.* the discussion surrounding eq. (1.6) – this also divides into point-nucleus and a nuclear-structure piece, $\varepsilon_{nFj\varpi}^{\text{rec}} = \varepsilon_{nFj\varpi}^{\text{pt-rec}} + \varepsilon_{nFj\varpi}^{\text{N-rec}}$, both of which contribute at the order we work.

The next two sections compute the energy shifts $\delta\omega$ and $\varepsilon^{(1)}$ in some detail, with a view to counting systematically the number of relevant nuclear parameters. While both types of QED corrections are relevant to modern experiments, as are recoil corrections, we argue in §4 why these contribute only to predictions for the *value* of the two nuclear parameters, rather than introducing new independent parameters themselves. As such they are not conceptual obstacles to identifying nucleus-free observables.

2.3.2 Effects of the nuclear magnetic dipole

This section reviews the form of Dirac mode functions in the presence of the nuclear dipole magnetic field, with the magnetic field treated perturbatively. Discussions of this perturbation expansion are given in the literature [101–103], though for point-like nuclei (*i.e.* where the unperturbed radial-mode integration constants satisfy $\mathcal{D}/\mathcal{C} = 0$). We redo these calculations here explicitly however because nonzero \mathcal{D}/\mathcal{C} is required by finite-size nuclear effects. Because this is conceptually straightforward (though tedious) only the main features of the calculations are described here, with more details given in Appendix D.

As described below, for the present purposes we need work only to linear order in the nuclear spin-dependent effects. For the point nucleus it would therefore suffice to compute the linear-order energy shift without also needing the first-order change to the Dirac mode functions. An important change relative to the point-nucleus problem is that the determination of \mathcal{D}/\mathcal{C} to first-order also requires knowing the leading perturbative corrections to the mode functions as well.

We choose a basis of zeroth-order energy eigenstates, $|nFF_zj\varpi\rangle$, that also diagonalize total atomic angular momentum, $\mathbf{F} = \mathbf{J} + \mathbf{I}$, that sums nuclear spin \mathbf{I} with the total leptonic angular momentum \mathbf{J} . We do so by combining the Dirac-Coulomb states described above with nuclear spin states to make states that take definite values for \mathbf{F}^2 and F_z ,

$$\psi_{nFj\varpi}(r, \theta, \phi) := \langle r, \theta, \phi | nF f_z; I, j; \varpi \rangle_0 = \begin{pmatrix} \mathcal{Y}_{Ff_z}^{j,\varpi} \mathfrak{f}_{nj\varpi}(r) \\ i\mathcal{Y}_{Ff_z}^{j,-\varpi} \mathfrak{g}_{nj\varpi}(r) \end{pmatrix}, \quad (2.26)$$

where the functions $\mathcal{Y}_{Ff_z}^{j,\pm\varpi}$ are defined in eq.(D.20) to be

$$\mathcal{Y}_{F=j+\frac{\alpha}{2},f_z}^{j,\varpi} = \begin{bmatrix} \alpha \sqrt{\frac{j+\frac{1}{2}+\alpha f_z}{2j+1}} \Omega_{j,l,f_z-\frac{1}{2},\varpi} \\ \sqrt{\frac{j+\frac{1}{2}-\alpha f_z}{2j+1}} \Omega_{j,l,f_z+\frac{1}{2},\varpi} \end{bmatrix}. \quad (2.27)$$

with $\Omega_{jlj_z\varpi}$ defined in (2.17) and the nuclear 2-component spinors defined by

$$\eta_{\frac{1}{2},+\frac{1}{2}} = \begin{bmatrix} 1 \\ 0 \end{bmatrix} \quad \text{and} \quad \eta_{\frac{1}{2},-\frac{1}{2}} = \begin{bmatrix} 0 \\ 1 \end{bmatrix}. \quad (2.28)$$

To avoid confusion we use square brackets to denote spinors in nuclear-spin space and round brackets to denote the same in electron-spin space.

First-order energy shift

States with different F_z are degenerate at zeroth-order in the magnetic-moment field, necessitating the use of degenerate perturbation theory. Consequently one seeks a basis that diagonalizes the perturbing interaction $\mathcal{L}_{\text{int}} = -e\gamma^0\boldsymbol{\gamma} \cdot \mathbf{A}_{\text{nuc}}$ within the degenerate subspace of interest. For a degenerate eigenspace with fixed j the states with definite values of F and F_z provide precisely the required basis.¹⁷

The first-order energy shift for these states becomes

$$\begin{aligned} \varepsilon_{nFj\varpi}^{(1)} &= - \left(\frac{e}{4\pi} \right) \frac{\int d^3x r^{-2} \psi^\dagger \gamma^0 \boldsymbol{\gamma} \cdot (\boldsymbol{\mu} \times \hat{\mathbf{r}}) \psi}{\int d^3x \psi^\dagger \psi}, \\ &= \left(\frac{e\mu_N}{4\pi} \right) \frac{1}{\mathcal{D}} \int d^2\Omega_2 \left[(\mathcal{Y}_{F,f_z}^{j,\varpi})^\dagger \Sigma \mathcal{Y}_{F,f_z}^{j,-\varpi} - (\mathcal{Y}_{F,f_z}^{j,-\varpi})^\dagger \Sigma \mathcal{Y}_{F,f_z}^{j,\varpi} \right] \int dr \mathbf{f} \cdot \mathbf{g}, \end{aligned} \quad (2.29)$$

where

$$\Sigma := i(\mathbf{I} \times \hat{\mathbf{r}}) \cdot \boldsymbol{\sigma} \quad \text{and} \quad \mathcal{D} := \int dr r^2 (\mathbf{f}^2 + \mathbf{g}^2), \quad (2.30)$$

and we suppress the quantum numbers $\{n, F, j, \varpi\}$ on ψ and the radial functions to avoid notational clutter.

This can be further simplified using the property $\mathcal{Y}_{F,f_z}^{j,-\varpi} = -\sigma^r \mathcal{Y}_{F,f_z}^{j,\varpi}$, where $\sigma^r := \hat{\mathbf{r}} \cdot \boldsymbol{\sigma}$ is the radially-pointing Pauli matrix acting on the leptonic spin space, and a

¹⁷This is not to say that eigenstates with fixed F, F_z, j, j_z diagonalize the entire perturbing Hamiltonian, since mixing between opposite parity states that share the same values of F, F_z but with different j quantum numbers, can still occur, as has been known for some time [104, 105]. This mixing first appears in the energy at second order in the magnetic moment, and at first-order in the corrections to the wave-functions (as we describe in more detail later). Because its contributions to nuclear finite-size energy shifts are smaller than the precision to which we work in this paper, we do not calculate them in detail.

$(2I + 1) \times (2I + 1) = 2 \times 2$ unit matrix acting in nuclear-spin space is not written explicitly. Additionally, using

$$\begin{aligned} \boldsymbol{\sigma}\boldsymbol{\sigma}^r &= \{\mathbb{1}, -i\sigma^\phi, i\sigma^\theta\}, \quad \sigma^r\boldsymbol{\sigma} = \{\mathbb{1}, i\sigma^\phi, -i\sigma^\theta\}, \\ (\mathbf{I} \times \hat{\mathbf{r}}) \cdot (\boldsymbol{\sigma}\boldsymbol{\sigma}^r - \sigma^r\boldsymbol{\sigma}) &= -2i(I^\theta\sigma^\theta + I^\phi\sigma^\phi), \end{aligned} \quad (2.31)$$

the first-order mode-energy shift simplifies to

$$\varepsilon_{nFj\varpi}^{(1)} = \left(\frac{e\mu_N}{4\pi}\right) \mathfrak{K}X_F \left\{ \frac{\int dr \mathbf{f} \cdot \mathbf{g}}{\int dr r^2 (\mathbf{f}^2 + \mathbf{g}^2)} \right\}. \quad (2.32)$$

This expression evaluates the angular integration as in the literature [102]

$$2 \int d^2\Omega_2 (\mathcal{Y}_{F,f_z}^{j,\varpi})^\dagger (I^\theta\sigma^\theta + I^\phi\sigma^\phi) \mathcal{Y}_{F,f_z}^{j,\varpi} = -\mathfrak{K}X_F, \quad (2.33)$$

where the variable X_F is defined by

$$X_F := \frac{F(F+1) - j(j+1) - I(I+1)}{j(j+1)} = \begin{cases} (j+1)^{-1} & \text{if } F = j + \frac{1}{2} \\ -j^{-1} & \text{if } F = j - \frac{1}{2} \end{cases}, \quad (2.34)$$

and the final equality specializes to $I = \frac{1}{2}$.

The numerator of (2.34) arises ubiquitously in what follows because it is the eigenvalue of $2\mathbf{I} \cdot \mathbf{J} = (\mathbf{I} + \mathbf{J})^2 - \mathbf{J}^2 - \mathbf{I}^2$ evaluated in a state with definite nuclear, electronic and total atomic angular momentum quantum numbers I , j and F . In all of the energy shifts discussed below the dependence on F appears through this combination, as is ultimately required by rotational invariance.

It is convenient to extract the dimensionless combination

$$\mathfrak{s} := \frac{me\mu_N}{4\pi} \ll 1, \quad (2.35)$$

where m is (as usual) the lepton mass, because this is the small quantity that controls the size of nuclear-spin effects. Because our focus is on nuclear finite-size effects, and because current experimental precision for both atomic and muonic Hydrogen is insensitive to finite-size effects at order \mathfrak{s}^2 , for our purposes it suffices in what follows to work to linear order in \mathfrak{s} . At this order (2.32) implies the energy shift is

$$\varepsilon_{nFj\varpi}^{(1)} = \frac{\mathfrak{s}\mathfrak{K}X_F}{m} \left\{ \frac{\int dr \mathbf{f} \cdot \mathbf{g}}{\int dr r^2 (\mathbf{f}^2 + \mathbf{g}^2)} \right\} =: -4\mathfrak{s}\mathfrak{K}X_F \left(\frac{\kappa^3}{m^2}\right) \left(\frac{\mathfrak{N}}{\mathfrak{D}}\right). \quad (2.36)$$

The last equality of (2.36) evaluates the radial matrix elements inside the braces, for which both numerator and denominator naturally divide up into three parts. That is, defining

$$\int_0^\infty dr \mathbf{f} \cdot \mathbf{g} =: -\frac{\mathcal{C}^2}{2} \mathfrak{N} \quad (2.37)$$

one finds

$$\mathfrak{N} = \mathfrak{N}_{\text{pt}} + \left(\frac{\mathcal{D}}{\mathcal{L}}\right) \mathfrak{N}_1 + \left(\frac{\mathcal{D}}{\mathcal{L}}\right)^2 \mathfrak{N}_2, \quad (2.38)$$

and defining \mathfrak{D} as in (2.30),

$$\mathfrak{D} := \int dr r^2 (\mathfrak{f}^2 + \mathfrak{g}^2) = \frac{\mathcal{L}^2 m}{(2\kappa)^3} \mathfrak{D}, \quad (2.39)$$

implies it can be written

$$\mathfrak{D} = \mathfrak{D}_{\text{pt}} + \left(\frac{\mathcal{D}}{\mathcal{L}}\right) \mathfrak{D}_1 + \left(\frac{\mathcal{D}}{\mathcal{L}}\right)^2 \mathfrak{D}_2. \quad (2.40)$$

In these expressions the subscript ‘pt’ labels the contribution of a point-like nucleus (*i.e.* one for which the radial mode functions have $\mathcal{D} = 0$) and the remaining \mathcal{D} -dependent terms represent the nuclear-size dependent contributions (described in more detail below). An explicit factor of the integration constant \mathcal{L}^2 is factorized out of these definitions to emphasize how the energy shift depends only on the ratio \mathcal{D}/\mathcal{L} , and not on each of these constants separately.

The contributions to (2.38) and (2.40) are given in terms of a basic class of integrals of the form,

$$\mathcal{I}_{ij}^{(p)} := \int_0^\infty d\rho e^{-\rho} \rho^p \mathcal{M}_i \mathcal{M}_j, \quad (2.41)$$

where $i, j = 1, 2, 3, 4$, corresponding to the functions \mathcal{M}_i defined in (2.19), and p is a real number that depends on which of the \mathcal{M}_i appearing in (2.18) are relevant. For some of the choices of p encountered below the integrals $\mathcal{I}_{ij}^{(p)}$ diverges at the $\rho \rightarrow 0$ limit, a divergence that below gets renormalized into the effective coupling c_F .

Explicit formulae for \mathfrak{N} and \mathfrak{D} obtained by performing these integrals are given in eqs. (E.14) and (E.15) of Appendix §E, which state

$$\mathfrak{N}_{\text{pt}} = \left[\mathcal{I}_{11}^{(2\zeta-2)} - \left(\frac{a}{c}\right)^2 \mathcal{I}_{22}^{(2\zeta-2)} \right], \quad (2.42)$$

and

$$\begin{aligned} \mathfrak{N}_1 &= 2 \left[\mathcal{I}_{13}^{(-2)} - \left(\frac{aa'}{c^2}\right) \mathcal{I}_{24}^{(-2)} \right] \\ \mathfrak{N}_2 &= \mathcal{I}_{33}^{(-2\zeta-2)} - \left(\frac{a'}{c}\right)^2 \mathcal{I}_{44}^{(-2\zeta-2)}, \end{aligned} \quad (2.43)$$

while

$$\mathfrak{D}_{\text{pt}} = \left[2\mathcal{I}_{11}^{(2\zeta)} - \frac{4\omega}{m} \left(\frac{a}{c}\right) \mathcal{I}_{12}^{(2\zeta)} + 2 \left(\frac{a}{c}\right)^2 \mathcal{I}_{22}^{(2\zeta)} \right], \quad (2.44)$$

and

$$\begin{aligned}\mathfrak{D}_1 &= 2 \left[2\mathcal{I}_{13}^{(0)} - \frac{2\omega}{m} \left(\frac{a'}{c} \right) \mathcal{I}_{14}^{(0)} - \frac{2\omega}{m} \left(\frac{a}{c} \right) \mathcal{I}_{23}^{(0)} + 2 \left(\frac{aa'}{c^2} \right) \mathcal{I}_{24}^{(0)} \right] \\ \mathfrak{D}_2 &= 2 \left[\mathcal{I}_{33}^{(-2\zeta)} - \frac{2\omega}{m} \left(\frac{a'}{c} \right) \mathcal{I}_{34}^{(-2\zeta)} + \left(\frac{a'}{c} \right)^2 \mathcal{I}_{44}^{(-2\zeta)} \right].\end{aligned}\quad (2.45)$$

The integrals appearing in \mathfrak{N}_1 , \mathfrak{N}_2 , \mathfrak{D}_1 and \mathfrak{D}_2 are the ones that can diverge as $\rho \rightarrow 0$, and when present this divergence is regularized by restricting the integration to $\rho > \eta$ (or, more simply, using dimensional regularization) as described in Appendix E.

As a check, consider first the point-nucleus contributions, \mathfrak{N}_{pt} and \mathfrak{D}_{pt} . These involve only the confluent hypergeometric profiles, \mathcal{M}_1 and \mathcal{M}_2 and converge in the limit $\rho \rightarrow 0$, making them easy to evaluate (for details see Appendix E), leading to

$$\begin{aligned}\mathfrak{N}_{\text{pt}} &= \frac{(-2) [\Gamma(1+2\zeta)]^2 \Gamma[1-\zeta + \frac{Z\alpha\omega}{\kappa}] \left(\frac{Z\alpha m}{\kappa} \right)}{(4\zeta^2 - 1)(2\zeta)\Gamma[1+\zeta + \frac{Z\alpha\omega}{\kappa}] \left(\mathfrak{K} - \frac{Z\alpha m}{\kappa} \right)} \left(1 - \frac{2\mathfrak{K}\omega}{m} \right), \\ \mathfrak{D}_{\text{pt}} &= -\frac{4 [\Gamma(1+2\zeta)]^2 \Gamma(1-\zeta + \frac{Z\alpha\omega}{\kappa}) \left(\frac{Z\alpha m}{\kappa} \right)}{\Gamma(1+\zeta + \frac{Z\alpha\omega}{\kappa}) \left(\mathfrak{K} - \frac{Z\alpha m}{\kappa} \right)}.\end{aligned}\quad (2.46)$$

Using these, the energy shift for a point-like spin-half nucleus obtained from (2.36) by using (2.46) and $\mathcal{D} = 0$ in (2.38) and (2.40) is

$$\begin{aligned}\varepsilon_{nFj\varpi}^{\text{hfs}} &= -\mathfrak{s}\mathfrak{K}X_F \left(\frac{\kappa^3}{m^2} \right) \frac{(1 - 2\mathfrak{K}\omega/m)}{\zeta(4\zeta^2 - 1)} \\ &= -\mathfrak{K}X_F \frac{g_p m^2 (Z\alpha)^4}{2M} \left(\frac{m_r}{m} \right)^3 \left[\frac{1 - 2\mathfrak{K}\sqrt{1 - (Z\alpha)^2/\mathcal{N}^2}}{\mathcal{N}^3 \zeta(4\zeta^2 - 1)} \right] \quad (\text{Hydrogen}),\end{aligned}\quad (2.47)$$

where the second line specializes to Hydrogen and evaluates κ using $\kappa = m_r Z\alpha/\mathcal{N}$ with reduced mass $m_r = mM/(m+M)$ (where M is the nuclear mass) and \mathcal{N} as defined in (2.24) with \mathfrak{K} given in (2.21). Also used are the definition (2.35) of \mathfrak{s} and $\mu_p = g_p(Ze/2M)$ with g_p the proton's g -factor. When evaluated to compute the energy difference between the $nS_{j=1/2}^{F=1}$ and $nS_{j=1/2}^{F=0}$ states in Hydrogen, this expression agrees with standard results for relativistic hyperfine splitting [102, 103, 106].

So far so good, but what about non-point-like nuclei? To capture the finite-size effects we must use the modified near-nucleus boundary condition for Ψ implied by the nuclear effective interactions in S_p (which imply $\mathcal{D}/\mathcal{C} \neq 0$). This also requires dealing with the divergent integrals that appear in expressions (2.43) and (2.45) for the

magnetic-moment dependent energy shift, whose explicit form becomes

$$\begin{aligned}\varepsilon_{nFj\varpi}^{(1)} &= \varepsilon_{nFj\varpi}^{\text{hfs}} \left[\frac{1 + (\mathcal{D}/\mathcal{C})(\mathfrak{N}_1/\mathfrak{N}_{\text{pt}}) + (\mathcal{D}/\mathcal{C})^2(\mathfrak{N}_2/\mathfrak{N}_{\text{pt}})}{1 + (\mathcal{D}/\mathcal{C})(\mathfrak{D}_1/\mathfrak{D}_{\text{pt}}) + (\mathcal{D}/\mathcal{C})^2(\mathfrak{D}_2/\mathfrak{D}_{\text{pt}})} \right] \\ &\simeq -\mathfrak{s}\mathfrak{K}X_F \left(\frac{\kappa^3}{m^2} \right) \frac{(1 - 2\mathfrak{K}\omega/m)}{\zeta(4\zeta^2 - 1)} \left[1 + C_\eta - \frac{\mathfrak{c}}{n} + \dots \right],\end{aligned}\quad (2.48)$$

and in the second line \mathfrak{c} and C_η are n -independent constants. Of these \mathfrak{c} is defined below in (3.9) and so contains the various nuclear effective couplings. Unlike \mathfrak{c} , the constant C_η depends on the regularization parameter, η , associated with the near-nucleus divergences described above. In practice the detailed form of C_η does not matter in what follows because it gets absorbed into the nuclear effective coupling c_F .

What makes possible the absorption of C_η into a counterterm is the fact that neither \mathfrak{c} nor C_η depend on the principal quantum number and so the n -dependence in (2.48) is either explicit or contained within the standard expressions (2.23) and (2.24) for κ and ω . As shown in detail in §3, it is only because C_η does not come together with additional n dependence that its contribution to the energy is proportional to $1/n^3$ and so can be absorbed into a counterterm like c_F for an interaction localized at the nucleus' position (whose contribution to the energy is proportional to $|\psi(0)|^2$ and so is also $\propto 1/n^3$).

The same is not true of the term \mathfrak{c}/n in (2.48), whose n -dependence is a genuine prediction. As argued below (see also Appendix E) matching to nuclear properties implies $\mathfrak{c} \sim \mathcal{O}[(mRZ\alpha)^2]$ and so given that $\varepsilon^{\text{hfs}} \sim \mathcal{O}[(Z\alpha)^4(m^2/M)] \sim \mathcal{O}[(Z\alpha)^4m^2R]$ – with $M \sim 1/R$ being the nuclear mass, see *e.g.* (E.40) – the constant \mathfrak{c} turns out to contribute to the energy at order $m(Z\alpha)^3(mRZ\alpha)^3$. For electrons this is smaller than the $\mathcal{O}[m(Z\alpha)^4(mRZ\alpha)^2]$ and $\mathcal{O}[m(Z\alpha)^2(mRZ\alpha)^3]$ contributions computed here.¹⁸

First-order mode-function correction

As described above, eq. (2.48) is not the whole story. Previously we have mentioned – *c.f.* (2.25) – that at the accuracy of interest here finite nuclear size contributes to electron energies in two different ways: through the contributions of \mathcal{D}/\mathcal{C} to¹⁹ $\delta\omega_{nFj\varpi}$ and to $\varepsilon_{nFj\varpi}^{(1)}$.

In both of these contributions nuclear properties enter through the values implied for \mathcal{D}/\mathcal{C} by the near-nucleus boundary conditions – such as (2.14). Since it turns

¹⁸This also makes this contribution competitive with the $\mathcal{O}[m(Z\alpha)^2(mRZ\alpha)^4]$ contributions that are also not computed here, but which can be important for muonic Hydrogen.

¹⁹Because we compute by perturbing using zeroth-order Coulomb bound-state wave-functions, each of which satisfies (2.22), the new eigenstates found by perturbing with \mathbf{A}_{nuc} are automatically normalizable assuming only that (2.22) is satisfied.

out that calculating the implications of (2.14) for \mathcal{D}/\mathcal{C} requires knowing the first-order correction to the radial wave-functions, \mathbf{f} and \mathbf{g} , due to the magnetic moment interaction, we now pause to compute this.

Using standard first-order Rayleigh-Schrödinger perturbation theory, we find the following leading correction to the relativistic Dirac state due to the nuclear magnetic field:

$$|nFF_zj\varpi\rangle_1 = \sum_{\tilde{n} \neq n} \frac{\mathcal{C}_{\tilde{n}nFF_zj\varpi}}{E_{nFj\varpi}^{(0)} - E_{\tilde{n}Fj\varpi}^{(0)}} |\tilde{n}FF_zj\varpi\rangle_0 + (\tilde{j} \text{ terms}), \quad (2.49)$$

where ‘(\tilde{j} terms)’ denote contributions coming from summing states with $\tilde{j} \neq j$; terms that can be neglected in what follows as explained in Appendix E. The displayed sum is only over principal quantum numbers that differ from that of the state being perturbed, and the coefficients are

$$\begin{aligned} \mathcal{C}_{\tilde{n}nFF_zj\varpi} &= - \left(\frac{e}{4\pi\tilde{\mathcal{D}}} \right) \int d^3x r^{-2} \tilde{\psi}_{\tilde{n}Fj\tilde{\varpi}}^\dagger \gamma^0 \boldsymbol{\gamma} \cdot (\boldsymbol{\mu} \times \hat{\mathbf{r}}) \psi_{nFj\varpi}, \\ &= - \left(\frac{\mathbf{s}}{m\tilde{\mathcal{D}}} \right) \int d\Omega_2 \left(\mathcal{Y}_{F,fz}^{\tilde{j}\tilde{\varpi}} \right)^\dagger (I^\theta \sigma^\theta + I^\phi \sigma^\phi) \mathcal{Y}_{F,fz}^{j\varpi} \int dr \left(\tilde{\mathbf{f}} \mathbf{g} + \tilde{\mathbf{g}} \mathbf{f} \right), \end{aligned} \quad (2.50)$$

with

$$\tilde{\mathcal{D}} := \int dr r^2 \left(\tilde{\mathbf{f}}^2 + \tilde{\mathbf{g}}^2 \right) = \frac{\tilde{\mathcal{C}}^2 m}{(2\tilde{\kappa})^3} \tilde{\mathcal{D}}. \quad (2.51)$$

defined in the same way as is \mathcal{D} – in eq. (2.30) – but evaluated for the state $\tilde{\psi}$ (for more detail see Appendix D).

Notice that the integrals $\tilde{\mathcal{D}}_{\text{pt}}$, $\tilde{\mathcal{D}}_1$ and $\tilde{\mathcal{D}}_2$ appearing in $\tilde{\mathcal{D}}$, are defined in terms of $\tilde{\mathcal{D}}$ using (2.39) and (2.40) – *i.e.* with $\mathcal{C} \rightarrow \tilde{\mathcal{C}}$, $\kappa \rightarrow \tilde{\kappa}$, $n \rightarrow \tilde{n}$ and so on – the only new quantity here is the radial integral in the numerator. Defining

$$\begin{aligned} \mathfrak{N}^s &:= - \frac{1}{\tilde{\mathcal{C}}\tilde{\mathcal{C}}} \int_0^\infty dr \left(\tilde{\mathbf{f}} \mathbf{g} + \tilde{\mathbf{g}} \mathbf{f} \right) \\ &= m(2\tilde{\kappa})^{\tilde{\zeta}-1} (2\kappa)^{\zeta-1} (\tilde{\kappa} + \kappa)^{1-\tilde{\zeta}-\zeta} \\ &\quad \times \left\{ \mathfrak{N}_{\text{pt}}^s + \left(\frac{\mathcal{D}}{\tilde{\mathcal{C}}} \right) \mathfrak{N}_1^s + \left(\frac{\tilde{\mathcal{D}}}{\tilde{\mathcal{C}}} \right) \tilde{\mathfrak{N}}_1^s + \left(\frac{\tilde{\mathcal{D}}\mathcal{D}}{\tilde{\mathcal{C}}\tilde{\mathcal{C}}} \right) \mathfrak{N}_2^s \right\}, \end{aligned} \quad (2.52)$$

and evaluating the angular integral for $(\tilde{j}, \tilde{\varpi}) = (j, \varpi)$ the first-order state correction given in (2.49) becomes

$$\begin{aligned} |nFF_zj\varpi\rangle_1 &= - \sum_{\tilde{n} \neq n} \frac{\mathbf{s}(2\tilde{\kappa})^3 \mathfrak{K} X_F}{2m^2 \left(E_{nFj\varpi}^{(0)} - E_{\tilde{n}Fj\varpi}^{(0)} \right)} \left(\frac{\tilde{\mathcal{C}} \mathfrak{N}^s}{\tilde{\mathcal{C}} \tilde{\mathcal{D}}} \right) |\tilde{n}FF_zj\varpi\rangle_0 + (\tilde{j} \text{ terms}) \\ &=: \mathbf{s} X_F \widehat{\sum}_{\tilde{n}} |\tilde{n}FF_zj\varpi\rangle_0 + (\tilde{j} \text{ terms}), \end{aligned} \quad (2.53)$$

where the last equality defines the $\widehat{\Sigma}$ operator, which is therefore given by

$$\widehat{\Sigma}_{\tilde{n}} |\tilde{n} F F_{zj\varpi}\rangle_0 := - \sum_{\tilde{n} \neq n} \frac{4\tilde{\kappa}^3 \mathfrak{R}(4\tilde{\kappa}\kappa)^{\zeta-1} (\tilde{\kappa} + \kappa)^{1-2\zeta}}{m \left(E_{nFj\varpi}^{(0)} - E_{\tilde{n}Fj\varpi}^{(0)} \right)} \left(\frac{\mathcal{C} \mathfrak{N}_{\text{pt}}^s}{\mathcal{C} \tilde{\mathfrak{D}}_{\text{pt}}} \right) \quad (2.54)$$

$$\times \left\{ \frac{1 + \left(\frac{\mathcal{D}}{\mathcal{C}} \right) \mathfrak{N}_1^s / \mathfrak{N}_{\text{pt}}^s + \left(\frac{\tilde{\mathcal{D}}}{\mathcal{C}} \right) \tilde{\mathfrak{N}}_1^s / \mathfrak{N}_{\text{pt}}^s + \left(\frac{\tilde{\mathcal{D}} \mathcal{D}}{\mathcal{C}^2} \right) \mathfrak{N}_2^s / \mathfrak{N}_{\text{pt}}^s}{1 + \left(\frac{\tilde{\mathcal{D}}}{\mathcal{C}} \right) \tilde{\mathfrak{D}}_1 / \tilde{\mathfrak{D}}_{\text{pt}} + \left(\frac{\tilde{\mathcal{D}}}{\mathcal{C}} \right)^2 \tilde{\mathfrak{D}}_2 / \tilde{\mathfrak{D}}_{\text{pt}}} \right\} |\tilde{n} F F_{zj\varpi}\rangle_0 .$$

The integrals $\mathfrak{N}_{\text{pt}}^s$, \mathfrak{N}_1^s , $\tilde{\mathfrak{N}}_1^s$ and \mathfrak{N}_2^s appearing here are given explicitly in terms of integrals similar to $\mathcal{I}_{ij}^{(p)}$ in Appendix E, in eqs. (E.87) and (E.89) and subsequent paragraphs.

The solution to the leptonic equations of motion correct to first order in \mathfrak{s} then is,

$$\psi_{nFj\varpi} = \left[\begin{array}{l} \mathcal{Y}_{F,f_z}^{j,\varpi} \left(\mathfrak{f}_{nj\varpi}^{(0)}(r) + \mathfrak{s} X_F \mathfrak{f}_{nj\varpi}^{(1)}(r) + \dots \right) \\ i \mathcal{Y}_{F,f_z}^{j,-\varpi} \left(\mathfrak{g}_{nj\varpi}^{(0)}(r) + \mathfrak{s} X_F \mathfrak{g}_{nj\varpi}^{(1)}(r) + \dots \right) \end{array} \right] \quad (2.55)$$

with the ellipses representing terms of order $\mathcal{O}(\mathfrak{s}^2)$ or higher and the first-order function corrections are given by

$$\mathfrak{f}_{nj\varpi}^{(1)}(r) := \widehat{\Sigma}_{\tilde{n}} \mathfrak{f}_{nj\varpi}^{(0)}(r) \quad \text{and} \quad \mathfrak{g}_{nj\varpi}^{(1)}(r) := \widehat{\Sigma}_{\tilde{n}} \mathfrak{g}_{nj\varpi}^{(0)}(r). \quad (2.56)$$

This concludes our perturbative calculations of the lepton modes to linear order in \mathfrak{s} .

2.4 Near-nucleus fermion boundary conditions

We next determine the values of \mathcal{D}/\mathcal{C} required by the fermionic boundary conditions, obtained by a more careful treatment of the delta-function terms in the fermionic field equation (2.12). This section quotes the main results, with more details given in Appendix B. Because it happens that the dominant effects arise from boundary conditions for $j = \frac{1}{2}$ modes, we focus here on these. The relevant near-nucleus boundary condition – applied at distance $r = \epsilon$ from the nucleus – is given in (2.14), repeated here for convenience

$$0 = \int d^2\Omega_2 \epsilon^2 \left[\gamma^r + \hat{c}_s - i\gamma^0 \hat{c}_v + \hat{c}_F \mathbf{I} \cdot \boldsymbol{\Sigma} \right] \psi_{nFj\varpi}(\epsilon), \quad (2.57)$$

where (as before) $\hat{c}_i = c_i / (4\pi\epsilon^2)$.

As applied to the positive parity $j = \frac{1}{2}$ state, performing the angular integration implies the boundary condition for the radial function becomes

$$\hat{c}_s - \hat{c}_v + \mathcal{Z}_F \hat{c}_F = \frac{\mathfrak{g}_{n\frac{1}{2}+}(\epsilon)}{\mathfrak{f}_{n\frac{1}{2}+}(\epsilon)}, \quad (2.58)$$

where $\mathcal{Z}_F := \frac{1}{2} [F(F+1) - \frac{3}{2}] = \mathcal{Z}_{F+}$ where $\mathcal{Z}_{F\varpi}$ is defined for $j = \frac{1}{2}$ states as (see Appendix B)

$$\mathcal{Z}_{F\varpi} := \frac{2\varpi + 1}{6} \left[F(F+1) - I(I+1) - \frac{3}{4} \right] = \frac{2\varpi + 1}{8} X_F, \quad (2.59)$$

where the last equality uses the definition (2.34) of X_F . Repeating the same exercise for the negative parity, $j = \frac{1}{2}$ state similarly gives (see Appendix B)

$$\hat{c}_s + \hat{c}_v + \mathcal{Z}_F \hat{c}_F = \frac{\mathfrak{f}_{n\frac{1}{2}-}(\epsilon)}{\mathfrak{g}_{n\frac{1}{2}-}(\epsilon)}. \quad (2.60)$$

As elaborated in Appendix B, both eqs. (2.58) and (2.60) use a compact notation that suppresses an implicit dependence of the couplings on both F and ϖ (see *e.g.* eq. (2.61)).

As usual, there are two equivalent ways to read these last two equations. The simplest way is to evaluate the right-hand side of these equations using the solutions (2.18) to the radial equation, and regard them as being solved for \mathcal{D}/\mathcal{C} as a function of the \hat{c}_i . This shows explicitly how the integration constants are determined by the effective nuclear couplings. Because physical quantities (like leptonic energy levels) can be expressed as functions of \mathcal{D}/\mathcal{C} they also acquire a dependence on the \hat{c}_i .

The other way to interpret these equations is as renormalization-group equations that define the running of the renormalized couplings, \hat{c}_i . That is, if the value of ϵ is to be changed without modifying physical quantities (like electron energy levels), then the explicit ϵ -dependence visible in (2.58) and (2.60) must cancel against an ϵ -dependence that is implicit in the couplings \hat{c}_i [64, 70–72].

The remainder of this section focuses on the first of these two points of view, and we return to the second approach in §3 below.

2.4.1 Solution for \mathcal{D}/\mathcal{C}

The goal is to solve eqs. (2.58) and (2.60) for the integration constant \mathcal{D}/\mathcal{C} , to linear order in \mathfrak{s} . Because the explicitly calculable terms of eqs. (2.58) and (2.60) depend on nuclear spin only through the spin-dependence of X_F this suggests that the same should also be true for the couplings $\hat{c}_{s,v}$ and integration constants \mathcal{D}/\mathcal{C} at $\mathcal{O}(\mathfrak{s})$. This leads to the ansatz

$$\hat{c}_{s,v} = \hat{c}_{s,v}^{(0)} + \mathfrak{s} X_F \hat{c}_{s,v}^{(1)} + \mathcal{O}(\mathfrak{s}^2), \quad (2.61)$$

where the first terms are the couplings found in [64] for spinless nuclei that are independent of the total atomic angular momentum, F . The second terms are the first-order corrections whose F -dependence is guaranteed by rotation invariance to be proportional to $[F(F+1) - j(j+1) - I(I+1)]$. The integration constants are then solved

perturbatively in \mathfrak{s} , using

$$\left(\frac{\mathcal{D}}{\mathcal{C}}\right) = \left(\frac{\mathcal{D}}{\mathcal{C}}\right)^{(0)} + \mathfrak{s}X_F \left(\frac{\mathcal{D}}{\mathcal{C}}\right)^{(1)} + \dots, \quad (2.62)$$

where the F -independent part of eqs. (2.58) and (2.60) determine $(\mathcal{D}/\mathcal{C})^{(0)}$ and $(\mathcal{D}/\mathcal{C})^{(1)}$ is fixed by their X_F -dependent terms.

With this in mind we also expand the right-hand side of these boundary conditions to linear order in \mathfrak{s} , using the state-correction result from first-order perturbation theory in (2.55), to write it as,

$$\frac{\mathfrak{g}_\varpi}{\mathfrak{f}_\varpi} = \frac{\mathfrak{g}_\varpi^{(0)} + \mathfrak{s}X_F \mathfrak{g}_\varpi^{(1)} + \dots}{\mathfrak{f}_\varpi^{(0)} + \mathfrak{s}X_F \mathfrak{f}_\varpi^{(1)} + \dots} \simeq \frac{\mathfrak{g}_\varpi^{(0)}}{\mathfrak{f}_\varpi^{(0)}} \left[1 + \mathfrak{s}X_F \left(\frac{\mathfrak{g}_\varpi^{(1)}}{\mathfrak{g}_\varpi^{(0)}} - \frac{\mathfrak{f}_\varpi^{(1)}}{\mathfrak{f}_\varpi^{(0)}} \right) + \mathcal{O}(\mathfrak{s}^2) \right], \quad (2.63)$$

where $\varpi = \pm$ is the electron state's parity, $\mathfrak{g}_\varpi^{(0)}, \mathfrak{f}_\varpi^{(0)}$ are given by (2.18) and $\mathfrak{g}_\varpi^{(1)}, \mathfrak{f}_\varpi^{(1)}$ are given by (2.56). Because the functions $\mathfrak{g}_\varpi^{(0)}, \mathfrak{f}_\varpi^{(0)}$ and $\mathfrak{g}_\varpi^{(1)}, \mathfrak{f}_\varpi^{(1)}$ are themselves functions of the ratio $\mathcal{D}_\varpi/\mathcal{C}_\varpi$, which itself can depend on nuclear spin – *c.f.* (2.62) – to find all terms that appear at $\mathcal{O}(\mathfrak{s})$ requires using (2.62) in (2.63), expanding in powers of \mathfrak{s} and grouping terms.

What is important when doing so is this: because all of the $\mathcal{O}(\mathfrak{s})$ terms in (2.63) are proportional to X_F both sides of eqs. (2.58) and (2.60) share the same dependence on nuclear spin out to linear order in \mathfrak{s} . This is no accident because, to linear order, rotation invariance implies the nuclear spin appears only through the combination $\mathbf{I} \cdot \mathbf{J}$, whose matrix elements give the spin-dependence in both X_F and $\mathcal{Z}_{F\varpi} \propto X_F$. This shows how $(\mathcal{D}/\mathcal{C})^{(0)}$ is determined in terms of the coefficients $\hat{c}_s^{(0)}$ and $\hat{c}_v^{(0)}$ and by $\mathfrak{f}_\varpi^{(0)}/\mathfrak{g}_\varpi^{(0)} -$ as in [64]. Similarly $(\mathcal{D}/\mathcal{C})^{(1)}$ is given in terms of the $\mathcal{O}(\mathfrak{s})$ parts of $\hat{c}_F, \hat{c}_s^{(1)}$ and $\hat{c}_v^{(1)}$ together with $(\mathfrak{f}_\varpi^{(1)}/\mathfrak{f}_\varpi^{(0)}) - (\mathfrak{g}_\varpi^{(1)}/\mathfrak{g}_\varpi^{(0)})$ and $\mathfrak{f}_\varpi^{(0)}/\mathfrak{g}_\varpi^{(0)}$.

The details of this calculation can be found at the end of Appendix F and here we only quote the results, separately for each parity choice $\varpi = \pm$.

Positive parity states

Using the small- r asymptotic form for the radial solutions of eqs. (2.18) in the parity-even boundary condition (2.58) then gives, at zeroth order in \mathfrak{s} ,

$$\hat{c}_s^{(0)} - \hat{c}_v^{(0)} = -\chi \left[\frac{(c+a) + (c+a') (\mathcal{D}_+/\mathcal{C}_+)^{(0)} (2\kappa\epsilon)^{-2\zeta}}{(c-a) + (c-a') (\mathcal{D}_+/\mathcal{C}_+)^{(0)} (2\kappa\epsilon)^{-2\zeta}} \right], \quad (2.64)$$

where the parameters on the right-hand side are given in eqs. (2.20) and

$$\chi := \sqrt{\frac{m-\omega}{m+\omega}}. \quad (2.65)$$

Inverting (2.64) then gives the integration constants in terms of $\hat{c}_s^{(0)} - \hat{c}_v^{(0)}$:

$$\left(\frac{\mathcal{D}_+}{\mathcal{E}_+}\right)^{(0)} = - \left[\frac{\left(\hat{c}_s^{(0)} - \hat{c}_v^{(0)}\right) (c - a) + \chi(c + a)}{\left(\hat{c}_s^{(0)} - \hat{c}_v^{(0)}\right) (c - a') + \chi(c + a')} \right] (2\kappa\epsilon)^{2\zeta}, \quad (2.66)$$

as is also found in [64] for spinless nuclei.

Next, consider the $\mathcal{O}(\mathfrak{s})$ terms on both sides of the boundary condition (2.58) which reads – using $\mathcal{Z}_F = \mathcal{Z}_{F+} = \frac{3}{8} X_F$,

$$\begin{aligned} \mathfrak{s} \left(\hat{c}_s^{(1)} - \hat{c}_v^{(1)} \right) + \frac{3}{8} \hat{c}_F & \quad (2.67) \\ & = \mathfrak{s} \left\{ \frac{(-2)\chi c (a' - a) (2\kappa\epsilon)^{-2\zeta}}{\left[(c - a) + (c - a') \left(\frac{\mathcal{D}_+}{\mathcal{E}_+}\right)^{(0)} (2\kappa\epsilon)^{-2\zeta} \right]^2} \left(\frac{\mathcal{D}_+}{\mathcal{E}_+}\right)^{(1)} + \Lambda_+ \right\}, \end{aligned}$$

where Λ_+ is given by

$$\begin{aligned} \Lambda_+ & = -\sqrt{\frac{m + \tilde{\omega}}{m + \omega}} \sum_{\tilde{n}} \left[\frac{\tilde{\mathcal{E}}_+(2\tilde{\kappa}\epsilon)^{\zeta-1} c}{\tilde{\mathcal{E}}_+(2\tilde{\kappa}\epsilon)^{\zeta-1} \tilde{c}} \right] \left[\frac{(\tilde{c} - \tilde{a}) + (\tilde{c} - \tilde{a}') \left(\frac{\tilde{\mathcal{D}}_+}{\tilde{\mathcal{E}}_+}\right)^{(0)} (2\tilde{\kappa}\epsilon)^{-2\zeta}}{(c - a) + (c - a') \left(\frac{\mathcal{D}_+}{\mathcal{E}_+}\right)^{(0)} (2\kappa\epsilon)^{-2\zeta}} \right] \\ & \times \left\{ \tilde{\chi} \left[\frac{(\tilde{c} + \tilde{a}) + (\tilde{c} + \tilde{a}') \left(\frac{\tilde{\mathcal{D}}_+}{\tilde{\mathcal{E}}_+}\right)^{(0)} (2\tilde{\kappa}\epsilon)^{-2\zeta}}{(\tilde{c} - \tilde{a}) + (\tilde{c} - \tilde{a}') \left(\frac{\tilde{\mathcal{D}}_+}{\tilde{\mathcal{E}}_+}\right)^{(0)} (2\tilde{\kappa}\epsilon)^{-2\zeta}} \right] \right. \\ & \quad \left. - \chi \left[\frac{(c + a) + (c + a') \left(\frac{\mathcal{D}_+}{\mathcal{E}_+}\right)^{(0)} (2\kappa\epsilon)^{-2\zeta}}{(c - a) + (c - a') \left(\frac{\mathcal{D}_+}{\mathcal{E}_+}\right)^{(0)} (2\kappa\epsilon)^{-2\zeta}} \right] \right\}, \quad (2.68) \end{aligned}$$

and comes from evaluating the terms involving $\mathfrak{g}_+^{(1)}$ and $\mathfrak{f}_+^{(1)}$ in the square bracket of (2.63). In particular, Λ_+ does not depend on $(\mathcal{D}_+/\mathcal{E}_+)^{(1)}$.

As shown in detail in the paragraph surrounding (3.9) below, the two quantities in the final braces in (2.68) cancel one another – at least to leading order in $(Z\alpha)^2$ – which in turn ensures that Λ_+ vanishes to the order we require. This simplifies enormously the above boundary condition, whose solution for $\mathcal{D}_+/\mathcal{E}_+$ becomes

$$\begin{aligned} \mathfrak{s} \left(\frac{\mathcal{D}_+}{\mathcal{E}_+}\right)^{(1)} & = - \frac{\left[\mathfrak{s} \left(\hat{c}_s^{(1)} - \hat{c}_v^{(1)} \right) + \frac{3}{8} \hat{c}_F \right]}{4\chi c (a' - a)} \\ & \times \left[(c - a) + (c - a') \left(\frac{\mathcal{D}_+}{\mathcal{E}_+}\right)^{(0)} (2\kappa\epsilon)^{-2\zeta} \right]^2 (2\kappa\epsilon)^{2\zeta}. \quad (2.69) \end{aligned}$$

Eqs. (2.66) and (2.69) solve the problem of obtaining the integration constant ratio \mathcal{D}/\mathcal{C} as functions of the effective couplings, c_s , c_v and c_F , for positive-parity $j = \frac{1}{2}$ states. The next step, in principle, is to use these expressions in formulae like (2.36) and (C.10) for atomic energy shifts to predict how these are influenced by finite nuclear size. Before taking this step we first repeat the above exercise for parity-odd $j = \frac{1}{2}$ states.

Negative parity states

Returning now to the boundary condition (2.60), repeating the same steps as before (*i.e.* expanding the radial functions and integration constants to linear order in \mathfrak{s}) leads to two separate relations that determine $(\mathcal{D}_-/\mathcal{C}_-)^{(0)}$ and $(\mathcal{D}_-/\mathcal{C}_-)^{(1)}$ in terms of \hat{c}_s , \hat{c}_v and \hat{c}_F . The parity-odd counterpart to (2.64) is given by

$$\hat{c}_s^{(0)} + \hat{c}_v^{(0)} = -\frac{1}{\chi} \left[\frac{(c-a) + (c-a') (\mathcal{D}_-/\mathcal{C}_-)^{(0)} (2\kappa\epsilon)^{-2\zeta}}{(c+a) + (c+a') (\mathcal{D}_-/\mathcal{C}_-)^{(0)} (2\kappa\epsilon)^{-2\zeta}} \right], \quad (2.70)$$

which, when solved for the integration constants, gives

$$\left(\frac{\mathcal{D}_-}{\mathcal{C}_-} \right)^{(0)} = - \left[\frac{\chi (\hat{c}_s^{(0)} + \hat{c}_v^{(0)}) (c+a) + (c-a)}{\chi (\hat{c}_s^{(0)} + \hat{c}_v^{(0)}) (c+a') + (c-a')} \right] (2\kappa\epsilon)^{2\zeta}. \quad (2.71)$$

as the counterpart to eq. (2.66).

Similarly, the $\mathcal{O}(\mathfrak{s})$ terms of the parity-odd boundary condition (2.60) are, again using $\mathcal{Z}_F = \frac{3}{8} X_F$,

$$\mathfrak{s} (\hat{c}_s^{(1)} + \hat{c}_v^{(1)}) + \frac{3\hat{c}_F}{8} = \mathfrak{s} \left\{ \frac{2\chi^{-1}c(a'-a)(2\kappa\epsilon)^{-2\zeta}}{\left[(c+a) + (c+a') (\mathcal{D}_-/\mathcal{C}_-)^{(0)} (2\kappa\epsilon)^{-2\zeta} \right]^2} \left(\frac{\mathcal{D}_-}{\mathcal{C}_-} \right)^{(1)} + \Lambda_- \right\}, \quad (2.72)$$

with Λ_- given by

$$\begin{aligned} \Lambda_- = & -\sqrt{\frac{m-\tilde{\omega}}{m-\omega}} \sum_{\tilde{n}} \left[\frac{\tilde{\mathcal{C}}_- e^{-\tilde{\kappa}\epsilon} (2\tilde{\kappa}\epsilon)^{\zeta-1} c}{\tilde{\mathcal{C}}_- e^{-\kappa\epsilon} (2\kappa\epsilon)^{\zeta-1} \tilde{c}} \right] \left[\frac{(\tilde{c}+\tilde{a}) + (\tilde{c}+\tilde{a}') (\tilde{\mathcal{D}}_-/\tilde{\mathcal{C}}_-)^{(0)} (2\tilde{\kappa}\epsilon)^{-2\zeta}}{(c+a) + (c+a') (\mathcal{D}_-/\mathcal{C}_-)^{(0)} (2\kappa\epsilon)^{-2\zeta}} \right] \\ & \times \left\{ \frac{1}{\tilde{\chi}} \left[\frac{(\tilde{c}-\tilde{a}) + (\tilde{c}-\tilde{a}') (\tilde{\mathcal{D}}_-/\tilde{\mathcal{C}}_-)^{(0)} (2\tilde{\kappa}\epsilon)^{-2\zeta}}{(\tilde{c}+\tilde{a}) + (\tilde{c}+\tilde{a}') (\tilde{\mathcal{D}}_-/\tilde{\mathcal{C}}_-)^{(0)} (2\tilde{\kappa}\epsilon)^{-2\zeta}} \right] \right. \\ & \left. - \frac{1}{\chi} \left[\frac{(c-a) + (c-a') (\mathcal{D}_-/\mathcal{C}_-)^{(0)} (2\kappa\epsilon)^{-2\zeta}}{(c+a) + (c+a') (\mathcal{D}_-/\mathcal{C}_-)^{(0)} (2\kappa\epsilon)^{-2\zeta}} \right] \right\}, \quad (2.73) \end{aligned}$$

coming from evaluating the terms involving $\mathbf{g}_-^{(1)}$ and $\mathbf{f}_-^{(1)}$ in the square bracket of (2.63). As before, Λ_- does not depend on $(\mathcal{D}_-/\mathcal{C}_-)^{(1)}$ and, as argued in the discussion surrounding (3.13), the two terms in the final braces of (2.73) cancel to leading order, ensuring that Λ_- vanishes to the order we require. This allows the solution

$$\mathfrak{s} \left(\frac{\mathcal{D}_-}{\mathcal{C}_-} \right)^{(1)} = \frac{\chi \left[\mathfrak{s} \left(\hat{c}_s^{(1)} + \hat{c}_v^{(1)} \right) + \frac{3}{8} \hat{c}_F \right]}{2c(a' - a)} \times \left[(c + a) + (c + a') \left(\frac{\mathcal{D}_-}{\mathcal{C}_-} \right)^{(0)} (2\kappa\epsilon)^{-2\zeta} \right]^2 (2\kappa\epsilon)^{2\zeta}. \quad (2.74)$$

3 Renormalization

So far so good. But as things stand it looks like all predictions of nucleus-induced shifts on atomic energy levels depend explicitly on the arbitrary parameters ϵ (the position where the boundary conditions (2.58) and (2.60) are imposed) and η (the regularization scale associated with the divergent integrals \mathfrak{N}_1 , \mathfrak{N}_2 , \mathfrak{D}_1 and \mathfrak{D}_2 – introduced *e.g.* below eq. (E.42)). We now address how sensible predictions are possible despite the presence of these arbitrary scales.

Physical predictions are possible because all of the dependence on these arbitrary scales can be renormalized into the definitions of effective couplings like c_s , c_v and c_F . That is to say: what counts are physical predictions that relate observables to other observables, and effective couplings just play a role in intermediate steps when making these relations. For instance, in practice measurements of some observables are usually used to determine the values of the effective couplings, and any real physical content only emerges once these values are used to infer the numerical size of other observables (that can themselves be measured). What is important is that all of the arbitrary dependence on ϵ and η cancels out once observables are related to observables. In detail, this cancellation happens because any explicit dependence on ϵ and η cancels with an implicit dependence that is hidden in the values that are used for $\hat{c}_s(\epsilon, \eta)$, $\hat{c}_v(\epsilon, \eta)$ and $\hat{c}_F(\epsilon, \eta)$. If ϵ and η were varied then the inferred values these couplings acquire on comparison to measurements also change, and they do so (by construction) in precisely the way that is required to keep physical observables fixed.

3.1 Cancellation of ϵ -dependence

To see how this works, start first with the cancellation of ϵ -dependence. We do so first for those nuclear finite-size contributions that do not depend on nuclear spin and then repeat the exercise at linear order in nuclear spin.

3.1.1 Contributions independent of nuclear spin

At one level the dependence on ϵ that is required of the couplings $\hat{c}_s^{(0)}$ and $\hat{c}_v^{(0)}$ is simply given by the boundary condition itself: eq. (2.58), provided this is interpreted as giving the left-hand side as a function of ϵ , with the parameter $(\mathcal{D}_+/\mathcal{C}_+)^{(0)}$ held fixed. In this point of view most of the information contained in (2.58) specifies the class of trajectories along which any couplings like $\hat{c}_s^{(0)}$ and $\hat{c}_v^{(0)}$ must evolve in order to keep observables independent of ϵ . The constant $(\mathcal{D}_+/\mathcal{C}_+)^{(0)}$ is then regarded as specifying precisely which trajectory within this class the couplings of a particular nucleus lie.

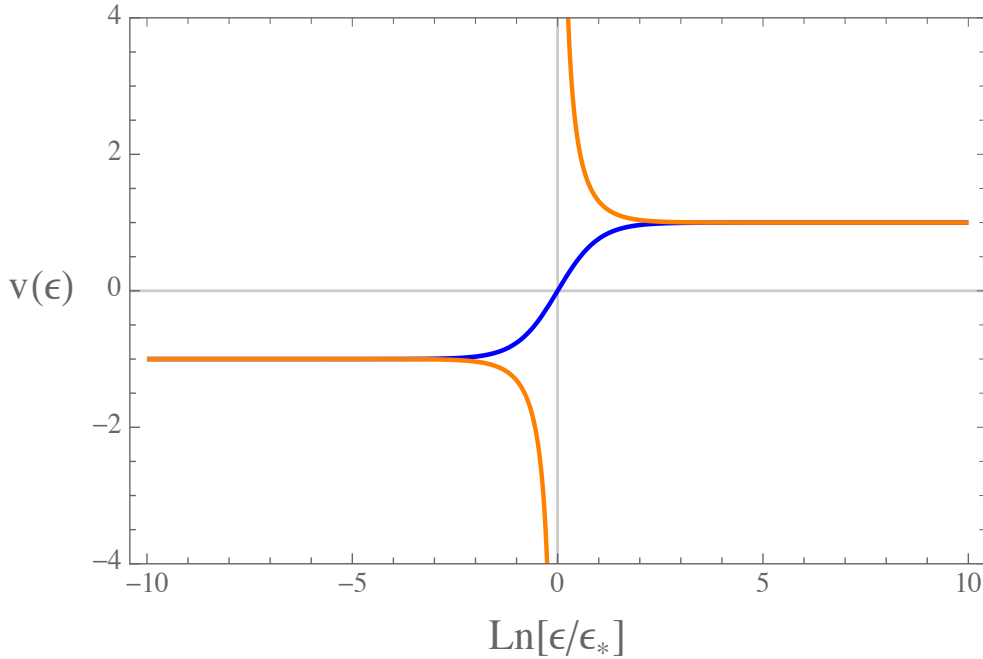


Figure 1: Illustration of the two categories of RG flow described by the solutions (F.13) to the evolution equation (F.11). This figure plots the universal variable $v(\epsilon)$ against the logarithmic variable $\ln(\epsilon/\epsilon_*)$. An example of each of the two categories of flow is shown.

This picture is laid out in more detail in [64, 70–73] and briefly summarized for convenience in Appendix F. The upshot is that relations like (2.64) and (2.70) can all be regarded as special cases of equations of the form:

$$g(\epsilon) = \frac{A(2\kappa\epsilon)^{2\zeta} + B}{C(2\kappa\epsilon)^{2\zeta} + D}, \quad (3.1)$$

where A, B, C and D are known parameters and g is a representative coupling (*i.e.* a specific combination of the couplings c_s, c_v and c_F). For *any* such evolution it is possible

to define a universal coupling $v(\epsilon)$, such that

$$g(\epsilon) = \frac{1}{2} \left(\frac{A}{C} - \frac{B}{D} \right) v(\epsilon) + \frac{1}{2} \left(\frac{A}{C} + \frac{B}{D} \right). \quad (3.2)$$

and for which the evolution of v with ϵ is simple. As is easily shown (*e.g.* in Appendix F), eqs. (3.1) and (3.2) ensure that v satisfies

$$\epsilon \frac{dv}{d\epsilon} = \zeta(1 - v^2). \quad (3.3)$$

whose general solution is

$$v(\epsilon) = \frac{(v_0 + 1)(\epsilon/\epsilon_0)^{2\zeta} + (v_0 - 1)}{(v_0 + 1)(\epsilon/\epsilon_0)^{2\zeta} - (v_0 - 1)} = \frac{(\epsilon/\epsilon_\star)^{2\zeta} + y_\star}{(\epsilon/\epsilon_\star)^{2\zeta} - y_\star}. \quad (3.4)$$

Here the first equality chooses the integration constant to ensure $v(\epsilon_0) = v_0$, and the second equality instead chooses $v(\epsilon_\star) = 0$ (if $y_\star = -1$) or $v(\epsilon_\star) = \infty$ (if $y_\star = +1$), where $y_\star = \text{sign}(|v| - 1) = \pm 1$ is a universal constant along the trajectory (in the sense that it does not depend on ϵ).

For $\zeta > 0$ eq. (3.4) describes a universal flow that runs from $v_0 = -1$ to $v_\infty = +1$ as ϵ flows from 0 to ∞ , corresponding to the initial variable flowing from $g_0 = B/D$ when $\epsilon = 0$ to $g_\infty = A/C$ as $\epsilon \rightarrow \infty$. Plots of these flows for each choice of $y_\star = \pm 1$ are given explicitly in Fig. 1. Physically, this flow describes the crossover between the two independent solutions to the radial mode equation with increasing distance from the source at the origin [73] (*i.e.* in the present case, from the nucleus). This crossover happens because the two radial solutions have different small- r asymptotic forms (typically power laws, with powers related to the two fixed points of the above flow equation), with one solution or the other dominating at large or small radius.

To keep things concrete we next show how things work for positive-parity $j = \frac{1}{2}$ states, and then return to describe the extension to negative-parity states.

Positive parity

For the specific case of $j = \frac{1}{2}$ parity-even states the evolution equation predicted by (2.58) has the form of (3.1) if we identify $g = -\left(\hat{c}_s^{(0)} - \hat{c}_v^{(0)}\right)/\chi$ and use $\zeta = \sqrt{1 - (Z\alpha)^2}$ and

$$\begin{aligned} \frac{A}{C} &= \frac{c + a}{c - a} = \frac{-1 + \zeta - (m + \omega)Z\alpha/\kappa}{-1 - \zeta - (m - \omega)Z\alpha/\kappa} \simeq n + \dots \\ \frac{B}{D} &= \frac{c + a'}{c - a'} = \frac{-1 - \zeta - (m + \omega)Z\alpha/\kappa}{-1 + \zeta - (m - \omega)Z\alpha/\kappa} \simeq \frac{4n}{(Z\alpha)^2} + \dots \end{aligned} \quad (3.5)$$

The approximate equalities here specialize to the leading Coulomb expression $m - \omega \simeq (Z\alpha)^2 m / (2n^2) + \dots$ and so $\kappa \simeq Z\alpha m / n + \dots$ as well as $\zeta \simeq 1 - \frac{1}{2}(Z\alpha)^2 + \dots$, with ellipses describing contributions suppressed by additional powers of $(Z\alpha)^2$.

Applying these expressions – as well as $\chi = \sqrt{(m - \omega)/(m + \omega)} \simeq Z\alpha / (2n) + \dots$ – to (3.2) then shows that the evolution of the quantity

$$\bar{\lambda}_+^{(0)} := \hat{c}_s^{(0)} - \hat{c}_v^{(0)} = -\chi \left[\frac{(c + a) + (c + a') (\mathcal{D}_+ / \mathcal{C}_+)^{(0)} (2\kappa\epsilon)^{-2\zeta}}{(c - a) + (c - a') (\mathcal{D}_+ / \mathcal{C}_+)^{(0)} (2\kappa\epsilon)^{-2\zeta}} \right], \quad (3.6)$$

has the equivalent form

$$\begin{aligned} \bar{\lambda}_+^{(0)} &= -\frac{\chi}{2} \left(\frac{c + a}{c - a} - \frac{c + a'}{c - a'} \right) v_+^{(0)}(\epsilon) - \frac{\chi}{2} \left(\frac{c + a}{c - a} + \frac{c + a'}{c - a'} \right) \\ &= -\frac{\chi}{2} \left(\frac{c + a}{c - a} - \frac{c + a'}{c - a'} \right) \left[\frac{(\epsilon/\epsilon_{\star+})^{2\zeta} + y_{\star+}}{(\epsilon/\epsilon_{\star+})^{2\zeta} - y_{\star+}} \right] - \frac{\chi}{2} \left(\frac{c + a}{c - a} + \frac{c + a'}{c - a'} \right). \end{aligned} \quad (3.7)$$

Using the values given in (2.20) for the parameters a , a' and c then gives

$$\bar{\lambda}_+^{(0)} \simeq \frac{1}{Z\alpha} (v_+^{(0)} - 1) = \frac{1}{Z\alpha} \left\{ \left[\frac{(\epsilon/\epsilon_{\star+})^{2\zeta} + y_{\star+}}{(\epsilon/\epsilon_{\star+})^{2\zeta} - y_{\star+}} \right] - 1 \right\}, \quad (3.8)$$

which drops terms suppressed by $(Z\alpha)^2$ relative to those shown.

Comparing eqs. (3.6) and (3.7) reveals something interesting. Although the integration constant $(\mathcal{D}_+ / \mathcal{C}_+)^{(0)}$ appears in both B and D , it completely cancels out of the differential evolution equations, which depend only on the ratios A/C and B/D . This shows that $(\mathcal{D}_+ / \mathcal{C}_+)^{(0)}$ can also be regarded as the integration constant obtained when integrating (3.3), and so carries the same information as do the parameters $\epsilon_{\star+}$ and $y_{\star+}$. Rewriting (3.7) to have the form eq. (3.6) makes this explicit:

$$\begin{aligned} \left(\frac{\mathcal{D}_+}{\mathcal{C}_+} \right)^{(0)} &= -y_{\star+} \left(\frac{c - a}{c - a'} \right) (2\kappa\epsilon_{\star+})^{2\zeta} \simeq -\frac{16y_{\star+}(m\epsilon_{\star+})^2}{n(n+1)} \left(\frac{2Z\alpha m\epsilon_{\star+}}{n} \right)^{2\zeta-2} + \dots \\ &=: -\frac{\mathfrak{c}}{n(n+1)} + \mathcal{O}[(Z\alpha)^2], \end{aligned} \quad (3.9)$$

where the last equality defines the n -independent constant $\mathfrak{c} = 16y_{\star+}(m\epsilon_{\star+})^2$. Since observable quantities (like electron energy shifts) depend on the boundary conditions only through the value \mathcal{D}/\mathcal{C} , eq. (3.9) shows that observables also only depend on the renormalization-group invariant parameters, like $(\epsilon_{\star}, y_{\star})$, that characterize the effective couplings.

Another important property of (3.8) is its n -independence, at least at leading order in $(Z\alpha)^2$. This considerably simplifies the $\mathcal{O}(\mathfrak{s})$ renormalization story, starting with

being responsible for the vanishing of Λ_+ as defined in (2.68). In particular, notice that the contents of the final braces in (2.68) have the form $\bar{\lambda}_+^{(0)} - \tilde{\lambda}_+^{(0)}$ where $\tilde{\lambda}_+^{(0)}$ and $\bar{\lambda}_+^{(0)}$ differ only by being evaluated using different quantum numbers – such as \tilde{n} and \tilde{j} as opposed to n and j and so on. But because (3.8) is independent of these state quantum numbers it follows that $\tilde{\lambda}_+^{(0)} = \bar{\lambda}_+^{(0)}$ to the accuracy to which we work. Furthermore, as mentioned above (and is seen explicitly below), the n -dependence appearing in (3.9) is precisely what is required to reproduce the proper energy shifts found in the literature for non-Coulomb nuclear structure related energy shifts [29, 106].

Negative parity

We next repeat the above story for nuclear-spin independent interactions, but for $j = \frac{1}{2}$ negative-parity states. At zeroth order in \mathfrak{s} the relevant boundary condition [64, 72] is as given in (2.70)

$$\bar{\lambda}_-^{(0)} := \hat{c}_s^{(0)} + \hat{c}_v^{(0)} = -\frac{1}{\chi} \left[\frac{(c-a) + (c-a') (\mathcal{D}_-/\mathcal{C}_-)^{(0)} (2\kappa\epsilon)^{-2\zeta}}{(c+a) + (c+a') (\mathcal{D}_-/\mathcal{C}_-)^{(0)} (2\kappa\epsilon)^{-2\zeta}} \right], \quad (3.10)$$

which defines the variable $\bar{\lambda}_-^{(0)}$. This again shows how $\hat{c}_s^{(0)} + \hat{c}_v^{(0)}$ must depend on ϵ to ensure that physical quantities do not. It also falls into the category of evolution considered in (3.1), with $g = -\bar{\lambda}_-^{(0)}\chi = -(\hat{c}_s^{(0)} + \hat{c}_v^{(0)})\chi$ and

$$\begin{aligned} \frac{A}{C} &= \frac{c-a}{c+a} = \frac{1-\zeta - (m-\omega)Z\alpha/\kappa}{1+\zeta - (m+\omega)Z\alpha/\kappa} \simeq -\frac{1}{4n}(Z\alpha)^2 + \dots \\ \frac{B}{D} &= \frac{c-a'}{c+a'} = \frac{1+\zeta - (m-\omega)Z\alpha/\kappa}{1-\zeta - (m+\omega)Z\alpha/\kappa} \simeq -\frac{1}{n} + \dots \end{aligned} \quad (3.11)$$

The universal evolution equivalent to (3.10) then is

$$\begin{aligned} \bar{\lambda}_-^{(0)} &= -\frac{1}{2\chi} \left(\frac{c-a}{c+a} - \frac{c-a'}{c+a'} \right) v_-^{(0)}(\epsilon) - \frac{1}{2\chi} \left(\frac{c-a}{c+a} + \frac{c-a'}{c+a'} \right) \\ &= -\frac{1}{2\chi} \left(\frac{c-a}{c+a} - \frac{c-a'}{c+a'} \right) \left[\frac{(\epsilon/\epsilon_{*-})^{2\zeta} + y_{*-}}{(\epsilon/\epsilon_{*-})^{2\zeta} - y_{*-}} \right] - \frac{1}{2\chi} \left(\frac{c-a}{c+a} + \frac{c-a'}{c+a'} \right), \end{aligned} \quad (3.12)$$

whose leading form for small $Z\alpha$ is

$$\bar{\lambda}_-^{(0)} \simeq -\frac{1}{Z\alpha} \left(v_-^{(0)} - 1 \right) = -\frac{1}{Z\alpha} \left\{ \left[\frac{(\epsilon/\epsilon_{*-})^{2\zeta} + y_{*-}}{(\epsilon/\epsilon_{*-})^{2\zeta} - y_{*-}} \right] - 1 \right\}, \quad (3.13)$$

which again drops terms suppressed by $(Z\alpha)^2$ relative to those shown. Rewriting (3.12) to have the form eq. (3.10) allows $(\mathcal{D}_-/\mathcal{C}_-)^{(0)}$ to be expressed in terms of ϵ_{*-} and y_{*-} , giving

$$\begin{aligned} \left(\frac{\mathcal{D}_-}{\mathcal{C}_-}\right)^{(0)} &= -y_{*-} \left(\frac{c+a}{c+a'}\right) (2\kappa\epsilon_{*-})^{2\zeta} \\ &\simeq -4y_{*-} \left(\frac{n-1}{n^3}\right) (Z\alpha m\epsilon_{*-})^2 \left(\frac{2Z\alpha m\epsilon_{*-}}{n}\right)^{2\zeta-2} + \dots \end{aligned} \quad (3.14)$$

Note the $\mathcal{O}[(Z\alpha)^2]$ suppression of this relative to the corresponding result (3.9) in the parity-even case, as expected due to the near-nucleus suppression of $l = 1$ electronic states relative to $l = 0$ wave functions.

3.1.2 Nuclear-spin dependent contributions

The arguments made to this point are special cases of those used for spinless nuclei in [64]. This section now extends these considerations to include terms at linear order in \mathfrak{s} , focussing in turn on $j = \frac{1}{2}$ states with even and odd parity.

Positive parity

Consider first the apparent ϵ -dependence coming from the $\mathcal{O}(\mathfrak{s})$ part of the boundary condition (2.58), as given explicitly in (2.67). As in previous sections the ϵ -dependence of the couplings can be read off directly from the boundary condition, which in this case states that

$$\begin{aligned} \bar{\lambda}_+^{(1)} &:= \hat{c}_s^{(1)} - \hat{c}_v^{(1)} + \frac{3}{8} \left(\frac{\hat{c}_F}{\mathfrak{s}}\right) \\ &= -\chi \left(\frac{\mathcal{D}_+}{\mathcal{C}_+}\right)^{(1)} \frac{2c(a'-a)(2\kappa\epsilon)^{-2\zeta}}{\left[(c-a) + (c-a')(\mathcal{D}_+/\mathcal{C}_+)^{(0)}(2\kappa\epsilon)^{-2\zeta}\right]^2}. \end{aligned} \quad (3.15)$$

This expression uses the positive-parity results $\varpi = +1$ and $2\varpi + 1 = 3$. It is useful to trade the dependence on $(\mathcal{D}_+/\mathcal{C}_+)^{(0)}$ in this expression for ϵ_{*+} using (3.9), leading to

$$\bar{\lambda}_+^{(1)} = - \left[\frac{2\chi c(a'-a)}{(c-a)^2} \right] \frac{(\epsilon/\epsilon_{*+})^{2\zeta}}{[(\epsilon/\epsilon_{*+})^{2\zeta} - y_{*+}]^2} \left(\frac{\mathcal{D}_+}{\mathcal{C}_+}\right)^{(1)} (2\kappa\epsilon_{*+})^{-2\zeta}. \quad (3.16)$$

Just like in previous sections, the requirement that observables remain ϵ -independent requires $\bar{\lambda}_+^{(1)}$ (and so also its particular combination of $\hat{c}_s^{(1)}$, $\hat{c}_v^{(1)}$ and \hat{c}_F) must vary with ϵ as indicated in this expression, with $(\mathcal{D}_+/\mathcal{C}_+)^{(1)}$ held fixed. Notice, in particular, that this coupling evolution does not require any new invariant parameters beyond ϵ_{*+} and

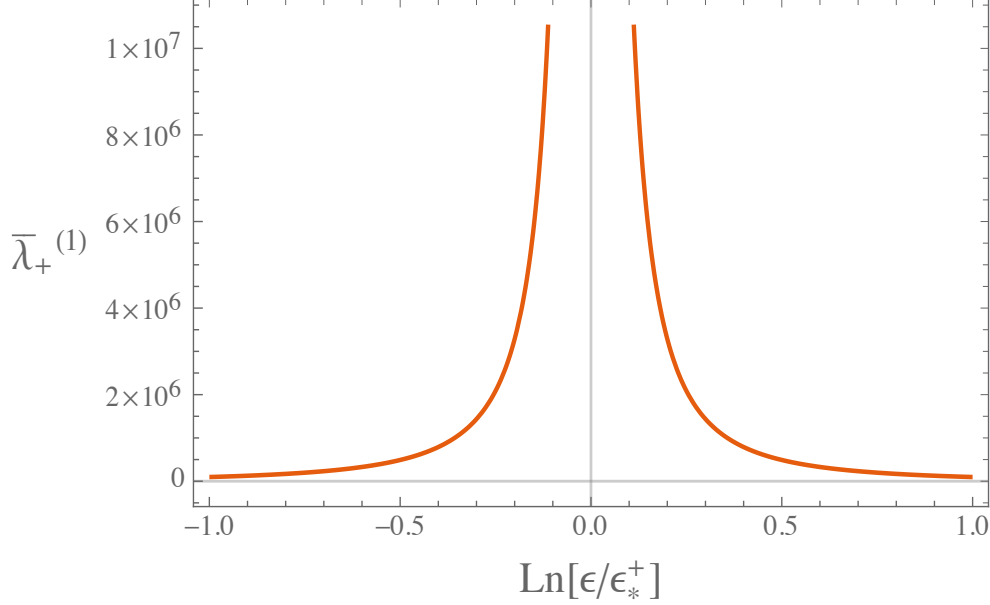


Figure 2: A plot of how $\bar{\lambda}_+^{(1)}(\epsilon, \eta)$ runs as a function of ϵ (with η fixed), based on (3.16). The RG-invariant scale ϵ_{*+} appearing here is the same one that also labels the running of the spin-independent interactions in $\bar{\lambda}_+^{(0)}$. The vertical scale is arbitrary because this depends on choices made for the value of η , as described in the main text.

y_{*+} already encountered in the running of $\bar{\lambda}_+^{(0)}$. With these definitions the expression (2.69) for $(\mathcal{D}_+/\mathcal{C}_+)^{(1)}$ becomes

$$\begin{aligned} \mathfrak{s} \left(\frac{\mathcal{D}_+}{\mathcal{C}_+} \right)^{(1)} &= -\frac{(c-a)^2 (2\kappa\epsilon_{*+})^{2\zeta}}{2\chi c(a'-a)} \left[\left(\frac{\epsilon}{\epsilon_{*+}} \right)^{2\zeta} - y_{*+} \right]^2 \left(\frac{\epsilon_{*+}}{\epsilon} \right)^{2\zeta} \left[\mathfrak{s} (\hat{c}_s^{(1)} - \hat{c}_v^{(1)}) + \frac{3\hat{c}_F}{8} \right], \\ &\simeq -\frac{8Z\alpha(m\epsilon_{*+})^2}{n(n+1)} \left(\frac{2Z\alpha m\epsilon_{*+}}{n} \right)^{2\zeta-2} \left[\left(\frac{\epsilon}{\epsilon_{*+}} \right)^{2\zeta} - y_{*+} \right]^2 \left(\frac{\epsilon_{*+}}{\epsilon} \right)^{2\zeta} \\ &\quad \times \left[\mathfrak{s} (\hat{c}_s^{(1)} - \hat{c}_v^{(1)}) + \frac{3\hat{c}_F}{8} \right]. \end{aligned} \quad (3.17)$$

There is an important difference between this expression and previous discussions. The difference is that $\mathfrak{s} (\hat{c}_s^{(1)} - \hat{c}_v^{(1)}) + \frac{3}{8} \hat{c}_F = \bar{\lambda}_+^{(1)} = \bar{\lambda}_+^{(1)}(\epsilon, \eta)$ must also depend on the other regularization parameter, η , in order to cancel the explicit η -dependence hidden in C_η in expressions like (2.48). This η -dependence is hidden in the couplings $\hat{c}_s^{(1)}$, $\hat{c}_v^{(1)}$ and \hat{c}_F since these are the parameters whose renormalization absorbs this particular dependence. So although the ϵ -dependence of $\mathfrak{s} (\hat{c}_s^{(1)} - \hat{c}_v^{(1)}) + \frac{3}{8} \hat{c}_F$ cancels the explicit ϵ -dependence in (3.17), the same cannot be true for the η dependence, implying $(\mathcal{D}_+/\mathcal{C}_+)^{(1)}$ is implicitly a function of η . The ultimate cancellation of this

η -dependence is described below after first summarizing how the ϵ -dependence cancels for parity-odd states at $\mathcal{O}(\mathfrak{s})$.

Negative parity

Consider first the apparent ϵ -dependence coming from the $\mathcal{O}(\mathfrak{s})$ part of the boundary condition (2.60), as given explicitly in (2.72). For negative parity this states that

$$\begin{aligned}\bar{\lambda}_-^{(1)} &:= \hat{c}_s^{(1)} + \hat{c}_v^{(1)} + \frac{3}{8} \left(\frac{\hat{c}_F}{\mathfrak{s}} \right) \\ &= \frac{1}{\chi} \left(\frac{\mathcal{D}_-}{\mathcal{L}_-} \right)^{(1)} \frac{2c(a' - a) (2\kappa\epsilon)^{-2\zeta}}{\left[(c + a) + (c + a') (\mathcal{D}_-/\mathcal{L}_-)^{(0)} (2\kappa\epsilon)^{-2\zeta} \right]^2}.\end{aligned}\quad (3.18)$$

Trading the dependence on $(\mathcal{D}_-/\mathcal{L}_-)^{(0)}$ in this expression for ϵ_{*-} using (3.14) then gives

$$\bar{\lambda}_-^{(1)} = \left[\frac{2c(a' - a)}{\chi(c + a)^2} \right] \frac{(\epsilon/\epsilon_{*-})^{2\zeta}}{\left[(\epsilon/\epsilon_{*-})^{2\zeta} - y_{*-} \right]^2} \left(\frac{\mathcal{D}_-}{\mathcal{L}_-} \right)^{(1)} (2\kappa\epsilon_{*-})^{-2\zeta}.\quad (3.19)$$

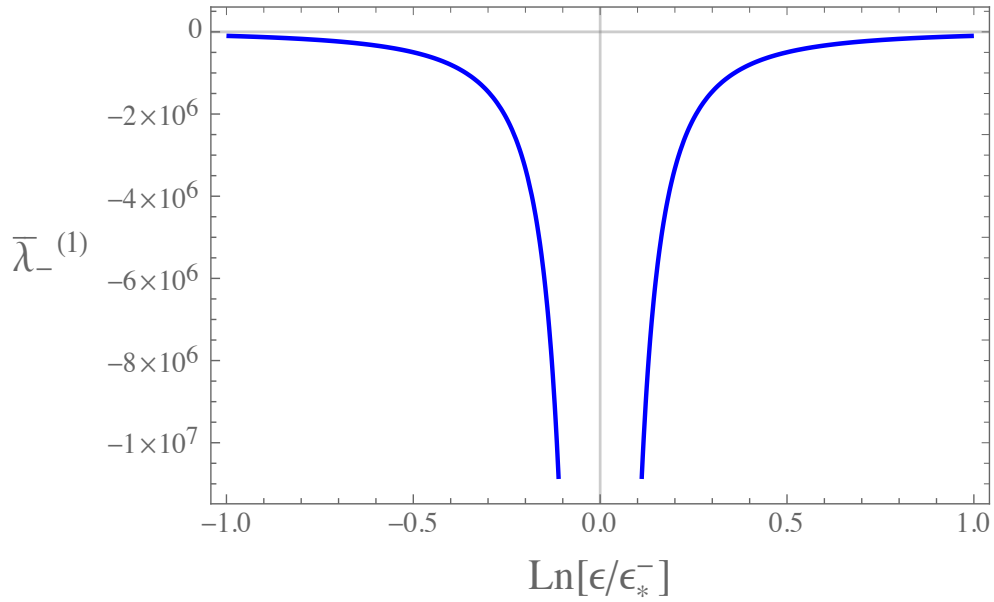


Figure 3: The running of $\bar{\lambda}_-^{(1)}$ as a function of ϵ , based on (3.19). The RG-invariant scale ϵ_{*-} is the same as the scale controlling the running of $\bar{\lambda}_-^{(0)}$. For plotting purposes we hold η fixed and so the vertical axis has an arbitrary scale that depends on the precise values chosen for η .

As before, this shows how $\bar{\lambda}_-^{(1)}$ (and so also the particular combination of $\hat{c}_s^{(1)}$, $\hat{c}_v^{(1)}$ and \hat{c}_F characteristic of negative parity states) must vary with ϵ , with $(\mathcal{D}_-/\mathcal{L}_-)^{(1)}$ held

fixed, in order to keep observables ϵ -independent. The solution, (2.74), for $(\mathcal{D}_-/\mathcal{C}_-)^{(1)}$ then becomes

$$\begin{aligned} \mathfrak{s} \left(\frac{\mathcal{D}_-}{\mathcal{C}_-} \right)^{(1)} &= \frac{\chi(c+a)^2(2\kappa\epsilon_{\star-})^{2\zeta}}{2c(a'-a)} \left[\left(\frac{\epsilon}{\epsilon_{\star-}} \right)^{2\zeta} - y_{\star-} \right]^2 \left(\frac{\epsilon_{\star-}}{\epsilon} \right)^{2\zeta} \left\{ \mathfrak{s} [\hat{c}_s^{(1)} + \hat{c}_v^{(1)}] + \frac{3\hat{c}_F}{8} \right\}, \\ &\simeq \frac{2(n-1)(Z\alpha)^3(m\epsilon_{\star-})^2}{n^3} \left(\frac{2Z\alpha m\epsilon_{\star-}}{n} \right)^{2\zeta-2} \\ &\quad \times \left[\left(\frac{\epsilon}{\epsilon_{\star-}} \right)^{2\zeta} - y_{\star-} \right]^2 \left(\frac{\epsilon_{\star-}}{\epsilon} \right)^{2\zeta} \left\{ \mathfrak{s} [\hat{c}_s^{(1)} + \hat{c}_v^{(1)}] + \frac{3\hat{c}_F}{8} \right\}, \end{aligned} \quad (3.20)$$

again exhibiting a P -wave $(Z\alpha)^2$ suppression relative to the parity-even case. This evolution is shown in Figure 3.

3.2 Cancellation of η -dependence

We now return to describing how divergent η -dependence found in earlier sections gets renormalized.

To this end recall that to linear order in \mathfrak{s} the nuclear-structure contribution to electronic energy levels has the form given in (2.25), of which the main focus in this section is on the first two terms on the right-hand side:

$$\delta\omega_{nFj\varpi} + \varepsilon_{nFj\varpi}^{(1)} = \left(\delta\omega_{nFj\varpi}^{(0)} + \delta\omega_{nFj\varpi}^{(1)} \right) + \left(\varepsilon_{nFj\varpi}^{\text{hfs}} + \delta\varepsilon_{nFj\varpi}^{(1)} \right). \quad (3.21)$$

Here $\delta\omega_{nFj\varpi}^{(0)}$ and $\delta\omega_{nFj\varpi}^{(1)}$ are the spin-independent and $\mathcal{O}(\mathfrak{s})$ contributions to $\delta\omega_{nFj\varpi}$, given by using $\mathcal{D}/\mathcal{C} = (\mathcal{D}/\mathcal{C})^{(0)} + \mathfrak{s}(\mathcal{D}/\mathcal{C})^{(1)}$ in the energy expression (C.10), while $\varepsilon_{nFj\varpi}^{\text{hfs}}$ is the hyperfine (point-nucleus but nuclear-spin dependent) energy shift of eq. (2.47) and

$$\begin{aligned} \delta\varepsilon_{nFj\varpi}^{(1)} &= \varepsilon_{nFj\varpi}^{\text{hfs}} \left[\frac{1 + (\mathcal{D}/\mathcal{C})(\mathfrak{N}_1/\mathfrak{N}_{\text{pt}}) + (\mathcal{D}/\mathcal{C})^2(\mathfrak{N}_2/\mathfrak{N}_{\text{pt}})}{1 + (\mathcal{D}/\mathcal{C})(\mathfrak{D}_1/\mathfrak{D}_{\text{pt}}) + (\mathcal{D}/\mathcal{C})^2(\mathfrak{D}_2/\mathfrak{D}_{\text{pt}})} - 1 \right] \\ &= \varepsilon_{nFj\varpi}^{\text{hfs}} \left[\left(\frac{\mathcal{D}}{\mathcal{C}} \right)^{(0)} \left(\frac{\mathfrak{N}_1}{\mathfrak{N}_{\text{pt}}} - \frac{\mathfrak{D}_1}{\mathfrak{D}_{\text{pt}}} \right) + \dots \right] \\ &\simeq \varepsilon_{nFj\varpi}^{\text{hfs}} \left[C_\eta - \frac{\mathfrak{c}}{n} + \dots \right], \end{aligned} \quad (3.22)$$

is the nuclear-structure part of the contribution to $\varepsilon_{nFj\varpi}^{(1)}$ of eq. (2.48) once $\varepsilon_{nFj\varpi}^{\text{hfs}}$ has been subtracted out.

The issue to be addressed arises because the integrations appearing in $\delta\varepsilon_{nFj\varpi}^{(1)}$ diverge in the near-nucleus ($r \rightarrow 0$) limit; a divergence that is dealt with using a regulation

parameter η . This section traces how this unphysical η -dependence is renormalized by the effective couplings $\hat{c}_s^{(1)}$, $\hat{c}_v^{(1)}$ and \hat{c}_F that appear in $\delta\omega_{nFj\varpi}^{(1)}$ through its dependence on $(\mathcal{D}/\mathcal{C})^{(1)}$ (such as, *e.g.*, eq. (3.17)).

To display this cancellation explicitly we require the dependence of $\delta\omega_{nFj\varpi}^{(1)}$ on $(\mathcal{D}_+/\mathcal{C}_+)^{(1)}$. This is found by expanding the general result (C.10) of Appendix C – found by solving (2.22) for nonzero \mathcal{D}/\mathcal{C} . Specializing (C.10) to positive-parity, $j = \frac{1}{2}$ states one finds

$$\begin{aligned}\delta\omega_{n\frac{1}{2}+}^{(0)} &\simeq -\frac{\kappa_D^3 n(n+1) (\mathcal{D}_+/\mathcal{C}_+)^{(0)} \left[1 - (2-2\zeta)(H_{n+1} + \gamma)\right]}{2m^2 Z\alpha \mathfrak{H}} \\ &\simeq \frac{8y_{\star+} (Z\alpha)^2 m(m\epsilon_{\star+})^2}{n^3 \mathfrak{H}} \left(\frac{2Z\alpha m\epsilon_{\star+}}{n}\right)^{2\zeta-2} + \dots,\end{aligned}\quad (3.23)$$

and

$$\begin{aligned}\delta\omega_{nF\frac{1}{2}+}^{(1)} &\simeq -\mathfrak{s} X_F \left[\frac{\kappa_D^3 n(n+1)}{2m^2 Z\alpha} \left(\frac{\mathcal{D}_+}{\mathcal{C}_+}\right)^{(1)} + \dots \right] \\ &\simeq \frac{4(Z\alpha)^3 m(m\epsilon_{\star+})^2}{n^3} \left(\frac{2Z\alpha m\epsilon_{\star+}}{n}\right)^{2\zeta-2} \\ &\quad \times \left[\left(\frac{\epsilon}{\epsilon_{\star+}}\right)^\zeta - y_{\star+} \left(\frac{\epsilon_{\star+}}{\epsilon}\right)^\zeta \right]^2 \left[\mathfrak{s} (\hat{c}_s^{(1)} - \hat{c}_v^{(1)}) + \frac{3\hat{c}_F}{8} \right] X_F + \dots,\end{aligned}\quad (3.24)$$

where the second lines of (3.23) and (3.24) respectively use (3.9) and (3.17), as well as

$$\begin{aligned}\mathfrak{H} &:= 1 - \frac{n(n+1) (\mathcal{D}_+/\mathcal{C}_+)^{(0)} [1 - 4(1-\zeta)(H_{n+1} + \gamma)]}{4(1-\zeta)} - 5(1-\zeta) + \dots \\ &\simeq 1 + \frac{4y_{\star+} (m\epsilon_{\star+})^2}{(Z\alpha)^2} + \dots,\end{aligned}\quad (3.25)$$

with $H_n = \sum_{k=1}^n 1/k$ being the harmonic numbers and γ being Euler's constant. As we shall see, matching implies $m\epsilon_{\star+} \propto mRZ\alpha$ and so the ratio $m\epsilon_{\star+}/(Z\alpha)$ proves to be small for electrons (though only order $\frac{1}{2}$ for muons). The ellipses in these expressions represent terms that involve additional powers of one or both of the small quantities $(\mathcal{D}_+/\mathcal{C}_+)^{(0)}$ or $(Z\alpha)^2$.

The η -dependence of the couplings is now determined by requiring physical quantities not depend on η . This implies

$$\frac{d}{d\eta} \left[-\mathfrak{s} X_F \frac{(Z\alpha)^2 m(n+1)}{2n^2} \left(\frac{\mathcal{D}_+}{\mathcal{C}_+}\right)^{(1)} + \delta\epsilon_{nF\frac{1}{2}+}^{(1)} + \dots \right] = 0,\quad (3.26)$$

and so, using (3.22)

$$\frac{d}{d\eta} \left(\frac{\mathcal{D}_+}{\mathcal{C}_+} \right)^{(1)} X_F \simeq \frac{2n^2}{(Z\alpha)^2(n+1)} \left(\frac{\varepsilon_{nF\frac{1}{2}+}^{\text{hfs}}}{\mathfrak{s}m} \right) \frac{dC_\eta}{d\eta} \simeq \frac{2X_F Z\alpha}{n(n+1)} \frac{dC_\eta}{d\eta}. \quad (3.27)$$

Since C_η is n -independent (at leading order in $Z\alpha$) and since eq. (3.17) implies the same is also true of $n(n+1)(\mathcal{D}_+/\mathcal{C}_+)^{(1)}$, it follows that the η -dependence can be cancelled by performing an η -dependent but n -independent shift of the combination $\mathfrak{s} \left(\hat{c}_s^{(1)} - \hat{c}_v^{(1)} \right) + \frac{3}{8} \hat{c}_F$. The integral of (3.27) then is

$$\begin{aligned} \left(\frac{\mathcal{D}_+}{\mathcal{C}_+} \right)^{(1)} &= \left(\frac{\mathcal{D}_+}{\mathcal{C}_+} \right)_{\text{phys}}^{(1)} + \frac{2n^2}{(Z\alpha)^2(n+1)} \left(\frac{\varepsilon_{nF\frac{1}{2}+}^{\text{hfs}}}{\mathfrak{s}X_F m} \right) C_\eta \\ &\simeq \left(\frac{\mathcal{D}_+}{\mathcal{C}_+} \right)_{\text{phys}}^{(1)} + \frac{2Z\alpha}{n(n+1)} C_\eta, \end{aligned} \quad (3.28)$$

where the first term is both ϵ - and η -independent and inversely proportional to $n(n+1)$.

Although the above discussion cancels the η -dependent part of $\delta\varepsilon_{nF\frac{1}{2}+}^{(1)}$, there is (as always) clearly considerable freedom in choosing the finite parts of the counterterms. We here use this freedom to define the new n -independent RG-invariant parameter ϵ_{F+} , through the definition (notice the resemblance to (3.9), apart from overall sign)

$$\left(\frac{\mathcal{D}_+}{\mathcal{C}_+} \right)_{\text{phys}}^{(1)} := \left(\frac{c-a}{c-a'} \right) \left(\frac{2Z\alpha m \epsilon_{F+}}{n} \right)^{2\zeta} \simeq \frac{16(m\epsilon_{F+})^2}{n(n+1)} \left(\frac{2Z\alpha m \epsilon_{F+}}{n} \right)^{2\zeta-2}. \quad (3.29)$$

With this definition the net spin-dependent energy shift at this order simply becomes,

$$\begin{aligned} \delta\omega_{nF\frac{1}{2}+}^{(1)} + \delta\varepsilon_{nF\frac{1}{2}+}^{(1)} &\simeq -\mathfrak{s}X_F \frac{\kappa_D^3 n(n+1)}{2m^2 Z\alpha} \left(\frac{\mathcal{D}_+}{\mathcal{C}_+} \right)^{(1)} + \varepsilon_{nF\frac{1}{2}+}^{\text{hfs}} \left(C_\eta - \frac{\mathfrak{c}}{n} \right) \\ &= -\mathfrak{s}X_F \left(\frac{\kappa_D^3}{m^2} \right) \left[\frac{n(n+1)}{2Z\alpha} \left(\frac{\mathcal{D}_+}{\mathcal{C}_+} \right)_{\text{phys}}^{(1)} + \frac{\mathfrak{c}}{n} \right] \\ &\simeq -\mathfrak{s}X_F \left[\frac{(Z\alpha)^2 m}{n^3} \right] 8(m\epsilon_{F+})^2 \left(\frac{2Z\alpha m \epsilon_{F+}}{n} \right)^{2\zeta-2} + \dots, \end{aligned} \quad (3.30)$$

where the last line drops the \mathfrak{c}/n term, as appropriate at the order we work. This is to be compared, say, with (3.23) for $\delta\omega_{nF\frac{1}{2}+}^{(0)}$.

A similar story goes through as well for $j = \frac{1}{2}$ negative parity states, in principle involving the definition of a new parameter ϵ_{F-} , however we do not pursue this further because the additional $(Z\alpha)^2$ suppression of P -wave states makes the contribution of this new parameter to atomic energy shifts too small to be relevant to the order we work. We therefore drop the parity label and in what follows simply use $\epsilon_F := \epsilon_{F+}$ to denote the parameter relevant to nuclear spin-dependence.

3.3 Matching to nuclear moments

The previous sections show that without loss of generality all nuclear finite-size effects can be described – at least out to contributions with dimension (length)³ – in terms of the three RG-invariant parameters $\epsilon_{\star+}$, $\epsilon_{\star-}$ and ϵ_F .

In this section our goal is to illustrate how the values of these parameters can in principle be calculable in terms of known nuclear moments from an underlying nuclear model. Later sections describe how our parameters can also be obtained from precision measurements of atomic energy levels. Besides providing some intuition for how big our parameters should be, relating them to nuclear moments allows a check on our energy-level calculations, which must reproduce those of specific models once specialized to the model’s assumptions.

3.3.1 Nuclear moments

Perhaps the simplest nuclear models replace the nucleus with specified charge and magnetization distributions, ρ_c and ρ_m , and although these are over-simplifications of the real quantum systems, they do allow explicit calculation of finite-size effects in the nucleus’ electromagnetic response. These distributions are normalized such that

$$Ze = \int d^3\mathbf{x}' \rho_c(\mathbf{x}'), \quad \mu_N = \int d^3\mathbf{x}' \rho_m(\mathbf{x}'), \quad (3.31)$$

where (as in earlier sections) Ze is the total nuclear charge and μ_N is the nuclear magnetic moment (including the g -factor). Because atoms are so much larger than nuclei, atomic observables tend to sample only the first few moments of these distributions, defined by

$$\langle r^k \rangle_c = \frac{1}{Ze} \int d^3\mathbf{x}' r^k \rho_c(\mathbf{x}'), \quad \langle r^k \rangle_m = \frac{1}{\mu_N} \int d^3\mathbf{x}' r^k \rho_m(\mathbf{x}'). \quad (3.32)$$

For instance, the first model-independent parameterization of a nuclear-size atomic energy shift was written down by Karplus, Klein and Schwinger for Hydrogen in [27] for the $nS_{1/2}$ ²⁰ state, giving

$$\delta\omega_{n\frac{1}{2}+}^{(0)} \simeq \frac{2}{3}(Z\alpha)^4 m_r^3 \langle r^2 \rangle_c, \quad (3.33)$$

where m_r is the reduced mass.

²⁰Here, and in the rest of the paper we use the spectroscopic notation, nL_j^F , where n is the principal quantum number, L is the orbital angular momentum quantum number, j is the total angular momentum quantum number of the orbiting lepton and F is the total atomic angular momentum quantum number (if appropriate and necessary).

A further step was taken by Zemach in [28], who computed the influence of the magnetization distribution to find (for total atomic spin $F = 0, 1$)

$$\delta\omega_{1F\frac{1}{2}+}^{(1)} \simeq -2\mathfrak{s}X_F \left(\frac{m_r}{m}\right)^3 (Z\alpha)^4 m^2 \langle r \rangle_{cm} + \dots, \quad (3.34)$$

with \mathfrak{s} as defined in (2.35) and the first Zemach moment, $\langle r \rangle_{cm}$, being one of many such moments defined by

$$\langle r^k \rangle_{cm} = \frac{1}{Ze\mu_N} \int d^3\mathbf{x}' \int d^3\mathbf{y}' r^k \rho_c(\mathbf{x}') \rho_m(\mathbf{y}'). \quad (3.35)$$

Friar categorized finite-size effects [29] out to third-order perturbation theory in $Z\alpha$ as a function of nuclear moments and showed (among other things) that for positive-parity $j = \frac{1}{2}$ (*i.e.* $nS_{1/2}$) states they can be written as,

$$\begin{aligned} \delta\omega_{n\frac{1}{2}+}^{(0)} = & \frac{2}{3}(Z\alpha)^4 \frac{m_r^3}{n^3} \left\{ \langle r^2 \rangle_c - \frac{1}{2}m_r(Z\alpha)\langle r^3 \rangle_{cc} - (Z\alpha)^2 \left[\frac{\langle r^3 \rangle_c \langle r^{-1} \rangle_c}{3} - I_2^{\text{REL}} - I_3^{\text{REL}} \right. \right. \\ & \left. \left. + \langle r^2 \rangle_c \left(H_{n-1} + \gamma - \frac{13n^2 + 4n - 9}{4n^2} + \left\langle \ln \left[\frac{2m_r(Z\alpha)r}{n} \right] \right\rangle_c \right) \right] \right. \\ & \left. + m_r^2(Z\alpha)^2 \left[I_2^{\text{NR}} + I_3^{\text{NR}} + \frac{2}{3}\langle r^2 \rangle_c \left(\left\langle r^2 \ln \left[\frac{2m_r(Z\alpha)r}{n} \right] \right\rangle_c \right. \right. \right. \\ & \left. \left. \left. + \langle r^2 \rangle_c \left(H_{n-1} + \gamma - \frac{4n + 3}{3n} \right) \right) \right] + \langle r^3 \rangle_c \langle r \rangle_c + \frac{\langle r^4 \rangle_c}{10n^2} + \langle r^5 \rangle_c \langle r^{-1} \rangle_c \right\} + \dots, \end{aligned} \quad (3.36)$$

where H_n are again the harmonic numbers – defined below (3.25) – while γ is Euler’s constant, the ellipses represent terms of order $(Z\alpha)^7$ or higher, and $I_2^{\text{NR}}, I_3^{\text{NR}}, I_2^{\text{REL}}, I_3^{\text{REL}}$ are parametric integrals whose detailed form plays no role in what follows (but, for those interested, can be found in [29]).

Calculations like these based on fixed distributions of charge and magnetization miss dynamical effects, such as those due to nucleon motion and polarizability (that are not included in [29]). These effects are included in the modern approaches to precision atomic calculations that dominate the more recent literature [50, 52, 55, 57], which involve more detailed modelling of nucleon substructure, nucleon motion and inter-nucleon interactions. Some of the results of these more sophisticated calculations nonetheless overlap with eqs. (3.36) and (3.38), typically when describing ‘elastic’ contributions (for which the nucleus is assumed to remain unexcited within internal lines when evaluating the relevant Feynman graphs – such as those describing virtual photon exchange with the orbiting lepton). Other contributions fall outside the above expression, such as those inelastic contributions that sum over excited nuclear states and are related to the electric and magnetic polarizabilities of the nucleus. As can be

seen in calculations for deuterium in [45, 57], the split between elastic and inelastic contributions can be artificial, and they are better considered together.

Combining these dynamical effects [57] with the results given above then gives (for the nuclear-spin independent shift of $nS_{1/2}$ states),

$$\begin{aligned} \delta\omega_{n\frac{1}{2}+}^{(0)} = & \frac{2}{3}(Z\alpha)^4 \frac{m_r^3}{n^3} \left\{ \langle r^2 \rangle_c - \frac{1}{2}m_r(Z\alpha)\langle r^3 \rangle_{cc}^{\text{eff}} - (Z\alpha)^2 \langle r^2 \rangle_c \left(H_{n-1} + \gamma + \frac{9}{4n^2} - \frac{1}{n} \right. \right. \\ & \left. \left. - 3 + \ln \left[\frac{2m_r(Z\alpha)}{n} \right] + \ln[\langle r_{c2} \rangle] \right) + m_r^2(Z\alpha)^2 \left[\frac{\langle r^4 \rangle_c}{15n^5} \right. \right. \\ & \left. \left. + \frac{2}{3} \langle r^2 \rangle_c \langle r^2 \rangle_c \left(H_{n-1} + \gamma - \frac{1}{n} + 2 + \ln \left(\frac{2Z\alpha m_r \langle r_{c1} \rangle}{n} \right) \right) \right] \right\} + \dots, \end{aligned} \quad (3.37)$$

where the ellipses now only denote terms of order $\mathcal{O}((Z\alpha)^7)$ or higher, $\langle r^3 \rangle_{cc}^{\text{eff}}$ is an effective radius that takes into account the inelastic contributions of the two-photon Coulomb exchange²¹, and $\langle r_{c2} \rangle, \langle r_{c1} \rangle$ are again other nuclear moments, whose definitions from [57] we do not repeat here as they do not qualitatively contribute to our discussion.

For some purposes it is also necessary to know similar results for the nucleus-induced energy shift for parity-negative $j = \frac{1}{2}$ states ($nP_{1/2}$). These are suppressed by the small size of the wave-function at the nucleus, which introduces two more powers of $Z\alpha$, with the result coming from a static nuclear charge distribution [29] to order $\mathcal{O}[(Z\alpha)^6]$ given by

$$\delta\omega_{n\frac{1}{2}-}^{(0)} = \frac{n^2 - 1}{3n^5} (Z\alpha)^4 m_r^3 \left\{ \frac{1}{2} (Z\alpha)^2 \langle r^2 \rangle_c + \frac{1}{15} (Z\alpha)^2 m_r^2 \langle r^4 \rangle_c \right\} + \dots, \quad (3.38)$$

where the ellipses again denote terms higher order in $(Z\alpha)$. Nuclear finite-size related polarizability contributions for Hydrogen do not yet contribute at order $(Z\alpha)^6$ for P -states and so can be ignored. (Even if present, such terms would not change the arguments made below.)

Energy shifts sensitive to nuclear spin – such as (3.34) – are also relevant at order $(Z\alpha)^6$, since – *c.f.* eq. (2.35) – for Hydrogen $\mathfrak{s} \sim (m/M)(Z\alpha)$. Since $m/M \sim Z\alpha$ for electrons the result (3.34) suffices to present experimental accuracy for ordinary Hydrogen, but the larger muon mass (and high experimental precision) implies that corrections involving both nuclear structure and spin can also be important for muonic Hydrogen. These are written in terms of momentum-space integrals over the proton

²¹There is a cancellation between the original $\langle r^3 \rangle_{cc}$ term in (3.36) (known as the Friar moment) and a certain part of the polarizability [45] but since the inelastic contributions at this order depend on the lepton quantum numbers the same way as the elastic contributions they can be combined to define the effective nuclear moment, $\langle r^3 \rangle_{cc}^{\text{eff}}$.

form-factors in [107], and a position-space equivalent is calculated in [56] as a part of elastic nuclear-structure corrections, leading (in our notation – see eq. (2.25) and (3.21)) to the total spin-dependent result

$$\delta\omega_{nF\frac{1}{2}+}^{(1)} + \delta\varepsilon_{nF\frac{1}{2}+}^{(1)} \simeq -\frac{\mathfrak{s}X_F}{n^3} \left\{ 2 \left(\frac{m_r}{m} \right)^2 (Z\alpha)^4 m_r^2 \langle r \rangle_{cm} - \frac{4}{3} (Z\alpha)^5 m_r^3 \langle r^2 \rangle_c \left[-\frac{1}{n} + \gamma + H_{n-1} \right. \right. \\ \left. \left. + \ln \left(\frac{2Z\alpha m \langle r_{pp} \rangle}{n} \right) + \frac{\langle r^2 \rangle_m}{4n^2 \langle r^2 \rangle_c} \right] \right\} + \dots \quad (3.39)$$

with atomic spin $F = 0, 1$ and with ellipses representing terms of $(Z\alpha)^7$ or higher. Here $\langle r_{pp} \rangle$ is yet another nuclear parameter (whose detailed form is found in [56], but whose precise definition is not needed in what follows).

3.3.2 Matching to RG-invariants

Eqs. (3.37), (3.38) and (3.39) seem to involve a lot of nuclear parameters. But while it is true that these parameters all capture something different (and in principle measurable) about the electromagnetic properties of nuclei, a major point in this paper (and of [64]) is that these nuclear parameter do not all appear independently if one’s interest is only the very low energies accessed by atomic energy shifts.

The formalism used in this paper captures nuclear effects using dramatically fewer parameters, and can do so because it expands from the get-go in powers of the small ratio of nuclear to atomic size. It is the timely use of this low-energy approximation that underlies its simplicity. Furthermore, it does *not* make assumptions about the validity of any particular nuclear models (including dynamical effects, such as polarizabilities). It is therefore guaranteed to capture all possible nuclear effects for atomic levels, and must in particular include the predictions of any specific model. In particular, this means that the energy-shift formulae (3.37), (3.38) and (3.39) must agree with those computed in earlier sections, for some choice of the parameters $\epsilon_{\star+}$, $\epsilon_{\star-}$ and ϵ_F .

In this section we compare our predictions for the nucleus-generated $nS_{1/2}$ and $nP_{1/2}$ energy shifts to the above results and by doing so identify (or ‘match’) how the parameters $\epsilon_{\star+}$, $\epsilon_{\star-}$ and ϵ_F are related to the various moments appearing in (3.37), (3.38) and (3.39). Doing so also shows that the traditional moments always appear together in these three combinations, so for the purposes of calculating atomic energy shifts there are fewer independent ‘effective’ nuclear moments than one might naively think.

To this end, the energy shift computed for $nS_{1/2}$ and $nP_{1/2}$ states using the steps above starting from (C.10), for the spin-independent nuclear-size contribution – accurate to order $(Z\alpha)^5 m^4 R^3$ and $(Z\alpha)^6 m^3 R^2$ – written using the RG-invariant $\epsilon_{\star\pm}$ is given

by [64]

$$\delta\omega_{n\frac{1}{2}+}^{(0)} = \frac{8(Z\alpha)^2}{n^3} \left(\frac{m_r}{m}\right)^2 m_r^3 y_{\star+} \epsilon_{\star+}^2 \left\{ 1 + (Z\alpha)^2 \left[\frac{12n^2 - n - 9}{4n^2(n+1)} - \ln\left(\frac{2Z\alpha m_r \epsilon_{\star+}}{n}\right) + 2 - \gamma - H_{n+1} \right] \right\} + \dots \quad (3.40)$$

$$\delta\omega_{n\frac{1}{2}-}^{(0)} = +2 \left(\frac{n^2 - 1}{n^5}\right) (Z\alpha)^4 \left(\frac{m_r}{m}\right)^2 m_r^3 \epsilon_{\star-}^2 + \dots, \quad (3.41)$$

where the ellipses represent terms of higher order in $(Z\alpha)^2$ and $(m\epsilon_{\star})$ than those written. In this expression we evaluate $\kappa_{nj}^D = Z\alpha m_r / \mathcal{N} \simeq Z\alpha m_r / n + \dots$, with $m_r = mM / (m + M)$ being the system's reduced mass.

Earlier sections in this paper also compute the nuclear-size-related effects at linear order in the nuclear spin – *i.e.* linear in \mathfrak{s} – using the effective couplings with dimension (length)² in S_p . The result obtained from (3.30) and (3.29) gives,

$$\delta\omega_{nF\frac{1}{2}+}^{(1)} = -\mathfrak{s} X_F \frac{8(Z\alpha)^2}{n^3} \left(\frac{m_r}{m}\right)^2 m_r^3 \epsilon_F^2 + \dots, \quad (3.42)$$

where ellipses represent terms higher order in $m\epsilon_F$ and $(Z\alpha)^2$ than those written (such as the mixed hyperfine, finite-size effects for negative-parity, $j = \frac{1}{2}$ states found in [30]). To this same accuracy no finite-size corrections enter into the $j = \frac{1}{2}$ negative-parity energy shift.

We now can compare formulae to read off expressions for the RG-invariant scales $\epsilon_{\star\pm}$ and ϵ_F . We do so starting with the parity-even spin-independent shifts – *i.e.* equating (3.37) to (3.40), excluding the terms suppressed relative to the leading one by $(R/a_B)^2$, – which requires the following terms to agree for all n :

$$\begin{aligned} & \frac{8(Z\alpha)^2}{n^3} \left(\frac{m_r}{m}\right)^2 m_r^3 y_{\star+} \epsilon_{\star+}^2 \left\{ 1 + (Z\alpha)^2 \left[\frac{12n^2 - n - 9}{4n^2(n+1)} + 2 - \gamma - H_{n+1} - \ln\left(\frac{2Z\alpha m_r \epsilon_{\star+}}{n}\right) \right] \right\} \\ &= \frac{2}{3} (Z\alpha)^4 \frac{m_r^3}{n^3} \langle r^2 \rangle_c \left\{ 1 + (Z\alpha)^2 \left[\frac{1}{n} + 3 - H_{n-1} - \gamma - \frac{9}{4n^2} - \ln\left(\frac{2Z\alpha m_r \langle r_{c2} \rangle}{n}\right) \right] \right\} - \frac{m_r^4}{3n^3} (Z\alpha)^5 \langle r^3 \rangle_{cc}^{\text{eff}}. \end{aligned} \quad (3.43)$$

First off, agreement on the overall sign requires $y_{\star+} = +1$. Second, although these at first sight appear to differ in their n dependence, writing H_{n+1} in terms of H_{n-1} (and a little algebra) shows this to be an illusion. They agree provided only that the

RG-invariant $\epsilon_{\star+}$ is chosen to be (at this order)

$$\epsilon_{\star+}^2 := \frac{(Z\alpha)^2}{12} \left(\frac{m}{m_r}\right)^2 \left\{ \langle r^2 \rangle_c \left[1 + (Z\alpha)^2 \left(1 + \frac{1}{2} \ln \left[\left(\frac{m}{m_r}\right)^2 \frac{(Z\alpha)^2 \langle r^2 \rangle_c}{12 \langle r_{c2} \rangle^2} \right] \right) \right] - \frac{1}{2} m_r (Z\alpha) \langle r^3 \rangle_{cc}^{\text{eff}} \right\}. \quad (3.44)$$

A similar exercise for the parity odd states compares the leading term in (3.38) to (3.41), giving agreement when

$$\epsilon_{\star-}^2 := \frac{(Z\alpha)^2}{12} \left(\frac{m}{m_r}\right)^2 \langle r^2 \rangle_c, \quad (3.45)$$

to the order required. Several things are noteworthy about these expressions

- First, notice that to the order we work this also implies

$$\epsilon_{\star+} = \epsilon_{\star-} =: \epsilon_{\star}, \quad (3.46)$$

as perhaps might have been expected for a parity-preserving nucleus. In particular, to the order we work only a single parameter controls the entire contribution to spin-independent nuclear-size-related energy shifts.

- Second, nuclear effects ultimately enter through so few parameters because they can only influence atomic properties by changing the value of the integration constant \mathcal{D}/\mathcal{C} arising when integrating the radial mode equation. The total number of independent parameters necessary is therefore given by the number of integration constants available. Although each partial wave contributes an independent integration constant, each partial wave is also suppressed at the nuclear position by additional powers of $Z\alpha$. Constants associated with higher partial waves can only enter energy shifts once a minimal precision is required in powers of $Z\alpha$.
- Third, notice that matching implies the overall size $\epsilon_{\star} \sim Z\alpha R$, where $R \sim 1$ fm is a typical nuclear-physics scale (that arises from $\langle r^2 \rangle_c \sim R^2$). This shows how ϵ_{\star} encodes both the nucleus' intrinsic size, but also the strength with which this size is probed. Because electromagnetic forces are weak it follows that $\epsilon_{\star} \ll R$.
- Finally, matching shows that the independent parameters ϵ_{\star} and ϵ_F depend explicitly on the lepton mass, and so parameters as measured using atomic Hydrogen do not directly apply to muonic Hydrogen. Although in principle this mass dependence can be computed, its calculation involves more detailed information about

the nuclear moments. From the point of view of minimizing nuclear-physics related errors we therefore treat parameters like ϵ_* as being independent for muonic and electronic Hydrogen.

A similar comparison can be done for the spin-dependent nuclear-size contributions – *i.e.* eqs. (3.42) and (3.39). Since (3.42) only works to leading-order accuracy we restrict to comparing only with the first term in (3.39) when inferring the value for ϵ_F^+ . Doing so shows they agree provided we identify

$$\epsilon_F^2 = \frac{(Z\alpha)^2 \langle r \rangle_{cm}}{4m_r} + \dots \quad (3.47)$$

The ellipses show that this comparison can receive corrections once the matching is done at higher orders in the ratio of nuclear to atomic size (R/a_B), or of α .

4 Predictions for energy shifts

This section takes the previous section's results for how atomic energy levels depend on finite nuclear size, and uses them to identify observables from which nuclear effects can be eliminated. Most of the discussion is aimed at electrons orbiting a proton (ordinary Hydrogen), but (motivated by the prospects of improving measurements) implications are also explored for muonic Hydrogen.

4.1 Isolating finite-nucleus effects

The main idea is simple: electronic energy levels are given (to the accuracy needed here) by (2.25) – and the discussion immediately following (2.25) – using also (3.21). The result is rewritten here as

$$\omega_{nFj\varpi} = \omega_{nFj\varpi}^{\text{pt}} + \omega_{nFj\varpi}^{\text{NS}}, \quad (4.1)$$

where

$$\begin{aligned} \omega_{nFj\varpi}^{\text{pt}} &= \omega_{nj}^D + \varepsilon_{nFj\varpi}^{\text{hfs}} + \varepsilon_{nFj\varpi}^{(ho)} + \varepsilon_{nFj\varpi}^{\text{QED}} + \varepsilon_{nFj\varpi}^{\text{pt-rec}} \\ \omega_{nFj\varpi}^{\text{NS}} &= \delta\omega_{nj\varpi}^{(0)} + \delta\omega_{nFj\varpi}^{(1)} + \delta\varepsilon_{nFj\varpi}^{(1)} + \varepsilon_{nFj\varpi}^{\text{N-QED}} + \varepsilon_{nFj\varpi}^{\text{N-rec}}. \end{aligned} \quad (4.2)$$

Here $\omega_{nFj\varpi}^{\text{pt}}$ contains all terms that would be present for a spinning point nucleus: ω_{nj}^D being the Dirac-Coulomb energy levels of (2.23) and (2.24); $\varepsilon_{nFj\varpi}^{\text{hfs}}$ given by the hyperfine structure (2.47) caused by the point-nucleus's magnetic moment; $\varepsilon_{nFj\varpi}^{(ho)}$ containing the higher-order magnetic moment effects for a point nucleus; $\varepsilon_{nFj\varpi}^{\text{QED}}$ describing the series in powers of α that give all the QED corrections to the first two (including the Lamb

shift), also computed for a point nucleus; and $\varepsilon_{nFj\varpi}^{\text{pt-rec}}$ containing all point-nucleus recoil corrections [108] to the assumed order. All of these contributions are under good theoretical control and can be calculated in principle with very high precision. For our purposes all these contributions are conveniently summarized to our assumed precision in [105] for electronic Hydrogen and in [116] for its muonic counterpart.

All of the influence of nuclear size resides in $\omega_{nFj\varpi}^{NS}$ of (4.2). Of these, the first two terms, $\delta\omega_{nFj\varpi}^{(0)} + \delta\omega_{nFj\varpi}^{(1)}$, give the change of energy – *c.f.* eq. (C.10) – induced by the change in the small- r boundary condition that the presence of the nucleus generates. The superscripts on these expressions indicate their dependence on nuclear spin, with $\delta\omega^{(k)}$ being proportional to \mathfrak{s}^k , with \mathfrak{s} given in (2.35). For $nS_{1/2}$ and $nP_{1/2}$ states these are given explicitly by eqs. (3.40), (3.41) and (3.42). The contribution $\delta\varepsilon_{nFj\varpi}^{(1)}$, on the other hand, describes the nuclear-structure modifications to the hyperfine energy, given by the ϵ_F -dependent (and, in principle, \mathfrak{c} -dependent) terms in (3.30).

The rest of this section exploits the fact that nuclear effects enter into these quantities (to the order computed here) only through the two independent parameters ϵ_\star and ϵ_F .

The remaining nuclear terms, $\varepsilon_{nFj\varpi}^{N-QED}$ and $\varepsilon_{nFj\varpi}^{N-rec}$, complicate the details (but not the logic) of this exploitation, by complicating the formulae involved. These terms represent the non-pointlike nuclear finite-size contributions to the QED corrections and to recoil corrections, which are calculable (see below) but only depend on the value of ϵ_\star (or change the relationship between ϵ_\star , ϵ_F and nuclear moments), but do not introduce any new parameters of principle.

4.1.1 Nuclear corrections to QED contributions

There are several ways that QED corrections enter into the above story. The most direct way is as the perturbative expansion in the bulk interaction $\mathcal{L}_{QED\text{int}} = ieA_\mu \bar{\Psi}\gamma^\mu\Psi$ of the bulk lagrangian (1.4). For graphs involving only electrons and photons these may be evaluated in the usual way, with the usual results.

What is unusual about the QED Feynman rules obtained from the action given in (1.4) and (1.5) is the Feynman rules for the nuclear degrees of freedom. In the effective theory used here the only nuclear degrees of freedom are its first-quantized center-of-mass position, $y^\mu(\tau)$, and its spin, $\xi^\mu(\tau)$. In deriving this action all other nuclear degrees of freedom are integrated out, leaving them to contribute to low-energy observables only through their contributions to effective interactions like c_s , c_v , c_F and so on. But the graphs can nonetheless be evaluated, with the functional integration over y^μ capturing in particular nuclear-recoil effects associated with the nucleus' motion in response to electron/photon interactions.

From this point of view the nuclear finite-size corrections to long-distance QED effects are calculated by evaluating Feynman graphs involving the nuclear effective couplings c_s , c_v and so on. No new independent constants enter in these corrections because they are explicitly built from the same couplings that are used to define the parameters ϵ_\star and ϵ_F , implying the existence of a formula of the form $\epsilon_{nFj\varpi}^{N-QED} = \epsilon_{nFj\varpi}^{N-QED}(\epsilon_\star, \epsilon_F)$, whose explicit form we require in the steps outlined below.

Rather than evaluating the c_i -dependent Feynman graphs (with $i = s, v, F$) to compute this function ab-initio, we instead are able to infer the result using standard evaluations of nuclear corrections to QED effects found in the literature. The procedure is very different for electrons and muons, so we treat them separately in what follows.

Electrons

For atomic Hydrogen one-loop QED corrections involve a vacuum polarization loop as well as one-loop vertex corrections for both the electron and nuclear couplings. The energy shift obtained by evaluating these graphs in a second-quantized theory of nucleons coupled to QED gives the following nucleus-dependent QED energy corrections [106],

$$\begin{aligned} \epsilon_{nF\frac{1}{2}^+}^{N-QED}(e) = & \frac{2}{3} (4 \ln 2 - 5) \alpha (Z\alpha)^5 \frac{m_r^3}{n^3} \langle r^2 \rangle_c \\ & + \mathfrak{s} X_F \left(\frac{m_r}{m} \right)^2 \frac{\alpha (Z\alpha)^4}{\pi n^3} m_r^2 \langle r \rangle_{cm} \left\{ \frac{5}{2} - \frac{4}{3} \left[\ln \left(\frac{\Lambda^2}{m^2} \right) - \frac{317}{105} \right] \right\}. \end{aligned} \quad (4.3)$$

Here Λ is a nuclear energy scale related to the dipole parameterization of the nuclear form factors used when evaluating the nuclear electromagnetic vertices in these graphs. To translate this into a useful form for the present purposes, all of the model-dependent variables – like Λ and the moments $\langle r^2 \rangle_c$ and $\langle r \rangle_{cm}$ – must be traded for a dependence on the existing variables ϵ_\star and ϵ_F (as we know must be possible).

This is a particularly simple process for electrons, and it is simple because the important scales circulating within the QED loops have energies of order the electron mass. As a result they involve very high energies relative to the scales allowed in our low-energy effective description. Because of this any QED loop-generated effects that explicitly involve nuclear properties can only influence physics within a Compton wavelength of the nucleus, and so from the point of view of the EFT can be described by a local operator localized at the nuclear position. But because the action S_p of (1.5) and (2.5) contains the most general local interactions involving the given degrees of freedom, *any* nucleus-dependent QED loops can simply be regarded as shifting the values of the effective couplings that are conceived to be functions of nuclear properties, and so correcting the formulae (3.44) and (3.47).

Because of this the nucleus-dependent energy shift contributed by QED loops are given by precisely the same formulae as above – *i.e.* eqs. (3.40) and (3.39). Within this picture the spin-independent and spin-dependent parts of (4.3) are completely captured by *omitting* $\varepsilon_{nF\frac{1}{2}+}^{N-QED}$ and then simply by using the modified results

$$\epsilon_{\star}^2 = \frac{(Z\alpha)^2}{12} \left(\frac{m}{m_r}\right)^2 \left\{ \langle r^2 \rangle_c \left[1 + (Z\alpha)^2 \left(1 + \frac{1}{2} \ln \left[\left(\frac{m}{m_r}\right)^2 \frac{(Z\alpha)^2 \langle r^2 \rangle_c}{12 \langle r_{C2} \rangle^2} \right] \right) + \alpha(Z\alpha)(4 \ln 2 - 5) \right] - \frac{1}{2} m_r (Z\alpha) \langle r^3 \rangle_{cc}^{\text{eff}} + \dots \right\}, \quad (4.4)$$

and

$$\epsilon_F^2 := \frac{(Z\alpha)^2 \langle r \rangle_{cm}}{4m_r} \left\{ 1 + \frac{\alpha}{\pi} \left(\frac{2}{3} \left[\ln \left(\frac{\Lambda^2}{m^2} \right) - \frac{317}{105} \right] - \frac{5}{4} \right) + \dots \right\} \quad (4.5)$$

instead of (3.44) and (3.47) in the remainder of the energy shifts: eqs. (3.40), (3.41) and (3.42).

Muons

Incorporation of nucleus-dependent one-loop QED corrections can be done in a similar way for muonic Hydrogen, though with an important difference. The explicit one-loop calculation has been done for muonic Hydrogen, with the result [30, 106, 109, 110]

$$\begin{aligned} \varepsilon_{nF\frac{1}{2}+}^{N-QED}(\mu) &= \frac{2}{3} (4 \ln 2 - 5) \alpha (Z\alpha)^5 \frac{m_r^3}{n^3} \langle r^2 \rangle_c \\ &+ X_{F5} \left(\frac{m_r}{m}\right)^2 \frac{\alpha (Z\alpha)^4}{\pi n^3} m_r^2 \langle r \rangle_{cm} \left\{ \frac{5}{2} - \frac{4}{3} \left[\ln \left(\frac{\Lambda^2}{m^2} \right) - \frac{317}{105} \right] \right\} \\ &+ \frac{4}{9n^3} \left[\frac{\alpha (Z\alpha)^4}{\pi} \right] m_r^3 \left\{ \langle r^2 \rangle_c - \frac{1}{2} Z\alpha m_r \langle r^3 \rangle_{cc}^{\text{eff}} \right\} \Xi_{n\frac{1}{2}+}, \end{aligned} \quad (4.6)$$

and

$$\varepsilon_{nF\frac{1}{2}-}^{N-QED}(\mu) = + \frac{4}{9n^3} \left[\frac{\alpha (Z\alpha)^4}{\pi} \right] m_r^3 \left\{ \langle r^2 \rangle_c - \frac{1}{2} Z\alpha m_r \langle r^3 \rangle_{cc}^{\text{eff}} \right\} \Xi_{n\frac{1}{2}-}. \quad (4.7)$$

The quantity $\Xi_{n_j\varpi}$ appearing here vanishes (to the order we work) for $j \neq \frac{1}{2}$, and is given for $j = \frac{1}{2}$ by

$$\begin{aligned}
 (Z\alpha)^2 \Xi_{n\frac{1}{2}\varpi} := & \left\{ \left(\frac{\mathbf{m}_e}{m_r} \right)^2 \frac{n(n-l-1)!}{[(n+l)!]^3} \int_0^\infty d\rho_0 e^{-\rho_0} \rho_0^{2l+1} [L_{n-l-1}^{2l+1}(\rho_0)]^2 \right. \\
 & \left. \times \int_1^\infty dx e^{-\left(\frac{\mathbf{m}_e}{m_r}\right)\frac{nx}{(Z\alpha)}\rho_0} \left(1 + \frac{1}{2x^2}\right) \sqrt{x^2-1} \right\} \\
 & + \left\{ \frac{(n-1)!}{n[(n)!]^3} \left(\frac{n}{2m_r}\right)^3 \left(\frac{2Z\alpha m_r}{n}\right) \right. \\
 & \left. \times \int \frac{d^3\rho_0}{\rho_0} e^{-\rho_0} L_{n-1}^1(\rho_0) G'(\rho_0, 0) L_{n-1}^1(0) \right. \\
 & \left. \times \int_1^\infty dx e^{-\left(\frac{\mathbf{m}_e}{m_r}\right)\frac{nx}{(Z\alpha)}\rho_0} \left(1 + \frac{1}{2x^2}\right) \frac{\sqrt{x^2-1}}{x^2} \right\} \delta_{\varpi+}, \tag{4.8}
 \end{aligned}$$

in which the factor of $(Z\alpha)^2$ is extracted so that $\Xi_{n\frac{1}{2}\varpi}$ is order unity.²²

In these expressions m and m_r denote, as usual, the muon mass and the muon-proton reduced mass, $m_r = mM/(m+M)$. The electron mass is here (and only here) denoted \mathbf{m}_e to emphasize that it is *not* the orbital lepton's mass, and enters through the contribution of electrons in virtual loops. The orbital-angular momentum quantum number l is the unique one consistent with $j = l \pm \frac{1}{2}$ and $\varpi = (-)^l$, while $\rho_0 = 2m_r Z\alpha r/n$ is the non-relativistic dimensionless radial variable of the Schrödinger-Coulomb problem and $L_n^k(x)$ are the associated Laguerre polynomials,

$$L_n^k(x) = \sum_{p=0}^n (-1)^p \frac{(n+k)!}{(n-p)!(k+p)!p!} x^p. \tag{4.9}$$

Finally $G'(x, 0)$ is the reduced Schrödinger-Coulomb Green's function for $nS_{1/2}$ states, which is not known for general n but is computed for $n = 2$ in [110] to calculate the above radiative corrections for the $2P - 2S$ Lamb shift in muonic Hydrogen.

All of the terms in (4.6) that do not involve $\Xi_{n\frac{1}{2}\varpi}$ come from the contributions of virtual muon loops, and so have the same functional form as did the electron loops for electronic Hydrogen. Because the important loop momenta for these graphs is set by the muon mass, their contribution to nucleus-dependent effects can also be captured by modifying the effective nuclear couplings. They consequently contribute to a shift in ϵ_\star and ϵ_F of the same form as in eqs. (4.4) and (4.5), but with m and m_r denoting the muon mass and the muon-proton reduced mass.

²²This factor of $(Z\alpha)^2$ can be displayed more explicitly by rescaling the integration variable $x \rightarrow \hat{x} := x/(Z\alpha)$.

It is the $\Xi_{n\frac{1}{2}\varpi}$ terms that are the key difference between the result (4.4) for electronic Hydrogen and (4.6) for muonic Hydrogen. These terms come from the vacuum polarization graph, in which virtual electrons circulate within the loop. Although the dominant momenta in this loop still have magnitudes of order the electron mass, the electron Compton wavelength is not much smaller than the muonic Bohr radius. This precludes absorbing this graph into the value of an effective coupling like ϵ_\star or ϵ_F .

To summarize, the full calculation of nucleus-induced energy shifts in muonic Hydrogen, including QED contributions [59, 106, 110], is captured by using the modified parameters ϵ_\star and ϵ_F of (4.4) and (4.5) in the energy shift (3.40), (3.41) and (3.42), *and* including only the electron loop separately, using

$$\epsilon_{nF\frac{1}{2}+}^{N-QED}(\mu) = \frac{16}{3n^3} \left[\frac{\alpha(Z\alpha)^2}{\pi} \right] \left(\frac{m_r}{m} \right)^2 m_r^3 \epsilon_\star^2 \Xi_{n\frac{1}{2}+}. \quad (4.10)$$

For electronic Hydrogen this last contribution is not separately required.

4.1.2 Structure-dependent recoil corrections

The arguments used above for QED corrections apply equally well to recoil corrections. Recoil corrections for a point nucleus are well-known, $\epsilon_{nFj\varpi}^{\text{pt-rec}}$, $\epsilon_{nFj\varpi}^{N\text{-rec}}$ [111–114] as are many explicit nuclear-size contributions, the leading ones of these that are not simply due to substitutions of reduced mass into the charge-radius term give [29, 52, 108, 109]

$$\epsilon_{nFj\varpi}^{N\text{-rec}} = -\frac{(Z\alpha)^5}{n^3} \left(\frac{m_r^3}{M} \right) \langle r \rangle_{cm}, \quad (4.11)$$

where we see the Zemach radius, $\langle r \rangle_{cm}$ emerge in a spin-independent context.

What matters is that to this order the n -dependence of this result is precisely the same as that of eqs. (3.40), and so it can be absorbed into $\delta\omega_{nFj\varpi}^{(0)}$ by shifting ϵ_\star from the value given in (4.4) by adding the new contribution

$$\delta\epsilon_\star^2 = -\frac{(Z\alpha)^3}{12} \left(\frac{m}{m_r} \right)^2 \frac{\langle r \rangle_{cm}}{M}. \quad (4.12)$$

The upshot is that these nuclear recoil terms, though numerically significant, only modify the relationship between ϵ_\star and nuclear properties; what they do not change is the functional form of (3.40) as a function of ϵ_\star .

4.1.3 Observables

The above sections use a first-quantized EFT to compute all spin-independent nuclear-size contributions to atomic energy levels that arise at orders $(Z\alpha)^4 m^3 R^2$, $(Z\alpha)^5 m^4 R^3$

and $(Z\alpha)^6 m^3 R^2$, plus all contributions linear in nuclear spin out to order $\mathfrak{s} m^2 R (Z\alpha)^4$. We show that the results agree with the extant calculations in the literature [105, 106, 116]. Most importantly these calculations show that, on very general grounds, the many nuclear moments that arise in standard calculations are all captured as contributions to only two independent effective parameters, our ϵ_\star and ϵ_F . In this section we use these results to predict the size of numerous atomic transition energies. By fitting the two parameters ϵ_\star and ϵ_F themselves from well-measured atomic transitions we remove the usual nuclear uncertainties from these calculations.

We focus first on atomic Hydrogen, since for this many more transitions are measured, but these same techniques can equally well be applied to muonic Hydrogen. The main difference for muonic Hydrogen is the relative scarcity of measured transitions, though those that have been measured have been done with spectacular accuracy. We provide a single prediction for a soon-to-be-measured muonic Hydrogen transition at the end of this section.

As ever, our starting point is the energy-level expressions (4.1) and (4.2), reproduced again here:

$$\omega_{nFj\varpi} = \omega_{nFj\varpi}^{\text{pt}} + \omega_{nFj\varpi}^{\text{NS}}, \quad (4.13)$$

where (4.2) gives the point-nucleus contribution, and is regarded here to be a known quantity (since our focus is on nuclear contributions), evaluated to any desired accuracy. Eq. (4.2) also gives the nuclear-size part of the level shifts as

$$\omega_{nFj\varpi}^{\text{NS}} := \delta\omega_{nFj\varpi}^{(0)} + \delta\omega_{nFj\varpi}^{(1)} + \delta\epsilon_{nFj\varpi}^{(1)} + \epsilon_{nFj\varpi}^{\text{N-QED}}, \quad (4.14)$$

where the first three terms are considered in detail in this paper given by (3.40), (3.41), (3.42) and (3.22), in which the parameters $y_{\star+} = +1$, as well as ϵ_\star and ϵ_F first arise. The final term is the nuclear QED radiative correction $\epsilon_{nFj\varpi}^{\text{N-QED}}$ of (4.10), that only need be considered for muonic Hydrogen (because, as shown above, all of the other nucleus-dependent QED effects can be absorbed into (3.40), (3.41) and (3.42) when one uses (4.4) and (4.5) for ϵ_\star and ϵ_F rather than (3.44) and (3.47)). $\epsilon_{nFj\varpi}^{\text{N-rec}}$ is omitted from this formula because it can also be absorbed into (3.40) through the shift (4.12). In practice the nuclear corrections of interest here are only important for $j = \frac{1}{2}$ states; the case to which we specialize below.

Of course, the observables of experimental interest are not atomic energies, they are the frequencies, $\nu(nL_j^F - n'L_{j'}^{F'})$, of radiation emitted in a transition between an initial state nL_j^F and a final state $n'L_{j'}^{F'}$. These are what can be measured with great precision, and are given in terms of energy differences of the initial and final states,

$$\nu(nL_j^F - n'L_{j'}^{F'}) = (\omega_{nFj\varpi}^{\text{pt}} - \omega_{n'F'j'\varpi'}^{\text{pt}}) + (\delta\omega_{nFj\varpi}^{\text{NS}} - \delta\omega_{n'F'j'\varpi'}^{\text{NS}}) + (\epsilon_{nFj\varpi}^{\text{N-QED}} - \epsilon_{n'F'j'\varpi'}^{\text{N-QED}}). \quad (4.15)$$

The next two sections use the two best-measured values for these frequencies to determine ϵ_\star and ϵ_F , from which predictions can be made for all other levels without introducing any uncertainties associated with the model-dependence of explicit nuclear calculations. What makes this strategy work is the observation that only these two parameters are needed, to the accuracy we work. All of the many potentially relevant nuclear moments that are naively needed to this accuracy actually only appear in atomic energy shifts through the two formulae (4.4) and (4.5) that predict the values for the two parameters ϵ_\star and ϵ_F . But one never need compute these two parameters from moments if one instead infers them directly from atomic experiments.

Precisely how many parameters are required for any given accuracy? The answer depends on the number of powers of $Z\alpha$ and in R/a_B one wishes to keep (where a_B is the relevant Bohr radius and $R \sim 1$ fm is a typical nuclear length scale), since this controls when the values of new integration constants like \mathcal{D}/\mathcal{C} for higher spherical harmonics become needed. Table 1 gives the size of various nuclear contributions to energy levels, obtained by estimating the size of nuclear moments to be $\langle r^k \rangle \sim R^k$. For each order in the expansion in powers of $Z\alpha$ and $R/a_B \sim mRZ\alpha$, this table also shows how many parameters are in principle required.

Estimates for the numerical size of each contribution is given in Table 1 for both atomic Hydrogen (for which $mRZ\alpha \ll Z\alpha$), and for muonic Hydrogen (for which $mRZ\alpha \sim Z\alpha$). We consider each of these two cases in turn.

4.2 Atomic Hydrogen

In atomic Hydrogen the three most accurately measured transitions are [6, 8, 105]

$$\begin{aligned} \nu \left(1S_{\frac{1}{2}}^{F=1} - 1S_{\frac{1}{2}}^{F=0} \right) &=: \nu_{1S_{hfs}} = 1\,420\,405.751\,768(1) \text{ kHz}, \\ \nu \left(2S_{\frac{1}{2}}^{F=1} - 2S_{\frac{1}{2}}^{F=0} \right) &=: \nu_{2S_{hfs}} = 177\,556.834\,3(67) \text{ kHz}, \\ \nu \left(2S_{\frac{1}{2}}^{F=1} - 1S_{\frac{1}{2}}^{F=1} \right) &=: \nu_{21} = 2\,466\,061\,102\,474.806(10) \text{ kHz}, \end{aligned} \tag{4.16}$$

which have experimental errors of size 10^{-6} kHz, 6.7×10^{-3} kHz and 10^{-2} kHz respectively. A large library of other measured transitions having experimental errors of 1 kHz or worse is given in [6], and similar precision also arises in more recent experiments, such as the recent $3S_{\frac{1}{2}}^{F=1} - 1S_{\frac{1}{2}}^{F=1}$ and Lamb shift measurements of atomic Hydrogen in [25] and [26] respectively. Many of these transitions are reproduced here in Tables 5 through 7.

As Table 1 shows, for atomic Hydrogen the two parameters ϵ_\star and ϵ_F suffice to describe nuclear contributions to atomic energy shifts down to an accuracy of about 10^{-3} kHz, which is much smaller than the ~ 1 kHz experimental accuracy listed [6]

for most of the transitions appearing in Tables 5 through 7. For ease of comparison, contributions of order 10^{-3} kHz are shaded in green in Table 1. Notice in particular that these estimates show that the contributions of $\delta\varepsilon_{nFj\varpi}^{(1)}$ coming from \mathbf{c} in (2.48), which first arise at order $\mathfrak{s} m^3 R^2 (Z\alpha)^5$, are too small to be relevant at an accuracy of a Hz, and so can be neglected in what follows.

Fitting for ϵ_{\star} and ϵ_F

Before providing more precise numerical estimates for nuclear transitions we provide the explicit formulae to be used to obtain them. Recalling that all ϵ_{\star} and ϵ_F dependence appears in eqs. (3.40), (3.41) and (3.42) and that (3.22) can be neglected, and that we can set $y_{\star+} = +1$ and (for electrons) $\varepsilon_{nFj\varpi}^{N-QED} = 0$, the nucleus-dependence of the parity-even $j = \frac{1}{2}$ levels is

$$\delta\omega_{nF\frac{1}{2}+}^{\text{NS}}(e) = \frac{8}{n^3} \left(\frac{m_r}{m_e}\right)^2 (Z\alpha)^2 m_r^3 \left\{ \epsilon_{\star,e}^2 \left[1 + (Z\alpha)^2 \left(2 - \gamma - H_{n+1} - \ln \left(\frac{2Z\alpha m_r \epsilon_{\star,e}}{n} \right) + \frac{12n^2 - n - 9}{4n^2(n+1)} \right) \right] - \left(\frac{g_N m_e}{2M} \right) Z\alpha \epsilon_{F,e}^2 X_F \right\} \quad (4.17)$$

where the subscript ‘e’ again emphasizes that this expression applies only for electronic (and not muonic) Hydrogen-like atoms with spin-half nuclei. Here X_F is defined in (2.34) and we leave factors of nuclear charge, Z , explicit in the answer (for applications to general spin-half nuclei), although take $Z = 1$ for our numerical applications to Hydrogen. As above, M denotes the nuclear mass and we write its magnetic moment as $\mu_N = Zeg_N/(2M)$ (specializing to Hydrogen via the replacement $g_N \rightarrow g_p$). The analogous formula for parity-odd $j = \frac{1}{2}$ states is

$$\delta\omega_{nF\frac{1}{2}-}^{\text{NS}}(e) = 2(Z\alpha)^4 \left(\frac{n^2 - 1}{n^5}\right) \left(\frac{m_r}{m_e}\right)^2 m_r^3 \epsilon_{\star,e}^2. \quad (4.18)$$

Since terms not proportional to X_F cancel from any hyperfine interval, we fix $\epsilon_{F,e}$ using the experimentally measured $2S$ hyperfine splitting frequency (4.17). Using (for $j = \frac{1}{2}$ states) $X_F = +\frac{2}{3}$ for $F = 1$ and $X_F = -2$ for $F = 0$, gives

$$\nu_{2S_{hfs}} = \left(\omega_{21\frac{1}{2}+}^{\text{pt}} - \omega_{20\frac{1}{2}+}^{\text{pt}} \right) - \frac{8}{3} \left(\frac{m_r}{m_e}\right)^2 \left(\frac{g_N m_e}{2M}\right) (Z\alpha)^3 m_r^3 \epsilon_{F,e}^2. \quad (4.19)$$

It is convenient to group together the experimentally measured value and the theoretical point-nucleus effects, since these are both regarded as given when effects related to

nuclear size are of interest. Define therefore the precisely known quantity

$$\widehat{\Delta\omega}_{nS_{hfs}} := \left(\omega_{n1\frac{1}{2}+}^{\text{pt}} - \omega_{n0\frac{1}{2}+}^{\text{pt}} \right) - \nu_{nS_{hfs}}, \quad (4.20)$$

in terms of which $\epsilon_{F,e}$ is accurately determined by

$$\widehat{\Delta\omega}_{2S_{hfs}} = \frac{8}{3} \left(\frac{m_r}{m_e} \right)^2 \left(\frac{g_N m_e}{2M} \right) (Z\alpha)^2 m_r^3 \epsilon_{F,e}^2. \quad (4.21)$$

Notice also that these formulae also predict the nuclear-size contributions to the two hyperfine transitions given in (4.16) are related by

$$\widehat{\Delta\omega}_{1S_{hfs}} = 8 \widehat{\Delta\omega}_{2S_{hfs}}. \quad (4.22)$$

We similarly use ν_{21} to fix $\epsilon_{*,e}$, while using (4.21) to eliminate $\epsilon_{F,e}$, and so

$$\begin{aligned} \nu_{21} = & \left(\omega_{21\frac{1}{2}+}^{\text{pt}} - \omega_{11\frac{1}{2}+}^{\text{pt}} \right) \\ & + (Z\alpha)^2 \left(\frac{m_r}{m_e} \right)^2 m_r^3 \epsilon_{*,e}^2 \left\{ 1 + (Z\alpha)^2 \left[2 - \gamma - \frac{17}{16} - \ln(Z\alpha m_r \epsilon_{*,e}) \right] \right\} \\ & - 8(Z\alpha)^2 \left(\frac{m_r}{m_e} \right)^2 m_r^3 \epsilon_{*,e}^2 \left\{ 1 + (Z\alpha)^2 \left[2 - \gamma - \frac{5}{4} - \ln(2Z\alpha m_r \epsilon_{*,e}) \right] \right\} \\ & - \frac{1}{4} \widehat{\Delta\omega}_{2S_{hfs}} + 2 \widehat{\Delta\omega}_{2S_{hfs}}, \end{aligned} \quad (4.23)$$

which can be rewritten

$$\begin{aligned} \widehat{\Delta\omega}_{21} = & -\frac{7}{4} \widehat{\Delta\omega}_{2S_{hfs}} \\ & + 7(Z\alpha)^2 \left(\frac{m_r}{m_e} \right)^2 m_r^3 \epsilon_{*,e}^2 \left\{ 1 + (Z\alpha)^2 \left[\frac{81}{112} - \gamma - \frac{8}{7} \ln 2 - \ln(Z\alpha m_r \epsilon_{*,e}) \right] \right\}, \end{aligned} \quad (4.24)$$

which defines the precisely known quantity

$$\widehat{\Delta\omega}_{21} := \left(\omega_{21\frac{1}{2}+}^{\text{pt}} - \omega_{11\frac{1}{2}+}^{\text{pt}} \right) - \nu_{21}. \quad (4.25)$$

For numerical purposes it is useful to have numerical values for these quantities, which are [105]

$$\widehat{\Delta\omega}_{1S_{hfs}} = 58.07(57) \text{ kHz}, \quad \widehat{\Delta\omega}_{2S_{hfs}} = 7.22(57) \text{ kHz} \quad \text{and} \quad \widehat{\Delta\omega}_{21} = 955.31(57) \text{ kHz}, \quad (4.26)$$

which also shows that (4.22) is satisfied, within the errors.

Eq. (4.24), has the form

$$\mathfrak{x}_e = z_e (\eta_e - \ln z_e) = -z_e \ln (e^{-\eta_e} z_e), \quad (4.27)$$

with $z_e := (m_r \epsilon_{\star,e})^2$ and

$$\begin{aligned} \mathfrak{x}_e &:= 2 \left(\frac{m_e}{m_r} \right)^2 \frac{\left(\widehat{\Delta\omega}_{21} + \frac{7}{4} \widehat{\Delta\omega}_{2S_{hfs}} \right)}{7m_r (Z\alpha)^4}, \\ \eta_e &:= \frac{2}{(Z\alpha)^2} - 2 \ln(Z\alpha) + \frac{81}{56} - 2\gamma - \frac{16}{7} \ln 2. \end{aligned} \quad (4.28)$$

This is to be solved for z , and so has solutions given by branches of the Lambert W -function²³

$$(m \epsilon_{\star,e})^2 = e^{\mathcal{W}} \quad \text{with} \quad \mathcal{W} := W_{-1}(-\mathfrak{x}_e e^{-\eta_e}) + \eta_e. \quad (4.29)$$

The Lambert W -function returns real values only for real arguments in the range $x > -e^{-1}$, and is double valued for arguments $-e^{-1} < x < 0$. One of the branches takes values $-1 < W_0(x) < 0$ while the other satisfies $W_{-1} < -1$ in this range. We choose the branch, $W_{-1}(x)$, here because $(m_r \epsilon_{\star,e})^2$ is both real and small, and because $Z\alpha \ll 1$ implies $\eta_e \gg 1$. These two statements are only consistent with one another, and with eq. (4.29), if $W(x)$ is order $-\eta_e$ for x near zero. The numerical values inferred in this way for ϵ_{\star} and ϵ_F are given in Table 2.

Given these explicit solutions for $\epsilon_{\star,e}$ and $\epsilon_{F,e}$ as functions of the two well-measured energy differences (combined with well-understood point-nucleus theory contributions) we may now use these to directly express predictions for the nuclear part of the energy shift for any other energy levels, without direct reference to nuclear physics. For parity-even $j = \frac{1}{2}$ states this gives

$$\begin{aligned} \delta\omega_{nF\frac{1}{2}+}^{\text{NS}}(e) &= \frac{8}{n^3} (Z\alpha)^2 \left(\frac{m_r}{m_e} \right)^2 m_r e^{\mathcal{W}} \\ &\times \left\{ 1 + (Z\alpha)^2 \left[2 - \gamma - H_{n+1} - \ln \left(\frac{2Z\alpha}{n} \right) - \frac{\mathcal{W}}{2} + \frac{12n^2 - n - 9}{4n^2(n+1)} \right] \right\} \\ &- \frac{3}{n^3} X_F \widehat{\Delta\omega}_{2S_{hfs}}, \end{aligned} \quad (4.30)$$

while for parity-odd $j = \frac{1}{2}$ states one instead finds

$$\delta\omega_{nF\frac{1}{2}-}^{\text{NS}}(e) = 2 \left(\frac{n^2 - 1}{n^5} \right) (Z\alpha)^4 \left(\frac{m_r}{m_e} \right)^2 m_r e^{\mathcal{W}}. \quad (4.31)$$

²³ $W(z)$ is defined as the solution to $W(z) e^{W(z)} = z$, and is multiple-valued with branches labelled by an integer k . The branches relevant for real z are $W_0(z)$, which is defined for $z > 0$, and $W_{-1}(z)$, whose argument satisfies $e^{-1} < z < 0$.

Transition	$\left(2S_{1/2}^{F=1} - 2S_{1/2}^{F=0}\right)$	$\left(2S_{1/2}^{F=1} - 1S_{1/2}^{F=1}\right)$
Experimental value	177 556.834 3 (kHz)	2 466 061 102 474.806 (kHz)
Experimental error	0.0067 (kHz)	0.010 (kHz)
Pt. nucl. theory	177 564.05 (kHz)	2 466 061 103 430.12 (kHz)
Pt. nucl. error	0.57 (kHz)	0.57 (kHz)
Inferred param.	$(m\epsilon_{F,e})^2$	$(m\epsilon_{*,e})^2$
Fitted value	3.71×10^{-8}	2.1020×10^{-11}
Prop. exp. error	0.0035×10^{-8}	0.000034×10^{-11}
Prop. theory error	0.29×10^{-8}	0.0025×10^{-11}

Table 2: The experimental values (row 2), the experimental errors (row 3) and the point-nucleus theoretical values (row 4) and errors (row 5) for the reference transitions in atomic Hydrogen used for fixing the values of the two nuclear parameters listed in row 6. The last 3 rows give the values inferred for these parameters (row 7) and the errors they inherit due to the experimental uncertainty (row 8) and the precision of the point-nucleus calculation (row 9).

Transition frequencies are then simply given by differences of the above, for different choices for n and F .

There are three main sources of error when using expressions (4.30) and (4.31) for transition frequencies. One of these – the ‘truncation’ error – arises because the above expressions drop terms beyond a fixed order in $Z\alpha$ and $mRZ\alpha$. For electronic Hydrogen this truncation puts a floor of about 0.001 kHz to the nuclear contribution to atomic energy shifts. To this must also be added two other sources of error: the experimental accuracy with which the input quantities ν_{21} and $\nu_{2S_{hf_s}}$ are measured (with current values given in (4.16)), and the uncertainty with which the point-nucleus prediction for $\omega_{nFj\varpi}^{\text{pt}}$ is known (which is limited in principle by the persistence of theorists). All three sources of error can be much smaller than is permitted for explicit calculations of the nuclear moments using nuclear models, and can also expect to improve into the future unconstrained by limitations in nuclear modelling.

Table 3 lists several atomic levels (taken from [6] and [25, 26]) that are measured to better than 10 kHz accuracy, and compares for each the overall size of the nuclear-structure prediction of eqs. (4.30) and (4.31), as well as the three sources of error in this prediction described above. Tables 5 through 7 list these similar information for a larger class of measured transitions given in [6]. In all cases the nuclear error is much smaller than the current experimental uncertainties. Many rows of these tables share the same values because the only shift that is larger than 10^{-3} kHz in size arises from

Transition	ν_{exp}	ΔE^{fs}	ΔE^{exp}	ΔE^{th}	ΔE^{trunc}
$2P_{1/2}^{F=1} - 2S_{1/2}^{F=0}$	909 871.7(3.2)	-143.70	0.0069	0.57	0.00031
$1S_{1/2}^{F=1} - 1S_{1/2}^{F=0}$	1 420 405.751 768(1)	-57.8	0.054	4.5	0.0033
$8S_{1/2}^{F=1} - 2S_{1/2}^{F=1}$	770 649 350 012(9)	-134.348	0.0014	0.080	0.00010
$8D_{3/2}^{F=2,1} - 2S_{1/2}^{F=1}$	770 649 504 450(8)	-136.481	0.0014	0.081	0.00010
$8D_{5/2}^{F=3,2} - 2S_{1/2}^{F=1}$	770 649 561 584(6)	-136.481	0.0014	0.081	0.00010
$12D_{3/2}^{F=2,1} - 2S_{1/2}^{F=1}$	799 191 710 473(9)	-136.481	0.0014	0.081	0.00010
$12D_{5/2}^{F=3,2} - 2S_{1/2}^{F=1}$	799 191 727 404(7)	-136.481	0.0014	0.081	0.00010
$3S_{1/2}^{F=1} - 1S_{1/2}^{F=1}$	2 922 743 278 671.5 (2.6)	-1051.35	0.011	0.62	0.00079

Table 3: Transitions from [26] (row 2), from [6] (rows 3-8) and [25] (row 9) that are measured with better than 10 kHz accuracy in atomic Hydrogen. Column 2 gives their experimental values (with experimental errors in brackets); all values given in kHz. Column 4 gives the nuclear-finite-size contribution to the transition energy predicted by eqs. (4.30) and (4.31). Columns 5–7 give the uncertainties in this prediction: column 5 is the error from measurement errors in the reference transitions; column 6 gives the error due to theoretical uncertainty in the point-nucleus finite-size effects [105]; while column 7 is the error due to neglect of higher orders in \mathfrak{s} , $Z\alpha$ and $R/a_B = mRZ\alpha$ beyond those given by green squares in Table 1. Uncertainty in values for α and Ry give errors significantly smaller than those listed.

the shift of the S -wave state, which is common to many transitions in the list.

In our numerical evaluations of these formulae we use the values for binding energies as given in [105] to fit the two parameters $\epsilon_{*,e}, \epsilon_{F,e}$. The errors given in [105] for the point-nucleus parts of the theory are at the 0.1 kHz level (which as these authors report, is satisfactory for the current experimental precision). The implied uncertainty for transition energies (and so also for $\epsilon_{F,e}$) then is effectively twice as large because transition frequencies involve energy differences. The same large uncertainty inherently exists for $\epsilon_{*,e}$, which is found through a different interval of binding energies. Currently this error dominates both the experimental error and the ‘truncation’ uncertainty mentioned earlier. The good news is that the theoretical error in the point-nucleus part of the energy differences can be made much smaller simply by including higher-order calculations.

4.3 Muonic Hydrogen

Lastly, we comment on how the above calculations are adapted for muonic Hydrogen. The most accurate measurements of transitions in this system are [5, 19, 115]

$$\begin{aligned}\nu_t &:= \nu (2P_{3/2}^{F=2} - 2S_{1/2}^{F=1}) = 206.2927(27) \text{ meV}, \\ \nu_s &:= \nu (2P_{3/2}^{F=1} - 2S_{1/2}^{F=0}) = 225.8536(43) \text{ meV},\end{aligned}\tag{4.32}$$

with an experimental uncertainty of approximately 10^{-3} meV.

The last column of Table 1 shows the size for muonic Hydrogen of each term in the expansions in powers of $Z\alpha$ and $mRZ\alpha$, and in particular shows that the same orders considered above for electronic Hydrogen – *i.e.* spin-independent contributions at order $m^3R^2(Z\alpha)^4$, $m^4R^3(Z\alpha)^5$ and $m^3R^2(Z\alpha)^6$ together with the Zemach moment contribution at $m^2R\mathfrak{s}(Z\alpha)^4$ – also control nuclear effects in muonic Hydrogen down to a precision of about 0.01 meV. To this accuracy there are therefore only two nuclear parameters relevant, $\epsilon_{\star,\mu}$ and $\epsilon_{F,\mu}$, whose values can be inferred using the experimental results (4.32). Once a third transition frequency is measured nucleus-independent predictions can in principle be tested.

Calculations reaching the experimental precision of 10^{-3} meV, however, likely also require including contributions at order $m^5R^4(Z\alpha)^6$ (indicated in yellow in Table 1). Although these can be computed using the methods in this paper, we do not do so here, for several reasons. First, proper treatment of boundary conditions to this accuracy also requires generalizing S_p to include spin-independent effective couplings out to dimension (length)⁴, and spin-dependent couplings out to order (length)³. This in turn involves analyzing the running of the existing couplings out to higher accuracy in ρ_ϵ than was performed here. Furthermore, as Table 1 shows, this new term introduces the additional complication that corrections to the $j = \frac{3}{2}$ modes first become relevant at this order, potentially introducing a new integration constant, \mathcal{D}/\mathcal{C} , and possibly requiring the addition of a third RG invariant parameter. Although this requires nothing new conceptually, it is a considerable complication that we defer to future work.

In what follows we instead work only to the 0.01 meV accuracy that our calculations above already capture, and identify how the two independent parameters $\epsilon_{\star,\mu}$ and $\epsilon_{F,\mu}$ are determined by existing observations, and sketch how to use these to predict the nuclear-structure part of the predictions for any other muonic Hydrogen levels that might be measured in the future.

Determining ϵ_{\star} and ϵ_F

The finite-size effects in muonic Hydrogen, written in terms of RG-invariants and approximately accurate to order 10^{-3} meV in the spin-independent sector but only to

10^{-2} meV in the spin-dependent sector are captured by the sum of the contributions from (3.40), (3.41) and (3.42), as applied to the muon, as well as adding (4.10), giving

$$\begin{aligned} \delta\omega_{nF\frac{1}{2}+}^{\text{NS}}(\mu) + \varepsilon_{nF\frac{1}{2}+}^{N-QED}(\mu) = & \frac{8}{n^3} \left(\frac{m_r}{m_\mu}\right)^2 (Z\alpha)^2 m_r^3 \left\{ \epsilon_{*,\mu}^2 \left[1 + \left(\frac{2\alpha}{3\pi}\right) \Xi_{n\frac{1}{2}+} \right. \right. \\ & \left. \left. + (Z\alpha)^2 \left(2 - \gamma - H_{n+1} - \ln\left(\frac{2Z\alpha m_r \epsilon_{*,\mu}}{n}\right) + \frac{12n^2 - n - 9}{4n^2(n+1)} \right) \right] \right. \\ & \left. - \left(\frac{g_N m_\mu}{2M}\right) (Z\alpha) \epsilon_{F,\mu}^2 X_F \right\} \end{aligned} \quad (4.33)$$

which is of almost exactly the same form as in the electronic case, except for the term proportional to $\Xi_{nj\varpi}$ (defined in (4.8)) which encodes the radiative corrections to finite-size effects due to electron vacuum polarization. Similarly

$$\begin{aligned} \delta\omega_{nF\frac{1}{2}-}^{\text{NS}}(\mu) + \varepsilon_{nF\frac{1}{2}-}^{N-QED}(\mu) = & 2 \left(\frac{n^2 - 1}{n^5}\right) (Z\alpha)^4 \left(\frac{m_r}{m_\mu}\right)^2 m_r^3 \epsilon_{*,\mu}^2 \\ & + \frac{16}{3n^3} \left[\frac{\alpha(Z\alpha)^2}{\pi}\right] \left(\frac{m_r}{m_\mu}\right)^2 m_r^3 \epsilon_{*,\mu}^2 \Xi_{n\frac{1}{2}-}. \end{aligned} \quad (4.34)$$

We follow ref. [116] and define two useful combinations of the two measurements of (4.32), which help isolate the complications due to the electronic vacuum polarization. The first linear combination of measurements in [116] is largely dominated by the hyperfine energy contributions and is useful for extracting $\epsilon_{F,\mu}$ directly, much in the same way as was done for the $2S$ hyperfine splitting in the electronic case, leading to

$$\begin{aligned} \nu_s - \nu_t = & \left(\omega_{21\frac{3}{2}+}^{\text{pt}} - \omega_{20\frac{1}{2}+}^{\text{pt}}\right) - \left(\omega_{22\frac{3}{2}+}^{\text{pt}} - \omega_{21\frac{1}{2}+}^{\text{pt}}\right) \\ & - \frac{8}{3} \left(\frac{m_r}{m_\mu}\right)^2 \left(\frac{m_\mu e \mu_p}{4\pi}\right) (Z\alpha)^2 m_r^3 \epsilon_{F,\mu}^2. \end{aligned} \quad (4.35)$$

In this expression the point-nuclear theory terms combine into the hyperfine splitting combination for the $2S_{1/2}$ and the $2P_{3/2}$ states, motivating the definition

$$\widehat{\Delta\omega}_{hfs} := \left(\omega_{21\frac{1}{2}+}^{\text{pt}} - \omega_{20\frac{1}{2}+}^{\text{pt}}\right) - \left(\omega_{22\frac{3}{2}+}^{\text{pt}} - \omega_{21\frac{3}{2}+}^{\text{pt}}\right) - (\nu_s - \nu_t), \quad (4.36)$$

in terms of which a numerical value for $\epsilon_{F,\mu}$ can be obtained, since

$$\widehat{\Delta\omega}_{hfs} = \frac{8}{3} \left(\frac{m_r}{m_\mu}\right)^2 \left(\frac{m_\mu e \mu_p}{4\pi}\right) (Z\alpha)^2 m_r^3 \epsilon_{F,\mu}^2. \quad (4.37)$$

For later convenience we record the numerical value for the point-nucleus theoretical expressions, as collected by [116]. For the transitions ν_s and ν_t of (4.32) they are

$$\omega_{21\frac{3}{2}+}^{\text{pt}} - \omega_{20\frac{1}{2}+}^{\text{pt}} = 209.9450(26) \text{ meV} \quad \text{and} \quad \omega_{22\frac{3}{2}+}^{\text{pt}} - \omega_{21\frac{1}{2}+}^{\text{pt}} = 229.6813(34) \text{ meV}, \quad (4.38)$$

while for the hyperfine intervals one has

$$\omega_{21\frac{1}{2}+}^{\text{pt}} - \omega_{20\frac{1}{2}+}^{\text{pt}} = 22.9858 (26) \text{ meV} \quad \text{and} \quad \omega_{22\frac{3}{2}+}^{\text{pt}} - \omega_{21\frac{3}{2}+}^{\text{pt}} = 3.2480 (2) \text{ meV}, \quad (4.39)$$

which also include the state-mixing δ contribution²⁴ [116] that is part of $\varepsilon_{nFj\varpi}^{(ho)}$.

The second useful linear combination, $\frac{1}{4}(\nu_s + 3\nu_t)$ is defined so that the mixed hyperfine, finite-size effects tracked by the variable $\epsilon_{F,\mu}$ cancel – to the accuracy used here – and hence for our purposes also allows for a direct fit of the $\epsilon_{\star,\mu}$ parameter. The contributions that survive in this second combination are separated by the authors of [116] into various point-like theory effects including the traditional $(2P_{\frac{1}{2}} - 2S_{\frac{1}{2}})$ Lamb shift, and the nuclear-size dependent piece. In our present notation this second variable becomes

$$\begin{aligned} \frac{1}{4}(\nu_s + 3\nu_t) &= \frac{1}{4}(\omega_{21\frac{3}{2}+}^{\text{pt}} - \omega_{20\frac{1}{2}+}^{\text{pt}}) + \frac{3}{4}(\omega_{22\frac{3}{2}+}^{\text{pt}} - \omega_{21\frac{1}{2}+}^{\text{pt}}) \\ &\quad - \left(\frac{m_r}{m_\mu}\right)^2 (Z\alpha)^2 m_\mu^3 \epsilon_{\star,\mu}^2 \left\{ 1 + (Z\alpha)^2 \left[\frac{133}{48} - \gamma - H_3 - \ln(Z\alpha m_r \epsilon_{\star,\mu}) \right] \right. \\ &\quad \left. + \frac{2\alpha}{3\pi} (\Xi_{2\frac{1}{2}+} - \Xi_{2\frac{3}{2}+}) \right\}. \end{aligned} \quad (4.40)$$

Some useful numerical values as transcribed from [116] with the help of [115] are also quoted here for later use,

$$\begin{aligned} \frac{1}{4}(\omega_{21\frac{3}{2}+}^{\text{pt}} - \omega_{20\frac{1}{2}+}^{\text{pt}}) + \frac{3}{4}(\omega_{22\frac{3}{2}+}^{\text{pt}} - \omega_{21\frac{1}{2}+}^{\text{pt}}) &= 214.8846 (11) \text{ meV}, \\ \text{and} \quad \frac{2\alpha}{3\pi} (\Xi_{2\frac{1}{2}+} - \Xi_{2\frac{3}{2}+}) &= 0.0038556. \end{aligned} \quad (4.41)$$

These motivate the following definition

$$\widehat{\Delta\omega}_{Lamb} := \frac{1}{4}(\omega_{21\frac{3}{2}+}^{\text{pt}} - \omega_{20\frac{1}{2}+}^{\text{pt}} - \nu_s) + \frac{3}{4}(\omega_{22\frac{3}{2}+}^{\text{pt}} - \omega_{21\frac{1}{2}+}^{\text{pt}} - \nu_t), \quad (4.42)$$

which simplifies solving (4.40) for the value of $\epsilon_{\star,e}$. From here on in the argument proceeds much as for electrons, defining

$$\mathfrak{r}_\mu = z_\mu (\mathfrak{y}_\mu - \ln z_\mu), \quad (4.43)$$

with parameters

$$\begin{aligned} \mathfrak{r}_\mu &:= 2 \left(\frac{m_\mu}{m_r}\right)^2 \frac{\widehat{\Delta\omega}_{Lamb}}{(Z\alpha)^4 m_r}, \\ \mathfrak{y}_\mu &:= \frac{2}{(Z\alpha)^2} \left[1 + \frac{2\alpha}{3\pi} (\Xi_{2\frac{1}{2}+} - \Xi_{2\frac{3}{2}+}) \right] + \frac{15}{8} - 2\gamma - 2\ln(Z\alpha), \end{aligned} \quad (4.44)$$

²⁴This is a point-nucleus mixing of the $F = 1$ levels for $j = \frac{1}{2}$ and $j = \frac{3}{2}$ that arises at second order in the nuclear magnetic field.

Transition	$\nu_s - \nu_t$	$\frac{1}{4}(\nu_s + 3\nu_t)$
Exp. value (meV)	19.5609	211.1829
Exp. error (meV)	0.0051	0.0023
Pt. nucl. theory (meV)	19.7363	214.8791
Pt. nucl. error (meV)	0.0030	0.0025
Parameter	$(m\epsilon_{F,\mu})^2$	$(m\epsilon_{*,\mu})^2$
Inferred value	3.51×10^{-6}	3.30506×10^{-8}
Prop. exp. error	0.10×10^{-6}	0.00056×10^{-8}
Prop. theory error	0.060×10^{-6}	0.00064×10^{-8}

Table 4: Measured transitions in muonic Hydrogen and linear combinations of these measurements (row 2) that are useful for fitting finite-size effects. The experimental errors are given in row 3, the point-nucleus theoretical contributions in row 4 and the errors in these in row 5. The parameters that we fit for are given in row 6, their fitted values are in row 7, and their uncertainty coming from the propagated experimental error are in row 8, while that coming from propagated point-nucleus theoretical errors are in row 9.

leads to a solution involving the Lambert W -function

$$(m_r\epsilon_{*,\mu})^2 = e^{\mathcal{W}} \quad \text{where} \quad \mathcal{W} := W_{-1}(-\xi_\mu e^{-\eta_\mu}) + \eta_\mu. \quad (4.45)$$

This last equation, with (4.37), give the required solution for both $\epsilon_{*,\mu}$ and $\epsilon_{F,\mu}$ in terms of well-understood point-nucleus parts of the theory and experimental values. Using these in (4.33) and (4.34) for other energy levels allows other transition energies to be computed without the usual nuclear uncertainties. Predictions made in this way are completely independent of nuclear models and their associated inaccuracies.

As an application of the predictivity of these techniques consider the planned measurements of the ground state hyperfine splitting experiment of muonic Hydrogen, whose precision is expected to be $\sim 10^{-4}$ meV [23, 24], and whose value is expected to provide the Zemach moment of the proton to a higher accuracy. As discussed above, to obtain this same theoretical accuracy using the techniques pursued here requires including higher-order terms than have so far been computed. We nonetheless predict here, for illustrative purposes, the nuclear contribution to this amplitude to the accuracy possible with the calculations given above, and find

$$\delta\omega_{11\frac{1}{2}+}^{\text{NS}}(\mu) + \varepsilon_{11\frac{1}{2}+}^{N-QED}(\mu) - \delta\omega_{10\frac{1}{2}+}^{\text{NS}}(\mu) - \varepsilon_{10\frac{1}{2}+}^{N-QED}(\mu) = -1.415(48) \text{ meV}, \quad (4.46)$$

with the total uncertainty resulting from a net experimental error of (0.041) meV, net point-like theoretical error of (0.021) meV and a truncation error of (0.013) meV. For

comparison, a similar calculation directly using (3.39) and (4.6), and simply quoting the values of (and errors for) nuclear moments (and the parameter Λ) estimated from nuclear models [116] instead gives

$$\delta\omega_{11\frac{1}{2}+}^{\text{NS}}(\mu) + \varepsilon_{11\frac{1}{2}+}^{N-QED}(\mu) - \delta\omega_{10\frac{1}{2}+}^{\text{NS}}(\mu) - \varepsilon_{10\frac{1}{2}+}^{N-QED}(\mu) = -1.385(47) \text{ meV}, \quad (4.47)$$

which are consistent with comparable quoted errors. Even if one accepts that the errors in nuclear models used in (4.47) are well-understood, because the errors in (4.46) are controlled only by experiments and theory calculations using point nuclei, they can improve dramatically as these are improved, without needing new approaches to nuclear theory.

Although not yet at an accuracy of 10^{-4} meV for muonic Hydrogen, we regard the above exercise to be a proof of principle that nuclear-modelling uncertainties can be banished for muonic Hydrogen using essentially the same steps as for atomic Hydrogen.

5 Summary and Outlook

To summarize, this paper extends earlier arguments based on first-quantized EFTs for spinless nuclei (PPEFTs) [64, 72] to include nuclear spin. The response of ‘bulk’ electromagnetic fields and a Dirac lepton field to this point nucleus is computed in order to capture how nuclear structure alters leptonic energy levels.

Spin is included by supplementing the nuclear center-of-mass coordinate, $y^\mu(\tau)$, with Grassmann (anti-commuting) classical variables, $\xi^\mu(\tau)$, that are also localized on the nuclear world-line. Once quantized, the Grassmann variables ξ^μ fill out a finite-dimensional quantum state space that represents spatial rotations (and thereby encodes the finite-dimensional space of nuclear spin-states). General EFT principles ensure that such a first-quantized effective action can capture the low-energy behaviour of *any* spinning nucleus provided one includes all possible interactions in the first-quantized nuclear effective action, subject to the other symmetries of the problem and unitarity. The effects of the effective nuclear couplings get transferred to electromagnetic and lepton degrees of freedom through a set of matching boundary conditions [70–72] that govern the behaviour of bulk modes in the near-nucleus regime $r = \epsilon \ll a_B$, where a_B is the lepton’s Bohr radius.

Experience with spinless nuclei [64, 72] shows that although there are many effective couplings (or nuclear moments) these only turn out to contribute to atomic energy shifts through a limited number of combinations. Ref. [64] showed that when computing atomic energy shifts for spinless nuclei of size R , and if one is expanding energies in a powers series in $Z\alpha$ and $R/a_B \sim mRZ\alpha$, then up to and including effects of

order $m^4 R^3 (Z\alpha)^5$ or $m^3 R^2 (Z\alpha)^6$ all nuclear moments contribute only through a single parameter, ϵ_\star , that has dimensions of length. Although ϵ_\star can depend in a complicated way on nuclear moments – typically with $\epsilon_\star \sim (Z\alpha)R$ – the leptonic energies themselves are functions of these moments only through their dependence on ϵ_\star .

We here show that a similar statement also holds once nuclear spin is included. Working to the same order in $Z\alpha$ and $mRZ\alpha$, and also including similar sized nuclear-spin-dependent terms, shows that all nuclear moments appear in atomic energies only through two parameters, ϵ_\star and ϵ_F . We verify that we reproduce the explicit nuclear calculations in the literature (to the order we work) and provide explicit expressions for how these parameters depend on nuclear moments.

A technical issue that arises in these calculations concerns the divergences that one finds when computing matrix elements found when perturbing in the nuclear magnetic fields. These divergences arise because the presence of nonzero nuclear size makes modes external to the nucleus more singular near the origin. Strictly speaking this divergent behaviour stops once nuclear structure intervenes, but nuclear structure is not present to do so within the PPEFT formalism, wherein nuclei are replaced by point objects with many effective couplings. We show that sensible predictions can nonetheless be made, because the near-nucleus divergences can be renormalized into the values of the effective nuclear couplings.

We have carried through this EFT program and applied it to compute nuclear effects in atomic Hydrogen. We correctly capture existing results for the energy shifts due to the charge radius, nuclear polarizabilities, Friar and Zemach moments and others, and thereby verify that these all contribute through only the two independent parameters ϵ_\star and ϵ_F , down to contributions at the 10^{-2} kHz order in atomic Hydrogen. By fitting these two parameters to two particularly well-measured transitions, we can predict the nuclear-size contributions to a large number of energy levels listed in [6, 25, 26]. Our uncertainties are independent of nuclear models, and are currently dominated by the precision with which pure QED corrections have been computed for point nuclei. Our errors are reduced by at least one order of magnitude compared to what is reported in [105] for such finite-size effects. Our results are summarised in Tables 2 and 3 for the best measured transitions, and in Tables 5 through 7 for a broader class of transitions.

We repeat the exercise for muonic Hydrogen, with results given in Table 4. Again two parameters suffice to capture finite-size nuclear effects down to errors of order 0.01 meV, although this is not yet competitive with the accuracy of current (and upcoming) measurements. The required improvement is a straightforward extension of the methods used here, making them much easier to perform than are traditional nuclear methods.

We remark that the same techniques apply equally well to nuclear-structure con-

tributions to energy shifts for heavier and more complicated spinning nuclei such as deuterium, tritium, various helium isotopes, lithium and beryllium, with convergence of the low-energy EFT expansion expected to be quickest for those nuclei with the largest internal gap to exciting internal nuclear degrees of freedom.

In future work we hope to carry out a meta-analysis of available data for most low- Z electronic and muonic atoms and make predictions of the finite-size effects in transitions of these system that are relevant for future experiments [23, 24] that are equally well unclouded by inaccuracies of nuclear moments as they only depend on non-finite-size theory and experimental measurements.

Acknowledgements

We thank Marko Horbatsch, Eric Hessels, Krzysztof Pachucki and Randolph Pohl for helpful discussions. CB and PH thank the Mainz Institute for Theoretical Physics for its hospitality during the workshop *Precision Measurements and Fundamental Physics: The Proton Radius Puzzle and Beyond*. This work was partially supported by funds from the Natural Sciences and Engineering Research Council (NSERC) of Canada. Research at the Perimeter Institute is supported in part by the Government of Canada through NSERC and by the Province of Ontario through MRI.

Transition	ΔE^{fs} (kHz)	ΔE^{exp} (kHz)	ΔE^{th} (kHz)	ΔE^{trunc} (kHz)
$2P_{1/2}^{F=1} - 2S_{1/2}^{F=0}$	-143.70	0.0069	0.57	0.00031
$2P_{3/2}^{F=1} - 2S_{1/2}^{F=0}$	-143.70	0.0069	0.57	0.00031
$3P_{1/2}^{F=1} - 2S_{1/2}^{F=1}$	-136.480	0.0014	0.081	0.00010
$3P_{1/2}^{F=0} - 2S_{1/2}^{F=1}$	-136.480	0.0014	0.081	0.00010
$3P_{3/2}^{F=2} - 2S_{1/2}^{F=1}$	-136.481	0.0014	0.081	0.00010
$3P_{3/2}^{F=1} - 2S_{1/2}^{F=1}$	-136.481	0.0014	0.081	0.00010
$8S_{1/2}^{F=1} - 2S_{1/2}^{F=1}$	-134.348	0.0014	0.080	0.00010
$8D_{3/2}^{F=2} - 2S_{1/2}^{F=1}$	-136.481	0.0014	0.081	0.00010
$8D_{3/2}^{F=1} - 2S_{1/2}^{F=1}$	-136.481	0.0014	0.081	0.00010
$8D_{5/2}^{F=3} - 2S_{1/2}^{F=1}$	-136.481	0.0014	0.081	0.00010
$8D_{5/2}^{F=2} - 2S_{1/2}^{F=1}$	-136.481	0.0014	0.081	0.00010
$10D_{5/2}^{F=3} - 2S_{1/2}^{F=1}$	-136.481	0.0014	0.081	0.00010
$10D_{5/2}^{F=2} - 2S_{1/2}^{F=1}$	-136.481	0.0014	0.081	0.00010
$12D_{3/2}^{F=2} - 2S_{1/2}^{F=1}$	-136.481	0.0014	0.081	0.00010
$12D_{3/2}^{F=1} - 2S_{1/2}^{F=1}$	-136.481	0.0014	0.081	0.00010
$12D_{5/2}^{F=3} - 2S_{1/2}^{F=1}$	-136.481	0.0014	0.081	0.00010
$12D_{5/2}^{F=2} - 2S_{1/2}^{F=1}$	-136.481	0.0014	0.081	0.00010
$3P_{1/2}^{F=1} - 3S_{1/2}^{F=0}$	-42.58	0.0020	0.17	0.000092
$3P_{3/2}^{F=2} - 3S_{1/2}^{F=1}$	-40.439	0.00042	0.024	0.000031
$3P_{3/2}^{F=2} - 3S_{1/2}^{F=0}$	-42.58	0.0020	0.17	0.000092
$3P_{3/2}^{F=1} - 3S_{1/2}^{F=1}$	-40.439	0.00042	0.024	0.000031
$3P_{3/2}^{F=1} - 3S_{1/2}^{F=0}$	-42.58	0.0020	0.17	0.000092
$3D_{3/2}^{F=2} - 3S_{1/2}^{F=1}$	-40.439	0.00042	0.024	0.000031
$3D_{3/2}^{F=2} - 3S_{1/2}^{F=0}$	-42.58	0.0020	0.17	0.000092
$3D_{3/2}^{F=1} - 3S_{1/2}^{F=1}$	-40.439	0.00042	0.024	0.000031
$3D_{3/2}^{F=1} - 3S_{1/2}^{F=0}$	-42.58	0.0020	0.17	0.000092
$3D_{5/2}^{F=2} - 3S_{1/2}^{F=0}$	-42.58	0.0020	0.17	0.000092

Table 5: Finite-nuclear-size effects (column 2) with three sources of errors (columns 3–5) for Hydrogen transitions listed in ref. [6] that can be measured at the 0.01kHz level. See Table 6 (and main text) for more detailed descriptions of the column entries.

Transition	ΔE^{fs} (kHz)	ΔE^{exp} (kHz)	ΔE^{th} (kHz)	$\Delta E^{\text{trunc.}}$ (kHz)
$4P_{1/2}^{F=1} - 4S_{1/2}^{F=1}$	-17.060	0.00018	0.010	0.000013
$4P_{1/2}^{F=1} - 4S_{1/2}^{F=0}$	-17.962	0.00086	0.071	0.000039
$4P_{1/2}^{F=0} - 4S_{1/2}^{F=1}$	-17.060	0.00018	0.010	0.000013
$4P_{1/2}^{F=0} - 4S_{1/2}^{F=0}$	-17.962	0.00086	0.071	0.000039
$4D_{3/2}^{F=2} - 4S_{1/2}^{F=1}$	-17.060	0.00018	0.010	0.000013
$4D_{3/2}^{F=2} - 4S_{1/2}^{F=0}$	-17.962	0.00086	0.071	0.000039
$4D_{3/2}^{F=1} - 4S_{1/2}^{F=1}$	-17.060	0.00018	0.010	0.000013
$4D_{3/2}^{F=1} - 4S_{1/2}^{F=0}$	-17.962	0.00086	0.071	0.000039
$4P_{3/2}^{F=2} - 4S_{1/2}^{F=1}$	-17.060	0.00018	0.010	0.000013
$4P_{3/2}^{F=2} - 4S_{1/2}^{F=0}$	-17.962	0.00086	0.071	0.000039
$4P_{3/2}^{F=1} - 4S_{1/2}^{F=1}$	-17.060	0.00018	0.010	0.000013
$4P_{3/2}^{F=1} - 4S_{1/2}^{F=0}$	-17.962	0.00086	0.071	0.000039
$4D_{5/2}^{F=3} - 4S_{1/2}^{F=1}$	-17.060	0.00018	0.010	0.000013
$4D_{5/2}^{F=3} - 4S_{1/2}^{F=0}$	-17.962	0.00086	0.071	0.000039
$4D_{5/2}^{F=2} - 4S_{1/2}^{F=1}$	-17.060	0.00018	0.010	0.000013
$4D_{5/2}^{F=2} - 4S_{1/2}^{F=0}$	-17.962	0.00086	0.071	0.000039
$5P_{1/2}^{F=1} - 5S_{1/2}^{F=1}$	-8.7346	0.000091	0.0052	0.0000066
$5P_{1/2}^{F=1} - 5S_{1/2}^{F=0}$	-9.197	0.00044	0.037	0.000020
$5P_{1/2}^{F=0} - 5S_{1/2}^{F=1}$	-8.7346	0.000091	0.0052	0.0000066
$5P_{1/2}^{F=0} - 5S_{1/2}^{F=0}$	-9.197	0.00044	0.037	0.000020
$5P_{3/2}^{F=2} - 5S_{1/2}^{F=1}$	-8.7348	0.000091	0.0052	0.0000066
$5P_{3/2}^{F=2} - 5S_{1/2}^{F=0}$	-9.197	0.00044	0.037	0.000020
$5P_{3/2}^{F=1} - 5S_{1/2}^{F=1}$	-8.7348	0.000091	0.0052	0.0000066
$5P_{3/2}^{F=1} - 5S_{1/2}^{F=0}$	-9.197	0.00044	0.037	0.000020

Table 6: More nuclear-size effects listed in [6]. Column 2 gives the nuclear-finite-size contribution to the transition energy predicted by eq. (4.30). Columns 3–5 give errors inherent in column 2: column 3 is the error due to uncertainty in $\mathcal{D}_L/\mathcal{C}_L$ due to measurement errors in the reference transitions; column 4 gives the uncertainty due to uncertainty in the unperformed parts of the calculation not associated with nuclear finite-size effects; column 5 is the error due to neglect of higher orders in \mathfrak{s} , $Z\alpha$ and $R/a_B = mRZ\alpha$ beyond those given by green squares in Table 1. Uncertainty in values for α and Ry give errors significantly smaller than those listed.

Linear combination of transitions	ΔE^{fs} (kHz)	ΔE^{exp} (kHz)	ΔE^{th} (kHz)	ΔE^{trunc} (kHz)
$\left(4P_{1/2}^{F=1} - 2S_{1/2}^{F=1}\right) - \frac{1}{4} \left(2S_{1/2}^{F=1} - 1S_{1/2}^{F=1}\right)$	102.35	0.0029	0.16	0.00021
$\left(4P_{1/2}^{F=0} - 2S_{1/2}^{F=1}\right) - \frac{1}{4} \left(2S_{1/2}^{F=1} - 1S_{1/2}^{F=1}\right)$	102.35	0.0029	0.16	0.00021
$\left(4S_{1/2}^{F=1} - 2S_{1/2}^{F=1}\right) - \frac{1}{4} \left(2S_{1/2}^{F=1} - 1S_{1/2}^{F=1}\right)$	119.41	0.0028	0.16	0.00020
$\left(4P_{3/2}^{F=2} - 2S_{1/2}^{F=1}\right) - \frac{1}{4} \left(2S_{1/2}^{F=1} - 1S_{1/2}^{F=1}\right)$	102.35	0.0029	0.16	0.00021
$\left(4P_{3/2}^{F=1} - 2S_{1/2}^{F=1}\right) - \frac{1}{4} \left(2S_{1/2}^{F=1} - 1S_{1/2}^{F=1}\right)$	102.35	0.0029	0.16	0.00021
$\left(4D_{5/2}^{F=3} - 2S_{1/2}^{F=1}\right) - \frac{1}{4} \left(2S_{1/2}^{F=1} - 1S_{1/2}^{F=1}\right)$	102.35	0.0029	0.16	0.00021
$\left(4D_{5/2}^{F=2} - 2S_{1/2}^{F=1}\right) - \frac{1}{4} \left(2S_{1/2}^{F=1} - 1S_{1/2}^{F=1}\right)$	102.35	0.0029	0.16	0.00021
$\left(6S_{1/2}^{F=1} - 2S_{1/2}^{F=1}\right) - \frac{1}{4} \left(3S_{1/2}^{F=1} - 1S_{1/2}^{F=1}\right)$	131.41	0.0031	0.17	0.00022
$\left(6D_{5/2}^{F=3} - 2S_{1/2}^{F=1}\right) - \frac{1}{4} \left(3S_{1/2}^{F=1} - 1S_{1/2}^{F=1}\right)$	126.36	0.0031	0.18	0.00022
$\left(6D_{5/2}^{F=2} - 2S_{1/2}^{F=1}\right) - \frac{1}{4} \left(3S_{1/2}^{F=1} - 1S_{1/2}^{F=1}\right)$	126.36	0.0031	0.18	0.00022

Table 7: Contribution of nuclear-size effects and the errors in this prediction for specific linear combinations of transition energies (whose motivation comes from experimental considerations), as taken from [6], that are observable at the 0.001 kHz level. See Table 6 for more details on the definitions of each column.

A Spin formalism

This appendix summarizes the quantization procedure for the Grassmann fields, $\xi^\mu(s)$, and sketches the derivation of the final form for the nuclear action described in the main text.

Quantization

The free spinning particle has action

$$S = \int ds \mathcal{L} = - \int ds \left[M \sqrt{-\dot{y}^2} + i \xi^\mu \dot{\xi}_\mu \right], \quad (\text{A.1})$$

where the configuration variables are the bosonic coordinate $y^\mu(s)$ and the Grassmann variables $\xi^\mu(s)$. This proves to be a constrained system because the symmetries of the

problem (such as reparameterization invariance along the world-line) imply that these variables and their canonical momenta are not independent.

As described in detail in [95] the canonical quantization procedure for systems with constraints proceeds as follows. First identify the conjugate momenta and the Hamiltonian, using

$$\delta S = \int ds \left(\delta y^\mu p_\mu + \delta \dot{\xi}^\mu \pi_\mu \right), \quad (\text{A.2})$$

and so

$$p_\mu = \frac{\partial \mathcal{L}}{\partial \dot{y}^\mu} = \frac{M \dot{y}_\mu}{\sqrt{-\dot{y}^2}} \quad \text{and} \quad \pi_\mu = \frac{\partial \mathcal{L}}{\partial \dot{\xi}^\mu} = i \xi_\mu. \quad (\text{A.3})$$

In principle one wishes to invert these expressions to write the velocities, \dot{y}^μ and $\dot{\xi}^\mu$ as functions of the momenta, and to use these to construct the Hamiltonian from the Lagrangian. For constrained systems, like the one considered here, this inversion cannot be done. For instance, for the Grassmann field the $\dot{\xi}^\mu$ does not even appear in π_μ , while the bosonic momentum satisfies the identity

$$p^\mu p_\mu = -M^2, \quad (\text{A.4})$$

(which is the correct dispersion relation for a relativistic massive particle). The inability to solve for velocities in terms of positions and momenta arises because the system's positions and velocities are related by the following two *primary* constraints,

$$\phi_1 := p^2 + M^2 = 0, \quad \text{and} \quad \Phi_\mu := \pi_\mu - i \xi_\mu = 0. \quad (\text{A.5})$$

It is useful to incorporate the primary constraints into the Lagrangian,

$$\mathcal{L}_c = -M \sqrt{-\dot{y}^2} - i \xi^\mu \dot{\xi}_\mu - \theta \phi_1 - \Theta^\mu \Phi_\mu, \quad (\text{A.6})$$

where θ and Θ^μ are Lagrange multipliers. The variation of \mathcal{L} with respect to y^μ and ξ^μ subject to the constraints (A.5) is equivalent to the unconstrained variation of \mathcal{L}_c provided that the new variables θ and Φ_μ are also varied. The Hamiltonian of this theory including the constraints is then:

$$\begin{aligned} H_c &= \dot{y}^\mu p_\mu + \dot{\xi}^\mu \pi_\mu - \mathcal{L}_c, \\ &= \theta \phi_1 + \Theta^\mu \Phi_\mu. \end{aligned} \quad (\text{A.7})$$

Primary constraints like (A.5) need not exhaust all of the constraints because even if the primary constraints are imposed on any initial conditions, additional constraints might be necessary to ensure that (A.5) remain true for all times. The time evolution of any function of canonical variables, $A(q, p, t)$, is given by

$$\frac{dA}{dt} = \frac{\partial A}{\partial t} + (A, H)_P = 0, \quad (\text{A.8})$$

where $(\dots, \dots)_P$ denotes the Poisson bracket, defined for Grassmann even and odd variables by [96]:

$$\begin{aligned}
 (E_1, E_2)_P &= \left(\frac{\partial E_1}{\partial q^\alpha} \frac{\partial E_2}{\partial p_\alpha^q} - \frac{\partial E_2}{\partial q^\alpha} \frac{\partial E_1}{\partial p_\alpha^q} \right) + \left(\frac{\partial E_1}{\partial \xi^\alpha} \frac{\partial E_2}{\partial \pi_\alpha^\xi} - \frac{\partial E_2}{\partial \xi^\alpha} \frac{\partial E_1}{\partial \pi_\alpha^\xi} \right), \\
 (E, O)_P &= \left(\frac{\partial E}{\partial q^\alpha} \frac{\partial O}{\partial p_\alpha^q} - \frac{\partial O}{\partial q^\alpha} \frac{\partial E}{\partial p_\alpha^q} \right) + \left(\frac{\partial E}{\partial \xi^\alpha} \frac{\partial O}{\partial \pi_\alpha^\xi} + \frac{\partial O}{\partial \xi^\alpha} \frac{\partial E}{\partial \pi_\alpha^\xi} \right), \\
 (O, E)_P &= \left(\frac{\partial O}{\partial q^\alpha} \frac{\partial E}{\partial p_\alpha^q} - \frac{\partial E}{\partial q^\alpha} \frac{\partial O}{\partial p_\alpha^q} \right) - \left(\frac{\partial O}{\partial \xi^\alpha} \frac{\partial E}{\partial \pi_\alpha^\xi} + \frac{\partial E}{\partial \xi^\alpha} \frac{\partial O}{\partial \pi_\alpha^\xi} \right), \\
 (O_1, O_2)_P &= \left(\frac{\partial O_1}{\partial q^\alpha} \frac{\partial O_2}{\partial p_\alpha^q} + \frac{\partial O_2}{\partial q^\alpha} \frac{\partial O_1}{\partial p_\alpha^q} \right) - \left(\frac{\partial O_1}{\partial \xi^\alpha} \frac{\partial O_2}{\partial \pi_\alpha^\xi} + \frac{\partial O_2}{\partial \xi^\alpha} \frac{\partial O_1}{\partial \pi_\alpha^\xi} \right). \quad (\text{A.9})
 \end{aligned}$$

Any further constraints required to ensure that primary constraints hold for all times are called *secondary* constraints.

For the constraints of (A.5) we find:

$$\frac{d\phi_1}{ds} = (\phi_1, H)_P = \theta (p^2 + M^2, p^2 + M^2)_P + \Theta^\mu (p^2 + M^2, \pi_\mu - i\xi_\mu)_P = 0, \quad (\text{A.10})$$

and

$$\begin{aligned}
 \frac{d\Phi_\mu}{ds} &= (\Phi_\mu, H)_P = \theta (\pi^\mu - i\xi^\mu, p^2 + M^2)_P - \Theta^\nu (\pi^\mu - i\xi^\mu, \pi_\nu - i\xi_\nu)_P \\
 &= \Theta^\nu (-i\delta_\alpha^\mu \delta_\nu^\alpha - i\eta_{\beta\nu} \delta_\alpha^\beta \eta^{\mu\gamma} \delta_\gamma^\alpha) = -2i\Theta^\mu, \quad (\text{A.11})
 \end{aligned}$$

and so the evolution of the bosonic constraint yields no new restrictions while preservation of the fermionic constraint in time constrains the Grassmann Lagrange multiplier to vanish.

The primary constraints have the following Poisson brackets with one another

$$(\phi_1, \phi_1)_P = (\phi_1, \Phi^\mu)_P = (\Phi^\mu, \phi_1)_P = 0 \quad \text{and} \quad (\Phi_\mu, \Phi_\nu)_P = 2i\eta_{\mu\nu}. \quad (\text{A.12})$$

Writing these constraints as a 5-component column vector, $\phi_\alpha = \{\phi_1, \Phi_\mu\}$, these brackets can be arranged into a matrix,

$$\Delta_{\alpha\beta} := (\phi_\alpha, \phi_\beta)_P = \begin{bmatrix} 0 & \mathbf{0}^T \\ \mathbf{0} & 2i\eta_{\mu\nu} \end{bmatrix}. \quad (\text{A.13})$$

Zero eigenvectors of this matrix are called first-class constraints, and are obstructions to the program of quantizing by using commutators to replace Dirac brackets, defined by

$$(A, B)_D = (A, B)_P - (A, \phi_\alpha)_P (\Delta^{-1})_{\alpha\beta} (\phi_\beta, B)_P. \quad (\text{A.14})$$

Zero eigenvectors are associated with local symmetries for which gauge conditions must be chosen as supplementary constraints. In the above example Δ is diagonal and so its only zero vector corresponds to the bosonic constraint ϕ_1 , corresponding to the freedom to redefine the world-line parameterization. This symmetry can be removed by choosing a gauge condition and checking its time evolution. The freedom to reparameterize time can be removed by fixing a coordinate condition like

$$\varphi := y^0 - s = 0, \quad (\text{A.15})$$

and the evolution of this new condition now fixes the final Lagrange multiplier, since

$$\frac{d\varphi}{ds} = -1 + 2\theta p^0 = 0. \quad (\text{A.16})$$

With this choice the variable y^0 is no longer dynamical and only the spatial components of the position-vector need be quantized. Their conjugate momenta are

$$p_i = \frac{M\dot{y}_i}{\sqrt{1 - \dot{y}^2}}, \quad (\text{A.17})$$

which can now be inverted for the velocities:

$$\dot{y}^i = \frac{p^i}{\sqrt{p^i p_i + M^2}}. \quad (\text{A.18})$$

Finally, quantization proceeds by replacing Dirac brackets with commutators and anticommutators, so

$$i(E_1, E_2)_D \rightarrow [\hat{E}_1, \hat{E}_2], \quad i(O, E)_D \rightarrow [\hat{O}, \hat{E}] \quad \text{and} \quad i(O_1, O_2)_D \rightarrow \{\hat{O}_1, \hat{O}_2\}. \quad (\text{A.19})$$

Using this for the variables $\{y^i, \xi^\mu, p^i\}$ in the present instance leads to

$$[\hat{x}^i, \hat{p}_j] = i\delta_j^i \quad \text{and} \quad \{\hat{\xi}^\mu, \hat{\xi}^\nu\} = -\frac{1}{2}\eta^{\mu\nu}, \quad (\text{A.20})$$

as used in the main text.

Representations

The bosonic commutators in the previous section are easily represented using position and derivative operators, but it remains to choose how to represent the anti-commutator. Defining $\hat{\xi}^\mu := \frac{i}{2}\Gamma^\mu$, we see that the anti-commutator goes over to the Clifford algebra,

$$\{\Gamma^\mu, \Gamma^\nu\} = 2\eta^{\mu\nu}, \quad (\text{A.21})$$

and any representation of this Clifford algebra provides a quantization of the Grassmann fields.

In the main text we work in the rest-frame of the nucleus, making it convenient to choose a basis for the matrices that make it simple to distinguish particles from anti-particles, and so use the $2n \times 2n$ matrices

$$\Gamma^0 = -i \begin{bmatrix} \mathbb{1} & 0 \\ 0 & -\mathbb{1} \end{bmatrix} \quad \text{and} \quad \Gamma^k = (-i) \begin{bmatrix} 0 & \tau^k \\ -\tau^k & 0 \end{bmatrix} \quad (\text{A.22})$$

and so defining $\Gamma_5 := -i\Gamma^0\Gamma^1\Gamma^2\Gamma^3$ gives

$$\Gamma_5\Gamma^k = (-i) \begin{bmatrix} \tau^k & 0 \\ 0 & -\tau^k \end{bmatrix} \quad \text{and} \quad \Gamma_5 = - \begin{bmatrix} 0 & \mathbb{1} \\ \mathbb{1} & 0 \end{bmatrix}, \quad (\text{A.23})$$

while $\Gamma^{\mu\nu} := -\frac{i}{4} [\Gamma^\mu, \Gamma^\nu]$ implies

$$\Gamma^{0k} = \frac{i}{2} \begin{bmatrix} 0 & \tau^k \\ \tau^k & 0 \end{bmatrix} \quad \text{and} \quad \Gamma^{jl} = \frac{1}{2} \epsilon^{jlk} \begin{bmatrix} \tau^k & 0 \\ 0 & \tau^k \end{bmatrix}. \quad (\text{A.24})$$

In the above expressions $\mathbb{1}$ denotes the $n \times n$ unit matrix and τ^i denotes the $n \times n$ representation of the rotation generators, whose choice determines how nuclear spin is represented. For spin-half nuclei the τ^k are Pauli matrices,

$$\tau^x = \begin{pmatrix} 0 & 1 \\ 1 & 0 \end{pmatrix}, \quad \tau^y = \begin{pmatrix} 0 & -i \\ i & 0 \end{pmatrix}, \quad \tau^z = \begin{pmatrix} 1 & 0 \\ 0 & -1 \end{pmatrix}, \quad (\text{A.25})$$

while for spin-one nuclei the matrices

$$\tau_{(3)}^x = \frac{1}{\sqrt{2}} \begin{bmatrix} 0 & 1 & 0 \\ 1 & 0 & 1 \\ 0 & 1 & 0 \end{bmatrix}, \quad \tau_{(3)}^y = \frac{1}{\sqrt{2}} \begin{bmatrix} 0 & -i & 0 \\ i & 0 & -i \\ 0 & i & 0 \end{bmatrix}, \quad \tau_{(3)}^z = \begin{bmatrix} 1 & 0 & 0 \\ 0 & 0 & 0 \\ 0 & 0 & -1 \end{bmatrix}, \quad (\text{A.26})$$

are instead used, and so on.

In this basis the particle and antiparticle states in the particle rest frame are given by

$$|\psi\rangle = e^{ip \cdot x} \begin{bmatrix} \alpha \\ \beta \end{bmatrix}, \quad (\text{A.27})$$

where α and β represent the particle- and anti-particle solutions respectively. It is the state α for spin-half nuclei that appears in the main text, and for these only Γ^0 and Γ^{jl} have nonvanishing matrix elements for nuclei at rest.

Comparison with second-quantized nuclei

It is instructive to compare the first-quantized action found above with what a second-quantized field theory with two fermion species would yield. Let us write down the lowest order terms in each case, assuming the fermions are now also charged under electromagnetism.

The lowest-order second-quantized effective action that respects all the previously mentioned symmetries (and a U(1) gauge symmetry) for two charged fermions is:

$$S = - \int d^4x \left\{ \frac{1}{4} F_{\mu\nu} F^{\mu\nu} + \bar{\Psi} [\not{D} + m_e] \Psi + \bar{\Phi} [\not{D} + M] \Phi + a_N (\bar{\Phi} \Gamma^{\mu\nu} \Phi) F_{\mu\nu} + \dots \right\}, \quad (\text{A.28})$$

where $\not{D}\Psi = \gamma^\mu (\partial_\mu + ieA_\mu) \Psi$ and $\not{D}\Phi = \Gamma^\mu (\partial_\mu - iZeA_\mu) \Phi$, for a nucleus with charge $+Ze$. This action contains two parameters for each fermion species, the mass and the electric charge, just as does the leading first-quantized action

$$S = - \int ds \left\{ M\sqrt{-\dot{y}^2} + i\xi^\mu \dot{\xi}_\mu - q\dot{y}^\mu A_\mu - i\mu_N \xi^\mu \xi^\nu F_{\mu\nu} + \dots \right\}, \quad (\text{A.29})$$

and it contains the same number of parameters.

Notice that writing $F_{jk} = \epsilon_{jkl} B^l$ for a magnetic field \mathbf{B} turns the last term into

$$- i\mu_N \xi^j \xi^l F_{jl} = -\frac{\mu_N}{2} \Gamma^{jl} F_{jl} = -\frac{\mu_N}{4} \epsilon^{jlk} \epsilon_{jlm} B^m \begin{bmatrix} \tau_k & 0 \\ 0 & \tau_k \end{bmatrix} = \begin{bmatrix} -\boldsymbol{\mu} \cdot \mathbf{B} & 0 \\ 0 & -\boldsymbol{\mu} \cdot \mathbf{B} \end{bmatrix}, \quad (\text{A.30})$$

when the Hamiltonian is computed, confirming the identification of μ_N as the nuclear magnetic moment (and once the magnetic-moment contribution is extracted from $\bar{\Phi}(\not{D}+M)\Phi$ it transpires that a_N contains the contribution $g-2$ to the nuclear magnetic moment μ_N).

B Fermionic boundary conditions

In the text, the boundary condition (2.14) is described as arising as in the classic delta-function potential: by integrating the fermion field equations over a sphere of radius ϵ , and dropping all but the derivative and delta-function terms. This does not mean that it requires an explicit extrapolation of Ψ right into the nucleus, however. Indeed, the PPEFT formalism is designed expressly to *avoid* dealing with the physics in the core. Though qualitatively correct, the delta-function description is not really precisely defined. This appendix outlines the more detailed derivation of this boundary condition, following the discussion in Appendix A of [70] (and fleshed out in [64, 71–73, 76]), focussing specifically on the special issues that arise with first-order fermionic field equations.

Within the PPEFT approach used here all of the internal degrees of freedom for the nucleus are integrated out, leaving only the centre-of-mass position, $y^\mu(s)$, and spin, $\xi^\mu(s)$. These variables are regarded as collective coordinates: *i.e.* modes that appear in the low-energy theory because they are related to the action of Poincaré symmetries on the nuclear state (which in general is neither translation nor rotation invariant). The coupling between these two modes and the bulk fields given in the text is found by writing down the most general action that involves them all while properly realizing the symmetries, organized in an expansion in interactions of successively higher dimension – eq. (2.5). We reproduce the important interactions from that action for the electron field Ψ here for convenience:

$$S_p^{\text{int}} = - \int ds \bar{\Psi}(y(s)) \left[\sqrt{-\dot{y}^2} (c_s + i c_2 \epsilon_{\alpha\beta\gamma\delta} \xi^\alpha \xi^\beta \xi^\gamma \xi^\delta \gamma_5 + i c_F \xi^\mu \xi^\nu \gamma_{\mu\nu}) \right. \\ \left. + i \dot{y}^\mu (c_v \gamma_\mu + c_3 \epsilon_{\alpha\beta\gamma\delta} \xi^\alpha \xi^\beta \xi^\gamma \xi^\delta \gamma_5 \gamma_\mu) \right] \Psi(y(s)) + \dots \quad (\text{B.1})$$

In particular, Ψ is evaluated ‘on the world-line of the nucleus’, but in an EFT sense wherein spatial resolutions are limited to be only over distances $L \gg R$, where $R \sim 1$ fm is a representative size of the nucleus. Notice that to the dimensions of interest in this paper only terms bilinear in Ψ are required, which simplifies the discussion because it allows the neglect of any two- or higher-body contact interactions.

The task is to make precise how the effective couplings in (B.1) can be translated into the correct near-nucleus behaviour of Ψ . To this end define the world-tube swept out by a ball $\mathcal{B}_\epsilon(y)$ of radius ϵ that is instantaneously centred on the nucleus. The radius of this ball is chosen so that $R \ll \epsilon \ll a_B$ (where, as in the main text, a_B is the electronic Bohr radius). In principle one could imagine specifying the value of Ψ itself, or of its radial derivative, on the surface of this world-tube, but this is too prescriptive because the precise value of a bulk field at any particular position on this world-tube depends not only on the sources situated inside it, but also on any other sources or fields that are outside (though with an influence that falls off with that source’s distance from the ball). What is sought is a construction that is dynamical, in that it can respond to the presence of all sources that play a role in the path integral.

The required dynamical boundary condition is found by defining a ‘boundary’ action, $I_{\mathcal{B}}$, on the surface of a world-tube swept out by $\mathcal{B}_\epsilon(y)$, defined by the property that the path integral over Ψ , y^μ and ξ^μ exterior to $\mathcal{B}_\epsilon(y)$ reproduces all of the results of the full theory, and thereby makes precise the implications of an action like (B.1). The formulation of such an action is simplest in the limit where recoil corrections are neglected, because in this limit the position of $\mathcal{B}_\epsilon(y)$ does not move.

Concretely, writing the field as a sum over a basis of modes (as in the main text) $\Psi = \sum_\beta \Psi_\beta$, in the nuclear centre-of-mass frame the interactions in the boundary action

required to work to the same accuracy as (B.1) is

$$I_{\mathcal{B}}^{\text{int}} = \int d^2\Omega \epsilon^2 \sum_{\beta} \bar{\Psi}_{\beta}(\epsilon) (\hat{c}_s(\beta; \epsilon) - i\hat{c}_v(\beta; \epsilon)\gamma^0 + \hat{c}_F(\beta; \epsilon)\mathbf{I} \cdot \boldsymbol{\Sigma}) \Psi_{\beta}(\epsilon) \quad (\text{B.2})$$

where we discard c_2 and c_3 as in section 2.3 (since they are not relevant for a nucleus at rest after projecting out the anti-particle solution), and as in the text $\mathbf{I} = \frac{1}{2}\boldsymbol{\tau}$ and $\boldsymbol{\Sigma}$ satisfies $\gamma^{ij} = \epsilon^{ijk}\Sigma_k$. For applications to atoms we take $\beta = \{n, j, F, \dots\}$ to run over the mode labels described in the main text.

In principle there is an independent *boundary* coupling, \hat{c}_s, \hat{c}_v , and \hat{c}_F , for every mode β [73], and this is required because each eigenmode satisfies slightly different boundary conditions in the nuclear region. These all separately depend on ϵ because the boundary condition required to capture the effects of a nucleus depend on the size of the ball \mathcal{B}_{ϵ} that is used. In general the couplings in (B.2) are found by matching to nuclear properties (as usual for EFTs), but for S -wave modes the connection between the couplings of (B.2) and (B.1) is simply given by dimensional reduction: schematically $4\pi\epsilon^2\hat{c}_i = c_i$.

As usual the ϵ -dependence of these couplings is chosen to ensure nothing physical depends on the value of ϵ , and so changes in ϵ generate a renormalization-group (RG) flow amongst these couplings. What is important is that the RG-invariant parameters (like ϵ_{\star} and ϵ_F of the main text, on which physical observables depend) do *not* depend on the mode label β , for the reasons described in more detail in Appendix F. This independence of β expresses the fact that the physical effective properties of the nucleus should not depend on the quantum numbers of the electrons that are used as probes.

The boundary conditions implied by the action $I_{\mathcal{B}}$ are found when evaluating the path integral over Ψ , with the nucleus replaced by $I_{\mathcal{B}}$. In a semiclassical evaluation this involves computing the saddle point, against which the total action is stationary against variations of Ψ both away from and on the ball \mathcal{B}_{ϵ} . Stationarity with respect to variations that vanish at ϵ leads to the standard bulk field equations, with mode solutions as given in section 2.3. Stationarity with respect to variations on the boundary \mathcal{B}_{ϵ} then gives boundary conditions for each mode, of the form

$$\left[\gamma^r + \hat{c}_s(\beta; \epsilon) - i\hat{c}_v(\beta; \epsilon)\gamma^0 + \hat{c}_F(\beta; \epsilon)\mathbf{I} \cdot \boldsymbol{\Sigma} \right] \Psi_{\beta}(\epsilon) = 0, \quad (\text{B.3})$$

where the γ^r term comes from an integration by parts in the bulk action.

For a second-order field equation (like the Schrödinger or Klein-Gordon equations discussed in [70, 71]) this would be the whole story, since the analog of (B.3) then gives a relation between the field and its radial derivative at $r = \epsilon$. Interpreting (B.3) is trickier for fermions because it is not a differential condition, and has nontrivial

solutions for $\Psi_\beta(\epsilon)$ only if the matrix in the square brackets has a zero eigenvalue. To see the implications of this observation consider how (B.3) constrains the radial eigenmodes found in the main text.

Radial Boundary Conditions

For convenience, we restate here the eigenmodes given in (2.26). We do so working in the same Dirac basis for leptons as for nucleons (A.22), reproduced here for ease of reference:

$$\gamma^0 = -i \begin{pmatrix} \mathbb{1}_2 & 0 \\ 0 & -\mathbb{1}_2 \end{pmatrix}, \quad \text{and} \quad \gamma^r = -i \begin{pmatrix} 0 & \sigma^r \\ -\sigma^r & 0 \end{pmatrix}, \quad (\text{B.4})$$

where $\mathbb{1}_2$ is the 2×2 identity matrix. Writing $\Psi_\beta = e^{-i\omega_\beta t} \psi_\beta$, we define:

$$\psi_{nFj\varpi} = \begin{pmatrix} \mathcal{Y}_{Ff_z}^{j,\varpi} \mathfrak{f}_{nj\varpi}(r) \\ i\mathcal{Y}_{Ff_z}^{j,-\varpi} \mathfrak{g}_{nj\varpi}(r) \end{pmatrix}. \quad (\text{B.5})$$

These modes satisfy the useful identity for the action of σ^r ,

$$\sigma^r \mathcal{Y}_{F,f_z}^{j,\varpi} = -\mathcal{Y}_{F,f_z}^{j,-\varpi}. \quad (\text{B.6})$$

The action of $\mathbf{I} \cdot \boldsymbol{\Sigma}$ appearing in (B.3), restricted to a degenerate subspace with specific electronic angular momentum j , can be evaluated using the projection identity [117]:

$$\begin{aligned} \mathcal{Z}_{Fj\varpi} &:= \langle \mathbf{I} \cdot \boldsymbol{\Sigma} \rangle = \frac{\langle \mathbf{J} \cdot \mathbf{I} \rangle \langle \mathbf{J} \cdot \boldsymbol{\Sigma} \rangle}{\langle \mathbf{J} \cdot \mathbf{J} \rangle}, \quad (\text{B.7}) \\ &= \frac{1}{4j(j+1)} [F(F+1) - I(I+1) - j(j+1)] [j(j+1) - l(l+1) + s(s+1)], \\ &= \frac{1 + \varpi(2j+1)}{8j(j+1)} \left[F(F+1) - j(j+1) - I(I+1) \right] \quad (s = \tfrac{1}{2}) \\ &= \left[\frac{1 + \varpi(2j+1)}{8} \right] X_F. \end{aligned}$$

Here the first line defines the constant $\mathcal{Z}_{Fj\varpi}$, the second-last line specializes to $s = \frac{1}{2}$ and $l = j - \frac{1}{2}\varpi$ and the last line uses the definition (2.34) of X_F . Specialized to states with $j = \frac{1}{2}$ this gives

$$\mathcal{Z}_{F\varpi} := \mathcal{Z}_{F\frac{1}{2}\varpi} = \frac{2\varpi + 1}{8} X_F, \quad (\text{B.8})$$

which for $I = \frac{1}{2}$ becomes

$$\mathcal{Z}_{F\varpi} = \frac{2\varpi + 1}{6} \left[F(F+1) - \frac{3}{2} \right]. \quad (\text{B.9})$$

In general, $\mathbf{I} \cdot \boldsymbol{\Sigma}$ is not diagonalized by the states in (B.5) because it turns out that $\mathbf{I} \cdot \boldsymbol{\Sigma}$ mixes the same opposite parity states as does the hyperfine interaction, *i.e.* states whose angular momentum quantum numbers only differ in their value for j . Consequently the boundary condition needs to be handled with care. However, for the $j = \frac{1}{2}$ states relevant for this paper, the off-diagonal elements are suppressed by additional factors of $mRZ\alpha$ relative to the diagonal elements, and this puts them beyond the precision with which we work in this paper.²⁵

Restricted to the $j = \frac{1}{2}$ eigenspace we may treat $\mathbf{I} \cdot \boldsymbol{\Sigma}$ as if it were diagonal in the basis (B.5). Using the identity in (B.7) the boundary condition (B.3) for Ψ modes reads²⁶:

$$\begin{pmatrix} \hat{c}_s^{\varpi f} + \mathcal{Z}_{F,\varpi} \hat{c}_F^{\varpi f} - \hat{c}_v^{\varpi f} & -i\sigma^r \\ i\sigma^r & \hat{c}_s^{\varpi f} + \mathcal{Z}_{F,-\varpi} \hat{c}_F^{\varpi f} + \hat{c}_v^{\varpi f} \end{pmatrix} \begin{pmatrix} \mathcal{Y}_{Ff_z}^{\frac{1}{2},\varpi} \mathfrak{f}_{nF\frac{1}{2}\varpi}(\epsilon) \\ i\mathcal{Y}_{Ff_z}^{\frac{1}{2},-\varpi} \mathfrak{g}_{nF\frac{1}{2}\varpi}(\epsilon) \end{pmatrix} = 0. \quad (\text{B.10})$$

The superscript on the couplings $\hat{c}_{s,v,F}^{\varpi f}$ is meant as a reminder that they depend in principle on the mode's parity $\varpi = \pm$ and the atom's total spin²⁷ $F = j \pm \frac{1}{2} = 0, 1$.

Coupling constraint

For generic couplings the boundary condition (B.10) implies $\mathfrak{f}_{nF\frac{1}{2}\varpi}(\epsilon) = \mathfrak{g}_{nF\frac{1}{2}\varpi}(\epsilon) = 0$ whenever the pre-multiplying matrix is invertible. So having a nonvanishing spinor at $r = \epsilon$ requires the boundary couplings must satisfy

$$1 + \left(\hat{c}_v^{\varpi f} - \frac{\varpi}{3} \left[F(F+1) - \frac{3}{2} \right] \hat{c}_F^{\varpi f} \right)^2 = \left(\hat{c}_s^{\varpi f} + \frac{1}{6} \left[F(F+1) - \frac{3}{2} \right] \hat{c}_F^{\varpi f} \right)^2, \quad (\text{B.11})$$

for both $F = 0$ and $F = 1$. This shows that the couplings $\hat{c}_{s,v}^{\varpi f}$ and $\hat{c}_F^{\varpi f}$ are not all independent of one another.

This relationship amongst the effective couplings can be made explicit order-by-order in \mathfrak{s} , keeping in mind that $\hat{c}_F^{\varpi f}$ starts at $\mathcal{O}(\mathfrak{s})$ while $\hat{c}_{s,v}^{\varpi f} = (\hat{c}_{s,v}^{\varpi})^{(0)} + \mathfrak{s} (\hat{c}_{s,v}^{\varpi f})^{(1)} +$

²⁵This suppression arises because the negative-parity $j = 1/2$ Dirac-Coulomb mode-functions go as $\rho^{\zeta-1} \approx \rho^0$, which yields diagonal expectation values of $\langle \mathbf{I} \cdot \boldsymbol{\Sigma} \rangle_d \sim (mRZ\alpha)^{2(j+1/2)-2} \sim 1$ on the $\mathbf{I} \cdot \boldsymbol{\Sigma}$ operator, but leads to matrix elements mixing this state with the positive-parity $j = 3/2$ state that go as $\langle \mathbf{I} \cdot \boldsymbol{\Sigma} \rangle_{\text{off-d}} \sim (mRZ\alpha)^{j+j'-1} \sim (mRZ\alpha)$. As such, this mixing effect arises at the next order in the R/a_B expansion of the EFT action and is therefore not considered here.

²⁶It might seem unusual to assign an F -dependence to the Dirac mode functions, however this dependence arises because the integration constants \mathcal{D}/\mathcal{L} differ for different F , as we see from the boundary condition derived below.

²⁷We use lower-case f to denote dependence on nuclear spin F due to the unfortunate notational choice that already uses capital F to label the coupling \hat{c}_F .

... At $\mathcal{O}(\mathfrak{s}^0)$ the leading constraint shows that $(\hat{c}_{s,v}^{\varpi})^{(0)}$ satisfy the F -independent constraint found for spinless nuclei in [64]

$$1 = \left[(\hat{c}_s^{\varpi})^{(0)} \right]^2 - \left[(\hat{c}_v^{\varpi})^{(0)} \right]^2, \quad (\text{B.12})$$

while at first-order,

$$\mathfrak{s} \left[(\hat{c}_s^{\varpi})^{(0)} (\hat{c}_s^{\varpi f})^{(1)} - (\hat{c}_v^{\varpi})^{(0)} (\hat{c}_v^{\varpi f})^{(1)} \right] = -\frac{\hat{c}_F^{\varpi f}}{6} \left[F(F+1) - \frac{3}{2} \right] \left[(\hat{c}_s^{\varpi})^{(0)} + 2\varpi (\hat{c}_v^{\varpi})^{(0)} \right]. \quad (\text{B.13})$$

This last expression is consistent with c_F^{ϖ} being F -independent while $(\hat{c}_s^{\varpi f})^{(1)}$ and $(\hat{c}_v^{\varpi f})^{(1)}$ are proportional to $F(F+1) - \frac{3}{2}$.

Boundary condition

To identify more explicitly the implications of the boundary condition for the radial functions, rewrite (B.10) as the two conditions

$$\begin{aligned} & \left[(\hat{c}_s^{\varpi f} + \mathcal{Z}_{F,\varpi} \hat{c}_F^{\varpi f} - \hat{c}_v^{\varpi f}) \mathfrak{f}_{\varpi} - \mathfrak{g}_{\varpi} \right] \mathcal{Y}_{Ff_z}^{\frac{1}{2},\varpi} = 0 \\ & \left[-i\mathfrak{f}_{\varpi} + i (\hat{c}_s^{\varpi f} + \mathcal{Z}_{F,-\varpi} \hat{c}_F^{\varpi f} + \hat{c}_v^{\varpi f}) \mathfrak{g}_{\varpi} \right] \mathcal{Y}_{Ff_z}^{\frac{1}{2},-\varpi} = 0, \end{aligned} \quad (\text{B.14})$$

which for brevity writes $\mathfrak{f}_{\varpi} := \mathfrak{f}_{nF\frac{1}{2}\varpi}(\epsilon)$ and $\mathfrak{g}_{\varpi} := \mathfrak{g}_{n\frac{1}{2}\varpi}(\epsilon)$. Although this looks like two conditions for each choice of ϖ and F , they are not independent because of condition (B.11). The implications for the radial functions then are the ones used in eqs. (2.58) and (2.60) of the main text:

$$(\hat{c}_s^+ + \mathcal{Z}_F \hat{c}_F^+ - \hat{c}_v^+) \mathfrak{f}_+ - \mathfrak{g}_+ = 0, \quad \text{and} \quad (\hat{c}_s^- + \mathcal{Z}_F \hat{c}_F^- + \hat{c}_v^-) \mathfrak{g}_- - \mathfrak{f}_- = 0, \quad (\text{B.15})$$

where in both boundary conditions $\mathcal{Z}_F := \mathcal{Z}_{F+} = \frac{1}{2} [F(F+1) - \frac{3}{2}]$.

C Finite-size energy shift

In this section we compute the finite-size energy shifts in terms of \mathcal{D}/\mathcal{C} , including its $(Z\alpha)^2$ corrections, which allows us to capture finite-size energy shifts in electronic atoms of $\mathcal{O}(m^3 R^2 (Z\alpha)^6)$ magnitude.

Energy shift in the single-zero, single-pole approximation to $\mathcal{O}[(Z\alpha)^2]$

As described in the main text, the normalizability of the zeroth order wave-functions requires that the ratio of integration constants in the radial solutions satisfy:

$$-\left(\frac{\mathcal{D}}{\mathcal{C}} \right) = \frac{\Gamma[1+2\zeta] \Gamma[-\zeta - \frac{Z\alpha\omega}{\kappa}]}{\Gamma[1-2\zeta] \Gamma[\zeta - \frac{Z\alpha\omega}{\kappa}]}. \quad (\text{C.1})$$

Our goal in this Appendix is to solve this equation for ω as a function of \mathcal{D}/\mathcal{E} , following the steps taken in [64]. In particular, we seek solutions that are nearby to the standard Coulomb-Dirac expression for ω_D and $\kappa_D = \sqrt{m^2 - \omega_D^2}$, for a point nucleus, (2.23) and (2.24), that are the solutions when $\mathcal{D}/\mathcal{E} = 0$.

Since $\zeta = \sqrt{\mathfrak{K}^2 - (Z\alpha)^2}$, it is close to the value of $|\mathfrak{K}|$ and so $|\mathfrak{K}| - \zeta \approx \mathcal{O}[(Z\alpha)^2] \ll 1$. At the same time, the value of the poles of the gamma functions in the denominator are slightly shifted due to the nucleus having a finite-size, which we implement by taking $\omega = \omega_{nj}^D + \delta\omega$ and it is $\delta\omega \ll \omega_{nj}^D$ that this normalizability condition allows us to find as a function of the ratio of the integration constants. Additionally, as we have noted in the main text, the Dirac energies have the property that $\zeta - \frac{\omega_{nj}^D}{\kappa_D} = -N$, where N is a non-negative integer, related to the principal quantum number, n , through

$$N = n - |\mathfrak{K}|. \quad (\text{C.2})$$

Then, to first order in $\delta\omega$ this combination without the subscripts becomes

$$\zeta - \frac{Z\alpha\omega}{\kappa} \approx -N - \left(\frac{Z\alpha m^2}{\kappa_D^3} \right) \delta\omega, \quad (\text{C.3})$$

which allows us to write the condition in (C.1) as a function of the small quantities

$$\delta y = 2|\mathfrak{K}| - 2\zeta \simeq \mathcal{O}[(Z\alpha)^2] \quad \text{and} \quad \delta x = - \left(\frac{Z\alpha m^2}{\kappa_D^3} \right) \delta\omega, \quad (\text{C.4})$$

as

$$- \left(\frac{\mathcal{D}}{\mathcal{E}} \right) = \frac{\Gamma[2|\mathfrak{K}| + 1 - \delta y] \Gamma[-(N + 2|\mathfrak{K}|) + \delta x + \delta y]}{\Gamma[-(2|\mathfrak{K}| - 1) + \delta y] \Gamma[-N + \delta x]}. \quad (\text{C.5})$$

Now, to capture the energy shift to an accuracy of $\mathcal{O}[(Z\alpha)^2]$ we need to expand this formula for small $\delta x, \delta y$ and keep terms of order $\mathcal{O}(\delta x, \delta y, \delta x \delta y)$ and potentially $\mathcal{O}(\delta y^2)$ but not higher. In general, using the special property of gamma functions that $x\Gamma[x] = \Gamma[x + 1]$ we can expand them around their poles in the following way,

$$\begin{aligned} \Gamma[-N + \delta z] &= \frac{\Gamma[-N + 1 + \delta z]}{(-N + \delta z)} = \frac{\Gamma[1 + \delta z]}{(-N + \delta z)(-N + 1 + \delta z) \cdots \delta z} \\ &\approx \frac{\Gamma[1] \left(1 + \delta z \frac{\Gamma'[1]}{\Gamma[1]} + \cdots \right)}{(-1)^N N! \delta z (1 - \delta z H_N + \cdots)}, \end{aligned} \quad (\text{C.6})$$

where the ellipses of (C.6) contain terms higher order in δz . Carrying out this expansion for each gamma function²⁸ in (C.5) we end up with (after some algebra),

$$-\left(\frac{\mathcal{D}}{\mathcal{E}}\right) = -\frac{(2|\mathfrak{K}| - 1)!(2|\mathfrak{K}|)!N! (\delta x \delta y) \left(1 - \frac{\delta y}{2|\mathfrak{K}|} (1 + 4|\mathfrak{K}|H_{2|\mathfrak{K}|-1}) + \dots\right)}{(N + 2|\mathfrak{K}|)! (\delta x [1 - 2\delta y (H_{N+2|\mathfrak{K}|} + \gamma)] + \delta y - \delta y^2 [H_{N+2|\mathfrak{K}|} + \gamma])}, \quad (\text{C.7})$$

which uses the identities:

$$\frac{\Gamma'[1]}{\Gamma[1]} = -\gamma, \quad \frac{\Gamma'[2|\mathfrak{K}| + 1]}{\Gamma[2|\mathfrak{K}| + 1]} = H_{2|\mathfrak{K}|} - \gamma, \quad H_{2|\mathfrak{K}|} + H_{2|\mathfrak{K}|-1} = \frac{1}{2|\mathfrak{K}|} (1 + 4|\mathfrak{K}|H_{2|\mathfrak{K}|-1}). \quad (\text{C.8})$$

Pulling out a factor of δy from the denominator yields

$$\left(\frac{\mathcal{D}}{\mathcal{E}}\right) = \frac{(2|\mathfrak{K}| - 1)!(2|\mathfrak{K}|)!N! (\delta x) \left[1 - \frac{\delta y}{2|\mathfrak{K}|} (1 + 4|\mathfrak{K}|H_{2|\mathfrak{K}|-1}) + \dots\right]}{(N + 2|\mathfrak{K}|)! \left(1 + \delta x \left[\frac{1}{\delta y} - 2(H_{N+2|\mathfrak{K}|} + \gamma)\right] - \delta y (H_{N+2|\mathfrak{K}|} + \gamma) + \dots\right)}, \quad (\text{C.9})$$

and rearranging this for $\delta\omega$ (hidden inside δx) and writing it in terms of the principal quantum number n gives the desired result for the finite-size energy shift to order $\mathcal{O}(Z\alpha^2)$ as a function of the small parameter \mathcal{D}/\mathcal{E} :

$$\delta\omega \simeq -\frac{\kappa_D^3 \mathfrak{B}(\mathcal{D}/\mathcal{E}) [1 - \delta y (H_{n+|\mathfrak{K}|} + \gamma)]}{m^2(Z\alpha) \left[1 - \mathfrak{B}(\mathcal{D}/\mathcal{E}) [(\delta y)^{-1} - 2(H_{n+|\mathfrak{K}|} + \gamma)] - \frac{\delta y}{2|\mathfrak{K}|} (1 + 4|\mathfrak{K}|H_{2|\mathfrak{K}|-1}) + \dots\right]}, \quad (\text{C.10})$$

where the ellipses represent terms that involve higher powers of δx and

$$\mathfrak{B} := \frac{(n + |\mathfrak{K}|)!}{(n - |\mathfrak{K}|)!(2|\mathfrak{K}|)!(2|\mathfrak{K}| - 1)!}. \quad (\text{C.11})$$

D Perturbing in the magnetic dipole

This appendix derives the contributions to lepton-mode energy shifts due to the nuclear magnetic-dipole electromagnetic field. This is to be combined with the effects of finite-size nuclear effects in the main text. For the applications there we work to first order in the leptonic wave-functions, and energy shifts.

²⁸Note that the arguments of the gamma functions in (C.5) that depend on N in both numerator and denominator simultaneously approach negative integers in the limit $\delta x, \delta y \rightarrow 0$ and this necessitates expanding both gamma functions around their poles, hence the name “single-zero, single-pole” approximation.

Degenerate perturbation theory

The discussion of the main text shows that the leptonic mode functions satisfy the equation of motion (2.13), reproduced here (after multiplying through by $i\gamma^0$) as

$$\omega\psi = [i\gamma^0\boldsymbol{\gamma} \cdot \nabla + i\gamma^0m + eA_0^{\text{nuc}}] \psi - (e\gamma^0\boldsymbol{\gamma} \cdot \mathbf{A}_{\text{nuc}}) \psi, \quad (\text{D.1})$$

where A_0^{nuc} and \mathbf{A}_{nuc} are given by (2.10), also reproduced here:

$$A_0^{\text{nuc}} \simeq -\frac{Ze}{4\pi r}, \quad \mathbf{A}_{\text{nuc}} \simeq \frac{\boldsymbol{\mu} \times \mathbf{r}}{4\pi r^3}. \quad (\text{D.2})$$

This is to be solved perturbatively in \mathbf{A}_{nuc} . To do so we regard (D.1) as a special instance of the eigenvalue condition,

$$[H_0 + \lambda V] |\psi_A\rangle = \omega_A |\psi_A\rangle, \quad (\text{D.3})$$

with

$$H_0 = i\gamma^0\boldsymbol{\gamma} \cdot \nabla + i\gamma^0m + eA_0^{\text{nuc}} \quad \text{and} \quad V = -e\gamma^0\boldsymbol{\gamma} \cdot \mathbf{A}_{\text{nuc}}, \quad (\text{D.4})$$

and λ being a parameter that formally helps keep track of the order in V (but that is set to unity at the end) [118, 119]. Seeking eigenstates and eigenvalues order by order in λ ,

$$\omega = \omega^{(0)} + \lambda\omega^{(1)} + \lambda^2\omega^{(2)} + \dots \quad \text{and} \quad |\psi\rangle = |\psi\rangle_0 + \lambda|\psi\rangle_1 + \lambda^2|\psi\rangle_2 + \dots, \quad (\text{D.5})$$

gives the hierarchy of conditions,

$$\begin{aligned} \mathcal{O}(1) : \quad & H_0 |\psi\rangle_0 = \omega^{(0)} |\psi\rangle_0 \\ \mathcal{O}(\lambda) : \quad & H_0 |\psi\rangle_1 + V |\psi\rangle_0 = \omega^{(0)} |\psi\rangle_1 + \omega^{(1)} |\psi\rangle_0, \\ \mathcal{O}(\lambda^2) : \quad & H_0 |\psi\rangle_2 + V |\psi\rangle_1 = \omega^{(0)} |\psi\rangle_2 + \omega^{(1)} |\psi\rangle_1 + \omega^{(2)} |\psi\rangle_0, \end{aligned}$$

and so on.

Zeroth order

The leading equation is:

$$H_0 |\psi\rangle_0 = \omega^{(0)} |\psi\rangle_0, \quad (\text{D.6})$$

which in the present instance is the Dirac-Coulomb equation, whose eigenvalues, $\omega_{nj}^{(0)} = \omega_{nj}^D$ are given in (2.23), and whose eigenstates are labelled by the electronic principal, angular-momentum and parity quantum numbers described in the main text, and by the nuclear spin. That is, the zeroth-order eigenstates are

$$|njj_z\varpi; II_z\rangle_0 = |njj_z\varpi\rangle_0 \otimes |II_z\rangle_0, \quad (\text{D.7})$$

where $j = \frac{1}{2}, \frac{3}{2}, \dots$ and $j_z = -j, -j+1, \dots, j-1, j$ and $I_z = -I, -I+1, \dots, I-1, I$ and $\varpi = \pm$.

Notice that these energy levels are degenerate, with $(2I+1)(2j+1)$ states distinguished by j_z and I_z sharing the same energy. This makes it necessary to use degenerate perturbation theory in what follows. That is, within any degenerate eigenspace a basis $|E, a\rangle_0$ of energy E the zeroth-order eigenstates should be chosen to ensure that V is diagonal:

$${}_0\langle E, b | V | E, a \rangle_0 = \mathcal{V}(E, a) \delta_{ab}. \quad (\text{D.8})$$

In practice the required basis are the states that are eigenstates of the total (combined nuclear and leptonic) angular momentum $\mathbf{F} = \mathbf{J} + \mathbf{I}$ (see below for details).

First order

At first order in λ the eigenvalue equation is

$$[H_0 - \omega^{(0)}] |\psi\rangle_1 = [\omega^{(1)} - V] |\psi\rangle_0. \quad (\text{D.9})$$

Following the usual steps this implies the first-order energy shift for a state $|\omega^{(0)}, a\rangle_0$ is

$$\omega^{(1)} = \mathcal{V}(\omega^{(0)}, a) = \frac{{}_0\langle \omega^{(0)}, a | V | \omega^{(0)}, a \rangle_0}{{}_0\langle \omega^{(0)}, a | \omega^{(0)}, a \rangle_0}, \quad (\text{D.10})$$

and the corresponding zeroth-order energy eigenstate at this order is $|\omega^{(0)}, a\rangle_0$.

The first-order correction to this energy eigenstate implied by (D.9) is then

$$|\omega^{(0)}, a\rangle_1 = \bar{D} \frac{1}{[\omega^{(0)} - H_0]} \bar{D} V |\omega^{(0)}, a\rangle_0, \quad (\text{D.11})$$

where \bar{D} denotes the projection matrix onto all zeroth-order states that are *not* degenerate with the original state $|\omega^{(0)}, a\rangle_0$.

Eigenstates of total atomic spin

Although the nuclear magnetic moment splits some of the degeneracy of Dirac-Coulomb levels, rotational invariance ensures that the resulting states retain a residual $(2F+1)$ -dimensional degeneracy where F is the total angular momentum quantum number for the entire atom (nucleus plus lepton): $\mathbf{F} = \mathbf{J} + \mathbf{I}$.

This section writes these states out for the special case of a spin-half nucleus, as is relevant for our main application to muonic and atomic Hydrogen. We would like these functions to satisfy

$$\begin{aligned} \mathbf{F}^2 \mathcal{Y}_{F, f_z}^{j, \varpi} &= F(F+1) \mathcal{Y}_{F, f_z}^{j, \varpi}, & F_z \mathcal{Y}_{F, f_z}^{j, \varpi} &= f_z \mathcal{Y}_{F, f_z}^{j, \varpi}, & \mathbf{I}^2 \mathcal{Y}_{F, f_z}^{j, \varpi} &= I(I+1) \mathcal{Y}_{F, f_z}^{j, \varpi}, \\ \mathbf{J}^2 \mathcal{Y}_{F, f_z}^{j, \varpi} &= j(j+1) \mathcal{Y}_{F, f_z}^{j, \varpi}, & \mathbf{S}^2 \mathcal{Y}_{F, f_z}^{j, \varpi} &= s(s+1) \mathcal{Y}_{F, f_z}^{j, \varpi}, & \mathbf{L}^2 \mathcal{Y}_{F, f_z}^{j, \varpi} &= l(l+1) \mathcal{Y}_{F, f_z}^{j, \varpi}. \end{aligned} \quad (\text{D.12})$$

Any such state also diagonalizes $\mathbf{I} \cdot \mathbf{J}$ and $\mathbf{S} \cdot \mathbf{L}$, with

$$\begin{aligned} 2\mathbf{I} \cdot \mathbf{J} &= (\mathbf{I} + \mathbf{J})^2 - \mathbf{I}^2 - \mathbf{J}^2 = F(F + 1) - I(I + 1) - j(j + 1) \\ \text{and } 2\mathbf{S} \cdot \mathbf{L} &= (\mathbf{S} + \mathbf{L})^2 - \mathbf{S}^2 - \mathbf{L}^2 = j(j + 1) - s(s + 1) - l(l + 1). \end{aligned} \quad (\text{D.13})$$

The electron spinor harmonics, $\Omega_{jlj_z\varpi}$ satisfy the last three of conditions (D.12) for $s = \frac{1}{2}$, as well as $J_z \Omega_{jlj_z\varpi} = j_z \Omega_{jlj_z\varpi}$. These are defined in eqs. (2.16) and (2.17), repeated here for convenience:

$$\psi = \begin{pmatrix} \Omega_{jlj_z\varpi}(\theta, \phi) \mathbf{f}_{nj}(r) \\ i\Omega_{jl'j_z\varpi}(\theta, \phi) \mathbf{g}_{nj}(r) \end{pmatrix} \quad \text{with} \quad \Omega_{jlj_z\varpi} := \begin{pmatrix} \varpi \sqrt{\frac{l+\varpi j_z + \frac{1}{2}}{2l+1}} Y_{l, j_z - \frac{1}{2}}(\theta, \phi) \\ \sqrt{\frac{l-\varpi j_z + \frac{1}{2}}{2l+1}} Y_{l, j_z + \frac{1}{2}}(\theta, \phi) \end{pmatrix}, \quad (\text{D.14})$$

where the left-hand equality gives the 4-component electron spinor – in a basis for which γ^0 is diagonal, see (B.4) – in terms of the 2-component electron spinor harmonics Ω_{jlj_z} defined in terms of ordinary scalar spherical harmonics in the right-hand equality. In the right-hand equality $\varpi = \pm 1$ is the parity quantum number and in the left-hand equality l and l' are related to j and parity by $l = j - \frac{1}{2}\varpi$ and $l' = j + \frac{1}{2}\varpi$.

Similarly the nuclear I -states,

$$\eta_{\frac{1}{2}, +\frac{1}{2}} = \begin{bmatrix} 1 \\ 0 \end{bmatrix} \quad \text{and} \quad \eta_{\frac{1}{2}, -\frac{1}{2}} = \begin{bmatrix} 0 \\ 1 \end{bmatrix}, \quad (\text{D.15})$$

satisfy

$$\mathbf{I}^2 \eta_{II_z} = I(I + 1) \eta_{II_z} \quad \text{and} \quad I_z \eta_{II_z} = I_z \eta_{II_z}. \quad (\text{D.16})$$

We adopt the convention where square brackets denote nuclear-spin spinors while round brackets denote spinors in electron-spin space.

In general, states of definite total spin are built from product states with given j and I by

$$|F, f_z\rangle = \sum_j \sum_{j_z} \sum_{I_z} \langle j, j_z; I, I_z | F, f_z \rangle |j, j_z; I, I_z\rangle, \quad (\text{D.17})$$

for an appropriate set of Clebsch-Gordan coefficients, $\langle j, j_z; I, I_z | F, f_z \rangle$. For a spin-half nucleus, $I = \frac{1}{2}$, this reduces to [119],

$$\begin{aligned} \left| F = j \pm \frac{1}{2}, f_z \right\rangle &= \pm \sqrt{\frac{j + \frac{1}{2} \pm f_z}{2j + 1}} \left| j, f_z - \frac{1}{2}; \frac{1}{2}, +\frac{1}{2} \right\rangle + \\ &\quad + \sqrt{\frac{j + \frac{1}{2} \mp f_z}{2j + 1}} \left| j, f_z + \frac{1}{2}; \frac{1}{2}, -\frac{1}{2} \right\rangle. \end{aligned} \quad (\text{D.18})$$

Using the explicit position-space representation given above the new basis of spinor harmonics with definite F are the 4-component mixed electron/nuclear spin quantities

$$\mathcal{Y}_{F=j\pm\frac{1}{2},f_z}^{j,\varpi} = \pm \sqrt{\frac{j+\frac{1}{2}\pm f_z}{2j+1}} \Omega_{jlf_z-\frac{1}{2},\varpi} \eta_{\frac{1}{2},+\frac{1}{2}} + \sqrt{\frac{j+\frac{1}{2}\mp f_z}{2j+1}} \Omega_{jlf_z+\frac{1}{2},\varpi} \eta_{\frac{1}{2},-\frac{1}{2}}, \quad (\text{D.19})$$

and so using (D.15) the explicit 4-component spinors with fixed F are

$$\mathcal{Y}_{F=j+\frac{\nu}{2},f_z}^{j,\varpi} = \begin{bmatrix} \nu \sqrt{\frac{j+\frac{1}{2}+\nu f_z}{2j+1}} \Omega_{j,l,f_z-\frac{1}{2},\varpi} \\ \sqrt{\frac{j+\frac{1}{2}-\nu f_z}{2j+1}} \Omega_{j,l,f_z+\frac{1}{2},\varpi} \end{bmatrix}, \quad (\text{D.20})$$

where $\nu = \pm$ corresponds to the choice for $F = j \pm \frac{1}{2} = j + \frac{\nu}{2}$ and ϖ is the parity of the electron spinor harmonic, and $l = j - \frac{1}{2}\varpi$.

As a concrete example, consider $F = 1, f_z = 0, \pm 1$ and $j = \frac{1}{2}$ states with positive and negative parity, for which the above give the explicit positive-parity (S -wave) angular functions,

$$\mathcal{Y}_{1,0}^{\frac{1}{2},+} = \frac{1}{\sqrt{2}} \begin{bmatrix} \Omega_{\frac{1}{2},0,-\frac{1}{2},+} \\ \Omega_{\frac{1}{2},0,+\frac{1}{2},+} \end{bmatrix}, \quad \mathcal{Y}_{1,+1}^{\frac{1}{2},+} = \begin{bmatrix} \Omega_{\frac{1}{2},0,\frac{1}{2},+} \\ 0 \end{bmatrix}, \quad \mathcal{Y}_{1,-1}^{\frac{1}{2},+} = \begin{bmatrix} 0 \\ \Omega_{\frac{1}{2},0,-\frac{1}{2},+} \end{bmatrix}, \quad (\text{D.21})$$

while the negative-parity (P -wave) states instead are

$$\mathcal{Y}_{1,0}^{\frac{1}{2},-} = \frac{1}{\sqrt{2}} \begin{bmatrix} \Omega_{\frac{1}{2},1,-\frac{1}{2},-} \\ \Omega_{\frac{1}{2},1,+\frac{1}{2},-} \end{bmatrix}, \quad \mathcal{Y}_{1,+1}^{\frac{1}{2},-} = \begin{bmatrix} \Omega_{\frac{1}{2},1,\frac{1}{2},-} \\ 0 \end{bmatrix}, \quad \mathcal{Y}_{1,-1}^{\frac{1}{2},-} = \begin{bmatrix} 0 \\ \Omega_{\frac{1}{2},1,-\frac{1}{2},-} \end{bmatrix}. \quad (\text{D.22})$$

The orthonormality of the spherical spinors and of the nuclear spin states,

$$\int d^2\Omega_2 \Omega_{j',l',j'_z}^\dagger \Omega_{j,l,j_z} = \delta_{jj'} \delta_{ll'} \delta_{j_z j'_z} \quad \text{and} \quad \eta_{I,I_z}^\dagger \eta_{I',I'_z} = \delta_{I,I'} \delta_{I_z I'_z} \quad (\text{D.23})$$

ensure the above spinor harmonics are orthonormal

$$\int d^2\Omega_2 \left(\mathcal{Y}_{F',f'_z}^{j',\varpi'} \right)^\dagger \mathcal{Y}_{F,f_z}^{j,\varpi} = \delta_{FF'} \delta_{jj'} \delta_{f'_z f_z} \delta_{\varpi\varpi'}. \quad (\text{D.24})$$

E Evaluation of matrix elements

This section evaluates the radial integrals that arise when evaluating the magnetic-moment contributions to energy shifts. Some of these integrals diverge due to singularities in the integrands as $r \rightarrow 0$, and for these we also evaluate the regularization procedure we use when separating out the divergent and finite parts. The divergences

all have a specific dependence on the principal quantum number n , that is consistent with their being renormalized into shifts of the effective coupling \hat{c}_F . As a result the main content of the finite contributions is restricted to those terms that depend differently on n than do the divergent ones.

We consider in turn the integrals associated with both the first-order energy shift and the first-order state change.

Energy shift

The first order energy shift due to the nuclear dipole field is given by (2.36),

$$\varepsilon_{nFj\varpi}^{(1)} = -\frac{\mathfrak{K}\mathfrak{s}X_F}{m} \frac{(2\kappa)^3}{2m} \left(\frac{\mathfrak{N}}{\mathfrak{D}} \right) = -4\mathfrak{s}\mathfrak{K} X_F \frac{\kappa^3}{m^2} \left(\frac{\mathfrak{N}}{\mathfrak{D}} \right) = -4\mathfrak{s}\mathfrak{K} X_F m \left(\frac{Z\alpha}{\mathcal{N}} \right)^3 \left(\frac{\mathfrak{N}}{\mathfrak{D}} \right), \quad (\text{E.1})$$

where

$$\mathcal{N} = n\sqrt{1 - \frac{2(n - |\mathfrak{K}|)(Z\alpha)^2}{n^2(\zeta + |\mathfrak{K}|)}} \rightarrow n\sqrt{1 - \frac{2(n - 1)(Z\alpha)^2}{n^2(\zeta + 1)}}, \quad (\text{E.2})$$

and

$$\mathfrak{s} := \frac{me\mu_N}{4\pi} \rightarrow \frac{Z\alpha}{2} \left(\frac{m}{M} \right) g_p, \quad (\text{E.3})$$

where g_p is the proton g -factor and

$$\begin{aligned} X_F &:= \frac{F(F+1) - j(j+1) - I(I+1)}{j(j+1)} \\ &= \begin{cases} (j+1)^{-1} & \text{if } F = j + \frac{1}{2} \\ -j^{-1} & \text{if } F = j - \frac{1}{2} \end{cases} \rightarrow \begin{cases} 2/3 & \text{if } F = 1 \\ -2 & \text{if } F = 0 \end{cases}. \end{aligned} \quad (\text{E.4})$$

In these expressions the arrows specialize to the positive parity $\varpi = +$, $j = \frac{1}{2}$ states of Hydrogen.

The numerator and denominator functions are obtained as matrix elements of the interaction Hamiltonian (as described in the main text) and so contain the integrals we seek to evaluate. They both depend on the integration constant ratio, \mathcal{D}/\mathcal{C} , and so can be written

$$\begin{aligned} \mathfrak{N} &= \mathfrak{N}_{\text{pt}} + \left(\frac{\mathcal{D}}{\mathcal{C}} \right) \mathfrak{N}_1 + \left(\frac{\mathcal{D}}{\mathcal{C}} \right)^2 \mathfrak{N}_2 \\ \mathfrak{D} &= \mathfrak{D}_{\text{pt}} + \left(\frac{\mathcal{D}}{\mathcal{C}} \right) \mathfrak{D}_1 + \left(\frac{\mathcal{D}}{\mathcal{C}} \right)^2 \mathfrak{D}_2. \end{aligned} \quad (\text{E.5})$$

where eq. (3.9) gives the integration constant for parity-even $j = \frac{1}{2}$ states as

$$\begin{aligned} \left(\frac{\mathcal{D}_+}{\mathcal{E}_+}\right)^{(0)} &\simeq -\frac{16y_{\star+}(m\epsilon_{\star+})^2}{n(n+1)} \left(\frac{2Z\alpha m\epsilon_{\star+}}{n}\right)^{2\zeta-2} + \dots \\ &\simeq -\frac{\mathbf{c}}{n(n+1)} + \mathcal{O}[(Z\alpha)^2]. \end{aligned} \quad (\text{E.6})$$

which defines $\mathbf{c} = 16y_{\star+}(m\epsilon_{\star+})^2$. Since matching reveals that $\epsilon_{\star+} \sim \mathcal{O}(RZ\alpha)$ where $R \sim 1$ fm is a typical nuclear scale, we see that $\mathbf{c} \sim \mathcal{O}[(mRZ\alpha)^2]$. In particular $\mathfrak{N}_{\text{pt}}/\mathfrak{D}_{\text{pt}}$ is revealed to be the point-nucleus contribution to the hyperfine energy (which provides a useful check).

The functions \mathfrak{N}_{pt} , \mathfrak{N}_1 , \mathfrak{N}_2 , \mathfrak{D}_{pt} , \mathfrak{D}_1 and \mathfrak{D}_2 are given in terms of the following class of integrals, that the rest of this section evaluates in detail:

$$\mathcal{I}_{ij}^{(p)} := \int_0^\infty d\rho e^{-\rho} \rho^p \mathcal{M}_i \mathcal{M}_j, \quad (\text{E.7})$$

where we use the notation $\mathcal{M}(a; b; z) := {}_1F_1(a; b; z)$ for confluent hypergeometric functions and the integrands are as given in (2.19)

$$\begin{aligned} \mathcal{M}_1 &:= \mathcal{M}(a, b; \rho), \quad \mathcal{M}_2 := \mathcal{M}(a+1, b; \rho), \\ \mathcal{M}_3 &:= \mathcal{M}(a', b'; \rho), \quad \mathcal{M}_4 := \mathcal{M}(a'+1, b'; \rho). \end{aligned} \quad (\text{E.8})$$

with parameters defined as in (2.20)

$$\begin{aligned} a &:= \zeta - \frac{Z\alpha\omega}{\kappa}, \quad a' := -\left(\zeta + \frac{Z\alpha\omega}{\kappa}\right), \quad b := 1 + 2\zeta, \quad b' := 1 - 2\zeta, \\ c &:= \mathfrak{K} - \frac{Z\alpha m}{\kappa}, \quad \rho := 2kr, \quad \kappa := \sqrt{m^2 - \omega^2}, \quad \zeta := \sqrt{\mathfrak{K}^2 - (Z\alpha)^2}, \end{aligned} \quad (\text{E.9})$$

and $\mathfrak{K} = -\varpi(j + \frac{1}{2})$ where $\varpi = \pm 1$ is the state's parity.

Our main interest is in $j = \frac{1}{2}$ and $\varpi = +1$ states for which $\mathfrak{K} = -1$. For this choice we have

$$\zeta = \sqrt{1 - (Z\alpha)^2} = 1 + \mathfrak{z} \quad (\text{E.10})$$

where \mathfrak{z} is order $(Z\alpha)^2$. Similarly, for bound states one has

$$\kappa = \sqrt{m^2 - \omega^2} = \frac{Z\alpha m}{\mathcal{N}} \simeq \frac{Z\alpha m}{n} + \mathcal{O}[(Z\alpha)^2], \quad (\text{E.11})$$

where $n = 1, 2, \dots$ is the principal quantum number, and so

$$\frac{Z\alpha\omega}{\kappa} = n + \lambda \quad \text{and} \quad \frac{Z\alpha m}{\kappa} = n + \mu \quad (\text{E.12})$$

with λ and μ also order $(Z\alpha)^2$. In this regime the parameters of (E.9) are

$$\begin{aligned} a &= 1 - n + \mathfrak{z} - \lambda, & a' &= -1 - n - \mathfrak{z} - \lambda, & b &= 3 + 2\mathfrak{z} \\ b' &= -1 - 2\mathfrak{z} & \text{and} & & c &= -1 - n - \mu. \end{aligned} \quad (\text{E.13})$$

In terms of these quantities we have

$$\begin{aligned} \mathfrak{N}_{\text{pt}} &= \mathcal{I}_{11}^{(2\zeta-2)} - \left(\frac{a}{c}\right)^2 \mathcal{I}_{22}^{(2\zeta-2)} \\ \mathfrak{N}_1 &= 2 \left[\mathcal{I}_{13}^{(-2)} - \left(\frac{aa'}{c^2}\right) \mathcal{I}_{24}^{(-2)} \right] \\ \mathfrak{N}_2 &= \mathcal{I}_{33}^{(-2\zeta-2)} - \left(\frac{a'}{c}\right)^2 \mathcal{I}_{44}^{(-2\zeta-2)}, \end{aligned} \quad (\text{E.14})$$

and

$$\begin{aligned} \mathfrak{D}_{\text{pt}} &= 2\mathcal{I}_{11}^{(2\zeta)} - \frac{4\omega}{m} \left(\frac{a}{c}\right) \mathcal{I}_{12}^{(2\zeta)} + 2 \left(\frac{a}{c}\right)^2 \mathcal{I}_{22}^{(2\zeta)} \\ \mathfrak{D}_1 &= 2 \left[2\mathcal{I}_{13}^{(0)} - \frac{2\omega}{m} \left(\frac{a'}{c}\right) \mathcal{I}_{14}^{(0)} - \frac{2\omega}{m} \left(\frac{a}{c}\right) \mathcal{I}_{23}^{(0)} + 2 \left(\frac{aa'}{c^2}\right) \mathcal{I}_{24}^{(0)} \right] \\ \mathfrak{D}_2 &= 2 \left[\mathcal{I}_{33}^{(-2\zeta)} - \frac{2\omega}{m} \left(\frac{a'}{c}\right) \mathcal{I}_{34}^{(-2\zeta)} + \left(\frac{a'}{c}\right)^2 \mathcal{I}_{44}^{(-2\zeta)} \right]. \end{aligned} \quad (\text{E.15})$$

Hypergeometric facts

The relevant integrands depend on generalized hypergeometric functions, some of whose definitions and properties – taken from [120], [121] and online libraries such as [122] – are summarized here. These functions are defined within the domain of convergence by the following infinite series

$$\begin{aligned} {}_A\mathcal{F}_B \left[\begin{matrix} a_1, \dots, a_A \\ b_1, \dots, b_B \end{matrix}; z \right] &:= \sum_{k=0}^{\infty} \frac{(a_1)_k \cdots (a_A)_k}{(b_1)_k \cdots (b_B)_k} \frac{z^k}{k!} \\ &= 1 + \frac{a_1 \cdots a_A}{b_1 \cdots b_B} z + \frac{a_1(a_1+1) \cdots a_A(a_A+1)}{b_1(b_1+1) \cdots b_B(b_B+1)} \frac{z^2}{2} + \cdots \end{aligned} \quad (\text{E.16})$$

and are extended to general complex z by analytic continuation. Here $(a)_i$ are the Pochhammer symbols defined by

$$(a)_i := a(a+1) \cdots (a+i-1) \quad \text{when } i \geq 1, \quad (\text{E.17})$$

and $(a)_0 := 1$.

These definitions show that if any of the a -type arguments is a non-positive integer then the series expansion terminates after a finite number of terms. Similarly, the coefficients of the series are not well-defined if any of the b -type arguments is a non-positive integer. Both of these situations actually arise in Dirac-Coulomb wave-functions, which involve confluent hypergeometric functions (given by the special case $\mathcal{A} = \mathcal{B} = 1$). In particular

$${}_3\mathcal{F}_2 \left[\begin{matrix} a, b, -1 \\ c, d \end{matrix}; \rho \right] = 1 - \left(\frac{ab}{cd} \right) \rho \quad \text{and so} \quad {}_3\mathcal{F}_2 \left[\begin{matrix} a, b, -1 \\ c, d \end{matrix}; 1 \right] = \frac{cd - ab}{cd}. \quad (\text{E.18})$$

Also notice that

$${}_3\mathcal{F}_2 \left[\begin{matrix} a, b, d \\ c, d \end{matrix}; \rho \right] = {}_2\mathcal{F}_1 \left[\begin{matrix} a, b \\ c \end{matrix}; \rho \right] = {}_2\mathcal{F}_1(a, b; c; \rho), \quad (\text{E.19})$$

is a standard hypergeometric function, and so

$${}_3\mathcal{F}_2 \left[\begin{matrix} a, b, d \\ c, d \end{matrix}; 1 \right] = {}_2\mathcal{F}_1 \left[\begin{matrix} a, b \\ c \end{matrix}; 1 \right] = {}_2\mathcal{F}_1(a, b; c; 1) = \frac{\Gamma(c)\Gamma(c-a-b)}{\Gamma(c-a)\Gamma(c-b)}. \quad (\text{E.20})$$

Strictly speaking the last equality only holds for $\Re(c-a-b) > 0$, and is defined for other values by analytic continuation.

Basic integrals

Because $\mathcal{M}(a; c; \rho) \rightarrow 1$ as $\rho \rightarrow 0$, the basic integral of interest, (E.7), converges at $\rho = 0$ if $\Re p > -1$. Although the exponential factor $e^{-\rho}$ might seem to ensure automatic convergence as $\rho \rightarrow \infty$, the large- ρ asymptotic expansion

$$\mathcal{M}(a; b; \rho) \sim \frac{e^\rho \rho^{a-b}}{\Gamma(a)} \sum_{k=0}^{\infty} \frac{(1-a)_k (1-b)_k}{k!} \rho^{-k}, \quad (\text{E.21})$$

shows that convergence actually depends on the values of a, b, a' and b' and p .

The integral can be evaluated by expanding one of the hypergeometric functions and formally integrating term-by-term [120]:

$$\begin{aligned} \mathcal{I}_d(a, b; a', b') &:= \int_0^\infty d\rho e^{-\rho} \rho^{d-1} \mathcal{M}[a; b; \rho] \mathcal{M}[a'; b'; \rho], \\ &= \frac{\Gamma(b')}{\Gamma(a')} \sum_{k=0}^{\infty} \frac{\Gamma(a' + k)}{k! \Gamma(b' + k)} \int_0^\infty d\rho e^{-\rho} \rho^{d-1+k} \mathcal{M}(a, b; \rho) \\ &= \frac{\Gamma(d)\Gamma(b')\Gamma(b' - d - a')}{\Gamma(b' - a')\Gamma(b' - d)} {}_3\mathcal{F}_2 \left[\begin{matrix} a, d, 1 + d - b' \\ b, 1 + d + a' - b' \end{matrix}; 1 \right] \\ &= \frac{\Gamma(d)\Gamma(b)\Gamma(b - d - a)}{\Gamma(b - a)\Gamma(b - d)} {}_3\mathcal{F}_2 \left[\begin{matrix} a', d, 1 + d - b \\ b', 1 + d + a - b' \end{matrix}; 1 \right], \end{aligned} \quad (\text{E.22})$$

where the last equality uses the manifest symmetry of the original integrand under $(a, b) \leftrightarrow (a', b')$. A useful special case that arises sometimes is $d = b'$, in which case (E.22) simplifies to

$$\begin{aligned} \mathcal{I}_d(a, b; a', b') &= \frac{\Gamma(b)\Gamma(b')\Gamma(b-a-b')}{\Gamma(b-a)\Gamma(b-b')} {}_3\mathcal{F}_2 \left[\begin{matrix} a', b', 1+b'-b \\ b', 1+b'+a-b \end{matrix}; 1 \right] \\ &= \frac{\Gamma(b)\Gamma(b')\Gamma(b-a-b')}{\Gamma(b-a)\Gamma(b-b')} {}_2\mathcal{F}_1 \left[\begin{matrix} a', 1+b'-b \\ 1+b'+a-b \end{matrix}; 1 \right] \\ &= \frac{\Gamma(b)\Gamma(b')\Gamma(b-a-b')\Gamma(1+a+b-b)\Gamma(a-a')}{\Gamma(b-a)\Gamma(b-b')\Gamma(1+b'-b+a-a')\Gamma(a)}. \end{aligned} \quad (\text{E.23})$$

Integrals appearing in \mathfrak{N}_{pt} and \mathfrak{D}_{pt}

Consider first the convergent integrals that give the standard hyperfine structure. This tests that we are evaluating things properly.

The integral \mathcal{I}_{11}^p

We start with the integral

$$\begin{aligned} \mathcal{I}_{11}^{(p)} &= \int_0^\infty d\rho e^{-\rho} \rho^p \mathcal{M}(a, b; \rho) \mathcal{M}(a, b; \rho) = \mathcal{I}_{p+1}(a, b; a, b) \\ &= \frac{\Gamma(p+1)\Gamma(b)\Gamma(b-a-p-1)}{\Gamma(b-a)\Gamma(b-p-1)} {}_3\mathcal{F}_2 \left[\begin{matrix} a, p+1, p+2-b \\ b, p+2+a-b \end{matrix}; 1 \right], \end{aligned} \quad (\text{E.24})$$

which with

$$a = \zeta - \frac{Z\alpha\omega}{\kappa}, \quad b = 1 + 2\zeta, \quad b - a = 1 + \zeta + \frac{Z\alpha\omega}{\kappa}, \quad (\text{E.25})$$

gives

$$\mathcal{I}_{11}^{(p)} = \frac{\Gamma(p+1)\Gamma(1+2\zeta)\Gamma(\zeta-p+Z\alpha\omega/\kappa)}{\Gamma(2\zeta-p)\Gamma(1+\zeta+Z\alpha\omega/\kappa)} {}_3\mathcal{F}_2 \left[\begin{matrix} \zeta - Z\alpha\omega/\kappa, p+1, p+1-2\zeta \\ 1+2\zeta, p+1-\zeta-Z\alpha\omega/\kappa \end{matrix}; 1 \right]. \quad (\text{E.26})$$

This integral arises in \mathfrak{N}_{pt} and \mathfrak{D}_{pt} with the two cases $p = 2\zeta$ and $p = 2\zeta - 2$. We consider each of these cases in turn.

Specializing to $p = 2\zeta$ and simplifying the result using (E.20) gives

$$\begin{aligned} \mathcal{I}_{11}^{(2\zeta)} &= \frac{[\Gamma(1+2\zeta)]^2\Gamma(-\zeta+Z\alpha\omega/\kappa)}{\Gamma(0)\Gamma(1+\zeta+Z\alpha\omega/\kappa)} {}_3\mathcal{F}_2 \left[\begin{matrix} \zeta - Z\alpha\omega/\kappa, 1+2\zeta, 1 \\ 1+2\zeta, 1+\zeta-Z\alpha\omega/\kappa \end{matrix}; 1 \right] \\ &= \frac{[\Gamma(1+2\zeta)]^2\Gamma(1-\zeta+Z\alpha\omega/\kappa)}{\Gamma(1+\zeta+Z\alpha\omega/\kappa)} \end{aligned} \quad (\text{E.27})$$

which survives despite the $\Gamma(0)$ in the denominator of the prefactor²⁹ because of a compensating factor of $\Gamma(0)$ in the numerator coming from using (E.20) in the limit $c = b + a$. Expanding to lowest order in $(Z\alpha)^2$ then gives the result

$$\mathcal{I}_{11}^{(2\zeta)} = \frac{[\Gamma(3 + 2\mathfrak{z})]^2 \Gamma(n - \mathfrak{z} + \lambda)}{\Gamma(2 + n + \mathfrak{z} + \lambda)} = \frac{4}{n(n+1)} + \mathcal{O}[(Z\alpha)^2]. \quad (\text{E.28})$$

Specializing next to $p = 2\zeta - 2$ and using (E.18) to simplify the result leads to

$$\begin{aligned} \mathcal{I}_{11}^{(2\zeta-2)} &= \frac{\Gamma(2\zeta - 1)\Gamma(1 + 2\zeta)\Gamma(2 - \zeta + Z\alpha\omega/\kappa)}{\Gamma(2)\Gamma(1 + \zeta + Z\alpha\omega/\kappa)} {}_3\mathcal{F}_2 \left[\begin{matrix} \zeta - Z\alpha\omega/\kappa, 2\zeta - 1, -1 \\ 1 + 2\zeta, -1 + \zeta - Z\alpha\omega/\kappa \end{matrix}; 1 \right] \\ &= \frac{\Gamma(2\zeta - 1)\Gamma(1 + 2\zeta)\Gamma(1 - \zeta + Z\alpha\omega/\kappa)}{(1 + 2\zeta)\Gamma(1 + \zeta + Z\alpha\omega/\kappa)} \left(1 + \frac{2Z\alpha\omega}{\kappa} \right) \\ &= \frac{2(2n + 1)}{3n(n + 1)} + \mathcal{O}[(Z\alpha)^2]. \end{aligned} \quad (\text{E.29})$$

The integral \mathcal{I}_{12}^p

In this case we have the integral

$$\begin{aligned} \mathcal{I}_{12}^{(p)} &= \int_0^\infty d\rho e^{-\rho} \rho^p \mathcal{M}(a, b; \rho) \mathcal{M}(a + 1, b; \rho) = \mathcal{I}_{p+1}(a, b; a + 1, b) \\ &= \frac{\Gamma(p + 1)\Gamma(b)\Gamma(b - a - p - 1)}{\Gamma(b - a)\Gamma(b - p - 1)} {}_3\mathcal{F}_2 \left[\begin{matrix} a + 1, p + 1, p + 2 - b \\ b, p + 2 + a - b \end{matrix}; 1 \right], \end{aligned} \quad (\text{E.30})$$

in which we again use (E.25), leading to

$$\mathcal{I}_{12}^{(p)} = \frac{\Gamma(p + 1)\Gamma(1 + 2\zeta)\Gamma(\zeta - p + Z\alpha\omega/\kappa)}{\Gamma(2\zeta - p)\Gamma(1 + \zeta + Z\alpha\omega/\kappa)} {}_3\mathcal{F}_2 \left[\begin{matrix} 1 + \zeta - Z\alpha\omega/\kappa, p + 1, p + 1 - 2\zeta \\ 1 + 2\zeta, p + 1 - \zeta - Z\alpha\omega/\kappa \end{matrix}; 1 \right]. \quad (\text{E.31})$$

Specializing to the case $p = 2\zeta$ gives in this case

$$\begin{aligned} \mathcal{I}_{12}^{(2\zeta)} &= \frac{[\Gamma(1 + 2\zeta)]^2 \Gamma(-\zeta + Z\alpha\omega/\kappa)}{\Gamma(0)\Gamma(1 + \zeta + Z\alpha\omega/\kappa)} {}_3\mathcal{F}_2 \left[\begin{matrix} 1 + \zeta - Z\alpha\omega/\kappa, 1 + 2\zeta, 1 \\ 1 + 2\zeta, 1 + \zeta - Z\alpha\omega/\kappa \end{matrix}; 1 \right] \\ &= \frac{[\Gamma(1 + 2\zeta)]^2 \Gamma(-\zeta + Z\alpha\omega/\kappa)}{\Gamma(0)\Gamma(1 + \zeta + Z\alpha\omega/\kappa)} \left(-\zeta + \frac{Z\alpha\omega}{\kappa} \right) = 0, \end{aligned} \quad (\text{E.32})$$

²⁹More precisely, the expression contains the ill-defined quantity $\Gamma(a' - a)/\Gamma(b' - b) \rightarrow \Gamma(0)/\Gamma(0)$. This quantity requires regulating, and there is freedom in choosing how to do this. The easiest way is to choose $a' = a + \delta_a$ and $b' = b + \delta_b$ then take the limit that $\delta_a, \delta_b \rightarrow 0$, so that $\Gamma(\delta_a)/\Gamma(\delta_b) \rightarrow \delta_b/\delta_a = \pm 1$. The sign on the ratio depends on how δ_a and δ_b are taken to 0 and can be fixed by ensuring the results for the point-like integrals align with the standard Dirac-Coulomb wavefunctions, which turns out to require the negative sign.

which vanishes because of the uncanceled factor of $\Gamma(0)$ in the denominator.

By contrast, in the case $p = 2\zeta - 2$ one instead finds

$$\begin{aligned}
 \mathcal{I}_{12}^{(2\zeta-2)} &= \frac{\Gamma(2\zeta - 1)\Gamma(1 + 2\zeta)\Gamma(2 - \zeta + Z\alpha\omega/\kappa)}{\Gamma(2)\Gamma(1 + \zeta + Z\alpha\omega/\kappa)} {}_3\mathcal{F}_2 \left[\begin{matrix} 1 + \zeta - Z\alpha\omega/\kappa, 2\zeta - 1, -1 \\ 1 + 2\zeta, -1 + \zeta - Z\alpha\omega/\kappa \end{matrix}; 1 \right] \\
 &= \frac{2\Gamma(2\zeta - 1)\Gamma(1 + 2\zeta)\Gamma(1 - \zeta + Z\alpha\omega/\kappa)}{(1 + 2\zeta)\Gamma(1 + \zeta + Z\alpha\omega/\kappa)} \left(\zeta + \frac{Z\alpha\omega}{\kappa} \right) \\
 &= \frac{4}{3n} + \mathcal{O}[(Z\alpha)^2].
 \end{aligned} \tag{E.33}$$

The integral \mathcal{I}_{22}^p

Next up is

$$\begin{aligned}
 \mathcal{I}_{22}^{(p)} &= \int_0^\infty d\rho e^{-\rho} \rho^p \mathcal{M}(a + 1, b; \rho) \mathcal{M}(a + 1, b; \rho) = \mathcal{I}_{p+1}(a + 1, b; a + 1, b) \\
 &= \frac{\Gamma(p + 1)\Gamma(b)\Gamma(b - a - p - 2)}{\Gamma(b - a - 1)\Gamma(b - p - 1)} {}_3\mathcal{F}_2 \left[\begin{matrix} a + 1, p + 1, p + 2 - b \\ b, p + 3 + a - b \end{matrix}; 1 \right],
 \end{aligned} \tag{E.34}$$

in which we still use (E.25), finding

$$\mathcal{I}_{22}^{(p)} = \frac{\Gamma(p + 1)\Gamma(1 + 2\zeta)\Gamma(-1 + \zeta - p + Z\alpha\omega/\kappa)}{\Gamma(2\zeta - p)\Gamma(\zeta + Z\alpha\omega/\kappa)} {}_3\mathcal{F}_2 \left[\begin{matrix} 1 + \zeta - Z\alpha\omega/\kappa, p + 1, p + 1 - 2\zeta \\ 1 + 2\zeta, p + 2 - \zeta - Z\alpha\omega/\kappa \end{matrix}; 1 \right]. \tag{E.35}$$

In the case $p = 2\zeta$ this becomes

$$\begin{aligned}
 \mathcal{I}_{22}^{(2\zeta)} &= \frac{[\Gamma(1 + 2\zeta)]^2\Gamma(-1 - \zeta + Z\alpha\omega/\kappa)}{\Gamma(0)\Gamma(\zeta + Z\alpha\omega/\kappa)} {}_3\mathcal{F}_2 \left[\begin{matrix} 1 + \zeta - Z\alpha\omega/\kappa, 1 + 2\zeta, 1 \\ 1 + 2\zeta, 2 + \zeta - Z\alpha\omega/\kappa \end{matrix}; 1 \right] \\
 &= -\frac{[\Gamma(1 + 2\zeta)]^2\Gamma(-1 - \zeta + Z\alpha\omega/\kappa)}{\Gamma(\zeta + Z\alpha\omega/\kappa)} \left(1 + \zeta - \frac{Z\alpha\omega}{\kappa} \right) \\
 &= \frac{4}{n(n - 1)} + \mathcal{O}[(Z\alpha)^2]
 \end{aligned} \tag{E.36}$$

where again the $\Gamma(0)$ in the denominator cancels a similar factor in the numerator.

When $p = 2\zeta - 2$ the result instead is

$$\begin{aligned}
 \mathcal{I}_{22}^{(2\zeta-2)} &= \frac{\Gamma(2\zeta - 1)\Gamma(1 + 2\zeta)\Gamma(1 - \zeta + Z\alpha\omega/\kappa)}{\Gamma(2)\Gamma(\zeta + Z\alpha\omega/\kappa)} {}_3\mathcal{F}_2 \left[\begin{matrix} 1 + \zeta - Z\alpha\omega/\kappa, 2\zeta - 1, -1 \\ 1 + 2\zeta, \zeta - Z\alpha\omega/\kappa \end{matrix}; 1 \right] \\
 &= \frac{\Gamma(2\zeta - 1)\Gamma(1 + 2\zeta)\Gamma(-\zeta + Z\alpha\omega/\kappa)}{(1 + 2\zeta)\Gamma(\zeta + Z\alpha\omega/\kappa)} \left(-1 + \frac{2Z\alpha\omega}{\kappa} \right) \\
 &= \frac{2(2n - 1)}{3n(n - 1)} + \mathcal{O}[(Z\alpha)^2] \quad (\text{if } n \neq 1).
 \end{aligned} \tag{E.37}$$

At face value the singularity when $n = 1$ implies this goes like $1/(Z\alpha)^2$ for $n = 1$, but this doesn't matter since this integral ultimately appears in the energy shift premultiplied by factors of $(n - 1)$.

Combining results for \mathfrak{N}_{pt} and \mathfrak{D}_{pt}

Using the above integrals in (E.14) finally gives the expressions

$$\mathfrak{N}_{\text{pt}} = \mathcal{I}_{11}^{(2\zeta-2)} - \left(\frac{1-n+\mathfrak{z}-\lambda}{-1-n-\mu} \right)^2 \mathcal{I}_{22}^{(2\zeta-2)} = \frac{4}{(n+1)^2} + \mathcal{O}[(Z\alpha)^2], \quad (\text{E.38})$$

and

$$\begin{aligned} \mathfrak{D}_{\text{pt}} &= 2\mathcal{I}_{11}^{(2\zeta)} - \frac{4\omega}{m} \left(\frac{1-n+\mathfrak{z}-\lambda}{-1-n-\mu} \right) \mathcal{I}_{12}^{(2\zeta)} + 2 \left(\frac{1-n+\mathfrak{z}-\lambda}{-1-n-\mu} \right)^2 \mathcal{I}_{22}^{(2\zeta)} \\ &= \frac{16}{(n+1)^2} + \mathcal{O}[(Z\alpha)^2], \end{aligned} \quad (\text{E.39})$$

which together imply $\mathfrak{N}_{\text{pt}}/\mathfrak{D}_{\text{pt}} = \frac{1}{4} + \mathcal{O}[(Z\alpha)^2]$. Using this in (2.36) or (E.1) gives the prediction for hyperfine splitting for a point nucleus,

$$\begin{aligned} \varepsilon_{nF\frac{1}{2}+}^{\text{hfs}} &= -4\mathfrak{s}\mathfrak{K}X_F m \left(\frac{Z\alpha}{\mathcal{N}} \right)^3 \left(\frac{\mathfrak{N}_{\text{pt}}}{\mathfrak{D}_{\text{pt}}} \right) = -\mathfrak{s}\mathfrak{K}X_F m \left(\frac{Z\alpha}{n} \right)^3 + \mathcal{O}[(Z\alpha)^2] \\ &\rightarrow \frac{g_p m^2}{M} \left[\frac{(Z\alpha)^4}{2n^3} \right] X_F + \mathcal{O}[(Z\alpha)^2], \end{aligned} \quad (\text{E.40})$$

in agreement with the literature.

Integrals appearing in \mathfrak{N}_1 and \mathfrak{D}_1

We next apply the result (E.22) to the integrals appearing in \mathfrak{N}_1 and \mathfrak{D}_1 . In this case it is the cases $p = 0$ and $p = -2$ that are of interest, and it proves useful to specialize the general integral to these two cases for general a, b, a' and b' , keeping in mind that $b = 1 + 2\zeta$ and $b' = 1 - 2\zeta$ imply that $b' = 2 - b$.

For instance, taking $p = 0$ (*i.e.* $d = 1$) and $b' = 2 - b$ in (E.22), and simplifying using (E.20), gives

$$\begin{aligned} \mathcal{I}_1(a, b; a', 2 - b) &= \frac{\Gamma(b)\Gamma(1)\Gamma(b-a-1)}{\Gamma(b-a)\Gamma(b-1)} {}_3\mathcal{F}_2 \left[\begin{matrix} a', 1, 2-b \\ 2-b, 2+a-b \end{matrix}; 1 \right] \\ &= \frac{1-b}{1+a-a'-b}. \end{aligned} \quad (\text{E.41})$$

Similarly, taking $p = -2$ (and so $d = -1$) and $b' = 2 - b$ in (E.22) gives

$$\begin{aligned} \mathcal{I}_{-1}(a, b; a', 2 - b) &= \frac{\Gamma(b)\Gamma(d)\Gamma(b - a + 1)}{\Gamma(b - a)\Gamma(b + 1)} {}_3\mathcal{F}_2 \left[\begin{matrix} a', -1, -b \\ 2 - b, a - b \end{matrix}; 1 \right] \\ &= \frac{\Gamma(-1)}{b(b - 2)} \left[(2 - b)(a - b) + a'b \right], \end{aligned} \quad (\text{E.42})$$

which diverges (for all $Z\alpha$) due to the $\Gamma(d)$ factor as $d \rightarrow -1$. We regulate this divergence dimensionally, which in this instance merely means writing $d = -1 + \eta$ with the regularization parameter η taken to zero at the end, once the divergence has been renormalized away. With this in mind we write $\Gamma(-1) = \Gamma(-1 + \eta) = \Gamma(\eta)/(-1 + \eta) = -\Gamma(0)[1 + \mathcal{O}(\eta)]$ in what follows, in practice typically dropping the $\mathcal{O}(\eta)$ terms.

The integral \mathcal{I}_{13}^p

The general formula applies directly to $\mathcal{I}_{13}^{(p)}$, for which

$$\mathcal{I}_{13}^{(p)} := \int_0^\infty d\rho e^{-\rho} \rho^p \mathcal{M}(a, b; \rho) \mathcal{M}(a', b'; \rho) = \mathcal{I}_{p+1}(a, b; a', b'), \quad (\text{E.43})$$

in which we use

$$a = \zeta - \frac{Z\alpha\omega}{\kappa}, \quad b = 1 + 2\zeta, \quad a' = -\zeta - \frac{Z\alpha\omega}{\kappa}, \quad b' = 1 - 2\zeta. \quad (\text{E.44})$$

and so $b' = 2 - b$ and $a - a' = 2\zeta$. Again we require the cases $p = 0$ and $p = -2$ (or $d = 1$ and $d = -1$).

Specializing to $p = 0$ in (E.41) gives a divergent result because $1 + a - a' = 1 + 2\zeta = b$. Regularizing this divergence by deforming $a = \zeta - (Z\alpha\omega/\kappa) + \eta_a$ (with $\eta_a \rightarrow 0$ at the end) we have

$$\mathcal{I}_{13}^{(0)} = -\frac{2\zeta}{\eta_a} =: -\Gamma_a(0) 2\zeta = -2\Gamma_a(0) + \mathcal{O}[(Z\alpha)^2], \quad (\text{E.45})$$

which defines $\Gamma_a(0) = \eta_a^{-1}[1 + \mathcal{O}(\eta_a)]$. Similarly using the $p = -2$ in (E.42) gives

$$\mathcal{I}_{13}^{(-2)} = \frac{\Gamma(-1)}{(1 - 2\zeta)(1 + 2\zeta)} \left(1 + \frac{2Z\alpha\omega}{\kappa} \right) = -\left(\frac{2n + 1}{3} \right) \Gamma(-1) + \mathcal{O}[(Z\alpha)^2]. \quad (\text{E.46})$$

The integral \mathcal{I}_{14}^p

Next consider

$$\mathcal{I}_{14}^{(p)} := \int_0^\infty d\rho e^{-\rho} \rho^p \mathcal{M}(a, b; \rho) \mathcal{M}(a' + 1, b'; \rho) = \mathcal{I}_{p+1}(a, b; a' + 1, b'), \quad (\text{E.47})$$

evaluated using (E.44), which implies $b' = 2 - b$. In this case only $p = 0$ (or $d = 1$) is required and so using (E.41) gives

$$\mathcal{I}_{14}^{(0)} = \mathcal{I}_1(a, b; a' + 1, 2 - b) = \frac{1 - b}{a - a' - b} = 2\zeta = 2 + \mathcal{O}[(Z\alpha)^2]. \quad (\text{E.48})$$

The integral \mathcal{I}_{23}^p

The required integral in this case is

$$\mathcal{I}_{23}^{(p)} := \int_0^\infty d\rho e^{-\rho} \rho^p \mathcal{M}(a + 1, b; \rho) \mathcal{M}(a', b'; \rho) = \mathcal{I}_{p+1}(a + 1, b; a', b'), \quad (\text{E.49})$$

and only $p = 0$ (or $d = 1$) is required. Using (E.41) this time gives

$$\mathcal{I}_{23}^{(0)} = \mathcal{I}_1(a + 1, b; a', 2 - b) = \frac{1 - b}{2 + a - a' - b} = -2\zeta = -2 + \mathcal{O}[(Z\alpha)^2]. \quad (\text{E.50})$$

The integral \mathcal{I}_{24}^p

The final integral in this section is $\mathcal{I}_{24}^{(p)}$, for which

$$\mathcal{I}_{24}^{(p)} := \int_0^\infty d\rho e^{-\rho} \rho^p \mathcal{M}(a + 1, b; \rho) \mathcal{M}(a', b'; \rho) = \mathcal{I}_{p+1}(a + 1, b; a' + 1, b'), \quad (\text{E.51})$$

and both $p = 0$ (or $d = 1$) and $p = -2$ (or $d = -1$) are needed. In the case $p = 0$, using (E.41) and noting that $\mathcal{I}_1(a, b; a', 2 - b)$ depends on a and a' only through their difference, $a - a'$, implies $\mathcal{I}_{24}^{(0)} = \mathcal{I}_{13}^{(0)}$ and so

$$\mathcal{I}_{24}^{(0)} = \mathcal{I}_{13}^{(0)} = -\Gamma_a(0) 2\zeta = -2\Gamma_a(0) + \mathcal{O}[(Z\alpha)^2]. \quad (\text{E.52})$$

For $p = -2$, on the other hand, using (E.42) gives

$$\begin{aligned} \mathcal{I}_{24}^{(-2)} &= \mathcal{I}_{-1}(a + 1, b; a' + 1, 2 - b) = \frac{\Gamma(-1)}{b(b-2)} \left[(2-b)(1+a-b) + (1+a')b \right] \\ &= \frac{\Gamma(-1)}{(1+2\zeta)(-1+2\zeta)} \left(1 - \frac{2Z\alpha\omega}{\kappa} \right) = - \left(\frac{2n-1}{3} \right) \Gamma(-1) + \mathcal{O}[(Z\alpha)^2]. \end{aligned}$$

Combining results for \mathfrak{N}_1 and \mathfrak{D}_1

These integrals when combined in (E.14) give

$$\begin{aligned} \mathfrak{N}_1 &= 2\mathcal{I}_{13}^{(-2)} - 2 \left(\frac{1-n+\mathfrak{z}-\lambda}{-1-n-\mu} \right) \left(\frac{-1-n-\mathfrak{z}-\lambda}{-1-n-\mu} \right) \mathcal{I}_{24}^{(-2)} \\ &= -2 \left(\frac{2n+1}{3} \right) \Gamma(-1) + 2 \left(\frac{n-1}{n+1} \right) \left(\frac{2n-1}{3} \right) \Gamma(-1) + \mathcal{O}[(Z\alpha)^2] \quad (\text{E.53}) \\ &= - \left(\frac{4n}{n+1} \right) \Gamma(-1) + \mathcal{O}[(Z\alpha)^2], \end{aligned}$$

while (E.15) similarly becomes

$$\begin{aligned}
 \mathfrak{D}_1 &= 4\mathcal{I}_{13}^{(0)} - \frac{4\omega}{m} \left(\frac{-1-n-\mathfrak{z}-\lambda}{-1-n-\mu} \right) \mathcal{I}_{14}^{(0)} - \frac{4\omega}{m} \left(\frac{1-n+\mathfrak{z}-\lambda}{-1-n-\mu} \right) \mathcal{I}_{23}^{(0)} \\
 &\quad + 4 \left(\frac{1-n+\mathfrak{z}-\lambda}{-1-n-\mu} \right) \left(\frac{-1-n-\mathfrak{z}-\lambda}{-1-n-\mu} \right) \mathcal{I}_{24}^{(0)} \\
 &= -\frac{16}{n+1} \left[n\Gamma_a(0) + 1 \right] + \mathcal{O}[(Z\alpha)^2].
 \end{aligned} \tag{E.54}$$

Combining these with (E.38) and (E.39), which say $\mathfrak{N}_{\text{pt}} = 4/(n+1)^2 + \dots$ and $\mathfrak{D}_{\text{pt}} = 16/(n+1)^2 + \dots$ we finally get

$$\begin{aligned}
 \frac{\mathfrak{N}_1}{\mathfrak{N}_{\text{pt}}} &= -n(n+1) \Gamma(-1) + \mathcal{O}[(Z\alpha)^2] \\
 \frac{\mathfrak{D}_1}{\mathfrak{D}_{\text{pt}}} &= -(n+1) \left[n\Gamma_a(0) + 1 \right] + \mathcal{O}[(Z\alpha)^2].
 \end{aligned} \tag{E.55}$$

Keeping in mind that

$$\frac{\mathcal{D}}{\mathcal{E}} \simeq -\frac{\mathfrak{c}}{n(n+1)} \tag{E.56}$$

where $\mathfrak{c} \propto (m\epsilon_\star)^2$ is defined in (E.6), we see

$$\left(\frac{\mathcal{D}}{\mathcal{E}} \right) \frac{\mathfrak{N}_1}{\mathfrak{N}_{\text{pt}}} = \mathfrak{c} \Gamma(-1) + \mathcal{O}[(Z\alpha)^2] \tag{E.57}$$

and

$$\boxed{\left(\frac{\mathcal{D}}{\mathcal{E}} \right) \frac{\mathfrak{D}_1}{\mathfrak{D}_{\text{pt}}} = \mathfrak{c} \left[\Gamma_a(0) + \frac{1}{n} \right] + \mathcal{O}[(Z\alpha)^2]}. \tag{E.58}$$

What is important here is the divergent terms are n -independent, as is required for them to be absorbed into the counter-term c_F .

The finite contribution in \mathfrak{D}_1 does not cancel but it is small enough to be negligible for our purposes. To see why, recall that $\mathfrak{c} \sim (m\epsilon_\star)^2 \sim (mRZ\alpha)^2$ while the point hyperfine splitting is order $(m^2/M)(Z\alpha)^4$. Taking $m/M \sim mR$, the finite part of the \mathfrak{D}_1 piece contributes to the energy by an amount of order $m(Z\alpha)^3(mRZ\alpha)^3$. Keeping in mind that the charge radius contributes at order $m(Z\alpha)^2(mRZ\alpha)^2$ we see the finite part of \mathfrak{D}_1 is suppressed relative to the charge radius by a factor of order $mR(Z\alpha)^2$. For electrons this is smaller than the $(Z\alpha)^2 \sim mRZ\alpha$ order to which we work, and for muons it is comparable to the other $(mRZ\alpha)^2$ terms that have been neglected (but whose size is of practical interest for some experiments).

Integrals appearing in \mathfrak{N}_2 and \mathfrak{D}_2

Finally, consider the integrals in the $(\mathcal{D}/\mathcal{C})^2$ part of the hyperfine energy.

The integral \mathcal{I}_{33}^p

The first integral of interest here is

$$\begin{aligned} \mathcal{I}_{33}^{(p)} &:= \int_0^\infty d\rho e^{-\rho} \rho^p \mathcal{M}[a'; b'; \rho] \mathcal{M}[a'; b'; \rho] = \mathcal{I}_{p+1}(a', b'; a', b') \\ &= \frac{\Gamma(p+1)\Gamma(b')\Gamma(b'-a'-p-1)}{\Gamma(b'-a')\Gamma(b'-p-1)} {}_3\mathcal{F}_2 \left[\begin{matrix} a', p+1, p+2-b' \\ b', 2+p+a'-b' \end{matrix}; 1 \right], \end{aligned} \quad (\text{E.59})$$

in which we use

$$a' = -\zeta - \frac{Z\alpha\omega}{\kappa}, \quad b' = 1 - 2\zeta, \quad b' - a' = 1 - \zeta + \frac{Z\alpha\omega}{\kappa}. \quad (\text{E.60})$$

This is most easily obtained from the result for $\mathcal{I}_{11}^{(p)}$ found above by making the replacement $\zeta \rightarrow -\zeta$, leading to

$$\mathcal{I}_{33}^{(p)} = \frac{\Gamma(p+1)\Gamma(1-2\zeta)\Gamma(-\zeta-p+Z\alpha\omega/\kappa)}{\Gamma(-2\zeta-p)\Gamma(1-\zeta+Z\alpha\omega/\kappa)} {}_3\mathcal{F}_2 \left[\begin{matrix} -\zeta - Z\alpha\omega/\kappa, p+1, p+1+2\zeta \\ 1-2\zeta, p+1+\zeta - Z\alpha\omega/\kappa \end{matrix}; 1 \right], \quad (\text{E.61})$$

for which we require $p = -2\zeta$ and $p = -2\zeta - 2$.

In the case $p = -2\zeta$ using (E.20) allows the integral to be written

$$\begin{aligned} \mathcal{I}_{33}^{(-2\zeta)} &= \frac{[\Gamma(1-2\zeta)]^2\Gamma(\zeta+Z\alpha\omega/\kappa)}{\Gamma(0)\Gamma(1-\zeta+Z\alpha\omega/\kappa)} {}_3\mathcal{F}_2 \left[\begin{matrix} -\zeta - Z\alpha\omega/\kappa, 1-2\zeta, 1 \\ 1-2\zeta, 1-\zeta - Z\alpha\omega/\kappa \end{matrix}; 1 \right] \\ &= -\frac{[\Gamma(1-2\zeta)]^2\Gamma(1+\zeta+Z\alpha\omega/\kappa)}{\Gamma(1-\zeta+Z\alpha\omega/\kappa)}. \end{aligned}$$

Notice that in this expression the Gamma function $\Gamma(1-2\zeta)$ diverges when $Z\alpha \rightarrow 0$. What is important about this singularity is how it depends on n , since this allows it also to be absorbed into the effective coupling c_F . To see this explicitly, notice that for small $Z\alpha$ the above becomes

$$\mathcal{I}_{33}^{(-2\zeta)} = -\Gamma(-1-2\mathfrak{z})^2 \left[n(n+1) + \mathcal{O}[(Z\alpha)^2] \right]. \quad (\text{E.62})$$

The case $p = -2\zeta - 2$ similarly gives

$$\begin{aligned} \mathcal{I}_{33}^{(-2\zeta-2)} &= \frac{\Gamma(-1-2\zeta)\Gamma(1-2\zeta)\Gamma(2+\zeta+Z\alpha\omega/\kappa)}{\Gamma(2)\Gamma(1-\zeta+Z\alpha\omega/\kappa)} {}_3\mathcal{F}_2 \left[\begin{matrix} -\zeta - Z\alpha\omega/\kappa, -1-2\zeta, -1 \\ 1-2\zeta, -1-\zeta - Z\alpha\omega/\kappa \end{matrix}; 1 \right] \\ &= \frac{[\Gamma(1-2\zeta)]^2\Gamma(1+\zeta+Z\alpha\omega/\kappa)}{2\zeta(1+2\zeta)(1-2\zeta)\Gamma(1-\zeta+Z\alpha\omega/\kappa)} \left(1 + \frac{2Z\alpha\omega}{\kappa} \right). \end{aligned}$$

which as $Z\alpha \rightarrow 0$ becomes

$$\mathcal{I}_{33}^{(-2\zeta-2)} = [\Gamma(-1 - 2\zeta)]^2 \left[-\frac{1}{6} n(n+1)(2n+1) + \mathcal{O}[(Z\alpha)^2] \right].$$

The integral \mathcal{I}_{34}^p

Consider next

$$\begin{aligned} \mathcal{I}_{34}^{(p)} &:= \int_0^\infty d\rho e^{-\rho} \rho^p \mathcal{M}[a'; b'; \rho] \mathcal{M}[a'+1; b'; \rho] = \mathcal{I}_{p+1}(a', b'; a'+1, b') \quad (\text{E.63}) \\ &= \frac{\Gamma(p+1)\Gamma(b')\Gamma(b'-a'-p-1)}{\Gamma(b'-a')\Gamma(b'-p-1)} {}_3\mathcal{F}_2 \left[\begin{matrix} a'+1, p+1, p+2-b' \\ b', 2+p+a'-b' \end{matrix}; 1 \right], \end{aligned}$$

which becomes

$$\mathcal{I}_{34}^{(p)} = \frac{\Gamma(p+1)\Gamma(1-2\zeta)\Gamma(-\zeta-p+Z\alpha\omega/\kappa)}{\Gamma(-2\zeta-p)\Gamma(1-\zeta+Z\alpha\omega/\kappa)} {}_3\mathcal{F}_2 \left[\begin{matrix} 1-\zeta-Z\alpha\omega/\kappa, p+1, p+1+2\zeta \\ 1-2\zeta, p+1+\zeta-Z\alpha\omega/\kappa \end{matrix}; 1 \right]. \quad (\text{E.64})$$

In the case $p = -2\zeta$ this gives

$$\begin{aligned} \mathcal{I}_{34}^{(-2\zeta)} &= \frac{[\Gamma(1-2\zeta)]^2 \Gamma(\zeta+Z\alpha\omega/\kappa)}{\Gamma(0)\Gamma(1-\zeta+Z\alpha\omega/\kappa)} {}_3\mathcal{F}_2 \left[\begin{matrix} 1-\zeta-Z\alpha\omega/\kappa, 1-2\zeta, 1 \\ 1-2\zeta, 1-\zeta-Z\alpha\omega/\kappa \end{matrix}; 1 \right] \\ &= \frac{[\Gamma(1-2\zeta)]^2 \Gamma(\zeta+Z\alpha\omega/\kappa)}{\Gamma(0)\Gamma(1-\zeta+Z\alpha\omega/\kappa)} \left(\zeta + \frac{Z\alpha\omega}{\kappa} \right) = 0. \end{aligned}$$

which vanishes due to the uncanceled $\Gamma(0)$ in the denominator.

The integral \mathcal{I}_{44}^p

Finally consider the case

$$\begin{aligned} \mathcal{I}_{44}^{(p)} &:= \int_0^\infty d\rho e^{-\rho} \rho^p \mathcal{M}[a'+1; b'; \rho] \mathcal{M}[a'+1; b'; \rho] = \mathcal{I}_{p+1}(a'+1, b'; a'+1, b') \\ &= \frac{\Gamma(p+1)\Gamma(b')\Gamma(b'-a'-p-2)}{\Gamma(b'-a'-1)\Gamma(b'-p-1)} {}_3\mathcal{F}_2 \left[\begin{matrix} a'+1, p+1, p+2-b' \\ b', 3+p+a'-b' \end{matrix}; 1 \right], \quad (\text{E.65}) \end{aligned}$$

which becomes

$$\mathcal{I}_{44}^{(p)} = \frac{\Gamma(p+1)\Gamma(1-2\zeta)\Gamma(-1-\zeta-p+Z\alpha\omega/\kappa)}{\Gamma(-2\zeta-p)\Gamma(-\zeta+Z\alpha\omega/\kappa)} {}_3\mathcal{F}_2 \left[\begin{matrix} 1-\zeta-Z\alpha\omega/\kappa, p+1, p+1+2\zeta \\ 1-2\zeta, p+2+\zeta-Z\alpha\omega/\kappa \end{matrix}; 1 \right]. \quad (\text{E.66})$$

When $p = -2\zeta$ the above formula becomes

$$\begin{aligned} \mathcal{I}_{44}^{(-2\zeta)} &= \frac{[\Gamma(1-2\zeta)]^2 \Gamma(-1+\zeta+Z\alpha\omega/\kappa)}{\Gamma(0)\Gamma(-\zeta+Z\alpha\omega/\kappa)} {}_3\mathcal{F}_2 \left[\begin{matrix} 1-\zeta-Z\alpha\omega/\kappa, 1-2\zeta, 1 \\ 1-2\zeta, 2-\zeta-Z\alpha\omega/\kappa \end{matrix}; 1 \right] \\ &= \frac{[\Gamma(1-2\zeta)]^2 \Gamma(-1+\zeta+Z\alpha\omega/\kappa)}{\Gamma(-\zeta+Z\alpha\omega/\kappa)} \left(1-\zeta - \frac{Z\alpha\omega}{\kappa} \right). \quad (\text{E.67}) \end{aligned}$$

Expanding around $Z\alpha = 0$ shows the same divergent pole as for $\mathcal{I}_{33}^{(-2\zeta)}$, leading to

$$\mathcal{I}_{44}^{(-2\zeta)} = [\Gamma(-1 - 2\mathfrak{z})]^2 \left[-n(n-1) + \mathcal{O}[(Z\alpha)^2] \right]. \quad (\text{E.68})$$

Next take $p = -2\zeta - 2$ in which case

$$\begin{aligned} \mathcal{I}_{44}^{(-2\zeta-2)} &= \frac{\Gamma(-1 - 2\zeta)\Gamma(1 - 2\zeta)\Gamma(1 + \zeta + Z\alpha\omega/\kappa)}{\Gamma(2)\Gamma(-\zeta + Z\alpha\omega/\kappa)} {}_3\mathcal{F}_2 \left[\begin{matrix} 1 - \zeta - Z\alpha\omega/\kappa, -1 - 2\zeta, -1 \\ 1 - 2\zeta, -\zeta - Z\alpha\omega/\kappa \end{matrix}; 1 \right] \\ &= \frac{[\Gamma(1 - 2\zeta)]^2 \Gamma(\zeta + Z\alpha\omega/\kappa)}{2\zeta(1 + 2\zeta)(1 - 2\zeta)\Gamma(-\zeta + Z\alpha\omega/\kappa)} \left(-1 + \frac{2Z\alpha\omega}{\kappa} \right), \end{aligned} \quad (\text{E.69})$$

which expands out to give

$$\mathcal{I}_{44}^{(-2\zeta-2)} = [\Gamma(-1 - 2\mathfrak{z})]^2 \left[-\frac{1}{6}n(n-1)(2n-1) + \mathcal{O}[(Z\alpha)^2] \right]. \quad (\text{E.70})$$

Combining results \mathfrak{N}_2 and \mathfrak{D}_2

These integrals combine to give

$$\begin{aligned} \mathfrak{N}_2 &= \mathcal{I}_{33}^{(-2\zeta-2)} - \left(\frac{-1 - n - \mathfrak{z} - \lambda}{-1 - n - \mu} \right)^2 \mathcal{I}_{44}^{(-2\zeta-2)} \\ &= [\Gamma(-1 - 2\mathfrak{z})]^2 \left[-n^2 + \mathcal{O}[(Z\alpha)^2] \right], \end{aligned} \quad (\text{E.71})$$

and

$$\begin{aligned} \mathfrak{D}_2 &= 2 \left\{ \mathcal{I}_{33}^{(-2\zeta)} - \frac{2\omega}{m} \left(\frac{-1 - n - \mathfrak{z} - \lambda}{-1 - n - \mu} \right) \mathcal{I}_{34}^{(-2\zeta)} + \left(\frac{-1 - n - \mathfrak{z} - \lambda}{-1 - n - \mu} \right)^2 \mathcal{I}_{44}^{(-2\zeta)} \right\} \\ &= 2[\Gamma(-1 - 2\mathfrak{z})]^2 \left[-2n^2 + \mathcal{O}[(Z\alpha)^2] \right]. \end{aligned} \quad (\text{E.72})$$

and so

$$\frac{\mathfrak{N}_2}{\mathfrak{N}_{\text{pt}}} = [\Gamma(-1 - 2\mathfrak{z})]^2 \left[-\frac{n^2(n+1)^2}{4} + \mathcal{O}[(Z\alpha)^2] \right], \quad (\text{E.73})$$

and

$$\frac{\mathfrak{D}_2}{\mathfrak{D}_{\text{pt}}} = -[\Gamma(-1 - 2\mathfrak{z})]^2 \left[\frac{n^2(n+1)^2}{4} + \mathcal{O}[(Z\alpha)^2] \right]. \quad (\text{E.74})$$

Keeping in mind that

$$\frac{\mathcal{D}}{\mathcal{E}} \simeq -\frac{\mathfrak{c}}{n(n+1)} \quad (\text{E.75})$$

where $\mathfrak{c} \propto (m\epsilon_\star)^2$ so

$$\left(\frac{\mathcal{D}}{\mathcal{E}} \right)^2 \frac{\mathfrak{N}_2}{\mathfrak{N}_{\text{pt}}} = [\Gamma(-1 - 2\mathfrak{z})]^2 \left[-\frac{\mathfrak{c}^2}{4} + \mathcal{O}[(Z\alpha)^2] \right], \quad (\text{E.76})$$

and

$$\left(\frac{\mathcal{D}}{\mathcal{L}}\right)^2 \frac{\mathcal{D}_2}{\mathcal{D}_{\text{pt}}} = -[\Gamma(-1 - 2\mathfrak{z})]^2 \left[\frac{\mathfrak{c}^2}{4} + \mathcal{O}[(Z\alpha)^2] \right]. \quad (\text{E.77})$$

Combined result

Finally combining all terms gives

$$\begin{aligned} \frac{\mathfrak{N}}{\mathfrak{D}} &= \frac{\mathfrak{N}_{\text{pt}}}{\mathfrak{D}_{\text{pt}}} \left[\frac{1 + (\mathcal{D}/\mathcal{L})(\mathfrak{N}_1/\mathfrak{N}_{\text{pt}}) + (\mathcal{D}/\mathcal{L})^2(\mathfrak{N}_2/\mathfrak{N}_{\text{pt}})}{1 + (\mathcal{D}/\mathcal{L})(\mathfrak{D}_1/\mathfrak{D}_{\text{pt}}) + (\mathcal{D}/\mathcal{L})^2(\mathfrak{D}_2/\mathfrak{D}_{\text{pt}})} \right] \\ &\simeq \frac{\mathfrak{N}_{\text{pt}}}{\mathfrak{D}_{\text{pt}}} \left[1 + C - \frac{\mathfrak{c}}{n} + \dots \right], \end{aligned} \quad (\text{E.78})$$

where C is an n -independent but divergent constant whose precise value does not matter because it gets absorbed into the renormalization of c_F . The prediction beyond the contribution of c_F is completely contained in the \mathfrak{c}/n term, which is smaller than the order to which we work.

Radial matrix element of the first-order state correction

In the main text we have anticipated that the first-order wave-function corrections will lead to a more complicated RG behaviour of the combined PPEFT couplings $\hat{c}_s \pm \hat{c}_v + \langle \mathbf{I} \cdot \mathbf{S} \rangle \hat{c}_F$ of $j = 1/2$ states through the boundary conditions (B.15) (worked out in detail in Appendix B), repeated here for convenience

$$(\hat{c}_s^+ + \mathcal{Z}_F \hat{c}_F^+ - \hat{c}_v^+) = \frac{\mathfrak{g}_+}{\mathfrak{f}_+}, \quad \text{and} \quad (\hat{c}_s^- + \mathcal{Z}_F \hat{c}_F^- + \hat{c}_v^-) = \frac{\mathfrak{f}_-}{\mathfrak{g}_-}. \quad (\text{E.79})$$

This occurs because the radial functions on the right-hand sides of these conditions change under the perturbation of the nuclear magnetic dipole field and can be expanded in a perturbation series as $\mathfrak{f}_\varpi = \mathfrak{f}_\varpi^{(0)} + \mathfrak{s}\mathfrak{f}_\varpi^{(1)} + \dots$ and $\mathfrak{g}_\varpi = \mathfrak{g}_\varpi^{(0)} + \mathfrak{s}\mathfrak{g}_\varpi^{(1)} + \dots$, where the ellipses stand for the second- and higher-order corrections.

These corrections to the radial functions come about as a result of the state corrections, which we had formally calculated in (D.11) and as applied to the eigenstates of total atomic angular momentum $|nFF_z j \varpi\rangle$ reads

$$\begin{aligned} |nFF_z j \varpi\rangle_1 &= \frac{\mathcal{C}_{nnFF_z j' j(-\varpi)\varpi}}{\omega_{nj\varpi}^D - \omega_{nj'(-\varpi)}^D} |nFF_z j'(-\varpi)\rangle_0 + \sum_{\tilde{n} \neq n} \left[\frac{\mathcal{C}_{\tilde{n}nFF_z j j \varpi \varpi}}{\omega_{nj\varpi}^D - \omega_{\tilde{n}j\varpi}^D} |\tilde{n}FF_z j \varpi\rangle_0 \right. \\ &\quad \left. + \frac{\mathcal{C}_{\tilde{n}nFF_z j' j(-\varpi)\varpi}}{\omega_{nj\varpi}^D - \omega_{\tilde{n}j'(-\varpi)}^D} |\tilde{n}FF_z j'(-\varpi)\rangle_0 \right], \end{aligned} \quad (\text{E.80})$$

where the coefficients are defined as

$$\begin{aligned}
 \mathcal{C}_{\tilde{n}nFF_z\tilde{j}j\tilde{\varpi}\varpi} &:= {}_0 \langle \tilde{n}FF_z\tilde{j}\tilde{\varpi} | V | nFF_zj\varpi \rangle_0 = - \left(\frac{e\mu_N}{4\pi\tilde{\mathcal{D}}} \right) \int d^3x r^{-2} \tilde{\psi}^\dagger \boldsymbol{\gamma}^0 \boldsymbol{\gamma} \cdot (\mathbf{I} \times \hat{\mathbf{r}}) \psi, \\
 &= - \left(\frac{\mathfrak{s}}{m} \right) \int d\Omega_2 \left(\mathcal{Y}_{F,f_z}^{\tilde{j}\tilde{\varpi}} \right)^\dagger (I^\theta \sigma^\theta + I^\phi \sigma^\phi) \mathcal{Y}_{F,f_z}^{j\varpi} \frac{\int_0^\infty dr \left(\tilde{\mathfrak{f}}\mathfrak{g} + \tilde{\mathfrak{g}}\mathfrak{f} \right)}{\tilde{\mathcal{D}}}, \\
 &= \frac{(2\tilde{\kappa})^3 \mathfrak{s}}{m^2} \left(\frac{\mathcal{C}}{\tilde{\mathcal{C}}} \right) \int d\Omega_2 \left(\mathcal{Y}_{F,f_z}^{\tilde{j}\tilde{\varpi}} \right)^\dagger (I^\theta \sigma^\theta + I^\phi \sigma^\phi) \mathcal{Y}_{F,f_z}^{j\varpi} \left(\frac{\mathfrak{N}^s}{\tilde{\mathcal{D}}} \right), \quad (\text{E.81})
 \end{aligned}$$

with

$$\tilde{\mathcal{D}} = \int_0^\infty dr r^2 \left(\tilde{\mathfrak{f}}^2 + \tilde{\mathfrak{g}}^2 \right) = \frac{\tilde{\mathcal{C}}^2 m}{(2\tilde{\kappa})^3} \tilde{\mathcal{D}}. \quad (\text{E.82})$$

Notice that a total of three types of terms appear in the first-order wave-function correction: there are corrections coming from states that have the same angular momentum quantum numbers as the corrected state but that differ from it in their principal quantum number; there are corrections from states that have the same F, F_z and l quantum numbers but different n, j values and opposite parity; lastly there is a contribution from a state that shares the same n, F, F_z and l value as the corrected state and differs from it only in its j -value and parity. This medley of corrections occurs due to the fact that although the F eigenstates do diagonalize the degenerate subspaces of the combined nuclear and Dirac-Coulomb modes, they do *not* diagonalize the actual perturbation, $\mathcal{L}_{\text{int}} = -e\boldsymbol{\gamma}^0 \boldsymbol{\gamma} \cdot \mathbf{A}^{\text{nuc}}$ (except for S -states for which $\mathbf{J} = \mathbf{S}$); the hyperfine perturbation is known to mix states that share all their quantum numbers except for j and ϖ [104, 105]. This effect manifests in the corrections proportional to $\mathcal{C}_{nmFF_zj'j(-\varpi)\varpi}$ and $\mathcal{C}_{\tilde{n}nFF_zj'j(-\varpi)\varpi}$, which first appear for the negative-parity, $j = 1/2$ states that receive a correction from the positive-parity $j = 3/2$ states (and so we have $j = 1/2$, $j' = 3/2$ and $\varpi = -$ for these mixing corrections).

We can obtain a rough estimate for the sizes of these corrections knowing that the Dirac-Coulomb modes go as $\rho^{\zeta-1} \sim (mRZ\alpha)^{|\mathfrak{R}|-1}$ and so $|n, F, F_z, 1/2, -\rangle_0 \sim \mathcal{O}(1)$ whereas $|n, F, F_z, 3/2, +\rangle_0 \sim (mRZ\alpha)$, and assuming (as we will show below) $\mathcal{C}_{\tilde{n}nFF_z\tilde{j}j\tilde{\varpi}\varpi} \sim \mathfrak{s}(Z\alpha)^3$, while the energy differences are of size,

$$(\omega_{nj\varpi}^D - \omega_{\tilde{n}j\varpi}^D) \sim (Z\alpha)^2, \quad (\omega_{nj\varpi}^D - \omega_{\tilde{n}j'(-\varpi)}^D) \sim (Z\alpha)^2, \quad (\omega_{nj\varpi}^D - \omega_{nj'(-\varpi)}^D) \sim (Z\alpha)^4.$$

The large size of the last energy difference is due to the Dirac-Coulomb modes having the same principal quantum number, n but different angular momentum quantum numbers, j, j' .

Combining these estimates we find that the corrections coming from states with the same angular momentum quantum numbers but different principal quantum number

are of order,

$$\frac{\mathcal{C}_{\tilde{n}nFF_zjj\varpi\varpi}}{\omega_{nj\varpi}^D - \omega_{\tilde{n}j\varpi}^D} |\tilde{n}FF_zj\varpi\rangle_0 \sim \mathfrak{s} \frac{(Z\alpha)^3}{(Z\alpha)^2} = \mathfrak{s}(Z\alpha), \quad (\text{E.83})$$

those coming from states with the same F, F_z and l value but different n, j, ϖ values are of size,

$$\frac{\mathcal{C}_{\tilde{n}nFF_zj'j(-\varpi)\varpi}}{\omega_{nj\varpi}^D - \omega_{\tilde{n}j'(-\varpi)}^D} |\tilde{n}FF_zj'(-\varpi)\rangle_0 \sim \mathfrak{s} \frac{(Z\alpha)^3}{(Z\alpha)^2} (mRZ\alpha) = \mathfrak{s}(Z\alpha)(mRZ\alpha). \quad (\text{E.84})$$

and those coming from states with the same n, F, F_z but different j, ϖ quantum numbers as the corrected state yield a correction of size.

$$\frac{\mathcal{C}_{nnFF_zj'j(-\varpi)\varpi}}{\omega_{nj\varpi}^D - \omega_{nj'(-\varpi)}^D} |nFF_zj'(-\varpi)\rangle_0 \sim \mathfrak{s} \frac{(Z\alpha)^3}{(Z\alpha)^4} (mRZ\alpha) = \frac{\mathfrak{s}}{(Z\alpha)} (mRZ\alpha). \quad (\text{E.85})$$

Looking at these sizes we can see that the corrections coming from mixing states with different angular momentum quantum numbers are proportional to $(mRZ\alpha)$, which pushes them outside of the scope of this paper as their calculation would require the PPEFT action to be computed to the next order in R/a_B . Nevertheless, although we ignore these off-diagonal corrections to the negative parity, $j = 1/2$ state in what follows, we compute the most general matrix element $\mathcal{C}_{\tilde{n}nFF_z\tilde{j}\tilde{j}\tilde{\varpi}\tilde{\varpi}}$ next.

In the $\mathcal{C}_{\tilde{n}nFF_z\tilde{j}\tilde{j}\tilde{\varpi}\tilde{\varpi}}$ coefficients above, $\tilde{\mathfrak{D}}$ has the same functional form as \mathfrak{D} defined in (E.5) and (E.15) for the first-order energy shift with the parameters taken to be $n \rightarrow \tilde{n}, \zeta \rightarrow \tilde{\zeta}, \rho \rightarrow \tilde{\rho}$, etc. and so this part does not require further computation. What is new is the function in the numerator that integrates over the mixtures of the radial functions of the corrected and the correcting states that can be written in terms of the various integration constant ratios as,

$$\begin{aligned} \mathfrak{N}^s = & m(2\tilde{\kappa})^{\tilde{\zeta}-1} (2\kappa)^{\zeta-1} (\tilde{\kappa} + \kappa)^{1-\tilde{\zeta}-\zeta} \left\{ \mathfrak{N}_{\text{pt}}^s + \left(\frac{\mathcal{D}}{\mathcal{E}} \right) (2\kappa)^{-2\zeta} \mathfrak{N}_1^s + \left(\frac{\tilde{\mathcal{D}}}{\tilde{\mathcal{E}}} \right) (2\tilde{\kappa})^{-2\tilde{\zeta}} \tilde{\mathfrak{N}}_1^s \right. \\ & \left. + \left(\frac{\mathcal{D}\tilde{\mathcal{D}}}{\mathcal{E}\tilde{\mathcal{E}}} \right) (2\tilde{\kappa})^{-2\tilde{\zeta}} (2\kappa)^{-2\zeta} \mathfrak{N}_2^s \right\}. \end{aligned} \quad (\text{E.86})$$

Furthermore, similarly to the energy shift, the functions $\mathfrak{N}_{\text{pt}}^s, \mathfrak{N}_1^s, \tilde{\mathfrak{N}}_1^s$ and \mathfrak{N}_2^s can all be written as instances of the integral,

$$\mathcal{I}_{ij}^p := (\tilde{\kappa} + \kappa)^{\tilde{\zeta}+\zeta-1} \int_0^\infty dr e^{-(\tilde{\kappa}+\kappa)r} r^p \mathcal{M}_i \mathcal{M}_{\tilde{j}}, \quad (\text{E.87})$$

where the tilde on the subscript of the hypergeometric function means that in all of its arguments the parameters are to be transformed as $n \rightarrow \tilde{n}, \kappa \rightarrow \tilde{\kappa}, \zeta \rightarrow \tilde{\zeta}$ and so on.

This integral differs from that of the energy shift in (E.7) in that the integration variable is no longer the same as the argument of either of the hypergeometric functions and the exponential has a factor multiplying the integration variable and so is proportional to the more general form of (E.22)

$$\begin{aligned} \mathcal{I}_d(s; a, b, k; \tilde{a}, \tilde{b}, \tilde{k}) &:= \int_0^\infty dr e^{-sr} r^{d-1} \mathcal{M}[a; b; kr] \mathcal{M}[\tilde{a}; \tilde{b}; \tilde{k}r], \\ &= s^{-d} \Gamma[d] \sum_{q=0}^{\infty} \frac{(a)_q (k)^q (d)_q}{(b)_q q! s^q} {}_2\mathcal{F}_1 \left[\begin{matrix} \tilde{a}, d+q; \tilde{k} \\ \tilde{b}; s \end{matrix} \right], \end{aligned} \quad (\text{E.88})$$

which after taking the limit $\tilde{k} = k = s$ and redefining the integration variable to $\rho = kr$ becomes proportional to (E.22). The equality on the second line can again be found by writing out one of the hypergeometric functions in its series form and carrying out the resulting integral term by term using standard techniques found in [120, 121].

In terms of these integrals the functions of \mathfrak{N}^s can be written as,

$$\begin{aligned} \mathfrak{N}_{\text{pt}}^s &= \mathcal{I}_{11}^{(\tilde{\zeta}+\zeta-2)} \mathcal{S}_+ - \left(\frac{\tilde{a}}{\tilde{c}} \right) \mathcal{I}_{12}^{(\tilde{\zeta}+\zeta-2)} \mathcal{S}_- + \left(\frac{a}{c} \right) \mathcal{I}_{21}^{(\tilde{\zeta}+\zeta-2)} \mathcal{S}_- - \left(\frac{a\tilde{a}}{c\tilde{c}} \right) \mathcal{I}_{22}^{(\tilde{\zeta}+\zeta-2)} \mathcal{S}_+, \\ \mathfrak{N}_1^s &= \mathcal{I}_{31}^{(\tilde{\zeta}-\zeta-2)} \mathcal{S}_+ - \left(\frac{\tilde{a}}{\tilde{c}} \right) \mathcal{I}_{32}^{(\tilde{\zeta}-\zeta-2)} \mathcal{S}_- + \left(\frac{a'}{c} \right) \mathcal{I}_{41}^{(\tilde{\zeta}-\zeta-2)} \mathcal{S}_- - \left(\frac{a'\tilde{a}}{c\tilde{c}} \right) \mathcal{I}_{42}^{(\tilde{\zeta}-\zeta-2)} \mathcal{S}_+, \\ \tilde{\mathfrak{N}}_1^s &= \mathcal{I}_{13}^{(\zeta-\tilde{\zeta}-2)} \mathcal{S}_+ - \left(\frac{\tilde{a}'}{\tilde{c}} \right) \mathcal{I}_{14}^{(\zeta-\tilde{\zeta}-2)} \mathcal{S}_- + \left(\frac{a}{c} \right) \mathcal{I}_{23}^{(\zeta-\tilde{\zeta}-2)} \mathcal{S}_- - \left(\frac{a\tilde{a}'}{c\tilde{c}} \right) \mathcal{I}_{24}^{(\zeta-\tilde{\zeta}-2)} \mathcal{S}_+, \\ \mathfrak{N}_2^s &= \mathcal{I}_{33}^{(-\tilde{\zeta}-\zeta-2)} \mathcal{S}_+ - \left(\frac{\tilde{a}'}{\tilde{c}} \right) \mathcal{I}_{34}^{(-\tilde{\zeta}-\zeta-2)} \mathcal{S}_- + \left(\frac{a'}{c} \right) \mathcal{I}_{43}^{(-\tilde{\zeta}-\zeta-2)} \mathcal{S}_- - \left(\frac{a'\tilde{a}'}{c\tilde{c}} \right) \mathcal{I}_{44}^{(-\tilde{\zeta}-\zeta-2)} \mathcal{S}_+, \end{aligned} \quad (\text{E.89})$$

where the dimensionless quantities, \mathcal{S}_\pm are defined as

$$\mathcal{S}_\pm := \sqrt{\left(1 + \frac{\tilde{\omega}}{m}\right) \left(1 - \frac{\omega}{m}\right)} \pm \sqrt{\left(1 + \frac{\omega}{m}\right) \left(1 - \frac{\tilde{\omega}}{m}\right)} \sim \mathcal{O}(Z\alpha). \quad (\text{E.90})$$

In general, the integrals in \mathfrak{N}_1^s , $\tilde{\mathfrak{N}}_1^s$ and \mathfrak{N}_2^s will diverge and a more careful analysis of their divergence structure and the energy shifts is required to see if they can be absorbed into the PPEFT couplings through boundary conditions such as (B.15). However, the possible divergences appear along with ratios of integration constants such as $(\mathcal{D}/\mathcal{E})$ and $(\tilde{\mathcal{D}}/\tilde{\mathcal{E}})$ and so are suppressed by factors of $(m\epsilon_\star)^{2\zeta} \sim (mRZ\alpha)^{2|\Re|}$ and $(m\tilde{\epsilon}_\star)^{2\tilde{\zeta}} \sim (mRZ\alpha)^{2|\tilde{\Re}|}$, which makes them negligible to the order we work here and so we do not explicitly calculate the integrals in \mathfrak{N}_1^s , $\tilde{\mathfrak{N}}_1^s$ and \mathfrak{N}_2^s .

Then, it is sufficient for our purposes (which is to capture the leading order corrections to the wave-functions) to calculate $\mathfrak{N}_{\text{pt}}^s$, which contains integrals that integrate

over the point-nucleus parts of the radial functions of the Dirac-Coulomb modes. These evaluate to,

$$\begin{aligned}
 \mathcal{I}_{11}^{(\tilde{\zeta}+\zeta-2)} &= (\tilde{\kappa} + \kappa)^{\tilde{\zeta}+\zeta-1} \mathcal{I}_{(\tilde{\zeta}+\zeta-1)}(\tilde{\kappa} + \kappa; a, b, 2\kappa; \tilde{a}, \tilde{b}, 2\tilde{\kappa}) = \\
 &\Gamma[\tilde{\zeta} + \zeta - 1] \sum_{q=0}^{\infty} \frac{(a)_q (2\kappa)^q (\tilde{\zeta} + \zeta - 1)_q}{(b)_q q! (\tilde{\kappa} + \kappa)^q} {}_2\mathcal{F}_1 \left[\begin{matrix} \tilde{a}, \tilde{\zeta} + \zeta - 1 + q; \\ \tilde{b}; \end{matrix} \frac{2\tilde{\kappa}}{\tilde{\kappa} + \kappa} \right], \\
 \mathcal{I}_{12}^{(\tilde{\zeta}+\zeta-2)} &= (\tilde{\kappa} + \kappa)^{\tilde{\zeta}+\zeta-1} \mathcal{I}_{(\tilde{\zeta}+\zeta-1)}(\tilde{\kappa} + \kappa; a, b, 2\kappa; \tilde{a} + 1, \tilde{b}, 2\tilde{\kappa}) = \\
 &\Gamma[\tilde{\zeta} + \zeta - 1] \sum_{q=0}^{\infty} \frac{(a)_q (2\kappa)^q (\tilde{\zeta} + \zeta - 1)_q}{(b)_q q! (\tilde{\kappa} + \kappa)^q} {}_2\mathcal{F}_1 \left[\begin{matrix} \tilde{a} + 1, \tilde{\zeta} + \zeta - 1 + q; \\ \tilde{b}; \end{matrix} \frac{2\tilde{\kappa}}{\tilde{\kappa} + \kappa} \right], \\
 \mathcal{I}_{21}^{(\tilde{\zeta}+\zeta-2)} &= (\tilde{\kappa} + \kappa)^{\tilde{\zeta}+\zeta-1} \mathcal{I}_{(\tilde{\zeta}+\zeta-1)}(\tilde{\kappa} + \kappa; a + 1, b, 2\kappa; \tilde{a}, \tilde{b}, 2\tilde{\kappa}) = \\
 &\Gamma[\tilde{\zeta} + \zeta - 1] \sum_{q=0}^{\infty} \frac{(a + 1)_q (2\kappa)^q (\tilde{\zeta} + \zeta - 1)_q}{(b)_q q! (\tilde{\kappa} + \kappa)^q} {}_2\mathcal{F}_1 \left[\begin{matrix} \tilde{a}, \tilde{\zeta} + \zeta - 1 + q; \\ \tilde{b}; \end{matrix} \frac{2\tilde{\kappa}}{\tilde{\kappa} + \kappa} \right], \\
 \mathcal{I}_{22}^{(\tilde{\zeta}+\zeta-2)} &= (\tilde{\kappa} + \kappa)^{\tilde{\zeta}+\zeta-1} \mathcal{I}_{(\tilde{\zeta}+\zeta-1)}(\tilde{\kappa} + \kappa; a + 1, b, 2\kappa; \tilde{a} + 1, \tilde{b}, 2\tilde{\kappa}) = \\
 &\Gamma[\tilde{\zeta} + \zeta - 1] \sum_{q=0}^{\infty} \frac{(a + 1)_q (2\kappa)^q (\tilde{\zeta} + \zeta - 1)_q}{(b)_q q! (\tilde{\kappa} + \kappa)^q} {}_2\mathcal{F}_1 \left[\begin{matrix} \tilde{a} + 1, \tilde{\zeta} + \zeta - 1 + q; \\ \tilde{b}; \end{matrix} \frac{2\tilde{\kappa}}{\tilde{\kappa} + \kappa} \right],
 \end{aligned} \tag{E.91}$$

and then combine in $\mathfrak{N}_{\text{pt}}^{\text{s}}$ to

$$\begin{aligned}
 \mathfrak{N}_{\text{pt}}^{\text{s}} &= \Gamma[\tilde{\zeta} + \zeta - 1] \sum_{q=0}^{\infty} \frac{(2\kappa)^q (\tilde{\zeta} + \zeta - 1)_q}{(b)_q q! (\tilde{\kappa} + \kappa)^q} \times \\
 &\left\{ \mathcal{S}_+ \left((a)_{q2} \mathcal{F}_1 \left[\begin{matrix} \tilde{a}, \tilde{\zeta} + \zeta - 1 + q; \\ \tilde{b}; \end{matrix} \frac{2\tilde{\kappa}}{\tilde{\kappa} + \kappa} \right] - \right. \right. \\
 &\quad \left. \left. \left(\frac{\tilde{a}a}{\tilde{c}c} \right) (a + 1)_{q2} \mathcal{F}_1 \left[\begin{matrix} \tilde{a} + 1, \tilde{\zeta} + \zeta - 1 + q; \\ \tilde{b}; \end{matrix} \frac{2\tilde{\kappa}}{\tilde{\kappa} + \kappa} \right] \right) + \right. \\
 &\quad \left. \mathcal{S}_- \left(\frac{a(a + 1)_q}{c} {}_2\mathcal{F}_1 \left[\begin{matrix} \tilde{a}, \tilde{\zeta} + \zeta - 1 + q; \\ \tilde{b}; \end{matrix} \frac{2\tilde{\kappa}}{\tilde{\kappa} + \kappa} \right] - \right. \right. \\
 &\quad \left. \left. \frac{\tilde{a}(a)_q}{\tilde{c}} {}_2\mathcal{F}_1 \left[\begin{matrix} \tilde{a} + 1, \tilde{\zeta} + \zeta - 1 + q; \\ \tilde{b}; \end{matrix} \frac{2\tilde{\kappa}}{\tilde{\kappa} + \kappa} \right] \right) \right) \left. \right\}. \tag{E.92}
 \end{aligned}$$

A further simplification is possible thanks to $a = \zeta - Z\alpha\omega/\kappa = 1 - n$ and likewise $\tilde{a} = \tilde{\zeta} - Z\alpha\tilde{\omega}/\tilde{\kappa} = 1 - \tilde{n}$ being non-positive integers for all values of n, \tilde{n} and hence terminating both the explicit series and the series representation of the hypergeometric

functions. Then, using (E.16) and the identities $a(a+1)_q = (a)_{q+1} = (a)_q(a+q)$ and $(a)_q(a+q)_t = (a)_{q+t}$ we can write after a little bit of algebra,

$$\begin{aligned}
 \mathfrak{N}_{\text{pt}}^s &= \Gamma[\tilde{\zeta} + \zeta - 1] \sum_{q=0}^{\infty} \sum_{t=0}^{\infty} \frac{(2\kappa)^q (2\tilde{\kappa})^t (\tilde{\zeta} + \zeta - 1)_{q+t} (a)_q (\tilde{a})_t}{(\tilde{\kappa} + \kappa)^{q+t} q! t! (b)_q (\tilde{b})_t \tilde{c} c} \times \\
 &\quad \left\{ \mathcal{S}_+ (\tilde{c}c - (a+q)(\tilde{a}+t)) + \mathcal{S}_- (a - \tilde{a} + q - t) \right\}, \\
 &= \sum_{q=0}^{n-1} \sum_{t=0}^{\tilde{n}-1} \frac{\Gamma[\tilde{\zeta} + \zeta - 1] (2\kappa)^q (2\tilde{\kappa})^t (\tilde{\zeta} + \zeta - 1)_{q+t} (1-n)_q (1-\tilde{n})_t}{(\tilde{\kappa} + \kappa)^{q+t} q! t! (1+2\zeta)_q (1+2\tilde{\zeta})_t \left(\tilde{\mathfrak{K}} - \tilde{\mathcal{N}} \right) \left(\mathfrak{K} - \mathcal{N} \right)} \times \\
 &\quad \left\{ \mathcal{S}_+ \left[\left(\tilde{\mathfrak{K}} - \tilde{\mathcal{N}} \right) \left(\mathfrak{K} - \mathcal{N} \right) - (1-n+q)(1-\tilde{n}+t) \right] + \mathcal{S}_- (\tilde{n} - n + q - t) \right\},
 \end{aligned} \tag{E.93}$$

where the last two lines make use of the definitions of the hypergeometric parameters in (2.20) and $\kappa = mZ\alpha/\mathcal{N}$.

Lastly, let us estimate the size of the coefficients $\mathcal{C}_{\tilde{n}nFF_z\tilde{j}j\tilde{\omega}\omega}$. Assuming that the angular integral and the ratio $(\mathcal{C}/\tilde{\mathcal{C}})$ in (E.81) are $\mathcal{O}(1)$ numbers and estimating

$$\begin{aligned}
 \mathfrak{N}^s &\simeq m(2\tilde{\kappa})^{\tilde{\zeta}-1} (2\kappa)^{\zeta-1} \mathfrak{N}_{\text{pt}}^s \sim m(2\tilde{\kappa})^{\tilde{\zeta}-1} (2\kappa)^{\zeta-1} (\tilde{\kappa} + \kappa)^{1-\tilde{\zeta}-\zeta} \mathcal{S}_{\pm}, \\
 &\sim m(mZ\alpha)^{\tilde{\zeta}-1} (mZ\alpha)^{\zeta-1} (mZ\alpha)^{1-\tilde{\zeta}-\zeta} (Z\alpha) \sim \mathcal{O}(1)
 \end{aligned} \tag{E.94}$$

and also that $\tilde{\mathfrak{D}} \simeq \tilde{\mathfrak{D}}_{\text{pt}} \sim \mathcal{O}(1)$. In this case we obtain,

$$\begin{aligned}
 \mathcal{C}_{\tilde{n}nFF_z\tilde{j}j\tilde{\omega}\omega} &= \frac{(2\tilde{\kappa})^3 \mathfrak{s}}{m^2} \left(\frac{\mathcal{C}}{\tilde{\mathcal{C}}} \right) \int d\Omega_2 \left(\mathcal{Y}_{F,f_z}^{j\tilde{\omega}} \right)^\dagger (I^\theta \sigma^\theta + I^\phi \sigma^\phi) \mathcal{Y}_{F,f_z}^{j\omega} \left(\frac{\mathfrak{N}^s}{\tilde{\mathfrak{D}}} \right), \\
 &\sim m\mathfrak{s}(Z\alpha)^3.
 \end{aligned} \tag{E.95}$$

It turns out that a more careful calculation of $\mathcal{C}_{\tilde{n}nFF_z\tilde{j}j\tilde{\omega}\omega}$ is overkill because the leading corrections to the diagonal first-order state corrections of interest here (*i.e.* ignoring the corrections coming from mixing different angular momentum modes) vanish as is calculated in the next section and argued around (2.68) in the main text. As such, the leading size of the state corrections (or at least the diagonal contributions) gets suppressed by $(Z\alpha)^2$, making them negligible at the orders we work.

F RG evolution

This Appendix collects useful parts of the renormalization story told in the main text.

Universal evolution

The boundary conditions of the main text provide examples where the effective couplings are found to satisfy equations of the form

$$g(\epsilon) = \frac{A\rho_\epsilon^{2\zeta} + B}{C\rho_\epsilon^{2\zeta} + D}, \quad (\text{F.1})$$

where g is a representative coupling – such as $g = -(\hat{c}_s - \hat{c}_v)/\chi$ in eq. (2.64) or $g = -(\hat{c}_s + \hat{c}_v)\chi$ in (2.70) – and ϵ appears on the right-hand side through $\rho_\epsilon = 2\kappa\epsilon$ with $\kappa = \sqrt{m^2 - \omega^2}$. The power of ρ_ϵ appearing here is $\zeta = \sqrt{\mathfrak{K}^2 - (Z\alpha)^2}$ where $\mathfrak{K} = -\varpi(j + \frac{1}{2})$. For $j = \frac{1}{2}$ parity-even states, for example, comparison with (2.64) shows that the parameters A, B, C and D are given explicitly by

$$A = c + a, \quad B = (c + a') \left(\frac{\mathcal{D}_+}{\mathcal{E}_+} \right)^{(0)}, \quad C = c - a \quad \text{and} \quad D = (c - a') \left(\frac{\mathcal{D}_+}{\mathcal{E}_+} \right)^{(0)}, \quad (\text{F.2})$$

with parameters a, a' and c given in (2.20), and repeated here:

$$a = \zeta - \frac{Z\alpha\omega}{\kappa}, \quad a' = - \left(\zeta + \frac{Z\alpha\omega}{\kappa} \right), \quad c = \mathfrak{K} - \frac{Z\alpha m}{\kappa}, \quad (\text{F.3})$$

For later use, eq. (F.1) also inverts to give

$$\rho_\epsilon^{2\zeta} = \frac{B - Dg}{Cg - A}. \quad (\text{F.4})$$

The goal is to derive a universal differential version of this evolution (see, for example [64, 70–72] for more details). To start this off directly differentiate (F.1) holding A, B, C, D fixed, leading to

$$\epsilon \frac{dg}{d\epsilon} = 2\zeta \left[\frac{AD - BC}{(C\rho_\epsilon^{2\zeta} + D)^2} \right] \rho_\epsilon^{2\zeta} = 2\zeta \left[\frac{(Cg - A)(B - Dg)}{AD - BC} \right], \quad (\text{F.5})$$

where the second equality uses (F.4) to trade $\rho_\epsilon^{2\zeta}$ for g . This evolution equation has fixed points at $g = g_*$, where

$$g_* = \frac{A}{C} \quad \text{or} \quad g_* = \frac{B}{D}, \quad (\text{F.6})$$

which can also be seen as the $\rho_\epsilon \rightarrow 0$ and $\rho_\epsilon \rightarrow \infty$ limits of (F.1).

This equation can be put into a standard form by redefining g to ensure that $g_* = \pm 1$. To this end write

$$g(\epsilon) = u(\epsilon) + \frac{1}{2} \left(\frac{A}{C} + \frac{B}{D} \right), \quad (\text{F.7})$$

in terms of which the fixed points are

$$u_* = \pm \frac{1}{2} \left(\frac{A}{C} - \frac{B}{D} \right) = \pm \left(\frac{AD - BC}{2CD} \right), \quad (\text{F.8})$$

and (F.5) becomes

$$\epsilon \frac{du}{d\epsilon} = -\frac{2\zeta CD}{AD - BC} \left[u - \left(\frac{AD - BC}{2CD} \right) \right] \left[u + \left(\frac{AD - BC}{2CD} \right) \right]. \quad (\text{F.9})$$

Finally rescale

$$u = \left[\frac{AD - BC}{2CD} \right] v \quad (\text{F.10})$$

to see that

$$\epsilon \frac{dv}{d\epsilon} = \zeta(1 - v^2) \quad (\text{F.11})$$

is an automatic consequence of (F.1) once one defines

$$g = u + \frac{AD + BC}{2CD} = \frac{1}{2} \left(\frac{A}{C} - \frac{B}{D} \right) v + \frac{1}{2} \left(\frac{A}{C} + \frac{B}{D} \right). \quad (\text{F.12})$$

These expressions emphasize that although the positions of the fixed points for g depend on the ratios A/C and B/D , the speed of evolution along the RG flow depends only on ζ . Indeed the general solution to (F.11) is

$$v(\epsilon) = \frac{(v_0 + 1)(\epsilon/\epsilon_0)^{2\zeta} + (v_0 - 1)}{(v_0 + 1)(\epsilon/\epsilon_0)^{2\zeta} - (v_0 - 1)} \quad (\text{F.13})$$

where the integration constant is chosen to ensure $v(\epsilon_0) = v_0$. For $\zeta > 0$ this describes a universal flow that runs from $v = -1$ to $v = +1$ as ϵ flows from 0 to ∞ .

Since the trajectories given in (F.13) cannot cross the lines $v = \pm 1$ for any finite nonzero ϵ there are two categories of flow, distinguished by the flow-invariant sign of $|v| - 1$ (see Figure 1). That is, if $|v_0| - 1$ is negative (positive) for any $0 < \epsilon_0 < \infty$, then $|v(\epsilon)| - 1$ is negative (positive) for all $0 < \epsilon < \infty$. Every trajectory is therefore uniquely characterized by a pair of numbers. These can equally well be chosen to be the pair (ϵ_0, v_0) that specifies an initial condition $v_0 = v(\epsilon_0)$, or it can be taken to be the pair (ϵ_*, y_*) where $y_* = \text{sign}(|v| - 1) = \pm 1$ distinguishes the two classes of trajectories, and ϵ_* is defined as the value of ϵ for which $v(\epsilon_*) = 0$ (if $y_* = -1$) or the value for which $v(\epsilon_*) = \infty$ (if $y_* = +1$). The parameterization using (ϵ_*, y_*) is useful because physical observables turn out to have particularly transparent expressions in terms of these variables.

For the specific case of $j = \frac{1}{2}$ parity-even states these parameter combinations become $\zeta = \sqrt{1 - (Z\alpha)^2}$ and

$$\begin{aligned}\frac{A}{C} &= \frac{c+a}{c-a} = \frac{1-\zeta + (m+\omega)Z\alpha/\kappa}{1+\zeta + (m-\omega)Z\alpha/\kappa} \\ \frac{B}{D} &= \frac{c+a'}{c-a'} = \frac{1+\zeta + (m+\omega)Z\alpha/\kappa}{1-\zeta + (m-\omega)Z\alpha/\kappa}\end{aligned}\quad (\text{F.14})$$

Using, in these, the leading Coulomb expression $m - \omega \simeq (Z\alpha)^2 m / (2n^2)$ and so $\kappa \simeq Z\alpha m / n$ as well as $\zeta \simeq 1 - \frac{1}{2}(Z\alpha)^2$ then leads to the approximate forms

$$\frac{A}{C} \simeq n + \dots, \quad \frac{B}{D} \simeq \frac{2n}{(Z\alpha)^2} + \dots, \quad (\text{F.15})$$

up to terms suppressed by $(Z\alpha)^2$ compared to those shown.

Evolution for positive-parity $j = \frac{1}{2}$ states

The importance of calculating the first-order state corrections above is that the alternative boundary conditions in (2.58) and (2.60) set various combinations of the PPEFT couplings equal to the ratios of the full radial functions, $\mathbf{g}_{n\frac{1}{2}+}(\epsilon)/\mathbf{f}_{n\frac{1}{2}+}(\epsilon)$ and $\mathbf{f}_{n\frac{1}{2}-}(\epsilon)/\mathbf{g}_{n\frac{1}{2}-}(\epsilon)$ when applied to $j = 1/2$ positive- and negative parity states respectively. The new coupling c_F sits on the left-hand side of these equations, which we assume to be of size \mathfrak{s} and we further anticipate that the couplings present in the case of spinless nuclei c_s, c_v also receive spin-dependent corrections that first appear at this order. Matching powers of \mathfrak{s} on both sides of the boundary condition then requires us to compute all $\mathcal{O}(\mathfrak{s})$ contributions to the radial function ratios, which is what we will do now for both parities, starting with the positive-parity state. In what follows we will suppress both the arguments and the quantum number labels of the functions, except for parity.

Evolution for positive parity $j = 1/2$ states

On the right-hand side of the positive-parity, $j = 1/2$ states' boundary conditions in (2.58) sits the ratio $(\mathbf{g}_+/\mathbf{f}_+)$, which can be expanded to first order in degenerate perturbation theory schematically as,

$$\frac{\mathbf{g}_+}{\mathbf{f}_+} = \frac{\mathbf{g}_+^{(0)} + \mathfrak{s}\mathbf{g}_+^{(1)} + \dots}{\mathbf{f}_+^{(0)} + \mathfrak{s}\mathbf{f}_+^{(1)} + \dots} \approx \frac{\mathbf{g}_+^{(0)}}{\mathbf{f}_+^{(0)}} + \mathfrak{s} \left(\frac{\mathbf{g}_+^{(1)}}{\mathbf{f}_+^{(0)}} - \frac{\mathbf{g}_+^{(0)}}{\mathbf{f}_+^{(0)}} \frac{\mathbf{f}_+^{(1)}}{\mathbf{f}_+^{(0)}} \right) + \mathcal{O}(\mathfrak{s}^2), \quad (\text{F.16})$$

where $\mathbf{g}_+^{(0)}$ and $\mathbf{f}_+^{(0)}$ are given in (2.18) and $\mathbf{g}_+^{(1)}$ and $\mathbf{f}_+^{(1)}$ are given in (2.56) using appropriate substitutions for the quantum number labels. Before proceeding any further, it

is important to remember that the superscripts on these functions refer to their order in degenerate perturbation theory and not necessarily whether or not they are complete in any order in \mathfrak{s} . To emphasize, we had *defined* $\mathfrak{g}_+^{(1)}$ and $\mathfrak{f}_+^{(1)}$ to be the corrections to the radial solutions of the Dirac-Coulomb problem, $\mathfrak{g}_+^{(0)}, \mathfrak{f}_+^{(0)}$ that come about purely as a result of degenerate perturbation theory, but *not* including the expansion of the integration constant ratios in (2.62) and as such both $\mathfrak{g}_+^{(0)}, \mathfrak{g}_+^{(1)}$ and $\mathfrak{f}_+^{(0)}, \mathfrak{f}_+^{(1)}$ are still functions of the full $(\mathcal{D}_+/\mathcal{C}_+)$. This means that in order to get all the contributions to $\mathcal{O}(\mathfrak{s})$ in the ratio $(\mathfrak{g}_+/\mathfrak{f}_+)$ we still need to use (2.62) in $\mathfrak{g}_+^{(0)}$ and $\mathfrak{f}_+^{(0)}$, but not in $\mathfrak{g}_+^{(1)}, \mathfrak{f}_+^{(1)}$ since these are already $\mathcal{O}(\mathfrak{s})$. Then, focusing on the first term on the right-hand side of (F.16) we find

$$\begin{aligned}
 \frac{\mathfrak{g}_+^{(0)}}{\mathfrak{f}_+^{(0)}} &= -\chi \frac{[\mathcal{M}_1 + \frac{a}{c}\mathcal{M}_2] + \left(\frac{\mathcal{D}_+}{\mathcal{C}_+}\right)^{(0)} \rho^{-2\zeta} [\mathcal{M}_3 + \frac{a'}{c}\mathcal{M}_4] + \left(\frac{\mathcal{D}_+}{\mathcal{C}_+}\right)^{(1)} \rho^{-2\zeta} [\mathcal{M}_3 + \frac{a'}{c}\mathcal{M}_4]}{[\mathcal{M}_1 - \frac{a}{c}\mathcal{M}_2] + \left(\frac{\mathcal{D}_+}{\mathcal{C}_+}\right)^{(0)} \rho^{-2\zeta} [\mathcal{M}_3 - \frac{a'}{c}\mathcal{M}_4] + \left(\frac{\mathcal{D}_+}{\mathcal{C}_+}\right)^{(1)} \rho^{-2\zeta} [\mathcal{M}_3 - \frac{a'}{c}\mathcal{M}_4]}, \\
 &= -\chi \frac{[\mathcal{M}_1 + \frac{a}{c}\mathcal{M}_2] + \left(\frac{\mathcal{D}_+}{\mathcal{C}_+}\right)^{(0)} \rho^{-2\zeta} [\mathcal{M}_3 + \frac{a'}{c}\mathcal{M}_4]}{[\mathcal{M}_1 - \frac{a}{c}\mathcal{M}_2] + \left(\frac{\mathcal{D}_+}{\mathcal{C}_+}\right)^{(0)} \rho^{-2\zeta} [\mathcal{M}_3 - \frac{a'}{c}\mathcal{M}_4]} \\
 &\quad - \mathfrak{s} \frac{2 \left(\frac{\mathcal{D}_+}{\mathcal{C}_+}\right)^{(1)} \chi \rho^{-2\zeta} (a'\mathcal{M}_1\mathcal{M}_4 - a\mathcal{M}_2\mathcal{M}_3)}{c \left([\mathcal{M}_1 - \frac{a}{c}\mathcal{M}_2] + \left(\frac{\mathcal{D}_+}{\mathcal{C}_+}\right)^{(0)} \rho^{-2\zeta} [\mathcal{M}_3 - \frac{a'}{c}\mathcal{M}_4] \right)^2}. \tag{F.17}
 \end{aligned}$$

Substituting this into (F.16) along with the explicit functional forms from (2.18) and making use of (2.56) and (2.62) we can write the ratio of positive parity radial functions

as

$$\begin{aligned}
 \frac{\mathbf{g}_+}{\mathbf{f}_+} &\approx -\chi \frac{[\mathcal{M}_1 + \frac{a}{c}\mathcal{M}_2] + \left(\frac{\mathcal{D}_+}{\mathcal{E}_+}\right)^{(0)} \rho^{-2\zeta} [\mathcal{M}_3 + \frac{a'}{c}\mathcal{M}_4]}{[\mathcal{M}_1 - \frac{a}{c}\mathcal{M}_2] + \left(\frac{\mathcal{D}_+}{\mathcal{E}_+}\right)^{(0)} \rho^{-2\zeta} [\mathcal{M}_3 - \frac{a'}{c}\mathcal{M}_4]} \\
 &- \mathfrak{s} \left(\frac{2 \left(\frac{\mathcal{D}_+}{\mathcal{E}_+}\right)^{(1)} \chi \rho^{-2\zeta} (a'\mathcal{M}_1\mathcal{M}_4 - a\mathcal{M}_2\mathcal{M}_3)}{c \left([\mathcal{M}_1 - \frac{a}{c}\mathcal{M}_2] + \left(\frac{\mathcal{D}_+}{\mathcal{E}_+}\right)^{(0)} \rho^{-2\zeta} [\mathcal{M}_3 - \frac{a'}{c}\mathcal{M}_4]\right)^2} \right. \\
 &+ \widehat{\sum} \sqrt{\frac{m - \tilde{\omega}}{m + \omega}} \left(\frac{\tilde{\mathcal{E}}_+ e^{-\tilde{\rho}/2} \tilde{\rho}^{\zeta-1}}{\mathcal{E}_+ e^{-\rho/2} \rho^{\zeta-1}} \right) \frac{[\mathcal{M}_{\tilde{1}} + \frac{\tilde{a}}{c}\mathcal{M}_{\tilde{2}}] + \left(\frac{\tilde{\mathcal{D}}_+}{\tilde{\mathcal{E}}_+}\right)^{(0)} \tilde{\rho}^{-2\zeta} [\mathcal{M}_{\tilde{3}} + \frac{\tilde{a}'}{c}\mathcal{M}_{\tilde{4}}]}{[\mathcal{M}_1 - \frac{a}{c}\mathcal{M}_2] + \left(\frac{\mathcal{D}_+}{\mathcal{E}_+}\right)^{(0)} \rho^{-2\zeta} [\mathcal{M}_3 - \frac{a'}{c}\mathcal{M}_4]} \\
 &- \widehat{\sum} \chi \frac{[\mathcal{M}_1 + \frac{a}{c}\mathcal{M}_2] + \left(\frac{\mathcal{D}_+}{\mathcal{E}_+}\right)^{(0)} \rho^{-2\zeta} [\mathcal{M}_3 + \frac{a'}{c}\mathcal{M}_4]}{[\mathcal{M}_1 - \frac{a}{c}\mathcal{M}_2] + \left(\frac{\mathcal{D}_+}{\mathcal{E}_+}\right)^{(0)} \rho^{-2\zeta} [\mathcal{M}_3 - \frac{a'}{c}\mathcal{M}_4]} \\
 &\times \left. \sqrt{\frac{m + \tilde{\omega}}{m + \omega}} \left(\frac{\tilde{\mathcal{E}}_+ e^{-\tilde{\rho}/2} \tilde{\rho}^{\zeta-1}}{\mathcal{E}_+ e^{-\rho/2} \rho^{\zeta-1}} \right) \frac{[\mathcal{M}_{\tilde{1}} - \frac{\tilde{a}}{c}\mathcal{M}_{\tilde{2}}] + \left(\frac{\tilde{\mathcal{D}}_+}{\tilde{\mathcal{E}}_+}\right)^{(0)} \tilde{\rho}^{-2\zeta} [\mathcal{M}_{\tilde{3}} - \frac{\tilde{a}'}{c}\mathcal{M}_{\tilde{4}}]}{[\mathcal{M}_1 - \frac{a}{c}\mathcal{M}_2] + \left(\frac{\mathcal{D}_+}{\mathcal{E}_+}\right)^{(0)} \rho^{-2\zeta} [\mathcal{M}_3 - \frac{a'}{c}\mathcal{M}_4]} \right) + \mathcal{O}(\mathfrak{s}^2).
 \end{aligned} \tag{F.18}$$

With an eye to the future progression of this calculation in the main text, where the terms including the sums will cancel (to leading order in ρ), we can massage this into

the form,

$$\begin{aligned}
 \frac{\mathbf{g}_+}{\mathbf{f}_+} &\approx -\chi \frac{[c\mathcal{M}_1 + a\mathcal{M}_2] + \left(\frac{\mathcal{Q}_+}{\mathcal{E}_+}\right)^{(0)} \rho^{-2\zeta} [c\mathcal{M}_3 + a'\mathcal{M}_4]}{[c\mathcal{M}_1 - a\mathcal{M}_2] + \left(\frac{\mathcal{Q}_+}{\mathcal{E}_+}\right)^{(0)} \rho^{-2\zeta} [c\mathcal{M}_3 - a'\mathcal{M}_4]} \\
 &- \mathbf{s} \left(\frac{2 \left(\frac{\mathcal{Q}_+}{\mathcal{E}_+}\right)^{(1)} \chi \rho^{-2\zeta} (a'\mathcal{M}_1\mathcal{M}_4 - a\mathcal{M}_2\mathcal{M}_3) c}{\left([c\mathcal{M}_1 - a\mathcal{M}_2] + \left(\frac{\mathcal{Q}_+}{\mathcal{E}_+}\right)^{(0)} \rho^{-2\zeta} [c\mathcal{M}_3 - a'\mathcal{M}_4]\right)^2} \right. \\
 &+ \widehat{\Sigma} \sqrt{\frac{m + \tilde{\omega}}{m + \omega}} \left(\frac{\tilde{\mathcal{E}}_+ e^{-\tilde{\rho}/2} \tilde{\rho}^{\zeta-1} c}{\tilde{\mathcal{E}}_+ e^{-\rho/2} \rho^{\zeta-1} \tilde{c}} \right) \frac{[\tilde{c}\mathcal{M}_{\tilde{1}} - \tilde{a}\mathcal{M}_{\tilde{2}}] + \left(\frac{\tilde{\mathcal{Q}}_+}{\tilde{\mathcal{E}}_+}\right)^{(0)} \tilde{\rho}^{-2\zeta} [\tilde{c}\mathcal{M}_{\tilde{3}} - \tilde{a}'\mathcal{M}_{\tilde{4}}]}{[c\mathcal{M}_1 - a\mathcal{M}_2] + \left(\frac{\mathcal{Q}_+}{\mathcal{E}_+}\right)^{(0)} \rho^{-2\zeta} [c\mathcal{M}_3 - a'\mathcal{M}_4]} \\
 &\times \left\{ \tilde{\chi} \frac{[\tilde{c}\mathcal{M}_{\tilde{1}} + \tilde{a}\mathcal{M}_{\tilde{2}}] + \left(\frac{\tilde{\mathcal{Q}}_+}{\tilde{\mathcal{E}}_+}\right)^{(0)} \tilde{\rho}^{-2\zeta} [\tilde{c}\mathcal{M}_{\tilde{3}} + \tilde{a}'\mathcal{M}_{\tilde{4}}]}{[\tilde{c}\mathcal{M}_{\tilde{1}} - \tilde{a}\mathcal{M}_{\tilde{2}}] + \left(\frac{\tilde{\mathcal{Q}}_+}{\tilde{\mathcal{E}}_+}\right)^{(0)} \tilde{\rho}^{-2\zeta} [\tilde{c}\mathcal{M}_{\tilde{3}} - \tilde{a}'\mathcal{M}_{\tilde{4}}]} \right. \\
 &\left. - \chi \frac{[c\mathcal{M}_1 + a\mathcal{M}_2] + \left(\frac{\mathcal{Q}_+}{\mathcal{E}_+}\right)^{(0)} \rho^{-2\zeta} [c\mathcal{M}_3 + a'\mathcal{M}_4]}{[c\mathcal{M}_1 - a\mathcal{M}_2] + \left(\frac{\mathcal{Q}_+}{\mathcal{E}_+}\right)^{(0)} \rho^{-2\zeta} [c\mathcal{M}_3 - a'\mathcal{M}_4]} \right\}, \tag{F.19}
 \end{aligned}$$

where the leading small ϵ expansion (and identically small ρ expansion) yields,

$$\begin{aligned}
 \frac{\mathbf{g}_+}{\mathbf{f}_+} &\approx -\chi \frac{[c + a] + \left(\frac{\mathcal{Q}_+}{\mathcal{E}_+}\right)^{(0)} \rho^{-2\zeta} [c + a']}{[c - a] + \left(\frac{\mathcal{Q}_+}{\mathcal{E}_+}\right)^{(0)} \rho^{-2\zeta} [c - a']} - \mathbf{s} \left(\frac{2 \left(\frac{\mathcal{Q}_+}{\mathcal{E}_+}\right)^{(1)} \chi \rho^{-2\zeta} (a' - a) c}{\left([c - a] + \left(\frac{\mathcal{Q}_+}{\mathcal{E}_+}\right)^{(0)} \rho^{-2\zeta} [c - a']\right)^2} \right. \\
 &+ \widehat{\Sigma} \sqrt{\frac{m + \tilde{\omega}}{m + \omega}} \left(\frac{\tilde{\mathcal{E}}_+ \tilde{\rho}^{\zeta-1} c}{\tilde{\mathcal{E}}_+ \rho^{\zeta-1} \tilde{c}} \right) \frac{[\tilde{c} - \tilde{a}] + \left(\frac{\tilde{\mathcal{Q}}_+}{\tilde{\mathcal{E}}_+}\right)^{(0)} \tilde{\rho}^{-2\zeta} [\tilde{c} - \tilde{a}']}{[c - a] + \left(\frac{\mathcal{Q}_+}{\mathcal{E}_+}\right)^{(0)} \rho^{-2\zeta} [c - a']} \\
 &\times \left\{ \tilde{\chi} \frac{[\tilde{c} + \tilde{a}] + \left(\frac{\tilde{\mathcal{Q}}_+}{\tilde{\mathcal{E}}_+}\right)^{(0)} \tilde{\rho}^{-2\zeta} [\tilde{c} + \tilde{a}']}{[\tilde{c} - \tilde{a}] + \left(\frac{\tilde{\mathcal{Q}}_+}{\tilde{\mathcal{E}}_+}\right)^{(0)} \tilde{\rho}^{-2\zeta} [\tilde{c} - \tilde{a}']} - \chi \frac{[c + a] + \left(\frac{\mathcal{Q}_+}{\mathcal{E}_+}\right)^{(0)} \rho^{-2\zeta} [c + a']}{[c - a] + \left(\frac{\mathcal{Q}_+}{\mathcal{E}_+}\right)^{(0)} \rho^{-2\zeta} [c - a']} \right\} + \mathcal{O}(\mathbf{s}^2). \tag{F.20}
 \end{aligned}$$

Evolution for negative-parity $j = \frac{1}{2}$ states

Moving on to the negative parity, $j = 1/2$ states, the right-hand side of the boundary condition in (2.60) is equivalent to the ratio $(\mathbf{f}_-/\mathbf{g}_-)$, which using (2.55) can be

expanded to first order in \mathfrak{s} schematically as,

$$\frac{\mathfrak{f}_-}{\mathfrak{g}_-} = \frac{\mathfrak{f}_-^{(0)} + \mathfrak{s}\mathfrak{f}_-^{(1)} + \dots}{\mathfrak{g}_-^{(0)} + \mathfrak{s}\mathfrak{g}_-^{(1)} + \dots} \approx \frac{\mathfrak{f}_-^{(0)}}{\mathfrak{g}_-^{(0)}} + \mathfrak{s} \left(\frac{\mathfrak{f}_-^{(1)}}{\mathfrak{g}_-^{(0)}} - \frac{\mathfrak{f}_-^{(0)}}{\mathfrak{g}_-^{(0)}} \frac{\mathfrak{g}_-^{(1)}}{\mathfrak{g}_-^{(0)}} \right) + \mathcal{O}(\mathfrak{s}^2), \quad (\text{F.21})$$

where $\mathfrak{f}_-^{(0)}$ and $\mathfrak{g}_-^{(0)}$ are given in (2.18) and $\mathfrak{f}_-^{(1)}$ and $\mathfrak{g}_-^{(1)}$ are given in (2.56) using appropriate substitutions for the quantum number labels. A before, these functions still contain the full integration constant ratio $(\mathcal{D}_-/\mathcal{C}_-)$, therefore to complete the expansion of $(\mathfrak{f}_-/\mathfrak{g}_-)$ to linear order in \mathfrak{s} we need to make use of (2.62) in $\mathfrak{f}_-^{(0)}/\mathfrak{g}_-^{(0)}$. Concentrating on this term on the right-hand side of (F.21) we find

$$\begin{aligned} \frac{\mathfrak{f}_-^{(0)}}{\mathfrak{g}_-^{(0)}} &= -\chi^{-1} \frac{[\mathcal{M}_1 - \frac{a}{c}\mathcal{M}_2] + \left(\frac{\mathcal{D}_-}{\mathcal{C}_-}\right)^{(0)} \rho^{-2\zeta} [\mathcal{M}_3 - \frac{a'}{c}\mathcal{M}_4] + \left(\frac{\mathcal{D}_-}{\mathcal{C}_-}\right)^{(1)} \rho^{-2\zeta} [\mathcal{M}_3 - \frac{a'}{c}\mathcal{M}_4]}{[\mathcal{M}_1 + \frac{a}{c}\mathcal{M}_2] + \left(\frac{\mathcal{D}_-}{\mathcal{C}_-}\right)^{(0)} \rho^{-2\zeta} [\mathcal{M}_3 + \frac{a'}{c}\mathcal{M}_4] + \left(\frac{\mathcal{D}_-}{\mathcal{C}_-}\right)^{(1)} \rho^{-2\zeta} [\mathcal{M}_3 + \frac{a'}{c}\mathcal{M}_4]}, \\ &= -\chi^{-1} \frac{[\mathcal{M}_1 - \frac{a}{c}\mathcal{M}_2] + \left(\frac{\mathcal{D}_-}{\mathcal{C}_-}\right)^{(0)} \rho^{-2\zeta} [\mathcal{M}_3 - \frac{a'}{c}\mathcal{M}_4]}{[\mathcal{M}_1 + \frac{a}{c}\mathcal{M}_2] + \left(\frac{\mathcal{D}_-}{\mathcal{C}_-}\right)^{(0)} \rho^{-2\zeta} [\mathcal{M}_3 + \frac{a'}{c}\mathcal{M}_4]} \\ &\quad + \mathfrak{s} \frac{2 \left(\frac{\mathcal{D}_-}{\mathcal{C}_-}\right)^{(1)} \rho^{-2\zeta} (a'\mathcal{M}_1\mathcal{M}_4 - a\mathcal{M}_2\mathcal{M}_3)}{c\chi \left([\mathcal{M}_1 + \frac{a}{c}\mathcal{M}_2] + \left(\frac{\mathcal{D}_-}{\mathcal{C}_-}\right)^{(0)} \rho^{-2\zeta} [\mathcal{M}_3 + \frac{a'}{c}\mathcal{M}_4] \right)^2}. \end{aligned} \quad (\text{F.22})$$

Substituting this into (F.21) along with the explicit functional forms from (2.18) and making use of (2.56) and (2.62) we can write the ratio of negative parity radial functions

as

$$\begin{aligned}
 \frac{\mathbf{f}_-}{\mathbf{g}_-} &\approx -\chi^{-1} \frac{[\mathcal{M}_1 - \frac{a}{c}\mathcal{M}_2] + \left(\frac{\mathcal{D}_-}{\mathcal{E}_-}\right)^{(0)} \rho^{-2\zeta} [\mathcal{M}_3 - \frac{a'}{c}\mathcal{M}_4]}{[\mathcal{M}_1 + \frac{a}{c}\mathcal{M}_2] + \left(\frac{\mathcal{D}_-}{\mathcal{E}_-}\right)^{(0)} \rho^{-2\zeta} [\mathcal{M}_3 + \frac{a'}{c}\mathcal{M}_4]} \\
 &+ \mathfrak{s} \left(\frac{2 \left(\frac{\mathcal{D}_-}{\mathcal{E}_-}\right)^{(1)} \rho^{-2\zeta} (a'\mathcal{M}_1\mathcal{M}_4 - a\mathcal{M}_2\mathcal{M}_3)}{c\chi \left([\mathcal{M}_1 + \frac{a}{c}\mathcal{M}_2] + \left(\frac{\mathcal{D}_-}{\mathcal{E}_-}\right)^{(0)} \rho^{-2\zeta} [\mathcal{M}_3 + \frac{a'}{c}\mathcal{M}_4]\right)^2} \right. \\
 &- \widehat{\sum} \sqrt{\frac{m+\tilde{\omega}}{m-\omega}} \left(\frac{\tilde{\mathcal{E}}_- e^{-\tilde{\rho}/2} \tilde{\rho}^{\zeta-1}}{\mathcal{E}_- e^{-\rho/2} \rho^{\zeta-1}}\right) \frac{[\mathcal{M}_{\tilde{1}} - \frac{\tilde{a}}{c}\mathcal{M}_{\tilde{2}}] + \left(\frac{\tilde{\mathcal{D}}_-}{\tilde{\mathcal{E}}_-}\right)^{(0)} \tilde{\rho}^{-2\zeta} [\mathcal{M}_{\tilde{3}} - \frac{\tilde{a}'}{c}\mathcal{M}_{\tilde{4}}]}{[\mathcal{M}_1 + \frac{a}{c}\mathcal{M}_2] + \left(\frac{\mathcal{D}_-}{\mathcal{E}_-}\right)^{(0)} \rho^{-2\zeta} [\mathcal{M}_3 + \frac{a'}{c}\mathcal{M}_4]} \\
 &+ \widehat{\sum} \chi^{-1} \frac{[\mathcal{M}_1 - \frac{a}{c}\mathcal{M}_2] + \left(\frac{\mathcal{D}_-}{\mathcal{E}_-}\right)^{(0)} \rho^{-2\zeta} [\mathcal{M}_3 - \frac{a'}{c}\mathcal{M}_4]}{[\mathcal{M}_1 + \frac{a}{c}\mathcal{M}_2] + \left(\frac{\mathcal{D}_-}{\mathcal{E}_-}\right)^{(0)} \rho^{-2\zeta} [\mathcal{M}_3 + \frac{a'}{c}\mathcal{M}_4]} \\
 &\times \left. \sqrt{\frac{m-\tilde{\omega}}{m-\omega}} \left(\frac{\tilde{\mathcal{E}}_- e^{-\tilde{\rho}/2} \tilde{\rho}^{\zeta-1}}{\mathcal{E}_- e^{-\rho/2} \rho^{\zeta-1}}\right) \frac{[\mathcal{M}_{\tilde{1}} + \frac{\tilde{a}}{c}\mathcal{M}_{\tilde{2}}] + \left(\frac{\tilde{\mathcal{D}}_-}{\tilde{\mathcal{E}}_-}\right)^{(0)} \tilde{\rho}^{-2\zeta} [\mathcal{M}_{\tilde{3}} + \frac{\tilde{a}'}{c}\mathcal{M}_{\tilde{4}}]}{[\mathcal{M}_1 + \frac{a}{c}\mathcal{M}_2] + \left(\frac{\mathcal{D}_-}{\mathcal{E}_-}\right)^{(0)} \rho^{-2\zeta} [\mathcal{M}_3 + \frac{a'}{c}\mathcal{M}_4]} \right) + \mathcal{O}(\mathfrak{s}^2).
 \end{aligned} \tag{F.23}$$

With an eye to the future progression of this calculation in the main text, where the terms including the sums will cancel (to leading order in ρ), we can massage this into

the form,

$$\begin{aligned}
 \frac{\mathbf{f}_-}{\mathbf{g}_-} &\approx -\chi^{-1} \frac{[c\mathcal{M}_1 - a\mathcal{M}_2] + \left(\frac{\mathcal{D}_-}{\mathcal{E}_-}\right)^{(0)} \rho^{-2\zeta} [c\mathcal{M}_3 - a'\mathcal{M}_4]}{[c\mathcal{M}_1 + a\mathcal{M}_2] + \left(\frac{\mathcal{D}_-}{\mathcal{E}_-}\right)^{(0)} \rho^{-2\zeta} [c\mathcal{M}_3 + a'\mathcal{M}_4]} \\
 &+ \mathbf{s} \left(\frac{2\chi^{-1} \left(\frac{\mathcal{D}_-}{\mathcal{E}_-}\right)^{(1)} \rho^{-2\zeta} (a'\mathcal{M}_1\mathcal{M}_4 - a\mathcal{M}_2\mathcal{M}_3) c}{\left([c\mathcal{M}_1 + a\mathcal{M}_2] + \left(\frac{\mathcal{D}_-}{\mathcal{E}_-}\right)^{(0)} \rho^{-2\zeta} [c\mathcal{M}_3 + a'\mathcal{M}_4]\right)^2} \right. \\
 &- \widehat{\Sigma} \sqrt{\frac{m - \tilde{\omega}}{m - \omega}} \left(\frac{\tilde{\mathcal{E}}_- e^{-\tilde{\rho}/2} \tilde{\rho}^{\zeta-1} c}{\mathcal{E}_- e^{-\rho/2} \rho^{\zeta-1} \tilde{c}} \right) \frac{[\tilde{c}\mathcal{M}_{\tilde{1}} + \tilde{a}\mathcal{M}_{\tilde{2}}] + \left(\frac{\tilde{\mathcal{D}}_-}{\tilde{\mathcal{E}}_-}\right)^{(0)} \tilde{\rho}^{-2\zeta} [\tilde{c}\mathcal{M}_{\tilde{3}} + \tilde{a}'\mathcal{M}_{\tilde{4}}]}{[c\mathcal{M}_1 + a\mathcal{M}_2] + \left(\frac{\mathcal{D}_-}{\mathcal{E}_-}\right)^{(0)} \rho^{-2\zeta} [c\mathcal{M}_3 + a'\mathcal{M}_4]} \\
 &\times \left\{ \tilde{\chi}^{-1} \frac{[\tilde{c}\mathcal{M}_{\tilde{1}} - \tilde{a}\mathcal{M}_{\tilde{2}}] + \left(\frac{\tilde{\mathcal{D}}_-}{\tilde{\mathcal{E}}_-}\right)^{(0)} \tilde{\rho}^{-2\zeta} [\tilde{c}\mathcal{M}_{\tilde{3}} - \tilde{a}'\mathcal{M}_{\tilde{4}}]}{[\tilde{c}\mathcal{M}_{\tilde{1}} + \tilde{a}\mathcal{M}_{\tilde{2}}] + \left(\frac{\tilde{\mathcal{D}}_-}{\tilde{\mathcal{E}}_-}\right)^{(0)} \tilde{\rho}^{-2\zeta} [\tilde{c}\mathcal{M}_{\tilde{3}} + \tilde{a}'\mathcal{M}_{\tilde{4}}]} \right. \\
 &\left. - \chi^{-1} \frac{[c\mathcal{M}_1 - a\mathcal{M}_2] + \left(\frac{\mathcal{D}_-}{\mathcal{E}_-}\right)^{(0)} \rho^{-2\zeta} [c\mathcal{M}_3 - a'\mathcal{M}_4]}{[c\mathcal{M}_1 + a\mathcal{M}_2] + \left(\frac{\mathcal{D}_+}{\mathcal{E}_+}\right)^{(0)} \rho^{-2\zeta} [c\mathcal{M}_3 + a'\mathcal{M}_4]} \right\}, \tag{F.24}
 \end{aligned}$$

where the leading small ϵ expansion (and identically small ρ expansion) yields,

$$\begin{aligned}
 \frac{\mathbf{f}_-}{\mathbf{g}_-} &\approx -\chi^{-1} \frac{[c - a] + \left(\frac{\mathcal{D}_-}{\mathcal{E}_-}\right)^{(0)} \rho^{-2\zeta} [c - a']}{[c + a] + \left(\frac{\mathcal{D}_-}{\mathcal{E}_-}\right)^{(0)} \rho^{-2\zeta} [c + a']} + \mathbf{s} \left(\frac{2\chi^{-1} \left(\frac{\mathcal{D}_-}{\mathcal{E}_-}\right)^{(1)} \rho^{-2\zeta} (a' - a) c}{\left([c + a] + \left(\frac{\mathcal{D}_-}{\mathcal{E}_-}\right)^{(0)} \rho^{-2\zeta} [c + a']\right)^2} \right. \\
 &- \widehat{\Sigma} \sqrt{\frac{m - \tilde{\omega}}{m - \omega}} \left(\frac{\tilde{\mathcal{E}}_- e^{-\tilde{\rho}/2} \tilde{\rho}^{\zeta-1} c}{\mathcal{E}_- e^{-\rho/2} \rho^{\zeta-1} \tilde{c}} \right) \frac{[\tilde{c} + \tilde{a}] + \left(\frac{\tilde{\mathcal{D}}_-}{\tilde{\mathcal{E}}_-}\right)^{(0)} \tilde{\rho}^{-2\zeta} [\tilde{c} + \tilde{a}']}{[c + a] + \left(\frac{\mathcal{D}_-}{\mathcal{E}_-}\right)^{(0)} \rho^{-2\zeta} [c + a']} \\
 &\times \left\{ \tilde{\chi}^{-1} \frac{[\tilde{c} - \tilde{a}] + \left(\frac{\tilde{\mathcal{D}}_-}{\tilde{\mathcal{E}}_-}\right)^{(0)} \tilde{\rho}^{-2\zeta} [\tilde{c} - \tilde{a}']}{[\tilde{c} + \tilde{a}] + \left(\frac{\tilde{\mathcal{D}}_-}{\tilde{\mathcal{E}}_-}\right)^{(0)} \tilde{\rho}^{-2\zeta} [\tilde{c} + \tilde{a}']} - \chi^{-1} \frac{[c - a] + \left(\frac{\mathcal{D}_-}{\mathcal{E}_-}\right)^{(0)} \rho^{-2\zeta} [c - a']}{[c + a] + \left(\frac{\mathcal{D}_+}{\mathcal{E}_+}\right)^{(0)} \rho^{-2\zeta} [c + a']} \right\}. \tag{F.25}
 \end{aligned}$$

G List of symbols

Z	Atomic number of an element
$\alpha = \frac{e^2}{4\pi}$	Fine-structure constant
$N_{\text{exp}}, N_{\text{nuc}}$	The number of available experimental observables and the number of nuclear parameters
ε_n	Bohr energy level of a lepton
n	Principal quantum number of a leptonic energy level
m	Mass of the lepton orbiting the nucleus
M	Mass of the nucleus
m_r	Reduced mass of the nucleus-lepton system
e	Electric charge unit
\hbar	Reduced Planck's constant
c	Speed of light in vacuum
k_B	Boltzmann constant
$\mathbf{v}_e, v_e \sim (Z\alpha)$	Velocity and speed of the nucleus-orbiting lepton
R	A length-scale of approximately nuclear size, <i>i.e.</i> 1 fm
$a_B = (mZ\alpha)^{-1}$	Bohr radius of the atom
$\mathfrak{s} = \frac{m e \mu_N}{4\pi}$	The small parameter controlling the effects of the hyperfine interaction
j, j_z	Quantum numbers of the total leptonic angular momentum $\mathbf{J} = \mathbf{L} + \mathbf{S}$ and its projection

$S_{\Phi_{QED}}$	The renormalizable action of a theory treating the nucleus as a relativistic point-like particle interacting with photons and another lepton species
$F_{\mu\nu}$	Field strength of the U(1) gauge field, $A^\mu(x)$
$A^\mu(x)$	U(1) vector field
$D_\mu = \partial_\mu - iqA_\mu$	Covariant derivative of a field charged under the U(1) gauge group with charge q
$\Psi, \bar{\Psi}$	Leptonic Dirac field and its Dirac conjugate
$\Phi, \bar{\Phi}$	Nuclear Dirac field and its Dirac conjugate
γ^μ, γ_5	Dirac gamma matrices
$\gamma^{\mu\nu} = -\frac{i}{4} [\gamma^\mu, \gamma^\nu]$	Lorentz algebra generators for Dirac particles
$\not{D} = \gamma^\mu D_\mu$	Slashes indicate contraction with Dirac gamma matrices
S_{nuc}	The higher-dimensional extension of $S_{\Phi_{QED}}$ containing non-renormalizable interactions between the second-quantized nuclear and leptonic fields and a U(1) gauge field
$\tilde{c}_s, \tilde{c}_v, \tilde{c}_d$	Generic EFT couplings in S_{nuc} that are related to nuclear properties
\mathcal{P}	Curve mapping the real line, \mathbb{R} to the position of the nucleus
x^μ	Arbitrary position 4-vector
s	Arbitrary parameter along the world-line of the nucleus
$y^\mu(s)$	4-vector trajectory of the nucleus, parameterized by s
S_{QED}	The standard QED action describing the interaction between a Dirac particle and a U(1) gauge field
S_p	The 1-dimensional action of a point-particle

$S = S_{QED} + S_p$	Total action of the PPEFT
$\mathbf{v} \sim m(Z\alpha)/M$	Velocity of the nucleus
$\gamma := (1 - \mathbf{v}^2)^{-1/2}$	The relativistic conversion factor
$c_s, c_v, c_F, c_{em}, c_2, c_3$	Generic EFT couplings in the PPEFT arising at order (length) ²
τ	Proper time along the point-particle's trajectory
$\eta_{\mu\nu}, \eta^{\mu\nu}$	Minkowski metric and its inverse with signature (-, +, +, +)
\mathbf{e}_r	Radially pointing unit normal vector
$u_L(t, r, \theta, \varphi)$	Separable solution to the leptonic field equations
$\mathcal{R}_L(\kappa r)$	Radial part of the solution to the leptonic field equations
ω	Energy of the leptonic field mode
κ	A function of the leptonic mode's energy, ω . It is often given by the dispersion relation $\kappa = \sqrt{m^2 - \omega^2}$
L	Collection of angular momentum labels specific to the solution of the leptonic field equations
$Y_L(\theta, \varphi)$	The angular part of the solution to the leptonic field equations
l, l_z	Quantum numbers of the orbital angular momentum and its z -component in a solution to 3-dimensional field equations of spinless fields
$\mathcal{C}_L, \mathcal{D}_L$	Integration constants in the solution to the ordinary second-order differential equation satisfied by the radial component of the leptonic field multiplying the near-origin convergent and divergent solutions respectively

$\mathcal{R}_L^{\mathcal{C}(\mathcal{D})}(\kappa r)$	What are traditionally thought of as the near-origin convergent (divergent) radial solutions to leptonic field equations
μ_N	Nuclear magnetic moment (<i>not the nuclear magneton</i>) including the nuclear g -factor
g_N, g_l	The nuclear and leptonic g -factors
r_p, r_Z	Charge and Zemach radii of the proton as measured by [5]
\mathbf{I}	Nuclear spin vector
$\mathbf{F} = \mathbf{J} + \mathbf{I}$	Total atomic angular momentum operator
F	Quantum number of the total angular momentum of the atomic system, $\mathbf{F} = \mathbf{I} + \mathbf{J}$
S_B	The ‘bulk’ part of the PPEFT action, which for our purposes is the same as the QED action, $S_B = S_{QED}$
$\xi^\mu(s)$	Classical Grassmann field
$\{A, B\} = AB + BA$	The anticommutator
$[A, B] = AB - BA$	The commutator
S_{p0}	The lowest-order part of the PPEFT action that describes the kinematics of the point-particle
Γ^μ, Γ_5	Dirac gamma matrices acting on the Hilbert space of the nucleus
$\Gamma^{\mu\nu} = -\frac{i}{4} [\Gamma^\mu, \Gamma^\nu]$	The Lorentz algebra generators for the Hilbert space of the nucleus
$\epsilon_{\mu_1\mu_2\cdots\mu_n}$	n -dimensional totally antisymmetric tensor
$\mathbb{1}$	Identity operator

τ^i	The spin-matrices acting on nuclear-spin space
$\boldsymbol{\tau} = (\tau^1 \ \tau^2 \ \tau^3)^T$	The vector of spin matrices acting on nuclear-spin space
\mathbf{E}, \mathbf{B}	The electric and magnetic fields
$\boldsymbol{\mu} = \mu_N \mathbf{I}$	Nuclear magnetic moment
j^μ	Electromagnetic 4-current
$A_0^{\text{nuc}}, \mathbf{A}^{\text{nuc}}$	Electromagnetic fields directly generated by the nucleus
$A_0^{\text{rad}}, \mathbf{A}^{\text{rad}}$	Operator valued quantum field interaction of the electromagnetic field
$\boldsymbol{\Sigma} = \begin{bmatrix} \mathbf{S} & 0 \\ 0 & \mathbf{S} \end{bmatrix}$	The spin-operator for a Dirac-particle with $\mathbf{S} = \frac{1}{2}\boldsymbol{\sigma}$ the spin vector
σ^i	Pauli matrices acting on lepton-spin space
$\boldsymbol{\sigma} = (\sigma^1 \ \sigma^2 \ \sigma^3)^T$	Vector of spin-matrices acting on electron spin-space
$\psi(\mathbf{x})$	Spatial part of the solution to the leptonic field equations
l, l'	Quantum numbers of the orbital angular momentum of the leptons for both parities
$\varpi = \pm$	The parity quantum number, $(-)^l$ with $l = j - \frac{1}{2}\varpi$
$\Omega_{jlj_z}(\theta, \phi)$	2 component spherical spinors of the Dirac-Coulomb problem
$Y_{l_z}(\theta, \phi)$	Scalar spherical harmonics
$\mathfrak{f}_{nj\varpi}(r), \mathfrak{g}_{nj\varpi}(r)$	Solutions to the radial part of the Dirac-Coulomb field equations
$\mathcal{M}[\beta, \gamma; z] = {}_1\mathcal{F}_1[\beta; \gamma; z]$	Confluent hypergeometric function

\mathcal{M}_i	Denotes one of the confluent hypergeometric functions in $\mathbf{f}_{nj}(r)$ and $\mathbf{g}_{nj}(r)$ with $i = 1, 2, 3, 4$
$\rho = 2\kappa r$	Dimensionless radial variable of the Dirac-Coulomb problem
$\mathfrak{K} = \varpi \left(j + \frac{1}{2} \right)$	Eigenvalue of the operator $\boldsymbol{\sigma} \cdot \mathbf{p}$ in the Dirac-Coulomb problem, a.k.a. the Dirac quantum number (normally denoted by K in the literature)
\mathbf{p}	Momentum operator of the Dirac fields
$\zeta = \sqrt{\mathfrak{K}^2 - (Z\alpha)^2}$	Dimensionless combination appearing in the radial differential equations of the Dirac-Coulomb problem
$a = \zeta - \frac{Z\alpha\omega}{\kappa},$ $b = 1 + 2\zeta$	Arguments of the confluent hypergeometric functions that appear in the near-origin finite parts of $\mathbf{f}_{nj}(r)$, $\mathbf{g}_{nj}(r)$
$a' = -\left(\zeta + \frac{Z\alpha\omega}{\kappa} \right),$ $b' = 1 - 2\zeta$	Arguments of the confluent hypergeometric functions that appear in the near-origin divergent parts of $\mathbf{f}_{nj}(r)$, $\mathbf{g}_{nj}(r)$
$c = \mathfrak{K} - \frac{Z\alpha m}{\kappa}$	Factor appearing in both types of solutions (near-source convergent and divergent) of the radial functions $\mathbf{f}_{nj}(r)$, $\mathbf{g}_{nj}(r)$
$\mathcal{N} = n\sqrt{1 - \frac{2(n- \mathfrak{K})(Z\alpha)^2}{n^2(\zeta+ \mathfrak{K})}}$	Relativistic numerical factor appearing in the point-like source solutions to the Dirac-Coulomb problem
$\omega_{nj}^D = m\sqrt{1 - \frac{(Z\alpha)^2}{\mathcal{N}^2}}$	Bound state energy eigenvalue of Dirac particles in a Coulomb potential sourced by a point-like nucleus with charge (Ze)
$\kappa_{nj}^D = \frac{mZ\alpha}{\mathcal{N}}$	Function of the bound state lepton energy of a Dirac particle in a Coulomb potential sourced by a point-like nucleus with charge (Ze)
$\delta\omega_{nFj\varpi}$	Energy shifts of a nuclear origin to the leptonic mode functions with quantum numbers n, F, j, ϖ and Dirac-Coulomb energy ω_{nj}^D

$\varepsilon_{nFj\varpi}^{\text{mag}} = \varepsilon_{nFj\varpi}^{(1)} + \varepsilon_{nFj\varpi}^{(ho)}$	The energy shifts generated by the magnetic dipole moment of the nucleus at first and higher-order in \mathfrak{s} respectively
$\varepsilon_{nFj\varpi}^{\text{QED}} = \varepsilon_{nFj\varpi}^{\text{pt-QED}} + \varepsilon_{nFj\varpi}^{\text{N-QED}}$	The energy shifts coming from various QED processes in the point-nucleus limit and the radiative corrections to finite-size effects through loop processes respectively
$\varepsilon_{nFj\varpi}^{\text{rec}} = \varepsilon_{nFj\varpi}^{\text{pt-rec}} + \varepsilon_{nFj\varpi}^{\text{N-rec}}$	The energy shifts coming from nuclear recoil processes in the point-nucleus limit and the recoil corrections to the finite-size effects respectively
$\mathcal{Y}_{Ff_z}^{j,\varpi}(\theta, \phi)$	The new spinors that incorporate the hyperfine structure. They obey the eigenvalue relation $\mathbf{F}^2 \mathcal{Y}_F = F(F+1) \mathcal{Y}$ and others found in Appendix D
$\psi_{nFj\varpi} := nFf_z; I, j\rangle_0$	The correct zeroth-order atomic states that diagonalize the degenerate subspaces of the mixed electron and nuclear states under the hyperfine interaction
η_{I, I_z}	The nuclear spin states of a nucleus with spin, I
$\varepsilon_{nFj\varpi}^{(1)}$	The first-order energy shift caused by the presence of the nuclear magnetic dipole field calculated in perturbation theory
$\mathcal{D}, \tilde{\mathcal{D}}$	The explicit, normalization factor that emerges in the energy shift and state-corrections for unnormalized states
$\Sigma = i(\mathbf{I} \times \hat{\mathbf{r}}) \cdot \boldsymbol{\sigma}$	Angular operator acting on the hyperfine spinors $\mathcal{Y}_{F, f_z}^{j,\varpi}$
X_F	A combination of angular momentum quantum numbers defined in (2.34) that ubiquitously appears at first order in \mathfrak{s} due to rotational invariance
$\mathfrak{N}, \mathfrak{N}^s$	Collection of dimensionless integrals in the radial matrix elements appearing in the numerator of the first-order energy shift and the first-order state corrections respectively, due to the hyperfine interaction

$\mathfrak{D}, \tilde{\mathfrak{D}}$	Collection of dimensionless integrals appearing in the denominator of the first-order energy shift and state-corrections respectively, due to the hyperfine interaction
$\mathfrak{N}_{\text{pt}}, \mathfrak{N}_1, \mathfrak{N}_2,$ $\mathfrak{D}_{\text{pt}}, \mathfrak{D}_1, \mathfrak{D}_2$	Set of dimensionless integrals in $\mathfrak{N}, \mathfrak{D}$ split into three categories: integrals over only near-origin convergent functions ('pt' subscript); integrals accompanied by one power of the integration constant ratio \mathcal{D}/\mathcal{C} (labelled by the '1' subscript); integrals accompanied by two powers \mathcal{D}/\mathcal{C} (subscript '2')
$\mathfrak{N}_{\text{pt}}^s, \tilde{\mathfrak{N}}_1^s, \mathfrak{N}_1^s, \mathfrak{N}_2^s,$ $\tilde{\mathfrak{D}}_{\text{pt}}, \tilde{\mathfrak{D}}_1, \tilde{\mathfrak{D}}_2$	Set of dimensionless integrals in $\mathfrak{N}^s, \tilde{\mathfrak{D}}$ split into the same categories as those in $\mathfrak{N}, \mathfrak{D}$
$E_{n,j}^{(0)} = \omega_{nj}^D + \delta\omega_{nj}^{(0)}$	The zeroth-order energies of the atom with degeneracy $(2I + 1)(2j + 1)$
$\mathcal{C}_{\tilde{n}nFF_z\tilde{j}j\tilde{\omega}\varpi}$	Coefficient of the first-order state-corrections
$\delta\omega_{nj\varpi}^{(0)}$	The spin-independent, zeroth-order finite-size energy shift determined by the normalizability condition (2.22). This is the part of the energy shift that appears in our earlier work [64, 72] given by the zeroth-order, scalar part of the integration constant ratio $(\mathcal{D}/\mathcal{C})^{(0)}$
$\delta\omega_{nFj}^{(1)}$	The spin-dependent, first-order finite-size energy shift coming from the normalizability condition (2.22) through $(\mathcal{D}/\mathcal{C})^{(1)}$
$\mathcal{I}_{ij}^{(p)}$	Integrals that appear in the radial matrix elements of the first-order energy shift with $i, j \in [1, 4]$ denoting the four confluent hypergeometric functions in $\mathfrak{f}, \mathfrak{g}$
$\varepsilon_{nFj\varpi}^{\text{hfs}}$	The hyperfine-splitting energy shift with relativistic corrections included
C_η	A regularization-scale dependent function that needs to be absorbed into the effective couplings in order to keep $\varepsilon_{nFj\varpi}^{(1)}$ physical

$\mathbf{c} = 16(m\epsilon_{\star+})^2$	A function of the small dimensionless quantity $m\epsilon_{\star+}$ that controls finite-size effects in the PPEFT language
g_p	g-factor of the proton
μ_p	Magnetic moment of the proton
nL_j^F	Spectroscopic notation of an energy level with quantum numbers n, l, j, F
$\mathcal{I}_{ij}^{(p)}$	Integrals that appear in the \mathfrak{N}^s matrix-elements of the first-order state corrections. Here, the tilde signals the fact that the quantum numbers are different for the two hypergeometric functions in the integrand but the other indices are defined the same way as in $\mathcal{I}_{ij}^{(p)}$
$\widehat{\Sigma}$	The sum factor of (2.54) over all values of the principal quantum number that lie outside the degenerate subspace of the state whose corrections we are looking at
$\mathbf{f}_{nj\varpi}^{(0)}, \mathbf{g}_{nj\varpi}^{(0)}$	The Dirac-Coulomb wave-functions
$\mathbf{f}_{nj\varpi}^{(1)}, \mathbf{g}_{nj\varpi}^{(1)}$	First-order corrections to the Dirac-Coulomb wave-functions calculated in degenerate perturbation theory
$(\mathcal{D}/\mathcal{C})^{(0)}$	The ratio of integration constants found in the case of a scalar source
$(\mathcal{D}/\mathcal{C})^{(1)}$	The first order correction to the ratio of integration constants introduced as a compensation for the lack of new large- r normalizability conditions for the full states once the hyperfine interaction is turned on
ϵ	Radius of the Gaussian sphere on which the alternative boundary conditions implied by the PPEFT are set up
$\epsilon_{\star}, \epsilon_0$	RG-invariant scales associated with the finite-size effects of a scalar source and controlling the running of the PPEFT couplings c_s, c_v, c_F

ϵ_F	RG-invariant scale associated with the mixed finite-size, hyperfine effects
$\mathcal{Z}_{Fj\varpi}, \mathcal{Z}_{F\varpi}$	Another combination of angular momentum quantum numbers that appears in the matrix elements of the $\mathbf{I} \cdot \boldsymbol{\Sigma}$ operator.
$\hat{c}_i = \frac{c_i}{4\pi\epsilon^2}$	The generic EFT coupling divided by the surface area of the sphere on which the new boundary conditions are set up. Equivalently, these are the dimensionless couplings that appear in the boundary action of the PPEFT
$\hat{c}_s^{(0)}, \hat{c}_v^{(0)}$	The coupling coefficients appearing at zeroth order in \mathfrak{s} and so whose running is controlled by the spin-independent parts of the boundary-condition
$\hat{c}_s^{(1)}, \hat{c}_v^{(1)}$	Corrections to the $(length)^2$ coupling coefficients of scalar nuclei appearing at first order in \mathfrak{s}
$\chi = \sqrt{\frac{m-\omega}{m+\omega}}$	A numerical factor that appears in the ratios of radial functions $\mathbf{f}(r), \mathbf{g}(r)$
Λ_{\pm}	Contributions to the boundary conditions of leptonic modes that come from the first-order state-corrections
$g(\epsilon), u(\epsilon), v(\epsilon)$	Functions in terms of which the zeroth-order RG-flow can be universally determined
A, B, C, D	Constants in the universal evolution of coupling constants
$y_{\star} = \pm 1$	An RG-invariant that determines which type of curve the couplings flow on in the zeroth-order RG evolution
$\bar{\lambda}_{\pm}^{(0)}$	The n -independent linear combination of spin-independent PPEFT couplings $\hat{c}_s^{(0)}$ and $\hat{c}_v^{(0)}$ that follows from the leading-order RG behaviour of the couplings
$\bar{\lambda}_{\pm}^{(1)}$	The linear combination of spin-dependent PPEFT couplings $\hat{c}_s^{(1)}, \hat{c}_v^{(1)}$ and \hat{c}_F that follows from $cO(\mathfrak{s})$ RG behaviour of the couplings

$(\mathcal{D}/\mathcal{C})_{phys}^{(1)}$	The physical part of the normalizability compensating expansion of the ratio of leptonic integration constants at first order. This quantity controls the actual mixed hyperfine, finite-size effects coming from the large- r normalizability condition
$\delta\omega_{nFj\varpi} = \delta\omega_{nFj\varpi}^{(0)} + \delta\omega_{nFj\varpi}^{(1)}$	Nuclear-size dependent energy shift coming from the large- r normalizability condition at zeroth and first orders in \mathfrak{s}
H_n	Harmonic numbers
\mathfrak{H}	A function of \mathcal{D}/\mathcal{C} appearing in $\delta\omega_{nFj\varpi}$
γ	Euler-Mascheroni constant
$\rho_{c/m}(\mathbf{x}')$	The electric charge and magnetization densities of the proton
$\langle r^2 \rangle_c, \langle r^3 \rangle_{cc}, \langle r \rangle_{cm}, \dots$	The charge radius squared, the Friar and the Zemach moments and other nuclear moments that can be used to parameterize finite-size effects
$\langle r^3 \rangle_{cc}^{\text{eff}}$	The effective Friar moment, incorporating the finite-size parts of the nuclear polarizability contributions
$\langle r_{C1} \rangle, \langle r_{C2} \rangle, \langle r_{pp} \rangle$	Various moments used to capture elastic parts of the nuclear-structure effects from [57] and [56]
$\omega_{nFj\varpi}^{\text{pt}}$	Theoretical contributions to the energy shift of leptons in the point-nucleus limit
$\omega_{nFj\varpi}^{NS}$	Nuclear-size related energy shifts to the lepton energies
Λ	An arbitrary scale in radiative corrections to the leading mixed finite-size, hyperfine effects first derived in [30]
$\Xi_{nj\varpi}$	The radiative corrections to finite-size effects for muonic Hydrogen appearing in the traditional Lamb shift coming from the electronic vacuum polarization

$L_n^k(x)$	The associated Laguerre polynomials
$\rho_0 = \frac{2m_r(Z\alpha)r}{n}$	The dimensionless radial variable in the Schroedinger-Coulomb problem
$G'(x, 0)$	The reduced Schrödinger-Coulomb Green's function for $nS_{1/2}$ states
$\nu (nL_{j^F} - n'L'_{j'^F})$	The experimentally measured value of a transition between two energy levels
$\nu_{1S_{hfs}}, \nu_{2S_{hfs}}, \nu_{21}$	The experimentally measured energies of the $1S_{j=\frac{1}{2}}^{F=1} - 1S_{j=\frac{1}{2}}^{F=0}$, the $2S_{j=\frac{1}{2}}^{F=1} - 2S_{j=\frac{1}{2}}^{F=0}$ and the $2S_{j=\frac{1}{2}}^{F=1} - 1S_{j=\frac{1}{2}}^{F=1}$ transitions in atomic Hydrogen respectively
ν_t, ν_s	The experimentally measured $2P_{j=\frac{3}{2}}^{F=2} - 2S_{j=\frac{1}{2}}^{F=1}$ and the $2P_{j=\frac{3}{2}}^{F=1} - 2S_{j=\frac{1}{2}}^{F=0}$ transitions in muonic Hydrogen respectively
$z_\ell = (m_{r,(\ell)}\epsilon_{\star,\ell})^2$	A dimensionless combination of the RG-invariant $\epsilon_{\star,\ell}$ and the lepton ($\ell = e, \mu$) mass. We fit for this parameter in our numerical calculations
\mathfrak{r}_ℓ	An energy scale appearing in the fitting of z for the lepton $\ell = e, \mu$
η_ℓ	A dimensionless constant appearing in the fitting of z for the lepton $\ell = e, \mu$
$W(t)$	The Lambert- W function
$\mathcal{W} = W_{-1}(-\mathfrak{r}e^{-\eta}) + \eta$	The function of the Lambert-W function that determines $(m\epsilon_\star)^2$
$\widehat{\Delta\omega}_{2S_{hfs}}$	The difference, $\left[\omega_{21\frac{1}{2}+}^{\text{pt}} - \omega_{20\frac{1}{2}+}^{\text{pt}} \right] - \nu_{2S_{hfs}}$ between the experimentally measured value of the hyperfine-splitting of the $2S$ state in atomic Hydrogen and the size-independent contributions to this transition

$\widehat{\Delta\omega}_{21}$	The finite-size contribution to the $2S_{j=\frac{1}{2}}^{F=1} - 1S_{j=\frac{1}{2}}^{F=1}$ transition, expressed as the difference between point-like theory contributions and the experimentally measured value, $\left[\omega_{21\frac{1}{2}+}^{\text{pt}} - \omega_{11\frac{1}{2}+}^{\text{pt}}\right] - \nu_{21}$
$\widehat{\Delta\omega}_{hfs}$	The first linear combination of experimental values and point-like theoretical combinations to their measured intervals, $\left[\omega_{21\frac{1}{2}+}^{\text{pt}} - \omega_{20\frac{1}{2}+}^{\text{pt}}\right] - \left[\omega_{22\frac{3}{2}+}^{\text{pt}} - \omega_{21\frac{3}{2}+}^{\text{pt}}\right] - [\nu_s - \nu_t]$ that can be used to fit $\epsilon_{F,\mu}$ in muonic Hydrogen
$\widehat{\Delta\omega}_{Lamb}$	The second linear combination of experimental values and point-like theoretical combinations to their measured intervals, $\frac{1}{4} \left[\omega_{21\frac{3}{2}+}^{\text{pt}} - \omega_{20\frac{1}{2}+}^{\text{pt}}\right] - \nu_s + \frac{3}{4} \left[\omega_{22\frac{3}{2}+}^{\text{pt}} - \omega_{21\frac{1}{2}+}^{\text{pt}} - \nu_t\right]$ that can be used to fit $\epsilon_{F,\mu}$ in muonic Hydrogen
ΔE^{fs}	Finite-size contribution to a given energy shift
ΔE^{exp}	Experimental error on the value of ΔE^{fs}
ΔE^{th}	Error on ΔE^{fs} generated by the size-independent contributions to energy shifts
ΔE^{trunc}	The truncation error on ΔE^{fs} coming from ignoring terms in our finite-size series expansion
\mathcal{L}	The Lagrangian density
p^μ	Conjugate momentum to y^μ
π^μ	Conjugate momentum to ξ^μ
ϕ_1	Scalar constraint on the relativistic spinning point-particle
Φ^μ	Grassmann constraint on the relativistic spinning point-particle
\mathcal{L}_c, H_c	Constrained Lagrangian and Hamiltonian of the relativistic spinning point-particle

θ	The scalar Lagrange-multiplier for ϕ_1
Θ^μ	The Grassmann Lagrange multiplier for Φ^μ
$(A, B)_P$	The Poisson bracket, defined for a theory with only Grassmann-even quantities as $(A, B)_P = \frac{\partial A}{\partial q^i} \frac{\partial B}{\partial p_i} - \frac{\partial A}{\partial p_i^q} \frac{\partial B}{\partial q^i}$
$\Delta_{\alpha\beta} := (\phi_\alpha, \phi_\beta)_P$	A matrix built out of the Poisson brackets of constraints
$(A, B)_D$	The Dirac bracket
$\varphi := y^0 - s$	Imposed gauge condition to get rid of ϕ_1
α, β	Spinors of the Dirac field that are interpreted as the particle and anti-particle solutions in the rest-frame of the particle with the Dirac representation assumed. β can also be a set of generic angular momentum labels depending on context
S_p^{int}	The PPEFT action with the lepton field interactions
I_B^{int}	Boundary action of nucleus-lepton interactions
\mathcal{B}_ϵ	Ball of radius, ϵ where the boundary conditions are set up
$\delta x = -\delta\omega \frac{(Z\alpha)m^2}{(\kappa_{n,j}^D)^3}$	Convenient dimensionless quantity that appears when finding the energy shift through the normalizability condition
$\delta y = 2 \mathcal{K} - 2\zeta$	Another convenient difference of dimensionless quantities of size $\mathcal{O}((Z\alpha)^2)$ that appears when finding the energy shift from the normalizability condition
\mathfrak{B}	A function of the principal and Dirac quantum numbers appearing in the energy shift implied by the normalizability condition (2.22)
H_0	The zeroth-order Hamiltonian that can be solved exactly

V, λ	The perturbation to H_0 and a parameter that formally helps keep track of the orders in V and is eventually sent to 1
\bar{D}	Projection operator out of the degenerate subspace of a given state
$\mu, \lambda, \mathfrak{z}$	$\mathcal{O}[(Z\alpha)^2]$ parameters that help us keep track of the regularization of the divergent integrals in energy shifts and state-corrections
${}_A\mathcal{F}_B$	Hypergeometric function with \mathcal{A} numerator-type and \mathcal{B} denominator-type parameters
$(a)_i$	Pochhammer symbols
$\mathcal{I}_d(a, b; a', b')$	Generic integral appearing in \mathfrak{N} , \mathfrak{D} and $\tilde{\mathfrak{D}}$
η_a	The regularization parameter that controls the divergences in matrix elements
$\mathcal{I}_d(s; a, b, k; \tilde{a}, \tilde{b}, \tilde{k})$	Generic integral appearing in \mathfrak{N}^s
$\mathcal{S}_\pm := \frac{\sqrt{(1+\frac{\omega}{m})(1-\frac{\omega}{m})}}{\pm\sqrt{(1+\frac{\omega}{m})(1-\frac{\tilde{\omega}}{m})}}$	Frequently appearing numerical factors in the first order state corrections

References

- [1] A. van Wijngaarden, F. Holuj, G. W. F. Drake, “Lamb shift in He^+ : Resolution of a discrepancy between theory and experiment”, *Phys. Rev. A*, **63** (2000) 012505,
- [2] M. Fischer *et al.*, “Precision spectroscopy of atomic Hydrogen and variations of fundamental constants,” *Lect. Notes Phys.* **648** (2004) 209 [physics/0311128].
- [3] P. Indelicato, “Exotic atoms,” *Phys. Scripta T* **112** (2004) 20 [physics/0409058].
- [4] N. Kolachevsky, A. Matveev, J. Alnis, C. G. Parthey, S. G. Karshenboim and T. W. Hansch, “Measurement of the 2S Hyperfine Interval in Atomic Hydrogen”, *Phys. Rev. Lett.* **102** (2009) 213002,
- [5] R. Pohl, A. Antognini, F. Nez et. al. “The size of the proton”, *Nature*, **466** (2010) 213-216,
- [6] A. E. Kramida, “A Critical Compilation of Experimental Data on Spectral Lines and Energy Levels of Hydrogen, Deuterium and Tritium”, *At. Data Nucl. Data Tables*, **96**, (2010) 586-644,
- [7] R. Pohl *et al.*, “The size of the proton and the deuteron,” *J. Phys. Conf. Ser.* **264** (2011) 012008.
- [8] C. G. Parthey *et al.*, “Improved Measurement of the Hydrogen 1S - 2S Transition Frequency,” *Phys. Rev. Lett.* **107** (2011) 203001 [arXiv:1107.3101 [physics.atom-ph]].
- [9] A. Antognini *et al.*, “Illuminating the proton radius conundrum: The mu He^+ Lamb shift,” *Can. J. Phys.* **89** (2011) no.1, 47.
- [10] A. Antognini *et al.*, “The Lamb shift in muonic Hydrogen and the proton radius,” *Physics Procedia* **17** (2011) 10.
- [11] T. Nebel *et al.*, “The size of the proton,” *Hyperfine Interact.* **212** (2012) no.1-3, 185.
- [12] A. Beyer et. al., “Precision Spectroscopy of Atomic Hydrogen”, *J. Phys.: Conf. Ser.* **467** (2013) 012003,
- [13] A. Antognini, F. Nez, K. Schuhmann et. al., “Proton Structure from the Measurement of 2S-2P Transition Frequencies of Muonic Hydrogen”, *Science*, **339**, (2013) 417-420,
- [14] R. Pohl *et al.*, “Laser spectroscopy of muonic Hydrogen,” *Annalen Phys.* **525** (2013) no.8-9, 647.
- [15] M. Sato *et al.*, “Laser spectroscopy of the hyperfine splitting energy in the ground state of muonic Hydrogen,”
- [16] A. Antognini, “Muonic atoms and the nuclear structure,” arXiv:1512.01765 [physics.atom-ph].

- [17] A. Antognini, K. Schumann, F. D. Amaro, P. Amaro et. al. “Experiments towards resolving the proton charge radius puzzle”, EPJ Web Conf., **113** (2016) 01006,
- [18] M. Sato *et al.*, “Laser Spectroscopy of Ground State Hyperfine Splitting Energy of Muonic Hydrogen,” JPS Conf. Proc. **8** (2015) 025005.
- [19] R. Pohl [CREMA Collaboration], “Laser Spectroscopy of Muonic Hydrogen and the Puzzling Proton,” J. Phys. Soc. Jap. **85** (2016) no.9, 091003.
- [20] R. Pohl *et al.* [CREMA Collaboration], “Laser spectroscopy of muonic deuterium,” Science **353** (2016) no.6300, 669.
- [21] R. Pohl *et al.*, “Laser Spectroscopy of Muonic Atoms and Ions,” JPS Conf. Proc. **18** (2017) 011021 [arXiv:1609.03440 [physics.atom-ph]].
- [22] F. Nez *et al.*, “Laser spectroscopy of muonic deuterium: New contribution to the proton puzzle,”
- [23] S. Schmidt et. al., “The next generation of laser spectroscopy experiments using light muonic atoms”, J. Phys.: Conf. Ser. **1138** (2018) 012010,
- [24] S. Kanda et. al., “Measurement of the proton Zemach radius from the hyperfine splitting in muonic Hydrogen atom”, J. Phys.: Conf. Ser. **1138** (2018) 012009,
- [25] H. Fleurbaey *et al.*, “New Measurement of the $1S - 3S$ Transition Frequency of Hydrogen: Contribution to the Proton Charge Radius Puzzle,” Phys. Rev. Lett. **120** (2018) no.18, 183001 [arXiv:1801.08816 [physics.atom-ph]].
- [26] N. Bezginov, T. Valdez, M. Horbatsch, A. Marsman, A. C. Vutha and E. A. Hessels, “A measurement of the atomic Hydrogen Lamb shift and the proton charge radius,” Science **365** (2019) no.6457, 1007.
- [27] R. Karplus, A. Klein and J. Schwinger, “Electrodynamic Displacement of Atomic Energy Levels. 2. Lamb Shift,” Phys. Rev. **86** (1952), 288-301
- [28] A. C. Zemach, “Proton Structure and the Hyperfine Shift in Hydrogen,” Phys. Rev. **104** (1956) 1771.
- [29] J. L. Friar, “Nuclear finite-size effects in light muonic atoms”, Ann. Phys. **122** (1978) 152-196
- [30] S. G. Karshenboim, “Nuclear structure dependent radiative corrections to the Hydrogen hyperfine splitting,” Phys. Lett. A **225** (1997) 97 [hep-ph/9608484].
- [31] J. L. Friar and G. L. Payne, “Higher order nuclear size corrections in atomic Hydrogen,” Phys. Rev. A **56** (1997) 5173 [nucl-th/9705036].
- [32] K. Pachucki, “Proton structure effects in muonic Hydrogen,” Phys. Rev. A **60** (1999) 3593 [physics/9906002 [physics.atom-ph]].

- [33] A. V. Volotka, V. M. Shabaev, G. Plunien and G. Soff, “Nuclear size correction to the hyperfine splitting in low-Z Hydrogen-like atoms”, *Eur. Phys. J. D* **23** (2003) 51-56,
- [34] A. I. Milstein, O. P. Sushkov and I. S. Terekhov, “Finite nuclear size and Lamb shift of p wave atomic states,” *Phys. Rev. A* **67** (2003) 062111 [physics/0212018].
- [35] J. L. Friar and G. L. Payne, “Nuclear corrections to hyperfine structure in light Hydrogenic atoms,” *Phys. Rev. C* **72** (2005) 014002 [nucl-th/0504015].
- [36] A. V. Volotka, V. M. Shabaev, G. Plunien and G. Soff, “Zemach and magnetic radius of the proton from the hyperfine splitting in Hydrogen,” *Eur. Phys. J. D* **33** (2005) 23 [physics/0405118].
- [37] C. E. Carlson, V. Nazaryan and K. Griffioen, “Proton structure corrections to electronic and muonic Hydrogen hyperfine splitting,” *Phys. Rev. A* **78** (2008) 022517 [arXiv:0805.2603 [physics.atom-ph]].
- [38] C. E. Carlson, “Proton structure and atomic physics,” *AIP Conf. Proc.* **1155** (2009) no.1, 18.
- [39] J. Zatorski, K. Pachucki, “Electrodynamics of finite-size particles with arbitrary spin”, *Phys. Rev. A* **82** (2010) 052520,
- [40] K. Pachucki, “Nuclear structure corrections in muonic deuterium,” *Phys. Rev. Lett.* **106** (2011) 193007 [arXiv:1102.3296 [hep-ph]].
- [41] C. E. Carlson, V. Nazaryan and K. Griffioen, “Proton structure corrections to hyperfine splitting in muonic Hydrogen,” *Phys. Rev. A* **83** (2011) 042509 [arXiv:1101.3239 [physics.atom-ph]].
- [42] C. E. Carlson and M. Vanderhaeghen, “Higher order proton structure corrections to the Lamb shift in muonic Hydrogen,” *Phys. Rev. A* **84** (2011) 020102 [arXiv:1101.5965 [hep-ph]].
- [43] J. D. Carroll, A. W. Thomas, J. Rafelski and G. A. Miller, “Proton form-factor dependence of the finite-size correction to the Lamb shift in muonic Hydrogen,” arXiv:1108.2541 [physics.atom-ph].
- [44] J. D. Carroll, A. W. Thomas, G. A. Miller and J. Rafelski, “Non-perturbative Analysis of the Influence of the Proton Magnetization and Charge Densities on the Hyperfine Splitting of Muonic Hydrogen,” arXiv:1108.5785 [physics.atom-ph].
- [45] J. Friar, “Nuclear Polarization Corrections to $\mu - d$ Atoms in Zero-Range Approximation,” *Phys. Rev. C* **88** (2013) no.3, 034003 [arXiv:1306.3269 [nucl-th]].
- [46] C. E. Carlson, M. Gorchtein and M. Vanderhaeghen, “Nuclear structure contribution to the Lamb shift in muonic deuterium,” *Phys. Rev. A* **89** (2014) no.2, 022504 [arXiv:1311.6512 [nucl-th]].

- [47] B. Nickel, “Nuclear size effects on Hydrogenic atom energies: a semi-analytic formulation”, *J. Phys. B: At. Mol. Opt. Phys.* **46** (2013) 015001,
- [48] R. N. Faustov, A. P. Martynenko, G. A. Martynenko and V. V. Sorokin, “Radiative nonrecoil nuclear finite size corrections of order $\alpha(Z\alpha)^5$ to the hyperfine splitting of S-states in muonic Hydrogen,” *Phys. Lett. B* **733** (2014) 354 [arXiv:1402.5825 [hep-ph]].
- [49] C. Peset and A. Pineda, “The two-photon exchange contribution to muonic Hydrogen from chiral perturbation theory,” *Nucl. Phys. B* **887** (2014) 69 [arXiv:1406.4524 [hep-ph]].
- [50] K. Pachucki and A. Wienczek, “Nuclear structure effects in light muonic atoms,” *Phys. Rev. A* **91** (2015) no.4, 040503 [arXiv:1501.07451 [physics.atom-ph]].
- [51] C. Ji, O. J. Hernandez, N. Nevo Dinur, S. Bacca and N. Barnea, “Understanding the proton radius puzzle: Nuclear structure effects in light muonic atoms,” *EPJ Web Conf.* **113** (2016) 03006 [arXiv:1509.01430 [nucl-th]].
- [52] S. G. Karshenboim, E. Y. Korzinin, V. A. Shelyuto and V. G. Ivanov, “Recoil correction to the proton finite-size contribution to the Lamb shift in muonic Hydrogen,” *Phys. Rev. D* **91** (2015) no.7, 073003 [arXiv:1501.06539 [hep-ph]].
- [53] C. Peset and A. Pineda, “Model-independent determination of the two-photon exchange contribution to hyperfine splitting in muonic Hydrogen,” *JHEP* **1704** (2017) 060 [arXiv:1612.05206 [nucl-th]].
- [54] R. N. Faustov, A. P. Martynenko, F. A. Martynenko and V. V. Sorokin, “Radiative nonrecoil nuclear finite size corrections of order $\alpha(Z\alpha)^5$ to the Lamb shift in light muonic atoms,” *Phys. Lett. B* **775** (2017) 79 [arXiv:1706.01060 [hep-ph]].
- [55] A. E. Dorokhov, N. I. Kochelev, A. P. Martynenko, F. A. Martynenko and A. E. Radzhabov, “Corrections of two-photon interactions in the fine and hyperfine structure of the P-energy levels of muonic Hydrogen,” *Eur. Phys. J. A* **54** (2018) no.8, 131 [arXiv:1804.09749 [hep-ph]].
- [56] M. Kalinowski, K. Pachucki and V. A. Yerokhin, “Nuclear-structure corrections to the hyperfine splitting in muonic deuterium,” *Phys. Rev. A* **98** (2018) no.6, 062513 [arXiv:1810.06601 [physics.atom-ph]].
- [57] K. Pachucki, V. Patkóš and V. A. Yerokhin, “Three-photon exchange nuclear structure correction in Hydrogenic systems,” *Phys. Rev. A* **97** (2018) no.6, 062511 [arXiv:1803.10313 [physics.atom-ph]].
- [58] O. Tomalak, “Two-Photon Exchange Correction to the Lamb Shift and Hyperfine Splitting of S Levels,” *Eur. Phys. J. A* **55** (2019) no.5, 64 [arXiv:1808.09204 [hep-ph]].
- [59] S. G. Karshenboim, E. Y. Korzinin, V. A. Shelyuto and V. G. Ivanov, “ $\alpha(Z\alpha)^5 m$

- finite-nuclear-size contribution to the energy levels in light muonic atoms,” *Phys. Rev. A* **98** (2018) no.6, 062512.
- [60] N. Nevo Dinur, O. J. Hernandez, S. Bacca, N. Barnea, C. Ji, S. Pastore, M. Piarulli and R. B. Wiringa, “Zemach moments and radii of $^2,^3\text{H}$ and $^3,^4\text{He}$,” *Phys. Rev. C* **99** (2019) no.3, 034004 [arXiv:1812.10261 [nucl-th]].
- [61] S. G. Karshenboim, E. Y. Korzinin, V. A. Shelyuto and V. G. Ivanov, “Relativistic finite-nuclear-size corrections to the energy levels in light muonic atoms,” *Phys. Rev. A* **99** (2019) no.3, 032508.
- [62] C. Ji, “Ab Initio Calculation of Nuclear Structure Effects in Light Muonic Atoms,” *Springer Proc. Phys.* **238** (2020) 895.
- [63] C.P. Burgess, P. Hayman, Markus Rummel and László Zalavári, “Nuclear Predictions for H Spectroscopy without Nuclear Errors,” arXiv:2008.09719 [hep-ph].
- [64] C. P. Burgess, P. Hayman, M. Rummel and L. Zalavari, “Reduced theoretical error for $^4\text{He}^+$ spectroscopy,” *Phys. Rev. A* **98** (2018) no.5, 052510 [arXiv:1708.09768 [hep-ph]].
- [65] W. E. Caswell and G. P. Lepage, “Effective Lagrangians for Bound State Problems in QED, QCD, and Other Field Theories,” *Phys. Lett.* **167B** (1986) 437.
- [66] A. Pineda and J. Soto, “The Lamb shift in dimensional regularization,” *Phys. Lett. B* **420** (1998) 391 [hep-ph/9711292].
- [67] A. Pineda, “The Chiral structure of the Lamb shift and the definition of the proton radius,” *Phys. Rev. C* **71** (2005) 065205 [hep-ph/0412142].
- [68] R. J. Hill and G. Paz, “Model independent analysis of proton structure for Hydrogenic bound states,” *Phys. Rev. Lett.* **107** (2011) 160402 [arXiv:1103.4617 [hep-ph]].
- [69] G. Paz, “An Introduction to NRQED,” *Mod. Phys. Lett. A* **30** (2015) no.26, 1550128 [arXiv:1503.07216 [hep-ph]].
- [70] C. P. Burgess, P. Hayman, M. Williams and L. Zalavari, “Point-Particle Effective Field Theory I: Classical Renormalization and the Inverse-Square Potential,” *JHEP* **1704** (2017) 106 [arXiv:1612.07313 [hep-ph]].
- [71] C. P. Burgess, P. Hayman, M. Rummel, M. Williams and L. Zalavari, “Point-Particle Effective Field Theory II: Relativistic Effects and Coulomb/Inverse-Square Competition,” *JHEP* **1707** (2017) 072 [arXiv:1612.07334 [hep-ph]].
- [72] C. P. Burgess, P. Hayman, M. Rummel and L. Zalavari, “Point-Particle Effective Field Theory III: Relativistic Fermions and the Dirac Equation,” *JHEP* **1709** (2017) 007 [arXiv:1706.01063 [hep-ph]].
- [73] R. Plestid, C. P. Burgess and D. H. J. O’Dell, “Fall to the Centre in Atom Traps and

- Point-Particle EFT for Absorptive Systems,” *JHEP* **1808** (2018) 059 [arXiv:1804.10324 [hep-ph]].
- [74] C. P. Burgess, R. Plestid and M. Rummel, “Effective Field Theory of Black Hole Echoes,” *JHEP* **1809** (2018) 113 [arXiv:1808.00847 [gr-qc]].
- [75] P. Hayman and C. P. Burgess, “Point-Particle Catalysis,” *Front. in Phys.* **7** (2019) 167 [arXiv:1905.00103 [hep-th]].
- [76] C.P. Burgess, *Introduction to Effective Field Theory: Thinking effectively about hierarchies of scale*, Cambridge University Press 2020 (in press).
- [77] W. D. Goldberger and M. B. Wise, “Renormalization group flows for brane couplings,” *Phys. Rev. D* **65** (2002) 025011 [hep-th/0104170].
- [78] K. Agashe, A. Delgado and R. Sundrum, “Gauge coupling renormalization in RS1,” *Nucl. Phys. B* **643** (2002) 172 [hep-ph/0206099].
- [79] W. D. Goldberger and I. Z. Rothstein, “An Effective field theory of gravity for extended objects,” *Phys. Rev. D* **73** (2006) 104029 [hep-th/0409156].
- [80] C. de Rham, “The Effective field theory of codimension-two branes,” *JHEP* **0801** (2008) 060 [arXiv:0707.0884 [hep-th]].
- [81] C. P. Burgess, D. Hoover, C. de Rham and G. Tasinato, “Effective Field Theories and Matching for Codimension-2 Branes,” *JHEP* **0903** (2009) 124 [arXiv:0812.3820 [hep-th]].
- [82] A. Bayntun, C. P. Burgess and L. van Nierop, “Codimension-2 Brane-Bulk Matching: Examples from Six and Ten Dimensions,” *New J. Phys.* **12** (2010) 075015 [arXiv:0912.3039 [hep-th]].
- [83] J. G. Polchinski, “String Theory”, Cambridge University Press (1998) vol. I & II.
- [84] D. M. Gitman and I. V. Tyutin, “Quantization of Fields with Constraints,” Springer (1990), 291 p.
- [85] B. Zwiebach, “A first course in string theory,” Cambridge, UK: Univ. Pr. (2009) 673 p
- [86] R. Casalbuoni, “Relativity and Supersymmetries,” *Phys. Lett.* **62B** (1976) 49.
- [87] A. Barducci, R. Casalbuoni and L. Lusanna, “Supersymmetries and the Pseudoclassical Relativistic electron,” *Nuovo Cim. A* **35** (1976) 377.
- [88] F. A. Berezin and M. S. Marinov, “Particle Spin Dynamics as the Grassmann Variant of Classical Mechanics,” *Annals Phys.* **104** (1977) 336.
- [89] L. Brink, P. Di Vecchia, P. Howe, “A Lagrangian formulation of the classical and quantum dynamics of spinning particles”, *Nucl. Phys. B* **118** (1977) 76-94
- [90] P. Di Vecchia, F. Ravndal, “Supersymmetric Dirac Particles”, *Phys. Lett. A* **73** (1979) 371.

- [91] F. Ravndal, “Supersymmetric Dirac Particles in External Fields,” *Phys. Rev. D* **21** (1980) 2823.
- [92] P. A. M. Dirac, “Generalized Hamiltonian Dynamics”, *Can. J. Math.*, **2**, 129-148, 1950.,
- [93] P. A. M. Dirac, “Lectures on quantum mechanics”, New York, Belfer Graduate School of Science, Yeshiva University (1964), 87 p.
- [94] A. Hanson, T. Regge, C. Teitelboim, “Constrained Hamiltonian Systems”, RX-748, PRINT-75-0141 (IAS,PRINCETON) (1976).
- [95] M. Henneaux, C. Teitelboim, “Quantization of Gauge Systems”, Princeton, USA: Univ. Pr. 1992.
- [96] R. Casalbuoni, “On the quantization of systems with anticommuting variables”, *Il Nuovo Cimento A* **33** (1976) 115-125
- [97] B. De Witt, *Supermanifolds* Cambridge University Press (1992).
- [98] J. D. Jackson, “Classical Electrodynamics”, New York: Wiley, 2nd ed. (1975) 848 p.
- [99] D. J. Griffiths, “Introduction to electrodynamics”, Prentice Hall, 3rd ed. (1999) 576 p.
- [100] V. B. Berestetskii, E. M. Lifshitz and L. P. Pitaevskii, “Relativistic quantum theory”, Pergamon Press (1971-74) vol. I.
- [101] C. Schwartz, “Theory of Hyperfine Structure”, *Phys. Rev.* **97** (1955) 380,
- [102] E. Borie and G. A. Rinker, “The Energy Levels Of Muonic Atoms,” *Rev. Mod. Phys.* **54** (1982) 67.
- [103] J. Schwinger, “Particles, sources and fields”, Addison-Wesley Pub. Co. (1988-89), vol. II.
- [104] S. J. Brodsky and R. G. Parsons, “Precise Theory of the Zeeman Spectrum for Atomic Hydrogen and Deuterium and the Lamb Shift,” *Phys. Rev.* **163** (1967), 134-146 doi:10.1103/PhysRev.163.134
- [105] M. Horbatsch, E. A. Hessels, “Tabulation of the bound-state energies of atomic Hydrogen”, *Phys. Rev. A* **93** (2016) 022513,
- [106] M. I. Eides, H. Grotch and V. A. Shelyuto, “Theory of Light Hydrogenic Bound States,” *Springer Tracts Mod. Phys.* **222** (2007) pp. 1.
- [107] A. P. Martynenko and R. N. Faustov, “Hyperfine ground-state structure of muonic Hydrogen,” *J. Exp. Theor. Phys.* **98** (2004) no.1, 39 [*Zh. Eksp. Teor. Fiz.* **125** (2004) no.1, 48].
- [108] V. A. Yerokhin and V. M. Shabaev, “Nuclear Recoil Effect in the Lamb Shift of Light Hydrogenlike Atoms”, *Phys. Rev. Lett.*, **115** (2015) 233002,

- [109] E. Borie, “Lamb shift in light muonic atoms: Revisited,” *Annals Phys.* **327** (2012) 733 [arXiv:1103.1772 [physics.atom-ph]].
- [110] K. Pachucki, “Theory of the Lamb shift in muonic Hydrogen,” *Phys. Rev. A* **53** (1996) 2092.
- [111] G. T. Bodwin and D. R. Yennie, “Some Recoil Corrections to the Hydrogen Hyperfine Splitting,” *Phys. Rev. D* **37** (1988) 498.
- [112] R.N. Fell, I.B. Khriplovich, A.I. Milstein and A.S. Yelkhovsky, “On the Recoil Corrections in Hydrogen,” *Phys. Lett. A* **181** (1993) 172.
- [113] K. Pachucki and H. Grotch, “Pure Recoil Corrections to Hydrogen Energy Levels,” *Phys. Rev. A* **51** (1995) 1854.
- [114] R. N. Faustov, A. P. Martynenko, F. A. Martynenko and V. V. Sorokin, “Nuclear radiative recoil corrections to the hyperfine structure of S-states in muonic Hydrogen,” *Phys. Part. Nucl.* **48** (2017) no.5, 819.
- [115] S. G. Karshenboim, E. Y. Korzinin, V. A. Shelyuto and V. G. Ivanov, “Theory of Lamb Shift in Muonic Hydrogen”, *J. Phys. Chem. Ref. D.* **44** (2015) 031202,
- [116] A. Antognini, F. Kottmann, F. Biraben, P. Indelicato, F. Nez, R. Pohl, “Theory of the 2S-2P Lamb shift and 2S hyperfine splitting in muonic Hydrogen”, *Ann. Phys.*, **331** (2013) 127-145,
- [117] H. A. Bethe and E. E. Salpeter, *Quantum mechanics of one- and two-electron systems*, (Springer Berlin, Heidelberg, 1957) pp 88, 436.
- [118] D. J. Griffiths, “Introduction to quantum mechanics”, Pearson Prentice Hall, 2nd ed. (2005) 468 p.
- [119] J. J. Sakurai, “Modern quantum mechanics”, Addison-Wesley Pub. Co., Rev. ed. (1994) 500 p.
- [120] L. J. Slater, ‘Confluent Hypergeometric Functions’, Cambridge University Press, 1st ed. (1960) 260 p.
- [121] I. S. Gradshteyn and I. M. Ryzhik, “Table of Integrals, Series, and Products”, Academic Press, Seventh Ed. (2007) 1163 p.
- [122] F. W. J. Olver, A. B. Olde Daalhuis, D. W. Lozier, B. I. Schneider, R. F. Boisvert, C. W. Clark, B. R. Miller, B. V. Saunders, H. S. Cohl, and M. A. McClain, eds. “NIST Digital Library of Mathematical Functions”, <http://dlmf.nist.gov/> , Release 1.0.25 of 2019-12-15.

Chapter 5

Summary, Conclusion and Outlook

Summary and Conclusion

In the first chapter we started our discussion by presenting a review of EFTs that outlined how such theories emerge at low energies, E well-separated from some UV scale, Λ . We have seen that EFTs can be built by knowing the low-energy field content and symmetries of a theory and writing down all possible symmetry-preserving interactions between these fields and all their derivatives in an effective action that is essentially a multipole expansion of operators where higher-order terms are suppressed by increasing powers of the small ratio, $E/\Lambda \ll 1$. As such, these theories turned out to be non-renormalizable since they contain an infinite number of irrelevant operators in their actions, however due to the increasing suppression of terms by E/Λ to any given experimental accuracy it is only ever a finite-number of terms that enter into predictions of physical observables. These can be fit using measurements and used to make accurate predictions for other observables measurable with the same precision.

This was followed by constructing EFTs for lumps that are solutions to a given field's equations of motion that concentrate the energy into some region of spacetime and so have inherent size, R and are probed at some experimental scale, $a_{\text{exp}} \gg R$. The resulting EFTs turned out to depend only on the centre-of-mass coordinates of the lumps and their other internal degrees of freedom. When these lumps were coupled to external fields, their presence was shown to impose a set of near-source boundary conditions on these fields that specified the integration constants in the solutions to their equations of motion in such a way that the result would take into account the presence of the blob. Along the way of establishing this result we have identified PPEFTs as a class of these EFTs, where the lump is assumed to be a one-dimensional object.

Then, by drawing an analogy between a point-particle with centre-of-mass coordinates, $y^\mu(s)$ where s is some arbitrary parameter along the world-line of the particle, and one-dimensional lumps viewed from far away,

whose only low-energy fields are also their centre-of-mass coordinates, we have been able to identify the symmetries of such blobs to be that of Poincaré- and reparameterization invariance, hermiticity and symmetry under C-, P- and T-transformations. Afterwards, we charged this point-like object under a U(1) gauge field, $A^\mu(x)$ by introducing gauge-invariant interactions between the centre-of-mass coordinates of the lump and the gauge field. This gave rise to a Coulomb potential around the charged lump, which we have therefore identified to be a nucleus of charge, Ze . In this way we have found that a PPEFT with low-energy field content of only $y^\mu(s)$ governed by the symmetries of free point-particles and that of gauge-invariance are effective descriptions of spinless nuclei.

We then added the fermion field, $\Psi(x)$ of mass, m and charge $(-e)$ to the mix by minimally coupling them to the gauge field in the bulk to form the dynamics of QED and wrote down all their allowed effective interactions with the low-energy degrees of freedom of the nucleus. Then, we have found the bound-state solutions to the equations of motion of these fields with a Coulomb-potential that sample the nucleus at their Bohr radii, $a_B \sim (mZ\alpha)^{-1}$, meaning that the effective low-energy action of the nucleus for these states appear as a power series in the ratio, $R/a_B \sim (mRZ\alpha)$, revealing that the effective couplings in this action track the effects of the finite size of the nucleus. Then, we imposed the large- r boundary conditions on these solutions, which constrained the integration constant ratio, $\mathcal{D}_{j\varpi}/\mathcal{C}_{j\varpi}$ to satisfy (1.82). Consistency of this boundary condition with the one implied by the nuclear action lead to finite-size energy shifts as functions of $\mathcal{D}_{j\varpi}/\mathcal{C}_{j\varpi} \neq 0$. Then, it transpired that for these expressions to describe physical observables the PPEFT couplings had to flow in the RG sense and the energy shifts really only depended on the RG-invariant parameters of this running thanks to dimensional transmutation.

In the last section of the introduction we briefly introduced the history and current status of atomic bound-states with a special focus on finite-size effects to show that they are traditionally calculated as functions of numerous model-independent nuclear moments, and explained how these effects turn out to have such large uncertainties that they forbid accurately testing fundamental theory.

The first paper, presented in Chapter 2 detailed the above application of the PPEFT formalism to atomic bound-states of Dirac particles orbiting a heavy, scalar nucleus such as ${}^4_2\text{He}^{++}$. The new near-nucleus boundary conditions of $A^\mu(x)$ inferred from the nuclear action gave rise to the Coulomb field, which in turn lead to the Dirac-Coulomb bound-state solutions of (1.71) with (1.73). Then, by deriving the alternative near-nucleus boundary conditions for the lepton fields we have seen how the finite-size-related properties of the nucleus encoded by the PPEFT couplings enter bound-state energy shifts. We have further used these conditions to learn how these couplings have to depend on the fictitious scale, ϵ – the radius of the Gaussian sphere where we set up the boundary conditions – in order to keep energy shifts physical. Although we have advertised in the introduction

that it is through the RG-invariant parameters of this dependence that we should characterize the energy shifts, we instead chose here to parameterize them using effective moments, \hat{g}_i, \hat{f}_i . We have taken this parameterization out to subleading $(mRZ\alpha)$ and $(Z\alpha)^2$ orders relative to the leading term, which we have related to the charge-radius squared of nuclear moments found in the literature, such as those in eqs. (1.101), (1.102) and others. Lastly, we have worked out these effective moments for some specific charge distributions that had good analytical control.

In Chapter 3 we have expanded the nuclear action to include bulk-lump interactions suppressed by one additional factor of $R/a_B \sim (mRZ\alpha)$, *i.e.* operators with dimension $(length)^3$ coupling constants. By deriving the new near-nucleus boundary conditions for the fermionic field we have seen that trading their integration constant ratios $\mathcal{D}_{j\varpi}/\mathcal{C}_{j\varpi}$ for the PPEFT couplings introduced a more refined running of the couplings that was required to keep energy shifts physical but nevertheless, depended on the exact same RG-invariant parameters as its lower-order counterpart. We then used this more detailed RG-flow to write all the effective nuclear moments from the first paper as functions of the RG-invariant parameters, which in turn allowed us to write the nuclear-size energy shifts to the fermionic bound-states as a function of only one RG-invariant parameter, ϵ_\star . As such, we have been able to conclude that a single RG-invariant parameter, ϵ_\star is sufficient to capture finite nuclear-size effects in atoms out to and including subleading $(mRZ\alpha)$ and $(Z\alpha)^2$ orders relative to the leading term. This realization revealed that the PPEFT approach to these effects leads to fewer parameters than that of nuclear moments and we have shown what linear combinations of these moments ϵ_\star corresponds to. Finally, we have devised ways of exploiting the low number of these relevant parameters to make predictions in atoms with scalar nuclei whose nuclear-size related uncertainties were controlled by the errors of only the most precise measurements of spectroscopic transitions of the system and their corresponding theoretical contributions assuming a point-like nucleus, which therefore will only improve over time.

Lastly, in Chapter 4 we have detailed how to extend the PPEFT formalism to capture the effects of nuclei with spin, through the inclusion of a set of classically anti-commuting low-energy fields, $\xi^\mu(s)$ internal to the nucleus. This resulted in a small magnetic dipole field in the electromagnetic sector, which we treated in degenerate perturbation theory for the leptonic fields controlled by the parameter, $\mathfrak{s} := (me\mu_N)/4\pi \ll 1$. The correct zeroth order states that diagonalized this perturbation turned out to be the eigenstates of the total atomic angular momentum, $\mathbf{F} = \mathbf{I} + \mathbf{J}$ and their first-order energy shifts and state corrections were computed. This perturbation approach led to divergent matrix elements of the combined nuclear-Dirac-Coulomb modes, whose infinities we tracked through dimensional regularization and in the end were able to absorb into an $\mathcal{O}(\mathfrak{s})$ combination of PPEFT couplings thanks to the new near-nucleus boundary conditions also appearing at this order. These boundary conditions

also necessitated the running of this new coupling in the ϵ -parameter of the Gaussian sphere where they had been imposed, and we found that in addition to the familiar RG-invariant, ϵ_* a new RG-invariant parameter, ϵ_F had to be defined in order to capture spin-dependent finite-size-related energy shifts. We compared these energy shifts written in terms of our RG-invariant parameters to the same ones written as functions of the more traditional nuclear moments and were able to relate ϵ_F to the first Zemach-moment, $\langle r \rangle_{cm}$ of (1.99). In the end, exploiting the low number of RG-invariant scales the same way we had done for spinless nuclei we have used high-precision data for both electronic- and muonic Hydrogen to fit these parameters and make predictions for the finite-size effects of transitions in these systems. It so happened that due to the small mass of the electron we were able to make many predictions in atomic Hydrogen in which the uncertainties associated with nuclear-size effects were unusually small thanks to the errors on our parameters only being controlled by the most accurate measurements and their theoretical QED contributions that assume a point-like nucleus. While the latter point also applies to muonic Hydrogen, due to the larger mass of muons there are additional subleading effects relative to the ones we have included that need to be taken into account in order to accurately capture all finite-size effects to the accuracy of current measurements. Nevertheless, by fitting our two parameters we were able to make a prediction for the nuclear-size effects in the planned ground-state hyperfine splitting [49] with errors competitive with the same predictions made using nuclear moments.

In conclusion, we established that an effective description of atomic systems can be obtained through the low-energy effective theory of one-dimensional lumps of size, $R \sim 1$ fm and its implications for the surrounding bulk fields that probe its presence at scales of the fermionic Bohr radius, a_B . The interplay between these two components of the theory are captured by a hermitian one-dimensional effective action along the world-line of the nucleus that is a multipole expansion in the ratio, R/a_B of interactions between the bulk fields and the low-energy nuclear degrees of freedom. In line with our model-building algorithms we have found that the field content of the theory comprises of the bulk fields and the nuclear centre-of-mass coordinates, $y^\mu(s)$ and spin, $\xi^\mu(s)$, and that Poincaré, reparameterization, gauge, C, P and T-invariance make up the symmetries of the system. The bulk fields learn about the presence of the nucleus through the near-source boundary conditions this PPEFT action implies for them on a Gaussian pillbox of size, ϵ that obeys $R \ll \epsilon \ll a_B$ and in whose arbitrary radius the effective nuclear couplings turn out to flow in an RG-sense in order to keep observables physical. This flow is characterized by a handful of RG-invariant parameters that actual observables turn out to depend on, and in particular the bound-state energies depend on these parameters through requiring consistency between the new near-nucleus boundary conditions and the one demanding normalizability at large- r . Finally, we used this

newfound power to reduce the theoretical error floor in nuclear-size effect predictions of ${}^4_2\text{He}^+$, $\mu_2^4\text{He}^+$ H and μH .

Future Directions

Muonic Hydrogen

In order to capture all finite-size-related energy shifts in muonic Hydrogen relevant for current experiments we would need to include spin-independent contributions of $(mRZ\alpha)^2$ and spin-dependent finite-size effects of order $(mRZ\alpha)$ relative to their respective leading order terms. This amounts to expanding the nuclear action to include spin-independent nucleus-bulk couplings of dimension $(length)^4$ and spin-dependent ones of dimension $(length)^3$ that, however are still linear in nuclear spin. Then, by also capturing higher order terms in the energy shift coming from the large- r normalizability condition in (1.82), and analyzing the running of the new couplings implied by the alternative near-nucleus fermionic boundary conditions derived from the nuclear action, we could either find new RG-invariant parameters that account for these effects or find that no new RG-invariant parameters emerge and the existing ones become more refined, similarly to how it had happened in the work presented in Chapter 3. It should be noted however, that the RG-invariant parameter controlling the spin-independent finite-size effects of $j = 3/2$ states also become observable once effects of the targeted size are included, thereby enlarging our number of effective parameters. Nevertheless, this is a worthwhile and timely endeavour as it would allow for a more accurate prediction of the finite-size effects in the ground-state hyperfine splitting of this system.

Atoms other than hydrogen

There are many upcoming spectroscopic experiments – particularly on muonic atoms, such as muonic lithium, beryllium, *etc* [50] – to which our methods can be readily applied. Provided that we can capture all the relevant finite-size effects in these alternative systems it becomes possible to derive a floor on the nuclear-size related uncertainties that is controlled by the experimental precision and the point-like theoretical contributions to the energy transitions these experiments measure. With a systematic search for such systems we could largely expand the scope of PPEFT in atomic physics and potentially produce this low-error floor for all of them now that spin is not an obstruction to this program anymore.

Recoil effects

One of the major pieces missing in our calculations of atomic nuclear-size effects are the nuclear recoil corrections to them. The very leading parts of these can be easily included (and have been in our numerical studies)

by trading the lepton masses for their reduced mass counterparts, and the first non-trivial (*i.e.* not reproducible by a simple replacement of the lepton mass by its reduced mass factor) recoil corrections to finite-size effects were calculated in [28] and accounted for in Chapter 4. A more systematic inclusion of these mixed effects will involve assuming the nucleus to no longer be at rest and so $\dot{y}^\mu \neq \delta_0^\mu$, hence $\sqrt{-\dot{y}^2} = \sqrt{1 - \dot{\mathbf{y}}^2}$ and tracking the non-zero velocities $\dot{\mathbf{y}}^2$ will show us where the recoil effects hide.

Bound-states of other and more fields

Another missing piece from our framework is the inclusion of more orbiting leptons. This is a particularly important extension because for many atoms, obtaining highly ionized nuclei with a single electron is an experimentally difficult task; therefore, by including more orbiting leptons we could potentially expand our analysis to more experimentally testable systems.

Experiments that bind particles other than fermions to Hydrogen also exist and by choosing the bulk action to be different these can also be included in our PPEFT framework. Of particular importance could be the pionic and kaonic Hydrogen systems, where it is a spinless meson orbiting the nucleus, since for these systems we have already made some progress in [2]. However, note that due to the larger masses of these particles, recoil effects may feature in a more prominent role than we have given them credit for in the past.

Radiative corrections

In both the second and third papers, we have captured effects that are of the same order of magnitude as the radiative corrections to the leading and subleading finite-size effects. Our strategy to include these for our prediction algorithms has been to use the matching of the RG-invariants $\epsilon_\star, \epsilon_F$ to nuclear moments from the literature such as $\langle r^2 \rangle_c, \langle r \rangle_{cm}$ to write the radiative corrections written in terms of these moments in terms of the RG-invariant scales instead. However, since the external electron fields are assumed to be proper quantum fields in our framework, there is certainly room to explore the proper inclusion of radiative effects through the computation of loops, with the anticipated result that these will give us exactly the same energy shifts that we had used in our calculations based on the matching described above. In other words, in our PPEFT treatments so far we have modified the interaction picture evolutions of the fields from those of free fields to the integrable parts of their field equations and by taking into account Feynman diagrammatic expansions in the remaining interactions will allow us to account for the effects of second-quantization, such as self-energy and vacuum-polarization of the modified interaction-picture propagators.

Matching calculations

We have expressly avoided dealing with the specifics of how the background configurations for which we have developed our EFT methods were generated. However, this does not mean that such a calculation should not be done, and in fact this direction should definitely be pursued as it would tell us how more well-understood interactions of the UV theory lead to the effective couplings we have introduced by hand. In turn, this may be able to reveal in what way the RG-invariant parameters depend on the leptonic quantum numbers for example. At the moment, this is an active area of research that my esteemed colleague soon-to-be doctor Peter Hayman is working on, and if you are interested you will be able to read about it in his future publications.

Bibliography

- [1] C. P. Burgess, P. Hayman, M. Williams and L. Zalavari, “Point-Particle Effective Field Theory I: Classical Renormalization and the Inverse-Square Potential,” JHEP **1704** (2017) 106 doi:10.1007/JHEP04(2017)106 [arXiv:1612.07313 [hep-ph]].
- [2] C. P. Burgess, P. Hayman, M. Rummel, M. Williams and L. Zalavari, “Point-Particle Effective Field Theory II: Relativistic Effects and Coulomb/Inverse-Square Competition,” JHEP **1707** (2017) 072 doi:10.1007/JHEP07(2017)072 [arXiv:1612.07334 [hep-ph]].
- [3] C. P. Burgess, P. Hayman, M. Rummel and L. Zalavari, “Point-Particle Effective Field Theory III: Relativistic Fermions and the Dirac Equation,” JHEP **09** (2017), 007 doi:10.1007/JHEP09(2017)007 [arXiv:1706.01063 [hep-ph]].
- [4] C. P. Burgess, P. Hayman, M. Rummel and L. Zalavari, “Reduced theoretical error for ${}^4\text{He}^+$ spectroscopy,” Phys. Rev. A **98** (2018) no.5, 052510 doi:10.1103/PhysRevA.98.052510 [arXiv:1708.09768 [hep-ph]].
- [5] C. P. Burgess, R. Plestid and M. Rummel, “Effective Field Theory of Black Hole Echoes,” JHEP **09** (2018), 113 doi:10.1007/JHEP09(2018)113 [arXiv:1808.00847 [gr-qc]].
- [6] P. Hayman and C. P. Burgess, “Point-Particle Catalysis,” Front. in Phys. **7** (2019), 167 doi:10.3389/fphy.2019.00167 [arXiv:1905.00103 [hep-th]].
- [7] M. Rummel and C. P. Burgess, “Constraining Fundamental Physics with the Event Horizon Telescope,” JCAP **05** (2020), 051 doi:10.1088/1475-7516/2020/05/051 [arXiv:2001.00041 [gr-qc]].
- [8] R. Plestid, C. P. Burgess and D. H. J. O’Dell, “Fall to the Centre in Atom Traps and Point-Particle EFT for Absorptive Systems,” JHEP **18** (2020), 059 doi:10.1007/JHEP08(2018)059 [arXiv:1804.10324 [hep-ph]].
- [9] C. P. Burgess, P. Hayman, M. Rummel and L. Zalavári, “Nuclear Predictions for H Spectroscopy without Nuclear Errors,” [arXiv:2008.09719 [hep-ph]].

- [10] L. Zalavari, C. P. Burgess, P. Hayman and M. Rummel, “Precision Nuclear-Spin Effects in Atoms: EFT Methods for Reducing Theory Errors,” [arXiv:2008.09718 [hep-ph]].
- [11] K. G. Wilson and J. B. Kogut, “The Renormalization group and the epsilon expansion,” *Phys. Rept.* **12** (1974) 75. doi:10.1016/0370-1573(74)90023-4
- [12] A. Zee, “Quantum Field Theory in a Nutshell”, Princeton University Press, Second Edition (2010) 608 p.
- [13] Michael E. Peskin, Daniel V. Schroeder, “An Introduction to Quantum Field Theory”, Westview Press, First Edition (1995) 866 p.
- [14] Matthew D. Schwartz, “Quantum Field Theory and the Standard Model”, Cambridge University Press, First Edition (2014) 863 p.
- [15] C.P. Burgess, *Introduction to Effective Field Theory: Thinking effectively about hierarchies of scale*, Cambridge University Press 2020 (in press).
- [16] A. Hanson, T. Regge, C. Teitelboim, “Constrained Hamiltonian Systems”, RX-748, PRINT-75-0141 (IAS,PRINCETON) (1976).
- [17] D. M. Gitman and I. V. Tyutin, “Quantization of Fields with Constraints,” Springer (1990), 291 p.
- [18] M. Henneaux, C. Teitelboim, “Quantization of Gauge Systems”, Princeton, USA: Univ. Pr. 1992.
- [19] S. Carroll, “Spacetime and geometry: an introduction to general relativity”, Addison Wesley, (2004) 513 p.
- [20] J. G. Polchinski, “String Theory”, Cambridge University Press (1998) vol. I & II.
- [21] B. Zwiebach, “A First Course in String Theory”, Cambridge University Press, Second Edition, (2009) 694 p.
- [22] J. D. Jackson, “Classical Electrodynamics”, New York: Wiley, 2nd ed. (1975) 848 p.
- [23] V. B. Berestetskii, E. M. Lifshitz and L. P. Pitaevskii, “Relativistic quantum theory”, Pergamon Press (1971-74) vol. I.
- [24] Steven Weinberg, “The Quantum Theory of Fields: Foundations” Cambridge University Press, Vol. 1, First Edition (1998) 640 p.
- [25] M. I. Eides, H. Grotch and V. A. Shelyuto, “Theory of Light Hydrogenic Bound States,” *Springer Tracts Mod. Phys.* **222** (2007) pp. 1. doi:10.1007/3-540-45270-2

- [26] R. Karplus, A. Klein and J. Schwinger, “Electrodynamic Displacement of Atomic Energy Levels. 2. Lamb Shift,” *Phys. Rev.* **86** (1952) 288. doi:10.1103/PhysRev.86.288
- [27] A. C. Zemach, “Proton Structure and the Hyperfine Shift in Hydrogen,” *Phys. Rev.* **104** (1956) 1771. doi:10.1103/PhysRev.104.1771
- [28] J. L. Friar, “Nuclear finite-size effects in light muonic atoms”, *Ann. Phys.* **122** (1978) 152-196 doi:10.1016/0003-4916(79)90300-2
- [29] K. Pachucki, “Theory of the Lamb shift in muonic Hydrogen,” *Phys. Rev. A* **53** (1996) 2092.
- [30] S. G. Karshenboim, “Nuclear structure dependent radiative corrections to the Hydrogen hyperfine splitting,” *Phys. Lett. A* **225** (1997) 97 [hep-ph/9608484].
- [31] K. Pachucki and A. Wienczek, “Nuclear structure effects in light muonic atoms,” *Phys. Rev. A* **91** (2015) no.4, 040503 [arXiv:1501.07451 [physics.atom-ph]].
- [32] S. G. Karshenboim, E. Y. Korzinin, V. A. Shelyuto and V. G. Ivanov, “Theory of Lamb Shift in Muonic Hydrogen”, *J. Phys. Chem. Ref. D.* **44** (2015) 031202,
- [33] A. E. Dorokhov, N. I. Kochelev, A. P. Martynenko, F. A. Martynenko and A. E. Radzhabov, “Corrections of two-photon interactions in the fine and hyperfine structure of the P-energy levels of muonic Hydrogen,” *Eur. Phys. J. A* **54** (2018) no.8, 131 [arXiv:1804.09749 [hep-ph]].
- [34] K. Pachucki, V. Patkóš and V. A. Yerokhin, “Three-photon exchange nuclear structure correction in Hydrogenic systems,” *Phys. Rev. A* **97** (2018) no.6, 062511 [arXiv:1803.10313 [physics.atom-ph]].
- [35] J. Friar, “Nuclear Polarization Corrections to $\mu - d$ Atoms in Zero-Range Approximation,” *Phys. Rev. C* **88** (2013) no.3, 034003 [arXiv:1306.3269 [nucl-th]].
- [36] V. A. Yerokhin and V. M. Shabaev, “Nuclear Recoil Effect in the Lamb Shift of Light Hydrogenlike Atoms”, *Phys. Rev. Lett.*, **115** (2015) 233002,
- [37] A. P. Martynenko and R. N. Faustov, “Hyperfine ground-state structure of muonic Hydrogen,” *J. Exp. Theor. Phys.* **98** (2004) no.1, 39 [*Zh. Eksp. Teor. Fiz.* **125** (2004) no.1, 48].
- [38] M. Kalinowski, K. Pachucki and V. A. Yerokhin, “Nuclear-structure corrections to the hyperfine splitting in muonic deuterium,” *Phys. Rev. A* **98** (2018) no.6, 062513 [arXiv:1810.06601 [physics.atom-ph]].

- [39] M. Horbatsch, E. A. Hessels, “Tabulation of the bound-state energies of atomic Hydrogen”, *Phys. Rev. A* **93** (2016) 022513,
- [40] A. E. Kramida, “A Critical Compilation of Experimental Data on Spectral Lines and Energy Levels of Hydrogen, Deuterium and Tritium”, *At. Data Nucl. Data Tables*, **96**, (2010) 586-644,
- [41] A. Antognini, F. Nez, K. Schuhmann et. al., “Proton Structure from the Measurement of 2S-2P Transition Frequencies of Muonic Hydrogen”, *Science*, **339**, (2013) 417-420,
- [42] R. Pohl, A. Antognini, F. Nez et. al. “The size of the proton”, *Nature*, **466** (2010) 213-216, doi:10.1038/nature09250.
- [43] P. J. Mohr, D. B. Newell and B. N. Taylor, “CODATA Recommended Values of the Fundamental Physical Constants: 2014,” *Rev. Mod. Phys.* **88** (2016) no.3, 035009 doi:10.1103/RevModPhys.88.035009 [arXiv:1507.07956 [physics.atom-ph]].
- [44] R. J. Hill, “Review of Experimental and Theoretical Status of the Proton Radius Puzzle,” *EPJ Web Conf.* **137** (2017) 01023 doi:10.1051/epjconf/201713701023 [arXiv:1702.01189 [hep-ph]].
- [45] A. E. Dorokhov, A. P. Martynenko, F. A. Martynenko and A. E. Radzhabov, “The proton size puzzle: experiment vs theory.,” *EPJ Web Conf.* **191** (2018) 04001. doi:10.1051/epjconf/201819104001
- [46] G. Paz, “The Proton Radius Puzzle,” arXiv:1909.08108 [hep-ph].
- [47] National Institute of Standards and Technology, “2018 CODATA recommended values”, <https://physics.nist.gov/cgi-bin/cuu/Value?rp>
- [48] L. Brink, P. Di Vecchia, P. Howe, “A Lagrangian formulation of the classical and quantum dynamics of spinning particles”, *Nucl. Phys. B* **118** (1977) 76-94
- [49] S. Kanda et. al., “Measurement of the proton Zemach radius from the hyperfine splitting in muonic Hydrogen atom”, *J. Phys.: Conf. Ser.* **1138** (2018) 012009,
- [50] S. Schmidt et. al., “The next generation of laser spectroscopy experiments using light muonic atoms”, *J. Phys.: Conf. Ser.* **1138** (2018) 012010,